

Advances in neural reprogramming, disease modeling and therapeutic insights

Edited by

Shong Lau, Fred H. Gage, Shani Stern and
Janelle Drouin-Ouellet

Published in

Frontiers in Aging Neuroscience
Frontiers in Neuroscience
Frontiers in Cellular Neuroscience



FRONTIERS EBOOK COPYRIGHT STATEMENT

The copyright in the text of individual articles in this ebook is the property of their respective authors or their respective institutions or funders. The copyright in graphics and images within each article may be subject to copyright of other parties. In both cases this is subject to a license granted to Frontiers.

The compilation of articles constituting this ebook is the property of Frontiers.

Each article within this ebook, and the ebook itself, are published under the most recent version of the Creative Commons CC-BY licence. The version current at the date of publication of this ebook is CC-BY 4.0. If the CC-BY licence is updated, the licence granted by Frontiers is automatically updated to the new version.

When exercising any right under the CC-BY licence, Frontiers must be attributed as the original publisher of the article or ebook, as applicable.

Authors have the responsibility of ensuring that any graphics or other materials which are the property of others may be included in the CC-BY licence, but this should be checked before relying on the CC-BY licence to reproduce those materials. Any copyright notices relating to those materials must be complied with.

Copyright and source acknowledgement notices may not be removed and must be displayed in any copy, derivative work or partial copy which includes the elements in question.

All copyright, and all rights therein, are protected by national and international copyright laws. The above represents a summary only. For further information please read Frontiers' Conditions for Website Use and Copyright Statement, and the applicable CC-BY licence.

ISSN 1664-8714
ISBN 978-2-8325-3221-8
DOI 10.3389/978-2-8325-3221-8

About Frontiers

Frontiers is more than just an open access publisher of scholarly articles: it is a pioneering approach to the world of academia, radically improving the way scholarly research is managed. The grand vision of Frontiers is a world where all people have an equal opportunity to seek, share and generate knowledge. Frontiers provides immediate and permanent online open access to all its publications, but this alone is not enough to realize our grand goals.

Frontiers journal series

The Frontiers journal series is a multi-tier and interdisciplinary set of open-access, online journals, promising a paradigm shift from the current review, selection and dissemination processes in academic publishing. All Frontiers journals are driven by researchers for researchers; therefore, they constitute a service to the scholarly community. At the same time, the *Frontiers journal series* operates on a revolutionary invention, the tiered publishing system, initially addressing specific communities of scholars, and gradually climbing up to broader public understanding, thus serving the interests of the lay society, too.

Dedication to quality

Each Frontiers article is a landmark of the highest quality, thanks to genuinely collaborative interactions between authors and review editors, who include some of the world's best academicians. Research must be certified by peers before entering a stream of knowledge that may eventually reach the public - and shape society; therefore, Frontiers only applies the most rigorous and unbiased reviews. Frontiers revolutionizes research publishing by freely delivering the most outstanding research, evaluated with no bias from both the academic and social point of view. By applying the most advanced information technologies, Frontiers is catapulting scholarly publishing into a new generation.

What are Frontiers Research Topics?

Frontiers Research Topics are very popular trademarks of the *Frontiers journals series*: they are collections of at least ten articles, all centered on a particular subject. With their unique mix of varied contributions from Original Research to Review Articles, Frontiers Research Topics unify the most influential researchers, the latest key findings and historical advances in a hot research area.

Find out more on how to host your own Frontiers Research Topic or contribute to one as an author by contacting the Frontiers editorial office: frontiersin.org/about/contact

Advances in neural reprogramming, disease modeling and therapeutic insights

Topic editors

Shong Lau — Salk Institute for Biological Studies, United States

Fred H. Gage — Salk Institute for Biological Studies, United States

Shani Stern — University of Haifa, Israel

Janelle Drouin-Ouellet — Montreal University, Canada

Citation

Lau, S., Gage, F. H., Stern, S., Drouin-Ouellet, J., eds. (2023). *Advances in neural reprogramming, disease modeling and therapeutic insights*.

Lausanne: Frontiers Media SA. doi: 10.3389/978-2-8325-3221-8

Table of contents

- 05 **Editorial: Advances in neural reprogramming, disease modeling and therapeutic insights**
Shong Lau and Shani Stern
- 08 **The role of brain derived neurotrophic factor in central nervous system**
Yiyi Li, Fang Li, Dongdong Qin, Hongyu Chen, Jianhao Wang, Jiabei Wang, Shafei Song, Chao Wang, Yamei Wang, Songyan Liu, Dandan Gao and Zhi-Hao Wang
- 21 **A long-term high-fat diet influences brain damage and is linked to the activation of HIF-1 α /AMPK/mTOR/p70S6K signalling**
Fei Chen, Wen-min Yi, Sheng-yuan Wang, Ming-hao Yuan, Jie Wen, Hong-Yan Li, Qian Zou, Shu Liu and Zhi-you Cai
- 34 **CT-guided radiofrequency ablation of the extracranial cranial nerve for the treatment of Meige's syndrome**
Bing Huang, Xin-dan Du, Ming Yao, Hui-dan Lin, Wen-hua Yu and Qing-he Zhou
- 42 **Enhanced recruitment of glutamate receptors underlies excitotoxicity of mitral cells in acute hyperammonemia**
Mingxian Li, Zhenqi Liu, Ke Lai, Hanwei Liu, Lina Gong, Haosong Shi, Weitian Zhang, Hui Wang and Haibo Shi
- 57 **Pluripotent stem cell strategies for rebuilding the human brain**
Francesco Limone, Joseph R. Klim and Daniel A. Mordes
- 73 **Induced pluripotent stem cell-derived and directly reprogrammed neurons to study neurodegenerative diseases: The impact of aging signatures**
Simona Aversano, Carmen Caiazza and Massimiliano Caiazza
- 89 **Contrast-induced encephalopathy and permanent neurological deficit following cerebral angiography: A case report and review of the literature**
Yujing Zhang, Jiancheng Zhang, Shiyang Yuan and Huaqing Shu
- 111 **Upregulation of C-X-C motif chemokine 12 in the spinal cord alleviated the symptoms of experimental autoimmune encephalomyelitis in Lewis rats**
Dahe Lin, Hongjuan Liu, Honglu Song, Biye Chen, Junxia Fu, Mingming Sun, Huanfen Zhou, Wenhao Bai, Shihui Wei and Hongen Li
- 123 **Fountain of youth—Targeting autophagy in aging**
Lea Danics, Anna Anoir Abbas, Balázs Kis and Karolina Pircs
- 139 **The complex interplay of hypoxia and sleep disturbance in gray matter structure alterations in obstructive sleep apnea patients**
Jing Wang, Yezhou Li, Lirong Ji, Tong Su, Chaohong Cheng, Fei Han, Daniel J. Cox, Erlei Wang and Rui Chen

- 147 **Long-term survival benefits of intrathecal autologous bone marrow-derived mesenchymal stem cells (Neuronata-R®: lenzumestrocel) treatment in ALS: Propensity-score-matched control, surveillance study**
Jae-Yong Nam, Sehwan Chun, Tae Yong Lee, Yunjeong Seo, Kwijoo Kim, Jinseok Park, Wonjae Sung, Ki-Wook Oh, Sanggon Lee, Jin-Sung Park, Juyeon Oh, Kyung Cheon Chung, Hyonggin An, Hyeon Sik Chu, Bugyeong Son and Seung Hyun Kim
- 157 **Lactoferrin/sialic acid prevents adverse effects of intrauterine growth restriction on neurite length: investigations in an *in vitro* rabbit neurosphere model**
Britta Anna Kühne, Lara Gutierrez-Vázquez, Estela Sánchez Lamelas, Laia Guardia-Escote, Laura Pla, Carla Loreiro, Eduard Gratacós, Marta Barenys and Miriam Illa



OPEN ACCESS

EDITED AND REVIEWED BY
Jorge Busciglio,
University of California, Irvine, United States

*CORRESPONDENCE
Shani Stern
✉ sstern@univ.haifa.ac.il

RECEIVED 16 July 2023
ACCEPTED 20 July 2023
PUBLISHED 28 July 2023

CITATION
Lau S and Stern S (2023) Editorial: Advances in neural reprogramming, disease modeling and therapeutic insights.
Front. Aging Neurosci. 15:1259765.
doi: 10.3389/fnagi.2023.1259765

COPYRIGHT
© 2023 Lau and Stern. This is an open-access article distributed under the terms of the [Creative Commons Attribution License \(CC BY\)](#). The use, distribution or reproduction in other forums is permitted, provided the original author(s) and the copyright owner(s) are credited and that the original publication in this journal is cited, in accordance with accepted academic practice. No use, distribution or reproduction is permitted which does not comply with these terms.

Editorial: Advances in neural reprogramming, disease modeling and therapeutic insights

Shong Lau¹ and Shani Stern^{2*}

¹Laboratory of Genetics, Salk Institute for Biological Studies, La Jolla, CA, United States, ²Sagol Department of Neurobiology, Faculty of Natural Sciences, University of Haifa, Haifa, Israel

KEYWORDS

induced pluripotent stem cells, neurodegeneration, disease modeling, reprogramming, transplants, therapeutics

Editorial on the Research Topic

Advances in neural reprogramming, disease modeling and therapeutic insights

The human race advanced in the last century in an exponentially growing increase of knowledge. We can send rockets to space, use computers that can easily store terabytes of information and do billions of instructions per second, develop artificial intelligence that is hard to distinguish from a living human person and build smartphones that can communicate dozens of megabytes of information every second between distant places on earth. However, despite major advances in the medical field, many brain-related disorders and diseases still have no cures today, and often we cannot even understand why the disease has started. Disease modeling should therefore be a top priority. Stem cell models and regeneration using stem cells play an important role and hold great promise both for understanding disease and also for cures, especially in neurodegenerative disease. In this Research Topic of Frontiers in Aging Neuroscience, important advances in the field have been reported. This Research Topic includes models for neurodegenerative diseases, potential new therapeutics, and related reviews summarizing what is currently known in the field.

Patient-derived neurons are excellent models but in addition, are now considered also as a huge potential for transplantation and cell replacement in the cases of neurodegeneration or trauma. [Limone et al.](#) reviewed the literature on this important topic. The authors cover advances in methods used to differentiate human pluripotent stem cells into several highly specialized types of neurons, including cholinergic, dopaminergic, and motor neurons, and the potential clinical applications of stem cell-derived neurons for common neurodegenerative diseases, including Alzheimer's disease, Parkinson's disease, Huntington's disease, ataxia, and amyotrophic lateral sclerosis. Differentiation techniques for glial cell populations are also described in their review, including oligodendrocytes and microglia. Clinical trials of cell replacement therapies in the nervous system are underway holding great promise in regenerative medicine.

Mesenchymal stem cells have also been shown to incur regenerative possibilities ([Guo et al., 2019](#); [Margiana et al., 2022](#)). [Nam et al.](#) have sought to explore the regenerative potential of an autologous bone marrow-derived mesenchymal stem cell (BM-MSC) product (Neuronata-R[®] lenzumestrocel) in amyotrophic lateral sclerosis (ALS). The survival rate of 157 patients treated with intrathecal lenzumestrocel

was compared with placebo-treated patients. Remarkably, the treated patients' survival after 500 and 1,000 days were orders of magnitude higher than the placebo groups, even with a single dose. Therefore, lenzumestrol treatment is concluded to have a significant, long-term survival benefit in ALS patients.

Neurons derived through the reprogramming of somatic cells and differentiation have been shown to lack aging related signatures and are considered rejuvenated (Mertens et al., 2018). Studies show that even these young neurons carry information that relates to biological differences in the patients' brains (Choudhary et al., 2022; Hussein et al., 2023) and the case of neurodegenerative disease these probably occur long before the disease onset (Stern et al., 2022; Rike and Stern, 2023). However, other studies show also that especially in aging-related diseases, it may be important to use models where the age signatures persist through the differentiation (Mertens et al., 2021; Lau et al., 2022). Aversano et al. reviewed the latest literature on iPSC-derived neurons vs. directly converted neurons from somatic cells that retain the aging information and epigenetic modifications and listed the advantages and disadvantages of these methods.

Autophagy, a cellular process crucial for maintaining cellular homeostasis, takes center stage in the mini-review from Danics et al. It explores the role of autophagy in aging and age-related neurodegenerative diseases, such as Alzheimer's disease, Parkinson's disease, and Huntington's disease. Dysfunctional autophagy is commonly observed in these diseases, leading to the accumulation of toxic proteins and cellular imbalance. Danics et al. emphasize the potential of targeting autophagy as a therapeutic approach, opening doors to novel pharmacological interventions and clinical trials. Human-relevant models, including induced pluripotent stem cell-derived neurons and directly reprogrammed neurons, offer valuable insights into autophagy alterations and can aid in the development of effective treatments.

Chen et al. highlighted the detrimental effects of a long-term high-fat diet (HFD) on the brain and its link to the activation of specific signaling pathways. The study provides compelling evidence of the molecular pathology underlying obesity-related brain damage and cognitive impairment. It highlights the importance of understanding the impact of HFD on brain metabolism, especially in the context of aging and neurodegenerative diseases. These findings contribute to the development of diagnostic strategies and personalized treatment approaches for age-related conditions and neurodegenerative disorders.

Sleep disturbances have been previously associated with an increased probability of cognitive decline and neurodegeneration (Raggi and Ferri, 2010; Trotti and Karroum, 2016; Wennberg et al., 2017). Wang et al. have investigated Obstructive Sleep Apnea (OSA) that leads to hypoxia and sleep disturbance. The authors used structural equation modeling to investigate how hypoxia and sleep disturbance affect gray matter structures. For this, 74 participants underwent overnight polysomnography and T1-weighted Magnetic Resonance Imaging. The computational models revealed hypoxia-associated increases in gray matter volume, cortical thickness, and sulcal depth. Sleep disturbance on the other hand was shown to be largely associated with reduced gray matter volume and sulcal depth.

The dysfunction of BDNF signaling has central roles in neurological disorders including psychiatric and neurodegenerative diseases (Boulle et al., 2012; Lima Giacobbo et al., 2019; Miranda et al., 2019). Li Y. et al. explored the impact of Brain-derived neurotrophic factor (BDNF) dysfunctions that are mediated by the activation of two receptors, tropomyosin receptor kinase B (TrkB) receptor and the p75 neurotrophin receptor and are involved in physiological and pathological processes throughout life. Their review discusses the current knowledge and future directions in BDNF-associated research with an emphasis on the physiological and pathological functions in a long list of neurodegenerative diseases as well as other diseases such as diabetes and cancer. Methods to increase BDNF levels are discussed and BDNF-overexpressed stem cell transplantation is suggested as a possible promising therapeutic strategy.

In the study of Kühne et al. an *in vitro* rabbit neurosphere model was introduced to study the effects of intrauterine growth restriction (IUGR) on neuronal development. IUGR is known to cause neurodevelopmental abnormalities, and this model mimics the conditions seen in humans. The neuroprotective properties of lactoferrin, a potential therapeutic agent, were highlighted in preventing adverse effects on neurite length associated with IUGR. These findings provide valuable insights into the development of interventions to protect against IUGR-induced alterations in neuronal development and improve long-term cognitive outcomes.

Lin et al. unravel the role of C-X-C motif chemokine 12 (CXCL12) in experimental autoimmune encephalomyelitis (EAE), an animal model of multiple sclerosis (MS). The team used gene therapy to upregulate CXCL12 in the spinal cord of rats and induced EAE. They found that upregulated CXCL12 alleviated EAE symptoms and reduced clinical scores. The levels of myelin basic protein (MBP) and glial fibrillary acidic protein (GFAP) were higher in the CXCL12 group, indicating enhanced remyelination. Interestingly, the upregulation of CXCL12 did not induce significant leukocyte infiltration into the spinal cord. The study also demonstrated that CXCL12 promoted the differentiation of OPCs into oligodendrocytes *in vitro*. This study offers new avenues for targeting the CXCL12/CXCR4 axis as a potential therapeutic approach to enhance remyelination in MS and sheds light on the underlying mechanisms involved.

Contrast-induced encephalopathy (CIE) is a rare complication arising from exposure to iodinated contrast media during angiographic procedures. The review from Zhang et al. provides insights into the risk factors associated with prognosis. Female gender, younger age, higher contrast medium dose, and cerebral angiography procedure were linked to a poorer prognosis. Comorbidities such as hypertension, diabetes mellitus, renal insufficiency, and previous reactions to contrast media were also identified as potential risk factors. Neuroimaging and cerebrospinal fluid examination can aid in diagnosing CIE and distinguishing it from other neurological conditions. Supportive care, hydration, steroids, mannitol, and anti-epileptic medications are common treatment approaches. The review emphasizes that CIE can have lasting neurological effects, even with low doses of contrast media, and highlights the need for further research to better understand and manage this condition.

Meige's syndrome is a rare form of cranial dystonia. Current treatments such as oral medications and botulinum toxin injections have limitations. Deep brain stimulation is an alternative but has technical requirements and high costs. Huang et al. explore the use of CT-guided extracranial radiofrequency ablation for Meige's syndrome. They performed radiofrequency ablation on cranial nerves involved in the condition, targeting specific muscles. They found that the treatment resulted in symptom alleviation, although some patients experienced mild facial paralysis and sensory changes. Recurrences were observed in two cases. They suggested that CT-guided extracranial radiofrequency ablation could be a potential treatment option for Meige's syndrome, in addition to botulinum toxin injections and deep brain stimulation.

A major complication of liver disease is Hepatic encephalopathy. Through elevated levels of ammonia/ammonium in the blood and cerebrospinal fluid, the patients suffer from olfactory dysfunction. Li M. et al. performed patch-clamp recordings of mitral cells (MCs) in the mouse olfactory bulb (OB) and found involvement of glutamate receptors in NH_4^+ -induced hyperexcitability of MCs. NH_4^+ reduced the currents of voltage-gated K^+ channel (Kv) that may be linked to an attenuation of the spontaneous firing amplitudes. NH_4^+ also enhanced the amplitude of long-lasting spontaneous excitatory post-synaptic currents (sEPSCs) and increased the expression of NR1 and GluR1 on the membrane indicating an increased trafficking of glutamate receptors to the membrane. Importantly, the enhanced activity of glutamate receptors caused increased cell death through excitotoxicity, providing a potential pathological mechanism of the olfactory defects in patients with hyperammonemia and HE.

Author contributions

SS: Conceptualization, Writing—original draft, Writing—review and editing. SL: Conceptualization, Writing—original draft, Writing—review and editing.

Funding

SS was supported by Zuckerman STEM Leadership Program.

Conflict of interest

The authors declare that the research was conducted in the absence of any commercial or financial relationships that could be construed as a potential conflict of interest.

Publisher's note

All claims expressed in this article are solely those of the authors and do not necessarily represent those of their affiliated organizations, or those of the publisher, the editors and the reviewers. Any product that may be evaluated in this article, or claim that may be made by its manufacturer, is not guaranteed or endorsed by the publisher.

References

- Boulle, F., van den Hove, D. L., Jakob, S. B., Rutten, B. P., Hamon, M., van Os, J., et al. (2012). Epigenetic regulation of the BDNF gene: implications for psychiatric disorders. *Mol. Psychiatry* 17, 584–596. doi: 10.1038/mp.2011.107
- Choudhary, A., Peles, D., Nayak, R., Mizrahi, L., and Stern, S. (2022). Current progress in understanding schizophrenia using genomics and pluripotent stem cells: a meta-analytical overview. *Schizophr. Res.* doi: 10.1101/2022.08.18.504397
- Guo, S., Perets, N., Betzer, O., Ben-Shaul, S., Sheinin, A., Michalevski, I., et al. (2019). Intranasal delivery of mesenchymal stem cell derived exosomes loaded with phosphatase and tensin homolog siRNA repairs complete spinal cord injury. *ACS Nano* 13, 10015–10028. doi: 10.1021/acsnano.9b01892
- Hussein, Y., Tripathi, U., Choudhary, A., Nayak, R., Peles, D., Rosh, I., et al. (2023). Early maturation and hyperexcitability is a shared phenotype of cortical neurons derived from different ASD-associated mutations. *Transl. Psychiatry* 13, 246. doi: 10.1038/s41398-023-02535-x
- Lau, S., Stern, S., Linker, S., Silva, I. D., Nakatsuka, N., and Tampé, J. (2022). Identification of an age-related Parkinson's disease risk factor that regulates sulfur metabolism. *ResearchSquare*. doi: 10.21203/rs.3.rs-1168396/v1
- Lima Giacobbo, B., Doorduyn, J., Klein, H. C., Dierckx, R., Bromberg, E., de Vries, E. F., et al. (2019). Brain-derived neurotrophic factor in brain disorders: focus on neuroinflammation. *Mol. Neurobiol.* 56, 3295–3312. doi: 10.1007/s12035-018-1283-6
- Margiana, A., Markov, A., Zekiy, A. O., Hamza, M. U., Al-Dabbagh, K. A., Al-Zubaidi, S. H., et al. (2022). Clinical application of mesenchymal stem cell in regenerative medicine: a narrative review. *Stem Cell Res. Ther.* 13, 366. doi: 10.1186/s13287-022-03054-0
- Mertens, J., Herdy, J. R., Traxler, L., Schafer, S. T., Schlachetzki, J. C. M., Bohnke, L., et al. (2021). Age-dependent instability of mature neuronal fate in induced neurons from Alzheimer's patients. *Cell Stem Cell* 28, 1533–1548. e6. doi: 10.1016/j.stem.2021.04.004
- Mertens, J., Reid, D., Lau, S., Kim, Y., and Gage, F. H. (2018). Aging in a dish: iPSC-derived and directly induced neurons for studying brain aging and age-related neurodegenerative diseases. *Annu. Rev. Genet.* 52, 271–293. doi: 10.1146/annurev-genet-120417-031534
- Miranda, M., Morici, J. F., Zanoni, M. B., and Bekinschtein, P. (2019). Brain-derived neurotrophic factor: a key molecule for memory in the healthy and the pathological brain. *Front. Cell. Neurosci.* 13, 363. doi: 10.3389/fncel.2019.00363
- Raggi, A., and Ferri, R. (2010). Sleep disorders in neurodegenerative diseases. *Eur. J. Neurol.* 17, 1326–1338. doi: 10.1111/j.1468-1331.2010.03034.x
- Rike, W. A., and Stern, S. (2023). Proteins and transcriptional dysregulation of the brain extracellular matrix in Parkinson's disease: a systematic review. *Int. J. Mol. Sci.* 24, 7435. doi: 10.1101/2023.03.01.23286630
- Stern, S., Lau, S., Manole, A., Rosh, I., Percia, M. M., Ben Ezer, R., et al. (2022). Reduced synaptic activity and dysregulated extracellular matrix pathways in midbrain neurons from Parkinson's disease patients. *NPJ Parkinsons Dis.* 8, 103. doi: 10.1038/s41531-022-00366-z
- Trotti, L. M., and Karroum, E. G. (2016). Melatonin for sleep disorders in patients with neurodegenerative diseases. *Curr. Neurol. Neurosci. Rep.* 16, 63. doi: 10.1007/s11910-016-0664-3
- Wennberg, A. M. V., Wu, M. N., Rosenberg, P. B., and Spira, A. P. (2017). Sleep disturbance, cognitive decline, and dementia: a review. *Semin. Neurol.* 37, 395–406. doi: 10.1055/s-0037-1604351



OPEN ACCESS

EDITED BY

Shong Lau,
Salk Institute for Biological Studies,
United States

REVIEWED BY

Xavier Xifró,
University of Girona, Spain
Qiuwen Wang,
Salk Institute for Biological Studies,
United States

*CORRESPONDENCE

Zhi-Hao Wang
wangzh86@whu.edu.cn

SPECIALTY SECTION

This article was submitted to
Cellular and Molecular Mechanisms
of Brain-aging,
a section of the journal
Frontiers in Aging Neuroscience

RECEIVED 05 July 2022

ACCEPTED 23 August 2022

PUBLISHED 08 September 2022

CITATION

Li Y, Li F, Qin D, Chen H, Wang J,
Wang J, Song S, Wang C, Wang Y,
Liu S, Gao D and Wang Z-H (2022) The
role of brain derived neurotrophic
factor in central nervous system.
Front. Aging Neurosci. 14:986443.
doi: 10.3389/fnagi.2022.986443

COPYRIGHT

© 2022 Li, Li, Qin, Chen, Wang, Wang,
Song, Wang, Wang, Liu, Gao and
Wang. This is an open-access article
distributed under the terms of the
Creative Commons Attribution License
(CC BY). The use, distribution or
reproduction in other forums is
permitted, provided the original
author(s) and the copyright owner(s)
are credited and that the original
publication in this journal is cited, in
accordance with accepted academic
practice. No use, distribution or
reproduction is permitted which does
not comply with these terms.

The role of brain derived neurotrophic factor in central nervous system

Yiyi Li^{1,2}, Fang Li^{1,2}, Dongdong Qin^{1,2}, Hongyu Chen^{1,2},
Jianhao Wang^{1,2}, Jiabei Wang^{1,2}, Shafei Song^{1,2},
Chao Wang^{1,2}, Yamei Wang^{1,2}, Songyan Liu^{1,2}, Dandan Gao^{1,2}
and Zhi-Hao Wang^{1,2*}

¹Department of Neurology, Renmin Hospital of Wuhan University, Wuhan, China, ²Center for Neurodegenerative Disease Research, Renmin Hospital of Wuhan University, Wuhan, China

Brain derived neurotrophic factor (BDNF) has multiple biological functions which are mediated by the activation of two receptors, tropomyosin receptor kinase B (TrkB) receptor and the p75 neurotrophin receptor, involving in physiological and pathological processes throughout life. The diverse presence and activity of BDNF indicate its potential role in the pathogenesis, progression and treatment of both neurological and psychiatric disorders. This review is to provide a comprehensive assessment of the current knowledge and future directions in BDNF-associated research in the central nervous system (CNS), with an emphasis on the physiological and pathological functions of BDNF as well as its potential treatment effects in CNS diseases, including depression, Alzheimer's disease, Parkinson's disease, Huntington's disease, amyotrophic lateral sclerosis, multiple sclerosis, and cerebral ischemic stroke.

KEYWORDS

brain derived neurotrophic factor, physiological, pathological, treatment, central nervous system

Introduction

Brain derived neurotrophic factor, a member of the neurotrophin family, plays a critical role not only in the growth and development of the nervous system but also in supporting neurons survival and facilitating neurogenesis. In addition, it participates in glutamatergic and gamma-aminobutyric acid (GABA)-ergic synaptic plasticity and affects serotonergic and dopaminergic neurotransmission (Colucci-D'Amato et al., 2020). It is widely distributed in the cortical region, hippocampus, and visual cortex, as well as other parts of CNS such as substantia nigra, striatum, retrorubral region, and ventral tegmental area. The expression level of BDNF in brain tissues is determined by transcription of BDNF mRNA and translation of BDNF protein.

Brain derived neurotrophic factor signals are mediated by TrkB receptor and p75 neurotrophin receptor. The former is the key receptor for BDNF in adult brain since

its wide range of expression and a higher binding affinity for BDNF than the latter. TrkB receptor has tyrosine residues in its kinase domain, and phosphorylated-TrkB triggers downstream signaling cascades such as phospholipase C (PLC), mitogen-activated protein kinase (MAPK) and phosphatidylinositol 3-kinase (PI3K), exerting neuronal protective effects. However, truncated TrkB without intracellular kinase domain possesses inhibitory effect against mature BDNF signaling which activates full length TrkB. Furthermore, pro-BDNF is preferential to bind with p75 neurotrophin receptor, which has a low affinity to mature BDNF and leads to negative effects such as neuronal cell death (Teng and Hempstead, 2004).

It was reported that BDNF is highly active in cortex, hippocampus, and basal forebrain (Mirowska-Guzel et al., 2013). The diverse presence of BDNF leads to its important involvements in multiple neurological and psychiatric disorders. In this review, we briefly summarize the current state of knowledge regarding the physiological and pathological functions of BDNF as well as its potential treatment effects in CNS diseases.

Physiological functions of brain derived neurotrophic factor

Brain derived neurotrophic factor is mainly produced by neurons and glial cells and serves as a pleiotropic role in CNS (Lessmann and Brigadski, 2009). It is essential for neuronal genesis, differentiation, survival and growth, and acts as a mediator, modulator, or instructor of synaptic plasticity, viability and transmission (Kowiański et al., 2018). There are two forms of BDNF in human brain, the BDNF precursor (proBDNF) and mature BDNF (mBDNF). The proBDNF stored in either dendrites or axons (Lessmann et al., 2003), is synthesized as pre-proBDNF in endoplasmic reticulum followed by removing signal peptide in golgi apparatus to form proBDNF eventually (Wang M. et al., 2021). The mBDNF is converted from proBDNF which undergoes cleavage and strips off the pro-domain (BDNF pro-peptide, pBDNF) intracellularly (by furin or PC1/3/7) or extracellularly (by tPA/plasmin system or matrix metalloproteinases) (Lee et al., 2001; Mowla et al., 2001; Wang M. et al., 2021).

Brain derived neurotrophic factor was released both by presynaptic and postsynaptic terminals (Matsuda et al., 2009) as a mixture of pro- and mature forms in an activity dependent manner (Pang et al., 2004). Two types of BDNF maintain a dynamic balance and the ratio between them varies at different stages of brain development. During early postnatal period, proBDNF reaches a high concentration, while mBDNF is more dominant in adulthood (Yang et al., 2009, 2014). mBDNF takes effect by binding with two kinds of plasma membrane receptors, the TrkB receptor (Martin-Zanca et al., 1986) and the p75 neurotrophin receptor (Dechant and Barde, 2002). mBDNF,

as a member of the neurotrophin family, has a high affinity (dissociation constant $\sim 10^{11}$ M) to TrkB receptor (Rodríguez-Tébar and Barde, 1988), which promotes cell survival (Volosin et al., 2006), facilitates long term potentiation (LTP) and increases spine complexity (Zagrebelsky et al., 2005). However, mBDNF has a low affinity (dissociation constant $\sim 10^9$ M) to p75 neurotrophin receptor (Meeker and Williams, 2015), which preferentially binds to proBDNF, and the latter signal involves in brain development, facilitates long term depression (LTD) and induces apoptosis (Woo et al., 2005; Friedman, 2010). Due to its critical role in LTP, BDNF has been assumed to be an essential part of supporting memory formation and maintenance by promoting synaptic integration (Bramham and Messaoudi, 2005). Furthermore, BDNF increases neurogenesis by promoting cell survival and proliferation (Katoh-Semba et al., 2002; Lee S. H. et al., 2007).

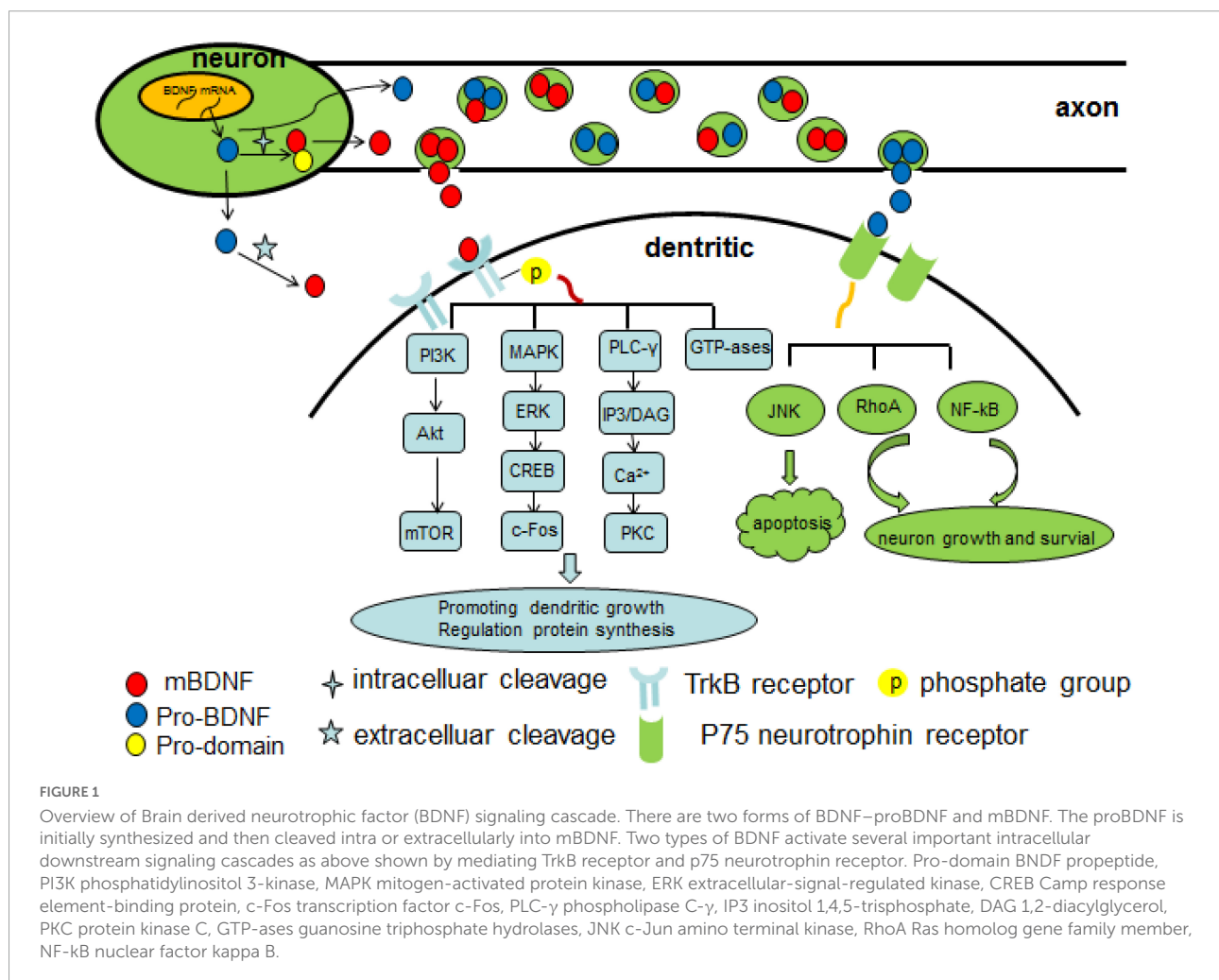
As is mentioned above, BDNF takes actions mainly by binding to TrkB, which is abundantly expressed in hippocampal neurons. After binding, the BDNF/TrkB complex is then internalized into the neuron and serves as a docking site for diverse signaling cascades, protein phosphorylation cascades, and secondary signaling systems (Huang and Reichardt, 2003; Nykjaer et al., 2005; Yoshii and Constantine-Paton, 2010). The binding of BDNF to TrkB receptor leads to phosphorylation of TrkB, thus activating several important intracellular downstream signaling cascades, including PLC, phosphatidylinositol 3-kinase/protein kinase B (PI3K/AKT), mitogen-activated protein kinase/extracellular signal-related kinase (MAPK/ERK) and guanosine triphosphate hydrolases (GTP-ases) of the Ras homolog (Rho) gene family pathways (Minichiello, 2009; Mohammadi et al., 2018). The BDNF/TrkB/PKC signaling is essential for synaptic function and maintenance (Lanuza et al., 2019), and it links pre- and post-synaptic activity to maintain neuromuscular function, which can be affected by a decrease in neuromuscular activity such as occurring neuromuscular disorders (Hurtado et al., 2017). BDNF/TrkB/PI3K/Akt pathway has an antiapoptotic effect and suppresses autophagy by which further inhibits the degradation of three important postsynaptic proteins (PSD-95, PICK1, and SHANK3) that is essential for N-methyl-D-aspartate receptor (NMDAR)-dependent synaptic plasticity (Nikoletopoulou et al., 2017). Synaptic plasticity is a dynamic process that involves in competition between Ca^{2+} /calmodulin-dependent protein kinase II (CaMKII) and PSD-95 for binding to the NR2A NMDAR subunit, while LTP is associated with an increase of α CaMKII binding with the NR2A/B subunit of the NMDA receptor and a concomitant decrease binding with PSD-95 (Stachowicz, 2022). In addition, BDNF also has direct effect on NMDA receptor subunits but with different level. Acute stimulation of hippocampal neurons with BDNF rapidly upregulated the protein levels and delivery to the plasma membrane of the NR1 and NR2B NMDA receptor subunits, while with a delayed increase of NR2A subunit

(Caldeira et al., 2007). Another study revealed that BDNF increased Girdin phosphorylation through the TrkB/PI3K/Akt pathway leading to phosphorylation of the NR2B subunit and NMDA receptor activation, which is crucial for synaptic plasticity and memory (Nakai et al., 2014). The PI3K/Akt/mTOR pathway promotes dendritic growing and branching through regulation of protein synthesis and cytoskeleton development (Jaworski et al., 2005; Kumar et al., 2005). The MAPK/ERK pathway is pivotal not only for early response gene expression such as c-Fos but also for cytoskeleton protein synthesis such as Arc and cypin (Gonzalez et al., 2016). Moreover, it plays a critical role in dendritic growth and branching of hippocampal neurons (Kwon et al., 2011). In addition, through BDNF/AMPA/mTOR signaling, ketamine induces structural plasticity in mouse mesencephalic and human induced pluripotent stem cells-derived dopaminergic neurons (Cavalleri et al., 2018). The BDNF/TrkB/GTP-ases pathway promotes actin and microtubule synthesis, resulting in growth of neuronal fibers (Gonzalez et al., 2016). The pro-BDNF/p75 neurotrophin receptor/sortilin binding complex initiates signaling cascades leading to activation of c-Jun amino terminal

kinase (JNK), ras homolog gene family member A (RhoA), and nuclear factor kappa B (NF- κ B) downstream, which involves in neuronal apoptosis (Anastasia et al., 2013), neuronal growth cone development and motility (Meeker and Williams, 2015), and neuronal survival (Lee et al., 2001; Figure 1).

Pathological functions of brain derived neurotrophic factor

The change of BDNF level in both peripheral blood and CNS and the imbalance or insufficient of pro-BDNF transformation into mBDNF have been found to be involved in the pathogenesis of multiple diseases such as depression, Alzheimer's disease, Parkinson's disease, Huntington's disease, amyotrophic lateral sclerosis, multiple sclerosis, and cerebral ischemic stroke (Eyileten et al., 2021; Wang M. et al., 2021). In these diseases, failure of the switch of pro-BDNF to mBDNF is due to the abnormal proteolytic cleavage. For example, altered expression and/or activities of components in the tPA/plasmin system



(extracellular cleavage proteases) participated in pathological processes related to depression and anxiety (Wang M. et al., 2021). Details will be summarized as below (Figure 2 and Table 1) and introduced in the following seven sections.

Brain derived neurotrophic factor and depression

Depression is not an unusual psychiatric disease at present. Major depressive disorder is characterized by emotional, motivational, cognitive and physiological domain symptoms, making it a complicated disease to treat. BDNF/TrkB signaling is involved in various psychiatric diseases and is widely studied in the context of depression, anxiety disorders, schizophrenia, autism, and addiction (Autry and Monteggia, 2012). Here, we mainly discuss the role of BDNF in depression. Clinical studies have shown that patients with severe depression have a low level of BDNF in the hippocampus and prefrontal cortex, accompanied by cerebral hippocampus atrophy, neuronal apoptosis and synaptic loss (Duman and Monteggia, 2006). In addition, the serum BDNF level was also found to be decreased in depression patients (Lee B. H. et al., 2007), and the level of plasma BDNF seems to be lower in patients with severe depression compared to mild depression patients (Kim et al., 2007). However, treatment with conventional antidepressant drugs as well as electroconvulsive therapy enhanced the mRNA expressions of BDNF and TrkB in the hippocampal and cortical

regions (Nibuya et al., 1995). Several intracellular signaling pathways such as mammalian target of rapamycin (mTOR) and glycogen synthase kinase 3 (GSK-3) have been implicated in the antidepressant effects of ketamine (Li et al., 2010; Beurel et al., 2011). Whereas, previous works examining the antidepressant effects of ketamine demonstrated that mTOR was a downstream target of BDNF (Autry et al., 2011). Animal model of depression revealed that BDNF signaling was rescued in the hippocampus after peripheral injection of BDNF for 14 consecutive days, and its mRNA level in the CA3 area of the hippocampus was also increased, suggesting the antidepressant-effect of BDNF (Schmidt and Duman, 2010). All these mentioned indicate that up-regulating BDNF level may have positive effect to the treatment of depression. Some clinical studies revealed that the serum proBDNF level in severe depression patients was apparently higher than that in healthy subjects, while the level of mBDNF shows the opposite trend. What's more, the ratio of mBDNF/proBDNF was much lower in depression patients compare to healthy control, while was increased after antidepressant drugs treatment (Zhou et al., 2013; Jiang et al., 2017). Another study showed that, in human cerebrospinal fluid, levels of pro-peptide BDNF (pro-domain of BDNF, pBDNF) were significantly lower in patients with major depressive disorder than in controls (Kojima et al., 2019). In addition, autopsy results of depression patients showed that the expressions of pBDNF and proBDNF increased in parietal cortex while mBDNF decreased (Yang et al., 2017). Furthermore, intraperitoneal or intraventricular injection of

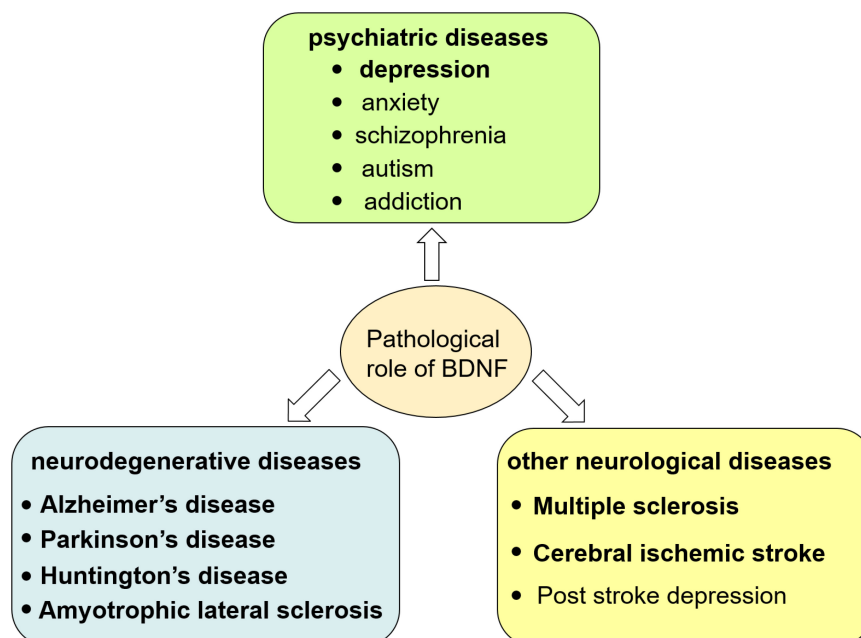


FIGURE 2

Pathological role of BDNF in central nervous system. The dysfunction of BDNF signaling causes neurological disorders including psychiatric, neurodegenerative diseases and other neurological diseases.

TABLE 1 Brain derived neurotrophic factor (BDNF) level in different brain disorders and BDNF associated therapy.

Disorders	BDNF level in patients and animal model	Therapy	References
Depression	↓BDNF in hippocampus and prefrontal cortex ↓BDNF in serum and plasma ↑Serum proBDNF ↓serum mBDNF ↓pBDNF in human cerebrospinal fluid ↑pBDNF and proBDNF ↓mBDNF in parietal cortex	antidepressant drugs electroconvulsive therapy peripheral injection of BDNF anti-proBDNF antibody 7,8-DHF	Nibuya et al., 1995; Duman and Monteggia, 2006; Kim et al., 2007; Lee B. H. et al., 2007; Schmidt and Duman, 2010; Zhou et al., 2013; Bai et al., 2016; Zhang et al., 2016; Jiang et al., 2017; Yang et al., 2017; Kojima et al., 2019
Alzheimer's disease	↓serum BDNF ↑proBDNF and proBDNF/BDNF in human cerebrospinal fluid ↑pBDNF and pBDNF/BDNF in hippocampal specimens Aβ impeded BDNF/TrkB downstream signaling Tau inhibited BDNF production	7,8-DHF CF3CN	Lim et al., 2015; Rosa et al., 2016; Aytan et al., 2018; Fleitas et al., 2018; Ng et al., 2019; Chen et al., 2021
Parkinson's disease	↓serum BDNF ↓BDNF in both brain and gut ↓Serum mBDNF and mBDNF/proBDNF	Dopamine neuron protective drugs intracerebral injection of BDNF non-invasive vagus nerve stimulation deep brain stimulation 7,8-DHF	Moreau and Destée, 2009; Chen et al., 2017; Ahn et al., 2021; Faust et al., 2021; Mondal et al., 2021; Yi et al., 2021; Tian et al., 2022
Huntington's disease	↓BDNF mRNA and protein levels in the cortex	BDNF overexpressing human neural stem cells transplantation bone-marrow mesenchymal stem cells transplantation P42 and BDNF combination treatment 7,8-DHF	Zuccato et al., 2008; Dey et al., 2010; Garcia-Diaz Barriga et al., 2017; Kim et al., 2020; Couly et al., 2021
Amyotrophic lateral sclerosis	↓BDNF protein level	stem cell therapy 7,8-DHF	Korkmaz et al., 2014; Schiaffino et al., 2018; Forostyak et al., 2020; Wang J. et al., 2021
Multiple sclerosis	↓BDNF protein level	stem cells transplantation 7,8-DHF	Makar et al., 2016; Naegelin et al., 2020; Brown et al., 2021
Cerebral ischemic stroke	↓BDNF in MCAO mice hippocampal ↓serum BDNF in post stroke depression patients ↓BDNF at the acute phase of CIS	stem cells therapy neuron protective drugs BDNF treatment	Nagahara and Tuszynski, 2011; Lasek-Bal et al., 2015; Cook et al., 2017; Kaur et al., 2021

anti-proBDNF antibody can neutralize proBDNF and alleviate depression-like behavior in rats (Bai et al., 2016). A research demonstrated that chronic 7,8-DHF (7,8-Dihydroxyflavone, a TrkB agonist) treatment rescued the depressive-like behaviors in sucrose preference test and novelty suppressed feeding test by regulating TrkB signaling, increasing BDNF levels and promoting synaptic protein expression (Zhang et al., 2016). In summary, overall consideration of the dynamic equilibrium and mutual interaction between proBDNF and mBDNF as well as pBDNF is of more significant than merely focusing on mBDNF.

Brain derived neurotrophic factor and Alzheimer's disease

Alzheimer's disease (AD) is the most common form of dementia, which was pathologically characterized by extracellular senile plaque (SP) formed by the deposition of β -amyloid (A β), and intracellular neurofibrillary tangles (NFTs) formed by the abnormally phosphorylated Tau protein

aggregation as well as vascular amyloidosis and loss of neurons in the cortex and hippocampus (Edler et al., 2017; Szaruga et al., 2017). Multiple studies showed that BDNF, proBDNF and pBDNF played important roles in the occurrence and development of AD. A meta-analysis indicated that AD patients, rather than mild cognitive impairment patients, have significantly lower serum BDNF levels compared to age-matched healthy controls, and a significant decrease in peripheral BDNF levels can only be detected at the late stage of dementia (Ng et al., 2019). A study on AD patients showed a negative correlation between cognitive decline and BDNF mRNA level in the dorsal lateral prefrontal cortex (Buchman et al., 2016). Furthermore, significant increases in proBDNF expression and the ratio of proBDNF/BDNF in AD patients' cerebrospinal fluid were detected, which led to an increase of pathogenicity and a decrease of trophic effect and caused neuronal apoptosis through p75 neurotrophin receptor (Fleitas et al., 2018). In hippocampal specimens of AD patients, the level of pBDNF was 16 times higher than that in healthy individuals, and the ratio of pBDNF/BDNF was 30 times higher compared to control. What's more, cell death rate increased

when treating cells with pBDNF and A β simultaneously compared to giving pBDNF solely, which indicated that they may cause synergistic toxicity in AD (Lim et al., 2015). In addition, A β promoted the production of shortened TrkB receptor mRNA and the decomposition of the full-length TrkB receptor, which impeded BDNF/TrkB downstream signaling (Jerónimo-Santos et al., 2015). Interestingly, we have found that deficiency in BDNF/TrkB neurotrophic signaling can increase CCAAT/enhancer binding protein β (C/EBP β) expression and then activate δ -secretase which leads to APP and Tau fragmentation and causes AD eventually (Wang et al., 2019). On the other hand, excessive or pathologically altered Tau can inhibit BDNF production and neurotoxicity without Tau gene mutation or neurofibrillary tangles formation (Rosa et al., 2016). Reversely, BDNF can also impede phosphorylation of Tau (Jiao et al., 2016).

In all, the interactions between BDNF and A β or Tau need further investigation to find an effective therapy for AD. In 5xFAD mice models, researchers found that 2 months' treatment of 7,8-DHF decreased cortical A β plaque deposition and protected dendritic arbor complexity in cortical neurons but without huge impact on the density of dendritic spines (Aytan et al., 2018). In addition, CF3CN, an optimized synthetic 7,8-DHF chemical, has the ability to activate TrkB neurotrophic signaling and inhibits the activation of delta-secretase, which attenuates AD pathologies and alleviates cognitive dysfunctions in 5xFAD mice. All these suggest that 7,8-DHF or CF3CN may be potential therapeutic agents for the treatment of AD (Chen et al., 2021).

Brain derived neurotrophic factor and Parkinson's disease

Parkinson's disease (PD), the second most prevalent neurodegenerative disease in the world, is characterized by progressive degeneration of nigrostriatal dopaminergic neurons and the development of intracellular proteinaceous aggregates. It is a combination of motor and non-motor symptoms. The former which weights most contains tremor, bradykinesia, rigidity, and postural instability, and the latter involves in hyposmia, sleep disorders, autonomic nervous dysfunction, and mental disorders. Study shows that the non-motor symptoms not only precede but often are accompanied by PD, of which neuropsychiatric symptoms including depression, anxiety, apathy, hallucinations and impulse control disorders are up to 60% in PD patients, in which almost 20-40% suffer from depression (Song et al., 2015). Many studies have shown that the mRNA and protein levels of serum BDNF in patients with depression and PD were significantly reduced. What's more, BDNF gene polymorphism, especially the Met allele, is associated with a higher neuropsychiatric burden in PD (Ramezani et al., 2020). An interesting clinical study has found

that PD patients with higher self-rating Depression Scale (SDS) score show lower serum BDNF level (Chen et al., 2017). On the other hand, the decrease of BDNF in PD patients may also affect neuronal function in hippocampus, prefrontal cortex and amygdala and eventually leads to depressive symptoms (Enomoto et al., 2016). Therefore, some researchers recognized serum BDNF as a clinical biomarker for motor severity in depressed PD patients, especially in female (Huang et al., 2021).

Except for these neuropsychiatric symptoms, BDNF also takes effect in motor symptoms and other non-motor symptoms. BDNF supports the midbrain dopaminergic neurons surviving, promotes differentiation, and protects dopamine neurons from neurotoxins (Minichiello et al., 2002). BDNF overexpression alleviated motor deficits and cognitive impairment in MPTP-induced PD mice through mitigating mitochondrial damage (Chang and Wang, 2021). What's more, BDNF level was significantly decreased in the colon of MPTP-treated group compared to the vehicle-treated group, indicating a role of BDNF in the gut-brain axis in PD (Choi et al., 2021). In accordance with this, BDNF and Netrin-1 are strongly decreased in both brain and gut of PD patients, and conditionally knocking out of these trophic factors in gut leads to dopaminergic neuronal loss, constipation and motor deficits (Ahn et al., 2021). A clinical study included one hundred and fifty-six patients with limb tremor and/or bradykinesia who meet the MDS Parkinson's diagnostic criteria and analyzed their serum level of proBDNF and mBDNF. They found that serum levels of mBDNF and mBDNF/proBDNF were significantly lower in the PD group compared with non-PD group, while the proBDNF showed opposite result. Thus, they supposed that mBDNF/proBDNF can be used as biomarker for early stage of PD and the combination of mBDNF and proBDNF has better diagnostic value than mBDNF alone in PD diagnosis (Yi et al., 2021).

Over the past decades, most of drugs for PD treatment mainly focus on modulating dopamine concentrations in the basal ganglia. Recently, studies of neurotrophic factors such as glial cell line-derived neurotrophic growth factor and BDNF, which are considered the primary factors for neuroprotection in PD, have gained a great attention. Intracerebral injection of BDNF markedly improves levodopa-induced dyskinesia in PD rat model without affecting the therapeutic effect of levodopa (Moreau and Destée, 2009). BDNF is being developed as a neuron protective drug, and the underlying mechanisms — include promoting neuronal regeneration, repairing the damaged neurons, promoting functional recovery, and enhancing the activity of antioxidant enzymes. However, exogenous BDNF cannot cross the blood-brain barrier, therefore, the treatment of PD is still under research. A recent study has shown that non-invasive vagus nerve stimulation, which is an established neurostimulation therapy used in the treatment of epilepsy, migraine and cluster headache, is demonstrated to improve gait and motor function in

PD patients, and it can significantly increase BDNF level (Mondal et al., 2021). What's more, the level of BDNF in the motor cortex increased after deep brain stimulation (DBS) in the subthalamic nucleus (STN), which is a powerful therapeutic alternative for the treatment of PD (Faust et al., 2021).

The α -Synuclein (α -Syn) is a major component of Lewy body which is a pathological marker of PD. Physiologically, α -Syn takes effect in intercellular dopamine storage, synaptic membrane biogenesis, and lipid transport (Lotharius and Brundin, 2002). Wild-type α -Syn induces BDNF expression, while α -Syn mutant (A30P and A53T) cannot induce BDNF expression (Kohno et al., 2004). These α -Syn mutants tend to form protofibrils and further aggregate into larger inclusion bodies associated with PD, which significantly inhibit axonal transport of BDNF/TrkB (Papapetropoulos and Mash, 2005; Volpicelli-Daley et al., 2014). However, BDNF reduces the degradation of TrkB through inhibiting the formation of the α -Syn–TrkB complex (Kang et al., 2017). Further studies are needed to clarify the crosstalk between BDNF/TrkB and the biomarkers of PD such as α -Syn and find effective treatment for neuronal degeneration. Recently, a study found that 7,8-DHF could ameliorate α -Syn 1-103-induced mitochondrial impairment and motor dysfunction, indicating a novel oral bioactive therapeutic agent for the treatment of PD (Tian et al., 2022).

All in all, BDNF plays an important role in the diagnosis and the treatment of PD, as well as involving in the development of PD through affecting PD pathology.

Brain derived neurotrophic factor and Huntington's disease

Huntington's disease (HD) is an autosomal dominant neurodegenerative disease caused by an expanded CAG repeat sequence in the huntingtin gene which leads to an abnormal expansion of the polyglutamine tract in the N-terminus of the protein huntingtin. This mutant huntingtin protein misfolds, aggregates, and disrupts proteostasis, which leads to degeneration of striatal medium spiny neurons (Rosas et al., 2003). Clinically, it is a progressive motor, cognitive, and mental dysfunction disease, whose mean onset age is 35 to 44 years and median survival time is 15 to 18 years once onset (Caron et al., 1993), and unfortunately, it affects the quality of life of their offspring and their partners.

The relationship between serum (or plasma) and cerebrospinal fluid levels of BDNF and HD has been controversial. A recent report concluded that levels of BDNF in plasma and cerebrospinal fluid are not a biomarker for HD (Ou et al., 2021). It is reported that the striatum cannot produce BDNF, and it maintains its function depending on BDNF from the cortex (about 95%), thalamus and mesencephalon (Bawari et al., 2019). BDNF, which is synthesized in cortical neurons and

then delivered into striatum by anterograde transportation, is essential for the cortico-striatal synaptic activity and the survival of GABAergic neurons. Depletion of BDNF in the cortex of HD patients may make striatal neurons more vulnerable to injury (Zuccato et al., 2001). A study showed significant reduction of BDNF mRNA and protein levels in the cortex of HD patients through a systematic and quantitative assessment (Zuccato et al., 2008). Additionally, it is found that the delivery of BDNF is attenuated while transferring from the cortex to the striatum in an animal model of HD. Therefore, the reduction of cortical BDNF delivery would result in decreased activity of the cortex and striatum synaptic activity and synaptic loss (Yu et al., 2018). BDNF pro-domain knockout mouse showed impaired righting reflex, abnormal motor behaviors, obvious weight loss and short lifespan, which displayed a Huntington's disease-like phenotype, supporting the BDNF hypothesis in the pathogenesis of HD (Li et al., 2020). Furthermore, low expression of BDNF in HD pathogenesis is potentially mediated by cAMP, MAPK and Ras signaling pathways (Zhou et al., 2021).

The astrocyte constitutes the largest population of brain cells and plays multiple roles, one of which is that it involves in neuronal dysfunction of HD. Expression mutant huntingtin with 160 polyQ specifically in astrocytes causes age-dependent neurological symptoms in transgenic mice, indicating a role of mutant huntingtin in exacerbating HD neuropathology (Bradford et al., 2009). What's more, the mutation of huntingtin gene affects the processing and secretion of the BDNF in astrocytes, leads to progressive degeneration of striatal GABAergic medium spiny neurons and decreases BDNF level in the brain of HD patients (Wang et al., 2012; Bawari et al., 2019). In return, BDNF modulates striatal astrocyte function by inducing astrocyte to secrete soluble neuroprotective factors that selectively protect neurons expressing mutant huntingtin (Saba et al., 2020).

The potential therapeutic effects of BDNF for HD have been reported in various rodent models. In a rat model of HD, researchers transplanted BDNF-overexpressing human neural stem cells (HB1.F3.BDNF) into the contralateral side of unilateral quinolinic acid-lesioned striatum, and found that BDNF can promote migration, differentiation and functional restoration of HD rat (Kim et al., 2020). Another research showed that transplantation bone-marrow mesenchymal stem cells with BDNF over-expressed into striatum slowed neurodegenerative processes and alleviated behavioral disorder in the YAC 128 mouse model of HD (Dey et al., 2010). However, the long-term safety and efficacy of this approach still need further research. A dual therapy that combines P42 treatment which increases TrkB expression in striatum, with BDNF-enhancing therapy such as environmental enrichment efficiently delayed HD pathology in R6/2 mice (Couly et al., 2021). Furthermore, bilateral expression of BDNF by adeno-associated virus1/2 in the striatum alleviated motor and cognitive dysfunction in transgenic HD rats, accompanied

by increased volume of the striatum and number of neural cells (Connor et al., 2016). In a more practical way, researchers found that oral 7,8-DHF ameliorated cognitive and motor deficits in a mouse model of HD through specific activation of the PLC γ 1 pathway (García-Díaz Barriga et al., 2017). These results suggest that BDNF has a compensating effect to HD and might be a promising treatment for HD.

Brain derived neurotrophic factor and amyotrophic lateral sclerosis

Amyotrophic lateral sclerosis (ALS) is an adult-onset neurodegenerative disorder, characterized by the loss and degeneration of both lower and upper motor neurons. The etiopathogenesis of ALS is still unknown, but the possible hypotheses include oxidative stress, inflammation, protein aggregation and miss-folding, as well as glutamate excitotoxicity, RNA processing and epigenetic dysregulation (Jankovic et al., 2021). Therefore, the treatments of ALS are of multi-level but with limited therapeutic effects.

As a member of the neurotrophin family, BDNF promotes cell regeneration and survival. A study conducted on spinal cord tissue in SOD1 G93A mice (a model of ALS) showed that the expression level of BDNF decreased significantly compared to control mice (Schiaffino et al., 2018). In addition, another study showed that physical exercise such as running and swimming can improve the BDNF/TrkB neurotrophic signaling at the neuromuscular junction and reduce the impact of ALS in mice (Just-Borràs et al., 2020). Based on the above evidence, recent studies have recognized the critical role of BDNF in maintaining motoneurons survival, and take BDNF as a potential treatment for ALS. BDNF have been used in ALS human clinical trials, but the results are disappointing due to the poor pharmacokinetics and pharmacodynamics of BDNF. Deletion of the BDNF receptor TrkB.T1 alleviated muscle weakness and motoneuron cell death of spinal cord in the G93A SOD1 animal model of ALS, indicating TrkB.T1 may limit the neuroprotective BDNF signaling to motoneurons via a non-cell autonomous mechanism, which providing new understanding of the reasons for past clinical failures (Yanpallewar et al., 2021). In a transgenic rat model, intraspinal transplantation of pluripotent stem cells might rescue or replace dying motoneurons and these cells display neuroprotective effects by regulating local gene expression and extracellular matrix plasticity of central nervous system, which means that stem cell therapy is a promising therapeutic strategy for ALS (Forostyak et al., 2020). Additionally, transplantation of BDNF-overexpressing human umbilical cord mesenchymal stem cell-derived motor neurons was capable of increasing motor ability and prolonging lifespan of hSOD1 G93A mice (Wang J. et al., 2021). What's more, chronic administration of 7,8-DHF significantly improved motor deficits, and preserved spinal motor neurons count and

dendritic spines in SOD1 G93A mice (Korkmaz et al., 2014). In summary, BDNF and its equivalent drugs may be a promising therapeutic strategy for ALS, but further researches are needed to overcome the difficulties of poor pharmacokinetics and pharmacodynamics of BDNF.

Brain derived neurotrophic factor and multiple sclerosis

Multiple sclerosis (MS) is a chronic autoimmune disease characterized by neuronal inflammation, degeneration and demyelinating lesions within brain and spinal cord (primarily in the white matter of the brain), which leads to motor dysfunction and cognitive decline. The mechanisms underlying the pathogenesis and progression of MS are not fully understood and current treatments have limited efficacy. Several molecules such as BDNF, IL-1 β , PDGF, and CB1Rs, are involved in functional recovery of MS from the acute phase and are thus taken as potential therapeutic targets (Ksiazek-Winiarek et al., 2015). Recently, a novel drug, 7,8-DHF was found to reduce the clinical and pathological severity of MS in a murine model through activation of TrkB/AKT/STAT3 signaling and reduction of inflammation and demyelination (Makar et al., 2016), which brought good news to this disease.

The versatile BDNF acts as a neuroprotective factor in the process of inflammation, degeneration and demyelination of MS. BDNF is required to drive the endogenous repair of regeneration and remyelination after demyelinating inflammatory injury in MS, which is crucial for neuronal preservation and prevention of clinical progression (Brod, 2022). Study showed that neural stem cells transplantation rescued the progression of MS by inducing anti-inflammation and promoting neurogenesis and myelination, possibly by modulating BDNF and FGF signaling pathways in an experimental autoimmune encephalomyelitis mouse model of MS (Brown et al., 2021). Another study revealed that BDNF is initially presented in T cells and macrophages in MS lesions to confirm the capability of producing BDNF in human immune system. However, high levels of cytokines tend to negatively regulate circulating BDNF levels indicating BDNF may act as an immune-mediated defense of neurons in MS lesions (Sorenson et al., 2014). To determine whether BDNF can serve as a biomarker for MS, a comparatively large cohort research found that the level of BDNF can be detected to have a difference between MS patients and healthy controls, with mean BDNF levels in the former were lower by 8% than the latter. However, the difference is minor and thus it is unlikely to effectively evaluate and inform decision-making processes at an individual patient level. Therefore, it is hard to claim that serum BDNF is a biomarker for MS although it has multifunction in this disease (Naegelin et al., 2020).

Brain derived neurotrophic factor and cerebral ischemic stroke

Cerebral stroke is one of the leading causes of death and long-term disability worldwide, of which cerebral ischemic stroke (CIS) takes up the overwhelming majority. Recently, BDNF has been focused on in CIS, especially its relationship with post-stroke mobility. A study found that the expression of BDNF and TrkB decreased both in oxygen glucose deprivation cells and in mice hippocampal experiencing surgery of middle cerebral artery occlusion (MCAO). Shuxuening injection reverses it and promotes the recovery of post-stroke cognitive and motor deficiencies via BDNF-mediated Neurotrophin/Trk Signaling (Li et al., 2021). Furthermore, intra-arterially mesenchymal stem cells therapy in post-stroke facilitates neuroprotection and regulates ER stress-mediated apoptosis via the BDNF/TrkB signaling pathway (Kaur et al., 2021). Additionally, BDNF is also involved in post stroke depression (PSD). PSD patients show lower level of serum BDNF compared to those without PSD. Furthermore, antidepressants could improve the expression of BDNF in brain, which further alleviates depression symptoms. However, the mechanisms of BDNF in the development of PSD are still unknown (Zhang and Liao, 2020).

Except for post-stroke, it has been reported that BDNF level was significantly decreased at the acute phase of CIS and it can act as a factor warning poor prognosis for the functional status of patients on the 90th day after onset (Lasek-Bal et al., 2015). In addition, when exogenous BDNF is given immediately (within hours) after CIS, it can act as a neuroprotective agent. Surprisingly, when it is given several days after ischemic injury, it can promote axons protruding budding and synapses formation (Nagahara and Tuszynski, 2011). However, BDNF cannot penetrate the undamaged blood-brain barrier, which makes peripheral BDNF injection ineffective. What's more, transcranial BDNF treatment makes the time of tissue distribution much too short. Therefore, the way of delivering BDNF need further research to achieve the optimal treatment (Cook et al., 2017).

Conclusion

In this review, we introduced the physiological and pathological functions of BDNF as well as its potential treatment effect in CNS diseases including depression, Alzheimer's disease, Parkinson's disease, Huntington's disease, multiple sclerosis, amyotrophic lateral sclerosis and cerebral ischemic stroke. We discussed the alteration of BDNF level and BDNF-based therapies in different disease models. Apart from the disorders above mentioned, the role of BDNF was also investigated in many other diseases such as diabetes and cancer (Eyileten et al., 2017; Guzel et al., 2021). Understanding the role of BDNF and its signaling as well as how they regulate repair

or regrowth of CNS will be useful. Myriad compelling studies reveal that enhancing BDNF levels or restoring its receptor's signaling cascades can improve the phenotype of animal models in different diseases. However, there are still many questions to be answered. Firstly, BDNF has a large molecular weight and is difficult to pass through the blood-brain barrier, so it cannot reach the CNS and play a role when intravenous administration. Intraventricular injection has high technical requirements for operators and is prone to cause huge damage, which leads to it difficult to popularize. Using BDNF agonists to increase the release of BDNF *in vivo* can solve this problem, but what agonists we should use is another problem. Recently, more and more researchers take their emphasis on BDNF-overexpressed stem cells transplantation in animal model, which might be a promising therapeutic strategy but it is on the try phase and further studies are needed. Secondly, at present, BDNF is still limited to animal experiments and cannot be applied in clinical practice on a large scale. Thirdly, there is no consensus on when and at what dose BDNF should be administered to specific diseases.

Author contributions

Z-HW conceived and revised the manuscript. YL, FL, DQ, and HC found the associated documents. JHW, JBW, SS, CW, YW, SL, and DG helped to draw the figures. YL wrote the manuscript with input from all authors. All authors contributed to the article and approved the submitted version.

Funding

This work was supported by the National Natural Science Foundation of China (No. 82101479) to Z-HW and National Key Research Projects of China (No. 2021YFA1302400) to Z-HW.

Conflict of interest

The authors declare that the research was conducted in the absence of any commercial or financial relationships that could be construed as a potential conflict of interest.

Publisher's note

All claims expressed in this article are solely those of the authors and do not necessarily represent those of their affiliated organizations, or those of the publisher, the editors and the reviewers. Any product that may be evaluated in this article, or claim that may be made by its manufacturer, is not guaranteed or endorsed by the publisher.

References

- Ahn, E. H., Kang, S. S., Liu, X., Cao, X., Choi, S. Y., Musazzi, L., et al. (2021). BDNF and Netrin-1 repression by C/EBP β in the gut triggers Parkinson's disease pathologies, associated with constipation and motor dysfunctions. *Prog. Neurobiol.* 198:101905. doi: 10.1016/j.pneurobio.2020.101905
- Anastasia, A., Deinhardt, K., Chao, M. V., Will, N. E., Irmady, K., Lee, F. S., et al. (2013). Val66Met polymorphism of BDNF alters prodomain structure to induce neuronal growth cone retraction. *Nat. Commun.* 4:2490. doi: 10.1038/ncomms3490
- Autry, A. E., Adachi, M., Nosyreva, E., Na, E. S., Los, M. F., Cheng, P. F., et al. (2011). NMDA receptor blockade at rest triggers rapid behavioural antidepressant responses. *Nature* 475, 91–95. doi: 10.1038/nature10130
- Autry, A. E., and Monteggia, L. M. (2012). Brain-derived neurotrophic factor and neuropsychiatric disorders. *Pharmacol. Rev.* 64, 238–258. doi: 10.1124/pr.111.005108
- Aytan, N., Choi, J. K., Carreras, I., Crabtree, L., Nguyen, B., Lehar, M., et al. (2018). Protective effects of 7,8-dihydroxyflavone on neuropathological and neurochemical changes in a mouse model of Alzheimer's disease. *Eur. J. Pharmacol.* 828, 9–17. doi: 10.1016/j.ejphar.2018.02.045
- Bai, Y. Y., Ruan, C. S., Yang, C. R., Li, J. Y., Kang, Z. L., Zhou, L., et al. (2016). ProBDNF Signaling Regulates Depression-Like Behaviors in Rodents under Chronic Stress. *Neuropsychopharmacology* 41, 2882–2892. doi: 10.1038/npp.2016.100
- Bawari, S., Tewari, D., Argüelles, S., Sah, A. N., Nabavi, S. F., Xu, S., et al. (2019). Targeting BDNF signaling by natural products: Novel synaptic repair therapeutics for neurodegeneration and behavior disorders. *Pharmacol. Res.* 148:104458. doi: 10.1016/j.phrs.2019.104458
- Beurel, E., Song, L., and Jope, R. S. (2011). Inhibition of glycogen synthase kinase-3 is necessary for the rapid antidepressant effect of ketamine in mice. *Mol. Psychiatry* 16, 1068–1070. doi: 10.1038/mp.2011.47
- Bradford, J., Shin, J. Y., Roberts, M., Wang, C. E., Li, X. J., and Li, S. (2009). Expression of mutant huntingtin in mouse brain astrocytes causes age-dependent neurological symptoms. *Proc. Natl. Acad. Sci. U.S.A.* 106, 22480–22485. doi: 10.1073/pnas.0911503106
- Bramham, C. R., and Messaoudi, E. (2005). BDNF function in adult synaptic plasticity: The synaptic consolidation hypothesis. *Prog. Neurobiol.* 76, 99–125. doi: 10.1016/j.pneurobio.2005.06.003
- Brod, S. A. (2022). A proposal: How to study pro-myelinating proteins in MS. *Autoimmun. Rev.* 21:102924. doi: 10.1016/j.autrev.2021.102924
- Brown, C., McKee, C., Halassy, S., Kojan, S., Feinstein, D. L., and Chaudhry, G. R. (2021). Neural stem cells derived from primitive mesenchymal stem cells reversed disease symptoms and promoted neurogenesis in an experimental autoimmune encephalomyelitis mouse model of multiple sclerosis. *Stem. Cell Res. Ther.* 12:499. doi: 10.1186/s13287-021-02563-8
- Buchman, A. S., Yu, L., Boyle, P. A., Schneider, J. A., De Jager, P. L., and Bennett, D. A. (2016). Higher brain BDNF gene expression is associated with slower cognitive decline in older adults. *Neurology* 86, 735–741. doi: 10.1212/wnl.0000000000002387
- Caldeira, M. V., Melo, C. V., Pereira, D. B., Carvalho, R. F., Carvalho, A. L., and Duarte, C. B. (2007). BDNF regulates the expression and traffic of NMDA receptors in cultured hippocampal neurons. *Mol. Cell Neurosci.* 35, 208–219. doi: 10.1016/j.mcn.2007.02.019
- Caron, N. S., Wright, G. E. B., and Hayden, M. R. (1993). "Huntington disease," in *Gene reviews* [Internet]. eds M. P. Adam, G. M. Mirzaa, R. A. Pagon, S. E. Wallace, L. J. H. Bean, K. W. Gripp, et al. (Seattle, WA: University of Washington).
- Cavalleri, L., Merlo Pich, E., Millan, M. J., Chiamulera, C., Kunath, T., Spano, P. F., et al. (2018). Ketamine enhances structural plasticity in mouse mesencephalic and human iPSC-derived dopaminergic neurons via AMPAR-driven BDNF and mTOR signaling. *Mol. Psychiatry* 23, 812–823. doi: 10.1038/mp.2017.241
- Chang, E., and Wang, J. (2021). Brain-derived neurotrophic factor attenuates cognitive impairment and motor deficits in a mouse model of Parkinson's disease. *Brain Behav.* 11:e2251. doi: 10.1002/brb3.2251
- Chen, C., Ahn, E. H., Liu, X., Wang, Z. H., Luo, S., Liao, J., et al. (2021). Optimized TrkB Agonist Ameliorates Alzheimer's Disease Pathologies and Improves Cognitive Functions via Inhibiting Delta-Secretase. *ACS Chem. Neurosci.* 12, 2448–2461. doi: 10.1021/acscchemneuro.1c00181
- Chen, H., Lombès, M., and Le Menuet, D. (2017). Glucocorticoid receptor represses brain-derived neurotrophic factor expression in neuron-like cells. *Mol. Brain* 10:12. doi: 10.1186/s13041-017-0295-x
- Choi, J. G., Jeong, M., Joo, B. R., Ahn, J. H., Woo, J. H., Kim, D. H., et al. (2021). Reduced Levels of Intestinal Neuropeptides and Neurotrophins in Neurotoxin-Induced Parkinson Disease Mouse Models. *J. Neuropathol. Exp. Neurol.* 80, 15–20. doi: 10.1093/jnen/nlaa113
- Colucci-D'Amato, L., Speranza, L., and Volpicelli, F. (2020). Neurotrophic Factor BDNF, Physiological Functions and Therapeutic Potential in Depression, Neurodegeneration and Brain Cancer. *Int. J. Mol. Sci.* 21:7777. doi: 10.3390/ijms21207777
- Connor, B., Sun, Y., von Hieber, D., Tang, S. K., Jones, K. S., and Maucksch, C. (2016). AAV1/2-mediated BDNF gene therapy in a transgenic rat model of Huntington's disease. *Gene Ther.* 23, 283–295. doi: 10.1038/gt.2015.113
- Cook, D. J., Nguyen, C., Chun, H. N., Chiu, A. S., Machnicki, M., Zarembinski, T. I., et al. (2017). Hydrogel-delivered brain-derived neurotrophic factor promotes tissue repair and recovery after stroke. *J. Cereb. Blood Flow Metab.* 37, 1030–1045. doi: 10.1177/0271678x16649964
- Couly, S., Carles, A., Denus, M., Benigno-Anton, L., Maschat, F., and Maurice, T. (2021). Exposure of R6/2 mice in an enriched environment augments P42 therapy efficacy on Huntington's disease progression. *Neuropharmacology* 186:108467. doi: 10.1016/j.neuropharm.2021.108467
- Dechant, G., and Barde, Y. A. (2002). The neurotrophin receptor p75(NTR): Novel functions and implications for diseases of the nervous system. *Nat. Neurosci.* 5, 1131–1136. doi: 10.1038/nn1102-1131
- Dey, N. D., Bombard, M. C., Roland, B. P., Davidson, S., Lu, M., Rossignol, J., et al. (2010). Genetically engineered mesenchymal stem cells reduce behavioral deficits in the YAC 128 mouse model of Huntington's disease. *Behav. Brain Res.* 214, 193–200. doi: 10.1016/j.bbr.2010.05.023
- Duman, R. S., and Monteggia, L. M. (2006). A neurotrophic model for stress-related mood disorders. *Biol. Psychiatry* 59, 1116–1127. doi: 10.1016/j.biopsych.2006.02.013
- Edler, M. K., Sherwood, C. C., Meindl, R. S., Hopkins, W. D., Ely, J. J., Erwin, J. M., et al. (2017). Aged chimpanzees exhibit pathologic hallmarks of Alzheimer's disease. *Neurobiol. Aging* 59, 107–120. doi: 10.1016/j.neurobiolaging.2017.07.006
- Enomoto, S., Shimizu, K., Nibuya, M., Toda, H., Yoshino, A., Suzuki, E., et al. (2016). Increased expression of endocytosis-Related proteins in rat hippocampus following 10-day electroconvulsive seizure treatment. *Neurosci. Lett.* 624, 85–91. doi: 10.1016/j.neulet.2016.05.015
- Eyileten, C., Kaplon-Cieslicka, A., Mirowska-Guzel, D., Malek, L., and Postula, M. (2017). Antidiabetic Effect of Brain-Derived Neurotrophic Factor and Its Association with Inflammation in Type 2 Diabetes Mellitus. *J. Diabetes Res.* 2017:2823671. doi: 10.1155/2017/2823671
- Eyileten, C., Sharif, L., Wicik, Z., Jakubik, D., Jarosz-Popek, J., Sopłinska, A., et al. (2021). The Relation of the Brain-Derived Neurotrophic Factor with MicroRNAs in Neurodegenerative Diseases and Ischemic Stroke. *Mol. Neurobiol.* 58, 329–347. doi: 10.1007/s12035-020-02101-2
- Faust, K., Vajkoczy, P., Xi, B., and Harnack, D. (2021). The Effects of Deep Brain Stimulation of the Subthalamic Nucleus on Vascular Endothelial Growth Factor, Brain-Derived Neurotrophic Factor, and Glial Cell Line-Derived Neurotrophic Factor in a Rat Model of Parkinson's Disease. *Stereotact. Funct. Neurosurg.* 99, 256–266. doi: 10.1159/000511121
- Fleitas, C., Piñol-Ripoll, G., Marfull, P., Rocandio, D., Ferrer, I., Rampon, C., et al. (2018). proBDNF is modified by advanced glycation end products in Alzheimer's disease and causes neuronal apoptosis by inducing p75 neurotrophin receptor processing. *Mol. Brain* 11:68. doi: 10.1186/s13041-018-0411-6
- Forostyak, S., Forostyak, O., Kwok, J. C. F., Romanyuk, N., Rehorova, M., Kriska, J., et al. (2020). Transplantation of Neural Precursors Derived from Induced Pluripotent Cells Preserve Perineuronal Nets and Stimulate Neural Plasticity in ALS Rats. *Int. J. Mol. Sci.* 21:9593. doi: 10.3390/ijms21249593
- Friedman, W. J. (2010). Proneurotrophins, seizures, and neuronal apoptosis. *Neuroscientist* 16, 244–252. doi: 10.1177/1073858409349903
- García-Díaz Barriga, G., Giral, A., Anglada-Huguet, M., Gaja-Capdevila, N., Orlandi, J. G., Soriano, J., et al. (2017). 7,8-dihydroxyflavone ameliorates cognitive and motor deficits in a Huntington's disease mouse model through specific activation of the PLC γ 1 pathway. *Hum. Mol. Genet.* 26, 3144–3160. doi: 10.1093/hmg/ddx198
- Gonzalez, A., Moya-Alvarado, G., Gonzalez-Billaut, C., and Bronfman, F. C. (2016). Cellular and molecular mechanisms regulating neuronal growth by brain-derived neurotrophic factor. *Cytoskeleton* 73, 612–628. doi: 10.1002/cm.21312
- Guzel, T. A., Mech, K., Wronski, M., Gerkowicz, K., Bednarczyk, A., Adamczyk, W., et al. (2021). Brain-derived neurotrophic factor in gastroenterology oncology

– short review of current literature. *Ann. Agric. Environ. Med.* 28, 367–371. doi: 10.26444/aaem/122628

Huang, E. J., and Reichardt, L. F. (2003). Trk receptors: Roles in neuronal signal transduction. *Annu. Rev. Biochem.* 72, 609–642. doi: 10.1146/annurev.biochem.72.121801.161629

Huang, Y., Huang, C., Zhang, Q., Wu, W., and Sun, J. (2021). Serum BDNF discriminates Parkinson's disease patients with depression from without depression and reflect motor severity and gender differences. *J. Neurol.* 268, 1411–1418. doi: 10.1007/s00415-020-10299-3

Hurtado, E., Cilleros, V., Nadal, L., Simó, A., Obis, T., García, N., et al. (2017). Muscle Contraction Regulates BDNF/TrkB Signaling to Modulate Synaptic Function through Presynaptic cPKCa and cPKCβI. *Front. Mol. Neurosci.* 10:147. doi: 10.3389/fnmol.2017.00147

Jankovic, M., Novakovic, I., Gamil Anwar Dawod, P., Gamil Anwar Dawod, A., Drinic, A., Abdel Motalab, F. I., et al. (2021). Current Concepts on Genetic Aspects of Mitochondrial Dysfunction in Amyotrophic Lateral Sclerosis. *Int. J. Mol. Sci.* 22:9832. doi: 10.3390/ijms22189832

Jaworski, J., Spangler, S., Seeburg, D. P., Hoogenraad, C. C., and Sheng, M. (2005). Control of dendritic arborization by the phosphoinositide-3'-kinase-Akt-mammalian target of rapamycin pathway. *J. Neurosci.* 25, 11300–11312. doi: 10.1523/jneurosci.2270-05.2005

Jerónimo-Santos, A., Fonseca-Gomes, J., Guimarães, D. A., Tanqueiro, S. R., Ramalho, R. M., Ribeiro, J. A., et al. (2015). Brain-derived neurotrophic factor mediates neuroprotection against Aβ-induced toxicity through a mechanism independent on adenosine 2A receptor activation. *Growth Factors* 33, 298–308. doi: 10.3109/08977194.2015.1080696

Jiang, H., Chen, S., Li, C., Lu, N., Yue, Y., Yin, Y., et al. (2017). The serum protein levels of the tPA-BDNF pathway are implicated in depression and antidepressant treatment. *Transl. Psychiatry* 7:e1079. doi: 10.1038/tp.2017.43

Jiao, S. S., Shen, L. L., Zhu, C., Bu, X. L., Liu, Y. H., Liu, C. H., et al. (2016). Brain-derived neurotrophic factor protects against tau-related neurodegeneration of Alzheimer's disease. *Transl. Psychiatry* 6:e907. doi: 10.1038/tp.2016.186

Just-Borràs, L., Hurtado, E., Cilleros-Mañé, V., Biondi, O., Charbonnier, F., Tomás, M., et al. (2020). Running and swimming prevent the deregulation of the BDNF/TrkB neurotrophic signalling at the neuromuscular junction in mice with amyotrophic lateral sclerosis. *Cell Mol. Life Sci.* 77, 3027–3040. doi: 10.1007/s00018-019-03337-5

Kang, S. S., Zhang, Z., Liu, X., Manfredsson, F. P., Benskey, M. J., Cao, X., et al. (2017). TrkB neurotrophic activities are blocked by α-synuclein, triggering dopaminergic cell death in Parkinson's disease. *Proc. Natl. Acad. Sci. U.S.A.* 114, 10773–10778. doi: 10.1073/pnas.1713969114

Katoh-Semba, R., Asano, T., Ueda, H., Morishita, R., Takeuchi, I. K., Inaguma, Y., et al. (2002). Riluzole enhances expression of brain-derived neurotrophic factor with consequent proliferation of granule precursor cells in the rat hippocampus. *FEBS J.* 16, 1328–1330. doi: 10.1096/fj.02-0143fe

Kaur, H., Sarmah, D., Veeresh, P., Datta, A., Kalia, K., Borah, A., et al. (2021). Endovascular Stem Cell Therapy Post Stroke Rescues Neurons from Endoplasmic Reticulum Stress-Induced Apoptosis by Modulating Brain-Derived Neurotrophic Factor/Tropomyosin Receptor Kinase B Signaling. *ACS Chem. Neurosci.* 12, 3745–3759. doi: 10.1021/acscchemneuro.1c00506

Kim, H. S., Jeon, I., Noh, J. E., Lee, H., Hong, K. S., Lee, N., et al. (2020). Intracerebral Transplantation of BDNF-overexpressing Human Neural Stem Cells (HB1.F3.BDNF) Promotes Migration, Differentiation and Functional Recovery in a Rodent Model of Huntington's Disease. *Exp. Neurobiol.* 29, 130–137. doi: 10.5607/en20011

Kim, Y. K., Lee, H. P., Won, S. D., Park, E. Y., Lee, H. Y., Lee, B. H., et al. (2007). Low plasma BDNF is associated with suicidal behavior in major depression. *Prog. Neuropsychopharmacol. Biol. Psychiatry* 31, 78–85. doi: 10.1016/j.pnpbp.2006.06.024

Kohno, R., Sawada, H., Kawamoto, Y., Uemura, K., Shibasaki, H., and Shimohama, S. (2004). BDNF is induced by wild-type alpha-synuclein but not by the two mutants, A30P or A53T, in glioma cell line. *Biochem. Biophys. Res. Commun.* 318, 113–118. doi: 10.1016/j.bbrc.2004.04.012

Kojima, M., Matsui, K., and Mizui, T. (2019). BDNF pro-peptide: Physiological mechanisms and implications for depression. *Cell Tissue Res.* 377, 73–79. doi: 10.1007/s00441-019-03034-6

Korkmaz, O. T., Aytan, N., Carreras, I., Choi, J. K., Kowall, N. W., Jenkins, B. G., et al. (2014). 7,8-Dihydroxyflavone improves motor performance and enhances lower motor neuronal survival in a mouse model of amyotrophic lateral sclerosis. *Neurosci. Lett.* 566, 286–291. doi: 10.1016/j.neulet.2014.02.058

Kowiański, P., Lietzau, G., Czuba, E., Waśkow, M., Steliga, A., and Moryś, J. (2018). BDNF: A Key Factor with Multipotent Impact on Brain Signaling and

Synaptic Plasticity. *Cell Mol. Neurobiol.* 38, 579–593. doi: 10.1007/s10571-017-0510-4

Książek-Winiarek, D. J., Szpakowski, P., and Glabinski, A. (2015). Neural Plasticity in Multiple Sclerosis: The Functional and Molecular Background. *Neural Plast.* 2015:307175. doi: 10.1155/2015/307175

Kumar, V., Zhang, M. X., Swank, M. W., Kunz, J., and Wu, G. Y. (2005). Regulation of dendritic morphogenesis by Ras-PI3K-Akt-mTOR and Ras-MAPK signaling pathways. *J. Neurosci.* 25, 11288–11299. doi: 10.1523/jneurosci.2284-05.2005

Kwon, M., Fernández, J. R., Zegarek, G. F., Lo, S. B., and Firestein, B. L. (2011). BDNF-promoted increases in proximal dendrites occur via CREB-dependent transcriptional regulation of cypin. *J. Neurosci.* 31, 9735–9745. doi: 10.1523/jneurosci.6785-10.2011

Lanuz, M. A., Just-Borràs, L., Hurtado, E., Cilleros-Mañé, V., Tomás, M., García, N., et al. (2019). The Impact of Kinases in Amyotrophic Lateral Sclerosis at the Neuromuscular Synapse: Insights into BDNF/TrkB and PKC Signaling. *Cells* 8:1578. doi: 10.3390/cells8121578

Lasek-Bal, A., Jędrzejowska-Szypułka, H., Różycka, J., Bal, W., Holecki, M., Duława, J., et al. (2015). Low Concentration of BDNF in the Acute Phase of Ischemic Stroke as a Factor in Poor Prognosis in Terms of Functional Status of Patients. *Med. Sci. Monit.* 21, 3900–3905. doi: 10.12659/msm.895358

Lee, B. H., Kim, H., Park, S. H., and Kim, Y. K. (2007). Decreased plasma BDNF level in depressive patients. *J. Affect. Disord.* 101, 239–244. doi: 10.1016/j.jad.2006.11.005

Lee, S. H., Kim, Y. J., Lee, K. M., Ryu, S., and Yoon, B. W. (2007). Ischemic preconditioning enhances neurogenesis in the subventricular zone. *Neuroscience* 146, 1020–1031. doi: 10.1016/j.neuroscience.2007.02.058

Lee, R., Kermani, P., Teng, K. K., and Hempstead, B. L. (2001). Regulation of cell survival by secreted proneurotrophins. *Science* 294, 1945–1948. doi: 10.1126/science.1065057

Lessmann, V., and Brigadski, T. (2009). Mechanisms, locations, and kinetics of synaptic BDNF secretion: An update. *Neurosci. Res.* 65, 11–22. doi: 10.1016/j.neures.2009.06.004

Lessmann, V., Gottmann, K., and Malsangio, M. (2003). Neurotrophin secretion: Current facts and future prospects. *Prog. Neurobiol.* 69, 341–374. doi: 10.1016/s0301-0082(03)00019-4

Li, H., Lin, L. Y., Zhang, Y., Lim, Y., Rahman, M., Beck, A., et al. (2020). Pro-BDNF Knockout Causes Abnormal Motor Behaviours and Early Death in Mice. *Neuroscience* 438, 145–157. doi: 10.1016/j.neuroscience.2020.05.007

Li, N., Lee, B., Liu, R. J., Banasr, M., Dwyer, J. M., Iwata, M., et al. (2010). mTOR-dependent synapse formation underlies the rapid antidepressant effects of NMDA antagonists. *Science* 329, 959–964. doi: 10.1126/science.1190287

Li, Z., Wang, H., Xiao, G., Du, H., He, S., Feng, Y., et al. (2021). Recovery of post-stroke cognitive and motor deficiencies by ShuXueJing injection via regulating hippocampal BDNF-mediated Neurotrophin/Trk Signaling. *Biomed. Pharmacother.* 141:111828. doi: 10.1016/j.biopha.2021.111828

Lim, J. Y., Reighard, C. P., and Crowther, D. C. (2015). The pro-domains of neurotrophins, including BDNF, are linked to Alzheimer's disease through a toxic synergy with Aβ. *Hum. Mol. Genet.* 24, 3929–3938. doi: 10.1093/hmg/ddv130

Lotharius, J., and Brundin, P. (2002). Pathogenesis of Parkinson's disease: Dopamine, vesicles and alpha-synuclein. *Nat. Rev. Neurosci.* 3, 932–942. doi: 10.1038/nrn983

Makar, T. K., Nimmagadda, V. K., Singh, I. S., Lam, K., Mubarez, F., Judge, S. I., et al. (2016). TrkB agonist, 7,8-dihydroxyflavone, reduces the clinical and pathological severity of a murine model of multiple sclerosis. *J. Neuroimmunol.* 292, 9–20. doi: 10.1016/j.jneuroim.2016.01.002

Martin-Zanca, D., Hughes, S. H., and Barbacid, M. (1986). A human oncogene formed by the fusion of truncated tropomyosin and protein tyrosine kinase sequences. *Nature* 319, 743–748. doi: 10.1038/319743a0

Matsuda, N., Lu, H., Fukata, Y., Noritake, J., Gao, H., Mukherjee, S., et al. (2009). Differential activity-dependent secretion of brain-derived neurotrophic factor from axon and dendrite. *J. Neurosci.* 29, 14185–14198. doi: 10.1523/jneurosci.1863-09.2009

Meeker, R. B., and Williams, K. S. (2015). The p75 neurotrophin receptor: At the crossroad of neural repair and death. *Neural. Regen. Res.* 10, 721–725. doi: 10.4103/1673-5374.156967

Minichiello, L. (2009). TrkB signalling pathways in LTP and learning. *Nat. Rev. Neurosci.* 10, 850–860. doi: 10.1038/nrn2738

Minichiello, L., Calella, A. M., Medina, D. L., Bonhoeffer, T., Klein, R., and Korte, M. (2002). Mechanism of TrkB-mediated hippocampal long-term potentiation. *Neuron* 36, 121–137. doi: 10.1016/s0896-6273(02)00942-x

- Mirowska-Guzel, D., Litwin, T., Gromadzka, G., Czlonkowski, A., and Czlonkowska, A. (2013). Influence of BDNF polymorphisms on Wilson's disease susceptibility and clinical course. *Metab. Brain Dis.* 28, 447–453. doi: 10.1007/s11011-013-9399-x
- Mohammadi, A., Amooeian, V. G., and Rashidi, E. (2018). Dysfunction in Brain-Derived Neurotrophic Factor Signaling Pathway and Susceptibility to Schizophrenia. *Parkinson's and Alzheimer's Diseases. Curr. Gene. Ther.* 18, 45–63. doi: 10.2174/1566523218666180302163029
- Mondal, B., Choudhury, S., Banerjee, R., Roy, A., Chatterjee, K., Basu, P., et al. (2021). Non-invasive vagus nerve stimulation improves clinical and molecular biomarkers of Parkinson's disease in patients with freezing of gait. *NPJ Parkinsons Dis.* 7:46. doi: 10.1038/s41531-021-00190-x
- Moreau, C., and Destée, A. (2009). A new perspective on brain derived neurotrophin factor polymorphism in L-dopa induced dyskinesia. *J. Neurol. Neurosurg. Psychiatry* 80:129. doi: 10.1136/jnnp.2008.163568
- Mowl, S. J., Farhadi, H. F., Pareek, S., Atwal, J. K., Morris, S. J., Seidah, N. G., et al. (2001). Biosynthesis and post-translational processing of the precursor to brain-derived neurotrophic factor. *J. Biol. Chem.* 276, 12660–12666. doi: 10.1074/jbc.M008104200
- Naegel, Y., Saeuberli, K., Schaedelin, S., Dingsdale, H., Magon, S., Baranzini, S., et al. (2020). Levels of brain-derived neurotrophic factor in patients with multiple sclerosis. *Ann. Clin. Transl. Neurol.* 7, 2251–2261. doi: 10.1002/acn3.51215
- Nagahara, A. H., and Tuszynski, M. H. (2011). Potential therapeutic uses of BDNF in neurological and psychiatric disorders. *Nat. Rev. Drug. Discov.* 10, 209–219. doi: 10.1038/nrd3366
- Nakai, T., Nagai, T., Tanaka, M., Itoh, N., Asai, N., Enomoto, A., et al. (2014). Girdin phosphorylation is crucial for synaptic plasticity and memory: A potential role in the interaction of BDNF/TrkB/Akt signaling with NMDA receptor. *J. Neurosci.* 34, 14995–15008. doi: 10.1523/jneurosci.2228-14.2014
- Ng, T. K. S., Ho, C. S. H., Tam, W. W. S., Kua, E. H., and Ho, R. C. (2019). Decreased Serum Brain-Derived Neurotrophic Factor (BDNF) Levels in Patients with Alzheimer's Disease (AD): A Systematic Review and Meta-Analysis. *Int. J. Mol. Sci.* 20:257. doi: 10.3390/ijms20020257
- Nibuya, M., Morinobu, S., and Duman, R. S. (1995). Regulation of BDNF and trkB mRNA in rat brain by chronic electroconvulsive seizure and antidepressant drug treatments. *J. Neurosci.* 15, 7539–7547. doi: 10.1523/jneurosci.15-11-07539.1995
- Nikoletopoulou, V., Sidiropoulou, K., Kallergi, E., Dalezios, Y., and Tavernarakis, N. (2017). Modulation of Autophagy by BDNF Underlies Synaptic Plasticity. *Cell Metab.* 26:230–242.e235. doi: 10.1016/j.cmet.2017.06.005
- Nykjaer, A., Willnow, T. E., and Petersen, C. M. (2005). p75NTR—live or let die. *Curr. Opin. Neurobiol.* 15, 49–57. doi: 10.1016/j.conb.2005.01.004
- Ou, Z. A., Byrne, L. M., Rodrigues, F. B., Tortelli, R., Johnson, E. B., Foiani, M. S., et al. (2021). Brain-derived neurotrophic factor in cerebrospinal fluid and plasma is not a biomarker for Huntington's disease. *Sci. Rep.* 11:3481. doi: 10.1038/s41598-021-83000-x
- Pang, P. T., Teng, H. K., Zaitsev, E., Woo, N. T., Sakata, K., Zhen, S., et al. (2004). Cleavage of proBDNF by tPA/plasmin is essential for long-term hippocampal plasticity. *Science* 306, 487–491. doi: 10.1126/science.1100135
- Papapetropoulos, S., and Mash, D. C. (2005). Alpha-synuclein aggregation and its relation to neurodegenerative diseases. *Ann. Neurol.* 57, 605;authorreply605–606. doi: 10.1002/ana.20414
- Ramezani, M., Ruskey, J. A., Martens, K., Kibreab, M., Javer, Z., Kathol, I., et al. (2020). Association Between BDNF Val66Met Polymorphism and Mild Behavioral Impairment in Patients With Parkinson's Disease. *Front. Neurol.* 11:587992. doi: 10.3389/fneur.2020.587992
- Rodriguez-Tébar, A., and Barde, Y. A. (1988). Binding characteristics of brain-derived neurotrophic factor to its receptors on neurons from the chick embryo. *J. Neurosci.* 8, 3337–3342. doi: 10.1523/jneurosci.08-09-03337.1988
- Rosa, E., Mahendram, S., Ke, Y. D., Ittner, L. M., Ginsberg, S. D., and Fahnstock, M. (2016). Tau downregulates BDNF expression in animal and cellular models of Alzheimer's disease. *Neurobiol. Aging* 48, 135–142. doi: 10.1016/j.neurobiolaging.2016.08.020
- Rosas, H. D., Koroshetz, W. J., Chen, Y. I., Skewe, C., Vangel, M., Cudkowicz, M. E., et al. (2003). Evidence for more widespread cerebral pathology in early HD: An MRI-based morphometric analysis. *Neurology* 60, 1615–1620. doi: 10.1212/01.wnl.0000065888.88988.6e
- Saba, J., López Couselo, F., Turati, J., Carniglia, L., Durand, D., de Laurentiis, A., et al. (2020). Astrocytes from cortex and striatum show differential responses to mitochondrial toxin and BDNF: Implications for protection of striatal neurons expressing mutant huntingtin. *J. Neuroinflammation* 17:290. doi: 10.1186/s12974-020-01965-4
- Schiaffino, L., Bonafede, R., Scambi, I., Parrella, E., Pizzi, M., and Mariotti, R. (2018). Acetylation state of RelA modulated by epigenetic drugs prolongs survival and induces a neuroprotective effect on ALS murine model. *Sci. Rep.* 8:12875. doi: 10.1038/s41598-018-30659-4
- Schmidt, H. D., and Duman, R. S. (2010). Peripheral BDNF produces antidepressant-like effects in cellular and behavioral models. *Neuropsychopharmacology* 35, 2378–2391. doi: 10.1038/npp.2010.114
- Song, X., Hu, X., Zhou, S., Xu, Y., Zhang, Y., Yuan, Y., et al. (2015). Association of specific frequency bands of functional MRI signal oscillations with motor symptoms and depression in Parkinson's disease. *Sci. Rep.* 5:16376. doi: 10.1038/srep16376
- Sorenson, M., Jason, L., Peterson, J., Herrington, J., and Mathews, H. (2014). Brain derived neurotrophic factor is decreased in chronic fatigue syndrome and multiple sclerosis. *J. Neurol. Neurophysiol.* s12:S12–S013.
- Stachowicz, K. (2022). Is PSD-95 entangled in the side effects of antidepressants? *Neurochem. Int.* 159:105391. doi: 10.1016/j.neuint.2022.105391
- Szaruga, M., Munteanu, B., Lismont, S., Veugelen, S., Horré, K., Mercken, M., et al. (2017). Alzheimer's-Causing Mutations Shift Aβ Length by Destabilizing γ-Secretase-Aβn Interactions. *Cell* 170, 443–456.e414. doi: 10.1016/j.cell.2017.07.004
- Teng, K. K., and Hempstead, B. L. (2004). Neurotrophins and their receptors: Signaling trios in complex biological systems. *Cell Mol. Life Sci.* 61, 35–48. doi: 10.1007/s00018-003-3099-3
- Tian, Y., Pan, L., Yuan, X., Xiong, M., Zhang, Z., Meng, L., et al. (2022). 7,8-Dihydroxyflavone ameliorates mitochondrial impairment and motor dysfunction in the α-synuclein 1-103 transgenic mice. *Neurobiol. Dis.* 169:105736. doi: 10.1016/j.nbd.2022.105736
- Volosin, M., Song, W., Almeida, R. D., Kaplan, D. R., Hempstead, B. L., and Friedman, W. J. (2006). Interaction of survival and death signaling in basal forebrain neurons: Roles of neurotrophins and proneurotrophins. *J. Neurosci.* 26, 7756–7766. doi: 10.1523/jneurosci.1560-06.2006
- Volpicelli-Daley, L. A., Gamble, K. L., Schultheiss, C. E., Riddle, D. M., West, A. B., and Lee, V. M. (2014). Formation of α-synuclein Lewy neurite-like aggregates in axons impedes the transport of distinct endosomes. *Mol. Biol. Cell* 25, 4010–4023. doi: 10.1091/mbc.E14-02-0741
- Wang, J., Hu, W., Feng, Z., and Feng, M. (2021). BDNF-overexpressing human umbilical cord mesenchymal stem cell-derived motor neurons improve motor function and prolong survival in amyotrophic lateral sclerosis mice. *Neurol. Res.* 43, 199–209. doi: 10.1080/01616412.2020.1834775
- Wang, M., Xie, Y., and Qin, D. (2021). Proteolytic cleavage of proBDNF to mBDNF in neuropsychiatric and neurodegenerative diseases. *Brain Res. Bull.* 166, 172–184. doi: 10.1016/j.brainresbull.2020.11.005
- Wang, L., Lin, F., Wang, J., Wu, J., Han, R., Zhu, L., et al. (2012). Expression of mutant N-terminal huntingtin fragment (htt552-100Q) in astrocytes suppresses the secretion of BDNF. *Brain Res.* 1449, 69–82. doi: 10.1016/j.brainres.2012.01.077
- Wang, Z. H., Xiang, J., Liu, X., Yu, S. P., Manfredsson, F. P., Sandoval, I. M., et al. (2019). Deficiency in BDNF/TrkB Neurotrophic Activity Stimulates δ-Secretase by Upregulating C/EBPβ in Alzheimer's Disease. *Cell Rep.* 28:655–669.e655. doi: 10.1016/j.celrep.2019.06.054
- Woo, N. H., Teng, H. K., Siao, C. J., Chiaruttini, C., Pang, P. T., Milner, T. A., et al. (2005). Activation of p75NTR by proBDNF facilitates hippocampal long-term depression. *Nat. Neurosci.* 8, 1069–1077. doi: 10.1038/nn1510
- Yang, B., Ren, Q., Zhang, J. C., Chen, Q. X., and Hashimoto, K. (2017). Altered expression of BDNF, BDNF pro-peptide and their precursor proBDNF in brain and liver tissues from psychiatric disorders: Rethinking the brain-liver axis. *Transl. Psychiatry* 7:e1128. doi: 10.1038/tp.2017.95
- Yang, J., Harte-Hargrove, L. C., Siao, C. J., Marinic, T., Clarke, R., Ma, Q., et al. (2014). proBDNF negatively regulates neuronal remodeling, synaptic transmission, and synaptic plasticity in hippocampus. *Cell Rep.* 7, 796–806. doi: 10.1016/j.celrep.2014.03.040
- Yang, J., Siao, C. J., Nagappan, G., Marinic, T., Jing, D., McGrath, K., et al. (2009). Neuronal release of proBDNF. *Nat. Neurosci.* 12, 113–115. doi: 10.1038/nn.2244
- Yanpallewar, S., Fulgenzi, G., Tomassoni-Ardori, F., Barrick, C., and Tessarollo, L. (2021). Delayed onset of inherited ALS by deletion of the BDNF receptor TrkB.T1 is non-cell autonomous. *Exp. Neurol.* 337:113576. doi: 10.1016/j.expneurol.2020.113576
- Yi, X., Yang, Y., Zhao, Z., Xu, M., Zhang, Y., Sheng, Y., et al. (2021). Serum mBDNF and ProBDNF Expression Levels as Diagnosis Clue for Early Stage Parkinson's Disease. *Front. Neurol.* 12:680765. doi: 10.3389/fneur.2021.680765
- Yoshii, A., and Constantine-Paton, M. (2010). Postsynaptic BDNF-TrkB signaling in synapse maturation, plasticity, and disease. *Dev. Neurobiol.* 70, 304–322. doi: 10.1002/dneu.20765

- Yu, C., Li, C. H., Chen, S., Yoo, H., Qin, X., and Park, H. (2018). Decreased BDNF Release in Cortical Neurons of a Knock-in Mouse Model of Huntington's Disease. *Sci. Rep.* 8:16976. doi: 10.1038/s41598-018-34883-w
- Zagrebelsky, M., Holz, A., Dechant, G., Barde, Y. A., Bonhoeffer, T., and Korte, M. (2005). The p75 neurotrophin receptor negatively modulates dendrite complexity and spine density in hippocampal neurons. *J. Neurosci.* 25, 9989–9999. doi: 10.1523/jneurosci.2492-05.2005
- Zhang, E., and Liao, P. (2020). Brain-derived neurotrophic factor and post-stroke depression. *J. Neurosci. Res.* 98, 537–548. doi: 10.1002/jnr.24510
- Zhang, M. W., Zhang, S. F., Li, Z. H., and Han, F. (2016). 7,8-Dihydroxyflavone reverses the depressive symptoms in mouse chronic mild stress. *Neurosci. Lett.* 635, 33–38. doi: 10.1016/j.neulet.2016.10.035
- Zhou, L., Xiong, J., Lim, Y., Ruan, Y., Huang, C., Zhu, Y., et al. (2013). Upregulation of blood proBDNF and its receptors in major depression. *J. Affect. Disord.* 150, 776–784. doi: 10.1016/j.jad.2013.03.002
- Zhou, Z., Zhong, S., Zhang, R., Kang, K., Zhang, X., Xu, Y., et al. (2021). Functional analysis of brain derived neurotrophic factor (BDNF) in Huntington's disease. *Aging* 13, 6103–6114. doi: 10.18632/aging.202603
- Zuccato, C., Ciammola, A., Rigamonti, D., Leavitt, B. R., Goffredo, D., Conti, L., et al. (2001). Loss of huntingtin-mediated BDNF gene transcription in Huntington's disease. *Science* 293, 493–498. doi: 10.1126/science.1059581
- Zuccato, C., Marullo, M., Conforti, P., MacDonald, M. E., Tartari, M., and Cattaneo, E. (2008). Systematic assessment of BDNF and its receptor levels in human cortices affected by Huntington's disease. *Brain Pathol.* 18, 225–238. doi: 10.1111/j.1750-3639.2007.00111.x



OPEN ACCESS

EDITED BY

Shong Lau,
Salk Institute for Biological Studies,
United States

REVIEWED BY

Leandro Ceotto Freitas Lima,
Academy of Sciences of the Czech
Republic (ASCR), Czechia
Karnam Shruthi,
University of California, Berkeley,
United States

*CORRESPONDENCE

Zhi-you Cai
caizhiyou@ucas.ac.cn

SPECIALTY SECTION

This article was submitted to
Neurodegeneration,
a section of the journal
Frontiers in Neuroscience

RECEIVED 26 June 2022

ACCEPTED 30 August 2022

PUBLISHED 16 September 2022

CITATION

Chen F, Yi W-m, Wang S-y, Yuan M-h,
Wen J, Li H-y, Zou Q, Liu S and Cai Z-y
(2022) A long-term high-fat diet
influences brain damage and is linked
to the activation of
HIF-1 α /AMPK/mTOR/p70S6K
signalling.
Front. Neurosci. 16:978431.
doi: 10.3389/fnins.2022.978431

COPYRIGHT

© 2022 Chen, Yi, Wang, Yuan, Wen, Li,
Zou, Liu and Cai. This is an
open-access article distributed under
the terms of the [Creative Commons
Attribution License \(CC BY\)](#). The use,
distribution or reproduction in other
forums is permitted, provided the
original author(s) and the copyright
owner(s) are credited and that the
original publication in this journal is
cited, in accordance with accepted
academic practice. No use, distribution
or reproduction is permitted which
does not comply with these terms.

A long-term high-fat diet influences brain damage and is linked to the activation of HIF-1 α /AMPK/mTOR/p70S6K signalling

Fei Chen^{1,2,3,4,5}, Wen-min Yi^{1,2,3,4,5}, Sheng-yuan Wang^{1,2,3,4,5},
Ming-hao Yuan^{1,2,3,4,5}, Jie Wen^{5,6}, Hong-Yan Li^{5,7}, Qian Zou^{4,5},
Shu Liu^{1,2,3,4,5} and Zhi-you Cai^{1,2,3,4,5*}

¹Department of Neurology, Chongqing Medical University, Chongqing, China, ²Chongqing Institute Green and Intelligent Technology, Chinese Academy of Sciences, Chongqing, China, ³Chongqing School, University of Chinese Academy of Sciences, Chongqing, China, ⁴Department of Neurology, Chongqing General Hospital, Chongqing, China, ⁵Chongqing Key Laboratory of Neurodegenerative Diseases, Chongqing, China, ⁶Department of Neurology, Guangdong Medical University, Zhanjiang, Guangdong, China, ⁷Department of Neurology, The Affiliated Hospital of Southwest Medical University, Luzhou, China

High-fat diets (HFDs) are related to the incidence of obesity and diabetes, but the effect of high-fat diet-induced brain damage remains to be clarified. In our study, we found that 24 weeks of a HFD effectively induced obesity and a change in fur color in mice. In addition, the mice also exhibited deficits in learning and memory. We further found that autophagic flux was impaired in mice after HFD feeding. Hypoxia-inducible factor 1 α (HIF-1 α) expression was significantly increased in HFD-fed mice, and HFD feeding inhibited adenosine monophosphate-activated protein kinase (AMPK) phosphorylation and induced mechanistic target of rapamycin (mTOR) phosphorylation and p70S6K expression. Treatment of HFD-induced BV2 cell model with palmitic acid (PA) was used to further verify a similar result. We concluded that improving tissue hypoxia or enhancing autophagy through the AMPK/mTOR/p70S6K pathway may be a relevant strategy for improving obesity- and ageing-related disorders.

KEYWORDS

ageing, obesity, high-fat (HF) diet, autophagy, HIF-1 α , AMPK/m TOR pathway

Introduction

With the increase in restaurant businesses and takeaway food outlets, the global epidemic of HFD structures continues unabated [Prentice and Jebb \(2003\)](#). It is clear that the human health span and life span have increases over the past three decades. However, prolonged overconsumption of a HFD induces obesity and may counteract the health benefits of modern civilization. Excessive fat intake makes people

more susceptible to obesity. Obesity in middle age significantly increases the risks of developing noncommunicable chronic diseases (NCDs), such as coronary artery diseases, cerebrovascular accidents, type-2 diabetes mellitus, dementia, hyperlipidaemia, Parkinson's disease (PD) and Alzheimer's disease (AD), later in life Knight et al. (2014) and Abbott et al. (2019). As a major manifestation of metabolic syndrome, obesity not only impairs aesthetic appearance but is also accompanied by low-grade systemic inflammation and elevated blood pressure, supraphysiological fasting plasma glucose, high serum triglycerides, and low high-density lipoprotein levels Hoffman et al. (2015). To date, there have been many epidemiological surveys conducted on abnormal lipid metabolism with cognitive impairment worldwide, but there have been few reports on the molecular pathology of obesity-related brain damage.

Accumulating evidence indicates that the accumulation of senescent cells in the brain can lead to disease pathology (Sikora et al., 2021). According to a previous report, excess adiposity is associated with local tissue hypoxia Hosogai et al. (2007). The cellular response to hypoxia is coordinated by HIF-1 α , a heterodimeric transcription factor thought to be a key regulator of the host response to hypoxia. HIF-1 α expression levels are increased in a hypoxic tissue microenvironment. Hypoxic stimuli increase HIF-1 α protein levels by inhibiting its degradation by the proteasome. AMPK is a highly evolutionarily conserved metabolic regulator that maintains energy homeostasis during metabolic stress Hardie (2015). The enzyme AMPK is a heterotrimeric protein composed of a catalytic α -subunit and regulatory β - and γ -subunits. The activation of AMPK requires the phosphorylation at threonine 172 of the α catalytic subunit by upstream kinases. AMPK plays a vital role in regulating obesity Carling et al. (2008). The mechanistic target of rapamycin (mTOR), a protein kinase, regulates mammalian metabolism and physiology especially in cell survival, protein synthesis and autophagy. mTOR exists in two multiprotein protein complexes, mTORC1 and mTORC2. Rapamycin-sensitive mTORC1 regulates protein synthesis and cell growth through the phosphorylation of p70 ribosomal S6 kinase 1 (p70S6K1: Thr389). Mammalian target of rapamycin complex 1 (mTORC1) can promote many anabolic processes, including the biosynthesis of proteins, lipids and organelles, and by limiting catabolic processes such as autophagy and apoptosis. According to previous reports, under physiological conditions, mTOR activation inhibits autophagy Wang and Zhang (2019). Moreover, as a classically regulated autophagy signaling factor, mTOR kinase activity may be suppressed by the phosphorylation of AMPK.

Herein, we hypothesized that diet-induced brain impairment may induce cellular senescence through the activation of AMPK and mTOR signaling and is involved in changes in autophagy in progressive disease occurrence, ultimately resulting in cognitive impairment.

Materials and methods

Animals and treatments

All procedures were approved by the Institutional Animal Care and Use Committee of Chongqing Medical University. Studies were conducted in accordance with institutional guidelines for the care and use of laboratory animals.

Male C57BL/6 mice (13 months old, weighing 25–33 g) were obtained from Chengdu Dossy Experimental Animals Co., Ltd. (Chengdu, China). The mice were maintained in individual cages under controlled light and environmental conditions (12 h light/12 h dark cycle at $23 \pm 2^\circ\text{C}$ and $50 \pm 10\%$ humidity). After 1 week of adaptation, the mice were randomly divided into one of two groups, balanced by weight, and the mice were fed a regular chow diet (10% kcal fat), referred to as a low-fat diet (LFD) or a HFD (60% kcal fat; D12492; Research Diets, New Brunswick, NJ, USA) Bartels et al. (2009) *ad libitum* for 24 weeks. The general condition of the mice was observed daily, including fur color, mental state, food intake and body weight, and these indices were examined every week. At the end of the study, the mice (18 months old) were tested in the Morris water maze (MWM) task and then were sacrificed by decapitation or deeply anaesthetized with isoflurane. After the mice were perfused with phosphate-buffered saline, the brain was immediately removed, and the tissues were stored at -80°C or 4°C until use.

Cell culture and treatments

BV2 cells were stored in our laboratory. BV2 cells were maintained in DMEM/F12 culture medium (Gibco Life Technologies, Carlsbad, CA, USA) supplemented with 10% fetal bovine serum (FBS, 187 Invigitech, Irvine, CA, USA) and antibiotics (100 U/ml penicillin and 100 $\mu\text{g/ml}$ streptomycin) and incubated in a humidified atmosphere with 5% CO_2 at 37°C . The cells were cultured in a 10-cm Petri dish. The HFD BV2 cell model was established by treating the cells with PA medium (containing 100 mM PA) for 24 h (HFD group). BV2 cells in the control (CON) group were treated with the corresponding concentrations of solvent. PA and its solvent (vehicle) were purchased from Kunchuang Biotechnology (Xi'an, Shanxi, China). The reagents were diluted to working concentrations using growth medium.

Morris water maze test

To assess the spatial learning and memory abilities of mice, the MWM test, which is a widely accepted paradigm, was performed. MWM training included two phases: the place navigation phase and the spatial probe phase. A clear escape

platform (8-cm diameter) was submerged 1 cm below the surface of the pool (1.2 m in diameter and 0.4 m in depth, $25 \pm 1^\circ\text{C}$). Behavioral data of the mice were acquired using ANY-maze software (Stoelting Co., Wood Dale, IL, USA) and a digital video camera installed on the ceiling above the center of the maze. Briefly, the mice were trained for 6 consecutive days, with four trials per day lasting 1 min each to spatially locate the submerged platform. Each trial was initiated by placing the mouse in the water. Upon finding and climbing onto the hidden platform, the animals were given 5 s during which they could rest on it. If a mouse failed to find the submerged platform within the allowed time (60 s), it was placed on the platform manually for 30 s. The average latency to reach the platform, average velocity, and mean distance from the platform were analyzed by comparing the average of four trials across each training day to determine the learning performance. On day 7, the mice were subjected to the probe trial to assess spatial memory. The hidden platform was removed for this trial, and then the mice were placed in the quadrant opposite the target quadrant (the previous location of the hidden platform). The number of entries to the platform and latency to reach the target quadrant were analyzed to assess spatial memory consolidation. The MWM test procedures were monitored with the Morris Image System (Shanghai DOIT Industrial Co., Ltd.) $n = 20$ (HFD), 4 (ND).

Western blot

The mice ($n = 4/\text{group}$) were sacrificed humanely after the behavioral experiment, and then the whole brain was quickly removed and stored at -80°C until use. Total protein was extracted from BV2 cells after the cells were treated with PA medium (100 mM) for 24 h and quantified with a BCA protein quantification kit (Beyotime Biyuntian Biotechnology Co., Ltd., China, Cat). Mouse brain tissue or cell lysates were loaded onto 7, 10, or 12% SDS-PAGE gels for separation, depending upon the molecular weight of the target proteins, and then transferred onto PVDF membranes (Bio-Rad, Hercules, CA, USA). The membrane was blocked at room temperature with 5% skim milk in TBST for 2 h on a shaker prior to being incubated with primary antibodies [HIF-1 α (1:1000, Proteintech Cat No. 20960-1-AP), mTOR (1:1000, CST, 2984), p-mTOR (Ser2448) (1:1000, CST, 5536), p70S6 kinase (1:1000, CST, 9202), LC3A/B, Beclin-1, Atg3 212 (1:1000, Autophagy Antibody Sampler Kit, CST, 4445)] at 4°C overnight. The membrane was then washed three times with TBST (10 min). The membrane was then incubated with the appropriate horseradish peroxidase-conjugated secondary antibody against rabbit IgG or mouse IgG. The membrane was washed with TBST (3×10 min), and the target protein was exposed with an ECL chemiluminescent system (Tanon-5200Multi, Shanghai, China). The grey value of the target protein band was calculated by ImageJ 1.8.0 software (NIH).

Immunofluorescence staining

The anaesthetized mice ($n = 3/\text{group}$) were intracardially perfused with ice-cold phosphate-buffered saline (PBS), and the tissues were paraffin-embedded and sectioned into 4- μm -thick slices using a Rotary Microtome (HM 340E, 9 Thermo Scientific). Following deparaffinization, antigen retrieval was carried out as recommended by the manufacturers with citrate buffer pH 6.0 in a microwave oven for 5 min under high heat and for 15 min under medium heat. For non-specific binding, the sections were blocked for 30 min with 1.5% normal goat serum in PBS containing 0.5% bovine serum albumin. The sections were incubated overnight at 4°C with HIF-1 α (1:300, Proteintech Cat No. 20960-1-AP) primary antibodies. After incubation with HRP-conjugated IgG secondary antibody (1:300, Alexa Fluor 488-conjugated goat anti-rabbit IgG, cat. ZF-0516, ZSGB-BIO, China), nuclei were stained with DAPI (10 $\mu\text{g}/\text{ml}$) (Beyotime, China) for 3 min. Then, the sections were washed three times in PBS, anti-quenching fluorescence mounting medium was added, and the samples were covered with coverslips. The frequency of apoptosis in the brain was determined using an *in situ* cell death detection kit (Beyotime) according to the manufacturer's protocol. All immunofluorescence slides were viewed, and images were acquired using a NEXCOPE microscope (NE900, USA).

Transmission electron microscopy

After the MWM test, the mice ($n = 3/\text{group}$) were euthanized, and the hippocampal tissues were quickly harvested. The samples were prefixed with a solution of 3% glutaraldehyde for TEM analysis. Then, the tissue was postfixed in 1% osmium tetroxide, dehydrated in acetone, infiltrated in Epox 812 for a long time, and embedded. The semithin sections were stained with methylene blue, and ultrathin sections were cut with a diamond knife and stained with uranyl acetate and lead citrate. The sections were examined with a JEM-1400-FLASH Transmission Electron Microscope.

SA- β -gal cytochemical staining

Staining for the activity of senescence-associated β -galactosidase (SA- β -gal) was performed using a senescence β -galactosidase commercial assay following the manufacturer's instructions (Beyotime, C0602). Mice ($n = 3/\text{group}$) were euthanized in tricaine anesthetic, embedded in Tissue-Tek O.C.T. compound and frozen at -80°C . Ten-micrometer frozen sections were cut onto slides using a cryostat (Thermo). The slides were allowed to dry, washed in PBS solution for 5 min at room temperature, and then fixed with fixative solution for 30 min. Next, the slides were rinsed with PBS, and then 1 ml

of β -galactosidase staining solution was added to each sample. After staining overnight at 37°C, blue senescent staining in the cytoplasm in senescent cells was observed at 200 \times magnification. To quantify the number of SA- β -gal-positive cells, four random visual fields per section were selected and counted with ImageJ software.

Immunohistochemistry

Prior to incubation with antibody, deparaffinization with xylene and antigen retrieval were performed in a microwave. Sections were incubated in endogenous peroxidase blocker for 10 min. After washing (PBS 3 \times 5 min), goat serum was added and blocked at 37°C for 20 min. Samples were incubated overnight at 4°C with mouse anti-human A β 1-42 monoclonal antibody (1:300, CST, 14974S). The next day, the sections were reheated for 30 min, and PBS was rinsed (3 \times 5 min). Then, the secondary antibody (goat anti-rabbit/mouse IgG) was added and incubated at room temperature for 10 min. After subsequent washing in PBS, the peroxidase-conjugated streptavidin-biotin complex was incubated at 37°C for 10 min. After washing with PBS, antigen-antibody complexes were visualized using the DAB horseradish peroxidase color development kit (Jiangsu Beyotime). The slides were then stained with haematoxylin for 5 min and differentiated with hydrochloric acid alcohol for 2 s. The staining results were analyzed by the image analysis software Proplus 6.0 and photographed by a NEXCOPE microscope $n = 3/\text{group}$.

Click-it TUNEL alexa fluor 488 imaging assay

We used the terminal deoxynucleotidyl transferase dUTP nick end labeling (TUNEL) staining method to detect apoptosis by using an *in situ* cell death detection kit (Jiangsu Beyotime). For *in situ* labeling, brain tissue slices were placed in 1 \times PBS for 10 min after dehydration. The samples were incubated in the presence of 50 ng/ μ l proteinase K for 30 min followed by 50 μ l of CytoninTM for 120 min. The samples treated with TACS nuclease were used as the positive control. TUNEL-positive cells were detected with a fluorescence microscope (NEXCOPE, NE900, USA). The percentage (%) of apoptotic cells in the TUNEL assay was obtained by dividing the number of apoptotic cells (TUNEL-positive cells) from the number of total cells (DAPI nuclear staining) in the microscopic field ($n = 3/\text{group}$).

Statistical analysis

Mouse randomization was based on the random number generator function (RANDBETWEEN) in Microsoft Excel. The

data were analyzed by GraphPad Prism Software version 8.3.0 (GraphPad Software, San Diego, CA, USA). One-way analyses of variance (ANOVA) and independent-sample *t*-tests were used to compare the differences in measurement data between two groups. The data are expressed as the means \pm standard errors of the means (SEM), and differences were considered statistically significant at $*P < 0.05$.

Results

A high-fat diet induced hippocampal-related behavioral changes in aged C57BL/6 mice

We fed 13-month-old male C57BL/6 mice a normal chow diet or a HFD for 24 weeks (6 months) and monitored body weight and food intake (Figure 1). The body weight of mice in the HFD group was significantly lower than those in the control group at week 61 ($P < 0.05$). Moreover, we observed an apparent progressive thinning of body hair, which had a lusterless and sharp appearance in HFD animals. However, the results showed no significant difference in brain weight and food intake between the two groups during the 6 months. Changes in diet have been widely linked to changes in behavior, including hippocampal-dependent cognition, which declines during ageing Daub et al. (2017). Thus, we performed the MWM test to examine whether a high-fat diet damaged brain health and hippocampus-associated behavioral abnormalities in aged mice. Previous research has shown that ageing is linked to impaired learning ability and an increase in the latency to enter the target platform zone. Compared with the ND group, the HFD group showed a significant difference in the number of entries to the target platform. The swim average velocity and average latency to reach the platform in the visible platform trials were similar in the two groups. Aged HFD-fed mice showed increases in the mean distance from the platform on training days 5 and 6. Overall, these data suggest that long-term exposure to a HFD exacerbated the impaired spatial learning and memory in naturally aged mice (Figure 2).

A high-fat diet increased tissue hypoxia and HIF-1 α levels

Then, we evaluated the effect of a hyperlipidaemic diet on the hypoxic environment in the mouse brain. In HFD-fed mice, the protein levels of HIF-1 α were significantly increased, as shown by western blotting. BV2 cells treated with PA yielded similar results. To determine the localization of HIF-1 α in the two groups, immunofluorescence analysis was performed (Figure 3). HIF-1 α was highly expressed, and the overlay images showed that HIF-1 α accumulated in the nucleus rather than

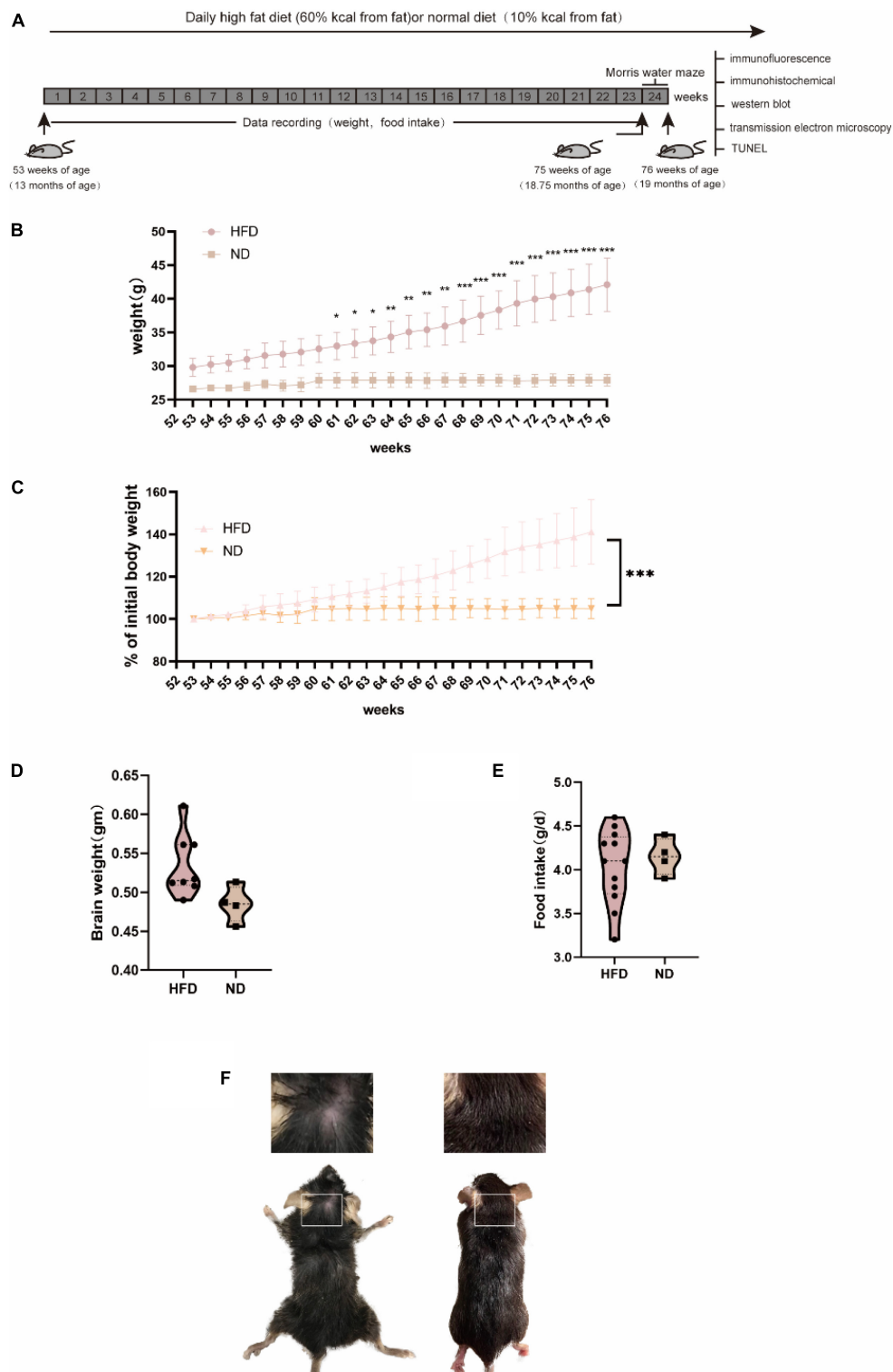


FIGURE 1

General characteristics of C57BL/6 mice fed with normal diet and high-fat diet. C57BL/6 mice (13 months old) were fed a HFD or ND for 24 weeks. **(A)** Experiment process overview. **(B)** Changes in body weight over time and body weight were significantly increased after 8 weeks of HFD. **(C)** A percentage of the initial body weight during the course of the experiment. Body weight percentage was calculated as (actual body weight/initial body weight) \times 100. **(D)** Alterations in food intake were not significantly different between groups. **(E)** (HFD, $n = 20$ mice; ND, $n = 10$ mice) **(E)** Brain weight did not differ between groups. **(F)** At the late stage, the HFD group exhibited an extremely poor status with increasingly sparse hair.

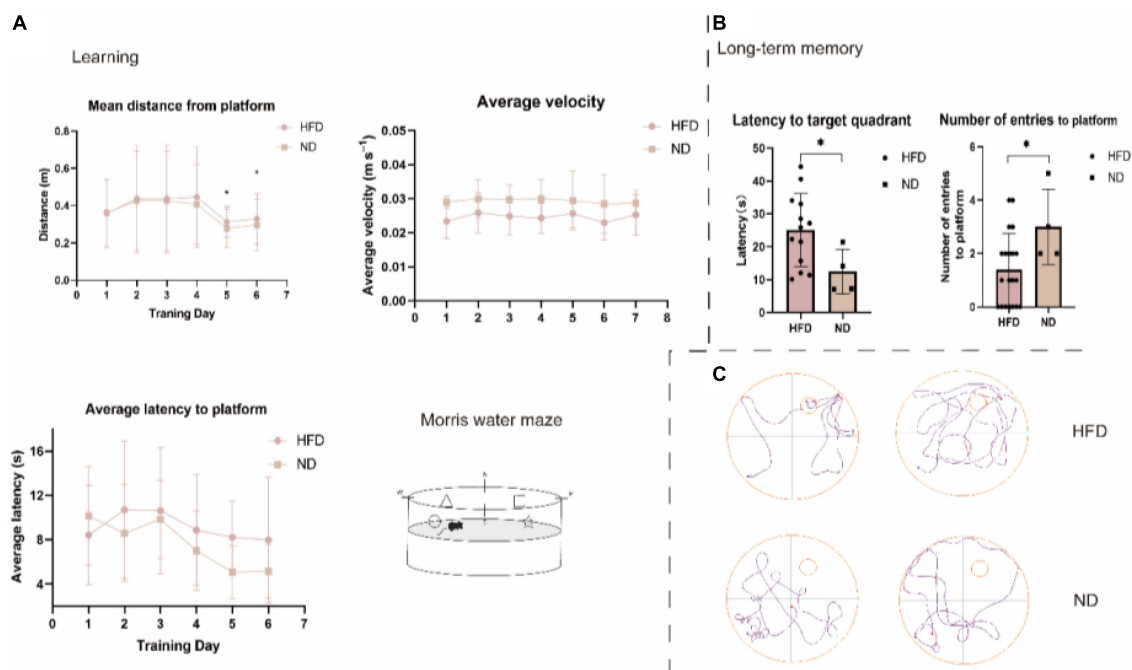


FIGURE 2

High-fat diet impairs spatial learning and memory in aged C57BL/6 mice. Long-term spatial memory assessed *via* MWM. **(A)** Learning ability. HFD significantly impacted the mean distance from the platform. ND mice spent more time closer to the platform than HFD mice. HFD mice were significantly different from ND mice on days 5 and 6 ($P = 0.047$, $P = 0.025$, respectively). There were no overall differences in average latency to platform or average velocity. $n = 20$ (HFD), 4 (ND), **(B)** Long-term memory. The probe trial revealed an age-related impairment in latency to target quadrant and number of entries to platform, wherein HFD mice were significantly slower to the target quadrant compared to ND mice ($P = 0.049$, $P = 0.023$, respectively). Swimming traces of mice in the probe trial are presented in panel **(C)**. p , two-sample t -test. Mean \pm SEM, $*p < 0.05$ compared with the ND group, HFD, high-fat diet; ND, normal diet.

the cytoplasm in the HFD group (Figure 3E). These results suggested that HIF-1 α was increased in hypoxic tissue in the hypoxic environment induced by the hyperlipidaemic diet.

A high-fat diet increased the expression of brain senescence markers

Senescence-associated β -galactosidase (SA- β -Gal) is a common marker for senescence. SA- β -gal staining of brain tissues was used as a brain senescence marker. Our results show that after 24 weeks of high-fat diet feeding, a significant increase in the number of SA- β -gal-positive cells was demonstrated in the mouse hippocampus when compared to that in the normal diet groups especially in region CA3 (Figure 4).

A high-fat diet triggers cellular apoptosis in mice brain

Cellular apoptosis plays numerous important age-related degenerative pathophysiological roles. We also performed

terminal deoxynucleotidyl transferase (TdT)-mediated dUTP nick-end labeling (TUNEL) staining shown in Figure 5. After 24 weeks of a high-fat diet, apoptosis was significantly increased in the brains of the HFD group.

A high-fat diet influences autophagic flux by suppressing the conversion of autophagosomes to autophagolysosomes

Autophagic flux was measured by examining the levels of the autophagy-related proteins LC3, Atg3, and Beclin1 by western blotting. The expression of LC3, Atg3, and Beclin1 was significantly increased; moreover, the expression of the elective autophagy receptor SQSTM1/p62 was also increased, suggesting that a HFD may affect autophagic flux by increasing autophagosome formation. To confirm the role of autophagosomes in the mouse hippocampus, we performed transmission electron microscopy, which is a standard method to examine autophagy activation. Under an electron microscope, the number of autophagosomes was increased in HFD-induced cells, and the number of autophagolysosomes was

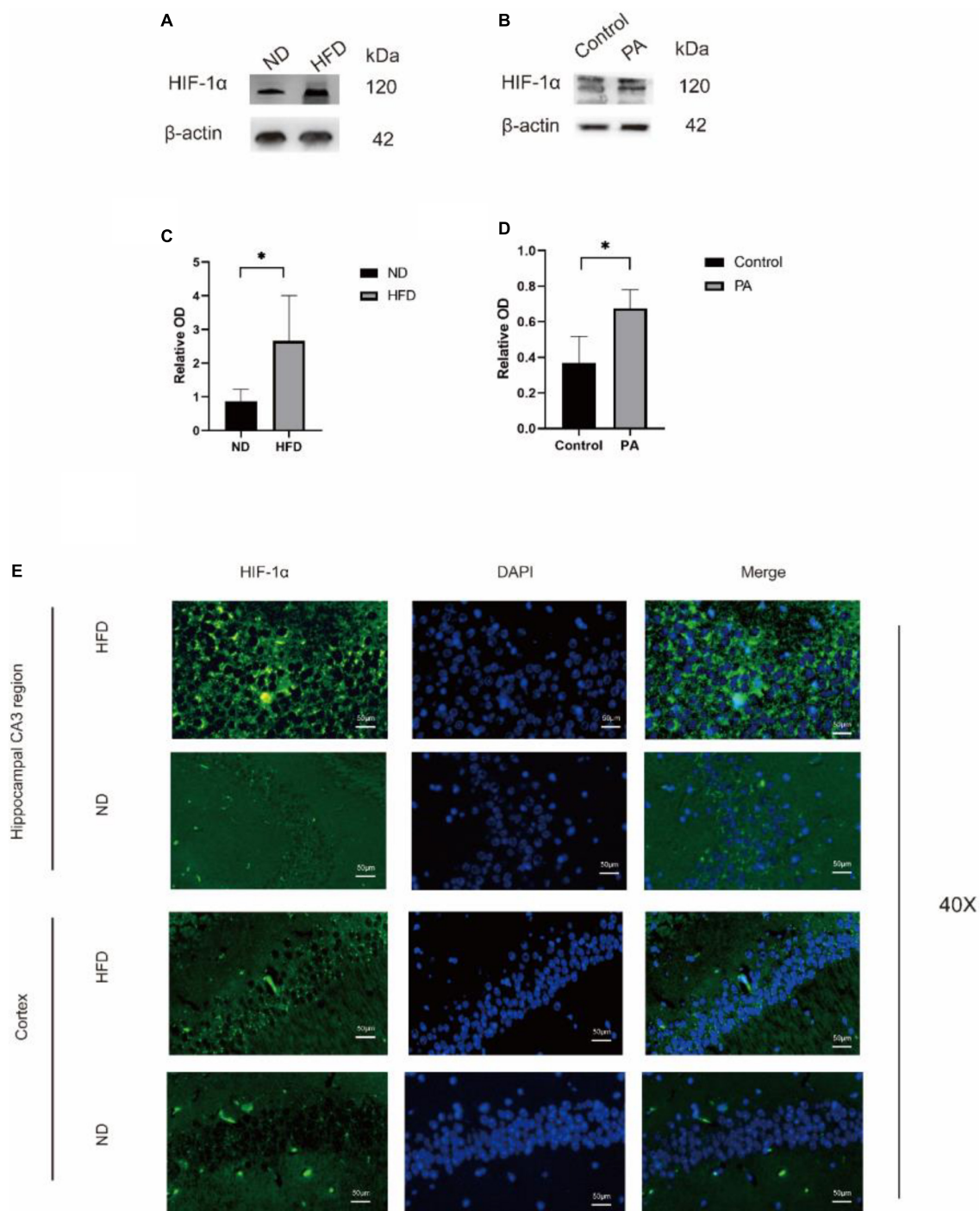


FIGURE 3

The expression of HIF-1α was observed in hippocampus of mice. Western blot results showing that high-fat diet upregulates the expression of HIF-1α in the hippocampus of aged brain C57BL/6 mice ($n = 4/\text{group}$, two-sample t -test) (A,B). (C,D), Graph showing the expression level of HIF-1α proteins expressed in BV2 cells after treatment with 100 mM PA. (E) Expression of HIF-1α in the CA3 of the hippocampus and cortex of mice in the two groups observed by immunofluorescence ($n = 3/\text{group}$). Scale bars = 50 μm .

decreased. Abnormal glial morphology and increased apoptosis in HFD-fed mice were accompanied by mitochondrial depolarization. **Figures 8Eb,d** shows a significantly abnormal

synaptic structure and blurred or missing synaptic clefts. We tested this hypothesis, and the results from our *in vitro* HFD model using BV2 cells was consistent with the *in vivo*

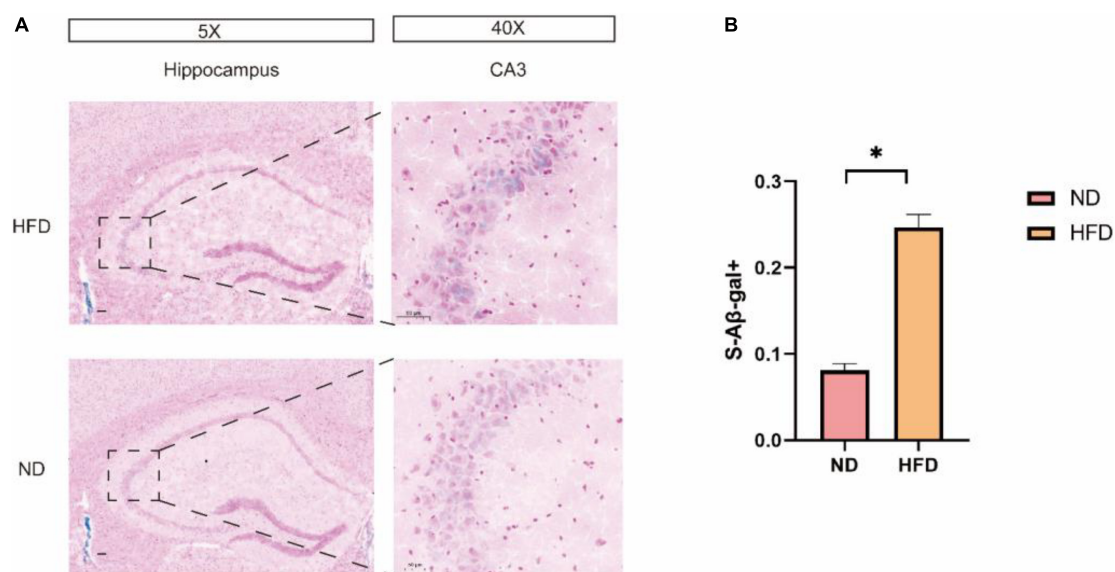


FIGURE 4
A HFD induced hippocampal cell senescence. **(A)** Representative images of SA-β-Gal⁺ in HFD mice and ND mice in the hippocampus. The enlarged boxed region (right) shows the region CA3-positive cells. Scale bars = 50 μm. **(B)** Quantification of SA-β-GalC in total cells in the hippocampus of ND and HFD mice (n = 3/group) *p < 0.05.

results. Western blotting showed that PA treatment significantly increased the expression of LC3II/LC3I, Atg3 and Beclin1 and increased the accumulation of p62 compared with those in the control group. These data suggest that a long-term HFD feeding can suppress autophagic degradation.

The AMPK-mTOR-p70S6K signaling pathway, which regulates autophagy, is activated by a high-fat diet

To confirm whether the increase in autophagy induced by HFD was dependent on the regulation of the AMPK-mTOR-p70S6K signaling pathway, C57BL/6J mice were fed a HFD for 6 months. Western blot analysis revealed that the levels of phosphorylated AMPK (Thr172) were decreased, and the levels of phosphorylated mTOR (Ser2448) and p70S6 were decreased, as shown in [Figure 7](#).

A high-fat diet caused hippocampal amyloidosis to increase in aged C57BL/6 mice

Amyloid-β (Aβ) peptides have been reported to impair synaptic function, long-term synaptic plasticity and memory performance [Walsh et al. \(2002\)](#) and [Cleary et al. \(2005\)](#). We performed immunohistochemistry to detect the expression of Aβ42 in the hippocampus of the ND group and HFD group. Interestingly, as shown in [Figure 6](#), compared with the ND

group, the HFD group had significantly increased expression of Aβ42 in the hippocampus, especially in the CA3 region.

Discussion

This study aimed to investigate HFD-induced obesity on the ageing process and cognitive or behavioral changes. In this study, we found that 24 weeks of a HFD effectively induced phenotypic changes, including obesity and changes in skin and fur, in mice. In addition, the mice also showed learning and memory deficits. Moreover, the HFD-induced obesity activated tissue hypoxia, upregulated the expression of HIF-1α, and influenced autophagy by decreasing the p-AMPK/AMPK ratio and increasing the p-mTOR/mTOR ratio in the hippocampus. The results of the *in vitro* experiment were consistent with those of the *in vivo* experiment. Overall, our results demonstrated that long-term HFD-induced obesity may increase HIF-1α levels, inhibit AMPK phosphorylation and promote mTOR phosphorylation to inhibit autophagy and increase apoptosis and cellular senescence, which eventually leads to a senescent phenotype and disturbances in cognitive function in mice. Accumulating evidence indicates that chronic HFD feeding can cause obesity, insulin resistance, and glucose intolerance [Forouhi et al. \(2018\)](#). However, research on how brain metabolic manipulations improve the quality of health and thus prolong life in elderly individuals is still in its infancy. Specifically, accelerated ageing and cognitive dysfunction following HFD feeding are poorly understood. Impaired autophagy is involved in neurodegenerative age-related diseases, such as AD, PD,

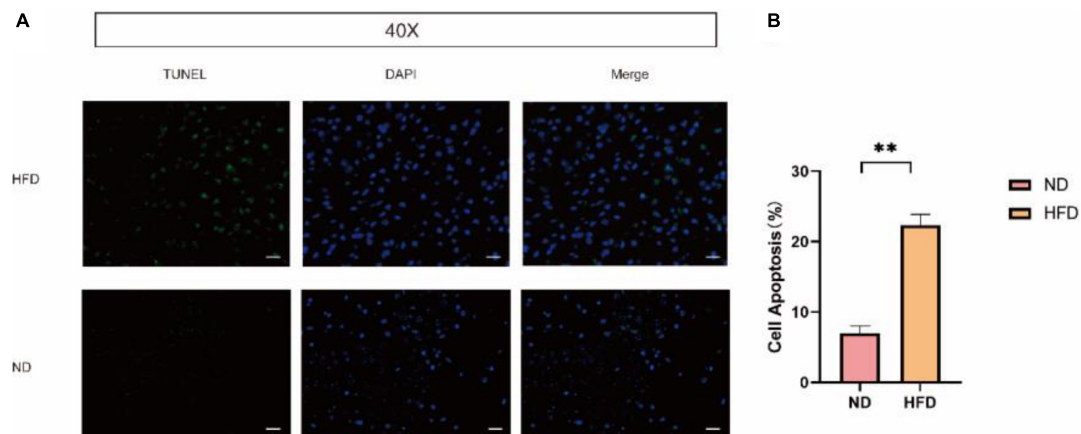


FIGURE 5

A HFD boosted cell apoptosis in mice brain. (A) TUNEL staining was applied to assess the effects of HFD induced on the apoptosis of brain cell. Scale bars = 50 μ m. (B) Percentage of TUNEL-positive cells by TUNEL staining ($n = 3/\text{group}$) $**p < 0.01$.

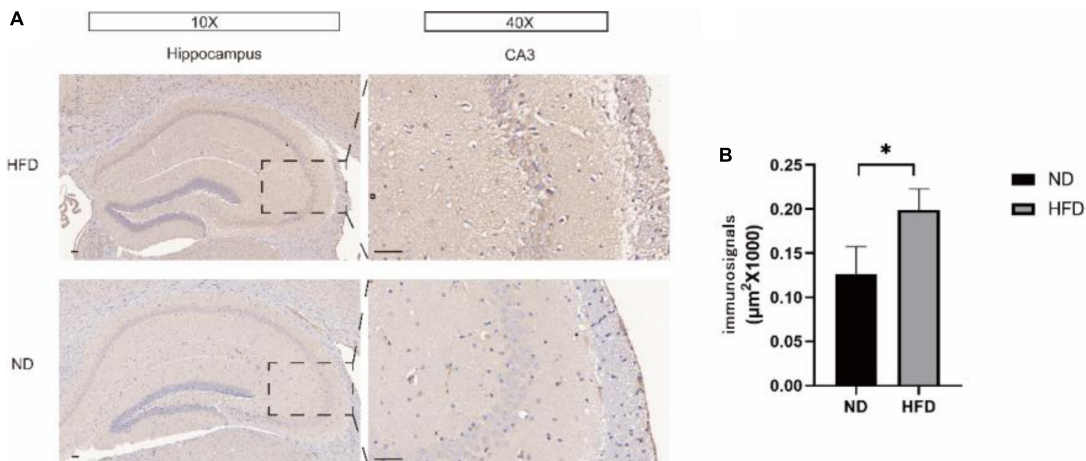


FIGURE 6

(A) Hippocampal immunohistochemical staining using an antibody against A β 42 was performed to detect the A β 42 load in hippocampal slices from the ND group and HFD group. The right panel shows representative A β 42 plaque staining in region CA3. (B) Immunohistochemical analysis of A β 42 protein expression. Significant differences compared with the ND group.

and HD, as well as in lysosomal storage disorders Hansen et al. (2018). It is widely accepted that autophagy is divided into three categories: macroautophagy, molecular chaperone-mediated autophagy and microautophagy. Among them, the most widely studied is macroautophagy. Autophagy is a dynamic process that consists of several steps, including (i) phagosome formation, (ii) autophagosome formation, (iii) lysosome fusion to autophagolysosomes, and (iv) the degradation of autophagolysosomes (Figure 9). Microtubule-associated protein light chain 3 β (also known as LC3) is an essential macroautophagy protein that is present from autophagosome formation to fusion with lysosomes. LC3 is divided into two subtypes: soluble LC3-I and lipidated LC3-II. LC3I is first activated by autophagy-related protein 7 (Atg7) and then transferred to Atg3 (a ubiquitin-2-like

protein), and the conversion of LC3 from the LC-I-cleaved form to the conjugated form (LC3II) is considered a key step in autophagosome formation Tanaka et al. (2012). Beclin1 is a crucial molecule in autophagy due to its ability to initiate autophagosome formation, mediate the recruitment of autophagy-related proteins and promote the formation and maturation of autophagosomes Choi et al. (2015). The mTOR signaling pathway is well known to be a negative regulator of autophagy. Activated AMPK (p-AMPK, phosphorylated AMPK) inhibits mTOR, resulting in enhanced autophagy. The major downstream target of mTOR is P70S6K. An adverse haemodynamic profile and diminished cerebral blood flow were observed in adipose tissue from obese humans, suggesting a hypoxic state in the tissue, which likely contributes to metabolic dysfunction.

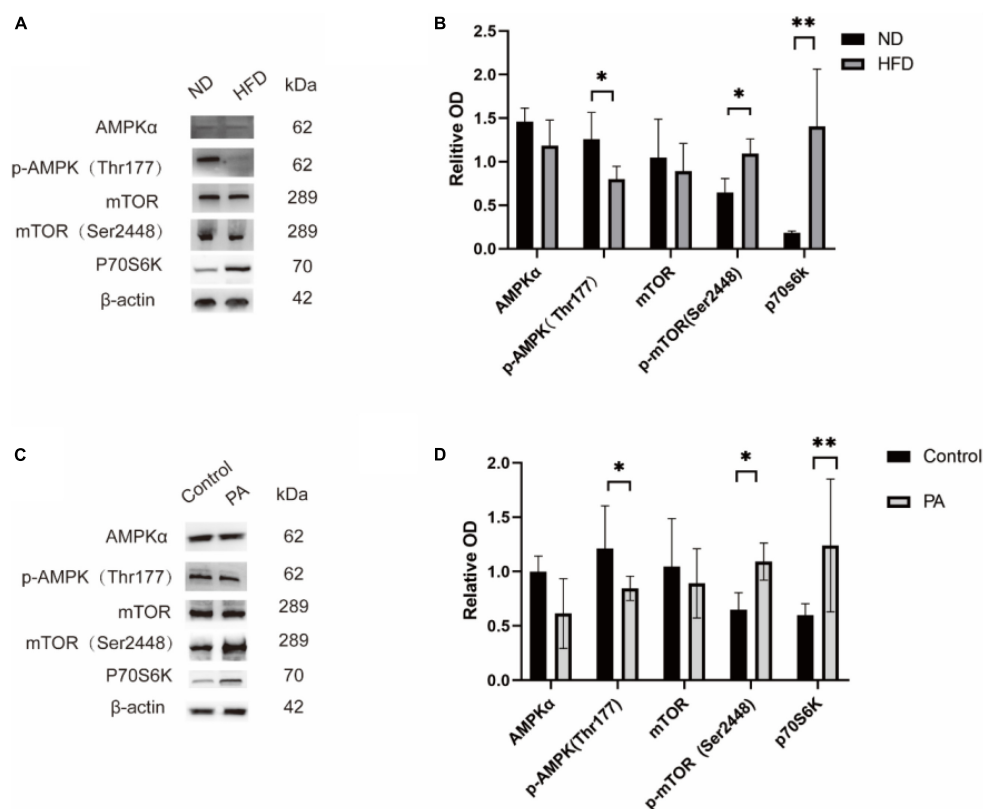


FIGURE 7

Effect of high-fat diet on AMPK/mTOR/p70S6K pathway protein levels. Representative western blotting bands of mTOR, p-mTOR, AMPK, p-AMPK, and p70S6K in the hippocampus of the ND and HFD groups (shown in panel A). Statistical results showed that a high-fat diet increased p-mTOR levels and the p-mTOR/mTOR ratio, decreased p-AMPK levels and the p-AMPK/AMPK ratio and decreased p70S6K in the hippocampus (ND, $n = 4$ mice; HFD, $n = 4$ mice) (shown in panel B). BV2 cells treated with were done with PA medium (100 mM), and showed the same result (C,D) * $p < 0.05$, ** $p < 0.01$.

Previous studies have established a link between obesity and an increased burden of senescent cells Tumasian et al. (2021). In addition, Shin et al. showed that an increase in HIF-1 α contributes to increased p-tau expression in neurons and astrocytes in the hippocampus, eventually resulting in cognitive impairment Shin et al. (2019). Moreover, it has been previously reported that autophagic flux is increased in the initial phase of hypoxia and later results in impaired autophagy-mediated clearance (Cui et al., 2017). Whereas AMPK depresses the activity of HIF-1 α , HIF-1 α promotes autophagic flux in an AMPK-independent manner Li et al. (2015). In the present study, our results showed that a HFD markedly induced the protein expression of p-AMPK and reduced the expression of p-mTOR in the mouse hippocampus, which might be due to eutrophication Hu et al. (2018). Emerging evidence suggests direct links between autophagy and A β , which may contribute to AD onset or progression Pickford et al. (2008). Normally, A β aggregates, can also be degraded by the autophagy-lysosomal pathway (ALP). Defective ALP, which is increased formation of autophagosomes not only leads to A β ₄₂ accumulation, but also hinders its degradation. In addition, it has been shown that

defective ALP can overproduce neurovirulent A β ₄₀ and A β ₄₂ Chu et al. (2013).

In summary, our results provide the first evidence that a long-term HFD causes accelerated ageing and cognitive dysfunction compared to a normal diet. Autophagy dysfunction caused by disrupted lipid metabolism and tissue hypoxia in the brain may be associated with dietary fat. In comparison, previous studies in this field mostly studied young mice fed a HFD for a shorter time. Thus, our study revealed that a HFD alters the rate of pathological autophagosomes *in vitro* and *in vivo*. Ageing is characterized by a progressive loss of physiological integrity in various organs throughout life. Dietary nutrients are among the most critical environmental factors that modulate health span and lifespan. However, how a HFD affects brain damage is still unclear. Our findings may provide a means for the diagnosis or personalized treatment of congenital premature ageing syndromes, AD and PD and resolve the challenges in the ageing population. Furthermore, our work provides novel insight into the importance of HFD feeding in midlife in mice.

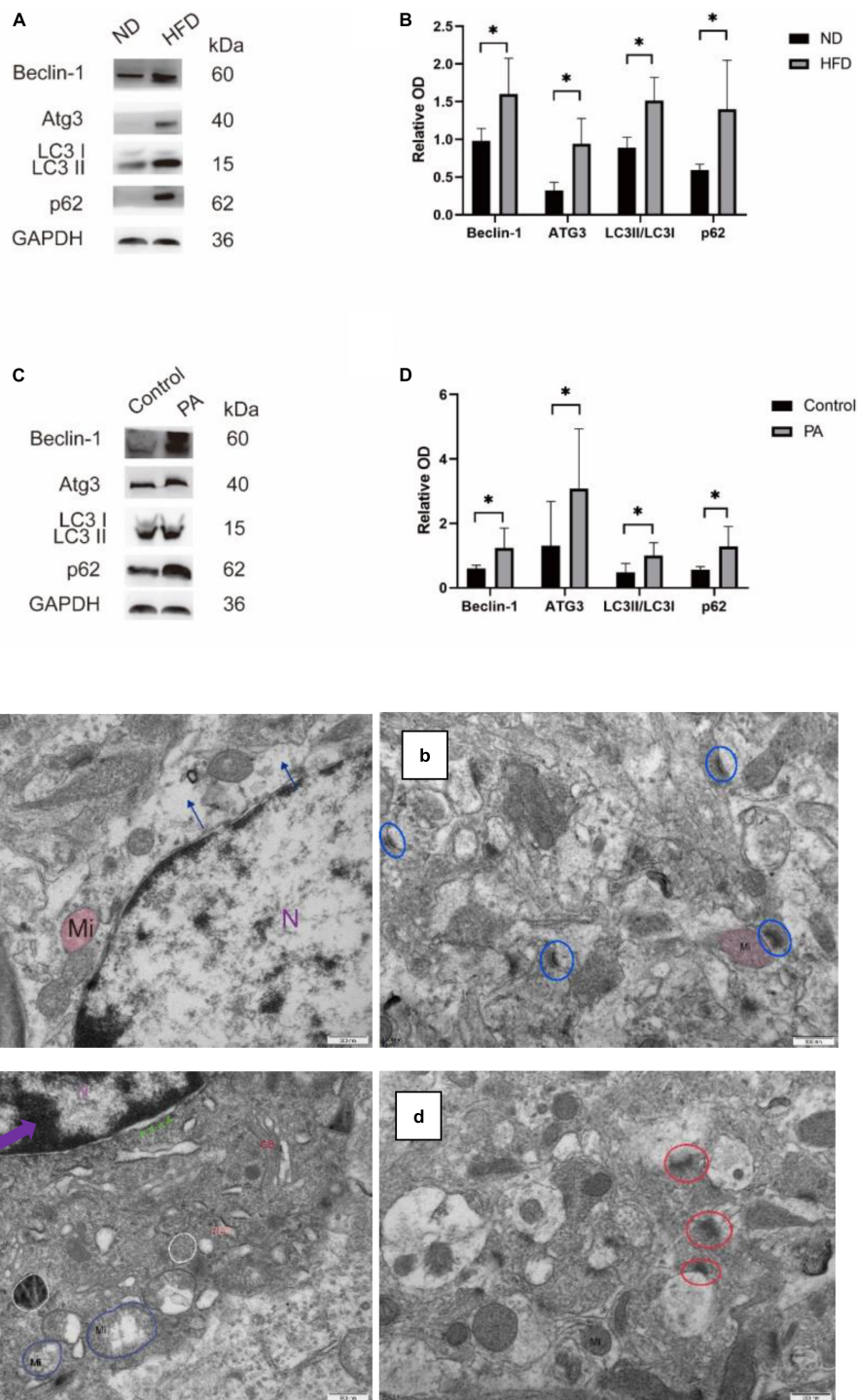
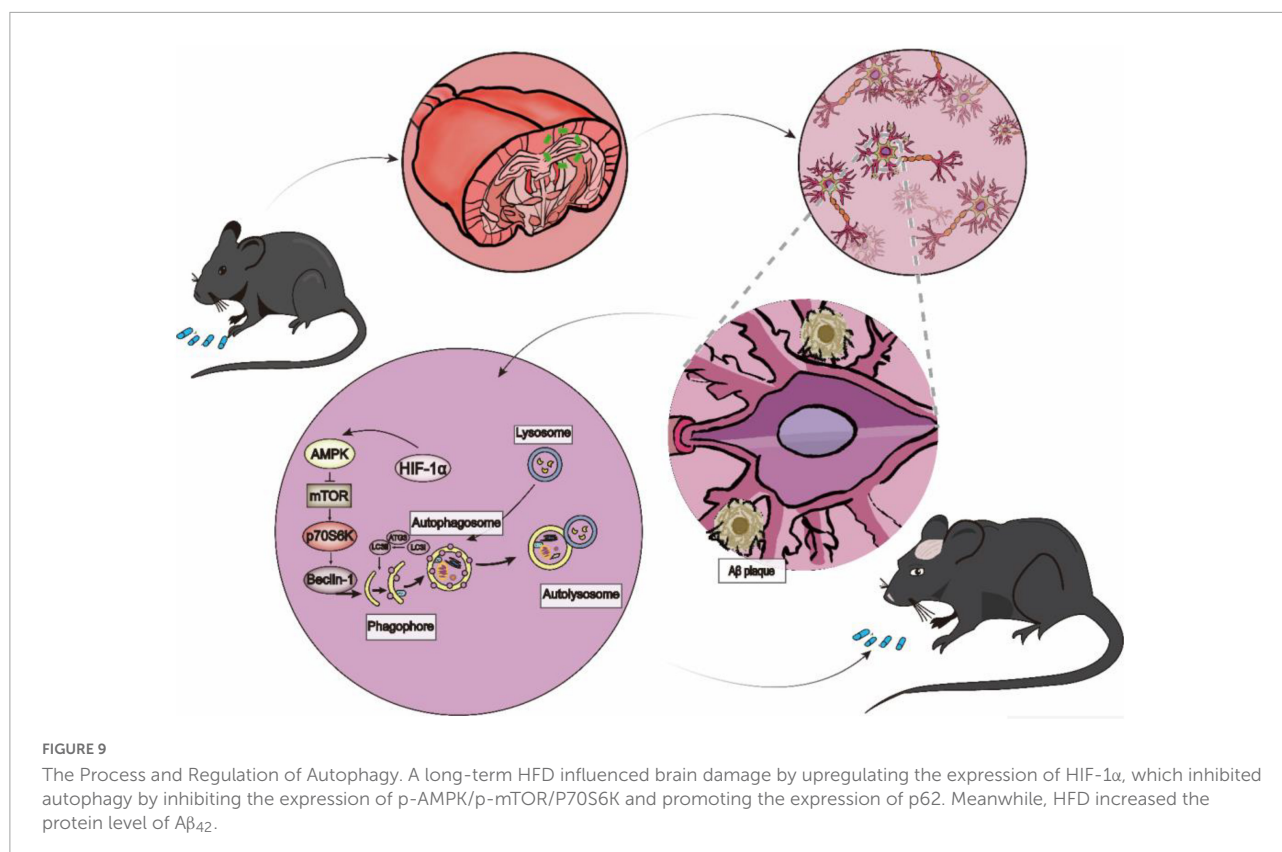


FIGURE 8

The expression levels of autophagy-associated proteins and the ultrastructure of autophagosomes in the hippocampus of mice under an electron microscope. (A,B) Representative western blotting bands of Beclin-1, ATG3, LC3, and P62 in the hippocampus of mice and their quantification. (C,D) BV2 cells treated with PA medium (100 mM) showed increased expression of Beclin-1, ATG3, LC3, and P62 compared with the CON group (ND, $n = 4$ mice; HFD, $n = 4$ mice). (E) Alterations in hippocampal ultrastructure were examined by transmission electron microscopy. (a) The gliocyte lost its cytosol (blue arrow) in ND. N, nucleus; Mi, mitochondria, $\times 30000$. (b) The synaptic structure was intact, with normal histological structure in ND (blue circle). (c) The nucleus condensed, and the chromosomes gathered to assemble chromatin (purple arrow) and widened the nuclear gap (green arrow) and mitochondrial mild swelling (blue circle) and autophagosomes (white circle) in the HFD group. RER, rough endoplasmic reticulum, GB, Golgi bodies $\times 30000$. (d) The structure of presynaptic membrane and synaptic gap is not clear in HFD (red circle) $\times 30000$, scalar bar = 500 μm .



Data availability statement

The raw data supporting the conclusions of this article will be made available by the authors, without undue reservation.

Ethics statement

The animal study was reviewed and approved by the Chongqing General Hospital.

Author contributions

ZC and FC were responsible for the conception of the idea, data analysis, and manuscript preparation. FC, WY, SW, MY, JW, HL, QZ, and SL performed the experimental work. ZC and FC prepared and revised the manuscript. All authors contributed to the article and approved the submitted version.

Funding

This work was supported by the Construction Project of Capacity Improvement Plan for Chongqing Municipal

Health Commission affiliated unit (2019NLT001)-ZS03174, operating grant to Chongqing Key Laboratory of Neurodegenerative Diseases (1000013), Chongqing Talent Project (2000062), Overseas Students entrepreneurial fund (2000079), and Plan for High-level Talent Introduction (2000055).

Conflict of interest

The authors declare that the research was conducted in the absence of any commercial or financial relationships that could be construed as a potential conflict of interest.

Publisher's note

All claims expressed in this article are solely those of the authors and do not necessarily represent those of their affiliated organizations, or those of the publisher, the editors and the reviewers. Any product that may be evaluated in this article, or claim that may be made by its manufacturer, is not guaranteed or endorsed by the publisher.

References

- Abbott, K. N., Arnott, C. K., Westbrook, R. F., and Tran, D. (2019). The effect of high fat, high sugar, and combined high fat-high sugar diets on spatial learning and memory in rodents: a meta-analysis. *Neurosci. Biobehav. Rev.* 107, 399–421. doi: 10.1016/j.neubiorev.2019.08.010
- Bartels, E. D., Bang, C. A., and Nielsen, L. B. (2009). Early atherosclerosis and vascular inflammation in mice with diet-induced type 2 diabetes. *Eur. J. Clin. Invest.* 39, 190–199. doi: 10.1111/j.1365-2362.2009.02086.x
- Carling, D., Sanders, M. J., and Woods, A. (2008). The regulation of AMP-activated protein kinase by upstream kinases. *Int. J. Obes.* 32(Suppl. 4), S55–S59. doi: 10.1038/ijo.2008.124
- Choi, J., Jo, M., Lee, E., Lee, D. Y., and Choi, D. (2015). Dienogest enhances autophagy induction in endometriotic cells by impairing activation of AKT, ERK1/2, and mTOR. *Fertil. Steril.* 104, 655–664. doi: 10.1016/j.fertnstert.2015.05.020
- Chu, C., Zhang, X., Ma, W., Li, L., Wang, W., Shang, L., et al. (2013). Induction of autophagy by a novel small molecule improves abeta pathology and ameliorates cognitive deficits. *PLoS One* 8:e65367. doi: 10.1371/journal.pone.0065367
- Cleary, J. P., Walsh, D. M., Hofmeister, J. J., Shankar, G. M., Kuskowski, M. A., Selkoe, D. J., et al. (2005). Natural oligomers of the amyloid-beta protein specifically disrupt cognitive function. *Nat. Neurosci.* 8, 79–84. doi: 10.1038/nn1372
- Cui, D., Sun, D., Wang, X., Yi, L., Kulikowicz, E., Reyes, M., et al. (2017). Impaired autophagosome clearance contributes to neuronal death in a piglet model of neonatal hypoxic-ischemic encephalopathy. *Cell Death Dis.* 8:e2919. doi: 10.1038/cddis.2017.318
- Daub, J. T., Moretti, S., Davydov, I. I., Excoffier, L., and Robinson-Rechavi, M. (2017). Detection of pathways affected by positive selection in primate lineages ancestral to humans. *Mol. Biol. Evol.* 34, 1391–1402. doi: 10.1093/molbev/msx083
- Forouhi, N. G., Krauss, R. M., Taubes, G., and Willett, W. (2018). Dietary fat and cardiometabolic health: evidence, controversies, and consensus for guidance. *BMJ* 361:k2139. doi: 10.1136/bmj.k2139
- Hansen, M., Rubinsztein, D. C., and Walker, D. W. (2018). Autophagy as a promoter of longevity: insights from model organisms. *Nat. Rev. Mol. Cell Biol.* 19, 579–593. doi: 10.1038/s41580-018-0033-y
- Hardie, D. G. (2015). AMPK: positive and negative regulation, and its role in whole-body energy homeostasis. *Curr. Opin. Cell Biol.* 33, 1–7. doi: 10.1016/j.ceb.2014.09.004
- Hoffman, E. L., VonWald, T., and Hansen, K. (2015). The metabolic syndrome. *S D Med. Spec No*, 24–28.
- Hosogai, N., Fukuhara, A., Oshima, K., Miyata, Y., Tanaka, S., Segawa, K., et al. (2007). Adipose tissue hypoxia in obesity and its impact on adipocytokine dysregulation. *Diabetes* 56, 901–911. doi: 10.2337/db06-0911
- Hu, H., Seung-Hwan, L., Inês, S., Sang, S. K., Won, M. H., Yossi, D., et al. (2018). Rho-kinase/AMPK axis regulates hepatic lipogenesis during overnutrition. *J. Clin. Invest.* 128, 5335–5350. doi: 10.1172/JCI63562
- Knight, E. M., Martins, I. V., Gumusgoz, S., Allan, S. M., and Lawrence, C. B. (2014). High-fat diet-induced memory impairment in triple-transgenic Alzheimer's disease (3xTgAD) mice is independent of changes in amyloid and tau pathology. *Neurobiol. Aging* 35, 1821–1832. doi: 10.1016/j.neurobiolaging.2014.02.010
- Li, H., Satriano, J., Thomas, J. L., Miyamoto, S., Sharma, K., Pastor-Soler, N. M., et al. (2015). Interactions between HIF-1alpha and AMPK in the regulation of cellular hypoxia adaptation in chronic kidney disease. *Am. J. Physiol. Renal Physiol.* 309, F414–F428. doi: 10.1152/ajprenal.00463.2014
- Pickford, F., Masliah, E., Britschgi, M., Lucin, K., Narasimhan, R., Jaeger, P. A., et al. (2008). The autophagy-related protein beclin 1 shows reduced expression in early Alzheimer disease and regulates amyloid beta accumulation in mice. *J. Clin. Invest.* 118, 2190–2199. doi: 10.1172/JCI33585
- Prentice, A. M., and Jebb, S. A. (2003). Fast foods, energy density and obesity: a possible mechanistic link. *Obes. Rev.* 4, 187–194. doi: 10.1046/j.1467-789x.2003.00117.x
- Shin, N., Kim, H. G., Shin, H. J., Kim, S., Kwon, H. H., Baek, H., et al. (2019). Uncoupled endothelial nitric oxide synthase enhances p-tau in chronic traumatic encephalopathy mouse model. *Antioxid Redox Signal.* 30, 1601–1620. doi: 10.1089/ars.2017.7280
- Sikora, E., Bielak-Zmijewska, A., Dudkowska, M., Krzystyniak, A., Mosieniak, G., Wesierska, M., et al. (2021). Cellular senescence in brain aging. *Front. Aging Neurosci.* 13:646924. doi: 10.3389/fnagi.2021.646924
- Tanaka, A., Jin, Y., Lee, S. J., Zhang, M., Kim, H. P., Stolz, D. B., et al. (2012). Hyperoxia-induced LC3B interacts with the Fas apoptotic pathway in epithelial cell death. *Am. J. Respir. Cell Mol. Biol.* 46, 507–514. doi: 10.1165/rcmb.2009-0415OC
- Tumasian, R. R., Harish, A., Kundu, G., Yang, J. H., Ubaida-Mohien, C., Gonzalez-Freire, M., et al. (2021). Skeletal muscle transcriptome in healthy aging. *Nat. Commun.* 12:2014. doi: 10.1038/s41467-021-22168-2
- Walsh, D. M., Klyubin, I., Fadeeva, J. V., Cullen, W. K., Anwyl, R., Wolfe, M. S., et al. (2002). Naturally secreted oligomers of amyloid beta protein potently inhibit hippocampal long-term potentiation in vivo. *Nature* 416, 535–539. doi: 10.1038/416535a
- Wang, Y., and Zhang, H. (2019). Regulation of autophagy by mTOR signaling pathway. *Adv. Exp. Med. Biol.* 1206, 67–83. doi: 10.1007/978-981-15-0602-4_3



OPEN ACCESS

EDITED BY
Shani Stern,
University of Haifa, Israel

REVIEWED BY
Michael Benjamin Larkin,
Baylor College of Medicine,
United States
Renato Juan Galzio,
University of Pavia, Italy

*CORRESPONDENCE
Qing-he Zhou
jxxmxy@163.com

SPECIALTY SECTION
This article was submitted to
Neurodegeneration,
a section of the journal
Frontiers in Neuroscience

RECEIVED 07 August 2022
ACCEPTED 20 September 2022
PUBLISHED 06 October 2022

CITATION
Huang B, Du X-d, Yao M, Lin H-d,
Yu W-h and Zhou Q-h (2022)
CT-guided radiofrequency ablation of
the extracranial cranial nerve for the
treatment of Meige's syndrome.
Front. Neurosci. 16:1013555.
doi: 10.3389/fnins.2022.1013555

COPYRIGHT
© 2022 Huang, Du, Yao, Lin, Yu and
Zhou. This is an open-access article
distributed under the terms of the
[Creative Commons Attribution License](https://creativecommons.org/licenses/by/4.0/)
(CC BY). The use, distribution or
reproduction in other forums is
permitted, provided the original
author(s) and the copyright owner(s)
are credited and that the original
publication in this journal is cited, in
accordance with accepted academic
practice. No use, distribution or
reproduction is permitted which does
not comply with these terms.

CT-guided radiofrequency ablation of the extracranial cranial nerve for the treatment of Meige's syndrome

Bing Huang¹, Xin-dan Du², Ming Yao¹, Hui-dan Lin³,
Wen-hua Yu⁴ and Qing-he Zhou^{1*}

¹Department of Pain Medicine, Affiliated Hospital of Jiaxing University, Jiaxing, China, ²Department of Pain Medicine, Redcross Hospital of Hangzhou, Hangzhou, China, ³Department of Pain Medicine, First Hospital of Ningbo, Ningbo, China, ⁴Department of Neurosurgery, Affiliated Hangzhou First People's Hospital, Zhejiang University School of Medicine, Hangzhou, China

Background: Meige's syndrome, a rare form of dystonia, lacks effective treatment. The purpose of this study was to determine the effects of CT-guided percutaneous extracranial radiofrequency ablation of the facial and/or trigeminal nerves in the treatment of Meige's syndrome.

Methods: A total of 10 patients were enrolled in this study, with the numbers of blepharospasm dystonia syndrome (BDS), oromandibular dystonia syndrome (ODS), and blepharospasm combined with oromandibular dystonia syndrome (B-ODS) being 7, 1, and 2, respectively. BDS patients underwent radiofrequency ablation of the bilateral stylomastoid foramen facial nerve; ODS patients underwent radiofrequency ablation of the bilateral foramen oval trigeminal mandibular branch, and B-ODS patients underwent radiofrequency ablation of the bilateral stylomastoid foramen facial nerve and foramen oval trigeminal mandibular branch. The therapeutic effects and complications were observed.

Results: All 10 patients in this series experienced improved Meige's syndrome-related symptoms after extracranial radiofrequency ablation of the cranial and/or mandibular branches of the extracranial trigeminal nerve. Adverse events included class II–III facial paralysis and/or mandibular skin numbness. Two patients had recurrences at the 18th and 22nd months postoperatively, respectively; the other patients were being followed up.

Conclusion: These results shown that CT-guided radiofrequency ablation of bilateral stylomastoid foramen facial nerve and/or oval foramen trigeminal mandibular branch can effectively treat the corresponding types of Meige's syndrome. According to preliminary observations, the therapeutic effect may last more than 18 months.

KEYWORDS

Meige's syndrome, radiofrequency ablation, facial nerve, trigeminal nerve, CT

Introduction

Meige's syndrome, also known as segmental craniometrical dystonia, is a rare form of cranial dystonia characterized by blepharospasm (BDS) and oromandibular dystonia (ODS), as well as complex movement of the lower facial muscles, jaw, mouth, tongue, pharyngeal, and cervical muscles (Pandey and Sharma, 2017). BDS is the most common and incapacitating manifestation in a patient with Meige's syndrome, which begins unilaterally in nearly 25% of patients and quickly progresses to bilateral (Tolosa and Klawans, 1979), with progressive worsening of BDS and spreading of symptoms involving the oromandibular, cervical, and limb muscles (Weiss et al., 2006; Abbruzzese et al., 2008). Meige's syndrome is classified into three subtypes based on the distinct craniometrical muscles involved: BDS, ODS, and blepharospasm combined with oromandibular dystonia (B-ODS) (Marsden, 1976).

Oral medications (LeDoux, 2009) and botulinum toxin injections (Bhidayasiri et al., 2006; Czyz et al., 2013), are currently used as therapeutic options but have not yet achieved the required level of clinical resolution. Although deep brain stimulation has emerged as an alternative treatment option for intractable patients (Markaki et al., 2010; Reese et al., 2011), the treatment necessitates excessive technical requirements and the cost is high.

Our previous studies established that CT-guided percutaneous stylomastoid foramen puncture and radiofrequency ablation are effective for treating hemifacial spasm (Huang et al., 2021), and that CT-guided percutaneous foramen oval puncture and radiofrequency ablation are effective for treating mandibular branch of trigeminal neuralgia and refractory V3 trigeminal neuralgia (Huang et al., 2019a; Lin et al., 2021). Based on these prior studies, here we report our experience with 10 patients who underwent CT-guided extracranial radiofrequency ablation of the cranial nerve for the treatment of Meige's syndrome.

Materials and methods

This study was approved by the Ethics Committee of the Affiliated Hospital of Jiaying University, Jiaying, China (LS2019-013) on 20 May 2019. A total of 10 patients diagnosed with Meige's syndrome were enrolled from April 2019. All study subjects volunteered to participate in this prospective, observational study and provided consent to use their health data and portraits for future publications.

Abbreviations: BDS, blepharospasm dystonia syndrome; ODS, oromandibular dystonia syndrome; B-ODS, blepharospasm combined with oromandibular dystonia syndrome.

Inclusion and exclusion criteria

This study enrolled patients with Meige's syndrome. Before surgery, all individuals consented to a cranial CT examination to rule out cerebral space-occupying lesions. All patients underwent a three-dimensional time of flight magnetic resonance angiography (3D-TOF MRA) and there was no concomitant vascular compression of bilateral facial nerves. Synchronous contraction of the bilateral orbicularis oculi muscle and explosive discharge of the bilateral orbicularis oris muscle were observed on facial electromyography before the operation, and no abnormal muscle response was noted. None of the subjects had a history of Parkinson's disease or tremor, long-term history of taking psychosedative drugs, craniocerebral trauma, cerebrovascular accident, or encephalitis. None of the patients had any history of deep brain stimulation. Contraindications to radiofrequency ablation treatment such as coagulation dysfunction, infection of the puncture site, and cardiac pacemaker were also excluded.

Treatment options

Patients with BDS were treated with radiofrequency ablation of bilateral stylomastoid foramen facial nerve under CT guidance; patients with ODS were treated with radiofrequency ablation of bilateral foramen oval trigeminal mandibular branch under CT guidance, and patients with B-ODS were treated with radiofrequency ablation of bilateral stylomastoid foramen facial nerve and foramen oval trigeminal mandibular branch under CT guidance.

Treatment of blepharospasm dystonia syndrome

Before the procedure, study participants fasted for 4–6 h. After entering the CT examination room, the subject was placed in the lateral decubitus position with the head supported on a pillow. Upper limb venous access was established, and standard ASA monitors were implemented. Following confirmation of the puncture site, CT positioning grids were placed anterior and posterior to the patient's ear (Figure 1). The mastoid region was scanned in 3-mm layers using a paranasal sinus CT scanning protocol. The stylomastoid foramen was identified on an image sequence [Syngo Multimodality Workplace (MMWP); Siemens] and set as the puncture target.

The CT layer with the stylomastoid foramen and without the bone barrier of the tympanic part of the temporal bone was selected as the puncture layer, and the CT measurement tool software was used to pull a straight line forward from the stylomastoid foramen. The intersection of the line and the skin is the puncture point (Figure 2). We determined

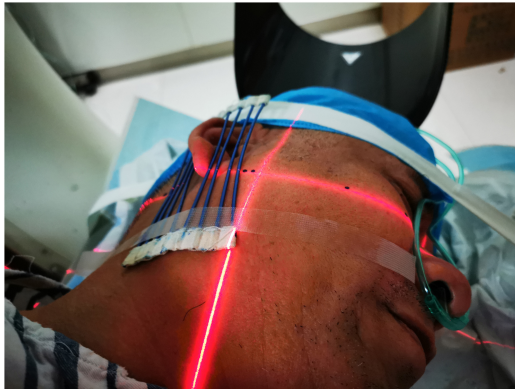


FIGURE 1
Placement of the CT positioning grids. CT positioning grids were placed anterior and posterior to the patient's ear.

the puncture depth (the distance from the puncture point to the target) and puncture angle (the angle between the puncture route and sagittal plane). After administering local anesthesia to the puncture site, a stylet 7-gauge radiofrequency needle with a length of 10 cm and an exposed end of 5 mm (Model 240100; Innomed Medical Technology Co., Ltd.) was gradually advanced toward the target under the guidance of intermittent CT inspection (**Figure 3**) and confirmed by three-dimensional reconstruction of CT scanning (**Figure 4**). The facial nerve was then stimulated with a radiofrequency probe

at a frequency of 2 Hz and a current capacity of 0.5 mA (RF instrument model PMG230; Baylis Medical Co., Inc.). The positive facial muscle twitches from the stimulation indicated that the facial nerve was in close proximity (**Supplementary Video 1**).

Patients were required to puff their cheeks and close their eyes while receiving continuous radiofrequency ablation at a preset temperature of 65°C for 30 s. Whether air leakage occurred when the patient's cheeks were bulging and the treatment side eye could be tightly closed during the treatment was closely observed. When the individual struggled to keep their eyes closed or their cheeks bulged, the ablation protocol was stopped, and the procedure was completed. After 30 s of radiofrequency ablation, if no air leakage occurred when puffing the cheeks and the eyes were tightly closed, there was an increase in the radiofrequency temperature by 5°C before the next cycle. Thus, a 5°C step heating radiofrequency was implemented until air leakage occurred on the treatment side during puffy cheeks and the eyes could not be tightly closed. Sedation was performed during the needle insertion process. The same method was used for contralateral treatment.

Treatment of oromandibular dystonia syndrome

The patient was positioned supine on the CT scaffold, with thin pillows beneath the shoulders to keep the head backward

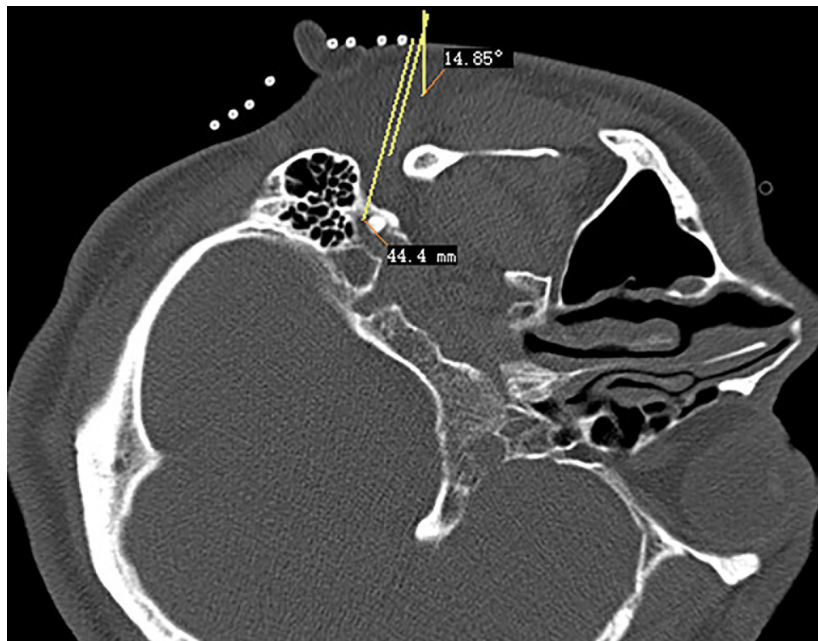


FIGURE 2
Puncture path design of stylomastoid foramen.

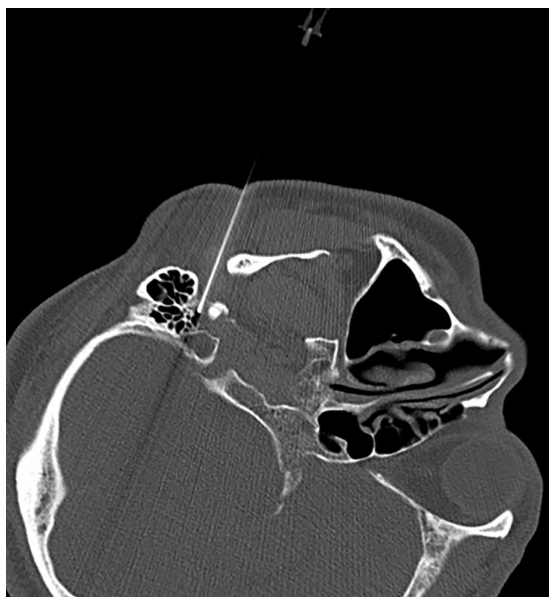


FIGURE 3
Puncturing of the stylomastoid foramen under intermittent CT guidance.

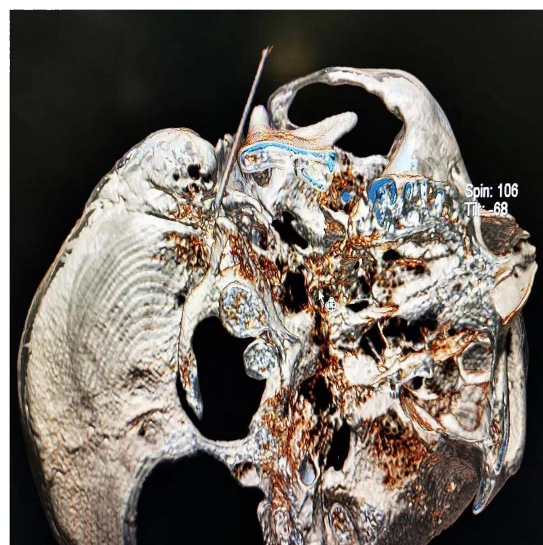


FIGURE 4
Three-dimensional reconstruction of the CT scans confirmed successful puncture of the stylomastoid foramen.

by 15–25°. The patient's head was fixed on the head frame of the CT table using a wide tape, and a CT positioning grid was placed on the lateral corner of the mouth of the affected side. The head positioning image was taken in the paranasal sinus mode, and the zygomatic face was scanned in the semi-coronal position with a 3 mm layer thickness. The scanning baseline was parallel to the line from the external earhole to the item point of the second molar, and the upper edge of the scanning frame reached the upper edge of the zygomatic arch. The scanned CT image was replayed, the layer containing foramen oval (puncture targets) on both sides selected as the puncture layer, the puncture path on this layer was designed by pulling a straight line from the target close to the inner edge of the coronal process to the facial soft tissue. The intersection of the straight line and skin was the puncture point. The distance from the target point to the puncture point (puncture depth) was measured, and the angle between the puncture direction and the sagittal plane (puncture angle) was determined using CT software.

Following routine disinfection and towel laying, local anesthesia at the puncture point was performed. A stylet 7-gauge radiofrequency needle with a length of 10 cm and an exposed end 5 mm close to the inner edge of the coronal process was inserted into the foramen oval along the designed puncture path, and the needle feeding was stopped when the needle tip was flat at the inner opening of the foramen oval to avoid the needle tip entering the brain.



FIGURE 5
Two puncture needles are inserted into the foramen ovale.

If stimulation with high frequency (50 Hz) current (0.5 mA) or voltage (0.3 V) could induce alloesthesia in the innervation area of the trigeminal mandibular branch (lower lip, mandible, ototemporal area), and stimulation with low a frequency (2 Hz) current (0.5–1 MA) or voltage (0.3–0.5 V) could induce

rhythmic jitter of the mandible (**Supplementary Video 2**), then standard radiofrequency thermocoagulation at 95°C was administered for 180 s (Lin et al., 2021).

The assumption was that CT scanning revealed the horizontal transverse diameter of the foramen oval on the affected side to be greater than 6 mm. In that case, double-needle bipolar RF ablation technology was used (Huang et al., 2019a): Two parallel puncture paths were designed with the inner and outer sides of the foramen oval as targets, respectively, and an RF needle was punctured into the inner and outer sides of the oval foramen along the designed path to the internal opening of the oval foramen. Double-needle bipolar radiofrequency ablation was performed after satisfactory electrophysiological testing (**Figure 5**).

Treatment of blepharospasm combined with oromandibular dystonia syndrome

After the radiofrequency ablation treatment of the facial nerve *via* the stylomastoid foramen was conducted under CT guidance, radiofrequency ablation of the left and right mandibular branches of the extracranial trigeminal nerve *via* the oval foramen was performed using the methods described above, respectively.

Following up and adverse events

All patients were followed up postoperatively to observe the therapeutic effects, and complications such as facial paralysis and skin numbness of the mandible were also observed. The definition facial paralysis was based on the report of House and Brackmann (1985).

Results

General characteristics

Ten patients (two men and eight women) were enrolled in this study. The average age was 57.6 ± 6.6 years, the average course of the disease was 3.1 ± 1.1 years, and the average follow-up time was 8.3 ± 10.5 months. The BDS, ODS, and B-ODS numbers were seven, one, and two, respectively.

Effects and complications

All 10 patients in this series experienced improved Meige's syndrome -related symptoms after extracranial radiofrequency ablation of a cranial nerve or/and mandibular branches of the

extracranial trigeminal nerve. Two patients had recurrences at the 18th and 22nd months, respectively; the remaining eight patients were followed up for 1–9 months, respectively, and no recurrence was found. The adverse events included facial paralysis class II-III and/or mandibular skin numbness, and these complications improved over time (see **Tables 1, 2**).

Discussion

Meige's syndrome is characterized by autonomic motor control dysfunction, basal ganglia thalamus cortical circuit interaction disorder, basal ganglia, and thalamus neurotransmitter imbalance, resulting in excitatory and inhibitory imbalance (LeDoux, 2009; Ribot et al., 2019; Ma et al., 2021). Jochim et al. (2020) reported that treating Meige's syndrome with botulinum toxin A is safe and effective, lasting for only 2–4 months, and only a few patients experience toxic reactions (Hassell and Charles, 2020). Deep brain stimulation can be used to treat Meige's syndrome by placing stimulation electrodes into the bilateral medial globus pallidus or the subthalamic nucleus. Nonetheless, only 50–70% of patients receive effective treatment. This technology requires stereotactic neuronavigation, which has stringent technical requirements and is too expensive for the majority of patients (Horisawa et al., 2018; Liu et al., 2021).

Dystonia is treated by blocking the generation and transmission of abnormal motor signals. Deep electrical stimulation is used to treat Meige's syndrome because it blocks or interferes with the generation of abnormal movement signals of the hypothalamic nuclei, which is equivalent to treating the pacing system (signal source). Local injection of botulinum toxin blocks the transmission of abnormal motor signals at the neuromuscular junction, which is equivalent to the treatment of effectors. Radiofrequency ablation of the cranial nerve blocks the transmission of abnormal motor signals in the cranial nerve, which is equivalent to the treatment of the intermediate links of the conduction system. Different types of Meige's syndrome affect different cranial nerves.

The facial nerve serves as the conduction system for BDS, whereas the mandibular branch of the trigeminal nerve serves as the main conduction system for ODS. The conduction system of BDS combined with ODS type involves the mandibular branch of the facial nerve and trigeminal nerve, involving pharyngeal muscle, lingual muscle, and neck muscle. The conduction system comprises glossopharyngeal, hypoglossal, and accessory nerves. Therefore, partial radiofrequency ablation of the above cranial nerves can theoretically block the transmission of abnormal motion signals to effectors (orbicularis oculi muscle, orbicularis oris muscle, and/or masticatory muscle, pharyngeal muscle, tongue muscle, sternocleidomastoid muscle, etc.), and thus alleviate Meige's symptoms.

TABLE 1 Characteristics and treatments of study patients.

Pt.	Diagnosis and relevant abnormal symptoms	Sex/age (years)	Duration of disease (years)	Previous treatment	Present treatment
1	BDS (blepharospasm)	Female/62	5	Botulinum toxin injection	Bilateral nerve radiofrequency ablation with 85°C for 30 s
2	BDS (blepharospasm)	Female/66	2	Botulinum toxin injection	Bilateral nerve radiofrequency ablation with 70°C for 23s
3	B-ODS (blepharospasm combined with oromandibular dystonia)	Female/60	3	Botulinum toxin injection	Bilateral nerve radiofrequency ablation with 65°C for 27 s combined with mandibular branch of bilateral trigeminal nerve radiofrequency ablation with 95°C for 180 s
4	BDS (blepharospasm)	Female/57	2	None	Bilateral nerve radiofrequency ablation with 65°C for 30 s
5	B-ODS (blepharospasm combined with oromandibular dystonia)	Male/54	4	Botulinum toxin injection	Bilateral nerve radiofrequency ablation with 90°C for 25 s combined with mandibular branch of bilateral trigeminal nerve radiofrequency ablation with 95°C for 180 s
6	BDS (blepharospasm)	Female/64	2	Botulinum toxin injection	Bilateral nerve radiofrequency ablation with 85°C for 20 s
7	ODS (oromandibular dystonia)	Male/43	3	None	Mandibular branch of bilateral trigeminal nerve radiofrequency ablation with 95°C for 180 s
8	BDS (blepharospasm)	Female/58	4	None	Bilateral nerve radiofrequency ablation with 70°C for 30 s
9	BDS (blepharospasm)	Female/53	4	Botulinum toxin injection	Bilateral nerve radiofrequency ablation with 95°C for 30 s
10	BDS (blepharospasm)	Female/59	2	None	Bilateral nerve radiofrequency ablation with 80°C for 23 s

BDS, blepharospasm dystonia syndrome; ODS, oromandibular dystonia syndrome; B-ODS, blepharospasm combined with oromandibular dystonia syndrome.

TABLE 2 The outcomes and adverse events of radiofrequency ablation for Meige's syndrome.

Pt.	Diagnosis and relevant abnormal symptoms	Follow up time	Treatment effect and recurrence	Adverse events	Adverse events lasted
1	BDS (blepharospasm)	31 months	Recurrence at the 18th month	Facial paralysis class II	Disappeared 2 months later
2	BDS (blepharospasm)	24 months	Recurrence at the 22th month	Facial paralysis class III	Disappeared 3 months later
3	B-ODS (blepharospasm combined with oromandibular dystonia)	9 months	No recurrence	Facial paralysis class III	Disappeared 3 months later; skin numbness of mandibular, lasted for 9 months
4	BDS (blepharospasm)	4 months	No recurrence	Facial paralysis class II	Disappeared 2 months later
5	B-ODS (blepharospasm combined with oromandibular dystonia)	4 months	No recurrence	Facial paralysis class II	Disappeared 3 months later; skin numbness of mandibular; lasted to now
6	BDS (blepharospasm)	3 months	No recurrence	Facial paralysis class III	Disappeared 2 months later
7	ODS (oromandibular dystonia)	3 months	No recurrence	Skin numbness of mandibular,	Numbness lasted to now
8	BDS (blepharospasm)	2 months	No recurrence	Facial paralysis class III, restored to class II	Lasted to now
9	BDS (blepharospasm)	2 months	No recurrence	Facial paralysis class II	Lasted to now
10	BDS (blepharospasm)	1 months	No recurrence	Facial paralysis class III	Lasted to now

BDS, blepharospasm dystonia syndrome; ODS, oromandibular dystonia syndrome; B-ODS, blepharospasm combined with oromandibular dystonia syndrome.

Our research group conducted an in-depth study on the treatment of trigeminal neuralgia using extracranial non-Gasser ganglion radiofrequency and discovered that radiofrequency

therapy directed at the extracranial trigeminal nerve trunk can also achieve a satisfactory therapeutic effect (Huang et al., 2014, 2019b; Chen et al., 2019). Additionally, while using extracranial

radio frequency, the puncture needle does not need to penetrate the skull to locate the semilunar ganglion. Nonetheless, the radio frequency for the mandibular branch can be realized at the foramen ovale (Huang et al., 2019a; Lin et al., 2021). Complications such as intracranial infection and intracranial hemorrhage associated with puncturing the semilunar segment of the intracranial trigeminal nerve can be avoided entirely, significantly improving the safety of radiofrequency treatment. Additionally, for the radiofrequency treatment of the facial nerve, we developed extracranial radio frequency technology, “CT-guided percutaneous puncture of the facial nerve in stylomastoid foramen for the treatment of facial spasm,” and successfully applied it in the clinic (Huang et al., 2021).

According to different syndrome types, this group adopted different cranial nerves for extracranial radiofrequency treatment: for BDS, which involves only the orbicularis oculi and orbicularis oris muscles innervated by the facial nerve, but not the masticatory muscle, the symptoms of eyelid spasm and perioral expression muscle twitch completely resolved after radiofrequency treatment of bilateral stylomastoid foramen facial nerve; for ODS, which involves only the masticatory muscle, bilateral foramen oval trigeminal mandibular branch radiofrequency could eliminate masticatory muscle spasm; and for B-ODS, which involves BDS combined with ODS, extracranial radiofrequency therapy of the mandibular branch of the facial nerve and trigeminal nerve was performed successively to eliminate BDS and masticatory muscle spasm, respectively. It is conceivable that if Meige’s syndrome affects more cranial muscles, the cranial nerves that transmit motor signals to the corresponding muscles will need to be treated with radiofrequency.

In contrast to facial spasm which is caused by irregular, involuntary, and painless clonus of unilateral facial muscles due to compression of the root of the facial nerve by accompanying blood vessels (Chaudhry et al., 2015), the cranial dystonia of Meige’s syndrome is often symmetrically distributed on both sides of the central axis of the face, and its pathogenesis is not caused by the accompanying vascular compression of the root of the facial nerve in the anterior pontine cistern. Therefore, Meige’s syndrome cannot be treated by craniotomy microvascular decompression (Pandey and Sharma, 2017).

In the current case series, we observed that after radiofrequency treatment of bilateral nerves, mild facial paralysis occurred simultaneously, there was no quarrel or skew, but the sucking ability significantly decreased, leaving the patient unable to complete the smiling action, and no other complications occurred. After radiofrequency surgery on the bilateral mandibular branches of the trigeminal nerve, there was no difficulty in opening the mouth. Nonetheless, hypoesthesia and numbness persisted in the innervation area of bilateral mandibular branches. However, two patients had recurrences at the 18th and 22nd months after 24 months of follow-up. No recurrence was reported in the other cases, which may be

attributable to the short follow-up time in these cases. However, in our previous experience with extracranial radiofrequency treatment of trigeminal neuralgia, 11–13, 22–24 the effects lasted for 2–5 years.

Conclusion

CT-guided extracranial radiofrequency ablation of the bilateral stylomastoid foramen facial nerve and/or foramen oval trigeminal mandibular branch may be a viable treatment option for Meige’s syndrome. Apart from botulinum toxin injection and deep brain stimulation, neuro-extracranial radio frequency technology may become a new treatment for Meige’s syndrome.

Data availability statement

The original contributions presented in this study are included in the article/**Supplementary material**, further inquiries can be directed to the corresponding author.

Ethics statement

This study was approved by the Ethics Committee of the Affiliated Hospital of Jiaying University, Jiaying, China (LS2019-013) on 20 May 2019. The patients/participants provided their written informed consent to participate in this study. Written informed consent was obtained from the individual(s) for the publication of any potentially identifiable images or data included in this article.

Author contributions

BH was responsible for the project conception and patients’ interviews. X-DD was responsible for the literature search. MY was responsible for the project conception. W-HY was responsible for the video. Q-HZ was responsible for the project conception and manuscript review. All authors contributed to the article and approved the submitted version.

Funding

This work was supported by Zhejiang Social Public Welfare Research and Development Project (LGF20H090021),

the Zhejiang Medical-Health Science and Technology Plan Project (2022ZH012), the Hangzhou Social Development Project (20201203B73), and the Key Discipline Established With Zhejiang Province and Jiaxing City Jointly (2019-ss-ttyx).

Conflict of interest

The authors declare that the research was conducted in the absence of any commercial or financial relationships that could be construed as a potential conflict of interest.

Publisher's note

All claims expressed in this article are solely those of the authors and do not necessarily represent those of their affiliated

organizations, or those of the publisher, the editors and the reviewers. Any product that may be evaluated in this article, or claim that may be made by its manufacturer, is not guaranteed or endorsed by the publisher.

Supplementary material

The Supplementary Material for this article can be found online at: <https://www.frontiersin.org/articles/10.3389/fnins.2022.1013555/full#supplementary-material>

SUPPLEMENTARY VIDEO 1

Facial muscles beat rhythmically with facial nerve stimulation.

SUPPLEMENTARY VIDEO 2

The mandibular joint beats rhythmically when the mandibular branch of the trigeminal nerve is stimulated.

References

- Abbruzzese, G., Berardelli, A., Girlanda, P., Marchese, R., Martino, D., Morgante, F., et al. (2008). Long-term assessment of the risk of spread in primary late-onset focal dystonia. *J. Neurol. Neurosurg. Psychiatry* 79, 392–396. doi: 10.1136/jnnp.2007.124594
- Bhidayasiri, R., Cardoso, F., and Truong, D. D. (2006). Botulinum toxin in blepharospasm and oromandibular dystonia: Comparing different botulinum toxin preparations. *Eur. J. Neurol.* 13, 21–29. doi: 10.1111/j.1468-1331.2006.01441.x
- Chaudhry, N., Srivastava, A., and Joshi, L. (2015). Hemifacial spasm: The past, present and future. *J. Neurol. Sci.* 356, 27–31. doi: 10.1016/j.jns.2015.06.032
- Chen, Y., Zhu, Q., Huang, B., Liu, Q., He, Q., Yao, Y., et al. (2019). The value and application of personalized needle modification in percutaneous infrazygomatic radiofrequency in isolated maxillary nerve pain through the foramen rotundum. *Pain Physician* 22, 377–387. doi: 10.36076/ppj/2019.22.377
- Czyz, C. N., Burns, J. A., Petrie, T. P., Watkins, J. R., Cahill, K. V., and Foster, J. A. (2013). Long-term botulinum toxin treatment of benign essential blepharospasm, hemifacial spasm, and Meige syndrome. *Am. J. Ophthalmol.* 156, 173–177.e2. doi: 10.1016/j.ajo.2013.02.001
- Hassell, T. J. W., and Charles, D. (2020). Treatment of blepharospasm and oromandibular dystonia with botulinum toxins. *Toxins* 12:269. doi: 10.3390/toxins12040269
- Horisawa, S., Ochiai, T., Goto, S., Nakajima, T., Takeda, N., Kawamata, T., et al. (2018). Long-term outcome of pallidal stimulation for Meige syndrome. *J. Neurosurg.* 130, 84–89. doi: 10.3171/2017.7.JNS17323
- House, J. W., and Brackmann, D. E. (1985). Facial nerve grading system. *Otolaryngol. Head Neck Surg.* 93, 146–147. doi: 10.1177/019459988509300202
- Huang, B., Xie, K., Chen, Y., Wu, J., and Yao, M. (2019a). Bipolar radiofrequency ablation of mandibular branch for refractory V3 trigeminal neuralgia. *J. Pain Res.* 12, 1465–1474. doi: 10.2147/JPR.S197967
- Huang, B., Yao, M., Liu, Q., Chen, Y., Ni, H., Li, Z., et al. (2019b). Personalized needle modification for CT-guided percutaneous infrazygomatic radiofrequency ablation of the maxillary nerve through the foramen rotundum in order to treat V2 trigeminal neuralgia. *J. Pain Res.* 12, 2321–2329. doi: 10.2147/JPR.S207297
- Huang, B., Yao, M., Chen, Q., Lin, H., Du, X., Huang, H., et al. (2021). Awake CT-guided percutaneous stylomastoid foramen puncture and radiofrequency ablation of facial nerve for treatment of hemifacial spasm. *J. Neurosurg.* 16, 1–7. doi: 10.3171/2020.10.JNS203209
- Huang, B., Yao, M., Feng, Z., Guo, J., Zereszki, A., Leong, M., et al. (2014). CT-guided percutaneous infrazygomatic radiofrequency neurolysis through foramen rotundum to treat V2 trigeminal neuralgia. *Pain Med.* 15, 1418–1428. doi: 10.1111/pme.12440
- Jochim, A., Meindl, T., Huber, C., Mantel, T., Zwirner, S., Castrop, F., et al. (2020). Treatment of blepharospasm and Meige's syndrome with abo- and onabotulinumtoxin A: Long-term safety and efficacy in daily clinical practice. *J. Neurol.* 267, 267–275. doi: 10.1007/s00415-019-09581-w
- LeDoux, M. S. (2009). Meige syndrome: What's in a name? *Parkinsonism Relat. Disord.* 15, 483–489. doi: 10.1016/j.parkreldis.2009.04.006
- Lin, H., Cao, G., Jin, G., Yang, Z., Huang, C., Shao, J., et al. (2021). Extracranial non-gasserian ganglion application of radiofrequency thermocoagulation on the mandibular branch of the trigeminal through the foramen ovale for trigeminal neuralgia. *Pain Physician* 24:E425–E432.
- Liu, J., Ding, H., Xu, K., Liu, R., Wang, D., Ouyang, J., et al. (2021). Pallidal versus subthalamic deep-brain stimulation for meige syndrome: A retrospective study. *Sci. Rep.* 11:8742. doi: 10.1038/s41598-021-88384-4
- Ma, H., Qu, J., Ye, L., Shu, Y., and Qu, Q. (2021). Blepharospasm, oromandibular dystonia, and Meige Syndrome: Clinical and genetic update. *Front. Neurol.* 12:630221. doi: 10.3389/fneur.2021.630221
- Markaki, E., Kefalopoulou, Z., Georgiopoulos, M., Paschali, A., and Constantoyannis, C. (2010). Meige's syndrome: A cranial dystonia treated with bilateral pallidal deep brain stimulation. *Clin. Neurol. Neurosurg.* 112, 344–346. doi: 10.1016/j.clineuro.2009.12.005
- Marsden, C. D. (1976). Blepharospasm-oromandibular dystonia syndrome (Brueghel's syndrome). A variant of adult-onset torsion dystonia? *J. Neurol. Neurosurg. Psychiatry* 39, 1204–1209. doi: 10.1136/jnnp.39.12.1204
- Pandey, S., and Sharma, S. (2017). Meige's syndrome: History, epidemiology, clinical features, pathogenesis and treatment. *J. Neurol. Sci.* 372, 162–170. doi: 10.1016/j.jns.2016.11.053
- Reese, R., Gruber, D., Schoenecker, T., Bänzner, H., Blahak, C., Capelle, H. H., et al. (2011). Long-term clinical outcome in meige syndrome treated with internal pallidum deep brain stimulation. *Mov. Disord.* 26, 691–698. doi: 10.1002/mds.23549
- Ribot, B., Aupy, J., Vidailhet, M., Mazère, J., Pisani, A., Bezard, E., et al. (2019). Dystonia and dopamine: From phenomenology to pathophysiology. *Prog. Neurobiol.* 182:101678. doi: 10.1016/j.pneurobio.2019.10.1678
- Tolosa, E. S., and Klawans, H. L. (1979). Meiges disease: A clinical form of facial convulsion, bilateral and medial. *Arch. Neurol.* 36, 635–637. doi: 10.1001/archneur.1979.00500460069010
- Weiss, E. M., Hershey, T., Karimi, M., Racette, B., Tabbal, S. D., Mink, J. W., et al. (2006). Relative risk of spread of symptoms among the focal onset primary dystonias. *Mov. Disord.* 21, 1175–1181. doi: 10.1002/mds.20919



OPEN ACCESS

EDITED BY

Shong Lau,
Salk Institute for Biological Studies,
United States

REVIEWED BY

Artur Llobet,
University of Barcelona, Spain
Joseph Zak,
University of Illinois at Chicago,
United States

*CORRESPONDENCE

Weitian Zhang
drzhangwt@163.com
Hui Wang
wangh2014@163.com
Haibo Shi
haibo99@hotmail.com

†These authors have contributed
equally to this work

SPECIALTY SECTION

This article was submitted to
Cellular Neuropathology,
a section of the journal
Frontiers in Cellular Neuroscience

RECEIVED 25 July 2022

ACCEPTED 05 October 2022

PUBLISHED 28 October 2022

CITATION

Li M, Liu Z, Lai K, Liu H, Gong L, Shi H,
Zhang W, Wang H and Shi H (2022)
Enhanced recruitment of glutamate
receptors underlies excitotoxicity
of mitral cells in acute
hyperammonemia.
Front. Cell. Neurosci. 16:1002671.
doi: 10.3389/fncel.2022.1002671

COPYRIGHT

© 2022 Li, Liu, Lai, Liu, Gong, Shi,
Zhang, Wang and Shi. This is an
open-access article distributed under
the terms of the [Creative Commons
Attribution License \(CC BY\)](#). The use,
distribution or reproduction in other
forums is permitted, provided the
original author(s) and the copyright
owner(s) are credited and that the
original publication in this journal is
cited, in accordance with accepted
academic practice. No use, distribution
or reproduction is permitted which
does not comply with these terms.

Enhanced recruitment of glutamate receptors underlies excitotoxicity of mitral cells in acute hyperammonemia

Mingxian Li[†], Zhenqi Liu[†], Ke Lai[†], Hanwei Liu, Lina Gong,
Haosong Shi, Weitian Zhang*, Hui Wang* and Haibo Shi*

Department of Otorhinolaryngology, Shanghai Sixth People's Hospital Affiliated to Shanghai Jiao Tong University School of Medicine, Shanghai, China

Hepatic encephalopathy (HE)—a major complication of liver disease—has been found to increase the risk of olfactory dysfunction, which may be attributed to elevated levels of ammonia/ammonium in the blood and cerebrospinal fluid. However, the cellular mechanisms underlying hyperammonemia-induced olfactory dysfunction remain unclear. By performing patch-clamp recordings of mitral cells (MCs) in the mouse olfactory bulb (OB), we found that 3 mM ammonium (NH_4^+) increased the spontaneous firing frequency and attenuated the amplitude, but synaptic blockers could prevent the changes, suggesting the important role of glutamate receptors in NH_4^+ -induced hyperexcitability of MCs. We also found NH_4^+ reduced the currents of voltage-gated K^+ channel (K_v), which may lead to the attenuation of spontaneous firing amplitude by NH_4^+ . Further studies demonstrated NH_4^+ enhanced the amplitude and integral area of long-lasting spontaneous excitatory post-synaptic currents (sEPSCs) in acute OB slices. This enhancement of excitatory neurotransmission in MCs occurred independently of pre-synaptic glutamate release and re-uptake, and was prevented by the exocytosis inhibitor TAT-NSF700. In addition, an NH_4^+ -induced increase in expression of NR1 and GluR1 was detected on cytoplasmic membrane, indicating that increased trafficking of glutamate receptors on membrane surface in MCs is the core mechanism. Moreover, NH_4^+ -induced enhanced activity of glutamate receptors in acute OB slices caused cell death, which was prevented by antagonizing glutamate receptors or chelating intracellular calcium levels. Our study demonstrates that the enhancement of the activity and recruitment of glutamate receptor directly induces neuronal excitotoxicity, and contributes to the vulnerability of OB to acute hyperammonemia, thus providing a potential pathological mechanism of olfactory defects in patients with hyperammonemia and HE.

KEYWORDS

olfactory dysfunction, ammonium, mitral cell, glutamate receptor, excitotoxicity

Introduction

Overwhelming evidence indicates that olfactory dysfunction is associated with liver disease (Burch et al., 1978; Deems et al., 1993; Landis et al., 2004; Temmel et al., 2005; Zucco et al., 2006; Heiser et al., 2018), and 27–76% of patients with liver diseases experience olfactory defects, which can severely affect patient food cravings and intake (Deems et al., 1993; Temmel et al., 2005; Heiser et al., 2018). Hepatic encephalopathy (HE) is a major complication of liver dysfunction, and poor olfactory function has been associated with severe cases. Even patients with minimal HE present with compromised thresholds of odor identification (Temmel et al., 2005; Zucco et al., 2006; Heiser et al., 2018). Ammonium (NH_4^+)—a proposed major determinants of HE—is toxic and can lead to functional disturbances in the central nervous system by altering neuronal excitability and synaptic transmission (Back et al., 2011; Oja et al., 2017; Jayakumar and Norenberg, 2018).

Ammonium exerts different neuronal effects in different brain regions. It influences the neuronal physiological properties through increasing intracellular calcium levels and altering cytoplasmic pH (Lazarenko et al., 2017). More importantly, NH_4^+ can affect glutamatergic and gamma-aminobutyric acid (GABA) neurotransmission and disturb intracellular signal transduction pathways (i.e., the glutamate-NO-cGMP pathway), resulting in impairment of neuronal plasticity, learning ability, memory, or even death in acute and chronic hyperammonemia (Sanchez-Perez and Felipo, 2006; Cabrera-Pastor et al., 2016; Lazarenko et al., 2017; Sancho-Alonso et al., 2022). In the CA1 region of rat hippocampus, acute NH_4^+ administration inhibits neuronal long-term potentiation through GABA-enhancing neurosteroids (Izumi et al., 2013). In the chronic hyperammonemia rat, decreased NR2A and NR2B subunit expressions in the hippocampus lead to impaired learning and memory (Yonden et al., 2010). Acute hyperammonemia in mice can impair cortical inhibitory network and trigger seizures by depolarizing neuronal GABA reversal potential (Rangroo Thrane et al., 2013). In rats with chronic hyperammonemia, the amount of GABA transporter GAT-3 is elevated, resulting in the increased extracellular accumulation of GABA leading to motor in-coordination (Cabrera-Pastor et al., 2018). Mitral cells (MCs), are the projecting neurons in the OB and responsible for olfactory encoding and transmission (Wang et al., 2003; Padmanabhan and Urban, 2010; Boyd et al., 2012; Nagayama et al., 2014). Its apical dendrites ramify in the glomerulus, where they receive glutamatergic inputs from the nerves of olfactory sensory neurons (OSNs) and external tufted cells (ETCs). And MCs also receive inhibitory inputs from the interneurons including periglomerular cells (PG) and granule cells (GCs) through dendrodendritic synapses. Despite compelling evidence of the effects of NH_4^+ on neurotransmission and neuronal excitability, its pathological mechanism in the olfactory system has never been explored.

In this study, we investigated whether NH_4^+ alters the excitability of MCs and explored the potential cellular mechanism of MC excitotoxicity by NH_4^+ . Our results demonstrated that 3 mM NH_4^+ increases the spontaneous firing rates and attenuates the amplitude by potentiating glutamate receptor activity and suppressing Kv currents, leading to MC hyperexcitability. Furthermore, not only have we found that NH_4^+ elevates the amplitude and integral area of spontaneous excitatory post-synaptic currents (sEPSCs), but also NH_4^+ administration leads to excitotoxicity and cell death through enhancing the activity and membrane trafficking of glutamate receptors, independently of the alteration in glutamate re-uptake and pre-synaptic glutamate release, suggesting elevated activity and expression of glutamate receptors by NH_4^+ underlie increased MC excitability and excitotoxicity in the OB.

Materials and methods

Ethical approval

All animal procedures were performed in accordance with the guiding principles of the National Institutes of Health Guide for the Care and Use of Laboratory Animals and were approved by the Ethics Committee of the Shanghai Sixth People's Hospital affiliated to Shanghai Jiao Tong University School of Medicine. All efforts were made to avoid causing unnecessary pain and suffering as possible.

Slice preparation and solutions

C57BL/6J mice (aged 15–20 days) were anesthetized with isoflurane before decapitation, as previously described (Chen et al., 2016). The brain was excised and immersed in ice-cold oxygenated artificial cerebrospinal fluid (aCSF) containing (in mM): 124 NaCl, 5 KCl, 1.2 KH_2PO_4 , 2.4 CaCl_2 , 1 MgCl_2 , 24 NaHCO_3 , and 10 glucose, saturated with 95% O_2 and 5% CO_2 . The forebrain containing the OB was dissected and sectioned into transverse 300 μm -thick slices using a vibratome (VT-1200s, Leica, Nussloch, Germany). The slices were incubated in aCSF with 95% O_2 and 5% CO_2 at 37°C for 40 min to recover cell viability and then maintained at room temperature (23–25°C) before patch-clamp recordings.

Reagents

All chemicals and drugs were purchased from Sigma-Aldrich (St. Louis, MO, USA), unless otherwise indicated. The common reagents used in the experiment were NH_4Cl , bicuculline (Bic), strychnine (Stry), DL-2-amino-5-phosphonopentanoic acid (APV) and 1,2,3,4-tetrahydro-6-nitro-2,3-dioxo-benzo[f]quinoxaline-7-sulfonamide disodium

salt hydrate (NBQX). We prepared different concentrations (1, 3, 5 and 10 mM) of NH_4Cl solution with an equimolar mass substitute of NaCl. The pH of NH_4Cl solution in aCSF saturated with 95% O_2 and 5% CO_2 was consistent with that of pure aCSF. DL-*threo*- β -benzyloxyaspartic acid (TBOA) and dynasore were purchased from Tocris (Bristol, United Kingdom). TAT-NSF700 was obtained from Anaspec (Fremont, CA, USA). Bic, Stry, APV, NBQX, TBOA, BAPTA-AM, TAT-NSF700, and dynasore were prepared in stock solution at -20°C and later diluted to a final concentration in aCSF before use. The final concentrations of Bic, Stry, APV, NBQX, TBOA, dynasore, TAT-NSF700, and BAPTA-AM were 10, 3, 50, 20, 30, 40, 5, and 40 μM , respectively. During physiological recordings, MCs were exposed to different reagents through a square-tube gravity perfusion system at a speed of 1 mL/min, continuously gassed with 95% O_2 and 5% CO_2 . All experiments were performed at room temperature.

Mitral cell identification

The MCs in the OB slices were identified by their location, size, shape, and primary dendrites of their cell bodies. MC cell bodies were located in the MC layer, had a diameter of $>20\text{ }\mu\text{m}$, and their soma structures were characterized by different shapes (triangles, polygons, or ovoids). The soma was readily identified using a CCD camera with a $60\times$ water immersion objective attached to an upright microscope (Examiner.A1, ZEISS, Gottingen, Germany).

Cell-attached recordings

Patch pipettes (resistance of 3–5 $\text{M}\Omega$) for the soma recordings were fabricated from borosilicate capillary glass (World Precision Instruments, Sarasota, FL, USA) using a vertical pipette puller (PC-10; Narishige, Tokyo, Japan). To record the physiological activity of MCs without causing perturbation of the intracellular homeostasis, spontaneous action potentials were recorded using a loose-patch cell-attached configuration in the current-clamp mode without any current injection. The pipette was only then filled with aCSF. Data were acquired using a MultiClamp 700B (Axon, 5 kHz low-pass-filtered; 1550, sampled at 50 kHz) and pClamp6 software. The gain of the amplifier was set to the highest possible range below saturation to increase the signal to noise ratio and improve data quality.

Whole-cell voltage-clamp recordings

To investigate the effects of NH_4^+ on the excitatory synaptic receptors of MC, we performed voltage-clamp recordings in a whole-cell configuration. The pipette solution used in all whole-cell recordings contained (in mM): 130 K-gluconate, 5 KCl, 0.6

ethylene glycol-bis(β -aminoethyl)-N,N,N',N'-tetraacetic acid (EGTA), 10 4-(2-hydroxyethyl)-1-piperazineethane sulfonic acid (HEPES), 4 MgCl_2 , 3 Na_2ATP and 0.3 Na_3GTP and 10 sodium creatine phosphate dibasic tetrahydrate (adjusted to pH 7.3 with KOH). The bath offset potential and electrode capacitance were compensated for before sealing the cell membrane. The series resistance varied from 5 to 15 $\text{M}\Omega$ among cells and was adjusted by 75–90% to maintain $<15\text{ }\text{M}\Omega$ throughout the recordings. Cells showing changes in series resistance of $>15\%$ during recording were omitted from the analysis. We recorded the spontaneous post-synaptic currents (sPSCs) that displayed long-lasting depolarization and continued to record spontaneous excitatory PSCs (sEPSCs) in the presence of Bic and Stry at a holding potential of -60 mV . Bic and Stry were used to suppress inhibitory currents mediated by GABA and glycine. sEPSCs were recorded in the control (Bic + Stry), drug solutions, and wash solution.

To examine the effect of NH_4^+ on excitatory inputs from OSNs to MCs, we placed a bipolar stimulation electrode at the OSN nerve stubs in a subset of experiments to stimulate afferent inputs to the recorded cell. Recordings were made 200–400 μm from the stimulation electrode. The threshold for evoked responses, defined as the stimulation threshold, was measured by gradually increasing the intensity until evoked EPSCs (eEPSCs) or burst firings were triggered. The average stimulation threshold was $2.55 \pm 0.23\text{ V}$. The eEPSC represents as “all or none” response (Gire and Schoppa, 2009). To evoke a stable eEPSC, we used a high intensity of stimulation. Single-pulse stimulations were performed with an interval of 20 s over a recording period of 100 s. Paired-pulse stimulation was conducted with an inter-pulse time interval of 2,000 ms, since evoked EPSCs (eEPSCs) displayed a long refractory period and needed more time to recover to baseline. The stimulations were repeated 10 times with an inter-trial interval of 15 s in the control, drug solutions, and wash solution. We further analyzed the paired-pulse ratio (PPR: P_2/P_1) to represent changes in pre-synaptic release probability.

Furthermore, raw voltage-gated sodium (Nav) and Kv currents were recorded in voltage-clamp mode at a holding potential of -70 mV and were activated by step depolarization from -70 to 40 mV in 10 mV increments, by using test pulses 500 ms in duration.

Whole-cell current-clamp recordings

We also recorded the spontaneous action potentials at I_0 in whole-cell current-clamp mode in the aCSF, and drug solutions. Resting membrane potential (RMP) was measured as well. To measure the membrane resistance (R_m), the evoked depolarized membrane potential was recorded through injecting a current of 10 pA at the holding potential of -60 mV . The rise time constant (τ) was measured by Clampfit 10.6 software. R_m

was calculated using the equation: $\tau = R_m C_m$, where C_m is membrane capacitance.

Membrane surface protein immunoblotting

The fresh mouse OB tissues were incubated in aCSF and 3 mM NH_4Cl respectively for 1 h and then washed with cold PBS (1×) and lysed in mild protein lysis buffer (Regent A in cell membrane protein extraction kit, Beyotime, Biotechnology, Shanghai, China) and supplemented with protease inhibitor (1×) (phenylmethanesulfonyl fluoride, Beyotime). This was followed by grinding using a glass homogenizer for 80 times, and subsequent centrifugation at $700 \times g$ for 10 min. The suspension was collected and centrifuged at $14,000 \times g$ for 30 min. As a result, the membrane proteins were pelleted at the bottom of the centrifuge tube. After discarding the supernatant, we added 200 μl Regent B and centrifuged the solution at $14,000 \times g$ for 5 min, and collected the membrane protein solution. The solution was boiled in 1× SDS sample buffer for 5 min and used for western blot. The samples were centrifuged and supernatant protein was separated on 7.5% sodium dodecyl sulfate-polyacrylamide gel electrophoresis (SDS-PAGE) Gel (Invitrogen, Carlsbad, CA, USA). Separated proteins were transferred onto a NC membrane, blocked in 5% non-fat dry milk for at least 1 h at room temperature and subsequently incubated overnight at 4°C on a shaker with primary antibody against rabbit anti-NR1, rabbit anti-GluR1 (purchased from abclonal, Wuhan, China, 1:1000 dilution) and rabbit anti-Na/K-ATPase (Servicebio, Wuhan, China, 1:1000 dilution). After incubation with primary antibodies, the membranes were incubated with goat anti-rabbit horseradish peroxidase conjugated secondary antibodies (abclonal, 1:5000 dilution) for 1 h at room temperature. Na/K-ATPase was chosen as the loading control. Western blots were performed for at least three times and the densitometry analysis was conducted using Image-J Software.

Assessment of cell vitality with calcein-AM/PI co-staining

To assess the levels of NH_4^+ -induced neurotoxicity in MCs, we sectioned OB slices to a thickness of 220 μm with a vibratome (Leica) and pre-treated the slices with control, NH_4Cl , APV + NBQX, APV + NBQX + NH_4Cl , TAT-NSF700, TAT-NSF700 + NH_4Cl , BAPTA-AM, or BAPTA-AM + NH_4Cl solution for 1 h before incubation with 1 μM calcein-AM and 2 μM propidium iodide (PI) (Solarbio, Beijing, China) for 15 min at 37°C. Following three washes with aCSF, the slices were fixed with 4% paraformaldehyde for 1 h and mounted, with a coverslip. Slices were observed by confocal microscopy

(LSM-710, ZEISS, Thornwood, NY, USA), and live cells and apoptotic nuclei were counted at $40 \times$ magnification. To evaluate the vitality of projecting neurons, we acquired the regions of interest, including the external plexiform and MC layers. The number of stained cells was measured using Image-J software (National Institutes of Health, Bethesda, MD, USA).

Statistical analysis

The amplitude, integral area, and frequency of sEPSCs were used to quantify synaptic events. All electrophysiological data were analyzed by Clampfit 10.2 software (Molecular Devices, San Jose, CA, USA). The parameter of minimum allowed duration in the threshold search was 0.001 or 300 ms to detect the peaks of spontaneous firing or EPSCs, respectively. Peaks were detected automatically, but each event was visually inspected to prevent the inclusion of stochastic artifacts. To quantify the features of spontaneous firing, we fitted the inter-event interval of each recording using a Gaussian function. The 3-min duration of the control period was used for quantitative evaluation after the electrophysiological activity of the cells reached stability. All drug treatments lasted for 10 min, and the time window used for analysis was 5 min, after confirming drug activity. The washout time was 6 min, and the last 3-min recording was used for analysis. The average eEPSC amplitude, integral area, and duration under control conditions were normalized to 1.0 for visual presentation and reported as absolute values in the text. Data were analyzed using SPSS 26.0 software (IBM SPSS, Chicago, IL, USA) and are presented as mean \pm standard error of the mean (SEM). GraphPad Prism 9 (GraphPad Software, San Diego, CA, USA) and Adobe Illustrator CC (Adobe Systems, San Jose, CA, USA) were used to generate graphics. Three-group comparisons were evaluated using one-way analysis of variance (ANOVA) with a *post hoc* least significant difference (LSD) test to determine intergroup differences. A paired or unpaired Student's *t*-test was used for two-group comparisons. Statistical significance was set at $p < 0.05$.

Results

Mitral cells exhibited typical spontaneous burst firings and long-lasting excitatory depolarized currents

Mitral cells, as one of the major neurons projecting to the piriform cortex, receive excitatory inputs from OSNs and ETCs, and inhibitory regulation from interneurons, including PG and GCs (Figure 1A). We first explored the

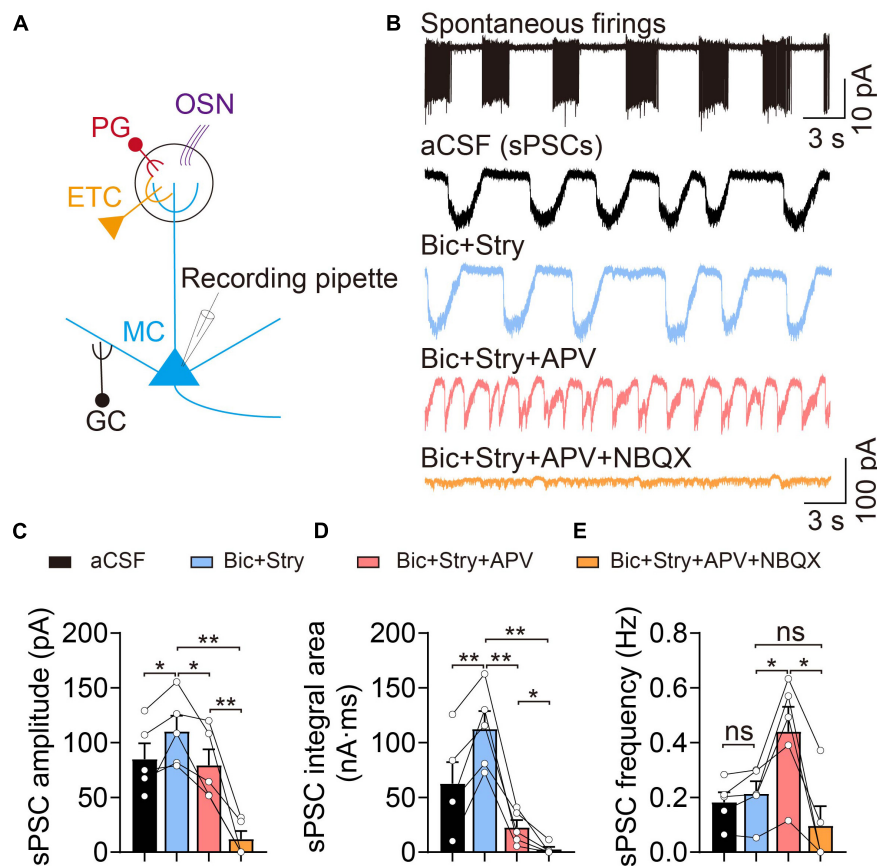


FIGURE 1

Electrophysiological properties of mitral cells (MCs). (A) Basic representation of MC morphology and electrophysiological recording using the patch-clamp technique; olfactory sensory neuron (OSN, purple), external tufted cell (ETC, yellow), periglomerular cell (PG, red), and granule cell (GC, black). (B) Cell-attached recording of spontaneous burst firings (upper) and corresponding whole-cell recordings of spontaneous post-synaptic currents (sPSCs) in aCSF, Bic + Stry, Bic + Stry + APV, and Bic + Stry + APV + NBQX in the same MC. (C–E) sPSC amplitude, integral area, and frequency in aCSF, Bic + Stry, Bic + Stry + APV, and Bic + Stry + APV + NBQX. Elevated sPSC amplitude and integral area in the presence of Bic + Stry and inhibition of sPSC by APV and NBQX revealed that the excitatory inputs in MC are regulated by glutamate receptors involving NMDA and AMPA receptors. Error bars represent standard error; * $p < 0.05$, ** $p < 0.01$; ns, not significant; one-way ANOVA with LSD *post-hoc* test.

electrophysiological properties of MCs in cell-attached voltage-clamp configurations. Previous studies have shown that MCs exert spontaneously active and heterogeneous firing patterns that encode olfactory cues. In our study, most MCs displayed spontaneous and rhythmic burst firing patterns, however other firing characteristics were also present, such as regular and irregular firing (Figure 1B). Interestingly, when the cell membrane was broken through in the voltage-clamp mode at a holding potential of -60 mV, they always appeared waved and long-lasting depolarized currents, defined as sPSCs (also LLD) (Figure 1B). Previous studies have shown the sPSCs consist of both *N*-methyl-D-aspartate (NMDA) and non-NMDA receptor components, and the non-NMDA receptor regulates the initiation of sPSCs (Carlson et al., 2000). The sPSCs are generated by a multistep, diffuse mechanism in the distal portion of the apical dendrite (Schoppa and Westbrook, 2001; Gire et al., 2012). The sPSC amplitude

(control: 84.97 ± 14.37 pA, Bic + Stry: 110.20 ± 14.32 pA, $n = 5$, $p = 0.042$) and integral area (control: 62.45 ± 19.66 nA·ms, Bic + Stry: 112.40 ± 16.48 nA·ms, $n = 5$, $p = 0.008$) were altered by inhibiting GABA_A and glycine receptors, while the sPSC frequency remained unchanged in this study ($n = 5$, $p = 0.150$, Figures 1C,D). After applying a cocktail of excitatory and inhibitory synaptic blockers, sEPSC amplitude (Bic + Stry + APV: 79.31 ± 14.54 pA, Bic + Stry + APV + NBQX: 11.96 ± 7.35 pA, $n = 5$), integral area (Bic + Stry + APV: 22.42 ± 6.87 nA·ms, Bic + Stry + APV + NBQX: 2.55 ± 2.45 nA·ms, $n = 5$), and frequency (Bic + Stry + APV: 0.44 ± 0.09 Hz, Bic + Stry + APV + NBQX: 0.10 ± 0.07 Hz, $n = 5$) were drastically reduced (all $p < 0.05$, Figures 1B–E). Interestingly, the frequency of sEPSCs was significantly increased before and after antagonizing NMDA receptor (Bic + Stry: 0.21 ± 0.04 Hz, Bic + Stry + APV: 0.44 ± 0.09 Hz, $n = 5$, $p = 0.022$). Consistent

with previous studies, our results demonstrate that MCs are mainly characterized by spontaneous rhythmic burst firing and long-lasting depolarized currents, which are mainly regulated by glutamate receptors involving NMDA and α -amino-3-hydroxy-5-methyl-4-isoxazole propionate (AMPA) receptors.

Ammonium enhanced mitral cell excitatory activity by accelerating spontaneous firing rates

To explore the acute effect of NH_4^+ on MC spontaneous firings, we continuously recorded spontaneous action potentials

for 10 min with a cell-attached configuration. To determine the appropriate concentration of NH_4Cl solution in the study, we perfused 1, 3, 5, and 10 mM NH_4Cl in the OB slices and observed its role in MCs spontaneous firings. We found that 3, 5, and 10 mM NH_4Cl increased the frequency of spontaneous firings by 89.88% ($n = 5$, $p = 0.003$), 66.42% ($n = 7$, $p < 0.001$), and 116.75% ($n = 7$, $p = 0.004$) over the initial 3-min period, which then weakened as the NH_4Cl application continued, and the amplitude of the depolarized and hyperpolarized action potential tended to decrease and even disappear (Figures 2A,B). In addition, application of 1 mM NH_4Cl also increased the spike frequency by 22.39% ($n = 5$, $p = 0.015$) but did not change the amplitude of action potentials.

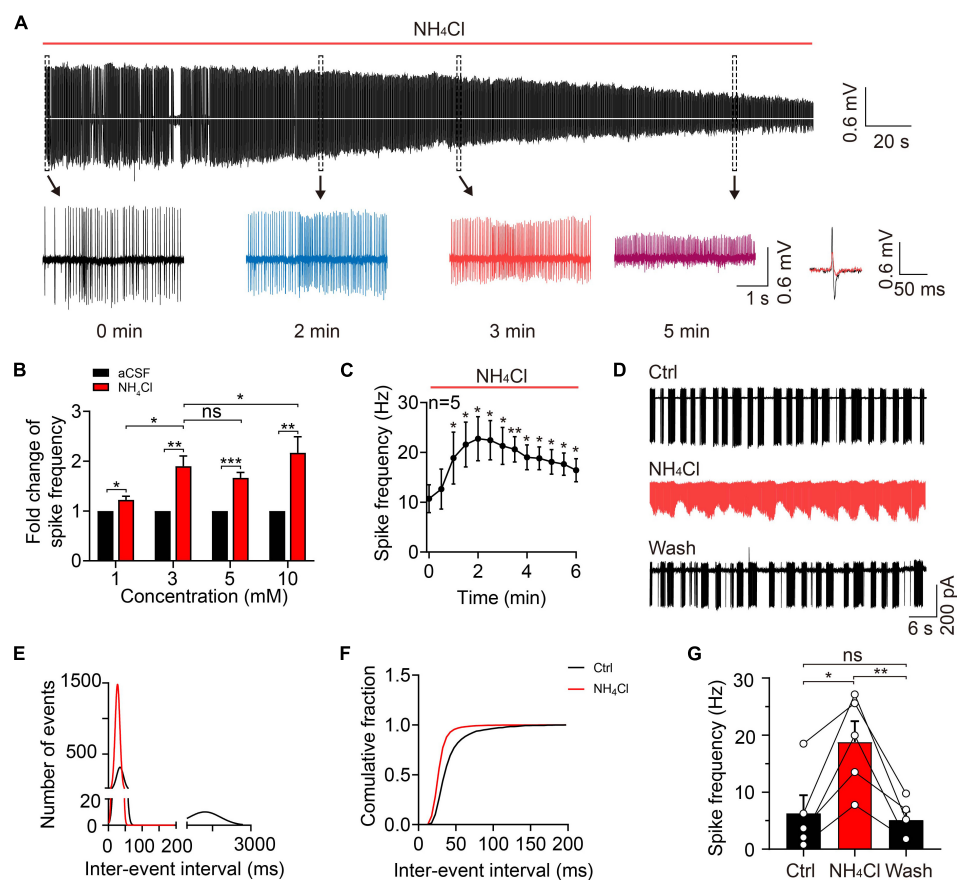


FIGURE 2

Ammonium enhanced MC excitability by increasing spontaneous firing frequency. (A) A typical trace showing spontaneous discharges in a cell-attached recording of a MC in an acute OB slice, showing continuous changes in spike frequency and amplitude with 3 mM NH_4Cl treatment. Insets below show the traces at 0, 2, 3, and 5 min (expanded from the dashed-line black boxes), as well as the superimposed spike waveforms at 0 (black) and 3 (red) min during NH_4Cl treatment. (B) Fold change in spike frequency in MCs treated with aCSF and NH_4Cl (1, 3, 5, and 10 mM) in cell-attached recordings. (C) Spike frequency of MCs in a cell-attached configuration within 6 min of perfusion with NH_4Cl solution, showing increased MC excitability. (D) An example of spontaneous firing in the cell-attached mode from a MC in control (Ctrl, aCSF solution), 3 mM NH_4Cl , and washing solution, respectively. (E) The relationship between the number of events and inter-event interval of spontaneous firings fitted by Gaussian equation before and after NH_4Cl application, showing two components in the Ctrl (bin of the first and second component is 5 and 200 ms, respectively) and only one component in NH_4Cl solution (bin: 5 ms). (F) The cumulative fraction of inter-event intervals before and after NH_4^+ application, showing much shorter mean intervals between events after NH_4Cl application. (G) The mean frequencies of spontaneous firings before and after NH_4Cl application, indicating a significant increase in the excitability of MCs by NH_4Cl . Error bars represent standard error; * $p < 0.05$, ** $p < 0.01$, *** $p < 0.001$; ns, not significant; unpaired Student's t -test and one-way ANOVA with LSD *post-hoc* test.

We also observed that high concentrations (e.g., 5 and 10 mM) of NH_4Cl induced an increment regarding spontaneous firing rates was not much higher than 3 mM NH_4Cl . Moreover, the percentage of cells with disappearing spikes, were positively associated with the increasing concentrations of NH_4Cl (0/5 cells in 1 mM NH_4Cl , 5/10 cells in 3 mM NH_4Cl , 4/7 cells in 5 mM NH_4Cl , and 7/7 cells in 10 mM NH_4Cl). However, these concentrations of NH_4Cl mentioned above, are higher than the concentration of NH_4Cl in patients with HE ($311 \pm 67 \mu\text{mol/L}$), and 3 mM NH_4Cl was an appropriate concentration to explore its acute neuronal excitotoxicity (Ong et al., 2003; Montes-Cortes et al., 2020). Moreover, we found the NH_4^+ -induced frequency alteration occurred in a time-dependent manner: At first, the frequency was accelerated to approximately three times that of the control and then decreased to a relatively stable frequency with persistent NH_4Cl application over 6 min at which the frequency was still higher than that in aCSF ($n = 5$, $p < 0.001$) (Figure 2C). Furthermore, to identify whether 3 mM NH_4Cl could induce a same phenomenon by using HEPES-dialyzed pipette solution, we recorded the spike frequency and RMP in whole-cell current-clamp mode, finding the change of spike frequency is same with cell-attached recordings and a depolarized trend of RMP with a significant transient depolarization within 4-min NH_4Cl (Supplementary Figure 1).

To clarify the effect of NH_4^+ on MC spike activity and whether the NH_4^+ -induced effect could be reversed, we recorded spontaneous firing in control (aCSF) buffer for 5 min, NH_4Cl solution for 10 min, and washing solution for 12 min. To analyze the spike frequency, we measured the inter-event interval of 3-min events in the control and NH_4Cl groups and plotted the data as binned and cumulative frequency histograms (Figures 2D–F). MCs with typical burst firing (in the control) had two components in the fitted curve, the first component representing the inter-event interval of intra-burst firings and the second component showing the inter-burst interval (first component 34.53 ± 10.14 ms, 5-ms bins, second component $1,210 \pm 610$ ms, 200-ms bins; $n = 5$); following the NH_4Cl treatment, the curve not only shifted toward zero but transformed into a single component (28.14 ± 6.94 ms, 5-ms bins; $n = 5$; Figure 2E), indicating elevated spike frequency. The left shift of the cumulative curve after NH_4Cl application indicated a reduction in the mean inter-event interval (Figure 2F). The NH_4^+ -induced excitation of MCs could be partially reversed by washing solution, but it took ~ 10 min for the spike frequency to return to baseline (control: 6.26 ± 3.19 Hz, NH_4Cl : 18.80 ± 3.65 Hz, Wash: 5.09 ± 1.54 Hz, $n = 5$, $p = 0.011$; Figure 2G). These results demonstrate that NH_4^+ can facilitate MC excitation by increasing spontaneous firing frequency, but the mechanisms behind the NH_4^+ -induced reduction in spike amplitude remain to be explored.

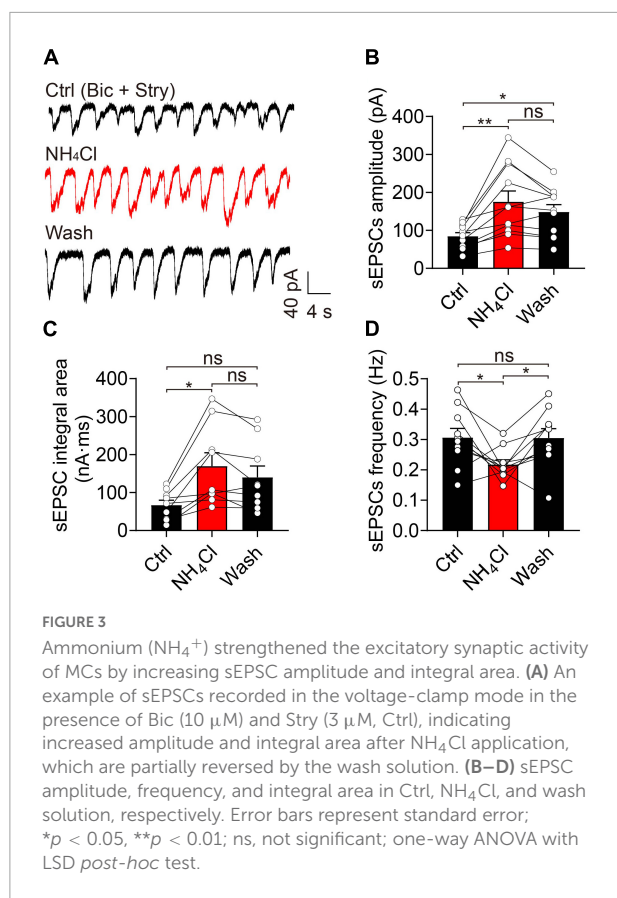
To explore the potential mechanism of NH_4^+ -induced effects on the frequency and amplitude of spontaneous firings, we conducted the electrophysiological recordings in the

presence of APV + NBQX + Bic + Stry. In the experiment, the results showed that NH_4^+ temporarily decreased the amplitudes of inward (I_{inward}) and outward (I_{outward}) currents of spontaneous action potentials and increased the spike frequency within 4-min of NH_4Cl perfusion which may be due to the depolarized membrane potential initially, but the amplitudes of I_{inward} and I_{outward} and the spike frequency gradually reversed to the baseline (in aCSF) 4-min after which was not consistent with those in the absence of post-synaptic receptors blockers (Supplementary Figures 2A–F). We further detected the effect of NH_4^+ on the raw currents of Nav (I_{Na}) and Kv (I_{K}) channels, showing that the amplitude of I_{Na} was decreased, and the number of I_{Na} events at -40 mV were increased by 4-min NH_4Cl perfusion, and the changes were recovered at 8-min, while the amplitude of I_{K} were attenuated with 4- and 8-min treatment (Supplementary Figures 3A–D). Interestingly, we also found that the gradual depolarization of RMP by NH_4^+ matched with the increased frequency and decreased amplitude of spontaneous firings, indicating NH_4^+ -induced changes of spontaneous firings may be attributed to the depolarized membrane potential (Supplementary Figures 2G,H). In the experiment, the membrane resistance remained unchanged during NH_4Cl application (Ctrl: 194.80 ± 18.92 M Ω , NH_4^+ : 195.30 ± 14.74 M Ω , $n = 5$, $p = 0.904$) (Supplementary Figures 2I,J). In summary, we consider NH_4^+ -induced changes of spike frequency and amplitude are caused by depolarized membrane potential, but the membrane potential is depolarized transiently when blocking excitatory and inhibitory synaptic inputs, which indicates that overactivity of glutamate receptors but not inhibitory receptors might be the potential factor to aggravate membrane depolarization and evoke MC excitotoxicity because the reversal potential of chloride ion is close to the RMP in the study.

Ammonium increased the amplitude and integral area of spontaneous excitatory post-synaptic currents

Elevated levels of NH_4^+ in the brain can increase glutamine synthesis, which can be catalyzed by glutaminase and decomposed to glutamate. NH_4^+ exerts neurotoxicity by facilitating NMDA receptor activation and activating the Ca^{2+} -NO-cGMP signaling pathway (Cauli et al., 2009). Spontaneous burst firing was mainly regulated by glutamate receptors in the OB and NH_4^+ -induced increment of spike frequency could be prevented by synaptic blockers (Hayar et al., 2004; Nagayama et al., 2014). Therefore, we hypothesized that the activity of glutamate receptors was upregulated by NH_4^+ resulting in depolarized membrane potential and increased spontaneous MC firing.

NH_4Cl increased the amplitude of sEPSCs to 168% that of the control, which was partially reversed by washing for



6 min (control: 84.54 ± 9.59 pA, NH_4Cl : 175.40 ± 28.28 pA, wash: 148.60 ± 19.11 pA, $n = 11$, $p = 0.012$; **Figures 3A,B**). NH_4Cl had a similar effect on sEPSC integral area (control: 66.86 ± 12.82 nA·ms, NH_4Cl : 169.40 ± 35.23 nA·ms, wash: 139.90 ± 29.95 nA·ms, $n = 9$, $p = 0.042$; **Figure 3C**). In contrast, the sEPSC frequency was reduced from 0.31 ± 0.03 Hz to 0.22 ± 0.02 Hz by NH_4Cl treatment, and could be reversed to 0.30 ± 0.03 Hz by washing ($n = 10$, $p = 0.037$; **Figure 3D**). These results indicate that NH_4^+ promotes MC neuronal excitability by increasing the amplitude and integral area of sEPSCs.

Ammonium boosted mitral cell synaptic activity independently of glutamate release from pre-synaptic terminals

To determine the potential mechanism of the NH_4^+ -induced increase of amplitude and integral area of sEPSCs, we recorded eEPSCs by stimulating the olfactory sensory nerves and examined whether NH_4^+ could facilitate glutamate release from pre-synaptic terminals. In this experiment, NH_4^+ substantially decreased the amplitude of eEPSCs to 46% that of the control during single-pulse stimuli with 20-s intervals

(control: 202.20 ± 66.21 pA, NH_4Cl : 93.61 ± 33.51 pA, wash: 287.30 ± 105.70 pA, $n = 4$, $p = 0.003$; **Figures 4A–C**), with no change observed in the integral area of eEPSCs ($n = 4$, $p = 0.250$). Washing recovered the amplitude of eEPSCs to an even greater extent than that of the control group (**Figure 4B**). To test whether the NH_4^+ -induced reduction in pre-synaptic glutamate release was due to changes in pre-synaptic release probability, we analyzed the PPR (P2/P1). We found that the amplitudes of both the first and second eEPSCs were markedly attenuated by NH_4Cl ($35.79 \pm 3.08\%$ that of the control in first EPSCs, $n = 7$, $p = 0.039$; $36.04 \pm 6.47\%$ that of the control in second EPSCs, $n = 5$, $p < 0.001$), while the mean PPR was unchanged ($n = 5$, $p = 0.826$; **Figures 4D–G**). These results suggest that NH_4^+ suppresses glutamate release from pre-synaptic terminals without influencing the release probability, which does not explain the enhanced activity of sEPSCs induced by NH_4^+ . Although we attempted to record miniature EPSCs (mEPSCs) and further confirm the above results, mEPSCs were particularly weak when perfusing 1 μM TTX.

Blocking glutamate re-uptake did not influence the ammonium-induced increase in excitatory synaptic activity

Ammonium can inhibit excitatory amino acid transporters (EAATs), which is likely one of the major factors influencing synaptic activity and neuronal excitation in a hyperammonemia model (Butterworth, 1993). Accordingly, we used TBOA to block EAATs in the OB and examined whether NH_4^+ could prevent intercellular glutamate re-uptake and, in so doing, promote overactivity of glutamate receptors. We recorded sEPSCs during the sequential application of control, NH_4Cl , and $\text{NH}_4\text{Cl} + \text{TBOA}$ solutions (**Figure 5A**). The TBOA + NH_4Cl treatment increased the amplitude (control: 96.70 ± 8.64 pA, NH_4Cl : 196.90 ± 25.10 pA, $\text{NH}_4\text{Cl} + \text{TBOA}$: 365.70 ± 42.72 pA, $n = 11$, $p < 0.001$) and integral area (control: 53.75 ± 10.78 nA·ms, NH_4Cl : 142.30 ± 32.52 nA·ms, $\text{NH}_4\text{Cl} + \text{TBOA}$: $1,067.00 \pm 238.10$ nA·ms, $n = 11$, $p < 0.001$) by 85.73 and 649.82% that of the NH_4Cl only group, respectively (**Figures 5B,C**). In contrast, the sEPSCs frequency was reduced by TBOA (control: 0.33 ± 0.02 Hz, NH_4Cl : 0.20 ± 0.02 Hz, $\text{NH}_4\text{Cl} + \text{TBOA}$: 0.10 ± 0.01 Hz, $n = 11$, $p < 0.001$; **Figure 5D**). Moreover, we first blocked EAATs and then applied NH_4Cl and found that the mean values of amplitude (control: 116.20 ± 14.41 pA, TBOA: 270.90 ± 45.06 pA, TBOA + NH_4Cl : 331.50 ± 42.41 pA, $n = 5$, $p = 0.004$) and integral area (control: 67.09 ± 17.37 nA·ms, TBOA: 420.50 ± 153.70 nA·ms, TBOA + NH_4Cl : 830.80 ± 325.60 nA·ms, $n = 5$, $p = 0.069$) of sEPSCs were also markedly increased by NH_4^+ though there were no significant statistical difference of integral area and frequency between only TBOA and TBOA + NH_4Cl with one way ANOVA analysis (**Figures 5E–H**). These results revealed

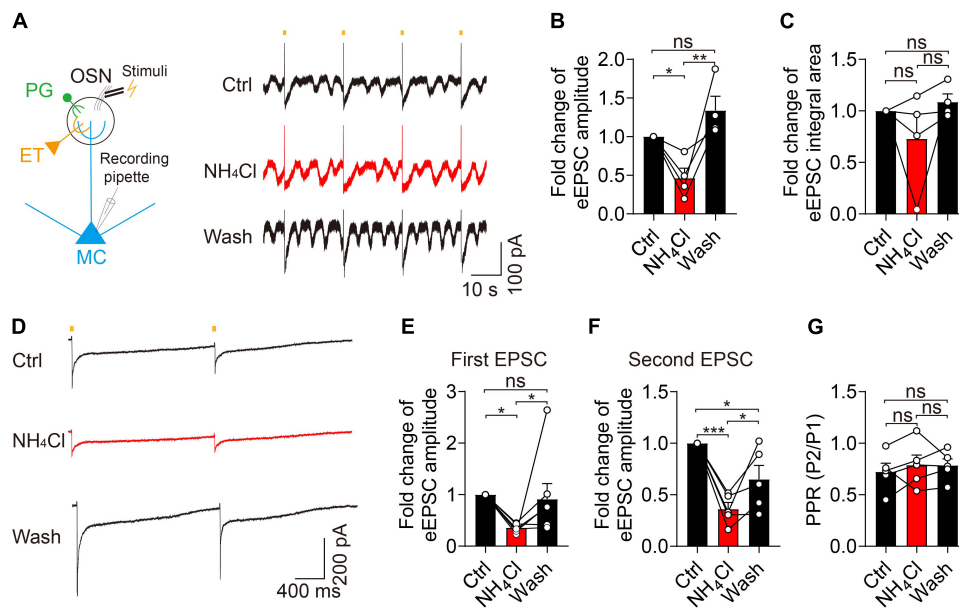


FIGURE 4

Ammonium (NH_4^+) reduced the pre-synaptic glutamate release in MCs without affecting pre-synaptic release probability. (A) Left panel showing MC recording of evoked EPSCs (eEPSCs) after stimulating OSN stubs with a bipolar electrode. Right panel showing eEPSCs from a MC by continuous single-pulse stimuli with 20 s intervals in Ctrl, NH_4Cl , and wash solution, respectively, in the presence of Bic + Stry. (B–C) Fold change of eEPSC amplitude, and integral area in Ctrl, NH_4Cl , and wash solution, respectively. (D) An example of eEPSCs recorded from a MC in Ctrl, NH_4Cl , and wash solution, respectively. EPSCs were evoked by paired-pulse stimuli with an interval of 2,000 ms (determined by the slow recovery course of eEPSCs). (E–G) Pooled data showing fold changes of the first and second eEPSC amplitude and PPR (paired-pulse ratio, P2/P1) in Ctrl, NH_4Cl , and wash solution, respectively. Error bars represent standard error; * $p < 0.05$, ** $p < 0.01$, *** $p < 0.001$; ns, not significant; one-way ANOVA with LSD *post-hoc* test.

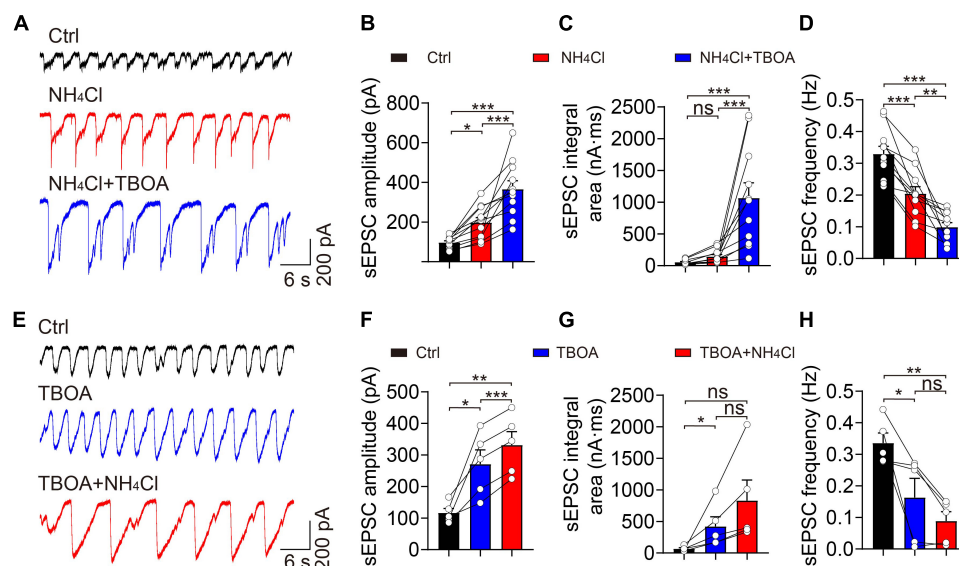


FIGURE 5

Blockade of EAATs did not attenuate NH_4^+ -induced potentiation of excitatory synaptic activity. (A) Representative traces showing sEPSCs recorded in a voltage-clamp configuration in the presence of Bic + Stry, showing the changes in sEPSC amplitude and integral area in Ctrl, NH_4Cl , and NH_4Cl + TBOA (30 μM), respectively. (B–D) sEPSC amplitude, integral area, and frequency in sequential treatments with Ctrl, NH_4Cl , and NH_4Cl + TBOA. (E) Typical sEPSC traces from a MC in sequential treatments of Ctrl, TBOA, and TBOA + NH_4Cl . (F–H) *Post hoc* analysis of sEPSC amplitude, integral area, and frequency in Ctrl, TBOA, and TBOA + NH_4Cl , respectively. Error bars represent standard error; * $p < 0.05$, ** $p < 0.01$, *** $p < 0.001$; ns, not significant; one-way ANOVA with LSD *post-hoc* test.

that the activity of EAATs in the OB was not inhibited by NH_4^+ and that sEPSCs could still be enhanced by NH_4^+ when blocking EAATs. In other words, the enhanced excitatory post-synaptic events induced by NH_4^+ in MCs was not attributed to the suppression of glutamate uptake.

Ammonium enhanced the trafficking of glutamate receptors to the cytoplasmic membrane

We hypothesized that NH_4^+ might increase the expression of glutamate receptors to potentiate excitatory synaptic transmission in MCs. We employed TAT-NSF700, an *N*-ethylmaleimide-sensitive factor (NSF) inhibitor fusion polypeptide that can permeate the cell membrane and interact with intracellular organelles, preventing vesicles from transporting intracellular proteins to the cytoplasmic membrane (Calvert et al., 2007). Pre-treatment of the OB slices with TAT-NSF700 for 30 min effectively alleviated the spontaneous excitatory synaptic activity induced by NH_4^+ (Figure 6A); NH_4^+ did not change the amplitude, integral area, or frequency of sEPSCs (amplitude: $n = 8$, $p = 0.052$; integral area: $n = 8$, $p = 0.225$; frequency: $n = 8$, $p = 0.163$; Figures 6B–D). This suggests that NH_4^+ increased the active recruitment of glutamate receptors from the cytosolic pool to the membrane.

Alternatively, slowed endocytosis of membrane glutamate receptors may also increase sEPSC activity. To explore this, we pre-incubated OB slices with 40 μM dynasore—a dynamin inhibitor that can block the internalization of membrane proteins—and found that NH_4^+ still increased the amplitude (control: 162.80 ± 32.85 pA, NH_4Cl : 264.40 ± 21.91 pA, $n = 5$, $p = 0.004$) and integral area (control: 133.10 ± 5.90 nA·ms, NH_4Cl : 182.90 ± 10.46 nA·ms, $n = 5$, $p = 0.033$) of sEPSCs by 62.41 and 37.42% that of the control group, respectively (Figures 6E–G). The frequency of sEPSCs was not affected by NH_4^+ ($n = 5$, $p = 0.955$) (Figure 6H). Interestingly, blocking the endocytosis of glutamate receptors with dynasore pre-treatment effectively increased NH_4^+ -induced excitatory synaptic activity (amplitude: NH_4^+ : 175.4 ± 28.28 pA, NH_4Cl with dynasore: 264.40 ± 21.91 pA, $p < 0.001$; integral area: NH_4Cl : 169.40 ± 35.23 nA·ms, NH_4Cl with dynasore: 182.90 ± 10.46 nA·ms, $p = 0.039$). These results demonstrate that when endocytosis is blocked, NH_4^+ can promote the accumulation of glutamate receptors on cell membrane as well as the recruitment of intracellular pool to the cell membrane, thereby synergistically enhancing excitability.

To directly demonstrate whether NH_4^+ can increase the recruitment of glutamate receptors to cell membrane surface, we carried out western blotting analysis of glutamate receptor subunits on cell membrane fractions after OB slices were treated with NH_4Cl solution. Considering that NR1 and GluR1 are the basic subunits of NMDA and AMPA receptor, respectively, we

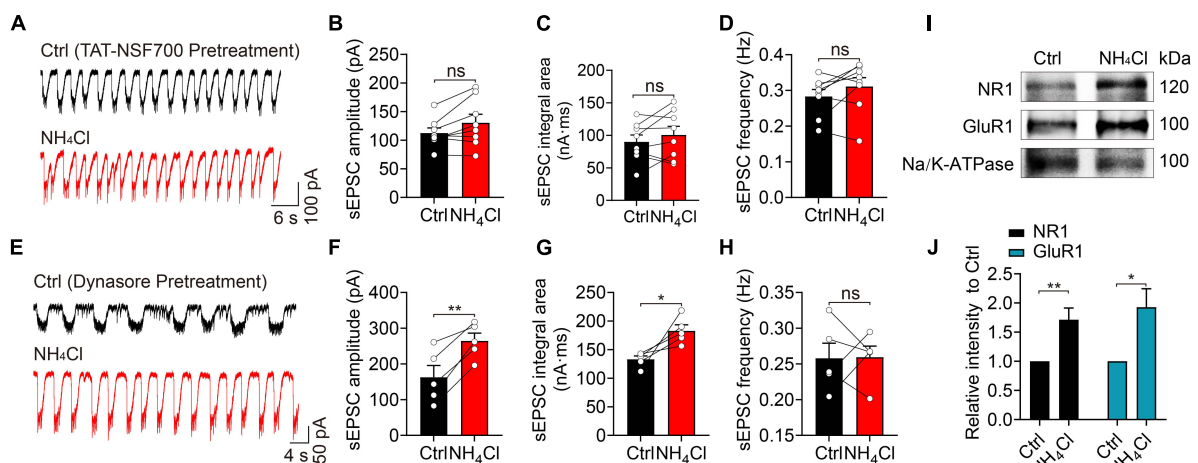


FIGURE 6

Blocking of exocytosis with TAT-NSF700 or blocking dynamin-dependent endocytosis changes the effect of NH_4^+ on the excitability of MCs.

(A) Example traces of sEPSCs from a MC in the presence of Bic + Stry, showing that the sEPSC amplitude, integral area, and frequency were unchanged by NH_4Cl after OB slices were pre-treated with TAT-NSF700 (5 μM , 30 min), a permeable thrombin-induced exocytosis inhibitor.

(B–D) Post hoc statistical analysis of sEPSC amplitude, integral area, and frequency in Ctrl and NH_4Cl solution after OB slices were pre-incubated with TAT-NSF700. (E) Typical sEPSC recordings from a MC in Ctrl (Bic + Stry in aCSF) and Ctrl + NH_4Cl buffer with OB slices pre-incubated with dynasore (40 μM , 30 min), an inhibitor for dynamin-dependent endocytosis. NH_4Cl effectively augmented sEPSC amplitude and integral area. (F–H) Mean sEPSC amplitude, integral area, and frequency in Ctrl (Bic + Stry in aCSF) and NH_4Cl solution in OB slices pre-incubated with dynasore. (I) Representative western blotting images of NR1, GluR1 and Na/K-ATPase from OB in the treatment of aCSF (Ctrl) and NH_4Cl , respectively. (J) Qualification of intensity of NR1 and GluR1 normalized to Ctrl (aCSF). Error bars represent standard error;

* $p < 0.05$, ** $p < 0.01$; ns, not significant; paired Student's *t*-test, unpaired Student's *t*-test.

tested the expression of NR1 and GluR1, with Na/K-ATPase as the internal reference. The immunoblotting analysis revealed that NH_4^+ significantly elevated the level of NR1 and GluR1 without affecting Na/K-ATPase expression on cytoplasmic membrane (NR1: elevated 1.71 ± 0.20 -fold in NH_4^+ , $n = 5$, $p = 0.007$; GluR1: elevated 1.93 ± 0.32 -fold in NH_4^+ , $n = 4$, $p = 0.027$) (Figures 6I,J). These results further demonstrated that NH_4^+ elevates the expression of glutamate receptors, resulting in enhanced MC excitability through promoting the recruitment of glutamate receptors to cytoplasmic membrane.

Upregulation of glutamate receptors induced by ammonium exacerbated cell death

To assess the effect of the upregulated membrane expression of glutamate receptors on cell viability, we assessed the neurotoxicity induced by NH_4^+ using a cell death assay. OB slices were pre-treated with control and NH_4^+ for 1 h, and then calcein-AM/PI co-staining was applied to quantify the ratio of dead/live cells. NH_4^+ increased the dead/live ratio from 1.97 ± 0.16 to 4.26 ± 0.22 that of the control (nine images from three slices, $p < 0.001$), while APV + NBQX, TAT-NSF700, and BAPTA-AM effectively attenuated NH_4^+ -induced cell death (NH_4Cl : 4.26 ± 0.22 , APV + NBQX + NH_4Cl : 2.47 ± 0.18 , TAT-NSF700 + NH_4Cl : 2.41 ± 0.16 , BAPTA-AM + NH_4Cl : 2.27 ± 0.29 , $p < 0.001$; Figures 7A,B). Interestingly, BAPTA-AM pre-treatment remarkably mitigated the NH_4^+ -induced cell death (NH_4Cl : 4.26 ± 0.22 , BAPTA-AM + NH_4Cl : 2.27 ± 0.29 , $p < 0.001$, Figures 7A,B). These results indicate that NH_4^+ can aggravate cell death, and buffering calcium can suppress the NH_4^+ -induced neurotoxicity.

Discussion

Growing evidence demonstrates that patients with liver diseases, especially those with HE, develop a poor olfactory ability to detect and identify odors (Temmel et al., 2005; Zucco et al., 2006). In these patients, serious liver dysfunction can lead to cognitive and motor impairment, coma, and death owing to the accumulation of many metabolic byproducts, among which NH_4^+ is a key contributor to cerebral dysfunction (Jayakumar and Norenberg, 2018). The present study provides evidence for NH_4^+ -induced excitotoxicity of MCs through the enhanced activity of glutamate receptors, revealing the potential mechanism of olfactory impairment in patients with HE.

In the olfactory system, MCs are characterized by burst firing patterns in complex neuronal circuits with neighboring cells (Nagayama et al., 2014). MC has a primary dendrite that forms a highly branched tufts within a single glomerulus, where these tufts receive a multistep signaling input forming glomerulus-specific slow and synchronized bursts or LLD (Gire et al., 2012). These signals include glutamatergic inputs from OSN axons and ETC dendrites, glutamate spillover and lateral excitation between MC-MC/MC-TC dendrodendritic connections, metabolic glutamate receptors, and electrical coupling between dendrites (Nicoll and Jahr, 1982; Isaacson and Strowbridge, 1998; Margrie et al., 2001; De Saint Jan et al., 2009; Gire and Schoppa, 2009; Moran et al., 2021). The initiation of a LLD driven by a glomerulus-specific network, is mainly mediated by AMPA receptors, and NMDA receptors modulate the amplitude and duration of the LLD (Carlson et al., 2000). Our observation that blocking the NMDA receptors results in an increased frequency, which may be attributed to the fast activation and desensitization kinetics of AMPA receptors (Figure 1B).

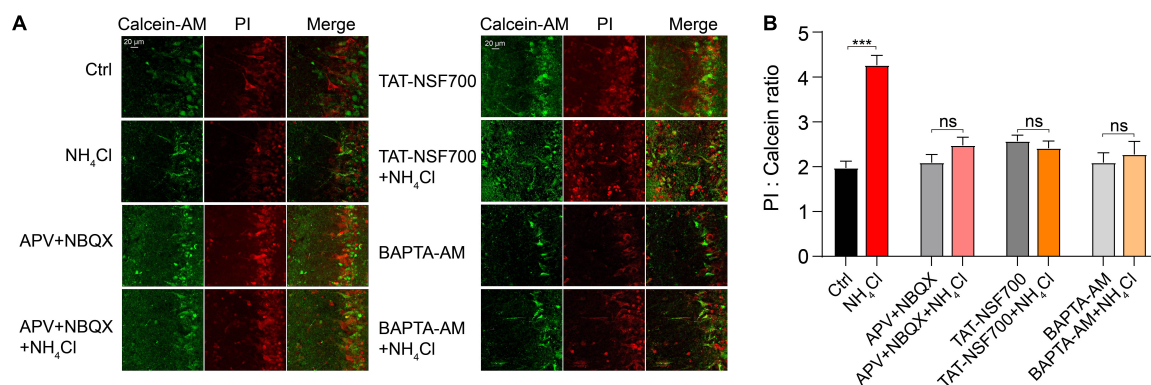


FIGURE 7

Ammonium (NH_4^+)-induced overactivation of glutamate receptors exacerbated MCs death. (A) Representative images of live (calcein-AM, Green) and dead cells (PI, Red), and overlay of fluorescence labeling under different experimental conditions with treatment of Ctrl, NH_4Cl , APV + NBQX, APV + NBQX + NH_4Cl , TAT-NSF700, TAT-NSF700 + NH_4Cl , BAPTA-AM, and BAPTA-AM + NH_4Cl for 1 h. (B) Ratio of dead (PI labeling) to live (calcein labeling) cells for all experiments. Error bars represent standard error; *** $p < 0.001$; ns, not significant; unpaired Student's t-test.

Interestingly, we also found that 3 mM NH_4Cl induced significant changes of spontaneous firings in MCs, showing increased frequency and decreased amplitude of spontaneous firings, whereas the increased frequency and decreased amplitude demonstrated to be transient and then recovered after blocking excitatory and inhibitory synaptic inputs. This phenomenon indicates that the enhanced activity of glutamate receptors by NH_4^+ plays an essential role in the continuous decrease of spike amplitude, as evidenced by the fact that activation of glutamate receptors in MCs can evoke a long-lasting membrane depolarization (Carlson et al., 2000). Furthermore, Nav and Kv channels are critical for spike initiation, propagation, and firing patterns in central neurons (Catterall et al., 2005; Bean, 2007). Lazarenko et al. has shown NH_4^+ depolarized neuronal membrane potential, probably by influencing Na^+ -sensitive background sodium leak channel NALCN (Lu et al., 2007; Lazarenko et al., 2017). NH_4Cl has been found to be one of the agonists of acid-sensitive ion channels, and may activate the channels contributing to the formation of the transient depolarization of membrane potential (Pidoplichko and Dani, 2006). In our study, transient membrane depolarization and the concurrent suppression of Nav and Kv currents by NH_4^+ , jointly lead to the amplitude attenuation during the initial NH_4^+ application. In addition, previous studies have shown NH_4^+ induced the decreased K^+ conductance and the elevation of extracellular K^+ which led to membrane depolarization (Allert et al., 1998; Rangroo Thrane et al., 2013). Except for the effect of glutamate receptors, the sustaining attenuation of Kv currents by NH_4^+ may be a necessary factor to depolarize membrane potential, resulting in progressive attenuation of amplitude in spontaneous firings.

In our study, we found that acute hyperammonemia can elevate the amplitude and integral area of sEPSCs in MCs, leading to neuronal hyperexcitability and neurotoxicity in OB slices, but the potential mechanism remains to be discussed. At first, olfactory sensory nerves in the superficial OB form monosynaptic connection to the apical dendrite tufts of MCs and the ETCs action potentials mediate the feedforward excitation of MCs in the specific glomerulus (Chen et al., 1997; Hayar et al., 2004; De Saint Jan et al., 2009). In our study, suprathreshold intensity stimulation of OSN stubs did not increase the eEPSC activity in the treatment of NH_4Cl , indicating the OSN-MC and OSN-ETC-MC synaptic transmission did not play an essential role in NH_4^+ -induced enhancement of sEPSCs. On the contrary, the pre-synaptic glutamate release was inhibited, consistently with the results of a previous study (Szerb and Butterworth, 1992). Second, it has been shown that ammonia facilitates the synthesis of glutamate and increase the accumulation of extracellular glutamate, which might boost the glutamate spillover and lateral excitation between MC-MC/MC-TC dendrodendritic synapses in the

glomeruli (Nicoll and Jahr, 1982; Aroniadou-Anderjaska et al., 1999; Cauli et al., 2009; Cabrera-Pastor et al., 2019). We excluded this possibility because the amplitude and integral area of sEPSCs were still enlarged by NH_4^+ after we blocked the uptake of glutamate with TBOA. Third, previous studies have revealed NH_4^+ plays a crucial role in triggering neuronal overexcitability by altering glutamate receptor expression in the central nervous system in acute and chronic hyperammonemia (Kosenkov et al., 2018; Sancho-Alonso et al., 2022). However, different results have been reported for glutamate receptor expression in the hippocampus and cerebellum of hyperammonemia rats. Some studies found that chronic hyperammonemia can elevate the membrane expression of NMDA receptors, and alter the expression of AMPA receptor subunits in the hippocampus (Cabrera-Pastor et al., 2016; Hernandez-Rabaza et al., 2016; Kosenkov et al., 2018). However, others found that ammonia reduces MK801 binding to NMDA receptors and the surface expression of the NR1 and NR2A subunits in ammonia-treated cerebellar neurons (Rao et al., 1991; Sanchez-Perez and Felipo, 2006). The C1 domain of NR1 has three serine residues (890, 896, and 897), whose phosphorylation has been implicated in modulating NMDA receptor trafficking and clustering (Llansola et al., 2005). The ammonia-induced increase in phosphorylation of these three serine residues is associated with the expression of NMDA receptors, but the potential mechanism is unclear. In our study, we demonstrated that NH_4^+ can dynamically regulate the recycling and trafficking of glutamate receptors and increase their expressions on the membrane in MCs. This process might be due to NH_4^+ -activated Ca^{2+} -dependent post-translational modifications of glutamate receptors on the membrane and/or the recruitment of a pre-existing pool of glutamate receptors.

We acknowledge some limitations to our study. For example, we did not identify the effect of NH_4^+ on the neurotransmission of MCs in a glutamate receptor-knockout mouse model. Our study was performed using *in vitro* acute OB slices, which revealed the cellular mechanism of NH_4^+ toxicity in the olfactory system; however, it did not consider pathological activity or the influence of NH_4^+ on olfactory function in an *in vivo* model.

In conclusion, we investigated the potential mechanisms underlying MC excitotoxicity in an *in vitro* model of acute hyperammonemia. We found that NH_4^+ increases spontaneous firing frequency and decreases the amplitude through the joint effects of enhanced glutamate receptor activity and reduced Kv currents. The results also demonstrated enhanced glutamate receptor activity by increasing the recruitment of glutamate receptors on the MC cytoplasmic membrane, contributing to cell overexcitability and neurotoxicity. This study implicates a potential pathological mechanism of olfactory defects in patients with hyperammonemia and HE, and glutamate receptors and their trafficking as potential molecular and

cellular targets for protection and intervention against NH_4^+ -induced neurotoxicity.

Data availability statement

The original contributions presented in the study are included in the article/**Supplementary material**, further inquiries can be directed to the corresponding authors.

Ethics statement

The animal study was reviewed and approved by Ethics Committee of the Shanghai Sixth People's Hospital Affiliated to Shanghai Jiao Tong University School of Medicine.

Author contributions

ML, ZL, and KL: experiments and data collection. HBS, HW, and WZ: data analysis and manuscript writing. WZ, HW, HBS, ZL, KL, HL, LG, HSS, and ML: experiment design and manuscript writing. All authors have reviewed the manuscript.

Funding

This work was sponsored by the International Cooperation and Exchange of the National Natural Science Foundation of China (82020108008) and the National Natural Science Foundation of China (82000993/82171140).

Acknowledgments

We would like to thank Editage (www.editage.cn) for English language editing.

Conflict of interest

The authors declare that the research was conducted in the absence of any commercial or financial relationships that could be construed as a potential conflict of interest.

Publisher's note

All claims expressed in this article are solely those of the authors and do not necessarily represent those of their affiliated organizations, or those of the publisher, the editors and the reviewers. Any product that may be evaluated in this article, or claim that may be made by its manufacturer, is not guaranteed or endorsed by the publisher.

Supplementary material

The Supplementary Material for this article can be found online at: <https://www.frontiersin.org/articles/10.3389/fncel.2022.1002671/full#supplementary-material>

SUPPLEMENTARY FIGURE 1

NH_4^+ increased MCs excitability in whole-cell current-clamp mode. (A) A recording of spontaneous firings in whole-cell current-clamp mode. (B,C) Pooled data showing the time course of resting membrane potential (RMP) and spike frequency during the 6-min application of NH_4Cl . Error bars represent standard error; * $p < 0.05$, ** $p < 0.01$, *** $p < 0.001$; one-way ANOVA with LSD *post hoc* test.

SUPPLEMENTARY FIGURE 2

NH_4^+ regulated MCs intrinsic excitability transiently. (A) Spontaneous firings in the presence of APV + NBQX + Bic + Stry (Ctrl, 1 min) and NH_4Cl + APV + NBQX + Bic + Stry (NH_4Cl , 8 min) in cell-attached mode. (B) Spontaneous firings during 0, 2, 4 and 6 min NH_4Cl application. (C–E) Scatter plots showing the amplitudes of inward current (I_{inward}), outward current (I_{outward}) and the ratio of I_{inward} to I_{outward} in spontaneous action potentials during the time course of NH_4Cl application. (F) Mean frequency during the time course of NH_4Cl application. (G) Whole-cell current-clamp recording of spontaneous action potentials with the injection current of 0 pA in the presence of APV + NBQX + Bic + Stry (Ctrl) and NH_4Cl + APV + NBQX + Bic + Stry (NH_4Cl). (H) Statistical curve showing the time course of RMP during the application of NH_4Cl . (I) The representative recording when injecting 10 pA current in current-clamp at a membrane potential of -60 mV before (Ctrl) and after NH_4Cl in the presence of APV + NBQX + Bic + Stry. (J) Histogram showing R_m before (Ctrl) and after NH_4Cl treatment from I, calculated using the function of $\tau = R_m C_m$, where τ is the time constant and C_m is the membrane capacitance. Error bars represent standard error; * $p < 0.05$, ** $p < 0.01$, *** $p < 0.001$; ns, not significant; one-way ANOVA with LSD *post hoc* test, paired Student's *t*-test.

SUPPLEMENTARY FIGURE 3

NH_4^+ -induced changes of voltage-gated sodium and potassium currents. (A) Raw electrophysiological traces showing inward currents (Na^+ current, I_{Na}) and outward currents (K^+ current, I_{K}) in Ctrl, 4-min and 8-min NH_4Cl . The protocol was performed by injecting step voltages from -70 mV to 40 mV with the increment of 10 mV at the holding potential of -70 mV in the presence of a cocktail of postsynaptic receptors blockers. Right panel representing the expanded I_{Na} in left panel. (B,C) Voltage-current relationship of I_{Na} and I_{K} in Ctrl, 4-min and 8-min NH_4Cl . (D) The number of activated I_{Na} events when injecting the voltage of -40 mV in Ctrl, 4-min and 8-min NH_4Cl . Error bars represent standard error; * $p < 0.05$, *** $p < 0.001$; one-way ANOVA with LSD *post hoc* test.

References

- Allert, N., Koller, H., and Siebler, M. (1998). Ammonia-induced depolarization of cultured rat cortical astrocytes. *Brain Res.* 782, 261–270. doi: 10.1016/s0006-8993(97)01288-2
- Aroniadou-Anderjaska, V., Ennis, M., and Shipley, M. T. (1999). Dendrodendritic recurrent excitation in mitral cells of the rat olfactory bulb. *J. Neurophysiol.* 82, 489–494. doi: 10.1152/jn.1999.82.1.489
- Back, A., Tupper, K. Y., Bai, T., Chirand, P., Goldenberg, F. D., Frank, J. L., et al. (2011). Ammonia-induced brain swelling and neurotoxicity in an organotypic slice model. *Neurol. Res.* 33, 1100–1108. doi: 10.1179/1743132811Y.0000000046
- Bean, B. P. (2007). The action potential in mammalian central neurons. *Nat. Rev. Neurosci.* 8, 451–465. doi: 10.1038/nrn2148
- Boyd, A. M., Sturgill, J. F., Poo, C., and Isaacson, J. S. (2012). Cortical feedback control of olfactory bulb circuits. *Neuron* 76, 1161–1174. doi: 10.1016/j.neuron.2012.10.020
- Burch, R. E., Sackin, D. A., Ursick, J. A., Jetton, M. M., and Sullivan, J. F. (1978). Decreased taste and smell acuity in cirrhosis. *Arch. Intern. Med.* 138, 743–746. doi: 10.1001/archinte.1978.03630290047017
- Butterworth, R. F. (1993). Portal-systemic encephalopathy: A disorder of neuron-astrocytic metabolic trafficking. *Dev. Neurosci.* 15, 313–319. doi: 10.1159/00011350
- Cabrera-Pastor, A., Arenas, Y. M., Taoro-Gonzalez, L., Montoliu, C., and Felipo, V. (2019). Chronic hyperammonemia alters extracellular glutamate, glutamine and GABA and membrane expression of their transporters in rat cerebellum. Modulation by extracellular cGMP. *Neuropharmacology* 161:107496. doi: 10.1016/j.neuropharm.2019.01.011
- Cabrera-Pastor, A., Balzano, T., Hernandez-Rabaza, V., Malaguarnera, M., Llansola, M., and Felipo, V. (2018). Increasing extracellular cGMP in cerebellum *in vivo* reduces neuroinflammation, GABAergic tone and motor in-coordination in hyperammonemic rats. *Brain Behav. Immun.* 69, 386–398. doi: 10.1016/j.bbi.2017.12.013
- Cabrera-Pastor, A., Hernandez-Rabaza, V., Taoro-Gonzalez, L., Balzano, T., Llansola, M., and Felipo, V. (2016). *In vivo* administration of extracellular cGMP normalizes TNF- α and membrane expression of AMPA receptors in hippocampus and spatial reference memory but not IL-1 β , NMDA receptors in membrane and working memory in hyperammonemic rats. *Brain Behav. Immun.* 57, 360–370. doi: 10.1016/j.bbi.2016.05.011
- Calvert, J. W., Gundewar, S., Yamakuchi, M., Park, P. C., Baldwin, W. M. III, Lefer, D. J., et al. (2007). Inhibition of N-ethylmaleimide-sensitive factor protects against myocardial ischemia/reperfusion injury. *Circ. Res.* 101, 1247–1254. doi: 10.1161/CIRCRESAHA.107.162610
- Carlson, G. C., Shipley, M. T., and Keller, A. (2000). Long-lasting depolarizations in mitral cells of the rat olfactory bulb. *J. Neurosci.* 20, 2011–2021. doi: 10.1523/JNEUROSCI.20-05-02011.2000
- Catterall, W. A., Goldin, A. L., and Waxman, S. G. (2005). International union of pharmacology. XLVII. Nomenclature and structure-function relationships of voltage-gated sodium channels. *Pharmacol. Rev.* 57, 397–409. doi: 10.1124/pr.57.4.4
- Cauli, O., Rodrigo, R., Llansola, M., Montoliu, C., Monfort, P., Piedrafita, B., et al. (2009). Glutamatergic and gabaergic neurotransmission and neuronal circuits in hepatic encephalopathy. *Metab. Brain Dis.* 24, 69–80. doi: 10.1007/s11011-008-9115-4
- Chen, W. R., Midtgaard, J., and Shepherd, G. M. (1997). Forward and backward propagation of dendritic impulses and their synaptic control in mitral cells. *Science* 278, 463–467. doi: 10.1126/science.278.5337.463
- Chen, X. J., Zhou, H. Q., Ye, H. B., Li, C. Y., and Zhang, W. T. (2016). The effect of bilirubin on the excitability of mitral cells in the olfactory bulb of the rat. *Sci. Rep.* 6:32872. doi: 10.1038/srep32872
- De Saint Jan, D., Hirnet, D., Westbrook, G. L., and Charpak, S. (2009). External tufted cells drive the output of olfactory bulb glomeruli. *J. Neurosci.* 29, 2043–2052. doi: 10.1523/JNEUROSCI.5317-08.2009
- Deems, R. O., Friedman, M. I., Friedman, L. S., Munoz, S. J., and Maddrey, W. C. (1993). Chemosensory function, food preferences and appetite in human liver disease. *Appetite* 20, 209–216. doi: 10.1006/appe.1993.1021
- Gire, D. H., and Schoppa, N. E. (2009). Control of on/off glomerular signaling by a local GABAergic microcircuit in the olfactory bulb. *J. Neurosci.* 29, 13454–13464. doi: 10.1523/JNEUROSCI.2368-09.2009
- Gire, D. H., Franks, K. M., Zak, J. D., Tanaka, K. F., Whitesell, J. D., Mulligan, A. A., et al. (2012). Mitral cells in the olfactory bulb are mainly excited through a multistep signaling path. *J. Neurosci.* 32, 2964–2975. doi: 10.1523/JNEUROSCI.5580-11.2012
- Hayar, A., Karnup, S., Shipley, M. T., and Ennis, M. (2004). Olfactory bulb glomeruli: External tufted cells intrinsically burst at theta frequency and are entrained by patterned olfactory input. *J. Neurosci.* 24, 1190–1199. doi: 10.1523/JNEUROSCI.4714-03.2004
- Heiser, C., Haller, B., Sohn, M., Hofauer, B., Knopf, A., Mühlh, T., et al. (2018). Olfactory function is affected in patients with cirrhosis depending on the severity of hepatic encephalopathy. *Ann. Hepatol.* 17, 822–829. doi: 10.5604/01.3001.0012.3143
- Hernandez-Rabaza, V., Cabrera-Pastor, A., Taoro-Gonzalez, L., Malaguarnera, M., Agusti, A., Llansola, M., et al. (2016). Hyperammonemia induces glial activation, neuroinflammation and alters neurotransmitter receptors in hippocampus, impairing spatial learning: Reversal by sulforaphane. *J. Neuroinflammation* 13:41. doi: 10.1186/s12974-016-0505-y
- Isaacson, J. S., and Strowbridge, B. W. (1998). Olfactory reciprocal synapses: Dendritic signaling in the CNS. *Neuron* 20, 749–761. doi: 10.1016/s0896-6273(00)81013-2
- Izumi, Y., Svrakic, N., O'Dell, K., and Zorumski, C. F. (2013). Ammonia inhibits long-term potentiation *via* neurosteroid synthesis in hippocampal pyramidal neurons. *Neuroscience* 233, 166–173. doi: 10.1016/j.neuroscience.2012.12.035
- Jayakumar, A. R., and Norenberg, M. D. (2018). Hyperammonemia in hepatic encephalopathy. *J. Clin. Exp. Hepatol.* 8, 272–280. doi: 10.1016/j.jceh.2018.06.007
- Kosenkov, A. M., Gaidin, S. G., Sergeev, A. I., Teplov, I. Y., and Zinchenko, V. P. (2018). Fast changes of NMDA and AMPA receptor activity under acute hyperammonemia *in vitro*. *Neurosci. Lett.* 686, 80–86. doi: 10.1016/j.neulet.2018.08.054
- Landis, B. N., Konnerth, C. G., and Hummel, T. (2004). A study on the frequency of olfactory dysfunction. *Laryngoscope* 114, 1764–1769. doi: 10.1097/00005537-200410000-00017
- Lazarenko, R. M., DelBove, C. E., Strothman, C. E., and Zhang, Q. (2017). Ammonium chloride alters neuronal excitability and synaptic vesicle release. *Sci. Rep.* 7:5061. doi: 10.1038/s41598-017-05338-5
- Llansola, M., Sanchez-Perez, A., Cauli, O., and Felipo, V. (2005). Modulation of NMDA receptors in the cerebellum. 1. Properties of the NMDA receptor that modulate its function. *Cerebellum* 4, 154–161. doi: 10.1080/14734220510007996
- Lu, B., Su, Y., Das, S., Liu, J., Xia, J., and Ren, D. (2007). The neuronal channel NALCN contributes resting sodium permeability and is required for normal respiratory rhythm. *Cell* 129, 371–383. doi: 10.1016/j.cell.2007.02.041
- Margrie, T. W., Sakmann, B., and Urban, N. N. (2001). Action potential propagation in mitral cell lateral dendrites is decremental and controls recurrent and lateral inhibition in the mammalian olfactory bulb. *Proc. Natl. Acad. Sci. U.S.A.* 98, 319–324. doi: 10.1073/pnas.98.1.319
- Montes-Cortes, D. H., Olivares-Corichi, I. M., Rosas-Barrientos, J. V., Manuel-Apolinar, L., Martinez-Godinez, M. L. A., Hernández-López, J. C., et al. (2020). Characterization of oxidative stress and ammonia according to the different grades of hepatic encephalopathy. *Dig. Dis.* 38, 240–250. doi: 10.1159/000503097
- Moran, A. K., Eiting, T. P., and Wachowiak, M. (2021). Dynamics of glutamatergic drive underlie diverse responses of olfactory bulb outputs *in vivo*. *eNeuro* 8. doi: 10.1523/ENEURO.0110-21.2021
- Nagayama, S., Homma, R., and Imamura, F. (2014). Neuronal organization of olfactory bulb circuits. *Front. Neural Circuits* 8:98. doi: 10.3389/fncir.2014.00098
- Nicoll, R. A., and Jahr, C. E. (1982). Self-excitation of olfactory bulb neurones. *Nature* 296, 441–444. doi: 10.1038/296441a0
- Oja, S. S., Saransaari, P., and Korpi, E. R. (2017). Neurotoxicity of ammonia. *Neurochem. Res.* 42, 713–720. doi: 10.1007/s11064-016-2014-x
- Ong, J. P., Aggarwal, A., Krieger, D., Easley, K. A., Karafa, M. T., Van Lente, F., et al. (2003). Correlation between ammonia levels and the severity of hepatic encephalopathy. *Am. J. Med.* 114, 188–193. doi: 10.1016/s0002-9343(02)01477-8
- Padmanabhan, K., and Urban, N. N. (2010). Intrinsic biophysical diversity decorrelates neuronal firing while increasing information content. *Nat. Neurosci.* 13, 1276–1282. doi: 10.1038/nn.2630

- Pidoplichko, V. I., and Dani, J. A. (2006). Acid-sensitive ionic channels in midbrain dopamine neurons are sensitive to ammonium, which may contribute to hyperammonemia damage. *Proc. Natl. Acad. Sci. U.S.A.* 103, 11376–11380. doi: 10.1073/pnas.0600768103
- Rangroo Thrane, V., Thrane, A. S., Wang, F., Cotrina, M. L., Smith, N. A., Chen, M., et al. (2013). Ammonia triggers neuronal disinhibition and seizures by impairing astrocyte potassium buffering. *Nat. Med.* 19, 1643–1648. doi: 10.1038/nm.3400
- Rao, V. L., Agrawal, A. K., and Murthy, C. R. (1991). Ammonia-induced alterations in glutamate and muscimol binding to cerebellar synaptic membranes. *Neurosci. Lett.* 130, 251–254. doi: 10.1016/0304-3940(91)90408-1
- Sanchez-Perez, A. M., and Felipo, V. (2006). Chronic exposure to ammonia alters basal and NMDA-induced phosphorylation of NMDA receptor-subunit NR1. *Neuroscience* 140, 1239–1244. doi: 10.1016/j.neuroscience.2006.03.004
- Sancho-Alonso, M., Taoro-Gonzalez, L., Cabrera-Pastor, A., Felipo, V., and Teruel-Martí, V. (2022). Hyperammonemia alters the function of AMPA and NMDA receptors in hippocampus: Extracellular cGMP reverses some of these alterations. *Neurochem. Res.* 47, 2016–2031. doi: 10.1007/s11064-022-03588-y
- Schoppa, N. E., and Westbrook, G. L. (2001). NMDA receptors turn to another channel for inhibition. *Neuron* 31, 877–879. doi: 10.1016/s0896-6273(01)00442-1
- Szerb, J. C., and Butterworth, R. F. (1992). Effect of ammonium ions on synaptic transmission in the mammalian central nervous system. *Prog. Neurobiol.* 39, 135–153. doi: 10.1016/0301-0082(92)90008-3
- Temmel, A. F., Pabinger, S., Quint, C., Munda, P., Ferenci, P., and Hummel, T. (2005). Dysfunction of the liver affects the sense of smell. *Wien. Klin. Wochenschr.* 117, 26–30. doi: 10.1007/s00508-004-0303-x
- Wang, J. W., Wong, A. M., Flores, J., Vossell, L. B., and Axel, R. (2003). Two-photon calcium imaging reveals an odor-evoked map of activity in the fly brain. *Cell* 112, 271–282. doi: 10.1016/s0092-8674(03)0004-7
- Yonden, Z., Aydin, M., Kilbas, A., Demirin, H., Sutcu, R., and Delibas, N. (2010). Effects of ammonia and allopurinol on rat hippocampal NMDA receptors. *Cell Biochem. Funct.* 28, 159–163. doi: 10.1002/cbf.1636
- Zucco, G. M., Amodio, P., and Gatta, A. (2006). Olfactory deficits in patients affected by minimal hepatic encephalopathy: A pilot study. *Chem. Senses* 31, 273–278. doi: 10.1093/chemse/bjj029



OPEN ACCESS

EDITED BY

Shong Lau,
Salk Institute for Biological Studies,
United States

REVIEWED BY

Adegbenro Omotuyi John Fakoya,
All Saints University School
of Medicine, Dominica
Qiuwen Wang,
Salk Institute for Biological Studies,
United States

*CORRESPONDENCE

Joseph R. Klim
jklim@fazemed.com
Daniel A. Mordes
daniel.mordes@ucsf.edu

SPECIALTY SECTION

This article was submitted to
Cellular and Molecular Mechanisms
of Brain-aging,
a section of the journal
Frontiers in Aging Neuroscience

RECEIVED 11 August 2022

ACCEPTED 27 September 2022

PUBLISHED 02 November 2022

CITATION

Limone F, Klim JR and Mordes DA
(2022) Pluripotent stem cell strategies
for rebuilding the human brain.
Front. Aging Neurosci. 14:1017299.
doi: 10.3389/fnagi.2022.1017299

COPYRIGHT

© 2022 Limone, Klim and Mordes. This
is an open-access article distributed
under the terms of the [Creative
Commons Attribution License \(CC BY\)](#).
The use, distribution or reproduction in
other forums is permitted, provided
the original author(s) and the copyright
owner(s) are credited and that the
original publication in this journal is
cited, in accordance with accepted
academic practice. No use, distribution
or reproduction is permitted which
does not comply with these terms.

Pluripotent stem cell strategies for rebuilding the human brain

Francesco Limone^{1,2,3,4}, Joseph R. Klim^{5*} and
Daniel A. Mordes^{6*}

¹Department of Stem Cell and Regenerative Biology, Harvard Stem Cell Institute, Cambridge, MA, United States, ²Department of Molecular and Cellular Biology, Harvard Stem Cell Institute, Cambridge, MA, United States, ³Stanley Center for Psychiatric Research, Broad Institute of MIT and Harvard, Cambridge, MA, United States, ⁴Leiden University Medical Center, Leiden, Netherlands, ⁵Faze Medicines, Cambridge, MA, United States, ⁶Institute for Neurodegenerative Diseases, Department of Pathology, University of California, San Francisco, San Francisco, CA, United States

Neurodegenerative disorders have been extremely challenging to treat with traditional drug-based approaches and curative therapies are lacking. Given continued progress in stem cell technologies, cell replacement strategies have emerged as concrete and potentially viable therapeutic options. In this review, we cover advances in methods used to differentiate human pluripotent stem cells into several highly specialized types of neurons, including cholinergic, dopaminergic, and motor neurons, and the potential clinical applications of stem cell-derived neurons for common neurodegenerative diseases, including Alzheimer's disease, Parkinson's disease, Huntington's disease, ataxia, and amyotrophic lateral sclerosis. Additionally, we summarize cellular differentiation techniques for generating glial cell populations, including oligodendrocytes and microglia, and their conceivable translational roles in supporting neural function. Clinical trials of specific cell replacement therapies in the nervous system are already underway, and several attractive avenues in regenerative medicine warrant further investigation.

KEYWORDS

neurodegeneration, aging, cell replacement therapies, regenerative medicine, pluripotent stem cells, developmental neuroscience, brain regeneration, neurological diseases

Introduction

Age—it's the one mountain you can't overcome, and as the average life expectancy extends into the eighth decade, neurodegenerative diseases are becoming increasingly prevalent. Despite their increasing incidence, preventative or disease-modifying strategies for these emotionally and financially draining disorders are lacking. Due to the fundamental lack of regeneration within the central nervous system (CNS), neurodegenerative diseases relentlessly attacking discrete populations of neurons are excellent candidates for cell replacement therapies. Here, we review the current

prospects on the application of pluripotent stem cell-derived cell types for the treatment of neurodegenerative disease.

Pluripotent stem cells provide a uniquely scalable source of functional somatic cells, including cells of the CNS, that can potentially replace damaged or diseased tissues. Although prospects for using stem cell derivatives seemed fanciful at the start of the millennium, approximately two decades later several clinical trials using cellular products of pluripotent stem cells are underway or about to reach the clinic (Gage and Temple, 2013; Kimbrel and Lanza, 2015; Steinbeck and Studer, 2015; Trounson and DeWitt, 2016). This progress has been facilitated through the development of robust methods for converting human pluripotent stem cells into the specific cell types that are lost in disease. Most techniques are based on fundamental principles learned from developmental biology and aim to recapitulate cell fate determination pathways in the culture dish, and these methods have been thoroughly reviewed elsewhere (Tao and Zhang, 2016). More recently, exogenous over-expression of transcription factors (TFs) has provided an alternative route to directed differentiation methodologies for generating specific classes of neurons. When appropriate, we will highlight both approaches that advance the field toward producing defined cellular populations, which are the ideal candidate for cell replacement therapies.

In this review, we summarize recent progress toward generating specific cell types from human pluripotent stem cells for regenerative medicine. The examples described herein are not intended to be all-inclusive, and readers are encouraged to examine other reviews on the clinical development of stem cell-based therapies (Gage and Temple, 2013; Kimbrel and Lanza, 2015; Steinbeck and Studer, 2015; Trounson and DeWitt, 2016). Rather, we focus on recent biotechnological advances in the derivation of human cells and their application as cell therapies in the field of neurodegeneration (Table 1). These selected studies illustrate the biological concepts, experimental approaches, and therapeutic possibilities of *in vitro* stem cell-derived cells of the neural (Figure 1) and glial (Figure 2) lineages. We conclude our review with a discussion of emerging technologies in the field, current limitations, and remaining challenges for regenerative medicine in translational neurosciences.

Parkinson's disease

Parkinson's disease (PD) is characterized by the degeneration of several neuronal subtypes, most notably the dopaminergic neurons of the substantia nigra pars compacta (SNpc), located in the ventral midbrain. These neurons project to the dorsal striatum of the basal ganglia and function in motor control, and the loss of these neurons contributes to the movement symptoms observed in the initial stages of PD. Fetal-derived dopamine neurons have had promising clinical

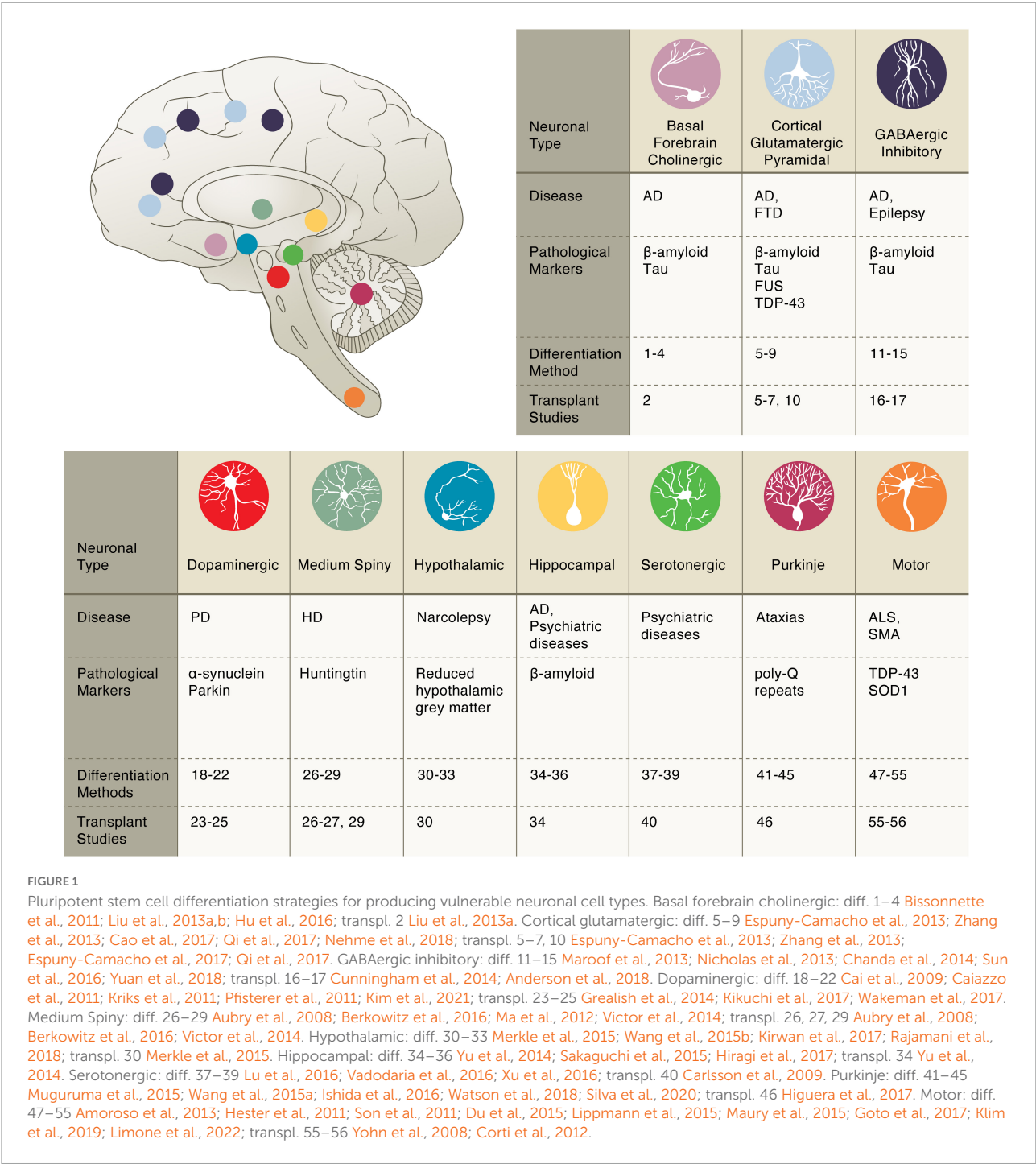
benefits for PD patients (Hallett et al., 2014). To avoid the ethical and logistical issues associated with fetal tissue transplants, the application of pluripotent stem cells to generate dopaminergic neurons has been a long-standing goal. Indeed, translational research to bring these specific neurons to the clinic has far exceeded the other cell replacement strategies discussed here and recent advances have extensively been discussed elsewhere (Barker et al., 2017; Kim et al., 2020). In this section we will provide a summary of the most relevant discoveries that led to the first transplantation studies with hiPSC-derived cells that established a road map for the field.

Dopaminergic neurons

From the initial basic science studies that furnished the directed differentiation strategies of dopaminergic neurons to their large-scale production in GMP-facilities for transplantation studies, the research program for midbrain dopamine neurons has made excellent progress. Several groups developed methods to produce FOXA2/LMX1A-positive midbrain neurons capable of releasing dopamine (Arenas et al., 2015). For example, the Studer group has developed a highly efficient protocol for producing these neurons by combining dual-SMAD inhibition with activation of SHH and FGF8 signaling. The critical step in midbrain specification is the strong activation of WNT signaling achieved using a GSK3 β inhibitor (Kriks et al., 2011; Kim et al., 2021). Transcription factors, such as LMX1A, can also be used to enhance directed differentiation approaches (Cai et al., 2009), or for the direct reprogramming of fibroblasts into dopaminergic neurons (Caiazzo et al., 2011; Pfisterer et al., 2011), and combined with cell sorting methods to further enrich for midbrain dopaminergic neurons (Arenas et al., 2015). Preclinical studies demonstrate that human iPSC cell-derived dopaminergic neurons are safe and efficacious in both rodent and primate PD models (Kikuchi et al., 2017; Wakeman et al., 2017) with similar efficacy to fetal-derived tissue (Grealish et al., 2014). A number of clinical trials with stem cell-based therapies are currently being planned with their details summarized at a recent consortium meeting (Barker et al., 2017). Although PD patients receiving the stem cell-derived dopaminergic neurons will likely show improvements in movement symptoms, their additional symptoms, including depression, fatigue, visual hallucinations, and sleep disturbances, might persist due to continued degeneration of other neuronal types. This has led to some to propose serotonergic neurons (Lu et al., 2016; Vadodaria et al., 2016; Xu et al., 2016) as an additive cellular therapy for PD (Politis and Loane, 2011). A delicate balance must be struck between dopaminergic and serotonergic neurons, however, as fetal grafts with high levels of serotonergic neurons have been associated with graft-induced dyskinesias in parkinsonian rats (Carlsson et al., 2009).

TABLE 1 Common neurodegenerative diseases characterized by selective vulnerability.

Disease	Prevalence	Main symptoms	Key brain regions affected	Main vulnerable neuronal subtypes	Pathological hallmarks (associated protein)	Therapies (symptomatic treatments)	Regenerative medicine cell-based approaches
Alzheimer's Disease (AD)	~5M	Cognitive impairments in memory, language, and behavior	Hippocampus, Basal Forebrain, Locus coeruleus (pons), Cortex	Pyramidal neurons, Cholinergic neurons	Neurofibrillary tangles (tau); neuritic plaques (beta-amyloid & tau)	acetylcholinesterase inhibitors, memantine	Cholinergic neurons, GABAergic Inhibitory neurons
Parkinson's Disease (PD) and Parkinson's Disease with Dementia (PDD)	~1M	Tremor, stiffness, slow movements, autonomic dysfunction, sleep problems, cognitive decline	Substantia nigra (midbrain), locus coeruleus (pons), Cortex (especially the cingulate)	Dopaminergic neurons	Lewy bodies and Lewy neurites (alpha-synuclein)	Levodopa, COMT inhibitors, dopamine agonists, deep brain stimulation	Dopaminergic neurons
Huntington's Disease (HD)	~30K	Uncontrolled movements (chorea), neuropsychiatric	Neostriatum, especially caudate (basal ganglia), cortex	Spiny neurons	Intranuclear & cytoplasmic neuronal inclusions (Htt)	Tetrabenazine, neuroleptics (off-label), antidepressants	Spiny neurons
Spinocerebellar Ataxias (SCAs)	~150K	Difficulty with walking and speech, lack of coordination	Cerebellum, brainstem, spinal cord (dorsal)	Purkinje neurons, pontine nuclei neurons	Intranuclear and cytoplasmic neuronal inclusions (various, e.g., ataxins)	Limited, physical therapy	Purkinje neurons
Amyotrophic Lateral Sclerosis (ALS)	~20K	Progressive weakness and muscle atrophy	Spinal cord (ventral), brainstem (motor nuclei), and frontal cortex	Upper and lower motor neurons	TDP-43 positive cytoplasmic neuronal inclusions	Riluzole, edaravone	Lower motor neurons



Dementia

Neurological conditions involving both memory loss and impaired judgment are classified as dementia ([Yue and Jing, 2015](#)). Alzheimer’s disease (AD) is the most common type of dementia in individuals older than 65 years old and the most prevalent neurodegenerative disease ([Table 1](#)). The incidence of AD dramatically increases with age, and with the aging US population, it is estimated that approximately 14 million individuals will be affected by 2050. AD often first manifests clinically as impairments with short-term memory, and later affects behavior and language. Current treatments are aimed at ameliorating these symptoms without substantially affecting disease course. Cognitive decline is associated with progressive degeneration of neurons in the limbic system (especially the hippocampus and connected entorhinal cortex),

the basal forebrain, and neocortical areas. Histologically, patient brains are characterized by the accumulation of extracellular beta-amyloid depositions and intracellular tau-positive neurofibrillary tangles as well as neuritic plaques that contain both tau within dystrophic neurites and beta-amyloid. Neuropathological studies strongly suggest that AD has well-defined and consistent spatiotemporal pattern of neurofibrillary degeneration, in most cases, that begins in the entorhinal cortex and spreads to pyramidal neurons in the hippocampus and then neocortical areas, with association areas affected sooner and more severely. Currently, there is no effective therapy to block the progression of AD making it a major looming public health challenge.

Basal forebrain cholinergic neurons

One of the earliest cell types perturbed by AD is the basal forebrain cholinergic neuron (BFCN). These neurons, which arise from the median ganglionic eminence (MGE) during development, are responsible for various aspects of cognition including learning, memory, and attention. At the molecular level, BFCNs are primary cholinergic neurons and innervate the cerebral cortex, hippocampus, and amygdala, and play critical roles in processing information related to cognitive function (Martinez et al., 2021). Transplantation of fetal cholinergic tissue from rats into the cortex of lesioned primates has been shown to restore memory deficits suggesting a potentially therapeutic roles for these cells (Ridley et al., 1994).

Several methods to differentiate pluripotent stem cells into BFCNs have been described (Bissonnette et al., 2011; Liu et al., 2013a,b; Hu et al., 2016). Typically, first forebrain neural progenitors are obtained and then treated with a SHH agonist and FGF8 to coax the cells into expressing the transcription factors Nkx2.1, consistent with a ventral medial ganglionic eminence (MGE) neural progenitor identity. Subsequent culture of these progenitor cells on glia or treatment with BMP9 then yields a mixture of neurons containing BFCNs (Bissonnette et al., 2011; Liu et al., 2013a,b; Hu et al., 2016). Alternatively, overexpression of the transcription factors Lhx8 and Gbx1 can convert the progenitors into BFCNs (Bissonnette et al., 2011). Cells produced using these methods express markers consistent with a cholinergic identity and exhibit expected electrophysiological profiles. In one study, MGE-progenitor cells transplanted into mouse brains differentiated into neurons, including BFCNs, and formed synaptic connections (Liu et al., 2013a). More importantly, injection of these precursor cells led to learning and memory improvements in lesioned mice (Liu et al., 2013a). Whether these improvements were the specific result of the BFCNs or other cell types remains to be

determined but this study provides an important proof-of-principle for the use of stem cell-based therapy to improve cognition.

Cortical glutamatergic pyramidal neurons

Cerebral cortex development consists of three major processes: cell proliferation, neuronal migration, and cortical organization into multiple well-defined layers. The cerebral cortex contains two major classes of neurons; a majority population of excitatory glutamatergic projection neurons that arise during development from the dorsal telencephalon, which is the developmental precursor to the cerebral cortex, and a minor population of inhibitory interneurons. Through successive waves of neurogenesis, these neurons generate the six layers of the neocortex, which can be further functionally divided based on specific patterns of axonal output and dendritic input. Due to their abundance and ability to project long distances, cortical pyramidal neurons, named for their shape, are able to integrate and send information across the entire nervous system (Bekkers, 2011).

The production of pyramidal neurons from pluripotent stem cells is considered to be a default differentiation fate because it occurs in the absence of exogenous signaling factors (Espuny-Camacho et al., 2013). Inhibiting certain signaling pathways, however, can enhance the yield of cortical glutamatergic neurons by suppressing the emergence of inhibitory interneurons (Cao et al., 2017). More recently, accelerated methods for generating cortical neurons have been reported. One method relies on a cocktail of molecules to both pattern the cells to dorsal forebrain lineage and then inhibit neural stem cell self-renewal to drive neurogenesis, which preliminary data suggests can be timed to achieve the production of neurons of different cortical layers (Qi et al., 2017). Forced expression of the transcription factor Ngn2 in stem cells further accelerates the differentiation to yield very pure populations of glutamatergic neurons (Zhang et al., 2013) that can be enhanced with the addition of developmental cues (Nehme et al., 2018). Transcriptional studies suggest this method favors the production of upper layer neurons, therefore additional methods to achieve the full diversity of cortical layers may still be necessary. After injecting into the postnatal mouse brain, human cortical neurons generated using the methodologies described above displayed proper, long-distance projection patterns and integrated functionally within the host's circuitry (Espuny-Camacho et al., 2013; Zhang et al., 2013; Qi et al., 2017). Whether they can ameliorate disease phenotypes in animal models remains an unanswered question, but neurons transplanted into a murine AD model display pathological hallmarks of the disease including altered tau biochemistry (Espuny-Camacho et al., 2017).

GABAergic inhibitory neurons

In both the brain and spinal cord, gamma-aminobutyric acid (GABA)-releasing interneurons are the major class of inhibitory neurons and play crucial roles in modulating neural circuits. There are many distinct subtypes of interneurons that differ in their synaptic connections, expression of neuropeptides, neurotransmitter machinery, and developmental origin with some immature interneurons having the remarkable ability to migrate and disperse long distances to integrate throughout the CNS (Southwell et al., 2014). This integrative property makes interneurons a promising candidate for cell replacement therapies.

Several groups have developed directed differentiation approaches for producing interneurons from human pluripotent stem cells (Liu et al., 2013b; Maroof et al., 2013; Nicholas et al., 2013). These approaches typically inhibit both branches of SMAD signaling as well as WNT signaling using small molecules to achieve robust forebrain induction into cells resembling the MGE, as suggested by expression of the transcription factor Nkx2.1. Careful timing of SHH activation then allows for induction of ventral cell fate in these progenitor cells that develop into GABAergic interneurons as opposed to basal forebrain cholinergic neurons (Liu et al., 2013b). In addition to directed differentiation approaches, transcription factor-mediated inductions of interneurons from stem cells have also been described (Chanda et al., 2014; Sun et al., 2016; Yuan et al., 2018). Minimally, transient expression of ASCL1 and DLX2 can convert stem cells into GABAergic interneurons. When injected into the mouse brain, these cells, migrated, integrated, and matured into a variety of interneuronal subtypes, including expression of the mature subtype markers parvalbumin or somatostatin. Further studies, such as single-cell transcriptomic approaches, are needed to characterize the full repertoire of subtypes of interneurons that can be obtained from pluripotent stem cells. Impressive studies have gone on to show that transplanted interneurons were capable of improving memory (Anderson et al., 2018) and in some cases suppressing seizures and abnormal behaviors in an epileptic mouse model (Cunningham et al., 2014). Based on these promising studies, one biotech company, Neurona Therapeutics, is pioneering the clinical uses for interneuron-based cell therapies for epilepsy and neuropathic pain.

Hippocampal neurons

Composed of granule and pyramidal neurons, the hippocampus plays a critical role in learning and memory. It is also an area of the brain that deteriorates in AD, additional forms of dementia, and other age-related cognitive

declines of distinct etiologies. Interestingly, in addition to the subventricular zone, the dentate gyrus of the hippocampus is a unique site of adult neurogenesis (although the absolute rate of neurogenesis remains controversial). Therefore, incorporation of immature stem cell-derived neurons into existing neural circuitry beyond embryonic development is a hopeful prospect.

To generate hippocampal neurons, stem cells are patterned to dorsal forebrain progenitors by inhibiting both branches of the SMAD signaling as well as factors to promote WNT and SHH signaling. Subsequently, WNT3a is applied along with BDNF to drive the neurogenesis of hippocampal granule neurons (Yu et al., 2014; Sakaguchi et al., 2015; Hiragi et al., 2017). Initial findings indicate concurrent WNT and BMP activation can drive the differentiation of the dorsal forebrain progenitors into pyramidal neurons (Sakaguchi et al., 2015). Rodent transplantation studies with hippocampal neural precursors revealed that the human neurons could integrate into the dentate gyrus (Yu et al., 2014), but it remains to be determined if these xenografts can affect disease-related phenotypes in animal models.

Huntington's disease

Huntington's disease (HD) is caused by a CAG trinucleotide repeat expansion within the coding region of the *HTT* gene, resulting in an extended polyglutamine (polyQ) tract within the Huntingtin protein. The progressive loss of neurons and gross atrophy in the neostriatum (caudate nucleus and putamen) disrupts neuronal circuits involving the basal ganglia and leads to gradually worsening motor impairment and, as additional brain regions are affected, significant cognitive and psychiatric symptoms.

Medium spiny neurons

Medium spiny neurons that reside in the striatum, contribute to the complex circuits that control movement and are particularly vulnerable in HD. During development, these inhibitory neurons arise from the lateral ganglionic eminence (LGE) and are marked by the expression of DARPP32 (dopamine- and cAMP-regulated phosphoprotein Mr~32 kDa) (Ejodorova et al., 2015). The relatively specific loss of DARPP32+ medium spiny class of neurons in the neostriatum makes HD a strong candidate for cell replacement therapies. Like for PD, fetal transplants have paved the way for stem cell-derived therapies for HD (Freeman et al., 2000).

Numerous groups have validated directed differentiation approaches for producing medium spiny neurons from stem cells (Aubry et al., 2008; Carri et al., 2012; Ma et al., 2012).

Like the methods for producing other inhibitory neurons from the neighboring MGE, combinatorial SHH/WNT signaling modulation induces an anterior-ventral fate. Of note, reduced activation of SHH signaling and the addition of Activin A can favor a LGE fate while inhibiting a MGE fate (Fjodorova et al., 2015). A direct conversion method has also recently been described for transforming fibroblasts into medium spiny neurons, specifically, with a combination of 4 transcription factors (CTIP2, DLX1, DLX2, and MYT1L) and two microRNAs (miR-9/9 and miR-124) (Victor et al., 2014). Whether these direct programming methods can be applied to pluripotent stem cells remains to be determined but could be used to improve the yield of medium spiny neurons from stem cells, which are at best ~50%. When transplanted into a murine striatum, the neurons integrate into the host circuit and project to the proper anatomical targets. In some cases, the transplanted cells neurons can rescue motor deficits in quinolinic acid, an excitotoxin, striatal-lesioned mice, a model of HD (Carri et al., 2012; Victor et al., 2014). In another study, however, the transplanted cells also resulted in cellular overgrowth (Aubry et al., 2008). Based on these studies, refined purification methods to yield more homogenous neuron populations followed by additional animal model studies seem warranted.

Ataxias

Spinocerebellar ataxias (SCAs) are a clinically and genetically heterogeneous group of neurological disorders associated with impairments in motor coordination due to degeneration of the cerebellum and connected neuronal pathways. Many SCAs are caused by CAG nucleotide repeat expansions within certain genes leading to the production of polyglutamine (polyQ)-containing proteins with putative toxic gain-of-function effects. For instance, an autosomal dominantly-inherited, abnormally long (>33 CAG repeats) trinucleotide repeat expansion within *ATXN-2* results in SCA2 that can manifest with ataxia, loss of neurological reflexes, and Parkinsonian symptoms. Ataxias can be associated with other inherited disorders. For examples, an autosomal recessively-inherited GAA trinucleotide repeat expansions in *FXN*, encoding frataxin, cause Friedrich's ataxia, which is characterized by progressive ataxia, impaired speech, loss of vibratory and proprioceptive sensation due to degeneration of spinal cord neurons and nerve fiber tracts connecting to the cerebellum. There are no effective treatments for these debilitating and often fatal diseases.

Purkinje cells

Purkinje cells are large inhibitory GABAergic neurons with extensive dendritic arbors that reside within the hindbrain

structure of the cerebellum. As the output neurons of the cerebellar cortex, they project to neurons within deep cerebellar nuclei and play an important role in motor coordination. Until recently, the differentiation of human PSCs into Purkinje neurons remained elusive, perhaps due to their late emergence during development. An initial directed differentiation approach for this cell type required several steps and many factors. First, exogenous factors were employed to stimulate endogenous Wnt1 and FGF8 signaling and promote a midbrain/hindbrain identity, and inhibition of SHH signaling was used to pattern cells toward a dorsal identity (Muguruma et al., 2015; Wang et al., 2015a). Then, the maturation process could be accomplished through several methods: plating precursors on mouse cerebellar slice cultures (Watson et al., 2018), within self-organizing, polarized cerebellar structures (Muguruma et al., 2015), or more recently in a defined basal medium optimized for cell culture (Bardy et al., 2015; Silva et al., 2020). Studies indicate that the stem cell-derived Purkinje cells are susceptible to genetic insults, such as the trinucleotide CAG repeat in *CACNA1A* associated with SCA6 (Ishida et al., 2016), that trigger their selective demise, and that they can also engraft into the mouse cerebellum (Wang et al., 2015a). Although more defined and robust methods are needed before cell replacement therapies should be considered clinically, the initial findings have paved the way for producing this neuronal type that is relevant to many neurological disorders.

Motor neuron diseases

The specific loss of motor neurons underlies several devastating neurological diseases including amyotrophic lateral sclerosis (ALS) and spinal muscular atrophy (SMA). Both diseases involve the progressive loss of motor function, eventually progressing to fatal paralysis. In nearly all (~97%) of cases of ALS, motor neurons in both the brain and spinal exhibit pathological changes in the cellular localization of the RNA binding protein TDP-43, which include loss of the normal nuclear localization and the formation of cytoplasmic inclusions (Klim et al., 2021).

Spinal motor neurons

Motor neurons represent a diverse group of neuronal subtypes and provide the pivotal link between mind and the animation of the body. Generally, there are two types of motor neurons; upper motor neurons that reside in the frontal cortex and project to lower motor neurons, found in the ventral brainstem and spinal cord, which in turn form synapses with the musculature. Decades of developmental studies and genetic analyses have illuminated the molecular

underpinnings of lower motor neuron specification during embryo development (Dasen and Jessell, 2009) with the morphological gradients well established (Davis-Dusenbery et al., 2014).

Leveraging this knowledge, stem cell scientists developed methods to generate motor neurons from mouse embryonic stem cells by applying retinoic acid (RA) to caudalize the cells toward a spinal cord (the distal or tail end of the neural tube) identity and activating SHH to ventralize them toward a motor, rather than sensory, identity (Wichterle et al., 2002). Several research groups have advanced these earlier findings to reproducibly convert human pluripotent stem cells into vast quantities of motor neurons (Amoroso et al., 2013; Du et al., 2015; Maury et al., 2015; Klim et al., 2019). These approaches typically rely on neural induction through small molecule dual-SMAD signaling inhibition, in some cases activation of WNT signaling, accelerated neurogenesis through inhibition of FGF or NOTCH signaling, all coupled with MN patterning described above (RA and SHH). Son et al. (2011) have used a large cadre of MN-related transcription factors (Isl1, Ascl1, Myt1l, Brn2, Ngn2, Lhx3, and Neurod1) to directly convert fibroblasts into induced motor neurons. Alternatively, simpler protocols were achieved that used a subset these factors to transform human stem cells into motor neurons (Hester et al., 2011; Goto et al., 2017). Recently, we have also shown that transcription factor-based and small molecule approaches could be combined to yield a highly pure population of cervical-like motor neurons from iPSCs with 100% efficiency through the inducible expression of Ngn2 (neurogenin-2) alone coupled with RA and SHH treatments (Limone et al., 2022). Interestingly, carefully varying the timing of retinoid application has been demonstrated to afford more caudal motor neuron fates (Lippmann et al., 2015), but methodologies for producing upper motor neurons, also known as cortical spinal motor neurons (CSMN), are still lacking. As degeneration of cortical and spinal cord motor regions occur in ALS, a full array of motor neuron subtypes might be needed as a cell replacement therapy.

So far, motor neuron transplant results have been encouraging. For example pioneering transplant studies demonstrate that mES-derived motor neurons injected into tibial nerve of adult mice can form functional NMJs and ameliorate muscle atrophy (Yohn et al., 2008). Another notable study was able to transplant human iPS cell-derived motor neurons into the ventral horns of an SMA mouse model (Corti et al., 2012). The transplanted motor neurons could survive and engraft into the murine spinal cord and could even ameliorate disease phenotypes and extend the life span relative to those receiving a fibroblast transplant (Corti et al., 2012). These exciting initial studies highlight the need for large animal models for testing motor neuron-based cell therapies.

Glial cells

Although glia are more abundant than neurons, nuances remain in our understanding of how their exact cellular identities are established and how glial developmental pathways can be recapitulated *in vitro* for cell replacement approaches. Three main types of glia exist in the CNS: astrocytes, oligodendrocytes (OLs), and microglia. In brief, astrocytes are responsible for forming and modulating the blood–brain barrier (BBB) and modifying the chemical microenvironment governing synaptic function. Microglia are the resident immune cells of the CNS that function in synaptic pruning during development, immune surveillance, debris clearance and defense from pathogens. Oligodendrocytes are responsible for myelinating axons in the CNS, thereby maintaining strong electrical connectivity of brain circuitry. Glia have been implicated in almost all neurodegenerative diseases, and their dysfunction in this context are more extensively reviewed elsewhere (Zheng et al., 2018). Glial transplantation for the treatment of neurodegenerative diseases has been explored much less than for neurons, though might be advantageous for ameliorating glial dysfunction as well as mitigating the loss of degenerating neurons by engaging in supportive roles. Like neurons, glial cells can be generated by activating development




Glial Type	 Astrocyte	 Oligodendrocyte	 Microglia
Disease	AD, ALS	MS, Epilepsy	AD, PD, ALS
Pathological Markers	Loss of neurotrophic support	Impaired myelinating functions	Disease Associated Microglia (DAM)
Differentiation Methods	1–8	12–17	20–28
Transplant Studies	9–11	12, 14, 18–19	29–30

FIGURE 2

Pluripotent stem cell differentiation strategies for producing glial cells. Astrocytes: diff. 1–8 Krencik and Zhang, 2011; Shaltouki et al., 2013; Tcw et al., 2017; Canals et al., 2018; Li et al., 2018; Tchieu et al., 2019; Barbar et al., 2020; transpl. 9–11 Lepore et al., 2008; Song et al., 2017; Baloh et al., 2022. Oligodendrocytes: diff. 12–17 Wang et al., 2013; Douvaras et al., 2014; Douvaras and Fossati, 2015; Ehrlich et al., 2017; García-León et al., 2018; Marton et al., 2019; transpl. 12, 14, 18–19 Wang et al., 2013; Douvaras et al., 2014; Thiruvalluvan et al., 2016; Windrem et al., 2020. Microglia: diff. 20–28 Muffat et al., 2016; Abud et al., 2017; Douvaras et al., 2017; Haenseler et al., 2017; Pandya et al., 2017; Takata et al., 2017; Chen et al., 2021; Limone et al., 2021; Dolan et al., 2022; transpl. 29–30 Svoboda et al., 2019; Xu et al., 2020.

cues or overexpression of cell type-specific transcription factors. We will discuss a selection of strategies to generate glia and their most promising applications to neurodegenerative diseases.

Astrocytes

Astrocytes are star-shaped glial cells that reside in both the brain and spinal cord to maintain BBB integrity, regulate nutrient flow, and govern neuronal function. They arise relatively early in neuronal development from radial glial progenitor cells usually after these cells have generated neurons. Broadly, differentiation protocols recapitulate developmental cues (Krencik et al., 2011; Shaltouki et al., 2013) by promoting neuronal stem cell (NSC) identity via dual SMAD inhibition and then gliogenesis with morphogens (Krencik and Zhang, 2011). Promoting gliogenesis after NSC differentiation has traditionally been a slow rate-limiting step in the generation of astrocytes, but recent transgenic and chemical strategies have greatly accelerated this process. Expansion of NSCs with Activin A, Heregulin 1 β (Neuregulin1), and IGFI (Shaltouki et al., 2013; Tcw et al., 2017), flow cytometry-based enrichment strategies (Barbar et al., 2020) or overexpression of TFs NFIA and SOX9 can dramatically shorten differentiation protocols (Canals et al., 2018; Tchieu et al., 2019). hPSC-derived astrocyte-like cells can be generated in as little as 30 days and show functional properties similar to primary astrocytes in that they uptake glutamate, promote neurite outgrowth, propagate calcium waves, and retain their identity *in vivo* (Krencik and Zhang, 2011; Shaltouki et al., 2013; Li et al., 2018). Many groups have recently developed methods to increase maturity and function of these cells by differentiating them from 3D structures coupled with cell sorting methods (Barbar et al., 2020).

Studies on ALS and PD animal models are laying the foundation for astrocyte transplantation therapies. In ALS models, astrocytes exert toxic gain-of-function effects that can act in a cell non-autonomous manner to contribute to motor neuron degeneration (Di Giorgio et al., 2007, 2008; Meyer et al., 2014; Hall et al., 2017). For instance, mice expressing human mutant SOD1 in astrocytes in addition to neurons had reduced to survival compared to mice only expressing mutant SOD1 in neurons, in other words, a wild-type astrocyte microenvironment may promote motor neuron survival (Bataveljić et al., 2012). Focal transplantation of glial-restricted NPCs (Neuronal Progenitor Cells) into the cervical spinal cord of SOD1 transgenic rats during disease progression extended survival and decreased motor neuron death, in part due to the partial rescue of GLT1 expression in astrocytes (Clement et al., 2003). Clinical trials are ongoing to prove the efficacy of transplanted PSC-derived astrocytes to boost neuronal survival and slow disease progression. For instance, a phase 1/2a trial in a small cohort of ALS patients

(NCT02943850) has shown that a single injection of human NPCs engineered to produce glial cell line-derived neurotrophic factor (GDNF) into the spinal cord is safe, and viable grafts differentiated into astrocytes that may be neuroprotective through increased GDNF production (Baloh et al., 2022).

Transplantation studies for PD also showed promising results. Co-transplantation of primary fetal NPCs and rat astrocytes increased long-term engraftment of mature midbrain dopaminergic neurons and increase anti-inflammatory markers in the brains of PD rats (Lepore et al., 2008). Transplantation of primary astrocytes into the SNpc increase synaptosomal dopamine uptake in the striatum, reduce ROS stress, and improved motor deficits of pharmacologically-induced PD rats (Song et al., 2017). These observations suggest hPSC-derived astrocytes may be used to slow disease progression and complement dopaminergic neuron transplantation.

Oligodendrocytes

Similar to astrocytes, oligodendrocytes are derived in development after neurogenesis. In both the forebrain and the spinal cord, oligodendroglial progenitor cells (OPCs) are generated from Nkx2.1⁺, SHH-derived progenitors and their differentiation is regulated by TFs Olig1 and Olig2. OPCs have an immense ability to migrate and populate the entire brain and spinal cord where most of them further differentiate into committed, myelinating oligodendrocytes (OLs) while a small subset of them are maintained in a progenitor state. Their great migratory abilities, plasticity and pivotal role in neuronal support render these cells ideal for transplantation studies and replacement therapies.

To generate OLs, hPSCs are first converted to a neural stem cell with small molecules or a neural epithelial identity through SHH activation and are then pushed toward an oligodendrocyte progenitors (OPCs) identity by the addition of PDGF-AA. These OPCs can be matured into OLs by various cocktails of small molecules, often containing IGF-1 and T3 (Wang et al., 2013; Douvaras et al., 2014; Douvaras and Fossati, 2015). Several groups have shown that complete maturation of OPCs into highly myelinating oligodendrocytes can be achieved either by injecting these cells *in vivo* (Douvaras et al., 2014) or by differentiating these cells in 3D structures (Marton et al., 2019). Protocols relying on overexpression of several transcription factors, including OLIG2, NKX6.2, and SOX10, were developed to be faster and similarly efficient (Ehrlich et al., 2017; García-León et al., 2018). García-León et al. (2018) found, however, that overexpression of SOX10 alone in NSCs was the most efficient at generating OLs in as little as 20 days, and the generated OLs were capable of myelinating cortical neurons both *in vitro* and *in vivo*.

Stem cell-derived OLs hold promise for both demyelinating diseases and spinal cord injury. Multiple sclerosis (MS) is

a chronic, autoimmune disease characterized by the loss of myelin and associated oligodendrocytes, often in a remitting and relapsing clinical course that results in gradual neurological decline. MS-iPSC-derived OPCs can myelinate the corpus callosum of immunocompromised hypomyelinated (shiver) mice (Wang et al., 2013; Douvaras et al., 2014), offering a potential regenerative route for re-myelination for cases of MS that are resistant to immune-suppressant treatment. Strikingly, human iPSC-derived OPCs can myelinate axons in a non-human primate marmoset model (Thiruvalluvan et al., 2016). Long term transplantation studies in both shiver mice and demyelinating cuprizone treatment also showed that these cells can not only migrate to distal regions of the CNS farther than previously believed but can also improve behavior and motor function in murine models (Windrem et al., 2020). These results highlight the feasibility of an iPSC-derived OL transplantation therapy for MS and perhaps for other demyelinating diseases.

Microglia

Unlike other glial cells, microglia are immune cells not derived from the neuroectoderm but originate from the embryonic yolk sac in early stages of development and then migrate to the neural tube (Ginhoux et al., 2010; Kierdorf et al., 2013). Chemical differentiation strategies generally generate early myeloid progenitors by isolation of delaminating cells from so-called yolk-sac embryoid bodies (Muffat et al., 2016; Haenseler et al., 2017) or by promoting hematopoiesis with hypoxic conditions and defined medias (Abud et al., 2017). Initial studies used co-cultures of these immature myeloid cells with human neurons or murine brain extracts to generate resident brain-like microglia (Takata et al., 2017). These protocols made scalability challenging so others have devised ways to further push immature myeloid progenitors toward microglia-like cells (MGLs) with defined medias containing M-CSF to generate myeloid cells coupled with CNS-enriched TGF-beta and CNS-specific, CSF1-receptor ligand IL34 to promote a brain-like specification of these myeloid progenitors. Generated MGLs show competence to phagocytose (Muffat et al., 2016; Abud et al., 2017; Douvaras et al., 2017; Haenseler et al., 2017; Pandya et al., 2017; Limone et al., 2021; Dolan et al., 2022) respond to IFN- γ and LPS stimulation via secretion of pro-inflammatory cytokines (Muffat et al., 2016; Abud et al., 2017), and migrate to sites of injury (Muffat et al., 2016). When co-cultured with neurons, MGLs have also been observed to secrete anti-inflammatory and pro-modeling cytokines (Haenseler et al., 2017). Like for other glial cells, transcription factor-based protocols may offer increased efficiency and decreased time for the generation of microglial-like cells. One study has shown that overexpression

of transcription factors CEBPA and PU.1 coupled with CNS-patterning molecules described above can generate Microglia-like cells from human iPSC (Chen et al., 2021) with a second one showing improved efficiency by overexpressing PU.1 from primitive hematopoietic progenitors (Sonn et al., 2022). A recent study has defined a set of six transcription factors for the generation of microglia-like cells at a scale sufficient for genetic screening (Drager et al., 2022). Following the progress in the derivation of specific neuronal populations, it is plausible that newer approaches might find that just a few transcriptional factors could be sufficient, when coupled with small molecules, for the generation of this cell type.

Long term engraftment studies have been rendered difficult by the lack of homology between murine and human CSF1, which is pivotal for long term microglial survival. However, initial studies have shown the feasibility of transplantation of hiPSC-derived iMGLs in humanized mouse models (Svoboda et al., 2019; Xu et al., 2020).

Technological advances

Directed differentiation approaches have evolved considerably since the initial derivation of neurons from human embryonic stem cells (Zhang et al., 2001). Although defined culture conditions that primarily employ small molecules instead of poorly defined co-culture systems are more robust, modern directed differentiation approaches still tend to yield highly heterogeneous cultures containing the cell type of interest along with developmentally related cells. Direct conversion strategies like the ones described above typically yield more homogenous cell populations, but viral integration could disrupt normal gene expression and thus might not be amenable to clinical applications. Alternatively, the use of cell surface antibodies for sorting different neural populations has been pioneered to enrich for more defined cell populations (Yuan et al., 2011), or dyes that are selectively taken up by specific cells could theoretically also be used to mark specific cell types as has been demonstrated for neural precursor cells (Yun et al., 2012). These advances have led to several of these differentiation protocols being used for modeling neurodegeneration in different cell types *in vitro* (Giacomelli et al., 2022), opening the door to their adaptation to transplantation studies in the future. Additionally, several groups have made significant progress in the development of protocols for the generation of 3D structures containing various CNS cell types (known as brain organoids) that can enhance cell type specification and maturation (Del Dosso et al., 2020). Whether this technology can be translated into reproducible, manufacturable products for transplantation studies remains unclear, though it does offer a myriad of intriguing possibilities for the field.

It is unclear whether nascent, immature neurons or elaborate, mature neurons will integrate more successfully into a degenerating brain to provide therapeutic benefit. Either way, the ability to control the functional maturation of stem cell-derived neurons would benefit many applications. For *in vitro* disease modeling studies, we have found that co-culture of human neurons with murine glial cells effectively increased neuronal activity, but co-culture with non-human cells is not an ideal strategy for cell replacement therapies. Instead, Gage and colleagues have developed a defined neuronal medium, BrainPhys, which better mimics the environment present in healthy human brains and enhances both spontaneous electrical and synaptic activity of human neurons (Bardy et al., 2015). Whether increased activity translates into increased survival after transplantation remains an unanswered but fascinating question.

The process of reprogramming adult cells back to the pluripotent state erases many aspects of aging that put vulnerable cells at risk in the first place (Mertens et al., 2018). Although resetting the biological clock makes disease modeling more challenging, it might rid the newly derived cells from the neurodegenerative stimuli of aging when transplanted. Still, there might be aspects of maturation that are critical for neuronal integration or function. Unlike stem cell-derived neurons, for example, neurons directly converted from adult fibroblasts capture the faithful expression of all tau isoforms detected in adult brains at the proper ratios (Capano et al., 2022). Direct conversion of adult cells to replace lost neurons might therefore be an alternative technology to consider and has even been shown to reverse symptoms of PD in a rodent model by converting midbrain astrocytes to dopaminergic neurons (Qian et al., 2020).

Limitations and challenges

Induced pluripotent stem cell technology marshaled in the possibility of personalized regenerative medicine using therapies based on an individual's own cells. To this end, investigators in Japan started a clinical trial to treat age-related macular degeneration using autologous transplants, however, the trial was eventually suspended after treating one patient (Mandai et al., 2017). Several hurdles generate significant headwinds for this type of approach including (1) the time and effort needed to generate iPS cells, (2) genomic instability of pluripotent stem cells, and (3) the cost of personalized therapeutics. Most of these hurdles have several potential solutions that we will describe here briefly.

Despite recent advances, the overall time to move from the collection of fibroblasts via skin biopsy in the clinic, the reprogramming of fibroblasts into PSCs with completion of appropriate quality controls, to the differentiation of individualized stem cells into a personal population of a

specific cell type, such as mature motor neurons, remains extensive, and hence possibly beyond the therapeutic window for rapidly progressive neurodegenerative diseases like ALS. To meet the demands of future clinical applications, state-of-the-art technologies for the cryopreservation of differentiated cell types are being tested to provide a ready to go off-the-shelf product (Holm et al., 2010; Nishiyama et al., 2016). Indeed, this approach is being pioneered within the PD cell replacement field, which has demonstrated that cryopreserved iPSC-derived neurons can maintain high viability and the molecular properties of a dopaminergic neuron. Moreover, these cryopreserved cells can be directly transplanted into a rat model of PD to reverse functional deficits (Wakeman et al., 2017).

For cell replacement therapies, even rare proliferating cells are especially worrisome because they could ultimately lead to the growth of tumors. Moreover, genomic instability of pluripotent stem cells has long been a concern for the field as aneuploid cells have readily been observed (Draper et al., 2004). To identify more subtle genetic changes, groups have performed whole-exome sequencing on many of the hES cell lines listed on the US National Institutes of Health registry and reported the acquisition of dominant negative p53 mutations, a mutation associated with many cancers, for several hES cell lines (Merkle et al., 2017), and other genomic changes associated with cancer and tumorigenesis (Merkle et al., 2022). Similar studies have also identified recurrent mutations that can occur during the reprogramming process and subsequent propagation (Pera, 2011). Therefore, thoughtful genetic characterization should be standard before stem cells or any of their derivatives are used in the clinic. This analysis will not only be useful to rule out stem cell lines with potentially dangerous mutations but could also be used after transplant to retrospectively identify the distribution of the donor cells.

To overcome the laborious nature of converting somatic cells into pluripotent stem cells, the New York Stem Cell Foundation has developed an automated platform for the high throughput conversion of skin biopsies into iPS cells (Paull et al., 2015). This high throughput platform can be used in conjunction with synthetic modified RNA to reprogram cells and avoid viral transduction (Warren et al., 2010). Finally, xenofree culture conditions have been developed and are now commercially available for deriving and propagating human pluripotent stem cells (Klim et al., 2010; Chen et al., 2011). Collectively, these innovations will help expedite the large-scale generation of clinical grade iPS cells.

Finally, widely applicable and efficient cell banking methods are needed to meet the demand of cell transplantation therapies. There are ongoing efforts in both Japan and the United States to screen and bank cells for allogeneic transplantations. Estimates from Cellular Dynamics International suggest that top 183 haplotypes could cover 95% of the US population. To gain maximum population coverage and provide social justice (Ellison, 2016), a universal stem cell donor could be part of the

banking effort. This tactic proposes to use genetic engineering to reduce immunogenicity by removing the MHC molecules from the surface of the cells while also introducing well-established tolerance-inducing molecules (Riolobos et al., 2013; Han et al., 2019). Ultimately, stem cell banking will facilitate regenerative therapies by providing a common and less costly off-the-shelf cellular materials that can be thoroughly characterized before regular and repeated clinical use.

Concluding remarks

It's an incredibly exciting time for stem cell-based regenerative medicine with a number of clinical trials started and more just on the horizon for neurodegenerative diseases, including one for PD (Kimbrel and Lanza, 2015). The International Society for Stem Cell Research (ISSCR) has established an updated set of guidelines (Daley et al., 2016) for the clinical translation of stem cell research to ensure safety and appropriate rigor while avoiding the real and present dangers of unregulated stem cell therapies (Berkowitz et al., 2016).

The demand for neurodegenerative disease therapeutics continues to grow as populations around the globe age. Currently, no pharmacological strategies exist that can significantly alter disease course for neurodegenerative diseases, thus cell replacement therapies remain an attractive avenue of exploration. Although the prospect of using stem cell-derived neurons to treat many of the diseases discussed above remains abstract, the PD clinical trials, grounded on years of fetal transplant studies and animal models with high fidelity, will provide important guideposts as others venture into these uncharted territories. In this review, we highlighted current methodologies for generating therapeutically relevant neuronal and glial cell types. Although directed differentiation strategies for some of these CNS cell types are in their nascent stage, they represent important first steps toward heralding in a new era of cellular therapeutics.

References

- Abud, E. M., Ramirez, R. N., Martinez, E. S., Healy, L. M., Nguyen, C. H. H., Newman, S. A., et al. (2017). iPSC-Derived human microglia-like cells to study neurological diseases. *Neuron* 94, 278–293. doi: 10.1016/j.neuron.2017.03.042
- Amoroso, M. W., Croft, G. F., Williams, D. J., O'Keeffe, S., Carrasco, M. A., Davis, A. R., et al. (2013). Accelerated high-yield generation of limb-innervating motor neurons from human stem cells. *J. Neurosci.* 33, 574–586. doi: 10.1523/jneurosci.0906-12.2013
- Anderson, N. C., Zandt, M. A. V., Shrestha, S., Lawrence, D. B., Gupta, J., Chen, C. Y., et al. (2018). Pluripotent stem cell-derived interneuron progenitors mature and restore memory deficits but do not suppress seizures in the epileptic mouse brain. *Stem Cell Res.* 33, 83–94. doi: 10.1016/j.scr.2018.10.007
- Arenas, E., Denham, M., and Villaescusa, J. C. (2015). How to make a midbrain dopaminergic neuron. *Development* 142, 1918–1936. doi: 10.1242/dev.097394
- Aubry, L., Bugi, A., Lefort, N., Rousseau, F., Peschanski, M., and Perrier, A. L. (2008). Striatal progenitors derived from human ES cells mature into DARPP32 neurons in vitro and in quinolinic acid-lesioned rats. *Proc. Natl. Acad. Sci. U. S. A.* 105, 16707–16712. doi: 10.1073/pnas.0808488105
- Baloh, R. H., Johnson, J. P., Avalos, P., Allred, P., Svendsen, S., Gowing, G., et al. (2022). Transplantation of human neural progenitor cells secreting GDNF into the spinal cord of patients with ALS: a phase 1/2a trial. *Nat. Med.* 28, 1813–1822. doi: 10.1038/s41591-022-01956-3

Author contributions

JK conceived of the review and drafted the figures. DM drafted the table. All authors drafted the original manuscript and read, edited, and approved the submitted version.

Acknowledgments

We would like to thank Katrina M. Wilbur and Renate G. E. Hellmiss from Harvard's MCB Graphics for their graphic design skills in preparing the figures, and Andrew Castillo for assisting in researching glial-related topics. DM acknowledges support from the NINDS (K08NS104270).

Conflict of interest

JK is an employee of Faze Medicines and a shareholder of Faze Medicines as well as QurAlis, and is an author on patent that describes surfaces for the long-term culture of pluripotent cells (US patent 8648170). JK and FL are authors on a patent application that describes methods and compositions for restoring STMN2 levels (US patent application 20220133848). DM is an author on a pending patent that describes compounds and methods for treating neurodegenerative diseases (WO2020107037).

Publisher's note

All claims expressed in this article are solely those of the authors and do not necessarily represent those of their affiliated organizations, or those of the publisher, the editors and the reviewers. Any product that may be evaluated in this article, or claim that may be made by its manufacturer, is not guaranteed or endorsed by the publisher.

- Barbar, L., Jain, T., Zimmer, M., Sadick, J. S., Wang, M., et al. (2020). CD49f Is a novel marker of functional and reactive human iPSC-derived astrocytes. *Neuron* 107, 436–453. doi: 10.1016/j.neuron.2020.05.014
- Bardy, C., van den Hurk, M., Eames, T., Marchand, C., Hernandez, R. V., Kellogg, M., et al. (2015). Neuronal medium that supports basic synaptic functions and activity of human neurons in vitro. *Proc. Natl. Acad. Sci. U.S.A.* 112, E2725–E2734. doi: 10.1073/pnas.1504393112
- Barker, R. A., Parmar, M., Studer, L., and Takahashi, J. (2017). Human trials of stem cell-derived dopamine neurons for Parkinson's Disease: Dawn of a New Era. *Cell Stem Cell* 21, 569–573. doi: 10.1016/j.stem.2017.09.014
- Bataveljić, D., Nikolić, L., Milosević, M., Todorović, N., and Andjus, P. R. (2012). Changes in the astrocytic aquaporin-4 and inwardly rectifying potassium channel expression in the brain of the amyotrophic lateral sclerosis SOD1 G93A rat model. *Glia* 60, 1991–2003. doi: 10.1002/glia.22414
- Bekkers, J. M. (2011). Pyramidal neurons. *Curr. Biol.* 21, R975. doi: 10.1016/j.cub.2011.10.037
- Berkowitz, A. L., Miller, M. B., Mir, S. A., Cagney, D., Chavakula, V., Guleria, I., et al. (2016). Glioproliferative lesion of the spinal cord as a complication of “stem-cell tourism”. *N. Engl. J. Med.* 375, 196–198. doi: 10.1056/nejmc1600188
- Bissonnette, C. J., Lyass, L., Bhattacharyya, B. J., Belmadani, A., Miller, R. J., and Kessler, J. A. (2011). The controlled generation of functional basal forebrain cholinergic neurons from human embryonic stem cells. *Stem Cells* 29, 802–811. doi: 10.1002/stem.626
- Cai, J., Donaldson, A., Yang, M., German, M. S., Enikolopov, G., and Iacovitti, L. (2009). The role of mx1a in the differentiation of human embryonic stem cells into midbrain dopamine neurons in culture and after transplantation into a Parkinson's Disease Model. *Stem Cells* 27, 220–229. doi: 10.1634/stemcells.2008-0734
- Caiazzo, M., Dell'Anno, M. T., Dvoretzskova, E., Lazarevic, D., Taverna, S., Leo, D., et al. (2011). Direct generation of functional dopaminergic neurons from mouse and human fibroblasts. *Nature* 476, 224–227. doi: 10.1038/nature10284
- Canals, I., Ginisty, A., Quist, E., Timmerman, R., Fritze, J., Miskinyte, G., et al. (2018). Rapid and efficient induction of functional astrocytes from human pluripotent stem cells. *Nat. Methods* 15, 693–696. doi: 10.1038/s41592-018-0103-2
- Cao, S.-Y., Hu, Y., Chen, C., Yuan, F., Xu, M., Li, Q., et al. (2017). Enhanced derivation of human pluripotent stem cell-derived cortical glutamatergic neurons by a small molecule. *Sci. Rep.* 7:3282. doi: 10.1038/s41598-017-03519-w
- Capano, L. S., Sato, C., Ficulie, E., Yu, A., Horie, K., Kwon, J. S., et al. (2022). Recapitulation of endogenous 4R tau expression and formation of insoluble tau in directly reprogrammed human neurons. *Cell Stem Cell* 29, 918–932 e918. doi: 10.1016/j.stem.2022.04.018
- Carlsson, T., Carta, M., Muñoz, A., Mattsson, B., Winkler, C., Kirik, D., et al. (2009). Impact of grafted serotonin and dopamine neurons on development of L-DOPA-induced dyskinesias in parkinsonian rats is determined by the extent of dopamine neuron degeneration. *Brain* 132, 319–335. doi: 10.1093/brain/awn305
- Carri, A. D., Onorati, M., Lelos, M. J., Castiglioni, V., Faedo, A., Menon, R., et al. (2012). Developmentally coordinated extrinsic signals drive human pluripotent stem cell differentiation toward authentic DARPP-32+ medium-sized spiny neurons. *Development* 140, 301–312. doi: 10.1242/dev.084608
- Chanda, S., Ang, C. E., Davila, J., Pak, C., Mall, M., Lee, Q. Y., et al. (2014). Generation of induced neuronal cells by the single reprogramming factor ASCL1. *Stem Cell Rep.* 3, 282–296. doi: 10.1016/j.stemcr.2014.05.020
- Chen, G., Gulbranson, D. R., Hou, Z., Bolin, J. M., Ruotti, V., Probasco, M. D., et al. (2011). Chemically defined conditions for human iPSC derivation and culture. *Nat. Methods* 8, 424–429. doi: 10.1038/nmeth.1593
- Chen, S.-W., Hung, Y.-S., Fuh, J.-L., Chen, N.-J., Chu, Y.-S., Chen, S.-C., et al. (2021). Efficient conversion of human induced pluripotent stem cells into microglia by defined transcription factors. *Stem Cell Rep.* 16, 1363–1380. doi: 10.1016/j.stemcr.2021.03.010
- Clement, A. M., Nguyen, M. D., Roberts, E. A., Garcia, M. L., Boilleie, S., Rule, M., et al. (2003). Wild-type nonneuronal cells extend survival of SOD1 mutant motor neurons in ALS Mice. *Science* 302, 113–117. doi: 10.1126/science.1086071
- Corti, S., Nizzardo, M., Simone, C., Falcone, M., Nardini, M., Ronchi, D., et al. (2012). Genetic correction of human induced pluripotent stem cells from patients with spinal muscular atrophy. *Sci. Transl. Med.* 4:165ra162. doi: 10.1126/scitranslmed.3004108
- Cunningham, M., Cho, J.-H., Leung, A., Savvidis, G., Ahn, S., Moon, M., et al. (2014). hPSC-Derived maturing GABAergic interneurons ameliorate seizures and abnormal behavior in epileptic mice. *Cell Stem Cell* 15, 559–573. doi: 10.1016/j.stem.2014.10.006
- Daley, G. Q., Hyun, I., Apperley, J. F., Barker, R. A., Benvenisty, N., and Bredenoord, A. L. (2016). Setting global standards for stem cell research and clinical translation: The 2016 ISSCR Guidelines. *Stem Cell Rep.* 6, 787–797. doi: 10.1016/j.stemcr.2016.05.001
- Dasen, J. S., and Jessell, T. M. (2009). Hox networks and the origins of motor neuron diversity. *Curr. Topics Dev. Biol.* 88, 169–200. doi: 10.1016/s0070-2153(09)88006-x
- Davis-Dusenbery, B. N., Williams, L. A., Klim, J. R., and Eggan, K. (2014). How to make spinal motor neurons. *Development* 141, 491–501. doi: 10.1242/dev.097410
- Del Dosso, A., Urenda, J. P., Nguyen, T., and Quadrato, G. (2020). Upgrading the physiological relevance of human brain organoids. *Neuron* 107, 1014–1028. doi: 10.1016/j.neuron.2020.08.029
- Di Giorgio, F. P., Boulting, G. L., Bobrowicz, S., and Eggan, K. C. (2008). Human embryonic stem cell-derived motor neurons are sensitive to the toxic effect of glial cells carrying an ALS-causing mutation. *Cell Stem Cell* 3, 637–648. doi: 10.1016/j.stem.2008.09.017
- Di Giorgio, F. P., Carrasco, M. A., Siao, M. C., Maniatis, T., and Eggan, K. (2007). Non-cell autonomous effect of glia on motor neurons in an embryonic stem cell-based ALS model. *Nat. Neurosci.* 10, 608–614. doi: 10.1038/nn1885
- Dolan, M. J., Therrien, M., Jereb, S., Kamath, T., Atkinson, T., Marsh, S., et al. (2022). A resource for generating and manipulating human microglial states in vitro. *bioRxiv*[Preprint] doi: 10.1101/2022.05.02.490100
- Douvaras, P., and Fossati, V. (2015). Generation and isolation of oligodendrocyte progenitor cells from human pluripotent stem cells. *Nat. Protoc.* 10, 1143–1154. doi: 10.1038/nprot.2015.075
- Douvaras, P., Sun, B., Wang, M., Kruglikov, I., Lallós, G., Zimmer, M., et al. (2017). Directed Differentiation of human pluripotent stem cells to microglia. *Stem Cell Rep.* 8, 1516–1524. doi: 10.1016/j.stemcr.2017.04.023
- Douvaras, P., Wang, J., Zimmer, M., Hanchuk, S., O'Bara, M. A., Sadiq, S., et al. (2014). Efficient generation of myelinating oligodendrocytes from primary progressive multiple sclerosis patients by induced pluripotent stem cells. *Stem Cell Rep.* 3, 250–259. doi: 10.1016/j.stemcr.2014.06.012
- Drager, N. M., Sattler, S. M., Huang, C. T., Teter, O. M., Leng, K., Hashemi, S. H., et al. (2022). A CRISPRi/a platform in human iPSC-derived microglia uncovers regulators of disease states. *Nat. Neurosci.* 25, 1149–1162. doi: 10.1038/s41593-022-01131-4
- Draper, J. S., Smith, K., Gokhale, P., Moore, H. D., Maltby, E., Johnson, J., et al. (2004). Recurrent gain of chromosomes 17q and 12 in cultured human embryonic stem cells. *Nat. Biotechnol.* 22, 53–54. doi: 10.1038/nbt922
- Du, Z.-W., Chen, H., Liu, H., Lu, J., Qian, K., Huang, C.-L., et al. (2015). Generation and expansion of highly pure motor neuron progenitors from human pluripotent stem cells. *Nat. Commun.* 6:6626. doi: 10.1038/ncomms7626
- Ehrlich, M., Mozafari, S., Glatza, M., Starost, L., Velychko, S., Hallmann, A.-L., et al. (2017). Rapid and efficient generation of oligodendrocytes from human induced pluripotent stem cells using transcription factors. *Proc. Natl. Acad. Sci. U. S. A.* 114, E2243–E2252. doi: 10.1073/pnas.1614412114
- Ellison, B. (2016). Stem Cell Research and Social Justice: Aligning Scientific Progress with Social Need. *Current Stem Cell Rep.* 2, 328–335. doi: 10.1007/s40778-016-0063-3
- Espuny-Camacho, I., Arranz, A. M., Fiers, M., Snellinx, A., Ando, K., Munck, S., et al. (2017). Hallmarks of Alzheimer's Disease in stem-cell-derived human neurons transplanted into mouse brain. *Neuron* 93, 1066–1081.e1068. doi: 10.1016/j.neuron.2017.02.001
- Espuny-Camacho, I., Michelsen, K. A., Gall, D., Linaro, D., Hasche, A., Bonnefont, J., et al. (2013). Pyramidal neurons derived from human pluripotent stem cells integrate efficiently into mouse brain circuits in vivo. *Neuron* 77, 440–456. doi: 10.1016/j.neuron.2012.12.011
- Fjodorova, M., Noakes, Z., and Li, M. (2015). How to make striatal projection neurons. *Neurogenesis* 2:e1100227. doi: 10.1080/23262133.2015.1100227
- Freeman, T. B., Cicchetti, F., Hauser, R. A., Deacon, T. W., Li, X.-J., Hersch, S. M., et al. (2000). Transplanted fetal striatum in Huntington's disease: Phenotypic development and lack of pathology. *Proc. Natl. Acad. Sci. U. S. A.* 97, 13877–13882. doi: 10.1073/pnas.97.25.13877
- Gage, F. H., and Temple, S. (2013). Neural stem cells: Generating and regenerating the brain. *Neuron* 80, 588–601. doi: 10.1016/j.neuron.2013.10.037
- García-León, J. A., Kumar, M., Boon, R., Chau, D., One, J., Wolfs, E., et al. (2018). SOX10 Single transcription factor-based fast and efficient generation of oligodendrocytes from human pluripotent stem cells. *Stem Cell Rep.* 10, 655–672. doi: 10.1016/j.stemcr.2017.12.014
- Giacomelli, E., Vahsen, B. F., Calder, E. L., Xu, Y., Scaber, J., Gray, E., et al. (2022). Human stem cell models of neurodegeneration: From basic science of

- amyotrophic lateral sclerosis to clinical translation. *Cell Stem Cell* 29, 11–35. doi: 10.1016/j.stem.2021.12.008
- Ginhoux, F., Greter, M., Leboeuf, M., Nandi, S., See, P., Gokhan, S., et al. (2010). Fate mapping analysis reveals that adult microglia derive from primitive macrophages. *Science* 330, 841–845. doi: 10.1126/science.1194637
- Goto, K., Imamura, K., Komatsu, K., Mitani, K., Aiba, K., Nakatsuji, N., et al. (2017). Simple derivation of spinal motor neurons from escs/ipscs using sendai virus vectors. *Mol. Ther. Methods Clin. Dev.* 4, 115–125. doi: 10.1016/j.omtm.2016.12.007
- Grealish, S., Diguett, E., Kirkeby, A., Mattsson, B., Heuer, A., Bramoulle, Y., et al. (2014). Human ESC-derived dopamine neurons show similar preclinical efficacy and potency to fetal neurons when grafted in a rat model of Parkinson's Disease. *Cell Stem Cell* 15, 653–665. doi: 10.1016/j.stem.2014.09.017
- Haenseler, W., Sansom, S. N., Buchrieser, J., Newey, S. E., Moore, C. S., Nicholls, F. J., et al. (2017). A Highly efficient human pluripotent stem cell microglia model displays a neuronal-co-culture-specific expression profile and inflammatory response. *Stem Cell Rep.* 8, 1727–1742. doi: 10.1016/j.stemcr.2017.05.017
- Hall, C. E., Yao, Z., Choi, M., Tyzack, G. E., Serio, A., Luisier, R., et al. (2017). Progressive motor neuron pathology and the role of astrocytes in a human stem cell model of VCP-Related ALS. *Cell Rep.* 19, 1739–1749. doi: 10.1016/j.celrep.2017.05.024
- Hallett, P. J., Cooper, O., Sadi, D., Robertson, H., Mendez, I., and Isacson, O. (2014). Long-Term health of dopaminergic neuron transplants in Parkinson's Disease Patients. *Cell Rep.* 7, 1755–1761. doi: 10.1016/j.celrep.2014.05.027
- Han, X., Wang, M., Duan, S., Franco, P. J., Kenty, J. H.-R., Hedrick, P., et al. (2019). Generation of hypoinmunogenic human pluripotent stem cells. *Proc. Natl. Acad. Sci. U. S. A.* 116, 10441–10446. doi: 10.1073/pnas.1902566116
- Hester, M. E., Murtha, M. J., Song, S., Rao, M., Miranda, C. J., Meyer, K., et al. (2011). Rapid and efficient generation of functional motor neurons from human pluripotent stem cells using gene delivered transcription factor codes. *Mol. Ther.* 19, 1905–1912. doi: 10.1038/mt.2011.135
- Higuera, G. A., Iaffaldano, G., Bedar, M., Shpak, G., Broersen, R., Munshi, S. T., et al. (2017). An expandable embryonic stem cell-derived Purkinje neuron progenitor population that exhibits in vivo maturation in the adult mouse cerebellum. *Sci. Rep.* 7, 8863. doi: 10.1038/s41598-017-09348-1
- Hiragi, T., Andoh, M., Araki, T., Shirakawa, T., Ono, T., Koyama, R., et al. (2017). Differentiation of human induced pluripotent stem cell (hiPSC)-derived neurons in mouse hippocampal slice cultures. *Front. Cell. Neurosci.* 11:143. doi: 10.3389/fncel.2017.00143
- Holm, F., Ström, S., Inzunza, J., Baker, D., Strömberg, A.-M., Rozell, B., et al. (2010). An effective serum- and xeno-free chemically defined freezing procedure for human embryonic and induced pluripotent stem cells. *Hum. Reprod.* 25, 1271–1279. doi: 10.1093/humrep/deq040
- Hu, Y., Qu, Z.-Y., Cao, S.-Y., Li, Q., Ma, L., Krencik, R., et al. (2016). Directed differentiation of basal forebrain cholinergic neurons from human pluripotent stem cells. *J. Neurosci. Methods* 266, 42–49. doi: 10.1016/j.jneumeth.2016.03.017
- Ishida, Y., Kawakami, H., Kitajima, H., Nishiyama, A., Sasai, Y., Inoue, H., et al. (2016). Vulnerability of purkinje cells generated from spinocerebellar ataxia type 6 patient-derived iPSCs. *Cell Rep.* 17, 1482–1490. doi: 10.1016/j.celrep.2016.10.026
- Kierdorf, K., Erny, D., Goldmann, T., Sander, V., Schulz, C., Perdiguer, E. G., et al. (2013). Microglia emerge from erythromyeloid precursors via Pu.1- and Irf8-dependent pathways. *Nat. Neurosci.* 16, 273–280. doi: 10.1038/nn.3318
- Kikuchi, T., Morizane, A., Doi, D., Magotani, H., Onoe, H., Hayashi, T., et al. (2017). Human iPS cell-derived dopaminergic neurons function in a primate Parkinson's disease model. *Nature* 548, 592–596. doi: 10.1038/nature23664
- Kim, T. W., Koo, S. Y., and Studer, L. (2020). Pluripotent stem cell therapies for Parkinson Disease: Present challenges and future opportunities. *Front. Cell Dev. Biol.* 8:729. doi: 10.3389/fcell.2020.00729
- Kim, T. W., Piao, J., Koo, S. Y., Kriks, S., Chung, S. Y., Betel, D., et al. (2021). Biphasic Activation of WNT Signaling Facilitates the Derivation of Midbrain Dopamine Neurons from hESCs for Translational Use. *Cell Stem Cell* 28, 343–355. doi: 10.1016/j.stem.2021.01.005
- Kimbrel, E. A., and Lanza, R. (2015). Current status of pluripotent stem cells: moving the first therapies to the clinic. *Nat. Rev. Drug Discov.* 14, 681–692. doi: 10.1038/nrd4738
- Kirwan, P., Jura, M., and Merkle, F. T. (2017). Generation and Characterization of Functional Human Hypothalamic Neurons. *Curr. Protoc. Neurosci.* 81, 33331–33324. doi: 10.1002/cpns.40
- Klim, J. R., Li, L., Wrighton, P. J., Piekarczyk, M. S., and Kiessling, L. L. (2010). A defined glycosaminoglycan-binding substratum for human pluripotent stem cells. *Nat. Methods* 7, 989–994. doi: 10.1038/nmeth.1532
- Klim, J. R., Pintacuda, G., Nash, L. A., Guerra San Juan, I., and Eggan, K. (2021). Connecting TDP-43 Pathology with Neuropathy. *Trends Neurosci.* 44, 424–440. doi: 10.1016/j.tins.2021.02.008
- Klim, J. R., Williams, L. A., Limone, F., Juan, I. G. S., Davis-Dusenbery, B. N., and Mordes, D. A. (2019). ALS-implicated protein TDP-43 sustains levels of STMN2, a mediator of motor neuron growth and repair. *Nat. Neurosci.* 22, 167–179. doi: 10.1038/s41593-018-0300-4
- Krencik, R., and Zhang, S.-C. (2011). Directed differentiation of functional astroglial subtypes from human pluripotent stem cells. *Nat. Protoc.* 6, 1710–1717. doi: 10.1038/nprot.2011.405
- Krencik, R., Weick, J. P., Liu, Y., Zhang, Z.-J., and Zhang, S.-C. (2011). Specification of transplantable astroglial subtypes from human pluripotent stem cells. *Nat. Biotechnol.* 29, 528–534. doi: 10.1038/nbt.1877
- Kriks, S., Shim, J.-W., Piao, J., Ganat, Y. M., Wakeman, D. R., Xie, Z., et al. (2011). Dopamine neurons derived from human ES cells efficiently engraft in animal models of Parkinson's disease. *Nature* 480, 547–551. doi: 10.1038/nature10648
- Lepore, A. C., Rauck, B., Dejea, C., Pardo, A. C., Rao, M. S., Rothstein, J. D., et al. (2008). Focal transplantation-based astrocyte replacement is neuroprotective in a model of motor neuron disease. *Nat. Neurosci.* 11, 1294–1301. doi: 10.1038/nn.2210
- Li, X., Tao, Y., Bradley, R., Du, Z., Tao, Y., Kong, L., et al. (2018). Fast generation of functional subtype astrocytes from human pluripotent stem cells. *Stem Cell Rep.* 11, 998–1008. doi: 10.1016/j.stemcr.2018.08.019
- Limone, F., Mitchell, J. M., Juan, I. G. S., Smith, J. L. M., Raghunathan, K., Couto, A., et al. (2022). Efficient generation of lower induced Motor Neurons by coupling Ngn2 expression with developmental cues. *bioRxiv* [Preprint] doi: 10.1101/2022.01.12.476020
- Limone, F., Mordes, D. A., Couto, A., Pietilainen, O., Joseph, B. J., Burberry, A., et al. (2021). Single-nucleus sequencing reveals enriched expression of genetic risk factors sensitises Motor Neurons to degeneration in ALS. *bioRxiv* [Preprint] doi: 10.1101/2021.07.12.452054
- Lippmann, E. S., Williams, C. E., Ruhl, D. A., Estevez-Silva, M. C., Chapman, E. R., Coon, J. J., et al. (2015). Deterministic HOX patterning in human pluripotent stem cell-derived neuroectoderm. *Stem Cell Rep.* 4, 632–644. doi: 10.1016/j.stemcr.2015.02.018
- Liu, Y., Liu, H., Sauvey, C., Yao, L., Zarnowska, E. D., and Zhang, S.-C. (2013b). Directed differentiation of forebrain GABA interneurons from human pluripotent stem cells. *Nat. Protoc.* 8, 1670–1679. doi: 10.1038/nprot.2013.106
- Liu, Y., Weick, J. P., Liu, H., Krencik, R., Zhang, X., Ma, L., et al. (2013a). Medial ganglionic eminence-like cells derived from human embryonic stem cells correct learning and memory deficits. *Nat. Biotechnol.* 31, 440–447. doi: 10.1038/nbt.2565
- Lu, J., Zhong, X., Liu, H., Hao, L., Huang, C. T.-L., Sherfat, M. A., et al. (2016). Generation of serotonin neurons from human pluripotent stem cells. *Nature Biotechnol.* 34, 89–94. doi: 10.1038/nbt.3435
- Ma, L., Hu, B., Liu, Y., Vermilyea, S. C., Liu, H., Gao, L., et al. (2012). Human embryonic stem cell-derived GABA neurons correct locomotion deficits in quinolinic acid-lesioned mice. *Cell Stem Cell* 10, 455–464. doi: 10.1016/j.stem.2012.01.021
- Mandai, M., Watanabe, A., Kurimoto, Y., Hirami, Y., Morinaga, C., Daimon, T., et al. (2017). Autologous induced stem-cell-derived retinal cells for macular degeneration. *N. Engl. J. Med.* 376, 1038–1046. doi: 10.1056/nejmoa1608368
- Maroof, A. M., Keros, S., Tyson, J. A., Ying, S.-W., Ganat, Y. M., Merkle, F. T., et al. (2013). Directed differentiation and functional maturation of cortical interneurons from human embryonic stem cells. *Cell Stem Cell* 12, 559–572. doi: 10.1016/j.stem.2013.04.008
- Martinez, J. L., Zammit, M. D., West, N. R., Christian, B. T., and Bhattacharyya, A. (2021). Corrigendum: basal forebrain cholinergic neurons: Linking down syndrome and Alzheimer's Disease. *Front. Aging Neurosci.* 13:742233. doi: 10.3389/fnagi.2021.742233
- Marton, R. M., Miura, Y., Sloan, S. A., Li, Q., Revah, O., Levy, R. J., et al. (2019). Differentiation and maturation of oligodendrocytes in human three-dimensional neural cultures. *Nat. Neurosci.* 22, 484–491. doi: 10.1038/s41593-018-0316-9
- Maury, Y., Côme, J., Piskrowski, R. A., Salah-Mohellibi, N., Chevalleyre, V., Peschanski, M., et al. (2015). Combinatorial analysis of developmental cues efficiently converts human pluripotent stem cells into multiple neuronal subtypes. *Nat. Biotechnol.* 33, 89–96. doi: 10.1038/nbt.3049
- Merkle, F. T., Ghosh, S., Genovese, G., Handsaker, R. E., Kashin, S., Meyer, D., et al. (2022). Whole-genome analysis of human embryonic stem cells enables rational line selection based on genetic variation. *Cell Stem Cell* 29, 472–486. doi: 10.1016/j.stem.2022.01.011

- Merkle, F. T., Ghosh, S., Kamitaki, N., Mitchell, J., Avior, Y., Mello, C., et al. (2017). Human pluripotent stem cells recurrently acquire and expand dominant negative P53 mutations. *Nature* 545, 229–233. doi: 10.1038/nature22312
- Merkle, F. T., Maroof, A., Wataya, T., Sasai, Y., Studer, L., Eggan, K., et al. (2015). Generation of neuropeptidergic hypothalamic neurons from human pluripotent stem cells. *Development* 142, 633–643. doi: 10.1242/dev.117978
- Mertens, J., Reid, D., Lau, S., Kim, Y., and Gage, F. H. (2018). Aging in a Dish: iPSC-Derived and directly induced neurons for studying brain aging and age-related neurodegenerative Diseases. *Annu. Rev. Genet.* 52, 271–293. doi: 10.1146/annurev-genet-120417-031534
- Meyer, K., Ferraiuolo, L., Miranda, C. J., Likhite, S., McElroy, S., Renusch, S., et al. (2014). Direct conversion of patient fibroblasts demonstrates non-cell autonomous toxicity of astrocytes to motor neurons in familial and sporadic ALS. *Proc. Natl. Acad. Sci. U. S. A.* 111, 829–832. doi: 10.1073/pnas.1314085111
- Muffat, J., Li, Y., Yuan, B., Mitalipova, M., Omer, A., Corcoran, S., et al. (2016). Efficient derivation of microglia-like cells from human pluripotent stem cells. *Nat. Med.* 22, 1358–1367. doi: 10.1038/nm.4189
- Muguruma, K., Nishiyama, A., Kawakami, H., Hashimoto, K., and Sasai, Y. (2015). Self-Organization of polarized cerebellar tissue in 3d culture of human pluripotent stem cells. *Cell Rep.* 10, 537–550. doi: 10.1016/j.celrep.2014.12.051
- Nehme, R., Zuccaro, E., Ghosh, S. D., Li, C., Sherwood, J. L., Pietilainen, O., et al. (2018). Combining NG2 programming with developmental patterning generates human excitatory neurons with NMDAR-mediated synaptic transmission. *Cell Rep.* 23, 2509–2523. doi: 10.1016/j.celrep.2018.04.066
- Nicholas, C. R., Chen, J., Tang, Y., Southwell, D. G., Chalmers, N., Vogt, D., et al. (2013). Functional maturation of hpsc-derived forebrain interneurons requires an extended timeline and mimics human neural development. *Cell Stem Cell* 12, 573–586. doi: 10.1016/j.stem.2013.04.005
- Nishiyama, Y., Iwanami, A., Kohyama, J., Itakura, G., Kawabata, S., Sugai, K., et al. (2016). Safe and efficient method for cryopreservation of human induced pluripotent stem cell-derived neural stem and progenitor cells by a programmed freezer with a magnetic field. *Neurosci. Res.* 107, 20–29. doi: 10.1016/j.neures.2015.11.011
- Pandya, H., Shen, M. J., Ichikawa, D. M., Sedlock, A. B., Choi, Y., Johnson, K. R., et al. (2017). Differentiation of human and murine induced pluripotent stem cells to microglia-like cells. *Nat. Neurosci.* 20, 753–759. doi: 10.1038/nn.4534
- Paull, D., Sevilla, A., Zhou, H., Hahn, A. K., Kim, H., Napolitano, C., et al. (2015). Automated, high-throughput derivation, characterization and differentiation of induced pluripotent stem cells. *Nat. Methods* 12, 885–892. doi: 10.1038/nmeth.3507
- Pera, M. F. (2011). Stem cells: The dark side of induced pluripotency. *Nature* 471, 46–47. doi: 10.1038/471046a
- Pfisterer, U., Kirkeby, A., Torper, O., Wood, J., Nelander, J., Dufour, A., et al. (2011). Direct conversion of human fibroblasts to dopaminergic neurons. *Proc. Natl. Acad. Sci. U. S. A.* 108, 10343–10348. doi: 10.1073/pnas.1105135108
- Politis, M., and Loane, C. (2011). Serotonergic dysfunction in Parkinson's Disease and its relevance to disability. *Sci. World J.* 11, 1726–1734. doi: 10.1100/2011/172893
- Qi, Y., Zhang, X.-J., Renier, N., Wu, Z., Atkin, T., Sun, Z., et al. (2017). Combined small-molecule inhibition accelerates the derivation of functional cortical neurons from human pluripotent stem cells. *Nat. Biotechnol.* 35, 154–163. doi: 10.1038/nbt.3777
- Qian, H., Kang, X., Hu, J., Zhang, D., Liang, Z., Meng, F., et al. (2020). Reversing a model of Parkinson's disease with in situ converted nigral neurons. *Nature* 582, 550–556. doi: 10.1038/s41586-020-2388-4
- Rajamani, U., Gross, A. R., Hjelm, B. E., Sequeira, A., Vawter, M. P., Tang, J., et al. (2018). Super-Obese patient-derived iPSC hypothalamic neurons exhibit obesogenic signatures and hormone responses. *Cell Stem Cell* 22, 698–712. doi: 10.1016/j.stem.2018.03.009
- Ridley, R. M., Baker, J. A., Baker, H. F., and MacLean, C. J. (1994). Restoration of cognitive abilities by cholinergic grafts in cortex of monkeys with lesions of the basal nucleus of meynert. *Neuroscience* 63, 653–666. doi: 10.1016/0306-4522(94)90512-6
- Riolobos, L., Hirata, R. K., Turtle, C. J., Wang, P.-R., Gornalusse, G. G., Zavajlevski, M., et al. (2013). HLA Engineering of Human Pluripotent Stem Cells. *Molecular Therapy* 21, 1232–1241. doi: 10.1038/mt.2013.59
- Sakaguchi, H., Kadoshima, T., Soen, M., Narii, N., Ishida, Y., Ohgushi, M., et al. (2015). Generation of functional hippocampal neurons from self-organizing human embryonic stem cell-derived dorsomedial telencephalic tissue. *Nat. Commun.* 6:8896. doi: 10.1038/ncomms.9896
- Shaltouki, A., Peng, J., Liu, Q., Rao, M. S., and Zeng, X. (2013). Efficient generation of astrocytes from human pluripotent stem cells in defined conditions. *Stem Cells* 31, 941–952. doi: 10.1002/stem.1334
- Silva, T. P., Bekman, E. P., Fernandes, T. G., Vaz, S. H., Rodrigues, C. A. V., Diogo, M. M., et al. (2020). . Maturation of human pluripotent stem cell-derived cerebellar neurons in the absence of co-culture. *Front. Bioeng. Biotechnol.* 8:70. doi: 10.3389/fbioe.2020.00070
- Son, E. Y., Ichida, J. K., Wainger, B. J., Toma, J. S., Rafuse, V. F., Woolf, C. J., et al. (2011). Conversion of mouse and human fibroblasts into functional spinal motor neurons. *Cell Stem Cell* 9, 205–218. doi: 10.1016/j.stem.2011.07.014
- Song, J.-J., Oh, S.-M., Kwon, O.-C., Wulnansari, N., Lee, H.-S., Chang, M.-Y., et al. (2017). Cografting astrocytes improves cell therapeutic outcomes in a Parkinson's disease model. *J. Clin. Invest.* 128, 463–482. doi: 10.1172/jci93924
- Sonn, I., Honda-Ozaki, F., Yoshimatsu, S., Morimoto, S., Watanabe, H., and Okano, H. (2022). Single transcription factor efficiently leads human induced pluripotent stem cells to functional microglia. *Inflamm. Regen.* 42:20. doi: 10.1186/s41232-022-00201-1
- Southwell, D. G., Nicholas, C. R., Basbaum, A. I., Stryker, M. P., Kriegstein, A. R., Rubenstein, J. L., et al. (2014). Interneurons from Embryonic Development to Cell-Based Therapy. *Science* 344:1240622. doi: 10.1126/science.1240622
- Steinbeck, J. A., and Studer, L. (2015). Moving stem cells to the clinic: potential and limitations for brain repair. *Neuron* 86, 187–206. doi: 10.1016/j.neuron.2015.03.002
- Sun, A. X., Yuan, Q., Tan, S., Xiao, Y., Wang, D., Khoo, A. T., et al. (2016). Direct Induction and functional maturation of forebrain GABAergic neurons from human pluripotent stem cells. *Cell Rep.* 16, 1942–1953. doi: 10.1016/j.celrep.2016.07.035
- Svoboda, D. S., Barrasa, M. I., Shu, J., Rietjens, R., Zhang, S., Mitalipova, M., et al. (2019). Human iPSC-derived microglia assume a primary microglia-like state after transplantation into the neonatal mouse brain. *Proc. Natl. Acad. Sci. U. S. A.* 116, 25293–25303. doi: 10.1073/pnas.1913541116
- Takata, K., Kozaki, T., Lee, C. Z. W., Thion, M. S., Otsuka, M., Lim, S., et al. (2017). Induced-Pluripotent-stem-cell-derived primitive macrophages provide a platform for modeling tissue-resident macrophage differentiation and function. *Immunity* 47, 183–198. doi: 10.1016/j.immuni.2017.06.017
- Tao, Y., and Zhang, S.-C. (2016). Neural subtype specification from human pluripotent stem cells. *Cell Stem Cell* 19, 573–586. doi: 10.1016/j.stem.2016.10.015
- Tchieu, J., Calder, E. L., Guttikonda, S. R., Gutzwiller, E. M., Aromolaran, K. A., Steinbeck, J. A., et al. (2019). NFIA is a gliogenic switch enabling rapid derivation of functional human astrocytes from pluripotent stem cells. *Nat. Biotechnol.* 37, 267–275. doi: 10.1038/s41587-019-0035-0
- Tcw, J., Wang, M., Pimenova, A. A., Bowles, K. R., Hartley, B. J., Lacin, E., et al. (2017). An efficient platform for astrocyte differentiation from human induced pluripotent stem cells. *Stem Cell Rep.* 9, 600–614. doi: 10.1016/j.stemcr.2017.06.018
- Thiruvalluvan, A., Czepl, M., Kap, Y. A., Mantingh-Otter, I., Vainchtein, I., Kuipers, J., et al. (2016). Survival and functionality of human induced pluripotent stem cell-derived oligodendrocytes in a nonhuman primate model for multiple sclerosis. *Stem Cells Transl. Med.* 5, 1550–1561. doi: 10.5966/sctm.2016-0024
- Trounson, A., and DeWitt, N. D. (2016). Pluripotent stem cells progressing to the clinic. *Nat. Rev. Mol. Cell Biol.* 17, 194–200. doi: 10.1038/nrm.2016.10
- Vadodaria, K. C., Mertens, J., Paquola, A., Bardy, C., Li, X., Jappelli, R., et al. (2016). Generation of functional human serotonergic neurons from fibroblasts. *Mol. Psychiatry* 21, 49–61. doi: 10.1038/mp.2015.161
- Victor, M. B., Richner, M., Hermansteyne, T. O., Ransdell, J. L., Sobieski, C., Deng, P.-Y., et al. (2014). Generation of human striatal neurons by microRNA-dependent direct conversion of fibroblasts. *Neuron* 84, 311–323. doi: 10.1016/j.neuron.2014.10.016
- Wakeman, D. R., Hiller, B. M., Marmion, D. J., McMahon, C. W., Corbett, G. T., Mangan, K. P., et al. (2017). Cryopreservation Maintains Functionality of Human iPSC Dopamine Neurons and Rescues Parkinsonian Phenotypes In Vivo. *Stem Cell Rep.* 9, 149–161. doi: 10.1016/j.stemcr.2017.04.033
- Wang, L., Meece, K., Williams, D. J., Lo, K. A., Zimmer, M., Heinrich, G., et al. (2015b). Differentiation of hypothalamic-like neurons from human pluripotent stem cells. *J. Clin. Invest.* 125, 796–808. doi: 10.1172/JCI79220
- Wang, S., Bates, J., Li, X., Schanz, S., Chandler-Militello, D., Levine, C., et al. (2013). Human iPSC-derived oligodendrocyte progenitor cells can myelinate and rescue a mouse model of congenital hypomyelination. *Cell Stem Cell* 12, 252–264. doi: 10.1016/j.stem.2012.12.002
- Wang, S., Wang, B., Pan, N., Fu, L., Wang, C., Song, G., et al. (2015a). Differentiation of human induced pluripotent stem cells to mature functional Purkinje neurons. *Sci. Rep.* 5:9232. doi: 10.1038/srep09232

- Warren, L., Manos, P. D., Ahfeldt, T., Loh, Y.-H., Li, H., Lau, F., et al. (2010). Highly efficient reprogramming to pluripotency and directed differentiation of human cells with synthetic modified mRNA. *Cell Stem Cell* 7, 618–630. doi: 10.1016/j.stem.2010.08.012
- Watson, L. M., Wong, M. M. K., Vowles, J., Cowley, S. A., and Becker, E. B. E. (2018). A Simplified method for generating purkinje cells from human-induced pluripotent stem cells. *Cerebellum* 17, 419–427. doi: 10.1007/s12311-017-0913-2
- Wichterle, H., Lieberam, I., Porter, J. A., and Jessell, T. M. (2002). Directed differentiation of embryonic stem cells into motor neurons. *Cell* 110, 385–397. doi: 10.1016/s0092-8674(02)00835-8
- Windrem, M. S., Schanz, S. J., Zou, L., Chandler-Militello, D., Kuypers, N. J., Nedergaard, M., et al. (2020). Human glial progenitor cells effectively remyelinate the demyelinated adult brain. *Cell Rep.* 31:107658. doi: 10.1016/j.celrep.2020.107658
- Xu, R., Li, X., Boreland, A. J., Posyton, A., Kwan, K., Hart, R. P., et al. (2020). Human iPSC-derived mature microglia retain their identity and functionally integrate in the chimeric mouse brain. *Nat. Commun.* 11:1577. doi: 10.1038/s41467-020-15411-9
- Xu, Z., Jiang, H., Zhong, P., Yan, Z., Chen, S., and Feng, J. (2016). Direct conversion of human fibroblasts to induced serotonergic neurons. *Mol. Psychiatry* 21, 62–70. doi: 10.1038/mp.2015.101
- Yohn, D. C., Miles, G. B., Rafuse, V. F., and Brownstone, R. M. (2008). Transplanted mouse embryonic stem-cell-derived motoneurons form functional motor units and reduce muscle atrophy. *J. Neurosci.* 28, 12409–12418. doi: 10.1523/jneurosci.1761-08.2008
- Yu, D. X., Di Giorgio, F. P., Yao, J., Marchetto, M. C., Brennand, K., Wright, R., et al. (2014). Modeling hippocampal neurogenesis using human pluripotent stem cells. *Stem Cell Rep.* 2, 295–310. doi: 10.1016/j.stemcr.2014.01.009
- Yuan, F., Chen, X., Fang, K.-H., Wang, Y., Lin, M., Xu, S.-B., et al. (2018). Induction of human somatostatin and parvalbumin neurons by expressing a single transcription factor LIM homeobox 6. *eLife* 7:e37382. doi: 10.7554/elife.37382
- Yuan, S. H., Martin, J., Elia, J., Flippin, J., Paramban, R. I., Hefferan, M. P., et al. (2011). Cell-Surface Marker Signatures for the Isolation of Neural Stem Cells, Glia and Neurons Derived from Human Pluripotent Stem Cells. *PLoS One* 6:e17540. doi: 10.1371/journal.pone.0017540
- Yue, C., and Jing, N. (2015). The promise of stem cells in the therapy of Alzheimer's disease. *Transl. Neurodegener.* 4:8. doi: 10.1186/s40035-015-0029-x
- Yun, S.-W., Leong, C., Zhai, D., Tan, Y. L., Lim, L., Bi, X., et al. (2012). Neural stem cell specific fluorescent chemical probe binding to FABP7. *Proc. Natl Acad. Sci. U. S. A.* 109, 10214–10217. doi: 10.1073/pnas.1200817109
- Zhang, S.-C., Wernig, M., Duncan, I. D., Brüstle, O., and Thomson, J. A. (2001). In vitro differentiation of transplantable neural precursors from human embryonic stem cells. *Nat. Biotechnol.* 19, 1129–1133. doi: 10.1038/nbt1201-1129
- Zhang, Y., Pak, C., Han, Y., Ahlenius, H., Zhang, Z., Chanda, S., et al. (2013). Rapid single-step induction of functional neurons from human pluripotent stem cells. *Neuron* 78, 785–798. doi: 10.1016/j.neuron.2013.05.029
- Zheng, W., Li, Q., Zhao, C., Da, Y., Zhang, H.-L., and Chen, Z. (2018). Differentiation of glial cells from hiPSCs: Potential applications in neurological diseases and cell replacement therapy. *Front. Cell Neurosci.* 12:239. doi: 10.3389/fncel.2018.00239



OPEN ACCESS

EDITED BY

Shong Lau,
Salk Institute for Biological Studies,
United States

REVIEWED BY

Nelly Olova,
University of Edinburgh,
United Kingdom
Adegbenro Omotuyi John Fakoya,
Louisiana State University Health
Shreveport, United States
Rajkumar P. Thummer,
Indian Institute of Technology Guwahati,
India
Krishna Kumar Haridhasapavalan,
Indian Institute of Technology
Guwahati, India,
in collaboration with reviewer RT

*CORRESPONDENCE

Massimiliano Caiazza
massimiliano.caiazza@unina.it

SPECIALTY SECTION

This article was submitted to
Cellular and Molecular Mechanisms
of Brain-aging,
a section of the journal
Frontiers in Aging Neuroscience

RECEIVED 13 October 2022

ACCEPTED 22 November 2022

PUBLISHED 20 December 2022

CITATION

Aversano S, Caiazza C and
Caiazza M (2022) Induced pluripotent stem
cell-derived and directly reprogrammed
neurons to study neurodegenerative
diseases: The impact of aging signatures.
Front. Aging Neurosci. 14:1069482.
doi: 10.3389/fnagi.2022.1069482

COPYRIGHT

© 2022 Aversano, Caiazza and Caiazza.
This is an open-access article distributed
under the terms of the [Creative Commons
Attribution License \(CC BY\)](#). The use,
distribution or reproduction in other
forums is permitted, provided the original
author(s) and the copyright owner(s) are
credited and that the original publication in
this journal is cited, in accordance with
accepted academic practice. No use,
distribution or reproduction is permitted
which does not comply with these terms.

Induced pluripotent stem cell-derived and directly reprogrammed neurons to study neurodegenerative diseases: The impact of aging signatures

Simona Aversano¹, Carmen Caiazza¹ and Massimiliano Caiazza^{1,2*}

¹Department of Molecular Medicine and Medical Biotechnology, University of Naples Federico II, Naples, Italy, ²Department of Pharmaceutics, Utrecht Institute for Pharmaceutical Sciences (UIPS), Utrecht University, Utrecht, Netherlands

Many diseases of the central nervous system are age-associated and do not directly result from genetic mutations. These include late-onset neurodegenerative diseases (NDDs), which represent a challenge for biomedical research and drug development due to the impossibility to access to viable human brain specimens. Advancements in reprogramming technologies have allowed to obtain neurons from induced pluripotent stem cells (iPSCs) or directly from somatic cells (iNs), leading to the generation of better models to understand the molecular mechanisms and design of new drugs. Nevertheless, iPSC technology faces some limitations due to reprogramming-associated cellular rejuvenation which resets the aging hallmarks of donor cells. Given the prominent role of aging for the development and manifestation of late-onset NDDs, this suggests that this approach is not the most suitable to accurately model age-related diseases. Direct neuronal reprogramming, by which a neuron is formed *via* direct conversion from a somatic cell without going through a pluripotent intermediate stage, allows the possibility to generate patient-derived neurons that maintain aging and epigenetic signatures of the donor. This aspect may be advantageous for investigating the role of aging in neurodegeneration and for finely dissecting underlying pathological mechanisms. Here, we will compare iPSC and iN models as regards the aging status and explore how this difference is reported to affect the phenotype of NDD *in vitro* models.

KEYWORDS

cell reprogramming, Parkinson's disease, Alzheimer's disease, Huntington's disease, ALS, *in vitro* model

Introduction

Aging is the natural process that progressively leads to the functional decline of the cell and ultimately of the whole organism. While its nature and causes still belong to a debated field, researchers mainly addressed the non-trivial question of defining aging at a biological level. Biological aging is very complex and involves genomic mutations, epigenetic changes, telomere shortening, and progressive decline in metabolic function and proteostasis, all reflecting different aspects of the process (Gladyshev, 2016). The aging signatures are crucial to correctly establish cellular age independently of chronological age and understand the impact of each factor on physiological and pathological aspects of aging itself. In this regard, aging has emerged as the leading risk factor for the late-onset diseases and particularly in neurodegenerative diseases (NDDs; Gudenschwager et al., 2021), thereby posing the urge to unveil its contribution in NDDs development. NDDs comprise a group of disorders that affect central nervous system (CNS) and have a higher incidence among the aged population. Among them, the most studied are Alzheimer's disease (AD), Parkinson's disease (PD), amyotrophic lateral sclerosis (ALS), and Huntington's disease (HD).

Although the genes involved in some early-onset familial forms of the diseases were identified, the overwhelming proportion of sporadic diagnosed cases remains unexplained (Wang et al., 2008; Fernández-Santiago et al., 2015) and effective treatment strategies to cure these diseases are missing. Aging hallmarks could account for the late-onset forms of NDDs, presumably interacting with genetic and environmental factors. Finding appropriate disease models that include aging information may help to achieve a comprehensive understanding of disease mechanisms and progression and to identify potential therapeutic targets.

Recently, the possibility of studying adult human neurons obtained by cell reprogramming strategies provided precious insights into the molecular mechanisms underlying neurodegeneration and other neurological disorders. Neurons can be derived from induced pluripotent stem cells (iPSCs) or directly induced from somatic cells such as fibroblasts (iNs) to make patient-tailored disease models. In the first strategy, primary human cells can be collected directly from patients, and the cells can then be reset to an embryonic-like state with the transient expression of the Yamanaka transcription factors (TFs), OCT4, KLF4, SOX2, and C-MYC (OKSM; Takahashi and Yamanaka, 2006). The generated iPSCs have the potential to differentiate into all three germ layers with the unlimited ability of self-renewal, providing a potential source of functional neurons that can be obtained either by using several developmental morphogens and small molecules (Kriks et al., 2011) or by forced expression of few neurogenic TFs. In the second case it is possible to apply forced expression of TFs directly to iPSCs to generate in a faster way (~3 weeks) dopamine, glutamate, GABA, and motor neurons (Dimos et al., 2008;

Chambers et al., 2009; Maroof et al., 2013; Theka et al., 2013; Chen et al., 2014; Yang et al., 2017).

The alternative route to obtain mature and functional neurons is the direct reprogramming of somatic cells into neurons, over-expressing combinations of neurogenic TFs. The first described example of this approach was the generation of glutamate neurons by applying ASCL1, BRN2, and MYT1L (BAM factors) on mouse embryonic fibroblasts (Vierbuchen et al., 2010).

Both strategies have also been used to obtain specific neural subtypes that are relevant for NDDs modeling; nevertheless, they can recapitulate different phenotypic properties of diseases. The differential maintenance of aging status of donor cells is the reason for this discrepancy and an aspect that has come to the attention of the researchers aiming to faithfully model NDDs.

Essentially, the reprogramming tools follow a different developmental program toward the neural fate. The induction of pluripotency entails an embryonic-like state which resets the cellular age and leads to cell rejuvenation (Lapasset et al., 2011) even in the finally differentiated neurons (Huh et al., 2016). Direct conversion of fibroblasts into neurons circumvents intermediate embryonic cell stages and has proven to preserve the cellular age of donor cells (Huh et al., 2016). Obligatory access to patient cell lines is a limitation of these approaches, since NDDs modeling needs the generation of iPSCs or iNs from large cohorts of patients, to comprise the genetic heterogeneity with respect to the disease-causing mutations. This limitation has been expunged by CRISPR/Cas9-edited disease models, which allow to introduce or correct any desired mutation, and to obtain isogenic cell lines carrying one or multiple disease-relevant mutations from a single iPSC background (Sen and Thummer, 2022). In this review, we describe in more detail the differences in the aging status of iN- and iPSC-derived neurons and discuss the impact of these features in the disease modeling of NDDs.

Aging features in directly converted and iPSC-derived neurons

Epigenetic and transcriptional memory

Age-associated changes in TFs and chromatin state represent a critical aspect of the aging process and a link between different aging hallmarks. Aging changes include reduced global heterochromatin, nucleosome loss and remodeling, changes in histone marks, global DNA hypomethylation with CpG island hypermethylation, and the relocalization of chromatin modifying factors (Oberdoerffer and Sinclair, 2007; Campisi and Vijg, 2009). Importantly, these factors were demonstrated to be correlated with age-related neurodegeneration (Booth and Brunet, 2016), albeit their contribution for disease development is far to be dissected. An *in vitro* model that reliably retains the epigenetic information is thus required to achieve a full comprehension of the sporadic as

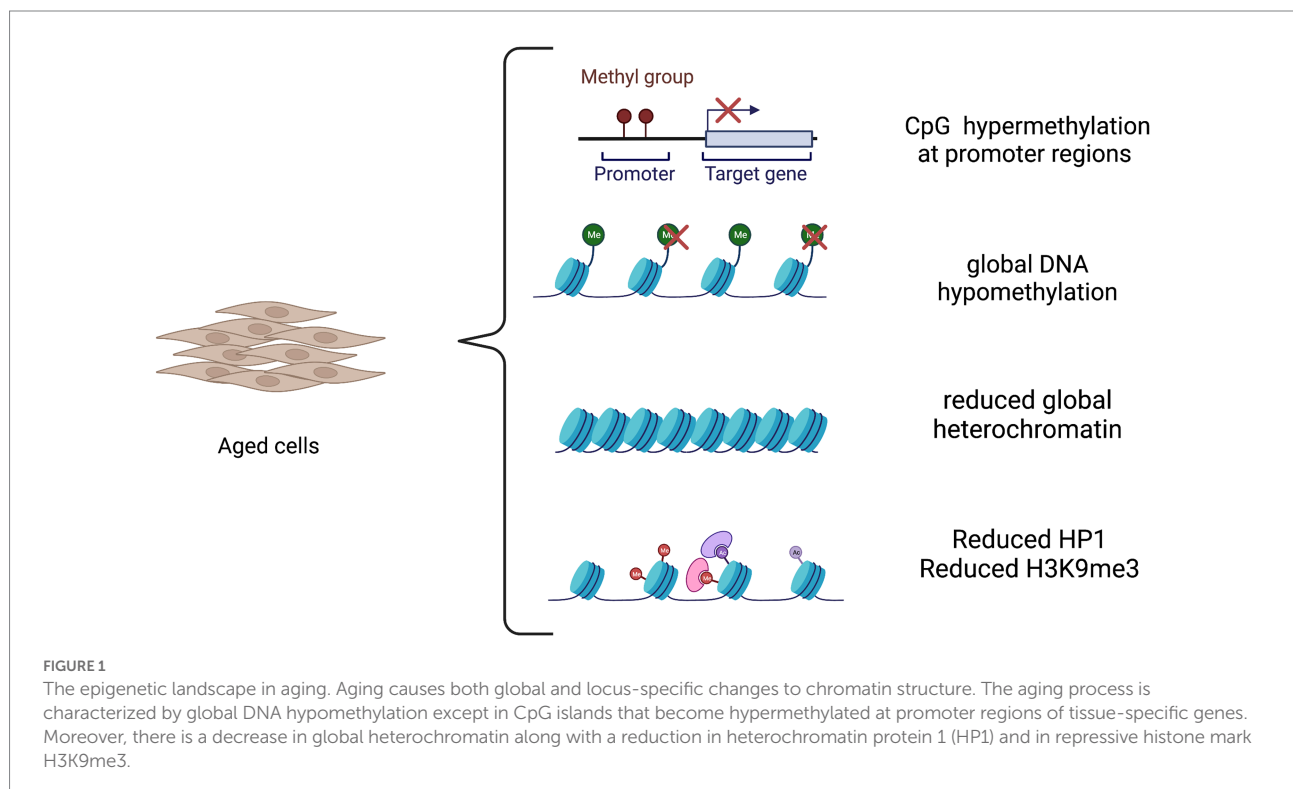
well genetic forms of the diseases. The epigenetic landscape in aging is depicted in [Figure 1](#).

The altered methylation landscape has been calibrated to accurately predict the age of cells ([Horvath, 2013](#)) and allowed for accurate aging characterization of iPSC-derived neurons and iNs, shedding light onto the epigenetic mechanisms governing the two different reprogramming strategies and the effects on the maintenance of cellular age. The induction of pluripotency resets the epigenetic clock to zero ([Horvath and Raj, 2018](#)) confirming previous evidence that demonstrated cell rejuvenation by reprogramming through the pluripotent state ([Maherali et al., 2007](#); [Meissner et al., 2008](#); [Lapasset et al., 2011](#)). Of note, epigenetic age is not restored upon neural induction, independently from the age of donor cells ([Huh et al., 2016](#)). This aspect can be explained by the hierarchical transcriptional and epigenetic mechanisms that occur during the TF-mediated induction of the pluripotent state. The reprogramming process involves the “off-target” cooperative chromatin binding of TFs, the OKSM factors identified by Yamanaka’s group ([Takahashi and Yamanaka, 2006](#)). TFs need to overcome a series of epigenetic barriers that have been gradually imposed on the genome during differentiation, including large, repressed chromatin domains enriched by H3K9me3 modification, to induce a huge chromatin remodeling that finally leads to the erasure of somatic acquired epigenetic marks and reactivation of pluripotent genes ([Takahashi and Yamanaka, 2006](#); [Takahashi et al., 2007](#); [Apostolou and Hochedlinger, 2013](#); [Wapinski et al., 2013](#)). It has been shown that age reset precedes de-differentiation during iPSC reprogramming

with OSKM factors ([Olova et al., 2019](#); [Gill et al., 2022](#)) and that combinations of two or three of those factors lead to similar rejuvenation effects, even after 2–3 days of exposure, where aging signatures are partially erased and restored to youthful states ([Lu et al., 2020](#)).

As expected, the epigenetic rejuvenation of iPSCs results in a population of reprogrammed neural cells that are epigenetically and transcriptionally different from their *in vivo* counterpart, hampering their potentiality for *in vitro* modeling and cell replacement therapy.

A genome-wide comparative gene-expression profiling demonstrated a clear correlation between iPSC-derived mesencephalic dopaminergic (mDA) neurons and embryonic mDA neurons, but less similarity was found between iPSC-derived mDA neurons and postnatal mDA neurons ([Roessler et al., 2014](#)). In stark contrast to iPSC-derived neurons, direct neuronal conversion from fibroblasts sampled at different ages has proven to retain the epigenetic age of the original donor cells ([Huh et al., 2016](#)). iNs do not follow the precise intermediate states of development but generate a unique intermediate state that is unrelated to the donor and the target cells. Despite this ‘shortcut’, iNs appear to arrive at the same state as neurons obtained by differentiation, preserving epigenetic information about age and disease ([Traxler et al., 2019](#)). It is worth noting that direct neural conversion is dependent on the activity of “on-target” pioneer TFs which immediately bind pro-neural target genes such as ASCL1 that facilitates the further action of BRN2 and MYT1L (BAM factors; [Wapinski et al., 2013](#); [Smith et al., 2016](#)) and that these



events do not erase the somatic epigenetic marks to induce an intermediate pluripotent cell stage. Therefore, direct reprogramming appears as the most suitable *in vitro* tool to obtain patient-specific neurons that also include the epigenetic information.

The concept of epigenetic memory was previously applied to iPSCs and neurons differentiated from iPSCs. These studies showed that iPSCs retain the epigenetic signatures of donor cells, which also predispose them to a preferential lineage-specific differentiation (Bar-Nur et al., 2011; Kim K. et al., 2011). DA neurons derived from iPSCs are somehow different from their primary counterpart, since they show a differential expression relative to fibroblast specific markers, suggesting remnants of a still active fibroblast gene program in iPSC-derived DA neurons (Roessler et al., 2014). However, these data were not conclusive and have to be read in the light of other studies showing that embryonic stem cells (ESCs) themselves exhibit variation in terms of their growth profiles and differentiation potential (Osafune et al., 2008; Sullivan et al., 2010). Finally, both iPSCs and ESCs share pluripotency and self-renewal capacity, indicating that transcriptional or epigenetic differences have no overall significant impact on stem-cell pluripotency *per se* nor are directly correlated to epigenetic memory. Instead, these subtle differences may well be compounded by culture conditions and laboratory practices (Sullivan et al., 2010).

Apart from the classical CpG DNA methylation which has an established role in gene regulation, some studies have underpinned the relevance of non-CpG methylation in the epigenetic landscape of adult mammalian brains, where mCH (where H = A, T, or C) and intermediates in the DNA demethylation pathway, in particular 5-hydroxymethylcytosine (5hmC; Xie et al., 2012; Guo et al., 2014; He and Ecker, 2015), are found at high levels.

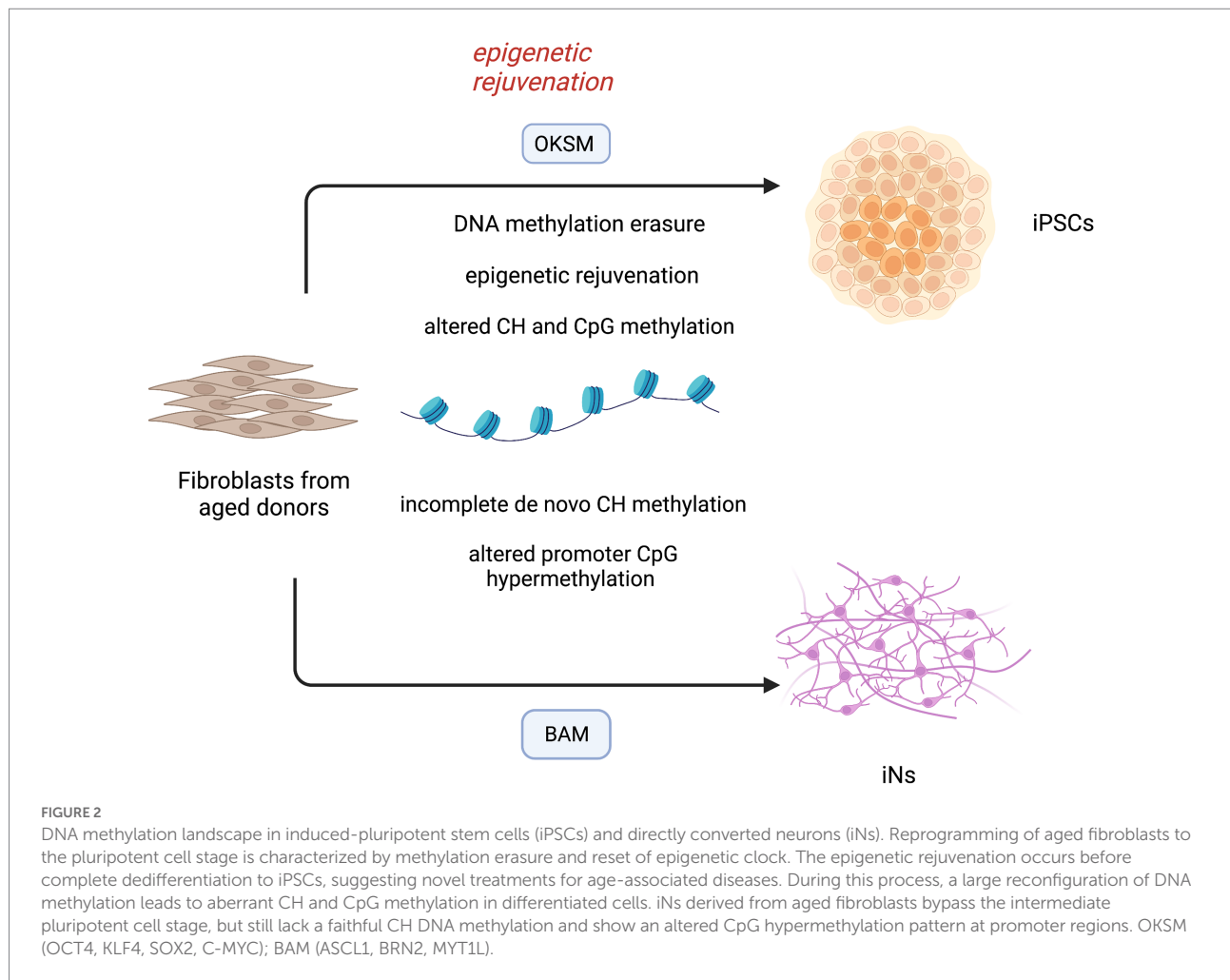
The precise role of these modifications is not fully understood; however, several evidence reported that mCH takes part in the modulation of gene expression in mature neurons (Xie et al., 2012; Mo et al., 2015; Stroud et al., 2017). mCH starts with birth and is targeted to constitutive repressed genes and to genes showing developmental downregulation in mature neurons (Luo et al., 2019), suggesting that this mechanism facilitates neuronal maturation through gene repression. Therefore, mCH represents an essential component of the epigenetic landscape of mature neurons, which has a profound implication in iPSC- and iN-based disease models. Whole-genome profiles of DNA methylation in iPSCs showed an aberrant methylation in the non-CpG context which is later transmitted to differentiated cells (Lister et al., 2011). Instead, base-resolution methylome of fully differentiated mouse iNs showed consistent mCH patterns; however, they did not recapitulate perfectly mCH and showed a different promoter CpG methylation compared to mature cortical neurons (Luo et al., 2019). This is in agreement with a recent investigation in which neurons differentiated from mouse ESCs have proven to acquire CH methylation in a similar time frame as their *in vivo* counterparts, but they still do not recapitulate this methylation context with fidelity (Martin et al., 2020). These data suggest that

other factors are necessary to fully develop *in vivo* methylation levels and patterns and this aspect must be deepened in order to faithfully recapitulate the aged neuronal methylome.

Importantly, human neurons have a much more extended developmental timeline compared to mouse neurons and reach the maximal *in vivo* mCH methylation in late adolescence (Lister et al., 2013). Therefore, an equal report that compares mCH methylation in ESC-derived human neurons and *in vivo* neurons is compelling and needs to be assessed in adult brain tissues. DNA methylation patterns of iPSCs and iNs have been recapitulated in Figure 2.

Mitochondrial function

Epigenetic changes may contribute to many of the hallmarks of aging, including mitochondrial dysfunction (Booth and Brunet, 2016). Mitochondria are a major generator of energy in our cells and a major target of cellular aging and age-related NDDs (Booth and Brunet, 2016; Mertens et al., 2018; Gudenschwager et al., 2021). In neurons, these organelles play a fundamental role in synaptic transmission and cell survival, by regulating energy metabolism, cell death, reactive oxygen species (ROS) production, calcium homeostasis, and macromolecule biosynthesis. Neurons rely almost completely on mitochondria-mediated oxidative phosphorylation of glucose to fulfill their energy requirements and a major part of this energy is used to maintain the electrochemical gradient across the plasma membrane which, in turn, is necessary for the synaptic transmission. Also, mitochondria contribute to homeostasis of calcium which is involved in neurotransmitters release and signal transmission. All these functions are accompanied by a modest increase in ROS which act as signaling molecules at physiological range but cause oxidative stress and cell death at higher concentrations. As cell ages, mitochondrial turnover declines, leading to alteration in glucose metabolism, increase in ROS and mutations in mitochondrial DNA, all contributing to neurodegeneration (Booth and Brunet, 2016; Mertens et al., 2018; Gudenschwager et al., 2021). Hence, mitochondrial function is another aspect that must be assessed in models of neurons derived from iPSCs and directly induced from fibroblasts. Suhr and colleagues firstly examined the properties of mitochondria in fibroblast-derived iPSCs and in fibroblasts re-derived from iPSCs, finding a dramatic improvement of mitochondrial quality and function in both cells (Suhr et al., 2010). iPSCs were induced from aged fibroblasts, indicating that iPSCs reset the mitochondrial age to an embryonic-like state. Noteworthy, fibroblasts re-differentiated from iPSCs show an improvement in mitochondrial functionality with respect to both iPSCs and parental fibroblasts lines (Suhr et al., 2010). This result was confirmed by another study showing that the induction of pluripotency can reset the metabolic age of senescent and centenarian cells (Lapasset et al., 2011). Cellular reprogramming to the pluripotent state has also proven to rejuvenate the mitochondrial-associated cell death mechanisms to an embryo stage, even from starting fibroblasts that harbor chromosomal aberrations



(Prigione et al., 2011). These cells restore mitochondrial function and the mitochondrial-mediated apoptotic signaling, crucial to prevent the oncogenic transformation that may occur in presence of chromosomal and genomic mutations. Despite being promising for the safety profile, these data suggest that iPSCs may be not ideal to study the organellar dysfunction in age-related neurodegeneration.

Instead, a study conducted by Kim and colleagues showed that iNs exhibit mitochondrial aging defects (Kim et al., 2018). Neurons directly induced from old fibroblasts show decreased expression of oxidative phosphorylation genes and impaired mitochondrial function, as assessed by increased mitochondrial fragmentation and lower total ATP levels with respect to neurons derived from young fibroblasts. As expected by previous results, iPSC-derived neurons from aged donors show no age-related mitochondrial defects, extending the mitochondrial rejuvenation that follows iPSC induction to neuronal differentiation (Kim et al., 2018).

Surprisingly, although old fibroblast-derived iNs show severe mitochondrial defects, their parental fibroblasts show only mild age-related phenotypes (Kim et al., 2018), proposing that upon neuronal transdifferentiation, iNs acquire a neuronal-specific age-dependent mitochondrial dysfunction, rather than preserving a general age-related mitochondrial status. This aspect further

validates iNs as a valuable cell source for the study of age-related bioenergetic dysfunctions directly in human neurons and emphasizes the cell-type specificity of the aging process.

Telomeres

Telomeres are special regions of repeated nucleotide sequences at the end of the chromosomes. Associated with specific proteins, they ensure the protection of the chromosomal ends from progressive degradation occurring during replication and prevent DNA repair systems from mistaking the very ends of the DNA strand for a double-strand break. The chance of the latter increases as the average telomere length decreases. The average telomere length is set and maintained in cells of the germline which typically express high levels of telomerase, whereas in somatic cells, telomere length is very heterogeneous but typically declines with age. Thus, telomere length has emerged as an indicator of replicative senescence and advancement of aging process (Aubert and Lansdorp, 2008). Importantly, the rate of increase in the percentage of short telomeres over time rather than the absolute telomere length has emerged as predictor of lifespan in mice (Vera et al., 2012). The role of this factor

in replicative aging of somatic cells is evident; however, its contribution to the aging process of post-mitotic cells, such as neurons, remains obscure. Despite not being an accurate age-predictor, telomere shortening was found to be related to neurodegeneration (Martin-Ruiz et al., 2006; Wafar et al., 2011; Kume et al., 2012). Vera and colleagues showed that the pharmacological downregulation of telomerase and following telomere shortening results in disease-specific phenotypes in human iPSC-derived DA neurons (Vera et al., 2012). These cells exhibit a loss of tyrosine hydroxylase (TH) expression during differentiation, which is a characteristic feature of early PD.

Thus, manipulating telomere length may be a valuable strategy to model late-onset disease in human iPSC-derived lineages. Still, this represents only a feature of aging and how it reproduces the physiological and pathological aspects in aging and age-related diseases, respectively, needs to be further evaluated.

Proteostasis

Proteostasis or “protein homeostasis” ensures a balanced proteome within the cells, by promoting the correct protein folding, trafficking and degradation mediated by proteasomes or lysosomes. Biological mechanisms underlying these functions are reported to become progressively impaired with age. In virtue of the post-mitotic nature of the neurons and their highly vulnerability to protein accumulation, these mechanisms are strongly related to the late-onset neurodegenerative process.

Although a direct and full comparison between iPSC-derived neurons and iNs with respect to the age-related decline in proteostasis has not been conducted, some evidence shows that iNs are somehow different in this aspect, as they were found to recapitulate different phenotypic manifestations associated with HD (Victor et al., 2018). Medium spiny neurons (MSNs) that were differentiated from iPSCs were reported to be free of the classical huntingtin (HTT) aggregates that characterize HD and to lack an overt cell death phenotype (Victor et al., 2018).

Instead, patients directly converted MSNs consistently exhibited mutant HTT (mHTT) aggregates, mHTT-dependent DNA damage, mitochondrial dysfunction, and spontaneous degeneration over time in culture. It is likely that directly reprogrammed subtype-specific neurons, as well as iNs, retain age-associated features of patients' cells and these hallmarks finally result in a more reliable manifestation of the modeled disease. In addition, nuclear pore permeabilization is linked to the correct protein compartmentalization, including TFs and regulatory proteins, and has emerged as another factor impaired during the aging process (Mertens et al., 2015). Nuclear pores are composed of nucleoporins that control the flux of proteins, RNAs, and other information between the nucleus and the cytoplasm, acting as important regulator of gene transcription and global nuclear organization. With age increasing they get more permeable to cytoplasmic proteins entering the nucleus and are increasingly leaky for nuclear proteins, impacting the subcellular localization

of proteins and the chromatin architecture and transcription. In part, the altered permeability may be a consequence of the low turnover of extremely long-lived nucleoporins, hence, an effect of age-associated damage of proteins.

Interestingly, a significant impairment in nucleocytoplasmic compartmentalization was observed in iNs derived from old donor cells compared to iNs from young and middle-aged donors, proposing an age-dependent phenomenon (Mertens et al., 2015). In contrast, iPSC-derived neurons show no detectable impairment in nucleocytoplasmic functionality in iNs converted from young, middle-aged, and old donors, indicating that iPSC rejuvenation can restore this function in old cells (Mertens et al., 2015). Taken together, these data demonstrate that iNs retain the principal aging signatures of the primary cell, and manifest neuronal-specific aging signs compared to neurons derived from iPSCs, confirming that they are an age-equivalent *in vitro* model for neuronal degeneration. Finally, the aging hallmarks can hamper the reprogramming process, but some evidence shows an equal efficient direct conversion for young and old fibroblasts (Mertens et al., 2015).

Impact of aging signatures in brain disease models

iPSC-derived and directly converted neurons for disease modeling: impact on disease phenotype. Despite many of the NDD-causing mutations have been largely characterized, it still results very difficult to conduct studies of drug screening due to the lack of a model that correctly resemble the human neuronal physiology. The different complexity of human neurophysiology renders the use of animal models an unsuitable tool for these types of diseases as demonstrated from the unsuccessfully translation of drugs derived from animal screening to clinical application. For this reason, the pursuit for a more human resembling disease model remains a sensitive issue. Promising results have been reached in recent years by differentiating neurons *in vitro* from iPSCs or from somatic cells. The big advantage of differentiating neurons from iPSCs is related to an increased plasticity of undifferentiated cells that could be more efficiently induced toward a mature phenotype. However, iPSC-derived neurons phenotype is more similar to an embryonic stage and show a reset in the epigenetic aging so resulting not optimal for modeling diseases related to aging. To overcome this issue the best chance seems to be represented by the direct reprogramming. The first attempt of direct reprogramming toward neuronal lineage was accomplished in 2010 when the Wernig group successfully converted mouse fibroblasts into iNs by expressing three TFs, namely BRN2, ASCL1, and MYT1L (Vierbuchen et al., 2010). Since then, many efforts have been applied to directly reprogram somatic cells to specific neuron subtypes. Most of these protocols are based on the co-expression of neuron subtype-specific TFs together with BAM factors. By using this approach functional induced DA neurons (iDANs) expressing TH and other midbrain markers have been generated from different somatic cells (Addis

et al., 2011; Caiazzo et al., 2011; Pfisterer et al., 2011; Kim et al., 2012; Liu et al., 2012; Torper et al., 2013; Jiang et al., 2015; Park et al., 2015; Di Val et al., 2017; Yoo et al., 2017).

However, the conversion efficiency of iNs is relatively low, ranging from 5 to 30% depending on the starting cell type. To overcome this limit many protocols have been identified based on a semi-direct approach in which pluripotency factors for direct reprogramming (PDR) can generate expandable neuronal progenitor cells (iNPCs) that can be further differentiated into desired cells (Kim J. et al., 2011; Lu et al., 2013; Zhu et al., 2014; Lee et al., 2015). Still, the usage of pluripotency factors may alter the epigenetic and transcriptional aging signatures. The direct reprogramming from blood cells by using SOX2 and C-MYC has

been proven to cause a loss of age-related DNA methylation signatures at the early stages of induced neuronal stem cells (iNSCs) which further erode across extended passaging, eventually resembling the methylation profile of iPSC-derived neuronal precursors. Moreover, the epigenetic resetting is accompanied by a lack of age-associated transcriptional signatures and absence of cellular aging hallmarks. iNSCs derived from single colonies display differences in methylation signature suggesting that during the SOX2-dependent direct reprogramming each iNSC undergoes an independent epigenetic reprogramming process (Sheng et al., 2018). Here, we summarize the most relevant updates in neurodegenerative disease modeling by using the iPSC or direct reprogramming strategies (Table 1).

TABLE 1 Disease-associated phenotypes in iPSC-derived and direct reprogramming-derived neurons.

Disease	Study	Strategy	Disease-associated phenotype
PD	Nguyen et al. (2011) Sánchez-Danés et al. (2012)	iPSC	α-synuclein aggregates ↑ oxidative stress genes ↓ number of neurites
		iPSC	↑ mitochondrial stress
	Seibler et al. (2011) Miller et al. (2013)	iPSC + progerin	abnormal nuclear morphology DNA damage ↑ ROS dendritic degeneration ↓ TH expression ↑ Lewy body
		iPSC + telomerase inhibitor	DNA damage ↑ ROS ↓ dendrites
	Lee et al. (2019)	Direct reprogramming	Proteasomal stress ↑ cell death
	Yagi et al. (2011) Israel et al. (2012) Ochalek et al. (2017) Mertens et al. (2021)	iPSC	↑ Aβ42
		iPSC	↑ Aβ42
		Direct reprogramming	Tau phosphorylation GSK-3β activation ↑ immature neuronal signaling cell cycle re-entry ↑ ROS DNA damage aneuploid DNA contents
			↑ Aβ42 ↑ p-tau e tau
	Hu et al. (2015)	Direct reprogramming	↑ p-tau e tau
ALS	Chen et al. (2014)	iPSC	NF aggregation neurite swelling axonal degeneration
	Tang et al. (2017)	Direct reprogramming	DNA damage ↓ nuclear organization
	Liu et al. (2016)	Direct reprogramming	soma shrinkage hypoactivity ↓ action potential inability to form NMJs
HD	Jeon et al. (2012)	iPSC	Absent or slow protracted HTT aggregates
	Camnasio et al. (2012)	iPSC	no evident HD phenotype
	Liu et al. (2014a,b)	Direct reprogramming	HTT aggregation abnormal neurite outgrowth and branching
			HTT aggregates mitochondrial dysfunction
	Victor et al. (2018)	Direct reprogramming	spontaneous degeneration decline in proteostasis
	Pircs et al. (2022)	Direct reprogramming	Increased DNA methylation autophagic impairment

Parkinson's disease

PD is a neurodegenerative disorder caused by the progressive loss of DANs in the substantia nigra which manifests with alteration in motility as bradykinesia, resting tremor, rigidity, flexed posture, “freezing,” and loss of postural reflexes (Lees et al., 2009). The generation of DANs from iPSC has allowed the investigation of genetic mutations in the pathogenesis of the disease and has given a proof-of-concept of the beneficial effect of reverting such mutations. Several groups have successfully obtained DANs with specific mutation related to PD starting from patient-specific iPSCs (Nguyen et al., 2011; Seibler et al., 2011; Sánchez-Danés et al., 2012).

These DANs show some of the most common features of PD such as α -synuclein (SNCA) aggregates, overexpression of oxidative stress genes, lower number of neurites, caspase-3 activation (Nguyen et al., 2011; Sánchez-Danés et al., 2012), and upregulation of PGC-1 α (Seibler et al., 2011). However, the passage through the state of undifferentiated cells causes the loss of age-related phenotypes, and to overcome this issue, several groups are trying to manipulate iPSC-derived DANs to restore the aging. Lorenz Studer's group showed a restoration of age identity by overexpressing progerin, a truncated form of lamin A known to be associated with premature aging (Dechat et al., 2008). In iPSC-derived DANs, the overexpression of progerin results in aging-associated phenotypes as abnormal nuclear morphology, DNA damage, and ROS accumulation and more specific PD features as dendritic degeneration, TH expression loss, and Lewy body accumulation (Miller et al., 2013). Later, the same research group adopted another approach which employs the pharmacological inhibition of telomerase starting from the observation that during the process of mDAN differentiation there is a shortening of telomeres.

The treatment with this inhibitor does not interfere with DAN differentiation efficacy but results in neurons with shorter telomeres that mirrors the neuronal aging phenotype (Vera et al., 2016).

In 2015, the analysis of epigenome of iPSC-derived DANs from PD patients has highlighted the role of epigenetic modifications for the development of both monogenic and sporadic disease (Fernández-Santiago et al., 2015). They found that iPSC-derived DANs from PD patients present a DNA methylation enrichment in enhancers elements resulting in downregulation of TFs as FOXA1, NR3C1, HNF4, and FOSL2 which were already associated with the specification of substantia nigra (Ziller et al., 2013). They also found that the alteration of DNA methylation was absent in parental skin cells or iPSC and only reveal upon differentiation into DANs. The PD DAN DNA methylation profile resembles the one of neuronal culture not-enriched-in-DAN indicating a failure to fully acquire the epigenetic identity during the reprogramming (Fernández-Santiago et al., 2015). Kim's group was able to generate human iNPCs starting from patients' fibroblasts with familiar LRRK2-associated and sporadic PD. The cells so

generated showed a normal ploidy and expressed neuronal precursors markers as N-CAD, PAX6, PLZF, and ZO1 and more mature ones during the differentiation (TH, MAP2, NEUN, SYNAPSIN2). Most importantly, the neurons generated also mimic the pathological features of PD neurons as shown by an enhanced susceptibility to proteasome stress induced by proteasome inhibition treatment which results in increased apoptosis measured both by cell viability and caspase 3 cleavage (Lee et al., 2019). PD patient-derived human iNPCs of Kim's group also have been used to evaluate the therapeutic efficacy of cryptotanshinone (Lee et al., 2020), a drug that was already reported to prevent oxidative stress injury in 1-methyl-4-phenyl-1,2,3,6-tetrahydropyridine (MPTP)-induced mouse PD models (Yun et al., 2018). More recently, a breakthrough was made by Drouin-Ouellet et al., who generated functional iDANs from patients with idiopathic PD, showing specific age and PD-related impairments (Drouin-Ouellet et al., 2022).

They focused on autophagic impairments since its functions decrease with age and they have been previously implicated in PD pathophysiology. Both an alteration in baseline chaperone-mediated autophagy and stress-induced autophagy were demonstrated to be present in idiopathic PD-derived iDANs. Importantly, the altered response to starvation was specific to iDANs and was not observed in any other healthy or PD iNs.

To assess how the age-associated properties of the human donors affect PD-related pathology, the Drouin-Ouellet's group asked whether the accumulation of lysosomal structures in healthy and PD-iNs was associated with the age of the donor (Drouin-Ouellet et al., 2022). In fact, they found a positive correlation between the age and the accumulation of lysosomes in neurites and a tendency toward a positive correlation of the accumulation with age of onset at diagnosis. Moreover, alterations in stress-induced autophagy observed in iNs from idiopathic PD patients led to changes in the levels of phosphorylated SNCA at the serine 129 site, whose accumulation is a hallmark of PD pathology that has been recapitulated for the first time in idiopathic PD. By contrast, any pSer129 SNCA puncta were detected in the resulting iPSC-iNs, supporting that the maintenance of age in iNs is crucial for modeling SNCA pathology in idiopathic forms of PD. Finally, direct reprogramming of DANs that maintain age-related signatures provides a faithful tool to study idiopathic PD (Drouin-Ouellet et al., 2017).

Alzheimer's disease

AD is the most common neurodegeneration in the elderly. The hallmarks of the AD are the accumulation of amyloid beta (A β) plaques, intracellular neurofibrillary tangles of hyperphosphorylated tau, and loss of synaptic connections which result in neuronal death. The disease phenotype is manifested by cognitive decline and behavior changes with memory impairment, language disturbance, and mood swings.

Several genetic mutations in amyloid precursor protein (APP), presenilin 1/2 (PS1/2) and apolipoprotein E (APOE) have been associated with pathogenesis of familial AD (fAD). However, genetic cases represent the minority of the cases as most of AD develop as sporadic (sAD) without a clear genetic etiology with risk increasing exponentially with age (Deture and Dickson, 2019). Several groups have reported the successful generation of iPSC-derived neurons from AD patients' fibroblasts (Yagi et al., 2011; Yahata et al., 2011; Israel et al., 2012; Kondo et al., 2013; Mahairaki et al., 2014; Muratore et al., 2014; Sposito et al., 2015; Ochalek et al., 2017).

Yagi and colleagues pioneered the *in vitro* modeling of AD by generating neurons from patients with PS1/2 mutation. These neurons display increased levels of amyloid β 42 (A β 42) secretion (Yagi et al., 2011). Later, it was described the generation of neurons with APP mutation from fAD (Israel et al., 2012) and from sAD (Ochalek et al., 2017) patients' fibroblasts which similarly showed higher levels of A β 42 followed by τ phosphorylation and GSK-3 β activation.

Another important application of iPSC-derived AD neurons was found in drug screening. Their usage has been very useful in deeper understanding of the potential benefits of γ - and β -secretase inhibitors on A β accumulation (Yahata et al., 2011; Israel et al., 2012; Kondo et al., 2013; Mahairaki et al., 2014; Muratore et al., 2014).

However, iPSC-dependent AD modeling retains an important limitation as they mostly express the fetal 3R isoform of tau protein. The lack of mature tau could deeply affect the results obtained in terms of reversion of pathological phenotype and drug screening (Sposito et al., 2015). Modeling of AD was also accomplished by direct reprogramming fibroblasts of both fAD and sAD patients.

Fred Gage's group was able to generate sAD iNs resembling the physiopathological characteristics of the disease with decrease of synapsis and reduction of neuronal functionality. The iNs mirror the gene expression of AD brains with the activation of immature neuronal signaling patterns and induction of cell cycle re-entry (YAP/TAZ, Notch, HIF1 α , Nf-kB, c-Myc, p53, and TGF- β). Furthermore, AD iNs display elevated ROS, DNA damage, and aneuploid DNA contents which are responsible of inducing the undifferentiated state of neurons which is an important hallmark of the early stage of AD (Mertens et al., 2021).

Another seminal approach in generating AD iNs by direct reprogramming was described by Gang Pei's group. They were able to produce chemically induced neuronal cells (chiNs) from human fibroblasts only by using a cocktail of seven small molecules and reach the same results of iPSC-derived iNs in terms of morphology, gene expression, and electrophysiology. They accomplished the direct chemical conversion of fibroblasts derived from fAD patients with APP and PS1 mutations. iNs so generated displayed accumulation of A β 42 levels in two out of four patient-derived iNs and an accumulation of both phosphorylated and total level of tau in one out of four (Hu et al., 2015).

Amyotrophic lateral sclerosis

ALS is a fatal adult-onset neurodegenerative disease characterized by progressive degeneration of motor neurons (MNs), with approximately 10% of all cases being familial. A multitude of ALS genes was found to be related to the autophagic system, including *P62*, *OPTN*, *VCP*, *UBQLN2* and *TBK*. The remaining 90% of ALS cases are classified as sporadic disease. For these patients, results from family aggregation studies have identified an overlap between ALS and common neurodegenerative disorders, including AD and PD, suggesting the existence of susceptibility genes that might increase the overall risk of neurodegeneration among relatives.

However, attempts to establish the complex genetic basis for sporadic ALS by identifying susceptibility genes have had little success. Apart from genetic susceptibility, cellular aging process takes pivotal roles in the development of ALS, but the mechanisms leading to selective MN loss around the age of onset remain poorly understood (Robberecht and Philips, 2013). This is largely due to the difficulty to obtain patient MNs in order to faithfully recapitulate patient-specific phenotype. Moreover, there is no current approved treatment for the disease, and therapeutics developed with model animals even if proven successful in ALS animals, have failed when translated to clinical trials (Chen et al., 2014). This poses the necessity to use human neurons to accurately recapitulate the specific human cellular physiology and the age-related characteristics of patients' cells, with the crucial aim of investigating ALS molecular mechanisms and to develop new screening platforms for effective therapeutics.

In this effort, researchers used the iPSC strategy to obtain MNs that harbor ALS mutations. Chen and colleagues generated iPSC lines from fibroblasts that carry mutations in Cu/Zn superoxide dismutase (*SOD1*) gene, the primary genetic cause identified in both familial and sporadic ALS cases (Chen et al., 2014). They managed to model human ALS beyond the interindividual variability and heterogeneity of the reprogrammed cell population. They used iPSCs from ALS patients with different mutations (D90A and A4V *SOD1*) and employed transcription activator-like effector nucleases (TALEN)-based homologous recombination to correct the D90A *SOD1* mutation as well as to express the same mutation in human ESCs. In addition, they used an iPSC-based reprogramming system that simply adds three small molecules to the initial neuroepithelial differentiation protocol to generate MNs with 90% efficiency of generation overcoming the issue of heterogeneity and immaturity of disease target cells. By using these strategies, they could compare the mutants and controls under the same human genetic background and establish a cause-effect relationship between disease mutations and MN defects. *SOD1* mutations emerged as leading cause of selective neurofilament (NF) misregulation in MNs but not in other neurons, leading to NF aggregation, neurite swelling, and axonal degeneration.

Despite representing a useful tool to investigate the molecular mechanisms underlying monogenic forms of ALS, iPSC approach

is not suitable to model the late-onset phenotype. By reverting the donor cell age to an embryonic-like state, it is uncertain whether the defects identified in these young neurons resemble those of disease- stage degeneration in adult human patients. In this aspect, direct reprogramming approach appears to be a promising strategy to obtain mature and functional MNs that carry the age status apart from the genetic background of patient donor cells (Tang et al., 2017). Tang and colleagues efficiently generated MNs from iPSCs or directly induced from donor fibroblasts (iMNs) and made a comparative analysis of many aging-associated feature (Tang et al., 2017). They assessed aberrant nuclear morphology and DNA damage by the number of H2AX foci, and measured SA- β -Gal activity, nuclear and chromosome architectures by nuclear lamina-associated protein 2 α (LAP2 α), H3K9me3 and heterochromatin protein 1 γ (HP1 γ).

To minimize the potential complications due to methodological variances, the group developed a protocol consisting of the same cocktail of four TFs NSIL (NGN2, SOX11, ISL1, and LHX3) that could be employed to derive MNs both from iPSCs and directly from donor fibroblasts (Tang et al., 2017). Interestingly, they reported equal efficiency of derived neurons irrespective of derived from the iPSCs or donor fibroblasts. iMNs from old donor had a much higher number of cells containing H2AX foci, a dramatic increase in cells positive for SA- β -Gal, and concomitant reduced levels of markers associated with heterochromatin and nuclear organization (LAP2 α , H3K9me3, HP1 γ). Instead, no differences on aging-associated markers were detected between iPSC-MNs from different aged-cells.

Collectively, these data show that direct reprogramming to MNs preserves the principal aging-associated hallmarks of donor cells, whereas these are reset in MNs after passage through the pluripotent stage (Tang et al., 2017). The study of Liu et al. confirmed direct reprogramming of subtype-specific neurons is a valuable approach for disease modeling and drug screening (Liu et al., 2016). They defined an efficient method to directly obtain mature and functional MNs from adult human patients (hiMNs), which is based on viral transduction of NSIL factors, followed by administration of neuron-induction media containing the extrinsic factors forskolin, dorsomorphin, and basic fibroblast growth factor. These neurons exhibit the cytological and electrophysiological features of spinal MNs and form functional neuromuscular junctions (NMJs) with skeletal muscles. Noteworthy is that hiMNs converted from ALS-patient fibroblasts carrying FUS mutations show disease-specific morphological and functional defects. These were manifested through the soma shrinkage, the mislocalization of FUS protein in the cytosol, survival deficits, dramatic deficits in action potential firing, and the inability to form NMJs. Interestingly, comparing FUS levels and subcellular localization in fibroblasts obtained from both ALS patients and healthy controls failed to detect a significant difference, in sharp contrast to hiMNs, suggesting that upon motor neuronal differentiation, these cells acquire cell-type specific features. Together, the disease phenotypes observed in hiMNs matched the pathological features found in post-mortem tissues.

Finally, the study of Liu and colleagues suggested that patient-specific hiMNs can be employed for drug identification and validation (Liu et al., 2016). In a pilot screen of small molecules that promote the survival of ALS-hiMNs, Kenpaullone emerged as the best candidate drug which can greatly improve the morphology and the survival of patients' hiMNs, by promoting outgrowth and branching of neuronal processes, and can restore motor neuron excitability.

Huntington's disease

HD is caused by expansion of CAG repeats in the first exon of the huntingtin (HTT) gene. Mutant HTT is widely expressed and believed to induce neurodegeneration through abnormal interactions with other proteins, leading to many cellular alterations and ultimately cell death (Zuccato et al., 2010). Striatal MSNs expressing dopamine- and cAMP-regulated phosphoprotein (DARPP-32) undergo the greatest degeneration.

As other NDDs, modeling HD has been challenging with animal models since significant differences between rodent and human cells and between non-neuronal cells and neurons exist. Thus, iPSC-derived neurons and iNs from patients with HD have provided precious insights into pathological mechanisms.

Jeon and colleagues obtained striatal MSNs and GABAergic neurons from iPSC-derived from patients with a juvenile form of HD (Jeon et al., 2012). Although the differentiation of MSNs was finely assessed by the immunostaining of lateral ganglionic eminence progenitors specific-markers (GSH-2 and DLX2) and MSNs marker DARPP-32, the concrete value of the reprogrammed cells for disease modeling is questionable. By using an antibody which selectively binds to the toxic N-terminal fragment of the mutant HTT (EM48), they examined whether iPSC-derived neurons develop huntingtin aggregates, a neuropathological hallmark of HD, after differentiation or intracerebral transplantation.

Surprisingly, no EM48-positive aggregates were found in cultured or grafted HD-iPSC-derived cells, presumably because of the reprogramming process to obtain iPSCs which might have affected the development of a cellular HD phenotype. An alternative explanation may be that HD-iPSCs show slow protracted huntingtin aggregate formation and such aggregates might develop at later stages of transplantation. To test this hypothesis, HD iPSC-neural precursor cells (NPC) grafted into the lateral ventricle of mice were analyzed for EM48 expression after longer time survival (at 33 weeks and 40 weeks), showing that huntingtin aggregation was evident at these stages. However, it should be considered that this model reproduces a juvenile form of disease characterized by 72 repeats and this result is not representative for modeling of late-onset forms caused by a lower number of repeats. In fact, both genetics and age contribute to HD pathology, considering that the CAG repeat expansion in HTT correlates with age of disease onset, and disease manifestation is more prevalent with increasing age, independent of CAG repeat length. iPSC-based strategies to obtain MSNs are certainly useful

for HD forms in which the genetic factor is predominant, but these may lack precious information such as the age signature of donor cells and impact the disease phenotype observed especially for late-onset diseases. Microarray profiling of 14 iPSC lines from HD patients revealed gene expression patterns that distinguish early onset versus late-onset HD, and revealed that transcriptional changes specifically associated with HD pathogenesis were only present in lines carrying longer repeats (Mattis et al., 2012). Instead, pathways not previously associated with HD pathogenesis, such as changes in calcium signaling, showed effects specific to the 60-repeat range. These data suggest that iPSC-based technology may be unsuitable to reproduce all the features of late-onset HD carrying lower CAG repeats, and it is consistent with previous studies reporting only an enhanced lysosomal activity (Camnasio et al., 2012), but not an evident HD phenotype in neurons derived from iPSCs of HD patients.

By contrast, neuron-like cells directly converted from HD patient fibroblasts obtained through modulation of cell-lineage-specific TFs or RNA processing, were found to recapitulate the major aspects of neuropathological characteristics of HD, including mutant HTT aggregation, as assessed by immunostaining with EM48, increased cell death upon neural differentiation and abnormal neurite outgrowth and branching which is in accordance with a previous *in vivo* study in which abnormal dendritic arbors and increased dendritic branching in spiny striatal neurons were identified in post-mortem HD patients' brain sections (Liu et al., 2014a). Consistently, another investigation reported mutant HTT aggregates, mutant HTT-dependent DNA damage, mitochondrial dysfunction, and spontaneous degeneration in MSNs directly derived from patients' fibroblasts carrying CAG repeats lower than 50, as this range reflects most adult-onset cases (Victor et al., 2018). The same group demonstrated that iPSC-based protocol alters mutant HTT aggregation propensity. They derived HD-iPSCs from adult HD fibroblasts and differentiated these iPSCs back into embryonic fibroblast-like cells (HEFs). Upon direct conversion of HD-HEFs to MSNs little to no aggregated mutant HTT was detectable in these cells. More importantly, ubiquitin proteasome system (UPS), the main protein quality control machinery in the cell, was collapsed in HD-MSNs in comparison to embryonic MSNs, which retained the proteasome activity comparable to iPSCs. In addition, by comparing gene expression in young versus old fibroblasts and MSNs, fibroblasts did not display drastic changes in the expression of UPS-related genes with age, but MSNs from older individuals showed a dramatic increase in the number of downregulated UPS-related genes (Victor et al., 2018). The data suggest that the proteostasis collapse in adult MSNs, but not in originating fibroblasts or iPSC-derived neurons, is dependent on the cellular age of converted neurons (Victor et al., 2018). Therefore, age retention is crucial for HD modeling since the age-associated decline in proteostasis, which in turn reflects the downstream mutant HTT aggregates, is absent in iPSC-derived neurons. Eventually, mutant HTT aggregation is responsible for other HD-associated hallmarks, including increased DNA damage followed by spontaneous degeneration.

More direct evidence on the contribution of aging in HD phenotype manifestation was then provided by investigating the properties of MSNs reprogrammed from HD-fibroblasts sampled before the disease onset Pre-HD-MSNs. These neurons appeared less vulnerable to mHTT-induced toxicity, with lower levels of cell death and oxidative DNA damage, even though they still contained mutant HTT aggregates at a similar level as symptomatic HD-MSNs (Victor et al., 2018).

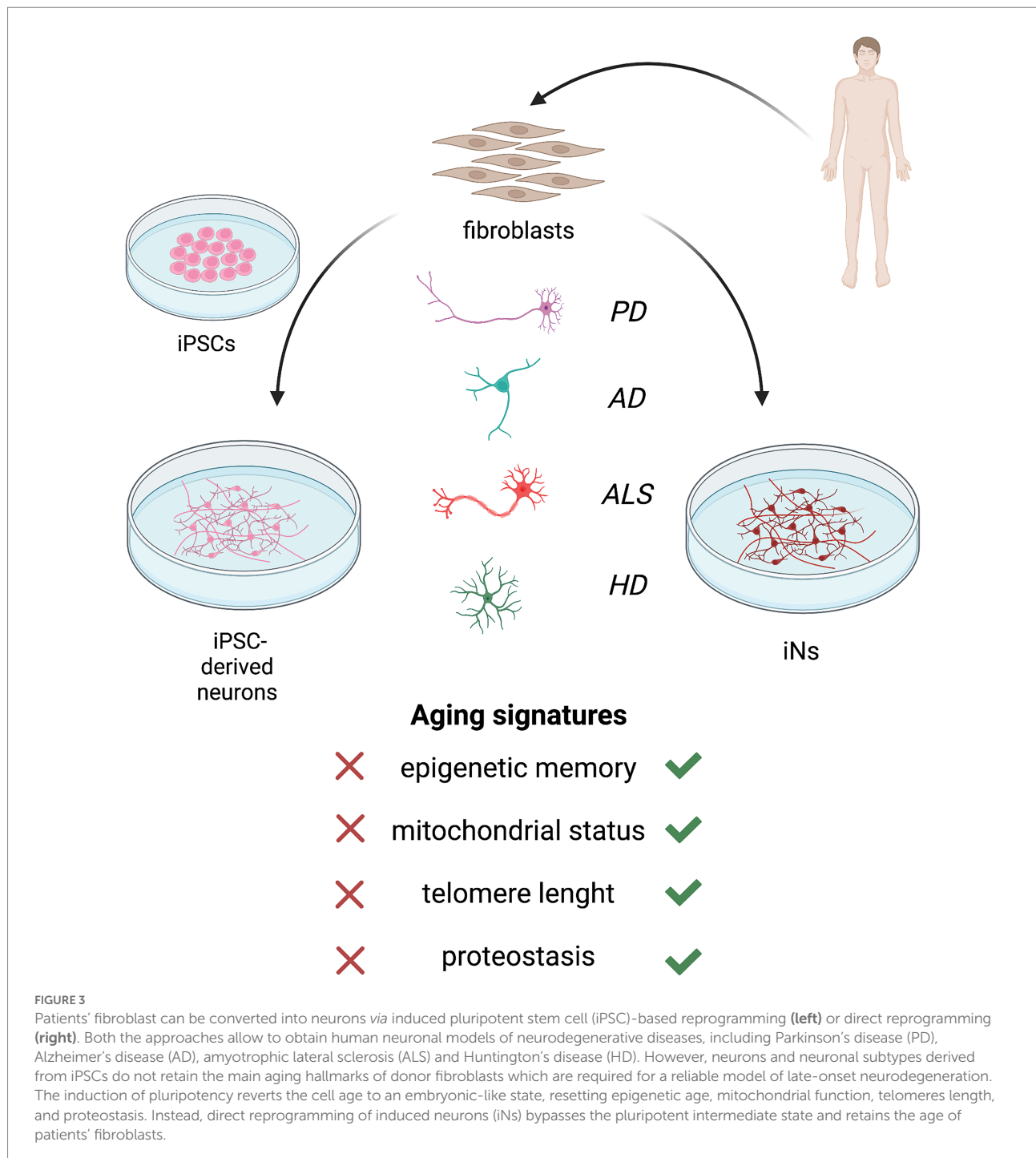
Therefore, directly converted HD-MSNs provide a human cellular model more suitable for examining the contribution of age and genetic factors to late-onset diseases. DARPP32⁺ neurons derived from adult-onset HD patients with clinically relevant CAG repeat lengths (41Q–57Q) showed a direct relationship between BDNF protein expression, CAG repeat length, and disease onset (Monk et al., 2021). BDNF plays a key role in the differentiation and maturation of striatal MSNs, with reduced BDNF signaling strongly implicated in HD neuropathogenesis. The protein expression negatively correlated to CAG repeat length and positively correlated to age of symptoms onset at days 30 and 45 of differentiation. Thus, at the individual patient level, BDNF levels directly relate to key HD pathological features, which can be modeled using direct-to-iNP reprogramming. Another age-associated hallmark in HD is the increase in epigenetic aging rates, which was previously described in post-mortem brain tissues (Steve Horvath et al., 2016). Since directly converted neurons from HD patients retain the age of donor cell (Pirces et al., 2022), this factor was investigated in this neuronal model. Pirces and colleagues examined the epigenetic age and confirmed a significantly increased DNA methylation predicted biological age in neurons induced from HD patients with respect to the control neurons (Pirces et al., 2022).

Interestingly, this model helped to unveil many of the molecular mechanisms underlying autophagic impairment, a factor widely associated with HD pathogenesis, and pointed to a combination of age-related epigenetic alterations and mutant HTT-mediated post transcriptional processes as a potential explanation for these defects.

Exactly how aging and the epigenetic alterations impact the disease pathology and autophagy impairments is currently unknown, but this model will allow further investigation of mechanistic links between these phenomena.

Current achievements and prospects

Aging hallmarks represent important contributors to neurodegeneration development and each aging feature differentially interacts with genetic and environmental factors in disease progression and manifestation. Also, its effect is related to the subtype-specific cell type/neuron (Kim et al., 2018; Victor et al., 2018; Pirces et al., 2022), underpinning the distinct involvement of aging in different NDDs. The relevance of age for late-onset NDDs development has been pictorially illustrated in Figure 3. Modeling neurodegeneration has been challenging due to the difficult accessibility in a source of human cells that could



serve as a platform to study molecular mechanisms and test pharmacological treatments.

In this scenario, iPSC differentiation and direct neural conversion methods have emerged as promising and relatively reliable tools to obtain neurons that can recapitulate human disease phenotypes *in vitro*. However, iPSC-based technologies were reported to lack the aging signature of donor cell lines and to revert the cellular age to an embryonic-like state. The induction of pluripotency before neural differentiation restores age-associated cellular features, including epigenetic age,

mitochondrial functions, telomere length, and proteostasis (Maherali et al., 2007; Meissner et al., 2008; Lapasset et al., 2011; Mertens et al., 2015).

Cell rejuvenation occurring in iPSCs and iPSC-derived neurons limits their use for disease modeling, since in some cases, they lack an overt disease-associated phenotype (Zhang et al., 2011; Camnasio et al., 2012; Mattis et al., 2012), whereas in other investigations, it is still uncertain whether the defects identified in young neurons resemble those of disease-stage degeneration in adult human patients.

Neurons resemble those of disease-stage degeneration in adult human patients (Chen et al., 2014). In the attempts of including aging features in iPSC-derived neurons to study late-onset diseases, some researchers used brief progerin exposure, a truncated form of lamin A involved in premature aging (Miller et al., 2013).

Despite observing several age- and PD-related phenotypes not seen in previous iPSC studies, the question of whether targeting pathways that trigger progeroid syndromes mimics pathological over physiological aging remains elusive.

A more physiological approach exploited telomere shortening, but only a preliminary disease-related feature such as TH loss was observed in PD-iPSC-derived neurons and a wider characterization of the effects on disease manifestation is required to confirm the validity of this approach (Vera et al., 2016).

Apart from NDD modeling, a new wave of studies has been performed in the field of iPSC-related rejuvenation, which may have the potential for application in cell replacement therapy of age-related diseases. Recent studies are focusing on the “transient reprogramming” strategy, in which OKSM factors are briefly expressed in order to restore epigenetic age while retaining starting cell identity, raising the possibility of inducing cell rejuvenation *in vivo* (Olova et al., 2019; Gill et al., 2022). Directly induced neurons appear the most suitable strategy to model late-onset NDDs. Retaining all the main aging hallmarks of primary fibroblasts, iNs have proven to recapitulate age-related features in PD models (Lee et al., 2019, 2020; Drouin-Ouellet et al., 2022), ALS (Liu et al., 2016), and HD (Liu et al., 2014b; Victor et al., 2018; Monk et al., 2021; Pircs et al., 2022).

A major hurdle for the use of iNs for studying age-related diseases is the poor reproducibility and efficiency. The development of a platform to study NDDs and to find potential drugs requires an adequate number of reproducible cells. Translating the tool to a larger scale is challenging by using a direct neural conversion protocol, since it does not include a highly expandable intermediate stage and the neurons generated are postmitotic. The expandable phase of iN conversion depends entirely on the proliferation of fibroblasts, whereas the resultant yield of iNs strictly depends on the conversion rate. This also brings to a higher degree of variability in the converted cells due to the absence of clone selection. In contrast, iPSCs, once derived, can theoretically be expanded infinitely, making them suitable for the generation of large numbers of neurons for subsequent applications that require relatively large amounts of material, such as drug screening.

Direct conversion approach can be used from patients' fibroblasts (Victor et al., 2018; Capano et al., 2022; Drouin-Ouellet et al., 2022; Pircs et al., 2022) and some evidence demonstrates that cells from all ages can be converted into iNs (Mertens et al., 2015). Noteworthy, a general difficulty in reaching equal conversion rates from adult or aged fibroblasts has been reported (Caiazzo et al., 2011; He et al., 2019), finally limiting the applicability of direct reprogramming for studying aging contribution in neurodegeneration. Improvements in conversion efficiencies especially from aged donors are needed before iN-based models can be translatable to large-scale investigations and pharmacological drug discovery in the treatment of age-related NDDs.

Interestingly, several studies are recently highlighting new molecular mechanisms involved in direct conversion process, therefore paving the way toward its optimization (Xie et al., 2018; Matsuda et al., 2019; Della Valle et al., 2020). Recently, Della Valle and colleagues proved that L1 retrotransposons are re-activated during the early stages of direct conversion in fully differentiated iDANs and inserted in specific regions of the genome relevant for neuronal lineage commitment and function (Della Valle et al., 2020). L1 retrotransposition is associated with increased chromatin accessibility and nearby lncRNA production in recipient loci. Moreover, blocking of L1 dynamics severely impairs the efficiency of iDAN transdifferentiation, suggesting that L1 retrotransposons are regulatory elements that elicit the expression of novel noncoding transcripts through chromatin remodeling. This confirms the role of both epigenetic mechanisms and non-coding RNAs (Pascale et al., 2022) in direct neural reprogramming and paves the way for a better understanding of the epigenetic mechanisms and their mechanistic link with downstream activation of lineage-specific genetic programs which can improve direct cell reprogramming-based technologies for future applications.

Author contributions

SA, CC, and MC contributed to conception and design of the article. CC created the table. SA created the figure. SA and CC wrote the first draft of the manuscript. All authors contributed to the article and approved the submitted version.

Funding

This work was supported by the H2020-FETOPEN-2018-2019-2020-01 ENLIGHT, Project number: 964497.

Acknowledgments

Figures were created with BioRender.

Conflict of interest

The authors declare that the research was conducted in the absence of any commercial or financial relationships that could be construed as a potential conflict of interest.

Publisher's note

All claims expressed in this article are solely those of the authors and do not necessarily represent those of their affiliated organizations, or those of the publisher, the editors and the reviewers. Any product that may be evaluated in this article, or claim that may be made by its manufacturer, is not guaranteed or endorsed by the publisher.

References

- Addis, R. C., Hsu, F. C., Wright, R. L., Dichter, M. A., Coulter, D. A., and Gearhart, J. D. (2011). Efficient conversion of astrocytes to functional midbrain dopaminergic neurons using a single Polycistronic vector. *PLoS One* 6:e28719. doi: 10.1371/journal.pone.0028719
- Apostolou, E., and Hochedlinger, K. (2013). Chromatin dynamics during cellular reprogramming. *Nature* 502, 462–471. doi: 10.1038/nature12749
- Aubert, G., and Lansdor, P. M. (2008). Telomeres and aging. *Physiol. Rev.* 88, 557–579. doi: 10.1152/physrev.00026.2007
- Bar-Nur, O., Russ, H. A., Efrat, S., and Benvenisty, N. (2011). Epigenetic memory and preferential lineage-specific differentiation in induced pluripotent stem cells derived from human pancreatic islet Beta cells. *Cell Stem Cell* 9, 17–23. doi: 10.1016/j.stem.2011.06.007
- Booth, L. N., and Brunet, A. (2016). The aging epigenome. *Mol. Cell* 62, 728–744. doi: 10.1016/j.molcel.2016.05.013
- Caiazzo, M., Dell'Anno, M. T., Dvoretzskova, E., Lazarevic, D., Taverna, S., Leo, D., et al. (2011). Direct generation of functional dopaminergic neurons from mouse and human fibroblasts. *Nature* 476, 224–227. doi: 10.1038/nature10284
- Camnasio, S., Carri, A. D., Lombardo, A., Grad, I., Mariotti, C., Castucci, A., et al. (2012). The first reported generation of several induced pluripotent stem cell lines from homozygous and heterozygous Huntington's disease patients demonstrates mutation related enhanced lysosomal activity. *Neurobiol. Dis.* 46, 41–51. doi: 10.1016/j.nbd.2011.12.042
- Campisi, J., and Vijg, J. (2009). Does damage to DNA and other macromolecules play a role in aging? If so how? *J. Gerontol.-Ser. A Biol. Sci. Med. Sci.* 64:175. doi: 10.1093/gerona/gln065
- Capano, L. S., Sato, C., Ficulle, E., Yu, A., Horie, K., Kwon, J. S., et al. (2022). Recapitulation of endogenous 4R tau expression and formation of insoluble tau in directly reprogrammed human neurons. *Cell Stem Cell* 29, 918–932.e8; 583. doi: 10.1016/j.stem.2022.04.018
- Chambers, S. M., Fasano, C. A., Papapetrou, E. P., Tomishima, M., Sadelain, M., and Studer, L. (2009). Highly efficient neural conversion of human ES and iPS cells by dual inhibition of SMAD signaling. *Nat. Biotechnol.* 27, 275–280. doi: 10.1038/nbt.1529
- Chen, H., Qian, K., Du, Z., et al. (2014). Modeling ALS with iPSCs reveals that mutant SOD1 Misregulates Neurofilament balance in motor neurons. *Cell Stem Cell* 14, 796–809. doi: 10.1016/j.stem.2014.02.004
- Dechat, T., Pflieger, K., Sengupta, K., Shimi, T., Shumaker, D. K., Solimando, L., et al. (2008). Nuclear Lamins: major factors in the structural organization and function of the nucleus and chromatin. *Genes Dev.* 22, 832–853. doi: 10.1101/gad.1652708
- Della Valle, F., Thimma, M. P., Caiazzo, M., et al. (2020). Transdifferentiation of mouse embryonic fibroblasts into dopaminergic neurons reactivates LINE-1 repetitive elements. *Stem Cell Rep.* 14, 60–74. doi: 10.1016/j.stemcr.2019.12.002
- Deture, M. A., and Dickson, D. W. (2019). The neuropathological diagnosis of Alzheimer's disease. *Mol. Neurodegener.* 14:32. doi: 10.1186/s13024-019-0333-5
- Di Val, R., Cervo, P., Romanov, R. A., Spigolon, G., et al. (2017). Induction of functional dopamine neurons from human astrocytes in vitro and mouse astrocytes in a Parkinson's disease model. *Nat. Biotechnol.* 35, 444–452. doi: 10.1038/nbt.3835
- Dimos, J. T., Rodolfa, K. T., Niakan, K. K., Weisenthal, L. M., Mitsumoto, H., Chung, W., et al. (2008). Induced pluripotent stem cells generated from patients with ALS can be differentiated into motor neurons. *Science* 321, 1218–1221. doi: 10.1126/science.1158799
- Drouin-Ouellet, J., Legault, E. M., Nilsson, F., Pircs, K., Bouquety, J., Petit, F., et al. (2022). Age-related pathological impairments in directly reprogrammed dopaminergic neurons derived from patients with idiopathic Parkinson's disease. *Stem Cell Rep.* 17, 2203–2219. doi: 10.1016/j.stemcr.2022.08.010
- Drouin-Ouellet, J., Pircs, K., Barker, R. A., Jakobsson, J., and Parmar, M. (2017). Direct neuronal reprogramming for disease modeling studies using patient-derived neurons: what have we learned? *Front. Neurosci.* 11:530. doi: 10.3389/fnins.2017.00530
- Fernández-Santiago, R., Carballo-Carbajal, I., Castellano, G., Torrent, R., Richaud, Y., Sánchez-Danés, A., et al. (2015). Aberrant epigenome in iPSC-derived dopaminergic neurons from Parkinson's disease patients. *EMBO Mol. Med.* 7, 1529–1546. doi: 10.15252/emmm.201505439
- Gill, D., Parry, A., Santos, F., Okkenhaug, H., Todd, C. D., Hernando-Herraez, I., et al. (2022). Multi-omic rejuvenation of human cells by maturation phase transient reprogramming. *elife* 11:e71624. doi: 10.7554/eLife.71624
- Gladyshev, V. N. (2016). Aging: progressive decline in fitness due to the rising Deleterious adjusted by genetic, environmental, and stochastic processes. *Aging Cell* 15, 594–602. doi: 10.1111/acel.12480
- Guidenschwager, C., Chavez, I., Cardenas, C., et al. (2021). Directly reprogrammed human neurons to understand age-related energy metabolism impairment and mitochondrial dysfunction in healthy aging and neurodegeneration. *Oxidative Med. Cell. Longev.* 2021, 1–14. doi: 10.1155/2021/5586052
- Guo, J. U., Yijing, S., Shin, J. H., Shin, J., Li, H., Xie, B., et al. (2014). Distribution, recognition and regulation of non-CpG methylation in the adult mammalian brain. *Nat. Neurosci.* 17, 215–222. doi: 10.1038/nn.3607
- He, Y., and Ecker, J. R. (2015). Non-CG methylation in the human genome. *Annu. Rev. Genomics Hum. Genet.* 16, 55–77. doi: 10.1146/annurev-genom-090413-025437
- He, M., Zhang, H., Li, Y., Tian, C., Tang, B., Huang, Y., et al. (2019). Direct and selective lineage conversion of human fibroblasts to dopaminergic precursors. *Neurosci. Lett.* 699, 16–23. doi: 10.1016/j.neulet.2019.01.033
- Horvath, S. (2013). DNA methylation age of human tissues and cell types. *Genome Biol.* 14:R115. doi: 10.1186/gb-2013-14-10-r115
- Horvath, S., Langfelder, P., Kwak, S., Aaronson, J., Rosinski, J., Vogt, T. F., et al. (2016). Huntington's disease accelerates epigenetic aging of human brain and disrupts DNA methylation levels. *Aging (Albany NY)* 8, 1485–1512. doi: 10.18632/aging.101005
- Horvath, S., and Raj, K. (2018). DNA methylation-based biomarkers and the epigenetic clock theory of ageing. *Nat. Rev. Genet.* 19, 371–384. doi: 10.1038/s41576-018-0004-3
- Hu, W., Qiu, B., Guan, W., Wang, Q., Wang, M., Li, W., et al. (2015). Direct conversion of Normal and Alzheimer's disease human fibroblasts into neuronal cells by small molecules. *Cell Stem Cell* 17, 204–212. doi: 10.1016/j.stem.2015.07.006
- Huh, C. J., Zhang, B., Victor, M. B., et al. (2016). Maintenance of age in human neurons generated by micro RNA-based neuronal conversion of fibroblasts. *elife* 5:e18648. doi: 10.7554/eLife.18648
- Israel, M. A., Yuan, S. H., Bardy, C., Reyna, S. M., Mu, Y., Herrera, C., et al. (2012). Probing sporadic and familial Alzheimer's disease using induced pluripotent stem cells. *Nature* 482, 216–220. doi: 10.1038/nature10821
- Jeon, I., Lee, N., Li, J. Y., et al. (2012). Neuronal properties, in vivo effects, and pathology of a Huntington's disease patient-derived induced pluripotent stem cells. *Stem Cells* 30, 2054–2062. doi: 10.1002/stem.1135
- Jiang, H., Xu, Z., Zhong, P., Ren, Y., Liang, G., Schilling, H. A., et al. (2015). Cell cycle and P 53 gate the direct conversion of human fibroblasts to dopaminergic neurons. *Nat. Commun.* 6:6. doi: 10.1038/ncomms10100
- Kim, J., Ambasudhan, R., and Ding, S. (2012). Direct lineage reprogramming to neural cells. *Curr. Opin. Neurobiol.* 22, 778–784. doi: 10.1002/stem.1135
- Kim, J., Efe, J. A., Zhu, S., Talantova, M., Yuan, X., Wang, S., et al. (2011). Direct reprogramming of mouse fibroblasts to neural progenitors. *Proc. Natl. Acad. Sci. U. S. A.* 108, 7838–7843. doi: 10.1073/pnas.1103113108
- Kim, K., Zhao, R., Doi, A., Ng, K., Unterhaeuer, J., Cahan, P., et al. (2011). Donor cell type can influence the epigenome and differentiation potential of human induced pluripotent stem cells. *Nat. Biotechnol.* 29, 1117–1119. doi: 10.1038/nbt.2052
- Kim, Y., Zheng, X., Ansari, Z., Bunnell, M. C., Herdy, J. R., Traxler, L., et al. (2018). Mitochondrial aging defects emerge in directly reprogrammed human neurons due to their metabolic profile. *Cell Rep.* 23, 2550–2558. doi: 10.1016/j.celrep.2018.04.105
- Kondo, T., Asai, M., Tsukita, K., Kutoku, Y., Ohsawa, Y., Sunada, Y., et al. (2013). Modeling Alzheimer's disease with iPSCs reveals stress phenotypes associated with intracellular A β and differential drug responsiveness. *Cell Stem Cell* 12, 487–496. doi: 10.1016/j.stem.2013.01.009
- Kriks, S., Shim, J. W., Piao, J., Ganat, Y. M., Wakeman, D. R., Xie, Z., et al. (2011). Dopamine neurons derived from human ES cells efficiently engraft in animal models of Parkinson's disease. *Nature* 480, 547–551. doi: 10.1038/nature10648
- Kume, K., Kikukawa, M., Hanyu, H., Takata, Y., Umahara, T., Sakurai, H., et al. (2012). Telomere length shortening in patients with dementia with Lewy bodies. *Eur. J. Neurol.* 19, 905–910. doi: 10.1111/j.1468-1331.2011.03655.x
- Lapasset, L., Milhavet, O., Prieur, A., Besnard, E., Babled, A., Ait-Hamou, N., et al. (2011). Rejuvenating senescent and centenarian human cells by reprogramming through the pluripotent state. *Genes Dev.* 25, 2248–2253. doi: 10.1101/gad.173922.111
- Lee, J. H., Mitchell, R. R., McNicol, J. D., et al. (2015). Single transcription factor conversion of human blood fate to NPCs with CNS and PNS developmental capacity. *Cell Rep.* 11, 1367–1376. doi: 10.1016/j.celrep.2015.04.056
- Lee, M., Sim, H., Ahn, H., Ha, J., Baek, A., Jeon, Y. J., et al. (2019). Direct reprogramming to human induced neuronal progenitors from fibroblasts of familial and sporadic Parkinson's disease patients. *Int. J. Stem Cells* 12, 474–483. doi: 10.15283/ijsc19075

- Lee, J. E., Sim, H., Yoo, H. M., Lee, M., Baek, A., Jeon, Y. J., et al. (2020). Neuroprotective effects of Cryptotanshinone in a direct reprogramming model of Parkinson's disease. *Molecules* 25:3602. doi: 10.3390/molecules25163602
- Lees, A. J., Hardy, J., and Revesz, T. (2009). Parkinson's disease. *Lancet* 373, 2055–2066. doi: 10.1016/S0140-6736(09)60492-X
- Lister, R., Mukamel, E. A., Nery, J. R., Urich, M., Puddifoot, C. A., Johnson, N. D., et al. (2013). Global epigenomic reconfiguration during mammalian brain development. *Science* 341:1237905. doi: 10.1126/science.1237905
- Lister, R., Pelizzola, M., Kida, Y. S., David Hawkins, R., Nery, J. R., Hon, G., et al. (2011). Hotspots of aberrant Epigenomic reprogramming in human induced pluripotent stem cells. *Nature* 471, 68–73. doi: 10.1038/nature09798
- Liu, X. J., Huang, Q., Li, F., and Li, C. Y. (2014a). Enhancing the efficiency of direct reprogramming of human primary fibroblasts into dopaminergic neuron-like cells through P 53 suppression. *Sci. China Life Sci.* 57, 867–875. doi: 10.1007/s11427-014-4730-2
- Liu, X., Li, F., Stubblefield, E. A., Blanchard, B., Richards, T. L., Larson, G. A., et al. (2012). Direct reprogramming of human fibroblasts into dopaminergic neuron-like cells. *Cell Res.* 22, 321–332. doi: 10.1038/cr.2011.181
- Liu, Y., Xue, Y., Ridley, S., Zhang, D., Rezvani, K., Fu, X. D., et al. (2014b). Direct reprogramming of Huntington's disease patient fibroblasts into neuron-like cells leads to abnormal neurite outgrowth, increased cell death, and aggregate formation. *PLoS One* 9:e109621. doi: 10.1371/journal.pone.0109621
- Liu, M. L., Zang, T., and Zhang, C. L. (2016). Direct lineage reprogramming reveals disease-specific phenotypes of motor neurons from human ALS patients. *Cell Rep.* 14, 115–128. doi: 10.1016/j.celrep.2015.12.018
- Lu, Y., Brommer, B., Tian, X., Krishnan, A., Meer, M., Wang, C., et al. (2020). Reprogramming to recover youthful epigenetic information and restore vision. *Nature* 588, 124–129. doi: 10.1038/s41586-020-2975-4
- Lu, J., Liu, H., Huang, C. T. L., Chen, H., du, Z., Liu, Y., et al. (2013). Generation of integration-free and region-specific neural progenitors from primate fibroblasts. *Cell Rep.* 3, 1580–1591. doi: 10.1016/j.celrep.2013.04.004
- Luo, C., Lee, Q. Y., Wapinski, O., Castanon, R., Nery, J. R., Mall, M., et al. (2019). Global DNA methylation remodeling during direct reprogramming of fibroblasts to neurons. *Life* 8:e40197. doi: 10.7554/eLife.40197
- Mahairaki, V., Ryu, J., Peters, A., Chang, Q., Li, T., Park, T. S., et al. (2014). Induced pluripotent stem cells from familial Alzheimer's disease patients differentiate into mature neurons with Amyloidogenic properties. *Stem Cells Dev.* 23, 2996–3010. doi: 10.1089/scd.2013.0511
- Maherali, N., Sridharan, R., Xie, W., Utikal, J., Eminli, S., Arnold, K., et al. (2007). Directly reprogrammed fibroblasts show global epigenetic remodeling and widespread tissue contribution. *Cell Stem Cell* 1, 55–70. doi: 10.1016/j.stem.2007.05.014
- Maroof, A. M., Keros, S., Tyson, J. A., Ying, S. W., Ganat, Y. M., Merkle, F. T., et al. (2013). Directed differentiation and functional maturation of cortical interneurons from human embryonic stem cells. *Cell Stem Cell* 12, 559–572. doi: 10.1016/j.stem.2013.04.008
- Martin, S., Poppe, D., Olova, N., O'Leary, C., Ivanova, E., Pflueger, J., et al. (2020). Conserved and divergent features of DNA methylation in embryonic stem cell-derived neurons. *BioRxiv* 2020:898429. doi: 10.1101/2020.01.08.898429
- Martin-Ruiz, C., Dickinson, H. O., Keys, B., Rowan, E., Kenny, R. A., and von Zglinicki, T. (2006). Telomere length predicts Poststroke mortality, dementia, and cognitive decline. *Ann. Neurol.* 60, 174–180. doi: 10.1002/ana.20869
- Matsuda, T., Irie, T., Katsurabayashi, S., Hayashi, Y., Nagai, T., Hamazaki, N., et al. (2019). Pioneer Factor NeuroD1 Rearranges Transcriptional and Epigenetic Profiles to Execute Microglia-Neuron Conversion. *Neuron* 101:472–485.e7. doi: 10.1016/j.neuron.2018.12.010
- Mattis, V. B., Svendsen, S. P., Ebert, A., et al. (2012). Induced pluripotent stem cells from patients with Huntington's disease show CAG repeat expansion associated phenotypes. *Cell Stem Cell* 11, 264–278. doi: 10.1016/j.stem.2012.04.027
- Meissner, A., Mikkelsen, T. S., Gu, H., Wernig, M., Hanna, J., Sivachenko, A., et al. (2008). Genome-scale DNA methylation maps of pluripotent and differentiated cells. *Nature* 454, 766–770. doi: 10.1038/nature07107
- Mertens, J., Herdy, J. R., Traxler, L., Schafer, S. T., Schlachetzki, J. C. M., Böhnke, L., et al. (2021). Age-dependent instability of mature neuronal fate in induced neurons from Alzheimer's patients. *Cell Stem Cell* 28, 1533–1548.e6. doi: 10.1016/j.stem.2021.04.004
- Mertens, J., Paquola, A. C. M., Ku, M., Hatch, E., Böhnke, L., Ladjevardi, S., et al. (2015). Directly reprogrammed human neurons retain aging-associated transcriptomic signatures and reveal age-related nucleocytoplasmic defects. *Cell Stem Cell* 17, 705–718. doi: 10.1016/j.stem.2015.09.001
- Mertens, J., Reid, D., Lau, S., Kim, Y., and Gage, F. H. (2018). Aging in a dish: iPSC-derived and directly induced neurons for studying brain aging and age-related neurodegenerative diseases. *Annu. Rev. Genet.* 52, 271–293. doi: 10.1146/annurev-genet-120417-031534
- Miller, J. D., Ganat, Y. M., Kishinevsky, S., Bowman, R. L., Liu, B., Tu, E. Y., et al. (2013). Human iPSC-based modeling of late-onset disease via Progerin-induced aging. *Cell Stem Cell* 13, 691–705. doi: 10.1016/j.stem.2013.11.006
- Mo, A., Mukamel, E. A., Davis, F. P., Luo, C., Henry, G. L., Picard, S., et al. (2015). Epigenomic signatures of neuronal diversity in the mammalian brain. *Neuron* 2015, 1369–1384. doi: 10.1016/j.neuron.2015.05.018
- Monk, R., Lee, K., Jones, K. S., and Connor, B. (2021). Directly reprogrammed Huntington's disease neural precursor cells generate striatal neurons exhibiting aggregates and impaired neuronal maturation. *Stem Cells* 39, 1410–1422. doi: 10.1002/stem.3420
- Muratore, C. R., Rice, H. C., Srikanth, P., Callahan, D. G., Shin, T., Benjamin, L. N. P., et al. (2014). The familial Alzheimer's disease APPV717I mutation alters APP processing and tau expression in iPSC-derived neurons. *Hum. Mol. Genet.* 23, 3523–3536. doi: 10.1093/hmg/ddu064
- Nguyen, H. N., Byers, B., Cord, B., Shcheglovitov, A., Byrne, J., Gujar, P., et al. (2011). LRRK2 mutant iPSC-derived Da neurons demonstrate increased susceptibility to oxidative stress. *Cell Stem Cell* 8, 267–280. doi: 10.1016/j.stem.2011.01.013
- Oberdoerffer, P., and Sinclair, D. A. (2007). The role of nuclear architecture in genomic instability and ageing. *Nat. Rev. Mol. Cell Biol.* 8, 692–702. doi: 10.1038/nrm2238
- Ochalek, A., Mihalik, B., Avci, H. X., Chandrasekaran, A., Téglási, A., Bock, I., et al. (2017). Neurons derived from sporadic Alzheimer's disease iPSCs reveal elevated TAU hyperphosphorylation, increased amyloid levels, and GSK3B activation. *Alzheimers Res. Ther.* 9:90. doi: 10.1186/s13195-0170317z
- Olova, N., Simpson, D. J., Marioni, R. E., and Chandra, T. (2019). Partial reprogramming induces a steady decline in epigenetic age before loss of somatic identity. *Aging Cell* 18:e12877. doi: 10.1111/acel.12877
- Osafune, K., Caron, L., Borowiak, M., Martinez, R. J., Fitz-Gerald, C. S., Sato, Y., et al. (2008). Marked differences in differentiation propensity among human embryonic stem cell lines. *Nat. Biotechnol.* 26, 313–315. doi: 10.1038/nbt1383
- Park, H., Kim, H., Yoo, J., Lee, J., Choi, H., Baek, S., et al. (2015). Homogeneous generation of iDA neurons with high similarity to Bona fide DA neurons using a drug inducible system. *Biomaterials* 72, 152–162. doi: 10.1016/j.biomaterials.2015.09.002
- Pascale, E., Caiazza, C., Paladino, M., Parisi, S., Passaro, F., and Caiazza, M. (2022). Micro RNA roles in cell reprogramming mechanisms. *Cells* 11:940. doi: 10.3390/cells11060940
- Pfisterer, U., Kirkeby, A., Torper, O., Wood, J., Nelander, J., Dufour, A., et al. (2011). Direct conversion of human fibroblasts to dopaminergic neurons. *Proc. Natl. Acad. Sci. U. S. A.* 108, 10343–10348. doi: 10.1073/pnas.1105135108
- Pircs, K., Drouin-Ouellet, J., Horváth, V., Gil, J., Rezel, M., Garza, R., et al. (2022). Distinct subcellular autophagy impairments in induced neurons from patients with Huntington's disease. *Brain* 145, 3035–3057. doi: 10.1093/brain/awab473
- Prigione, A., Hossini, A. M., Lichtner, B., Serin, A., Fauler, B., Megges, M., et al. (2011). Mitochondrial-associated cell death mechanisms reset to an embryonic-like state in aged donor derived IPS cells harboring chromosomal aberrations. *PLoS One* 6:e27352. doi: 10.1371/journal.pone.0027352
- Robberecht, W., and Philips, T. (2013). The changing scene of amyotrophic lateral sclerosis. *Nat. Rev. Neurosci.* 14, 248–264. doi: 10.1038/nrn3430
- Roessler, R., Smallwood, S. A., and Veenfliet, J. V., et al. (2014). Detailed analysis of the genetic and epigenetic signatures of iPSCs-derived Mesodiencephalic dopaminergic neurons. *Stem Cell Rep.* 2: 520–533; doi: 10.1016/j.stemcr.2014.03.001
- Sánchez-Danés, A., Richaud-Patin, Y., Carballo-Carbajal, I., Jiménez-Delgado, S., Caig, C., Mora, S., et al. (2012). Disease-specific phenotypes in dopamine neurons from human IPS-based models of genetic and sporadic Parkinson's disease. *EMBO Mol. Med.* 4, 380–395. doi: 10.1002/emmm.201200215
- Seibler, P., Graziotto, J., Jeong, H., Simunovic, F., Klein, C., and Krainc, D. (2011). Mitochondrial Parkin recruitment is impaired in neurons derived from mutant PINK1 induced pluripotent stem cells. *J. Neurosci.* 31, 5970–5976. doi: 10.1523/JNEUROSCI.4441-10.2011
- Sen, T., and Thummer, R. P. (2022). CRISPR and iPSCs: recent developments and future perspectives in neurodegenerative disease modelling, research, and therapeutics. *Neurotox. Res.* 40, 1597–1623. doi: 10.1007/s12640-022-00564-w
- Sheng, C., Jungverdorben, J., Wiethoff, H., Lin, Q., Flitsch, L. J., Eckert, D., et al. (2018). A stably self-renewing adult blood-derived induced neural stem cell exhibiting Patternability and epigenetic rejuvenation. *Nat. Commun.* 9:4047. doi: 10.1038/s41467-018-06398-5
- Smith, D. K., Yang, J., Liu, M. L., and Zhang, C. L. (2016). Small molecules modulate chromatin accessibility to promote NEUROG2-mediated fibroblast-to-neuron reprogramming. *Stem Cell Rep.* 7, 955–969. doi: 10.1016/j.stemcr.2016.09.013
- Sposito, T., Preza, E., Mahoney, C. J., et al. (2015). Developmental regulation of tau splicing is disrupted in stem cell-derived neurons from frontotemporal dementia patients with the 10 + 16 splice-site mutation in MAPT. *Hum. Mol. Genet.* 24, 5260–5269. doi: 10.1093/hmg/ddv246

- Stroud, H., Su, S. C., Hrvatin, S., Greben, A. W., Renthal, W., Boxer, L. D., et al. (2017). Early-life gene expression in neurons modulates lasting epigenetic states. *Cells* 171, 1151–1164.e16. doi: 10.1016/j.cell.2017.09.047
- Suhr, S. T., Chang, E. A., Tjong, J., Alcasid, N., Perkins, G. A., Goissis, M. D., et al. (2010). Mitochondrial rejuvenation after induced pluripotency. *PLoS One* 5:e14095. doi: 10.1371/journal.pone.0014095
- Sullivan, G. J., Bai, Y., Fletcher, J., and Wilmot, I. (2010). Induced pluripotent stem cells: epigenetic memories and practical implications. *Mol. Hum. Reprod.* 16, 880–885. doi: 10.1093/molehr/gaq091
- Takahashi, K., Tanabe, K., Ohnuki, M., Narita, M., Ichisaka, T., Tomoda, K., et al. (2007). Induction of pluripotent stem cells from adult human fibroblasts by defined factors. *Cells* 131, 861–872. doi: 10.1016/j.cell.2007.11.019
- Takahashi, K., and Yamanaka, S. (2006). Induction of pluripotent stem cells from mouse embryonic and adult fibroblast cultures by defined factors. *Cells* 126, 663–676. doi: 10.1016/j.cell.2006.07.024
- Tang, Y., Liu, M. L., Zang, T., and Zhang, C. L. (2017). Direct reprogramming rather than iPSC-based reprogramming maintains aging hallmarks in human motor neurons. *Front. Mol. Neurosci.* 10:359. doi: 10.3389/fnmol.2017.00359
- Theka, I., Caiazzo, M., Dvoretzskova, E., Leo, D., Ungaro, F., Curreli, S., et al. (2013). Rapid generation of functional dopaminergic neurons from human induced pluripotent stem cells through a single-step procedure using cell lineage transcription factors. *Stem Cells Transl. Med.* 2, 473–479. doi: 10.5966/sctm.2012-0133
- Torper, O., Pfisterer, U., Wolf, D. A., Pereira, M., Lau, S., Jakobsson, J., et al. (2013). Generation of induced neurons via direct conversion in vivo. *Proc. Natl. Acad. Sci. U. S. A.* 110, 7038–7043. doi: 10.1073/pnas.1303829110
- Traxler, L., Edenhofer, F., and Mertens, J. (2019). Next-generation disease modeling with direct conversion: a new path to old neurons. *FEBS Lett.* 593, 3316–3337. doi: 10.1002/1873-3468.13678
- Vera, E., Bernardes de Jesus, B., Foronda, M., Flores, J. M., and Blasco, M. A. (2012). The rate of increase of short telomeres predicts longevity in mammals. *Cell Rep.* 2, 732–737. doi: 10.1016/j.celrep.2012.08.023
- Vera, E., Bosco, N., and Studer, L. (2016). Generating late-onset human iPSC-based disease models by inducing neuronal age-related phenotypes through telomerase manipulation. *Cell Rep.* 17, 1184–1192. doi: 10.1016/j.celrep.2016.09.062
- Victor, M. B., Richner, M., Olsen, H. E., Lee, S. W., Monteys, A. M., Ma, C., et al. (2018). Striatal neurons directly converted from Huntington's disease patient fibroblasts recapitulate age-associated disease phenotypes. *Nat. Neurosci.* 21, 341–352. doi: 10.1038/s41593-018-0075-7
- Vierbuchen, T., Ostermeier, A., Pang, Z. P., Kokubu, Y., Südhof, T. C., and Wernig, M. (2010). Direct conversion of fibroblasts to functional neurons by defined factors. *Nature* 463, 1035–1041. doi: 10.1038/nature08797
- Wang, S. C., Oeize, B., and Schumacher, A. (2008). Age-specific epigenetic drift in late-onset Alzheimer's disease. *PLoS One* 3:e2698. doi: 10.1371/journal.pone.0002698
- Wapinski, O. L., Vierbuchen, T., Qu, K., Lee, Q. Y., Chanda, S., Fuentes, D. R., et al. (2013). Hierarchical mechanisms for direct reprogramming of fibroblasts to neurons. *Cells* 155, 621–635. doi: 10.1016/j.cell.2013.09.028
- Watfa, G., Dragonas, C., Brosche, T., Ditttrich, R., Sieber, C. C., Alecu, C., et al. (2011). Study of telomere length and different markers of oxidative stress in patients with Parkinson's disease. *J. Nutr. Health Aging* 15, 277–281. doi: 10.1007/s12603-010-0275-7
- Xie, W., Barr, C. L., Kim, A., Yue, F., Lee, A. Y., Eubanks, J., et al. (2012). Base-resolution analyses of sequence and parent-of-origin dependent DNA methylation in the mouse genome. *Cells* 148, 816–831. doi: 10.1016/j.cell.2011.12.035
- Xie, X., Jankauskas, R., Mazari, A. M. A., Drou, N., and Percipalle, P. (2018). β -actin regulates a heterochromatin landscape essential for optimal induction of neuronal programs during direct reprogramming. *PLoS Genet.* 14:e1007846. doi: 10.1371/journal.pgen.1007846
- Yagi, T., Ito, D., Okada, Y., Akamatsu, W., Nihei, Y., Yoshizaki, T., et al. (2011). Modeling familial Alzheimer's disease with induced pluripotent stem cells. *Hum. Mol. Genet.* 20, 4530–4539. doi: 10.1093/hmg/ddr394
- Yahata, N., Asai, M., Kitaoka, S., Takahashi, K., Asaka, I., Hioki, H., et al. (2011). Anti-A β drug screening platform using human IPS cell-derived neurons for the treatment of Alzheimer's disease. *PLoS One* 6:e25788. doi: 10.1371/journal.pone.0025788
- Yang, N., Chanda, S., Marro, S., Ng, Y. H., Janas, J. A., Haag, D., et al. (2017). Generation of pure GABAergic neurons by transcription factor programming. *Nat. Methods* 14, 621–628. doi: 10.1038/nmeth.4291
- Yoo, J., Lee, E., Kim, H. Y., Youn, D. H., Jung, J., Kim, H., et al. (2017). Electromagnetized gold nanoparticles mediate direct lineage reprogramming into induced dopamine neurons in vivo for Parkinson's disease therapy. *Nat. Nanotechnol.* 12, 1006–1014. doi: 10.1038/nnano.2017.133
- Yun, C. G., Hong, W. X., Ke, L. K., et al. (2018). Neuroprotective effects of Cryptotanshinone and 1, 2-Dihydrotanshinone I against MPTP induced mouse model of Parkinson's disease. *Phytochem. Lett.* 26, 68–73. doi: 10.1016/j.phytol.2018.05.016
- Zhang, S. F., Hennessey, T., Yang, L., Starkova, N. N., Beal, M. F., and Starkov, A. A. (2011). Impaired brain Creatine kinase activity in Huntington's disease. *Neurodegener. Dis.* 8, 194–201. doi: 10.1159/000321681
- Zhu, S., Ambasudhan, R., Sun, W., Kim, H. J., Talantova, M., Wang, X., et al. (2014). Small molecules enable OCT4-mediated direct reprogramming into expandable human neural stem cells. *Cell Res.* 24, 126–129. doi: 10.1038/cr.2013.156
- Ziller, M. J., Gu, H., Müller, F., et al. (2013). Charting a dynamic DNA methylation landscape of the human genome. *Nature* 500, 477–481. doi: 10.1038/nature12433
- Zuccato, C., Valenza, M., and Cattaneo, E. (2010). Molecular mechanisms and potential therapeutic targets in Huntington's disease. *Physiol. Rev.* 90, 905–981. doi: 10.1152/physrev.00041.2009805



OPEN ACCESS

EDITED BY

Shong Lau,
Salk Institute for Biological Studies,
United States

REVIEWED BY

Luis Rafael Moscote-Salazar,
Latinamerican Council of Neurocritical
Care (CLaNI), Colombia
Brandon Peter Lucke-Wold,
University of Florida, United States

*CORRESPONDENCE

Huaqing Shu
✉ huaqing_shu@163.com
Shiying Yuan
✉ yuan_shiying@163.com

†These authors have contributed
equally to this work

SPECIALTY SECTION

This article was submitted to
Cellular Neuropathology,
a section of the journal
Frontiers in Cellular Neuroscience

RECEIVED 14 October 2022

ACCEPTED 21 November 2022

PUBLISHED 04 January 2023

CITATION

Zhang Y, Zhang J, Yuan S and Shu H
(2023) Contrast-induced
encephalopathy and permanent
neurological deficit following cerebral
angiography: A case report
and review of the literature.
Front. Cell. Neurosci. 16:1070357.
doi: 10.3389/fncel.2022.1070357

COPYRIGHT

© 2023 Zhang, Zhang, Yuan and Shu.
This is an open-access article
distributed under the terms of the
[Creative Commons Attribution License
\(CC BY\)](https://creativecommons.org/licenses/by/4.0/). The use, distribution or
reproduction in other forums is
permitted, provided the original
author(s) and the copyright owner(s)
are credited and that the original
publication in this journal is cited, in
accordance with accepted academic
practice. No use, distribution or
reproduction is permitted which does
not comply with these terms.

Contrast-induced encephalopathy and permanent neurological deficit following cerebral angiography: A case report and review of the literature

Yujing Zhang^{1,2†}, Jiancheng Zhang^{1,2†}, Shiying Yuan^{1,2*} and
Huaqing Shu^{1,2*}

¹Department of Critical Care Medicine, Union Hospital, Tongji Medical College, Huazhong University of Science and Technology, Wuhan, China, ²Institute of Anesthesia and Critical Care Medicine, Union Hospital, Tongji Medical College, Huazhong University of Science and Technology, Wuhan, China

Contrast-induced encephalopathy (CIE) is an uncommon complication associated with contrast exposure during angiographic procedures that is usually transient but occasionally leads to permanent complications or death. Due to the low incidence of CIE, there are still insufficient reports. This study was used to summarize the clinical features of CIE through a case report and systematic review. We summarized and reviewed 127 patients with CIE, and we found that the total incidence of CIE between men and women had no difference (49.61 and 50.39%, respectively), but the average age in female patients with CIE was older than that in male patients (62.19 and 58.77 years, respectively). Interestingly, the incidence of female patients with CIE in the poor prognosis group was significantly higher than that in the good prognosis group (62.50 and 36.51%, respectively), and the average age of these female patients in the poor prognosis group was younger than that in the good prognosis group (61.39 and 62.82 years, respectively). The contrast medium types were mainly nonionic (79.69 and 73.02%, respectively) and low-osmolar (54.69 and 71.43%, respectively) in both groups. Importantly, the total contrast media administrated in patients with poor prognoses was greater than that administrated in patients with good prognoses (198.07 and 188.60 ml, respectively). In addition, comorbidities in both groups included hypertension (55.91%), diabetes mellitus (20.47%), previous contrast history (15.75%), renal impairment (11.81%), and hyperlipidemia (3.15%). The percentage of patients with cerebral angiography was significantly higher in the poor prognosis group than that in the good prognosis group (37.50 and 9.52%, respectively), whereas the percentage of patients with coronary angiography in both groups had the

opposite results (35.94 and 77.78%, respectively). In conclusion, CIE may not always have a benign outcome and can cause permanent deficits. Female gender, younger age, the higher dose of contrast medium, and the procedure of cerebral angiography may be related to the patient's poor prognosis.

KEYWORDS

cerebral angiography, contrast-induced encephalopathy, neurological deficit, prognosis, risk factor

Introduction

Contrast-induced encephalopathy (CIE) is an uncommon complication associated with intravenous or intra-arterial exposure to iodinated contrast media during angiographic procedures. The incidence of CIE ranges between 0.3 and 4.0% (de Bono, 1993; Potsi et al., 2012; Liu et al., 2020). Since the first description in 1970, the clinical features of CIE have included headache, memory loss, confusion, visual and speech impairment, seizures, hemiparesis, and even coma. The underlying mechanisms and causes of iodine-based CIE remain unclear. Studies suggest that this may be related to transient blood–brain barrier (BBB) breakdown and increased permeability, which may subsequently contribute to extravasation of contrast medium into the central nervous system, resulting in cerebral edema and altered neuronal excitability (Dangas et al., 2001; Babalova et al., 2021). In addition, some high concentrations of contrast media may cause the clumping of red blood cells and, consequently, occlusion of arterial branches, which may play a role in permanent neurological deficits (Cristaldi et al., 2021). Most patients with CIE have a good prognosis and resolve quickly within 1–2 days (Spina et al., 2017). A minority (approximately 15% of CIE) may develop permanent neurological deficits or fatal cerebral edema (Hamra et al., 2017; Donepudi and Trottier, 2018; Zhao et al., 2019). However, the development of an evidence-based consensus on CIE has been hindered by the low incidence of CIE. Although the current literature on CIE is extensive, only case reports in the literature describe CIE and further analyses on the risk factors of CIE prognosis have been rarely performed. Here, we provided a case report as a reference and summarized existing reports about CIE, aiming to explore pathogenesis, risk factors, diagnosis, treatment strategy, and future exploration direction of the disease.

Case report

A 51-year-old woman was admitted to our hospital with a suspected intracranial aneurysm. The patient had a history of hypertension. On admission, a physical examination showed no

signs of neurological deficits. Cerebral angiography was urgently performed through the right femoral approach. The procedure lasted for 60 min. A total of 50 ml iodixanol (Jiangsu Hengrui Pharmaceutical Co., Ltd., China), an iso-osmolar non-ionic dimeric hydrophilic contrast medium, was injected. Notably, 1% lignocaine was administered for local anesthesia prior to cerebral angiography. This was the patient's first exposure to a contrast medium, and no obvious aneurysm or vascular malformation was found.

Approximately 5 h after surgical completion, the patient developed a decrease in the upper and lower extremity motor strength, and the pupils were symmetric and reactive. The left muscle strength was grade 2, and the right muscle strength was grade 3. An emergency brain computed tomography (CT) scan was requested and revealed the diffuse contrast enhancement in brain sulci, fissures, cisterns, third ventricle, fourth ventricle, and subarachnoid space with mild global brain edema, and softening foci in the left basal ganglia-insular area (Figures 1A,B). On the second day, the patient's clinical symptoms further deteriorated and the upper and lower muscle strength was grade 0 with positive pathological signs. Brain CT was reviewed and showed diffuse enhancement disappeared, but the brain parenchyma was diffusely swollen and the lateral ventricles were slightly more compressed than that in the previous scan (Figures 1C,D). A diagnosis of CIE was suspected given the worsening of the clinical manifestations and symptoms compatible with higher functional impairment following the administration of the contrast medium.

The patient routinely received fluids to accelerate the excretion of contrast medium, 1,000 mg of intravenous methylprednisolone once daily for 2 days to mitigate inflammation, 250 ml of mannitol every 8 h to dehydrate and reduce intracranial pressure, 10 mg of nimodipine once daily to prevent vasospasm, 120 mg of sodium valproate once daily to prevent epilepsy, as well as strengthen nutrition to improve clinical symptoms. Furthermore, lumbar cistern drainage was performed to reduce intracranial pressure, and cerebrospinal fluid (CSF) was clear with increased white blood cell count and glucose level and decreased chloride level. In the following hours, the patient experienced further deterioration in

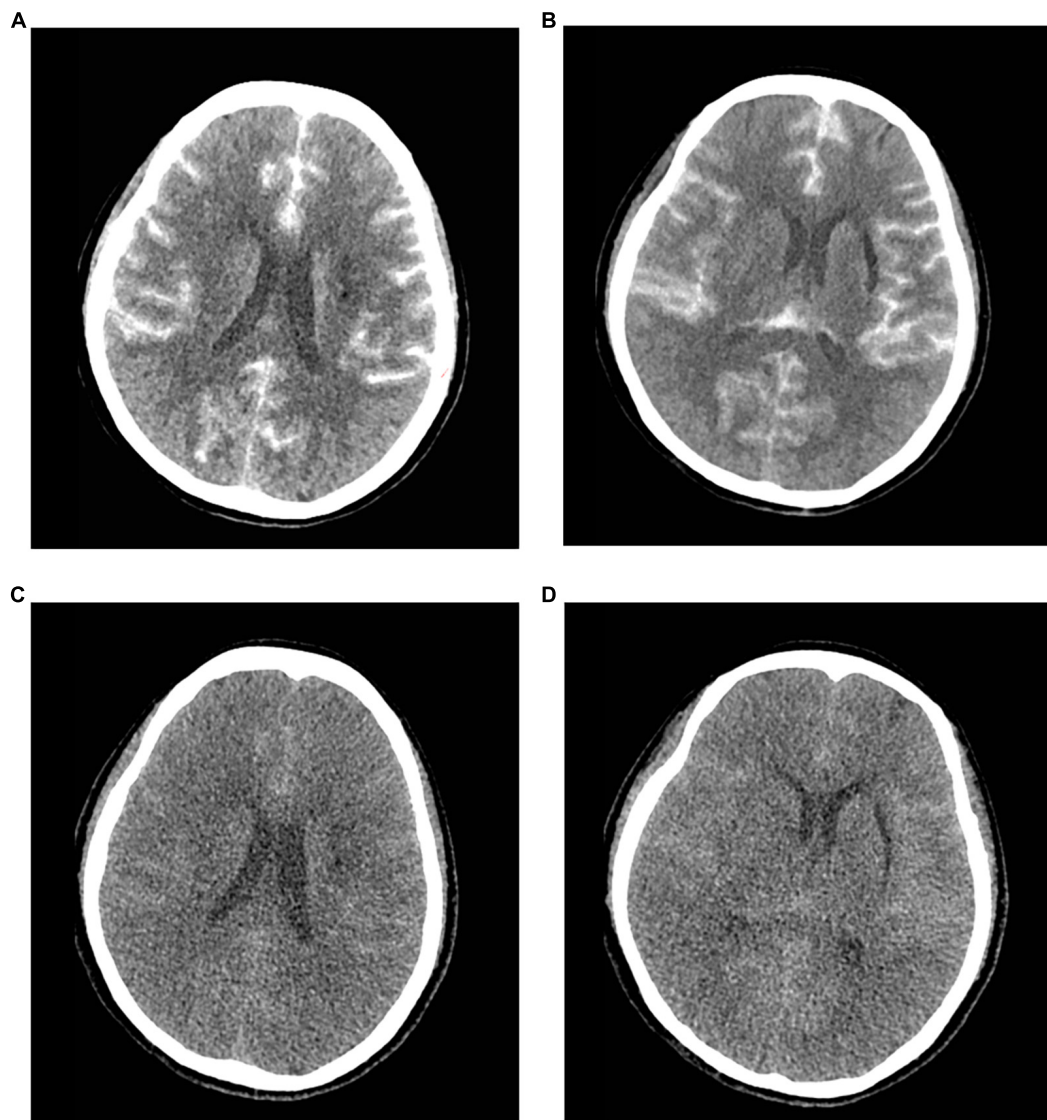


FIGURE 1

Contrast-induced encephalopathy in brain computed tomography (CT) scans. (A,B) Emergency brain CT 5 h after the procedure showed diffuse contrast enhancement in the brain parenchyma and subarachnoid space with mild global brain edema and the softening foci in the left basal ganglia-insular area. (C,D) Brain CT 2 days after the procedure indicated diffuse enhancement disappeared, and the brain parenchyma was diffusely swollen and the lateral ventricle was slightly more compressed.

mental status and fell into a coma with respiratory insufficiency. Therefore, the patient was transferred to the intensive care unit (ICU) where she underwent tracheal intubation with ventilator-assisted breathing, dehydration, anti-epileptic therapy, body temperature and blood pressure control, and close neurological observation.

On the second day after being admitted to the ICU, the patient regained consciousness, but her motor deficit was unchanged. A neurological examination showed muscle weakness in the upper and lower limbs and sensory loss below the T2 sensory level, which may be related to spinal cord edema. Considering that the patient was temporarily unable

to remove the tracheal tube, a tracheotomy was performed 4 days later. A magnetic resonance imaging (MRI) performed at 2 weeks revealed a diffuse hyperintense signal on FLAIR sequences in the cervical cord, which may be consistent with the patient's motor deficits and sensory disturbances, as well as a softening foci formation in the left basal ganglia-insular area (Figure 2). Dramatically, the patient suffered from a lung infection during hospitalization and was eventually discharged from the neurosurgery ward to another hospital for hyperbaric oxygen therapy after 20 days. A telephone follow-up after 2 months revealed that the patient's persistent neurological deficits had not improved.

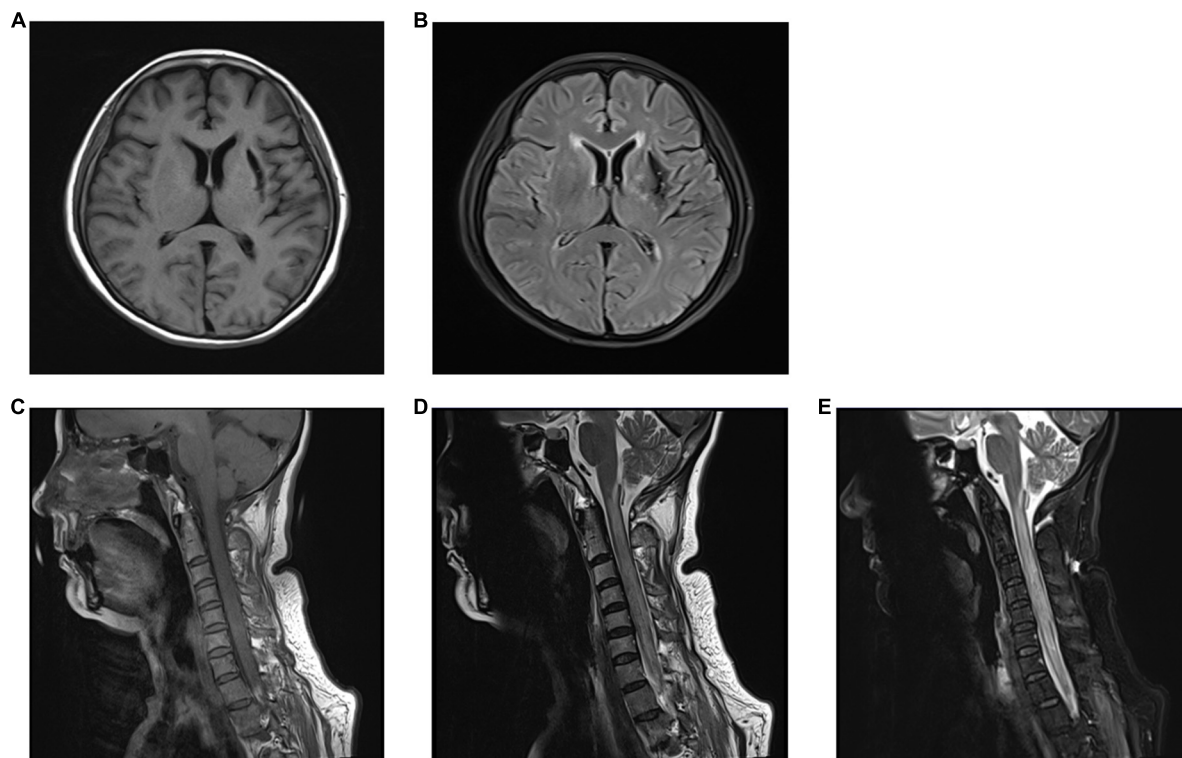


FIGURE 2

The brain and cervical spine magnetic resonance imaging (MRI) performed at 2 weeks. (A,B) Brain MRI showed the left basal ganglia-insular softening foci in T1 (A) and T2 (B) weighted image. (C–E) Cervical spine MRI showed diffuse hyperintense signal in the cervical cord in T2-weighted image (D) and fluid-attenuated inversion recovery (FLAIR) images (E), and normal findings were observed in T1-weighted image (C).

Literature review

In searching for the keywords “Contrast-induced encephalopathy” and “Angiography” in PubMed, 95 relevant articles were found. A total of 54 papers were selected after screening abstracts and titles. After reading through the whole paper, the reviews, editorial, and duplicate cases were excluded, and 40 papers were left. However, four of them were excluded because it was defined as allergic reactions, vasospasm, and posterior reversible encephalopathy syndrome, and complete data were not available in the other six papers. Finally, we accurately summarized 30 papers (Leong and Fanning, 2012; Yan and Ramanathan, 2013; Kocabay et al., 2014; Nagamine et al., 2014; Hamra et al., 2017; Park et al., 2017; Spina et al., 2017; Dattani et al., 2018; Heemelaar et al., 2018; Hirata et al., 2018; Kahyaoğlu et al., 2018; Tong et al., 2018; Renault and Rouchet, 2019; Riahi et al., 2019; Şimşek et al., 2019; Zhao et al., 2019, 2021; Fernando et al., 2020; Harada et al., 2020; Lei et al., 2020; Liu et al., 2020; Andone et al., 2021; Cristaldi et al., 2021; García-Pérez et al., 2021; Kamimura et al., 2021; Li et al., 2021; Vigano et al., 2021; Yao et al., 2021; Zhang et al., 2021; Rashid et al., 2022). A total of 127 patients were enrolled.

Figure 3 shows the screening process. Table 1 shows the basic information of 31 studies (including our case).

From the search results, we found that the total incidence of CIE between women and men has no difference. A total of 63/127 (49.61%) patients were women and 64/127 (50.39%) patients were men, and the average age in women was older than that in men (62.19 and 58.77 years, respectively). More importantly, we classified the statistical results according to prognosis, and patients who recovered less than or equal to 48 h were included in the good prognosis group and the remaining patients were included in the poor prognosis group. Eventually, 63 patients were included in the good prognosis group and 64 patients were included in the poor prognosis group, and the results are shown in Table 2. We found that the incidence of female patients with CIE in the poor prognosis group was significantly higher than that in the good prognosis group (62.50 and 36.51%, respectively), and the average age of these female patients in the poor prognosis group was younger than that in the good prognosis group (61.39 and 62.82 years, respectively). Furthermore, the poor prognosis group had a wider age range, ranging from 6 to 84 years.

In interventional procedures, the contrast types included non-ionic and ionic, or low-osmolar, high-osmolar, and

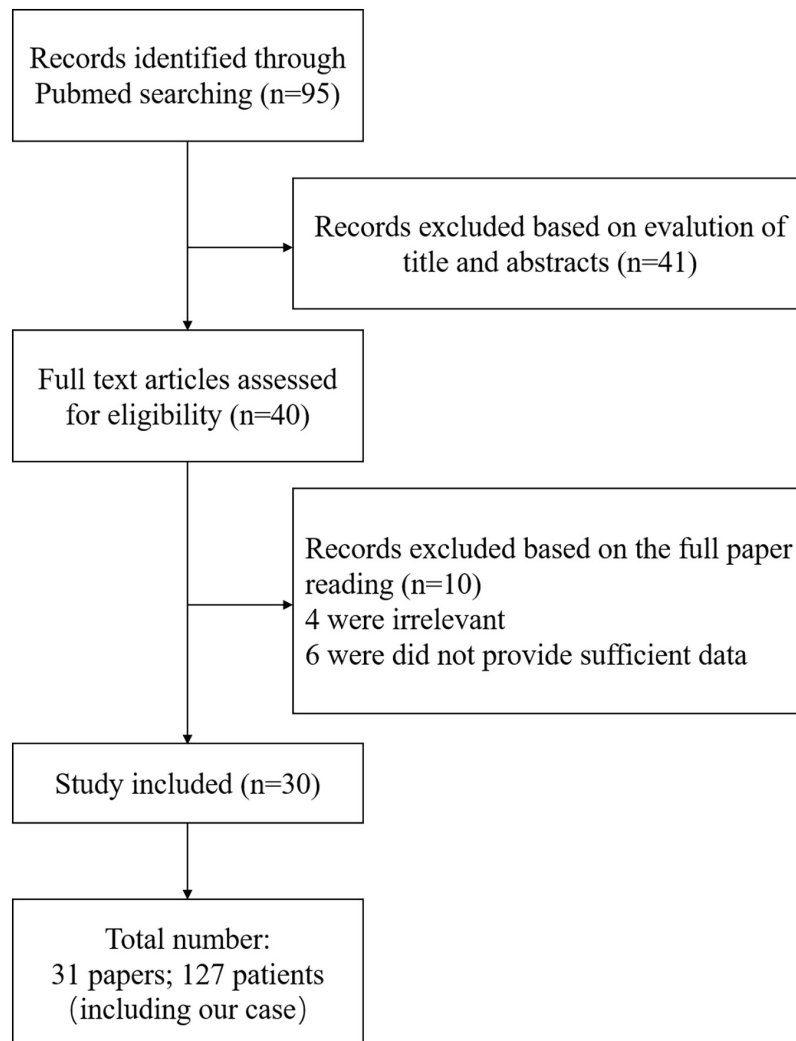


FIGURE 3
Screening process.

iso-osmolar in our present study, and we found that both groups were mainly non-ionic (79.69 and 73.02%, respectively) and low-osmolar (54.69 and 71.43%, respectively). Importantly, the total contrast media administrated and the non-ionic, ionic, low-osmolar, or high-osmolar contrast media administrated in patients with poor prognosis were greater than that administrated in patients with good prognosis (198.07 and 188.60 ml, 199.19 and 193.39 ml, 235.20 and 167.70 ml, 207.83 and 195.10 ml, and 194.20 and 117.83 ml, respectively), whereas the iso-osmolar contrast media administrated was lower in patients with poor prognosis compared to patients with good prognosis (152.56 and 167.50, respectively).

The comorbidities in the present study mainly included hypertension (55.91%), diabetes mellitus (20.47%), previous contrast history (15.75%), renal impairment (11.81%), and

hyperlipidemia (3.15%). Although there was no significant difference in comorbidities between the two groups, the percentages of hypertension, diabetes mellitus, previous contrast history, renal impairment, and hyperlipidemia in the poor prognosis group were higher than those in the good prognosis group (60.93 and 50.79%, 25.00 and 15.78%, 17.19 and 4.29%, 14.06 and 9.52%, and 4.69 and 3.17%, respectively). The angiography types, mainly coronary angiography (56.69%), cerebral angiography (23.62%), and carotid and vertebral angiography (7.87%), in both groups, were also analyzed. We found that the percentage of patients with cerebral angiography in the poor prognosis group was significantly higher than that in the good prognosis group (37.50 and 9.52%, respectively), whereas the percentage of patients with coronary angiography in both groups had the opposite results (35.94 and 77.78%, respectively). Moreover, brain CT or MRI

TABLE 1 Basic information of all patients.

Study	Number	Gender/ Age (year)	Procedure	Risk factor	Previous angio- graphy	Contrast medium	Contrast medium class	Volume (ml)	Presentation	Neuroimaging	Symptom duration	Complete resolution
Andone et al., 2021	1	M/70	Diagnostic coronary angiography	HT, DM	No	Ioversol	Non-ionic, monomer, low osmolar	100	Headache, behavioral changes and aggressive tendencies	CT: a mild hyper-density in the frontal lobes; MRI: normal	72 h	Yes
Dattani et al., 2018	2	M/76	Coronary angiography	HT, DM	No	Iohexol	Non-ionic, monomer, low osmolar	120	Confused and aggressive, expressing verbal profanities	CT: normal	9 days	Yes
	3	M/65	Diagnostic coronary angiography	Previous CIE, HT, Dyslipidaemia, Smoking.	Yes	Iopromide	Non-ionic, monomer, low osmolar	110	Global aphasia, bilateral limb weakness	CT and MRI: normal;	24 h	Yes
	4	M/49	Coronary angiography	–	–	Iopromide	Non-ionic, monomer, low osmolar	205	Confusion, decreased GCS	–	12 h	Yes
	5	M/32	Coronary angiography	–	–	Iopromide	Non-ionic, monomer, low osmolar	100	Cortical blindness	CT: normal	24 h	Yes
	6	F/39	Coronary angiography	–	No	Iopamidol	Non- ionic, monomer, low osmolar	100	Cortical blindness	CT: normal	1 h	Yes
	7	M/74	Coronary angiography + aortogram	HT, Obse	No	Iomeprol	Non-ionic, monomer, low osmolar	320	Cortical blindness	CT: normal	24 h	Yes
	8	M/73	Coronary angiography + PCI	Sleep apnea, Hypoventilation, Obese	–	None reported	N/A	240	Cortical blindness	CT: normal	7 h	Yes
	9	M/53	Coronary angiography	–	–	Ioversol	Non-ionic, monomer, low osmolar	100	Cortical blindness, catatonia	–	12 h	Yes
	10	M/45	Coronary angiography + PCI	HT	No	Ioversol	Non-ionic, monomer, low osmolar	167	Cortical blindness	–	24 h	Yes

(Continued)

TABLE 1 (Continued)

Study	Number	Gender/ Age (year)	Procedure	Risk factor	Previous angio- graphy	Contrast medium	Contrast medium class	Volume (ml)	Presentation	Neuroimaging	Symptom duration	Complete resolution
	11	M/59	Coronary angiography + PCI	HT	No	Ioversol	Non-ionic, monomer, low osmolar	220	Cortical blindness	–	12 h	Yes
	12	M/68	Coronary angiography + PCI	HT	No	Ioversol	Non-ionic, monomer, low osmolar	262	Homonymous hemianopia	–	15 min	Yes
	13	M/55	Coronary angiography	–	Yes	Diatrizoate	Ionic, monomer, high osmolar	280	Cortical blindness	CT: both occipital lobes enhancement	24 h	Yes
	14	M/61	Coronary angiography	–	Yes	Diatrizoate	Ionic, monomer, high osmolar	145	Cortical blindness	CT: normal	36 h	Yes
	15	M/44	Coronary angiography	–	No	Diatrizoate	Ionic, monomer, high osmolar	50	Cortical blindness	No brain CT	12 h	Yes
Kamimura et al., 2021	16	F/70	Diagnostic cerebral angiography	Not reported	No	Iopamidol	Non-ionic, monomer, low osmolar	43	Confusion and generalized tonic-clonic seizures	CT: high-density signaling in the cortex; MRI: high signal intensity in temporal lobe	24 h	Yes
	17	M/71	Cerebral angiography	Not reported	No	Iohexol	Non-ionic, monomer, low osmolar	46	Cortical blindness, confusion, and Ophthalmoplegia	No brain CT	10 days	N/A
	18	F/68	Cerebral angiography	Not reported	No	Iohexol	Non-ionic, monomer, low osmolar	24	Cortical blindness, confusion, and amnesia	No brain CT	6 days	N/A
	19	F/71	Cerebral angiography	HT, Transient ischemic attack	No	Iopromide	Non-ionic, monomer, low osmolar	25	Confusion, disorientation, and hemiparesis	CT: edema, right diffuse cortical hyperattenuation	24 h	Yes
Fernando et al., 2020	20	F/52	Coronary angiography	HT	N/A	Iopromide	Non-ionic, monomer, low osmolar	130	Left sided hemiparesis, disorientation, and decreased GCS	CT: cortical and subarachnoid hyper-densities	5day	Yes
Cristaldi et al., 2021	21	F/54	Cerebral angiography	HT, Cerebral ischemia	N/A	Iobitridol	Non-ionic, monomer, low osmolar	Not reported	Severe right hemiparesis and complete aphasia	CT: edema, abnormal subarachnoid contrast enhancement zone	>6 months	No

(Continued)

TABLE 1 (Continued)

Study	Number	Gender/ Age (year)	Procedure	Risk factor	Previous angio- graphy	Contrast medium	Contrast medium class	Volume (ml)	Presentation	Neuroimaging	Symptom duration	Complete resolution
	22	M/10	Angiocardiography	Fallot's tetralogy	Not stated	Urografin 76%	Ionic, monomer, high osmolar	76	Apnoea and cardiac arrest	No CT brain (autopsy showed brain edema)	During	Death
	23	F/7	Aortography	HT	No	Renografin 76%	Ionic, monomer, high osmolar	340	Seizures	CT: contrast enhancement of cortex, basal ganglia and thalamus	During	Death
	24	M/68	Bypass graft angiography	HT, DM	Yes	Iohexol	Non-ionic, monomer, low osmolar	180	Confusion, amnesia, aphasia, cortical blindness	CT: contrast enhancement of occipital lobes, temporal lobes, thalamus	During	No
	25	F/73	Coronary angiography	HT	No	Iohexol	Non-ionic, monomer, low osmolar	1150	Seizures, gait instability, postural tremor, dysphasia	CT: abnormal signal in bilateral frontal and occipital	During	No
	26	F/62	Cerebral angiography	None reported	No	Not specified	Non-ionic	297	Confusion, cortical blindness	CT: abnormal signal in bilateral occipital, basal ganglia, frontal	During	No
	27	M/41	Cerebral angiography	None reported	Yes	Not specified	Non-ionic	225	Bilateral visual loss, agitation	CT: right parietal abnormal signal	3 h	No
	28	F/54	Cerebral angiography	None reported	Yes	Not specified	Non-ionic	62	Cortical blindness with only light perception	MRI: bilateral occipital	1 months	Yes
	29	M/46	Cerebral angiography	None reported	Yes	Not specified	Non-ionic	225	Right homonymous hemianopia	CT and MRI: normal	1 months	Yes
	30	M/47	Cerebral angiography	None reported	No	Not specified	Non-ionic	384	Right homonymous hemianopia	CT: normal	7 days	Yes
	31	F/67	Coronary angiography	Angina, DM, HT	–	Iodixanol	Non-ionic, dimer, iso-osmolal	Not reported	Gradually GCS 3	N/A	During	Yes
	32	F/71	Cerebral angiography	HT, hyperlipidemia, Angina	–	Iopamidol	Non-ionic, monomer, low osmolar	110	Dizziness, nausea, vomiting; then respiratory distress, deep coma, GCS 3	CT: cerebral edema	56 days	Death

(Continued)

TABLE 1 (Continued)

Study	Number	Gender/ Age (year)	Procedure	Risk factor	Previous angio- graphy	Contrast medium	Contrast medium class	Volume (ml)	Presentation	Neuroimaging	Symptom duration	Complete resolution
	33	F/51	Carotid artery angioplasty	HT, DM, Coronary artery disease	–	Iohexol	Non-ionic, monomer, low osmolar	Not reported	Seizures, unconsciousness	N/A	During	Death
Spina et al., 2017	34	F/44	Diagnostic coronary angiography + PCI	End-stage kidney disease, HT, DM	–	Iohexol	Non-ionic, monomer, low osmolar	190	Left-sided weakness, seizure activity	CT: contrast enhancement of right cerebral hemisphere	72 h	Yes
	35	M/69	Diagnostic coronary angiography + PCI	HT, DM	–	Not reported	N/A	N/A	Aphasia, left-sided hemiparesis	CT: contrast enhancement of right cerebral hemisphere	12 h	Yes
	36	F/63	Diagnostic coronary angiography	HT, DM	–	Iopramide	Non-ionic, low osmolar	250	Cortical blindness	CT: contrast enhancement of occipital lobes; MRI: normal	72 h	Yes
	37	F/60	Diagnostic coronary angiography	HT	–	Not reported	N/A	N/A	Abrupt decrease in GCS score to 6/15	CT: cerebral edema confined to the right cerebral hemisphere; MRI: normal	10 days	Yes
	38	F/76	Diagnostic coronary angiography	HT, DM	–	Ioversol	Non-ionic, monomer, low osmolar	125	Aphasia, cortical blindness, right sided weakness	MRI: hyperintensity in frontoparietal regions	48 h	Yes
	39	F/69	Diagnostic coronary angiography + PCI	CKD, DM, Previous contrast reaction	Yes	Iodixanol	Non-ionic, dimer, iso-osmolal	320	Partial seizure, homonymous hemianopia, hemisensory loss, hemiparesis	CT: cerebral edema	24 h	Yes
	40	M/64	Diagnostic coronary angiography + PCI	HT, DM	–	Iopromide	Non-ionic, monomer, low osmolar	160	Confusion, irritability, limb paralysis, aphasia	CT: hyperdensity of sagittal sinus	28 h	Yes
	41	M/68	Diagnostic coronary angiography + PCI	HT	–	Iopromide	Non-ionic, monomer, low osmolar	250	Left lower extremity weakness and sensory loss	CT: contrast enhancement in sagittal sinus and occipital lobe	12 h	Yes
	42	M/47	Diagnostic coronary angiography + PCI	None reported	–	Iopromide	Non-ionic, monomer, low osmolar	150	Confusion, agitation, nausea, headache	CT: contrast enhancement in right occipital lobe	8 h	Yes

(Continued)

TABLE 1 (Continued)

Study	Number	Gender/ Age (year)	Procedure	Risk factor	Previous angio- graphy	Contrast medium	Contrast medium class	Volume (ml)	Presentation	Neuroimaging	Symptom duration	Complete resolution
	43	M/70	Diagnostic coronary angiography + PCI	DM	–	Iopromide	Non-ionic, monomer, low osmolar	120	Confusion; nausea	CT: contrast enhancement in occipital lobe	12 h	Yes
	44	F/76	PCI + carotid artery stenting	CKD, DM	–	Iodixanol	Non-ionic, dimer, iso-osmolal	200	Stupor, aphasia, hemiparesis	CT: hyperdensity of cerebral sulci and subarachnoid spaces	48 h	Yes
	45	F/39	Diagnostic coronary angiography	–	–	Iopamidol	Non-ionic, monomer, low osmolar	80	Cortical blindness	CT and vertebral angiogram: normal	1 h	Yes
	46	F/70	Diagnostic coronary angiography + PCI	–	–	None reported	N/A	N/A	Left-sided hemiparesis, conjugate gaze deviation to the right	CT: hyperdensity of cerebral sulci and right frontal lobe	72 h	Yes
	47	F/70	Diagnostic coronary angiography + PCI	–	–	Not specified	Ionic	1500	Myoclonus	CT: hyperdensity of cerebral sulci	<1 h	Yes
	48	F/52	Diagnostic coronary angiography	–	–	Iomeprol	Non-ionic, monomer, low osmolar	150	Cortical blindness	CT: contrast enhancement of occipital lobes	5 h	Yes
	49	F/70	Diagnostic coronary angiography	DM, HT	–	Iobitridol	Non-ionic, monomer, low osmolar	75	Cortical blindness	CT: contrast enhancement of occipital lobes	72 h	Yes
	50	M/56	Diagnostic coronary angiography	–	–	Iopromide	Non-ionic, monomer, low osmolar	135	Confusion, dysarthria, cortical blindness	CT: contrast enhancement of right occipital lobe	24 h	Yes
	51	F/82	Diagnostic coronary angiography + PCI	CKD, HT	–	Iomeprol	Non-ionic, monomer, low osmolar	500	Aphasia, right-sided hemiparesis	CT: hyperdensities filling the sulci of both cerebral hemispheres	40 h	Yes
	52	M/82	Diagnostic coronary angiography	CKD, DM, HT	–	Iopromide	Non-ionic, monomer, low osmolar	150	Right-sided hemiparesis, aphasia	CT: Left hemisphere cerebral edema and extravascular local contrast media	6 h	Yes
	53	M/63	Diagnostic coronary angiography + Aortogram	–	–	Iopremol	Non-ionic, monomers	450	Amnesia, numbness, right upper extremity numbness	CT: contrast enhancement of right occipital lobe	12 h	Yes

(Continued)

TABLE 1 (Continued)

Study	Number	Gender/ Age (year)	Procedure	Risk factor	Previous angio- graphy	Contrast medium	Contrast medium class	Volume (ml)	Presentation	Neuroimaging	Symptom duration	Complete resolution
	54	F/63	Diagnostic coronary angiography	DM, HT	–	Iopromide	Non-ionic, monomer, low osmolar	160	Cortical blindness, right homonymous hemianopia	CT and MRI: contrast enhancement of occipital lobes	48 h	Yes
	55	F/52	Diagnostic coronary angiography + PCI	HT	Yes	Ioversol	Non-ionic, monomer, low osmolar	280	Cortical blindness	CT: contrast enhancement of occipital lobes	36 h	Yes
	56	M/55	Diagnostic coronary angiography	–	–	Iomeprol	Non-ionic, monomer, low osmolar	280	Cortical blindness	CT: contrast enhancement of occipital lobes	5 days	Yes
	57	M/58	Diagnostic coronary angiography	HT	–	Iogaxate	Ionic, dimer, low osmolar	260	Cortical blindness	CT: normal	32 h	Yes
	58	M/64	Diagnostic coronary angiography	–	–	Iogaxate	Ionic, dimer, low osmolar	400	Cortical blindness	N/A	30 h	Yes
	59	M/49	Diagnostic coronary angiography	CKD, HT	–	Diatrizoate	Ionic, monomer, high osmolar	610	Seizures, encephalopathy	CT: contrast enhancement of left frontal gyri	4 h	Yes
	60	M/62	Diagnostic coronary angiography + PCI	CKD, HT	–	Iopamidol	Non-ionic, monomer, low osmolar	170	Headache, confusion, cortical blindness	CT: contrast enhancement of cerebellum, thalamus	12 h	Yes
	61	M/62	Diagnostic coronary angiography	HT	–	Iopamidol	Non-ionic, monomer, low osmolar	270	Cortical blindness, loss of coordination right arm	CT: contrast enhancement of occipital lobes	72 h	Yes
	62	F/57	Diagnostic coronary angiography	HT, Previous contrast reaction	Yes	Iogaxate	Ionic, dimer, low osmolar	200	Cortical blindness	CT: mild attenuation in occipital poles	48 h	Yes
	63	F/52	Diagnostic coronary angiography + aortogram	HT	–	Diatrizoate	Ionic, monomer, high osmolar	100	Cortical blindness	N/A	18 h	Yes
Hamra et al., 2017	64	M/62	Coronary angioplasty	HT	–	Iohexol	Non-ionic, monomer, low osmolar	200	Right-sided homonymous hemianopia	CT: contrast enhancement of the venous sinuses and cerebral arteries	48 h	Yes

(Continued)

TABLE 1 (Continued)

Study	Number	Gender/ Age (year)	Procedure	Risk factor	Previous angio- graphy	Contrast medium	Contrast medium class	Volume (ml)	Presentation	Neuroimaging	Symptom duration	Complete resolution
Vigano et al., 2021	65	F/56	Cerebral angiography	Migraine, Renal colic, Smoking, Previous heroin abuse	–	Iomeprol	Non-ionic, monomer, low osmolar	70	Global aphasia and right hemiplegia	CT: left cerebral edema	10 days	Yes
	66	F/74	Abdominal aorta and renal artery angiography + angioplasty	Renal impairment; HT	No	Diatrizoate	Ionic, monomer, high osmolar	250	Cortical blindness, left hemiparesis	CT: bilateral occipital and basal ganglia alterations	4–5 days	Yes
	67	M/64	Carotid artery and aorta angiography	HT	No	Iothalamate meeglumine	Ionic, monomer, high osmolar	12	Cortical blindness, fluent aphasia	CT: left temporo- parieto-occipital alterations	3 days	N/A
	68	F/71	Spinal angiography	–	No	Ioxaglate	Ionic dimer low osmolar	360	Right-sided visual neglect and Wernicke's aphasia	CT: bilateral occipital and left parietal lobe alterations	4 days	Yes
	69	M/82	Carotid artery angiography + stenting	HT	Yes	Ioxaglate	Ionic, dimer, low osmolar	50	Confusion, left hemiparesis, neglect	CT: right frontoparietal cortical enhancement and edema	2 days	Yes
	70	M/72	Carotid artery angiography + coiling anterior aneurysm	–	No	Iopamidol	Non-ionic, monomer, low osmolar	260	Right hemiparesis and motor aphasia	CT: enhancement throughout the left cerebral cortex and left basal ganglia, diffuse swelling of the left cerebral hemisphere	7 days	Yes
	71	M/80	Carotid and coronary angiography + stenting	HT	No	Iohexol	Non-ionic, monomer, low osmolar	250	Right hemiparesis	CT: left frontoparietal- occipital cortical enhancement	2 days	Yes
	72	M/51	Carotid artery angiography + right internal carotid artery	HT	No	Iopromide	Non-ionic, monomer, low osmolar	300	Gerstmann's left visual field deficit, hemiparesis, right gaze deviation	CT: cortical enhancement and edema in the right cerebral hemisphere	2 days	Yes

(Continued)

TABLE 1 (Continued)

Study	Number	Gender/ Age (year)	Procedure	Risk factor	Previous angio- graphy	Contrast medium	Contrast medium class	Volume (ml)	Presentation	Neuroimaging	Symptom duration	Complete resolution
	73	M/69	Coronary angiography + PCI	–	–	Iohexol	Non-ionic, monomer, low osmolar	100	Stupor, disorientation, left hemiplegia	CT: hyperdense lesion in the right frontoparietal region, parietal lobe and basal ganglia	6 h	Yes
	74	F/73	Aortic angiography + thoracic aortic aneurysm repair	Chronic kidney disease; HT	Yes	Iodixanol	Non-ionic, dimer, iso-osmolal	248	Seizure and left-sided hemiplegia	CT: hyperdensity of the right cortex, subarachnoid space and basal ganglia	7 days	N/A
	75	F/67	Cerebral angiography	HT	Yes	N/A	N/A	N/A	Right-sided hemiparesis and aphasia	CT: cortical edema of the left cerebral hemisphere and contrast medium leakage to the subarachnoid space	24 h	N/A
Liu et al., 2020	76	F/84	Coronary angiography	HT, Paroxysmal atrial fibrillation, Chronic bronchitis	–	Iopromide	Non-ionic, monomer, low osmolar	20	Lost consciousness, and exhibited left limb hemiplegia with muscle strength level 0 and eyes staring to the right, seizure	CT: high-density regions in the subarachnoid space	2 months	Yes
	77	F/57	Diagnostic coronary angiography + PCI	CKD, HT, DM	–	Iodixanol	Non-ionic, dimer, iso-osmolal	130	Tonic–clonic seizures	CT: right parenchymal edema	72 h	Yes
	78	M/6	Diagnostic coronary angiography	HT, DM	–	Iohexol	Non-ionic, monomer, low osmolar	120	Confused, aggressive, expressing verbal profanities	CT: normal	9 days	Yes
	79	M/62	Diagnostic coronary angiography + PCI	HT	–	Iohexol	Non-ionic, monomer, low osmolar	300	Right-sided homonymous hemianopia	CT: slight enhancement of the venous sinuses	48 h	Yes
	80	M/49	Diagnostic coronary angiography	–	–	Iopromide	Non-ionic, monomer, low osmolar	205	Confusion, decrease in level of consciousness	CT and MRI: normal	12 h	Yes

(Continued)

TABLE 1 (Continued)

Study	Number	Gender/ Age (year)	Procedure	Risk factor	Previous angio- graphy	Contrast medium	Contrast medium class	Volume (ml)	Presentation	Neuroimaging	Symptom duration	Complete resolution
	81	M/69	Diagnostic coronary angiography + PCI	–	–	Iohexol	Non-ionic, monomer, low osmolar	100	Confusion, headache, vomiting, left hemiplegia,	CT: focal hyperdense lesions	6 h	Yes
	82	M/74	Diagnostic coronary angiography + aortogram		–	Iomeprol	Non-ionic, monomer, low osmolar	320	Cortical blindness	CT: normal	24 h	Yes
Riahi et al., 2019	83	F/71	Coronary angiography	HT, DM	–	Iodixanol	Non-ionic, dimer, iso-osmolal	80	Aphasia, GCS score to 7/15	CT: normal	24 h	Yes
Rashid et al., 2022	84	F/76	Coronary angiography	DM, HT, Hyperlipidemia, Coronary artery disease	–	N/A	N/A	N/A	Confusion and aggressive behavior	CT and MRI: normal	16 days	Yes
Zhang et al., 2021	85	M/42	Coronary angiography	–	–	Iopromide	Non-ionic, monomer, low osmolar	200	Severe headache, cortical blindness and neuropsychiatric symptom	CT: normal	5 days	Yes
Park et al., 2017	86	F/58	Cerebral angiography	HT, Hypothyroidism, Peripheral artery occlusive disease, Depressive disorder	–	Iodixanol	Non-ionic, dimer, iso-osmolal	220	Tonic-clonic seizure, left hemiparesis involving face, arm and leg(grade 3/5), sensory loss, and left-sided neglect with drowsy mentality	CT:sulcal obliteration of right cerebral hemisphere; MRI: gyral swelling and hyperintensity in the right cerebral hemisphere	6 days	Yes
Kocabay et al., 2014	87	F/58	Diagnostic coronary angiography + PCI	HT, Hyperlipidemia	–	Iopromide	Non-ionic, monomer, low osmolar	220	Bilateral oculomotor ophthalmoplegia	N/A	>30 days	No
	88	M/68	Diagnostic coronary angiography + PCI	HT	–	Iopromide	Non-ionic, monomer, low osmolar	250	Monoplegia	N/A	12 h	Yes
	89	M/68	Diagnostic coronary angiography + PCI	HT, DM	–	Iopromide	Non-ionic, monomer, low osmolar	180	Unilateral oculomotor monoplegia	N/A	1 h	Yes

(Continued)

TABLE 1 (Continued)

Study	Number	Gender/ Age (year)	Procedure	Risk factor	Previous angio- graphy	Contrast medium	Contrast medium class	Volume (ml)	Presentation	Neuroimaging	Symptom duration	Complete resolution
	90	M/70	Diagnostic coronary angiography + PCI	HT	–	Iopromide	Non-ionic, monomer, low osmolar	130	Cerebellar dysfunction	N/A	14 h	Yes
Kahyaoglu et al., 2018	91	M/66	Lower extremity angiography	–	–	Iohexol	Non-ionic, monomer, low osmolar	Not reported	Confusion and cortical blindness, seizure	CT: normal	24 h	Yes
Zhao et al., 2019	92	F/71	Digital subtraction angiography	HT, Hyperlipemia, Angina	–	Iopamidol	Non-ionic, monomer, low osmolar	110	Headache, dizziness, nausea and vomiting, deep coma	CT: cerebral edema	56 days	Death
Li et al., 2021	93	F/77	Digital subtraction angiography	HT, Coronary heart disease	Yes	Visipaque	Non-ionic	200	Right hemiplegia, aphasia, and epilepsy	CT: hyperdensity in the left subarachnoid space	6 days	Yes
Zhao et al., 2021	94	F/50	Cerebral angiography	–	–	Iopromide	Non-ionic, monomer, low osmolar	6	Disturbance of consciousness, seizures, frequent blinking, and stiffness	CT: normal; MRI: swelling of the left cerebral cortex	10 days	Yes
Heemelaar et al., 2018	95	F/67	Coronary angiography	DM, HT, Adenocarcinoma of the left breast	–	Iso-osmolar iodinated contrast	Iso-osmolar	100	Acute-onset coma and respiratory insufficiency	CT: bilateral cerebral edema	23 days	Yes
García-Pérez et al., 2021	96	F/61	Diagnostic digital subtraction angiography	Migraine	–	Iodixanol	Non-ionic, dimer, iso-osmolar	70	Confused and drowsy, agitated and vomiting	MRI: lesions in the cerebellar hemispheres and parieto-occipital lobes;	36–48 h	Yes
	97	M/22	Diagnostic digital subtraction angiography	Left parietooccipital arteriovenous malformation	–	None reported	N/A	None reported	Disoriented, bilateral amaurosis and presented amnesia	CT and MRI: normal	48–72 h	Yes
Harada et al., 2020	98	F/72	Coronary angioplasty	HT, Hyperlipidemia	–	Iodinated contrast	None reported	210	Left hemiparesis, left sensory and visual hemineglect, and right gaze preference	CT: mild cerebral edema	2 days	Yes
Renault and Rouchet, 2019	99	M/49	Renal artery angiography	Chronic renal failure	–	Iohexol	Non-ionic, monomer, low osmolar		Cortical blindness, global amnesia disappeared	MRI: normal	6 days	Yes

(Continued)

TABLE 1 (Continued)

Study	Number	Gender/ Age (year)	Procedure	Risk factor	Previous angio- graphy	Contrast medium	Contrast medium class	Volume (ml)	Presentation	Neuroimaging	Symptom duration	Complete resolution
Hirata et al., 2018	100	M/75	Coronary angioplasty	DM	–	None reported	N/A	None reported	No neurological symptoms were observed because the patient was intubated	CT: high-density areas in the cortex, putamen, caudate nucleus and subarachnoid space of the right cerebral hemisphere	12 days	Yes
Yao et al., 2021	101	M/68	Contrast- enhanced chest CT examination	Rheumatoid arthritis	–	Iso-osmolar iodinated contrast	Iso-osmolar	70	Lost consciousness and experienced cardiorespiratory arrest	CT: abnormal cortical contrast enhancement and cerebral sulci hyperdensity	>17days	Yes
Leong and Fanning, 2012	102	F/50	Cerebral angiography	HT	No	Iopramide	Non-ionic, low osmolar	220	Right hemisindrome	CT: edema in the left cerebral hemisphere	During	No
	103	F/59	Aortic arch angiography	Renal impairment; HT	Yes	Diatrizoate	Ionic, monomer, high osmolar	150	Cortical blindness; headache, myoclonus or seizure	CT: bilateral parieto-occipital contrast enhancement	3 days	Yes
	104	F/53	Carotid artery angiography	Not reported	No	Diatrizoate meeglumine	Ionic, monomer, high osmolar	60	Partial motor seizure	CT: right temporo-parietal contrast enhancement	24 h	Yes
	105	M/70	Arch, Carotid & Vertebral arteries angiography	None reported	No	Diatrizoate	Ionic, monomer, high osmolar	72	Cortical blindness	CT: bilateral Occipital hyperdensity	2 days	Yes
	106	F/74	Abdominal aorta angiography	HT, Renal impairment	No	Iopamidol	Non-ionic, monomer, low osmolar	415	Visuospatial disorder	CT: bilateral parieto-occipital hyperdensity	4 days	Yes
	107	F/74	Diagnostic cerebral angiography	HT	No	Iohexol	Non-ionic, monomer, low osmolar	None reported	Complete bilateral blindness; confusion	CT: left parieto-occipital hyperdensity; MRI: left occipita hyperdensity	24 h	Yes
	108	F/45	Diagnostic cerebral angiography	HT	No	Iohexol	Non-ionic, monomer, low osmolar	None reported	Complete bilateral blindness; confusion	CT: normal; MRI: bilateral occipital hyperdensity	7 days	Yes

(Continued)

TABLE 1 (Continued)

Study	Number	Gender/ Age (year)	Procedure	Risk factor	Previous angio- graphy	Contrast medium	Contrast medium class	Volume (ml)	Presentation	Neuroimaging	Symptom duration	Complete resolution
	109	F/73	Diagnostic cerebral angiography	HT	No	Iohexol	Non-ionic, monomer, low osmolar	None reported	Cortical blindness	CT: normal; MRI: bilateral occipital hyperdensity	5 days	Yes
	110	F/70	Coronary artery angiography	HT	Yes	None reported	N/A	1500	Seizure	CT: hyperdensity of right frontal	24 h	Yes
	111	M/56	Coronary artery	None reported	Yes	Iohexol 350	Non-ionic, monomer, low osmolar	220	Bilateral cortical blindness	CT: high-density areas in the bilateral occipital and frontal lobes	4 days	Yes
Nagamine et al., 2014	112	F/58	Cerebral angiography	Unknown	N/A	Iohexol	Non-ionic, monomer, low osmolar	–	Agraphia, right hemiparesis	N/A	>20 days	No
Tong et al., 2018	113	F/64	Diagnostic cerebral angiography	HT	No	ioversol	Non-ionic, monomer, low osmolar	300	Lateral blindness	MRI: normal	6 days	Yes
	114	M/53	Diagnostic cerebral angiography	HT	Yes	Omnipaque	Non-ionic, monomer, high osmolar	155	Lateral blindness	CT: bilateral brain edema on frontal and occipital lobe	5 days	Yes
	115	F/61	Diagnostic cerebral angiography	HT	–	Omnipaque	Non-ionic, monomer, high osmolar	10	Lateral blindness	MRI: right occipital cerebellar infarction	3 months	Yes
	116	M/58	Carotid artery + vertebral artery angiography	–	Yes	Iopromide	Non-ionic, monomer, low osmolar	350	Cortical blindness	CT: cortical hyperdensity and vasogenic edema	10 days	Yes
	117	M/57	Vertebral artery angiography	–	Yes	Omnipaque	Non-ionic, monomer, high osmolar	20	Bilateral cortical blindness	CT: normal; MRI: abnormal bilateral parieto-occipital lobes	24 h	Yes
Lei et al., 2020	118	M/76	Coronary angiography	HT, DM, Transient ischemic attacks	Yes	Iodixanol	Non-ionic, dimer, iso-osmolar	150	Epileptic seizures	N/A	6 months	Yes
Yan and Ramanathan, 2013	119	M/63	Cerebral angiogram	HT, DM, Rheumatoid arthritis, End-stage renal disease	–	Iodixano	Non-ionic, dimer, iso-osmolar	910	Left-sided blindness and ophthalmoplegia	CT: bilateral subarachnoid hyper-attenuation over the cerebral sulci, and diffuse cerebral edema	72 h	Yes

(Continued)

TABLE 1 (Continued)

Study	Number	Gender/ Age (year)	Procedure	Risk factor	Previous angio- graphy	Contrast medium	Contrast medium class	Volume (ml)	Presentation	Neuroimaging	Symptom duration	Complete resolution
	120	F/58	Cerebral arteriogram	–	–	Iodixanol	Non-ionic, dimer, iso-osmolar	193	Left hemiparesis	CT: hyperdensity of right frontoparietal lobe	4 days	Yes
	121	F/61	Cerebral arteriogram	–	–	Iodixanol	Non-ionic, dimer, iso-osmolar	212	Left hemiparesis	CT: hyperdensity of right frontoparietal lobe	3 days	Yes
	122	F/ 58	Transfemoral cerebral angiography	–	–	Ioversol	Non-ionic, monomer, low osmolar	N / A	Global aphasia, right sided hemiparesis	CT: abnormal enhancement in left cerebral cortex and thalamus	3 days	Yes
	123	F/63	Right middle cerebral angiography	–	–	Iopromide	Non-ionic, monomer, low osmolar	150	N / A	CT: diffuse subarachnoid hyperdensity	2 days	Yes
	124	M/16	Angiography of the circle of Willis	–	–	Iopromide	Non-ionic, monomer, low osmolar	50	Cortical blindness	CT: occipital lobe hyperdensity	24 h	Yes
	125	F/69	Coronary angioplasty	–	–	Iopamidol 370	Non-ionic, monomer, low osmolar	260	Seizure, right hemiparesis.	CT: left cerebral cortex, left basal ganglia hyperdensity	18 h	Yes
Şimşek et al., 2019	126	M/68	Coronary angiography	HT, DM, Coronary artery disease, Severe renal impairment	No	Iohexol	Non-ionic, monomer, low osmolar	230	seizure	CT: hyperdense fields at the vertex and at the right frontal lobe	60 h	Yes
Our case	127	F/51	Cerebral angiography	HT	No	Iodixanol	Non-ionic, dimer, iso-osmolal	50	Dyskinesia, coma	CT:the diffuse hyperdensity in brain sulci, fissures, cisterns, third ventricle, fourth ventricle and subarachnoid space, and global brain edema	>3 months	No

abnormalities were found in most patients in both groups (68.83 and 62.00%, respectively).

Discussion

Contrast-induced encephalopathy is a rare and reversible complication that can cause neurotoxicity with a favorable prognosis and resolves within 24–48 h in most cases. Based on previous studies (Yan and Ramanathan, 2013; Spina et al., 2017; Cristaldi et al., 2021), the renal elimination of contrast medium, the regression of cerebral edema, and the recovery of BBB function were assumed to play an important role in the pathophysiology of neurological recovery. Here, we described a case of permanent neurological deficit

after cerebral angiography and provided a summary and analysis of a series of CIE cases to explore the probable reasons for permanent neurological deficit. Given that most patients resolved completely within 48 h, we performed a prognostic analysis using 48 h as the node. We found that the total incidence of CIE between female patients and male patients had no difference, but female patients were more likely to have a poor prognosis. In addition, the average age of patients with poor prognoses was younger than that of patients with good prognoses. Surprisingly, no reports are currently available on risk factors associated with prognosis in patients with CIE. Only two reports were found to analyze the relationship between the incidence of CIE and gender or age, and the conclusions of the two reports were inconsistent. One report found that the adverse drug reaction incidence of iodinated contrast medium (e.g., CIE) seemed to be associated with gender, with a significantly higher incidence in female patients than in male patients, and it was also associated with age, with a lower occurrence in older (>44 years) patients compared to younger patients (Jiang et al., 2021). The other report summarized 9 CIE cases in 2013 and proposed that male gender and advanced age are the greatest risk factors for developing CIE. These two reports just provide a reference for us, and further research and a more in-depth analysis are necessary.

Studies showed a correlation between contrast medium dose and CIE (Yu and Dangas, 2011; Vigano et al., 2021), and whether the more contrast medium used is related to the poor prognosis of patients has not been directly reported. Although our study showed that the patients with poor prognosis used more contrast medium among different types of contrast media, including the non-ionic, ionic, low-osmolar, and high-osmolar contrast media, as well as the total contrast media used, the results are not absolute. Because in our reported case and 4 other summarized cases, the patient presented with permanent neurological deficits (more than 10 days) after administrating only a low quantity of contrast medium (no more than 50 ml) for angiography. Among these cases, the contrast medium types included non-ionic, low-osmolar, high-osmolar, and iso-osmolar, suggesting that severe neurotoxic symptoms may occur in response to low doses and different types of contrast agents. A previous study has shown that a 49-year-old man developed CIE and completely resolved within 4 h after receiving 610 ml diatrizoate (an ionic high-osmolar contrast medium) for diagnostic coronary angiography (Muruve and Steinman, 1996), indicating that high-dose contrast media do not cause permanent neurological dysfunction. Therefore, we speculated that, in addition to volume, the poor prognosis is generally related to the route and number of administered, type of contrast medium, and individual patient characteristics.

TABLE 2 The relationship between prognosis with variable.

	≤2 days (n = 63)	>2 days (n = 64)
Gender		
Female (%)	23 (36.51)	40 (62.50)
Male (%)	40 (63.49)	24 (37.50)
Age (year)	62.82 ± 1.41	61.39 ± 1.45
Contrast types		
Non-ionic (%)	46 (73.02)	51 (79.69)
Ionic (%)	12 (19.05)	6 (9.38)
Low-osmolar (%)	45 (71.43)	35 (54.69)
High-osmolar (%)	8 (12.70)	7 (10.94)
Iso-osmolar (%)	4 (6.35)	11 (17.19)
Contrast doses (ml)	188.60 ± 13.99	198.07 ± 14.23
Non-ionic (ml)	193.39 ± 15.59	199.19 ± 14.73
Ionic (ml)	167.70 ± 37.91	235.20 ± 54.49
Low-osmolar (ml)	195.10 ± 16.18	207.83 ± 19.85
High-osmolar (ml)	117.83 ± 35.31	194.20 ± 45.73
Iso-osmolar (ml)	167.50 ± 58.79	152.56 ± 23.40
Comorbidities		
Hypertension (%)	32 (50.79)	39 (60.93)
Diabetes mellitus (%)	10 (15.78)	16 (25.00)
History of angiography (%)	9 (14.29) + 1	11 (17.19)
Renal impairment (%)	6 (9.52)	9 (14.06)
Dyslipidaemia (%)	2 (3.17)	3 (4.69)
Angiography types		
Coronary angiography (%)	49 (77.78)	23 (35.94)
Cerebral angiography (%)	6 (9.52)	24 (37.50)
Carotid and vertebral angiography (%)	6 (9.52)	4 (6.25)
Abnormal CT or MRI (%)	40 (63.49)	44 (68.75)

Previous research has shown that demographic risk factors for CIE are chronic hypertension, diabetes mellitus, renal insufficiency, and previous reactions to contrast media (Yu and Dangas, 2011; Zhao et al., 2019; Cristaldi et al., 2021). Our study showed that the majority of patients (55.91%) had hypertension, 20.47% had diabetes mellitus, 15.75% had a contrast history, and 11.81% had renal insufficiency. Although there is no statistical difference between the poor prognosis group and the good prognosis group, these risk factors have a higher proportion in patients with poor prognosis, suggesting they may be related to worse prognosis, and further research is needed by increasing the sample size.

For the types of angiographic procedures, the present study showed that the proportion of patients with cerebral angiography was significantly higher in the poor-prognosis group than in the good-prognosis group, whereas patients with coronary angiography had the opposite results. Whether the cerebral angiography procedure itself is more likely to aggravate the prognosis than coronary angiography is unclear. This study demonstrated that 170 ml is recommended as the maximum threshold level of toxicity for coronary angiography procedure, and a smaller volume of contrast media may damage the BBB during selective intracranial injection (Kocabay et al., 2014), suggesting that cerebral angiography may be more likely to damage the BBB than coronary angiography. Furthermore, it is unclear whether procedure-related factors and patient-related factors are involved.

The diagnosis of CIE often requires the exclusion of cerebrovascular accidents such as cerebral hemorrhage and cerebral infarction. Neuroimaging plays an important role in distinguishing CIE from other neurological pathologies such as thromboembolism and hemorrhage following angiography. Our research showed that the most common abnormalities on brain CT included cortical or subcortical contrast enhancement, cerebral edema, focal hyperdense lesions, and hyper-density in the cerebral sulci. MRI abnormalities included hyperintensity on T2, FLAIR, and DWI. This study has suggested that CSF examination is also useful to rule out subarachnoid hemorrhage through the absence of xanthochromia or red blood cells (Shahan et al., 2021). The simultaneous detection of high concentrations of iodinated contrast medium in CSF and serum supports contrast medium extravasation rather than hemorrhage. In addition, the exclusion of contrast allergy or allergic-like reactions is also essential for the diagnosis of CIE. A recent study showed that allergic-like or allergic reactions caused by contrast media are rare, which can be severe or even life-threatening (Fusco et al., 2022). It is important to obtain a history of immediate or delayed reactions to a specific contrast medium, which may contribute to predicting the risk for future reactions. Clinical manifestations such as

throat tightness, facial edema, and bronchospasm are helpful in distinguishing.

For the treatment of CIE, most patients with CIE have a good prognosis and a rapid recovery. Therefore, supportive care and observation are generally considered sufficient. Based on the literature summarized in the present study, it is recommended that appropriate hydration, steroids, and mannitol can be given immediately after surgery, and benzodiazepines can be used for epileptic seizures.

Conclusion

A contrast-induced encephalopathy is a form of neurotoxicity caused by contrast media that is usually transient but occasionally leads to permanent complications or death. We summarized a series of cases and found that the female gender, younger age, higher contrast medium dose, and cerebral angiography procedure were associated with poor prognosis in patients with CIE. However, the contrast medium types were not associated with the prognosis. In addition, there was no statistical difference between the poor prognosis group and the good prognosis group; hypertension, diabetes mellitus, renal insufficiency, and previous reactions to contrast media were also important risk factors for CIE. Our case and literature review highlight that CIE may not always have a benign outcome and has the potential to cause permanent neurological dysfunction, even with low-dose contrast media. We should not be overlooked, especially following procedures that use contrast medium.

Author contributions

YZ wrote the manuscript. JZ analyzed the data. HS and SY critically revised and edited the manuscript. All authors discussed the content and read and approved the final version.

Funding

This study was supported by the National Key Research and Development Program of China (2021YFC2501800) and the National Key Research and Development Program of China (2021YFC2501804).

Conflict of interest

The authors declare that the research was conducted in the absence of any commercial or financial relationships that could be construed as a potential conflict of interest.

Publisher's note

All claims expressed in this article are solely those of the authors and do not necessarily represent those of their affiliated

organizations, or those of the publisher, the editors and the reviewers. Any product that may be evaluated in this article, or claim that may be made by its manufacturer, is not guaranteed or endorsed by the publisher.

References

- Andone, S., Balasa, R., Barcutean, L., Bajko, Z., Ion, V., Motaitanu, A., et al. (2021). Contrast medium-induced encephalopathy after coronary angiography-case report. *J. Crit. Care Med.* 7, 145–149.
- Babalova, L., Ruzinak, R., Ballova, J., Sivak, S., Kantorova, E., Kurca, E., et al. (2021). Contrast-induced encephalopathy. *Bratisl. Lek. Listy* 122, 618–620.
- Cristaldi, P. M. F., Polistena, A., Patassini, M., de Laurentis, C., Giussani, C., and Remida, P. (2021). Contrast-induced encephalopathy and permanent neurological deficit: A case report and literature review. *Surg. Neurol. Int.* 12:273.
- Dangas, G., Monsein, L. H., Laureno, R., Peterson, M. A., Laird, J. R. Jr., Satler, L. F., et al. (2001). Transient contrast encephalopathy after carotid artery stenting. *J. Endovasc. Ther.* 8, 111–113.
- Dattani, A., Au, L., Tay, K. H., and Davey, P. (2018). Contrast-induced encephalopathy following coronary angiography with no radiological features: A case report and literature review. *Cardiology* 139, 197–201.
- de Bono, D. (1993). Complications of diagnostic cardiac catheterisation: Results from 34,041 patients in the United Kingdom confidential enquiry into cardiac catheter complications. The joint audit committee of the british cardiac society and royal college of physicians of london. *Br. Heart J.* 70, 297–300.
- Donepudi, B., and Trotter, S. (2018). A seizure and hemiplegia following contrast exposure: Understanding contrast-induced encephalopathy. *Case Rep. Med.* 2018:9278526.
- Fernando, T. G., Nandasiri, S., Mendis, S., Senanayake, S., Gooneratne, I. K., Navin, R., et al. (2020). Contrast-induced encephalopathy: A complication of coronary angiography. *Pract. Neurol.* 20, 482–485.
- Fusco, A., Pucci, L., Pierre, K., Wolberg, A., Small, C., Cerillo, J., et al. (2022). Contrast allergies for neurological imaging: When to proceed. *AIMS Allergy Immunol.* 6, 216–227.
- García-Pérez, D., Parra-Serrano, J., Panero, I., Moreno, L. M., Campollo, J., and Alén, J. F. (2021). Transient cortical blindness secondary to contrast-induced encephalopathy following diagnostic cerebral angiography: Report of 2 cases. *Acta Neurol. Belg.* 121, 585–589.
- Hamra, M., Bakhit, Y., Khan, M., and Moore, R. (2017). Case report and literature review on contrast-induced encephalopathy. *Future Cardiol.* 13, 331–335.
- Harada, Y., Kairamkonda, S. R., Ilyas, U., Pothineni, N. V. K., Samant, R. S., Shah, V. A., et al. (2020). Pearls & Oysters: Contrast-induced encephalopathy following coronary angiography: A rare stroke mimic. *Neurology* 94, e2491–e2494.
- Heemelaar, J. C., van der Hoeven, N. W., Muller, F. F., and Appelman, Y. (2018). Acute-onset coma after iso-osmolar iodinated contrast injection: A case report of contrast-induced encephalopathy after elective coronary angiography. *Eur. Heart J. Case Rep.* 2:tyt132.
- Hirata, S., Koga, M., and Iseki, H. (2018). Contrast-induced encephalopathy after coronary angioplasty in a patient with ST-elevation myocardial infarction. *Heart Asia* 10:e010987.
- Jiang, C., Li, J., Huang, Y., Huang, D., Lin, J., and Jiang, X. (2021). Clinical safety evaluation of contrast agents based on real-world evidence. *J. Clin. Pharm. Ther.* 46, 1600–1605.
- Kahyaoglu, M., Ağca, M., Çakmak, E., Geçmen, Ç., and İzgi, I. A. (2018). Contrast-induced encephalopathy after percutaneous peripheral intervention. *Türk Kardiyol. Dern. Ars.* 46, 140–142.
- Kamimura, T., Nakamori, M., Imamura, E., Hayashi, Y., Matsushima, H., Mizoue, T., et al. (2021). Low-dose contrast-induced encephalopathy during diagnostic cerebral angiography. *Intern. Med.* 60, 629–633.
- Kocabay, G., Karabay, C. Y., Kalayci, A., Akgun, T., Guler, A., Oduncu, V., et al. (2014). Contrast-induced neurotoxicity after coronary angiography. *Herz* 39, 522–527.
- Lei, P., He, W., Shi, Q., Sun, M., and Sun, Z. (2020). Recurrent epileptic seizures following cardiac catheterization with iodixanol: A case report. *BMC Cardiovasc. Disord.* 20:79. doi: 10.1186/s12872-020-01341-3
- Leong, S., and Fanning, N. F. (2012). Persistent neurological deficit from iodinated contrast encephalopathy following intracranial aneurysm coiling. A case report and review of the literature. *Interv. Neuroradiol.* 18, 33–41.
- Li, J., Qi, G., Zhang, H., Chen, G., Wang, S., Yan, M., et al. (2021). Contrast-induced encephalopathy mimicking stroke after a second cerebral DSA: An unusual case report. *BMC Neurol.* 21:430. doi: 10.1186/s12883-021-02457-5
- Liu, M. R., Jiang, H., Li, X. L., and Yang, P. (2020). Case report and literature review on low-osmolar, non-ionic iodine-based contrast-induced encephalopathy. *Clin. Interv. Aging* 15, 2277–2289.
- Murruve, D. A., and Steinman, T. I. (1996). Contrast-induced encephalopathy and seizures in a patient with chronic renal insufficiency. *Clin. Nephrol.* 45, 406–409.
- Nagamine, Y., Hayashi, T., Kakehi, Y., Yamane, F., Ishihara, S., Uchino, A., et al. (2014). Contrast-induced encephalopathy after coil embolization of an unruptured internal carotid artery aneurysm. *Intern. Med.* 53, 2133–2138.
- Park, J. C., Ahn, J. H., Chang, I. B., Oh, J. K., Kim, J. H., and Song, J. H. (2017). A case of unusual presentation of contrast-induced encephalopathy after cerebral angiography using iodixanol. *J. Cerebrovasc. Endovasc. Neurosurg.* 19, 184–188.
- Potsi, S., Chourmouzi, D., Moutzouoglou, A., Nikiforaki, A., Gkouvas, K., and Drevelgas, A. (2012). Transient contrast encephalopathy after carotid angiography mimicking diffuse subarachnoid haemorrhage. *Neurol. Sci.* 33, 445–448.
- Rashid, H., Brown, J., Nix, E., and Fisher Covin, A. (2022). Contrast-Induced encephalopathy following diagnostic coronary angiography. *Clin. Case Rep.* 10:e05624.
- Renault, P., and Rouchet, S. (2019). Transient global amnesia and transient cortical blindness secondary to contrast induced encephalopathy after renal artery angiography. *Rev. Neurol.* 175, 335–336.
- Riahi, L., Mediouni, M., Messelmani, M., and Fehri, W. (2019). A singular manifestation of contrast-induced encephalopathy following coronary angiography. *Neurol. India* 67, 1525–1527.
- Shahan, B., Choi, E. Y., and Nieves, G. (2021). Cerebrospinal fluid analysis. *Am. Fam. Phys.* 103, 422–428.
- Şimşek, E., Ertürk, E., Uçar, R., Yılmaz, A. O., Ekmekçi, C., Mutlu, I., et al. (2019). Transient contrast neurotoxicity after percutaneous coronary intervention mimicking subarachnoid hemorrhage in a patient with chronic kidney disease. *Clin. Med. Insights Case Rep.* 12:1179547619867671.
- Spina, R., Simon, N., Markus, R., Muller, D. W., and Kathir, K. (2017). Contrast-induced encephalopathy following cardiac catheterization. *Catheter. Cardiovasc. Interv.* 90, 257–268.
- Tong, X., Hu, P., Hong, T., Li, M., Zhang, P., Li, G., et al. (2018). Transient Cortical Blindness Associated with Endovascular Procedures for Intracranial Aneurysms. *World Neurosurg.* 119, 123–131.
- Vigano, M., Mantero, V., Basilico, P., Cordano, C., Sangalli, D., Reganati, P., et al. (2021). Contrast-induced encephalopathy mimicking total anterior circulation stroke: A case report and review of the literature. *Neurol. Sci.* 42, 1145–1150.
- Yan, J., and Ramanathan, V. (2013). Severe encephalopathy following cerebral arteriogram in a patient with end-stage renal disease. *Semin. Dial.* 26, 203–207.
- Yao, L. D., Zhu, X. L., Yang, R. L., and Zhang, M. M. (2021). Cardiorespiratory arrest after iso-osmolar iodinated contrast injection: A case report of contrast-induced encephalopathy following contrast-enhanced computed-tomography. *Medicine* 100:e24035.

Yu, J., and Dargas, G. (2011). Commentary: New insights into the risk factors of contrast-induced encephalopathy. *J. Endovasc. Ther.* 18, 545–546.

Zhang, W., Huang, H., Jiang, B., Liu, Z. Y., and He, Y. (2021). Iopromide-induced encephalopathy: A case report and literature review. *Sichuan Da Xue Xue Bao Yi Xue Ban* 52, 528–530.

Zhao, W., Zhang, J., Song, Y., Sun, L., Zheng, M., Yin, H., et al. (2019). Irreversible fatal contrast-induced encephalopathy: A case report. *BMC Neurol.* 19:46. doi: 10.1186/s12883-019-1279-5

Zhao, Z., Huang, L., Chen, J., and Zhu, H. (2021). Rapid contrast-induced encephalopathy after a small dose of contrast agent: Illustrative case. *J. Neurosurg. Case Lessons* 1:Case2052.



OPEN ACCESS

EDITED BY

Shong Lau,
Salk Institute for Biological Studies,
United States

REVIEWED BY

Qiuwen Wang,
Salk Institute for Biological Studies,
United States
Marija Mostarica-Stojkovic,
University of Belgrade, Serbia

*CORRESPONDENCE

Dahe Lin
✉ 416316606@qq.com
Hongen Li
✉ empyreal614@163.com
Shihui Wei
✉ weishihui706@hotmail.com

†These authors have contributed equally to this work and share first authorship

SPECIALTY SECTION

This article was submitted to
Neurodegeneration,
a section of the journal
Frontiers in Neuroscience

RECEIVED 22 November 2022

ACCEPTED 14 February 2023

PUBLISHED 16 March 2023

CITATION

Lin D, Liu H, Song H, Chen B, Fu J, Sun M,
Zhou H, Bai W, Wei S and Li H (2023)
Upregulation of C-X-C motif chemokine 12
in the spinal cord alleviated the symptoms
of experimental autoimmune
encephalomyelitis in Lewis rats.
Front. Neurosci. 17:1105530.
doi: 10.3389/fnins.2023.1105530

COPYRIGHT

© 2023 Lin, Liu, Song, Chen, Fu, Sun, Zhou, Bai,
Wei and Li. This is an open-access article
distributed under the terms of the [Creative
Commons Attribution License \(CC BY\)](#). The
use, distribution or reproduction in other
forums is permitted, provided the original
author(s) and the copyright owner(s) are
credited and that the original publication in this
journal is cited, in accordance with accepted
academic practice. No use, distribution or
reproduction is permitted which does not
comply with these terms.

Upregulation of C-X-C motif chemokine 12 in the spinal cord alleviated the symptoms of experimental autoimmune encephalomyelitis in Lewis rats

Dahe Lin^{1,2,3*†}, Hongjuan Liu^{1,4†}, Honglu Song^{1,5†}, Biyue Chen^{1†},
Junxia Fu¹, Mingming Sun⁶, Huanfen Zhou¹, Wenhao Bai¹,
Shihui Wei^{1*} and Hongen Li^{1*}

¹Department of Ophthalmology, The First Medical Center of Chinese People's Liberation Army (PLA) General Hospital, Beijing, China, ²Fujian Provincial Key Laboratory of Ecology-Toxicological Effects and Control for Emerging Contaminants, College of Environmental and Biological Engineering, Putian University, Putian, Fujian, China, ³Key Laboratory of Ecological Environment and Information Atlas, Fujian Provincial University (Putian University), Putian, Fujian, China, ⁴Department of Ophthalmology, Beijing Tongren Eye Center, Beijing Tongren Hospital, Beijing, China, ⁵Department of Ophthalmology, The 980th Hospital of the Chinese People's Liberation Army (PLA) Joint Logistics Support Force, Shijiazhuang, Hebei, China, ⁶Department of Ophthalmology, The Third Medical Center of Chinese People's Liberation Army (PLA) General Hospital, Beijing, China

Background: C-X-C motif chemokine 12 (CXCL12) is a chemokine that performs many functions. Studies have shown that CXCL12 can aggravate inflammatory symptoms in the central nervous system (CNS). Evidence also indicates that CXCL12 can promote the repair of myelin sheaths in the CNS in experimental autoimmune encephalomyelitis (EAE). Here, we investigated the function of CXCL12 in CNS inflammation by upregulating CXCL12 in the spinal cord and subsequently inducing EAE.

Materials and methods: CXCL12 upregulation in the spinal cords of Lewis rats was induced by the injection of adeno-associated virus 9 (AAV9)/eGFP-P2A-CXCL12 after intrathecal catheter implantation. Twenty-one days after AAV injection, EAE was induced and clinical score was collected; Immunofluorescence staining, WB and LFB-PAS staining were used to evaluate the effect of CXCL12 upregulation. In the *in vitro* study, oligodendrocyte precursor cells (OPCs) were harvested, cultured with CXCL12 and AMD3100, and subjected to immunofluorescence staining for functional assessment.

Results: CXCL12 was upregulated in the lumbar enlargement of the spinal cord by AAV injection. In each stage of EAE, upregulation of CXCL12 significantly alleviated clinical scores by inhibiting leukocyte infiltration and promoting remyelination. In contrast, the addition of AMD3100, which is a CXCR4 antagonist, inhibited the effect of CXCL12. *In vitro*, 10 ng/ml CXCL12 promoted the differentiation of OPCs into oligodendrocytes.

Conclusion: AAV-mediated upregulation of CXCL12 in the CNS can alleviate the clinical signs and symptoms of EAE and significantly decrease the infiltration of leukocytes in the peak stage of EAE. CXCL12 can promote the maturation and

differentiation of OPCs into oligodendrocytes *in vitro*. These data indicate that CXCL12 effectively promotes remyelination in the spinal cord and decreases the signs and symptoms of EAE.

KEYWORDS

CXCL12, EAE, AAV, neuroinflammation, remyelination

Introduction

As a common manifestation of multiple sclerosis (MS) and neuromyelitis optica spectrum disorders (NMOSDs), inflammatory demyelination make an important contribution to disability in the patients with demyelinating disorders (Kearney et al., 2015; Ciccarelli et al., 2019; Fadda et al., 2022). Chemokines are considered to be essential mediators that are secreted by many kinds of cells to activate G protein-mediated signaling pathways (Krumbholz et al., 2006; Huynh et al., 2020). Some of the chemokines guided inflammatory cells into the central nervous system (CNS) and played an important role in the myelin damage, but some are not. Notably, chemokine C-X-C motif ligand 12 (CXCL12) was revealed to play a crucial role in the maintenance of neural homeostasis, including the regulation of proliferation, differentiation and migration of oligodendrocyte precursor cells (OPCs) in the animal disease model system (Patel et al., 2010, 2012; Li et al., 2012; Zilkha-Falb et al., 2016). Additionally, CXCL12 could recruit other types of endogenous stem/progenitor cells, such as hematopoietic stem cells, mesenchymal stem cells, endothelial progenitor cells and neural progenitor cells (NPCs), mainly worked by interacting with CXCR4, which is one of its natural receptors (Klein and Rubin, 2004; Dziembowska et al., 2005; Patel et al., 2010; Carbajal et al., 2011; Huynh et al., 2020).

The observation that up-regulation of CXCL12 were found in the reactive astrocytes and endothelial cells in the lesions of patients with MS, and CXCR4-positive leukocytes could further infiltrated into CNS parenchyma (Calderon et al., 2006; McCandless et al., 2008; Moll et al., 2009). McCandless et al. (2008) suggested that the redistribution of CXCL12 at the blood-brain barrier (BBB), rather than up-regulation of CXCL12 expression in lesions of CNS, plays a more important role in leukocyte infiltration and demyelination in MS. These phenomenon are also observed in Experimental Autoimmune Encephalomyelitis (EAE), which may be the most frequently used animal model system of rodent for MS studying (McCandless et al., 2006; Cruz-Orengo et al., 2011; Zilkha-Falb et al., 2016). Inhibition of CXCL12 signaling could result in widespread white matter infiltration of mononuclear cells and aggravate EAE symptoms (McCandless et al., 2006). Therefore, it is rational to speculate that the ongoing progression of MS may result from the enhanced infiltration of leukocytes.

A series of studies have examined EAE in Dark Agouti (DA) and Albino Oxford (AO) rats (Miljković et al., 2011; Blaževski et al., 2013, 2015). The differential resistance of these two rat strains to EAE implies that CXCL12 is involved in the promotion of remyelination (Miljković et al., 2011; Blaževski et al., 2013).

Many of excellent studies have shown that CXCL12 plays a positive role in promoting the remyelination of EAE (McCandless et al., 2006; Patel et al., 2010, 2012; Miljković et al., 2011; Blaževski et al., 2013; Zilkha-Falb et al., 2016). The intense inflammation and macrophage phagocytosis aggregation in the active MS lesions are the main causes that leads to failure of remyelination, since sufficient OPCs were found within lesions (Kuhlmann et al., 2008; Lassmann et al., 2012; Chu et al., 2017). On the basis of the function of CXCL12 that promote migration and differentiation of OPCs, upregulation of CXCL12 in CNS may be a potential therapeutic strategy to MS. Several previous studies showed that CXCL12 acts as a T-cell chemoattractant at low doses and a chemorepellent at high doses (Poznansky et al., 2000; Vianello et al., 2006). So it is interesting to up-regulate CXCL12 before the onset of EAE, and observe whether the upregulated CXCL12 can alleviate the symptoms, or even inhibit the occurrence of EAE.

In this study, polyethylene catheters (PE-10 tubing) were placed into the subarachnoid space near the lumbar enlargement of rats, and overexpression of CXCL12-GFP in this area of CNS was induced by injection of AAV through the PE-10 tubing. 21 days after infection, EAE model was builded. The aim was to verify whether direct upregulation of CXCL12 gene in the spinal cord could promote the remyelination or exacerbate EAE symptoms by enhancing leukocyte infiltration.

Materials and methods

Animals and intrathecal catheter implantation

Ten-week-old female Lewis rats (180–220 g) were purchased from Vital river of China and raised under specific pathogen-free conditions. The rats were anesthetized with sodium pentobarbital (50 mg/kg), and then a polyethylene catheter was inserted through a hole made in the posterior atlantooccipital membrane (Chen et al., 2020). The catheter was threaded 7 cm caudally into the subarachnoid space of the spinal cord (Chen et al., 2020). The end of the tube opened approximately in the lumbar enlargement. The rostral part of the tube was sutured to the muscle for immobilization. After intrathecal catheter implantation, the rats were housed individually and allowed to recover for 7 days before AAV9 was injected into the subarachnoid space through a PE-10 tube (Portex Tubing PE 0.28*0.165 mm Bx, Scientific Laboratory Supplies, Nottingham).

AAV vector production

The AAV9 vectors (pAAV-CMV-bGlobin-EGFP-P2A) were used in this study to package rat CXCL12 (GenBank ID: NM_022177). AAV9 viral stocks with the recombinant AAV vector were produced according to the three-plasmid cotransfection method by Obio Technology Corp., Ltd., (Shanghai, China) (Beckman et al., 2021). The titers of purified AAV9/eGFP and AAV9/eGFP-P2A-CXCL12 were measured by quantitative polymerase chain reaction (qPCR) using SYBR green technology.¹ The AAVs were aliquoted and stored at -80°C until further use.

Study design

To determine the functions of CXCL12 in the rat CNS in EAE, an AAV9 vector expressing CXCL12 (AAV9/eGFP-P2A-CXCL12) was administered, as mentioned above; an eGFP vector (AAV9/eGFP) acted as the control. Each rat received 1×10^{12} vg/ml AAV9/eGFP-P2A-CXCL12 or AAV9/eGFP intrathecally *via* a polyethylene catheter that was inserted through a small hole made in the posterior atlantooccipital membrane. Then, the rats were divided into three groups: CXCL12, eGFP

and CXCL12 + AMD3100. AMD3100, a CXCR4 antagonist, was injected into the CNS through the catheter 2 days after immunization with spinal cord homogenate (SCH) and complete Freund's adjuvant (CFA). AMD3100 (Sigma-Aldrich, St. Louis, MO, USA), was dissolved in normal saline to an injection dose of $40 \mu\text{g}/10 \mu\text{l}$ per rat.

Induction of EAE

Twenty-one days after AAV injection, the rats were immunized with a $400\text{-}\mu\text{l}$ mixture containing $200 \mu\text{l}$ of spinal cord homogenate (SCH) and an equal volume of complete Freund's adjuvant (CFA, Sigma) by subcutaneous injection in the base of the tail. Forty-eight hours after immunization, the rats received 400 ng of pertussis toxin (Sigma) in $200 \mu\text{l}$ of PBS *via* intraperitoneal injection. The animals were observed and scored. Scoring was completed using a standard five-point scale: 0, no deficit; 0.5, partial loss of tail tone or slightly abnormal gait; 1.0, complete tail paralysis or both partial loss of tail tone and mild hind limb weakness; 1.5, complete tail paralysis and mild hind limb weakness; 2.0, tail paralysis with moderate hind limb weakness (evidenced by frequent foot dragging); 2.5, no weight bearing on hind limbs (dragging) but with some leg movement; 3.0, complete hind limb paralysis with no residual movement; 3.5, hind limb paralysis with mild weakness in forelimbs; 4.0, complete quadriplegia but with some movement of the head; 4.5, moribund; and 5.0, death.

¹ <https://www.addgene.org/protocols/aav-titration-qpcr-using-sybr-green-technology/>

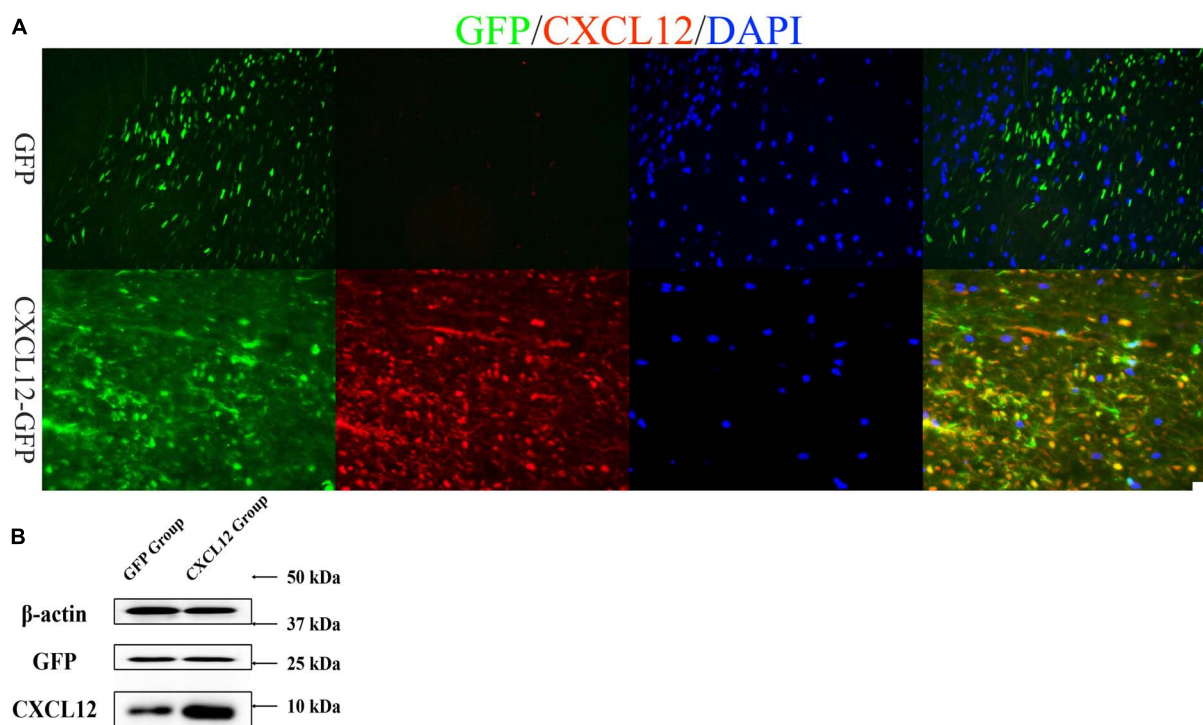


FIGURE 1

CXCL12-GFP and eGFP were upregulated in the lumbar enlargement of the spinal cord. (A) Adeno-associated virus (AAV)-mediated upregulation of CXCL12 and eGFP in the lumbar enlargement was robust. On the 21st day after infection, immunofluorescence showed that the level of CXCL12 in the lumbar enlargement was much higher in the CXCL12-GFP group than in the eGFP group, and the CXCL12 and eGFP signals in the white matter were stronger than those in the gray matter of the spinal cord. The bar in the lower right represents $50 \mu\text{m}$. (B) Western blot (WB) results also show that the expression of CXCL12 in spinal cord of CXCL12 group, particularly in regions surrounding the cannula tip, was higher than the eGFP group.

Histological and fluorescent immunostaining

First, the rats were anesthetized by intraperitoneal injection of pentobarbital sodium (50 mg/kg), and then the rats were perfused through heart with precooled PBS followed by precooled 4% paraformaldehyde (PFA) in PBS. The spinal cord was isolated and fixed for 6 h and then immersed in 30% sucrose for 48 h. After freezing in Tissue-Tek OCT compound (Sakura, Japan), the spinal cord was sliced by a freezing microtome (CM1850, Leica Biosystems, Heidelberg, Germany); 10- μ m-thick coronal sections were prepared and processed for Luxol fast blue periodic acid-Schiff (LFB-PAS) (Sigma-Aldrich, St. Louis, MO, USA) staining as well as fluorescent immunostaining for detect the severity of demyelination in each stages. The slides were dehydrated to 95% alcohol and incubated in 0.1% LFB solution about 10–16 h at 58°C, then sections were differentiated in 0.05% lithium carbonate solution and 70% alcohol then counterstained with PAS (Li et al., 2013). For fluorescent immunostaining, the slides were washed with PBS, treated with blocking solution (5% normal donkey serum in PBS) for 1 h at room temperature (25°C) and then stained with one of the following primary antibodies (diluted in blocking solution) in a humidified box overnight at 4°C: anti-MBP (1:100, Abcam, UK); anti-GFAP (1:200, CST, USA); anti-NG2 (1:100, Abcam, UK); anti-CD45 (1:100, Abcam, UK); anti-CXCR4 (1:100, Abcam, UK); and anti-CXCL12 (1:100, Abcam, UK). Finally, the slides were exposed to the appropriate secondary antibodies (1:200, Abcam, UK) for 1 h in a humidified box at room temperature. After immunostaining, the slides were stained with DAPI to visualize the nuclei.

Western blot analysis

The spinal cord tissue of Lewis rats about 0.5 cm upstream and downstream of the PE-10 tube's end was obtained, and then cut the tissue into 1–2 mm³ small pieces with ophthalmic scissors. After adding 3–5 times the volume of RIPA lysis buffer (Beyotime, China) and resuspending, the tissue was homogenized and then gets ultrasonication for 30 s. Centrifuged the homogenate at 14,000 g 4°C for 10 min for the supernatant and detected the protein concentration by the BCA kit (Beyotime, China). Diluted the sample protein concentration to 2 μ g/ μ l with RIPA lysis buffer. The protein samples (30 μ g/each) denatured in 5x loading buffer at 100°C for 5 min. Samples were loaded and separated electrophoretically using 8% SDS-PAGE gel operated at 100 V (for 1 h) and then 130 V (for 1.5 h), respectively. Following electrophoresis, samples were transferred to PVDF membranes (invitrogen, USA) using transfer buffer contain 25 mM Trisbase, 192 mM Glycine and 20% methanol. Membranes were blocked with 5% skimmed milk in Tris-buffered saline/0.1% Tween (TBST) for 1 h at room temperature, followed by incubation with primary antibody (rabbit anti-CXCL12, 1:1000, Abcam, UK; rabbit anti-GFP, 1:1000, Abcam, UK; mouse anti- β -actin, 1:1000, Abcam, UK) in blocking buffer (3%BSA in TBST) for 16 h at 4°C. Membranes were washed 3 \times 15 min in TBST, and then incubated with goat anti-rabbit or goat anti-mouse IgG (H + L) secondary antibodies conjugated to horse-radish peroxidase (1:1000, Beyotime, China)

for 1 h at room temperature, washed 3 \times 15 min in TBST, and then visualized with ECL substrate (Thermo Scientific, USA) and imaged with ChemiDoc MP system (Bio-Rad, USA).

Culture of OPCs

Oligodendrocyte precursor cells (OPCs) of WISTAR rats were purchased from CHI Scientific Co., Ltd., (1-5110). OPCs were cultured in Dulbecco's modified Eagle's medium (DMEM):F12 media (Gibco company, USA) supplemented with HEPES (Sigma, USA), bFGF (human recombinant, 20 ng/ml, PeproTech, USA) and EGF (mouse recombinant, 20 ng/ml, PeproTech, USA), all from PeproTech Company, USA. The culture medium was renewed every 2 days. For the differentiation experiments, OPCs were cultured in the presence or absence of 10 ng/ml CXCL12 (PeproTech, USA) in differentiation medium. To demonstrate the mechanism underlying the promotion of OPC differentiation, cells were treated with AMD3100 (100 ng/ml) and incubated for 12 days in differentiation medium. AMD3100 medium was replaced every day.

Image analysis

All images were captured using a Leica DM4000B microscope. The software settings for imaging kept exactly identical among spinal cord sections in each immunostaining. Areas of demyelination in the lumbar enlargement of spinal cords were quantified using a 0–4 points semiquantitative scale system (Zhang et al., 2019), where 0 = no demyelination; 1 = rare and focal demyelination; 2 = multiple focal demyelination; 3 = large or confluent demyelination; 4 = large and confluent demyelination. All slides were read in a blinded manner. The fluorescence intensity was calculated as the percentage of the antibody (anti-MBP, anti-GFAP, anti-NG2, and anti-CD45) positive stained area to the total area of spinal cord in the figure, and results from each rat were counted in three slides. Statistical analysis was undertaken using ImageJ software (version 1.39, NIH, USA).

Data statistics

The data were expressed as mean \pm SEM (standard error of mean). 1-way ANOVA (analysis of variance) was used to test significant differences among three groups, and 2-tailed unpaired Student's *t*-test was used for two groups at each time point. *P* < 0.05 was considered statistically significant.

Results

Upregulation of CXCL12 in the spinal cord lumbar enlargement of Lewis rats

After 21 days of the intrathecal injection of AAV9 (CXCL12 or eGFP), rats were sacrificed for immunofluorescence analysis and

Western blot (WB) tests (Figure 1). We found green fluorescence in both groups (CXCL12 and eGFP) in the lumbar enlargement of the spinal cord in Lewis rats (Figure 1A). The signal of CXCL12 were significantly higher in the CXCL12 group than in the control group (eGFP group) (Figure 1A), and WB of spinal cord tissue homogenates confirmed that (Figure 1B).

Upregulation of CXCL12 in the CNS can alleviate EAE clinical scores

Experimental autoimmune encephalomyelitis (EAE) was induced in the three groups: the eGFP group, CXCL12 group and CXCL12 + AMD3100-treated group. Each group contained nine rats. The clinical scores of all rats were collected and then statistically analyzed. The results indicated that the EAE symptoms of the AMD3100 treatment group were observed the earliest (8th day), followed by the eGFP group (10th day) and the CXCL12 group (13th day) (Figure 2A). At the peak stage of EAE (12–14 days), the mean of clinical scores of the CXCL12 group were significantly lower than that of the other two groups, and no relapse of EAE was observed in the CXCL12 group between the 24th and 30th day after EAE induction (Figure 2A). In addition, at the recovery stage (33–38 days), the clinical scores of CXCL12 group were still significantly lower than that of the other two groups (Figure 2A). Daily injection of 40 µg of AMD3100 after induction of EAE through a PE-10 tube inserted in the back of the head caused earlier onset of symptoms and extended the duration of remyelination. The LFB-PAS staining showed that there were no difference among three groups at the initial stage (2–4 days) of EAE, however, higher demyelination scores of eGFP and CXCL12 + AMD3100 groups compare to CXCL12 group in the spinal cord at the peak stage and the recovery stage (Figures 2B, C). The above results indicate that upregulation of CXCL12 in the white matter of the spinal cord can effectively reduce clinical scores and alleviate symptoms in the EAE model. Moreover, upregulated CXCL12 appeared to inhibit the recurrence of EAE (Figure 2A; 25–27 days).

Upregulation of CXCL12 can effectively reduce demyelination in EAE

Glia cells in the CNS, including microglia, astrocytes and oligodendrocytes, are very important for homeostasis maintaining and involved in the pathogenesis of MS directly (Stavropoulos et al., 2021). Oligodendrocytes are responsible for generating myelin sheaths and white matter tracts (Nave and Werner, 2014), and crosstalk between astrocytes and oligodendrocytes is closely related to the progress of MS (Patel et al., 2010; Stavropoulos et al., 2021). The immunofluorescence assay results revealed no significant differences in the expression levels of Myelin Basic Protein (MBP, a marker of mature oligodendrocytes) and Glial Fibrillary Acidic Protein (GFAP, a marker of astrocytes) among the three groups at the initial (Figure 3) and recovery stages (Figure 5) of EAE. However, at the peak stage of EAE, the fluorescence signals of MBP and GFAP in the spinal cord of the CXCL12 group were higher than those in the eGFP and CXCL12 + AMD3100 groups. The above

immunofluorescence results are consistent with LFB-PAS staining results. Taken together, the results indicate that upregulation of CXCL12 can effectively alleviate the symptoms of EAE by reducing myelin damage.

The infiltration of peripheral immune cell into the CNS are the early events in EAE development, and are also observed in brains of MS patients (Floris et al., 2004; Ortiz et al., 2014). To determine the underlying mechanisms of CXCL12's effects on the myelin sheath in the CNS, the signal of CD45 (a common leukocyte antigen) was detected in the three stages of EAE. At the initial stage, there were no significant differences in the CD45 signal among the three groups (Figure 3). However, during the peak stage and recovery stage, the CD45 signal in the CXCL12 group was significantly lower than that in the other groups (Figures 4, 5). Thus, there was less leukocyte infiltration in the CXCL12 group (Figures 3–5), which might be an important mechanism underlying the alleviation of the symptoms of EAE since lower leukocyte infiltration usually indicates reduced neuroinflammation.

CXCL12 upregulation promotes the differentiation of OPCs into oligodendrocytes

In the CNS, Oligodendrocytes is differentiated from OPCs. As shown in Figures 3, 4, NG2 (a biomarker of OPCs) was significantly upregulated in the spinal cord in the peak stage of EAE in the eGFP and CXCL12 + AMD3100 groups; the same trend was also observed in the recovery stage. This finding indicates that OPCs are actively involved in remyelination of the myelin sheath. However, in the CXCL12 group, it was difficult to detect OPCs at all stages of EAE, and the duration of the peak time (from the 13th to 22nd day) in the CXCL12 group was shorter than that of the other two groups (13 days on average), which might be because the upregulated CXCL12 promoted the mature differentiation of OPCs into oligodendrocytes, thus promoting regeneration of the spinal myelin sheath.

In vitro, OPCs of WISTAR rats were cultured in differentiation medium with either 0 or 10 ng/ml CXCL12. Exogenous CXCL12 (10 ng/ml) promoted the differentiation of OPCs into oligodendrocytes, as shown by immunostaining for MBP (Figure 6). AMD3100 was added to OPCs cultured in differentiation medium in the presence of CXCL12 (10 ng/ml). After 12 days, compared to the control differentiation culture (10 ng/ml CXCL12), AMD3100 administration strongly inhibited the differentiation of OPCs (Figure 6). Moreover, NG2 and CXCR4 coexpression in OPCs was assessed (Figure 7). The results were consistent with previous studies suggesting that the CXCL12/CXCR4 axis promotes the differentiation of OPCs *in vitro* and *in vivo* (Patel et al., 2010, 2012; Zilkha-Falb et al., 2016).

Discussion

Oligodendrocyte precursor cells (OPCs) originate in subventricular zones that region is distant from white matter areas within the CNS. The migration, proliferation, and differentiation of OPCs are essential for repairment of demyelinated lesions.

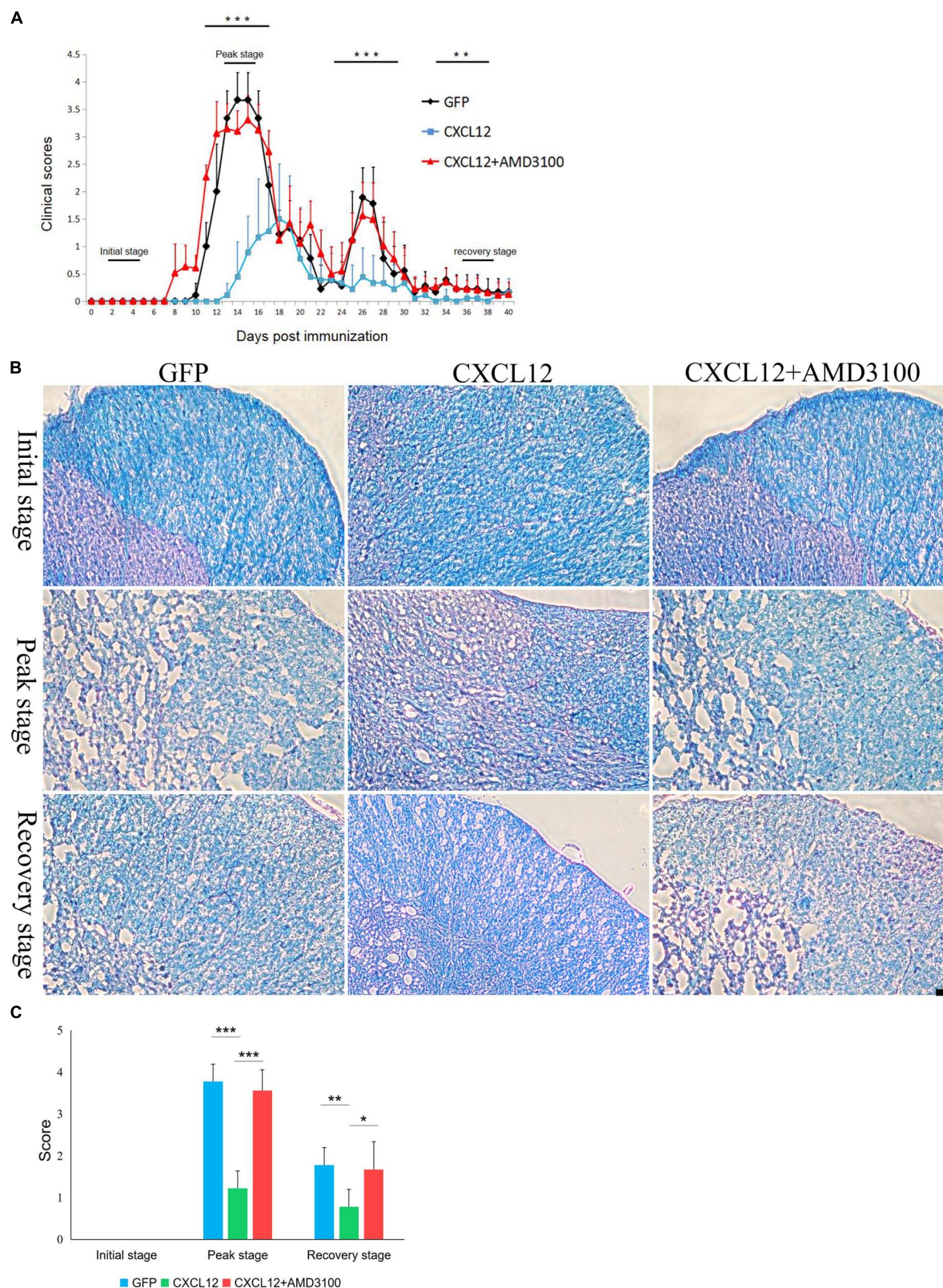


FIGURE 2

Upregulation of CXCL12 in the spinal cord can effectively reduce the clinical scores and demyelination of experimental autoimmune encephalomyelitis (EAE). (A) EAE was induced in Lewis rats ($n = 15$ in each group). The clinical scores were determined as described in the Methods section. The horizontal bars show the stages of EAE progression (the initial stage was 2–4 days, the peak stage was 12–14 days, and the recovery stage was 38–40 days). The rats were sacrificed for immunofluorescence detection at the each stage. (B) Representative images of Luxol fast blue periodic acid-Schiff (LFB-PAS) staining in the spinal cord at three stages in all three groups. The bar in the lower right represents 50 μm . (C) Demyelination score based on LFB-PAS staining in spinal cord. Data presented as the mean \pm SEM. “*” represents value of $P < 0.05$, “***” represents value of $P < 0.01$, “****” represents value of $P < 0.001$ by 2-tailed unpaired Student’s t -test or 1-way ANOVA.

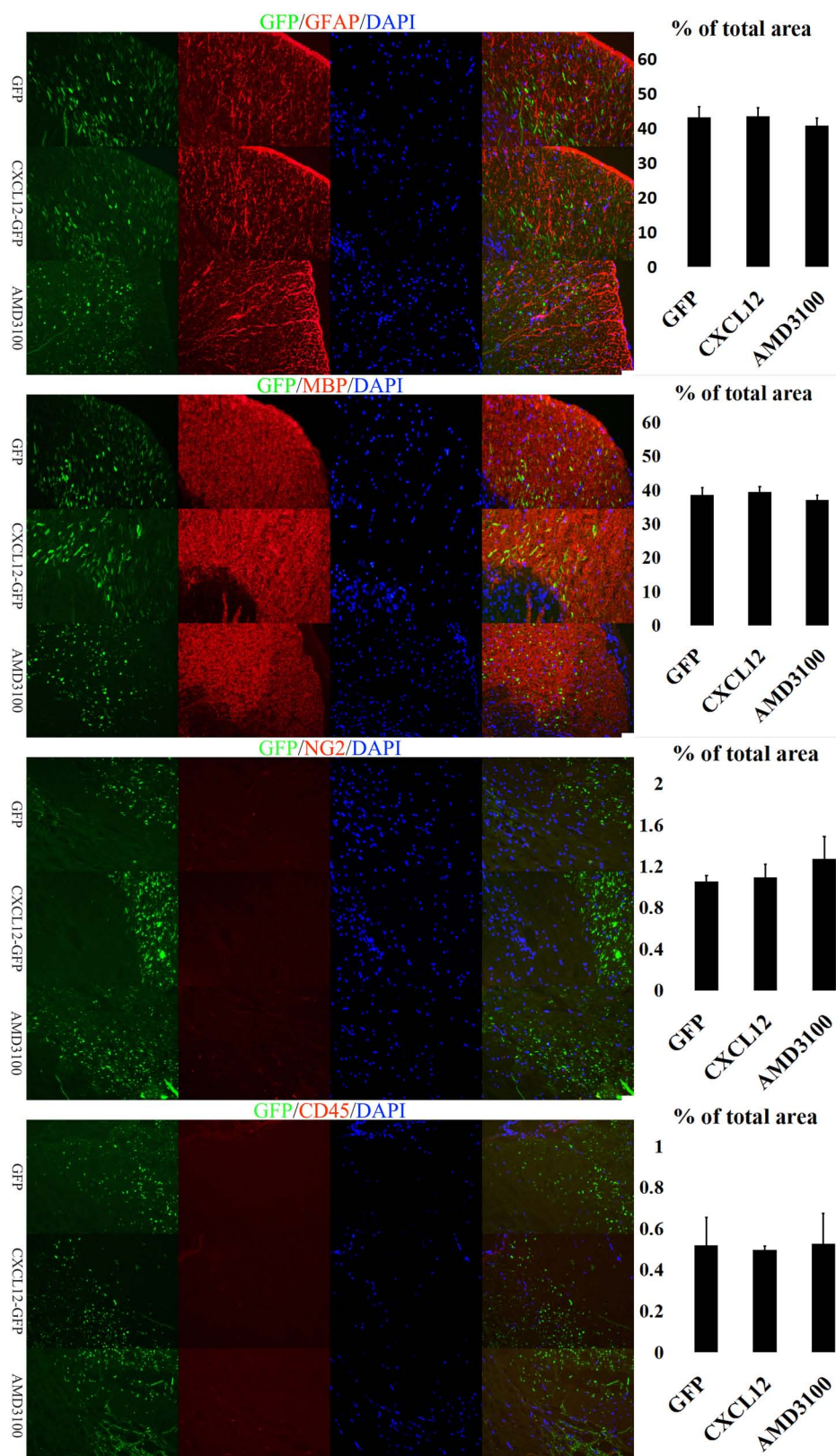


FIGURE 3

Upregulation of CXCL12 did not induced peripheral immune cell infiltration in the spinal cord at the initial stage. At the initiation stage of experimental autoimmune encephalomyelitis (EAE), the expression of glial fibrillary acidic protein (GFAP) and myelin basic protein (MBP) was similar in all three groups, indicating that the myelin sheath was intact. During this period, the OPC (NG2 +) and leukocyte (CD45 +) signals in the spinal cord were low. The bar charts show fluorescence intensity. Data presented as the mean \pm SEM. “*” represents value of $P < 0.05$, “***” represents value of $P < 0.01$, “****” represents value of $P < 0.001$ by 2-tailed Student’s *t*-test or 1-way ANOVA, $n = 4$ rats. The bar in the lower right represents 50 μ m.

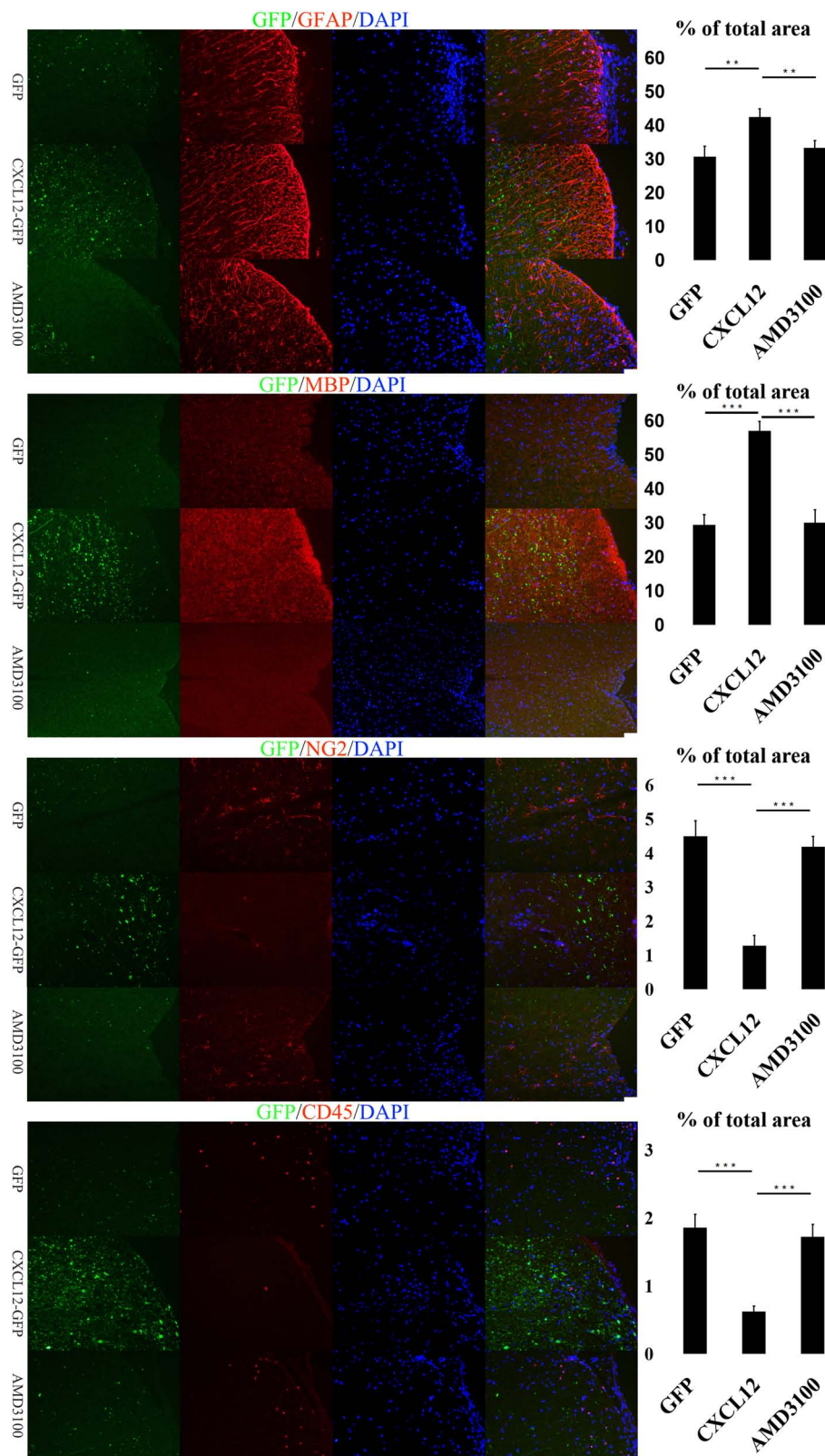


FIGURE 4

Upregulation of CXCL12 alleviated the spinal cord aberrations of experimental autoimmune encephalomyelitis (EAE) at the peak stage. At the peak stage of EAE, the significant differences in the glial fibrillary acidic protein (GFAP) and myelin basic protein (MBP) signals between the three groups showed that there was severe demyelination in the eGFP group and CXCL12-AMD3100 group. There were also significant differences in the CD45 and NG2 signals, suggesting that leukocyte infiltration likely led to deterioration of demyelination and that oligodendrocyte precursor cells (OPCs) were actively involved in remyelination. Data presented as the mean \pm SEM. "*" represents value of $P < 0.05$, "***" represents value of $P < 0.01$, "****" represents value of $P < 0.001$ by two-tailed Student's *t*-test or one-way ANOVA, $n = 4-6$ rats. The bar in the lower right represents 50 μm .

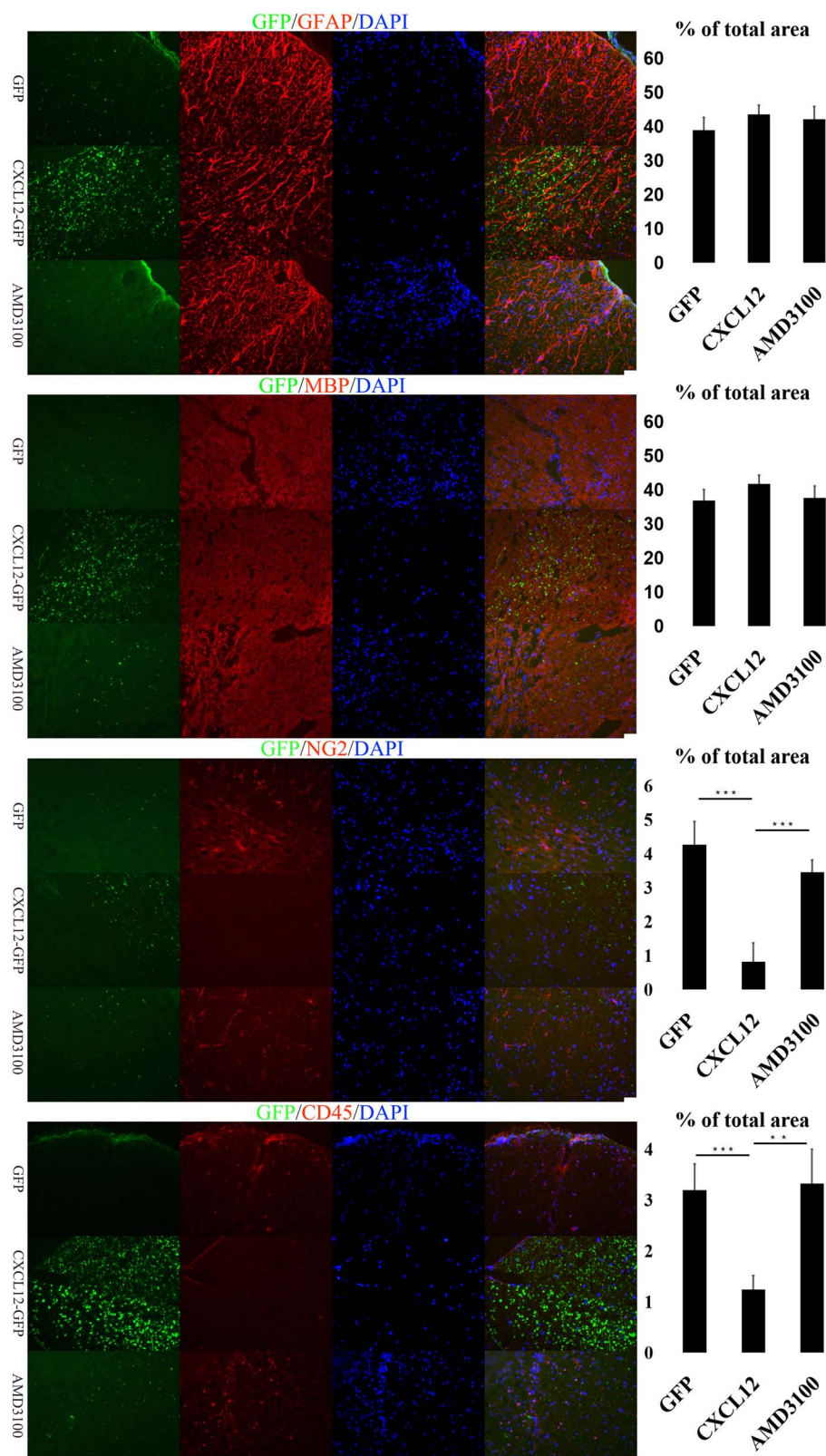
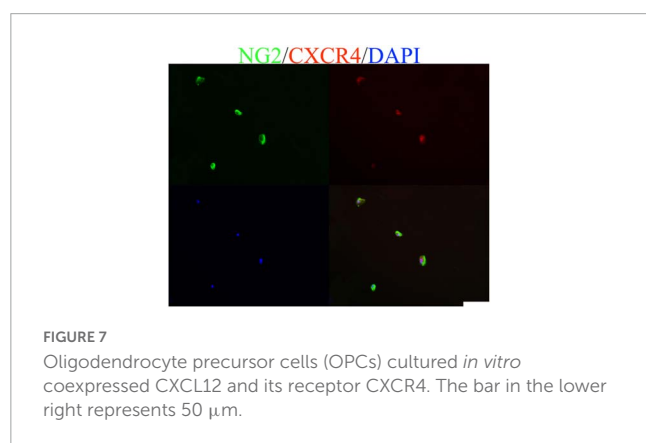
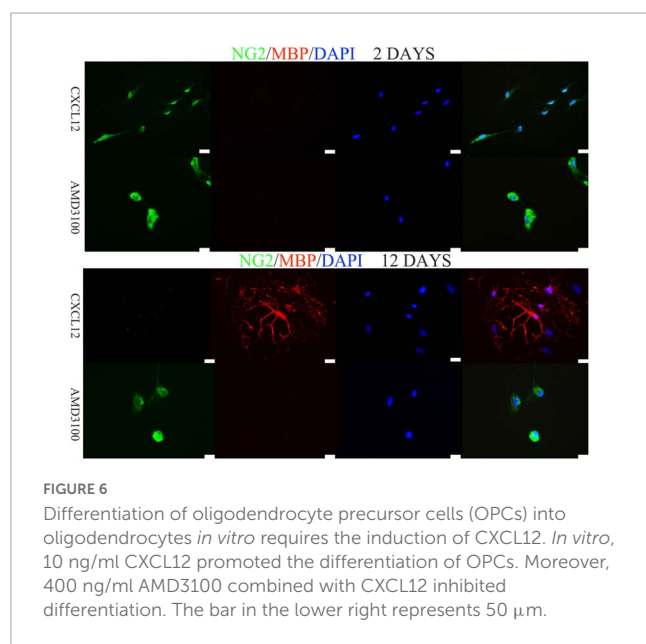


FIGURE 5

At the recovery stage of experimental autoimmune encephalomyelitis (EAE), upregulation of CXCL12 promoted the remyelination of spinal cord. During the recovery stage of EAE, the glial fibrillary acidic protein (GFAP) and myelin basic protein (MBP) signals indicated that the spinal myelin sheath was restored in the eGFP group and CXCL12 + AMD3100 group, but the infiltration of leukocytes (CD45 +) and the migration of OPCs (NG2 +) were still stronger than those in the CXCL12 group. Data presented as the mean \pm SEM. "*" represents value of $P < 0.05$, "***" represents value of $P < 0.01$, "****" represents value of $P < 0.001$ by two-tailed Student's t -test or one-way ANOVA, $n = 4-6$ rats. The bar in the lower right represents 50 μ m.



Therefore, the expression of chemoattractant which regulate neural precursor cells migrate and mature to replace damaged cells is essential for CNS injury response. CXCL12 and its receptors are widely expressed in the CNS and play an important role in the differentiation and maturation of NPCs and OPCs (Chu et al., 2017). Several previous studies have shown that CXCL12 can promote the migration of leukocytes to the lesion area of demyelination in the CNS during the progression of MS, thus aggravating the disease (Williams et al., 2014). In contrast, CXCL12 also promotes the migration and differentiation of OPCs to the lesion, thereby enhancing remyelination (Patel et al., 2010, 2012; Zilkha-Falb et al., 2016). In summary, the role of CXCL12 in the onset and progression of MS is complicated.

In this study, we up-regulated CXCL12 in the lumbar enlargement of spinal cord by AAV. This specific region was selected because the lesions of EAE predominantly distributed in the lumbosacral region of the spinal cord (Gibson-Corley et al., 2016). Immunofluorescence detection showed that the region of upregulated CXCL12 was limited to the vicinity of the PE-10 orifice. Immunofluorescence suggested that the level of CXCL12 in this region of the spinal cord was significantly higher in the CXCL12-GFP group than in the eGFP group (Figure 1A), and WB of SCH

also confirm that (Figure 1B). Upregulated CXCL12 effectively alleviated the symptoms of EAE, reduced the clinical scores, and inhibited recurrence between days 24 and 30 in the EAE model. The MBP and GFAP signals in the CXCL12 group were stronger than those in the eGFP group at the peak stage of EAE. Moreover, a high level of CXCL12 did not induce significant leukocyte infiltration into the white matter of the spinal cord. Taken together with the results of the CXCL12 + AMD3100 group, these findings suggest the effect of CXCL12 can alleviate the symptoms at peak stage of EAE and inhibited the relapse. However, since the high level of CXCL12 did not induce more leukocyte infiltration, CXCL12 overexpression may not be a necessary or sufficient condition to induce leukocyte migration into the CNS.

Previous studies have shown that remyelination in rodents is closely related to OPCs migration and differentiation (Lombardi et al., 2019). At the peak stage of the EAE model, the level of CXCL12 was upregulated in the spinal cord; this is consistent with several studies that have shown that CXCL12 enhanced the process of remyelination (Zeis et al., 2018; Gao et al., 2019; Beigi et al., 2020). Furthermore, the findings of the current study indicated that the NG2 signal (OPCs) in the spinal cord of the CXCL12 group was significantly lower than that of the other two groups at the peak stage and recovery stage, while the MBP signal was much stronger, suggesting that the differentiation of OPCs into oligodendrocytes in the CXCL12 group was due to the continuously upregulated CXCL12. *In vitro*, CXCL12 (10 ng/ml) promoted the differentiation of OPCs into oligodendrocytes (Figure 6), and the CXCR4 antagonist AMD3100 strongly inhibited the differentiation of OPCs (Figure 6). This finding suggests that CXCL12 protects the CNS of rats by promoting the differentiation of OPCs into oligodendrocytes.

The clinical scores of the CXCL12 group were significantly lower than those of the eGFP group and the AMD3100 treatment group, and there was no recurrence during days 24–30. *In vitro*, 10 ng/ml CXCL12 promoted the differentiation of OPCs into oligodendrocytes, which is consistent with previous studies (Zilkha-Falb et al., 2016). These results suggest that upregulation of CXCL12 can alleviate EAE symptoms and inhibit EAE recurrence through the underlying mechanism of initiating OPC maturation and differentiation. No significant difference in leukocyte infiltration in the EAE initial phase was found between the CXCL12 group and the other two groups using CD45 detection. At the EAE peak stage, the CXCL12 group had a significantly lower D45 + signal than the other groups. Yamasaki et al. (2014) reported that infiltrating monocyte-derived macrophages initiate demyelination; therefore, less infiltration of macrophages may delay the onset of EAE and alleviate the symptoms of EAE in the peak stage. *In vivo*, several previous studies have reported that CXCL12 acts as a T-cell chemoattractant at low doses and a chemorepellent at high doses (Poznansky et al., 2000; Vianello et al., 2006). Furthermore, Meiron et al. (2008) demonstrated that CXCL12 could transform effector Type 1 T helper (Th1) cells in the CNS into regulatory T cells that produce interleukin (IL)-10, an anti-inflammatory cytokine, thereby reducing neuroinflammation and further reducing the infiltration of leukocytes. This observation may explain why the infiltration of leukocytes was lower in the CXCL12 group than in the other groups.

The data presented in this study indicate that upregulation of CXCL12 in the lumbar enlargement of the spinal cord can

significantly reduce the symptoms and recurrence of EAE in a rat model. Furthermore, the CXCL12/CXCR4 axis may enhance remyelination by promoting the differentiation and maturation of OPCs, suggesting that the CXCL12/CXCR4 axis could be a promising therapeutic candidate to improve remyelination in MS.

Data availability statement

The original contributions presented in this study are included in the article/supplementary material, further inquiries can be directed to the corresponding authors.

Ethics statement

This animal study was reviewed and approved by the Ethics Committee of the Chinese PLA General Hospital.

Author contributions

DL, HJL, HS, and BC performed the experiments. DL, HJL, HS, and SW wrote the original manuscript. DL, JF, MS, HZ, WB, and HEL revised the manuscript. All authors contributed to the article and approved the submitted version.

Funding

This work was supported in part by the National Natural Science Foundation of China (No. 81870662), the National Key

Research and Development Program (No. 2018YFE0113900), the General Program of Fujian Provincial Department of Education (No. JAT170501), the General Project of Fujian Provincial Department of Science and Technology (No. 2022J011162), and the Research Project of Putian Science and Technology Bureau (2020NP001).

Acknowledgments

We thank Tingjun Chen for his excellent surgical support and advice. This manuscript was edited by American Journal Experts (AJE) for proper English language use.

Conflict of interest

The authors declare that the research was conducted in the absence of any commercial or financial relationships that could be construed as a potential conflict of interest.

Publisher's note

All claims expressed in this article are solely those of the authors and do not necessarily represent those of their affiliated organizations, or those of the publisher, the editors and the reviewers. Any product that may be evaluated in this article, or claim that may be made by its manufacturer, is not guaranteed or endorsed by the publisher.

References

- Beckman, D., Chakrabarty, P., Ott, S., Dao, A., Zhou, E., Janssen, W. G., et al. (2021). A novel tau-based rhesus monkey model of Alzheimer's pathogenesis. *Alzheimers Dement.* 17, 933–945. doi: 10.1002/alz.12318
- Beigi, F. B., Pasbakhsh, P., Mortezaee, K., Pirhajati, V., Alizadeh, R., Aryanpour, R., et al. (2020). Intranasal delivery of SDF-1 α -preconditioned bone marrow mesenchymal cells improves remyelination in the cuprizone-induced mouse model of multiple sclerosis. *Cell Biol. Int.* 44, 499–511. doi: 10.1002/cbin.11250
- Blaževski, J., Petković, F., Momčilović, M., Jevtić, B., Miljković, D., and Stojković, M. S. (2013). High interleukin-10 expression within the central nervous system may be important for initiation of recovery of Dark Agouti rats from experimental autoimmune encephalomyelitis. *Immunobiology* 218, 1192–1199. doi: 10.1016/j.imbio.2013.04.004
- Blaževski, J., Petković, F., Momčilović, M., Jevtić, B., Stojković, M. M., and Miljković, D. (2015). Tumor necrosis factor stimulates expression of CXCL12 in astrocytes. *Immunobiology* 220, 845–850. doi: 10.1016/j.imbio.2015.01.007
- Calderon, T. M., Eugenin, E. A., Lopez, L., Kumar, S. S., Hesselgesser, J., Raine, C. S., et al. (2006). A role for CXCL12 (SDF-1 α) in the pathogenesis of multiple sclerosis: Regulation of CXCL12 expression in astrocytes by soluble myelin basic protein. *J. Neuroimmunol.* 177, 27–39. doi: 10.1016/j.jneuroim.2006.05.003
- Carbajal K. S., Miranda Juan, L., Tsukamoto Michelle, R., and Lane Thomas, E. (2011). CXCR4 signaling regulates remyelination by endogenous oligodendrocyte progenitor cells in a viral model of demyelination. *Glia* 59, 1813–1821. doi: 10.1002/glia.21225
- Chen, T., Lennon, V. A., Liu, Y. U., Bosco, D. B., Li, Y., Yi, M. H., et al. (2020). Astrocyte-microglia interaction drives evolving neuromyelitis optica lesion. *J. Clin. Invest.* 130, 4025–4038. doi: 10.1172/jci134816
- Chu, T., Shields, L., Zhang, Y., Feng, S., Shields, C., and Cai, J. (2017). CXCL12/CXCR4/CXCR7 chemokine axis in the central nervous system: Therapeutic targets for remyelination in demyelinating diseases. *Neuroscientist* 23, 627–648. doi: 10.1177/1073858416685690
- Ciccarelli, O., Cohen, J. A., Reingold, S. C., Weinshenker, B. G., and International Conference on Spinal Cord Involvement and Imaging in Multiple Sclerosis and Neuromyelitis Optica Spectrum Disorders. (2019). Spinal cord involvement in multiple sclerosis and neuromyelitis optica spectrum disorders. *Lancet Neurol.* 18, 185–197. doi: 10.1016/S1474-4422(18)30460-5
- Cruz-Orrego, L., Holman, D. W., Dorsey, D., Zhou, L., Zhang, P., Wright, M., et al. (2011). CXCR7 influences leukocyte entry into the CNS parenchyma by controlling abluminal CXCL12 abundance during autoimmunity. *J. Exp. Med.* 208, 327–339. doi: 10.1084/jem.20102010
- Dziembowska, M., Tham, T. N., Lau, P., Vitry, S., Lazarini, F., and Dubois-Dalcq, M. (2005). A role for CXCR4 signaling in survival and migration of neural and oligodendrocyte precursors. *Glia* 50, 258–269. doi: 10.1002/glia.20170
- Fadda, G., Flanagan, E., Cacciaguerra, L., Jitrapakulsan, J., Solla, P., Zara, P., et al. (2022). Myelitis features and outcomes in CNS demyelinating disorders: Comparison between multiple sclerosis, MOGAD, and AQP4-IgG-positive NMOSD. *Front. Neurol.* 13:1011579. doi: 10.3389/fneur.2022.1011579
- Floris, S., Blezer, E. L., Schreibelt, G., Döpp, E., van der Pol, S. M., Schadee-Eestermans, I. L., et al. (2004). Blood-brain barrier permeability and monocyte infiltration in experimental allergic encephalomyelitis: A quantitative MRI study. *Brain* 127, 616–627. doi: 10.1093/brain/awh068
- Gao, D., Tang, T., Zhu, J., Tang, Y., Sun, H., and Li, S. (2019). CXCL12 has therapeutic value in facial nerve injury and promotes Schwann cells autophagy and migration via PI3K-AKT-mTOR signal pathway. *Int. J. Biol. Macromol.* 124, 460–468. doi: 10.1016/j.ijbiomac.2018.10.212
- Gibson-Corley, K., Boyden, A., Leidinger, M., Lambertz, A., Ofori-Amanfo, G., Naumann, P., et al. (2016). A method for histopathological study of the multifocal

nature of spinal cord lesions in murine experimental autoimmune encephalomyelitis. *PeerJ* 4:e1600. doi: 10.7717/peerj.1600

Huynh, C., Dingemans, J., Meyer Zu Schwabedissen, H., and Sidharta, P. (2020). Relevance of the CXCR4/CXCR7-CXCL12 axis and its effect in pathophysiological conditions. *Pharmacol. Res.* 161:105092. doi: 10.1016/j.phrs.2020.105092

Kearney, H., Miller, D., and Ciccarelli, O. (2015). Spinal cord MRI in multiple sclerosis—diagnostic, prognostic and clinical value. *Nat. Rev. Neurol.* 11, 327–338. doi: 10.1038/nrneurol.2015.80

Klein, R. S., and Rubin, J. B. (2004). Immune and nervous system CXCL12 and CXCR4: Parallel roles in patterning and plasticity. *Trends Immunol.* 25, 306–314. doi: 10.1016/j.it.2004.04.002

Krumbholz, M., Theil, D., Cepok, S., Hemmer, B., Kivisäkk, P., Ransohoff, R. M., et al. (2006). Chemokines in multiple sclerosis: CXCL12 and CXCL13 up regulation is differentially linked to CNS immune cell recruitment. *Brain* 129, 200–211. doi: 10.1093/brain/awn096

Kuhlmann, T., Miron, V., Cui, Q., Wegner, C., Antel, J., and Brück, W. (2008). Differentiation block of oligodendroglial progenitor cells as a cause for remyelination failure in chronic multiple sclerosis. *Brain* 131, 1749–1758. doi: 10.1093/brain/awn096

Lassmann, H., van Horssen, J., and Mahad, D. (2012). Progressive multiple sclerosis: Pathology and pathogenesis. *Nat. Rev. Neurol.* 8, 647–656. doi: 10.1038/nrneurol.2012.168

Li, C., Xiao, L., Liu, X., Yang, W., Shen, W., Hu, C., et al. (2013). A functional role of NMDA receptor in regulating the differentiation of oligodendrocyte precursor cells and remyelination. *Glia* 61, 732–749. doi: 10.1002/glia.22469

Li, M., Hale, J. S., Rich, J. N., Ransohoff, R. M., and Lathia, J. D. (2012). Chemokine CXCL12 in neurodegenerative diseases: An SOS signal for stem cell-based repair. *Trends Neurosci.* 35, 619–628. doi: 10.1016/j.tins.2012.06.003

Lombardi, M., Parolisi, R., Scaroni, F., Bonfanti, E., Gualerzi, A., Gabrielli, M., et al. (2019). Detrimental and protective action of microglial extracellular vesicles on myelin lesions: Astrocyte involvement in remyelination failure. *Acta Neuropathol.* 138, 987–1012. doi: 10.1007/s00401-019-02049-1

McCandless, E., Piccio, L., Woerner, B., Schmidt, R., Rubin, J., Cross, A., et al. (2008). Pathological expression of CXCL12 at the blood-brain barrier correlates with severity of multiple sclerosis. *Am. J. Pathol.* 172, 799–808. doi: 10.2353/ajpath.2008.070918

McCandless, E., Wang, Q., Woerner, B., Harper, J., and Klein, R. (2006). CXCL12 limits inflammation by localizing mononuclear infiltrates to the perivascular space during experimental autoimmune encephalomyelitis. *J. Immunol.* 177, 8053–8064. doi: 10.4049/jimmunol.177.11.8053

Meiron, M., Zohar, Y., Anunu, R., Wildbaum, G., and Karin, N. (2008). CXCL12 (SDF-1 α) suppresses ongoing experimental autoimmune encephalomyelitis by selecting antigen-specific regulatory T cells. *J. Exp. Med.* 205, 2643–2655. doi: 10.1084/jem.20080730

Miljković, D., Stanojević, Z., Momčilović, M., Odoardi, F., Flügel, A., and Mostarica-Stojković, M. (2011). CXCL12 expression within the CNS contributes to the

resistance against experimental autoimmune encephalomyelitis in Albino Oxford rats. *Immunobiology* 216, 979–987. doi: 10.1016/j.imbio.2011.03.013

Moll, N., Cossoy, M., Fisher, E., Staugaitis, S., Tucky, B., Rietsch, A., et al. (2009). Imaging correlates of leukocyte accumulation and CXCR4/CXCL12 in multiple sclerosis. *Arch. Neurol.* 66, 44–53. doi: 10.1001/archneurol.2008.512

Nave, K. A., and Werner, H. B. (2014). Myelination of the nervous system: Mechanisms and functions. *Annu. Rev. Cell Dev. Biol.* 30, 503–533.

Ortiz, G., Pacheco-Moisés, F., Macías-Islas, M., Flores-Alvarado, L., and Mireles-Ramírez, M. (2014). Role of the blood-brain barrier in multiple sclerosis. *Arch. Med. Res.* 45, 687–697. doi: 10.1016/j.arcmed.2014.11.013

Patel, J. R., McCandless, E. E., Dorsey, D., and Klein, R. S. (2010). CXCR4 promotes differentiation of oligodendrocyte progenitors and remyelination. *Proc. Natl. Acad. Sci. U.S.A.* 107, 11062–11067. doi: 10.1073/pnas.1006301107

Patel, J. R., Williams, J. L., Muccigrosso, M. M., Liu, L., Sun, T., Rubin, J. B., et al. (2012). Astrocyte TNFR2 is required for CXCL12-mediated regulation of oligodendrocyte progenitor proliferation and differentiation within the adult CNS. *Acta Neuropathol.* 124, 847–860. doi: 10.1007/s00401-012-1034-0

Poznansky, M., Olszak, I., Foxall, R., Evans, R., Luster, A., and Scadden, D. (2000). Active movement of T cells away from a chemokine. *Nat. Med.* 6, 543–548.

Stavropoulos, F., Georgiou, E., Sargiannidou, I., and Kleopa, K. (2021). Dysregulation of blood-brain barrier and exacerbated inflammatory response in Cx47-deficient mice after induction of EAE. *Pharmaceuticals* 14:621. doi: 10.3390/ph14070621

Vianello, F., Papeta, N., Chen, T., Kraft, P., White, N., Hart, W., et al. (2006). Murine B16 melanomas expressing high levels of the chemokine stromal-derived factor-1/CXCL12 induce tumor-specific T cell chemorepulsion and escape from immune control. *J. Immunol.* 176, 2902–2914. doi: 10.4049/jimmunol.176.5.2902

Williams, J., Patel, J., Daniels, B., and Klein, R. (2014). Targeting CXCR7/ACKR3 as a therapeutic strategy to promote remyelination in the adult central nervous system. *J. Exp. Med.* 211, 791–799. doi: 10.1084/jem.20131224

Yamasaki, R., Lu, H., Butovsky, O., Ohno, N., Rietsch, A., Cialic, R., et al. (2014). Differential roles of microglia and monocytes in the inflamed central nervous system. *J. Exp. Med.* 211, 1533–1549. doi: 10.1084/jem.20132477

Zeis, T., Howell, O. W., Reynolds, R., and Schaeren-Wiemers, N. (2018). Molecular pathology of multiple sclerosis lesions reveals a heterogeneous expression pattern of genes involved in oligodendroglialogenesis. *Exp. Neurol.* 305, 76–88. doi: 10.1016/j.expneurol.2018.03.012

Zhang, Y., Bi, X., Adebisi, O., Wang, J., Mooshekhian, A., Cohen, J., et al. (2019). Venlafaxine improves the cognitive impairment and depression-like behaviors in a cuprizone mouse model by alleviating demyelination and neuroinflammation in the brain. *Front. Pharmacol.* 10:332. doi: 10.3389/fphar.2019.00332

Zilkha-Falb, R., Kaushansky, N., Kawakami, N., and Ben-Nun, A. (2016). Post-CNS-inflammation expression of CXCL12 promotes the endogenous myelin/neuronal repair capacity following spontaneous recovery from multiple sclerosis-like disease. *J. Neuroinflammation* 13, 7. doi: 10.1186/s12974-015-0468-4



OPEN ACCESS

EDITED BY

Shani Stern,
University of Haifa, Israel

REVIEWED BY

Natalia L. Kononenko,
University of Cologne, Germany

*CORRESPONDENCE

Karolina Pircs
✉ karolina.pircs@hcemm.eu

†These authors have contributed equally to this work

SPECIALTY SECTION

This article was submitted to
Cellular and Molecular Mechanisms
of Brain-aging,
a section of the journal
Frontiers in Aging Neuroscience

RECEIVED 16 December 2022

ACCEPTED 14 March 2023

PUBLISHED 29 March 2023

CITATION

Danics L, Abbas AA, Kis B and Pircs K (2023)
Fountain of youth—Targeting autophagy
in aging.
Front. Aging Neurosci. 15:1125739.
doi: 10.3389/fnagi.2023.1125739

COPYRIGHT

© 2023 Danics, Abbas, Kis and Pircs. This is an
open-access article distributed under the terms
of the [Creative Commons Attribution License](#)
(CC BY). The use, distribution or reproduction
in other forums is permitted, provided the
original author(s) and the copyright owner(s)
are credited and that the original publication in
this journal is cited, in accordance with
accepted academic practice. No use,
distribution or reproduction is permitted which
does not comply with these terms.

Fountain of youth—Targeting autophagy in aging

Lea Danics^{1,2,3†}, Anna Anoir Abbas^{1,2†}, Balázs Kis^{1,2} and
Karolina Pircs^{1,2,4*}

¹Institute of Translational Medicine, Semmelweis University, Budapest, Hungary, ²Hungarian Centre of Excellence for Molecular Medicine – Semmelweis University (HCEMM-SU), Neurobiology and Neurodegenerative Diseases Research Group, Budapest, Hungary, ³Eötvös Loránd Research Network and Semmelweis University (ELKH-SU), Cerebrovascular and Neurocognitive Disorders Research Group, Budapest, Hungary, ⁴Laboratory of Molecular Neurogenetics, Department of Experimental Medical Science, Wallenberg Neuroscience Center and Lund Stem Cell Center, Lund University, Lund, Sweden

As our society ages inexorably, geroscience and research focusing on healthy aging is becoming increasingly urgent. Macroautophagy (referred to as autophagy), a highly conserved process of cellular clearance and rejuvenation has attracted much attention due to its universal role in organismal life and death. Growing evidence points to autophagy process as being one of the key players in the determination of lifespan and health. Autophagy inducing interventions show significant improvement in organismal lifespan demonstrated in several experimental models. In line with this, preclinical models of age-related neurodegenerative diseases demonstrate pathology modulating effect of autophagy induction, implicating its potential to treat such disorders. In humans this specific process seems to be more complex. Recent clinical trials of drugs targeting autophagy point out some beneficial effects for clinical use, although with limited effectiveness, while others fail to show any significant improvement. We propose that using more human-relevant preclinical models for testing drug efficacy would significantly improve clinical trial outcomes. Lastly, the review discusses the available cellular reprogramming techniques used to model neuronal autophagy and neurodegeneration while exploring the existing evidence of autophagy's role in aging and pathogenesis in human-derived *in vitro* models such as embryonic stem cells (ESCs), induced pluripotent stem cell derived neurons (iPSC-neurons) or induced neurons (iNs).

KEYWORDS

autophagy, aging, rejuvenation, clinical trial, neurodegenerative diseases, direct reprogramming, autophagy-modifying drugs, disease modeling

Introduction

Overcoming the effects of time has long since been one of the holy grails of science. Extending the human lifespan brings a lot of unforeseen consequences. By 2040, age-related neurodegenerative diseases will become the main cause of morbidity in industrialized countries, followed by cancer (Ferri et al., 2005). The extension of lifespan specifically that of healthy lifespan (healthspan) will have enormous effects on society, in both the quality of life and economical points of view. One of the promising “fountains of youth” is related to autophagy and its effects on age-related changes.

Organisms undergo a variety of changes during the process of aging, which impair cellular quality control via disturbed proteostasis, impaired clearance of

macromolecules, persistent cellular senescence, stem cell exhaustion, and telomere shortening. Macroautophagy (further referred to as autophagy) plays a key role in aging by maintaining cellular homeostasis through the degradation of unnecessary or dysfunctional components (Hansen et al., 2018; Tabibzadeh, 2023).

Autophagy is an evolutionarily conserved degradation process where cytoplasmic portions and organelles are sequestered into a double-membrane vesicle, an autophagosome (AP), followed by delivery into a degradative organelle, the lysosome, creating an autolysosome (AL) for breakdown and recycling of the resulting macromolecules (Klionsky et al., 2016). This highly dynamic, multi-step process characterized as the autophagic flux is the entire autophagic pathway, which cells can tune according to their metabolic needs (Klionsky et al., 2016).

The autophagic process is mediated by several protein complexes. The most important factors during initiation are the ULK1/2 (Unc-51 like autophagy activating kinase) initiation complex, BECN1 (Beclin1) and some key ATG (autophagy-related-genes) proteins. The main mediator of AP formation is the MAP1LC3B (Microtubule Associated Protein 1 Light Chain 3 Beta; further referred to as LC3B) complex, while SQSTM1 (Sequestosome 1; further referred to as p62) plays role in cargo engulfment (Klionsky et al., 2016; Hansen et al., 2018). In AP-lysosome fusion LAMP proteins (LAMP1 and 2; Lysosomal-associated membrane proteins) play a central role promoting AL formation and degradation.

Autophagy is a critical cellular process for preserving cellular homeostasis by clearance of debris and turnover of cellular compartments. The absence of essential autophagy genes or proteins, as well as impairments in their function cause perturbations in the autophagic flux leading to accumulation of certain autophagic structures and insufficient cellular clearance. Autophagic flux impairment is present in several human neurodegenerative diseases (Zhang et al., 2013).

Regulation of autophagy involves numerous interconnected signaling pathways. Main negative autophagy regulators of autophagy are: (i) the mTOR (mammalian target of Rapamycin), (ii) the PI3K/Akt (Phosphoinositide 3-kinase/Serine-threonine protein kinase), and (iii) the MAPK/ERK (Mitogen-activated protein kinase/Extracellular signal-regulated kinase) signaling pathways (Hansen et al., 2018). mTOR indirectly inhibits autophagy via reducing autophagic protein and lipid synthesis by suppressing transcription factor EB (TFEB) a key regulator of lysosomal biogenesis and autophagy (Hansen et al., 2018; Nnah et al., 2019). The MAPK/ERK signaling inhibits autophagy through enhancing mTOR activity, while the PI3K/Akt signaling blocks autophagy initiation via inhibiting the ULK1 complex (Zachari and Ganley, 2017). Major positive regulators of autophagy are: TFEB, regulating protein and lipid synthesis for autophagy-endolysosomal pathways, Adenosine-monophosphate activated-protein kinase (AMPK), and c-Jun N-terminal kinase (JNK), promoting the ULK1 complex and BECN1, respectively (Dhanasekaran and Reddy, 2017; Nnah et al., 2019; Wang et al., 2020).

Several studies indicated that activation of autophagy can efficiently extend the lifespan of various organisms such as yeast, worms, flies, and mammals (Hansen et al., 2018; Aman et al., 2021; Kaushik et al., 2021). Moreover, stem cell research revealed, that autophagy plays a critical role in maintaining cellular

stemness by regulating the mitochondrial content to help cellular adaptation to different metabolic requirements, and by reducing the accumulation of damaged mitochondria and reactive oxygen species (ROS) (Chang, 2020). Cellular stemness represents an extraordinary capability of self-renewal and escaping aging (Zhu et al., 2015). In stem cells the activity of the autophagic process is remarkably elevated which indicates a crucial role for stemness phenotype maintenance (Chang, 2020; Adelpour et al., 2022). Several studies have shown that induction of autophagy can accomplish rejuvenation of quiescent stem cells that can restore age-related molecular and functional features both *in vitro* and *in vivo* (Figures 1D–E; Chen et al., 2009; Zhu et al., 2015; Leeman et al., 2018; Fang et al., 2020; Navarro Negredo et al., 2020; Park et al., 2021; Tan et al., 2021).

Autophagy is not only a key element in lifespan expansion, but growing evidence indicates its pivotal role in age-related neurodegeneration, contributing to the development of late-onset disorders like Alzheimer's disease (AD), Parkinson's disease (PD), and Huntington's disease (HD) (Menziez et al., 2015). Altogether, growing number of evidence indicated autophagy activation as a potentially beneficial therapeutic target in aging and especially in age-related human specific diseases.

In this review we discuss the current clinical trials in which autophagy modulating therapies are applied to improve symptoms of neurodegenerative disorders. In addition, we summarize the available *in vitro* models that can recapitulate some key aspects of human neuronal aging (Figures 1A–C) and emphasize the need for more efficient tools in future neuronal rejuvenation studies targeting autophagy (Figures 1D–E).

Autophagy-modifying therapies in age-related neurodegenerative diseases

Basal and selective autophagy are both key mechanisms that ensure the clearance of toxic, cytoplasmic pathological agents like misfolded, mislocalized and aggregated proteins that contribute to many age-related neurodegenerative diseases. The number of damaged organelles and proteins increase progressively throughout human life. Autophagy has also been described as a cell survival mechanism with antiapoptotic properties (Noguchi et al., 2020). During aging autophagy declines progressively in human neurons (Aman et al., 2021). Downregulation of autophagy-related genes such as ATG5, ATG7, ATG16 (Lipinski et al., 2010), and BECN1 (Shibata et al., 2006; Lipinski et al., 2010) was shown in human glioblastoma cells and in postmortem brain tissue. The age-dependent reduction in the autophagic process contribute to impaired cellular homeostasis due to imbalance in cellular resources and accumulation of debris (Aman et al., 2021; Kaushik et al., 2021). Age is obviously the main risk factor for several disorders, including neurodegenerative diseases (Hou et al., 2019). Human studies demonstrate that autophagy dysfunction is present in almost all of the age-related neurodegenerative disorders, such as AD (Nixon et al., 2005; Nilsson et al., 2013; Sun et al., 2014), PD (Zhu et al., 2003; Tanji et al., 2011; Moors et al., 2016; Chang et al., 2017), and HD (Sapp et al., 1997; Martinez-Vicente et al., 2010;

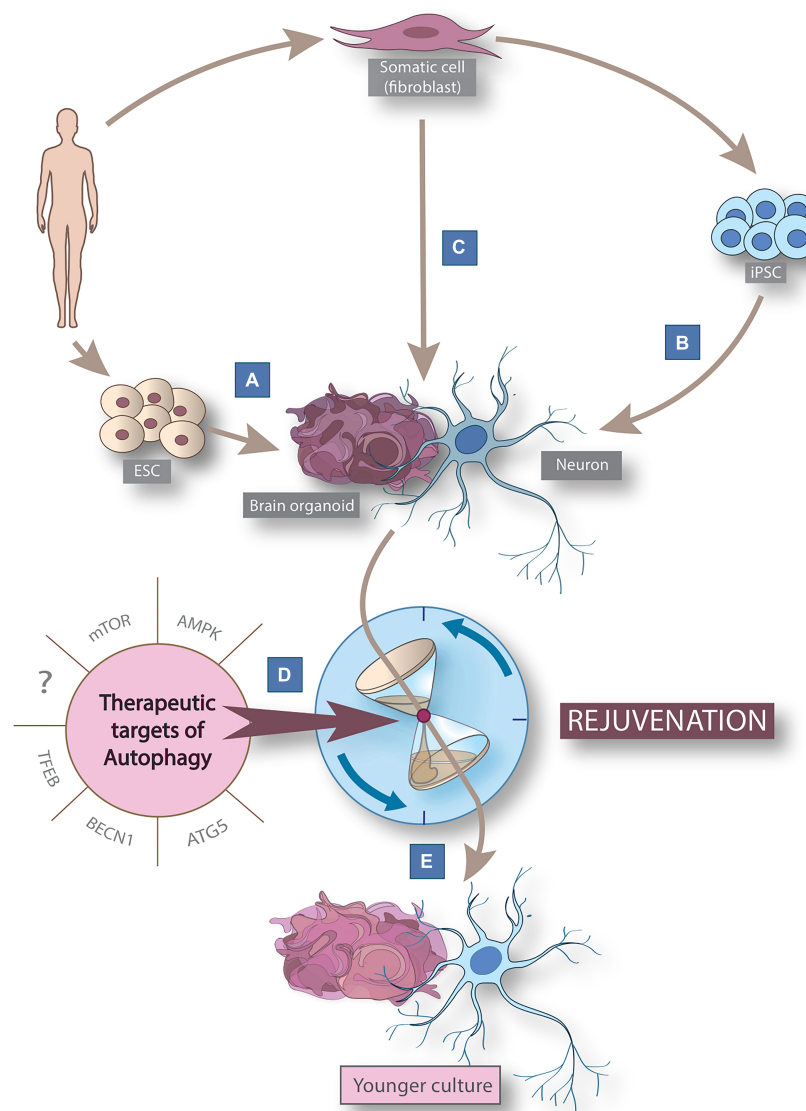


FIGURE 1

Cellular reprogramming models derived from human somatic cells to study aging and rejuvenation via autophagy modulation. Schematic figure summarizing cellular reprogramming models derived from human somatic cells to study neuronal rejuvenation via autophagy modulation. Human-derived *in vitro* 2D neuronal models can be generated from embryonic stem cells (ESCs) (A) or by post-differentiation reprogramming (B) from pluripotent stem cells (iPSCs) derived from somatic human cells. In addition, direct reprogramming (C) allows the generation of induced neurons (iNs). 3D brain organoids can be generated by 3 routes: from ESCs, iPSCs and iNs. The use of known (mTOR, AMPK, ATG5, BECN1, and TFEB) and yet undiscovered therapeutic autophagy targets (D) allows the rejuvenation (E) of neuron and brain organoid models for modeling neuronal aging. AMPK, AMP-activated protein kinase; BECN1, Beclin-1; ESC, embryonic stem cell; FOXO, forkhead box class o family member protein; iPSC, induced pluripotent stem cell; mTOR, mammalian target of rapamycin; TFEB, transcription factor EB.

Pircs et al., 2022), the question about the role of autophagy in disease development and progression arises.

Previously addressed preclinical studies suggest that autophagy activation can potentially prevent or halt age-related neurodegenerative diseases, thus autophagy targeting interventions may provide new therapeutic options for these patients. Here we summarize therapeutic approaches using pharmacological autophagy inducers targeting incurable age-related neurodegenerative human-specific diseases in currently ongoing or already completed clinical trials from the last five years dating from 2018 (Table 1). We conducted systematic search at ClinicalTrial.gov using key words for AD, PD or HD and sorted

out trials in which agents with autophagy modulating properties were administered in monotherapy as a primary intervention in the last five years between 2018 and 2022. We collected the most promising drugs—those that were tested in more than one trial in the last five years—in Table 1.

Alzheimer's disease

Alzheimer's disease is a neurodegenerative disease characterized by extracellular deposits of amyloid- β plaques and intracellular neurofibrillary tangles (tauopathies). Repeated

TABLE 1 Autophagy-modifying drugs used in clinical trials targeting age-related neurodegenerative disease.

Disease	Drug	Drug target	Effect on autophagy	Clinical outcome	Completed trials		Ongoing trials			References
					ID	Results posted	ID	Status	Study start	
AD	Bryostatins	PKC ϵ	ERK/JNK signaling pathway	improves cognition	NCT02431468	2018	NCT04538066	A	2020	Nelson et al., 2017; Mandic et al., 2022
					NCT03560245	2020				
	Donepezil	AChE inhibitor	BECN1 and LC3B-II induction	Improves cognition, activity and social behavior	NCT00571064	2018	NCT03810794	R	2019	Boada-Rovira et al., 2004; Zhao et al., 2013; Dasuri et al., 2016; Adlimoghaddam et al., 2018; Khuanjing et al., 2021; O'Bryant et al., 2021
					NCT03073876	2019	NCT04730635	R	2021	
					NCT01951118	2020	NCT04661280	R	2022	
					NCT00477659	2021	NCT05078944	R	2022	
	Idapiridin (Lu AE58054)	5-HT $_6$ receptor antagonist	mTOR inhibition	Delays memory impairment	NCT02079246	2018	NCT05592678	NYR	2023	Meffre et al., 2012; Wilkinson et al., 2014; Atri et al., 2018
					NCT02006641	2018				
					NCT02006654	2022				
	Levetiracetam	SV2A	BECN1 and LC3B-II induction	Improves spatial memory and executive function tasks	NCT01554683	2020	NCT03489044	A	2018	Sen et al., 2021; Vossel et al., 2021; Zheng et al., 2022
							NCT03875638	R	2019	
					NCT02002819	2022	NCT04004702	NYR	2020	
	Memantine	NMDA receptor antagonist	AMPK and VPS34 induction	Improves cognition and behavioral disturbances	NCT02553928	2019	NCT03703856	R	2019	Kishi et al., 2017; Hirano et al., 2019; McShane et al., 2019; Vucicevic et al., 2020
							NCT05063851	R	2021	
	Metformin	AMPK	AMPK activation	Moderate effect on cognitive impairment	NCT00620191	2020	NCT04098666	R	2021	Campbell et al., 2018; Farr et al., 2019
	Pimavanserin	5-HT $_{2A}$ receptor inverse agonist	ULK1, FIP200, ATG101, BECN1, ATG5, and LC3B modulation	Improves psychotic symptoms	NCT03118947	2020				Ballard et al., 2019; Srinivasan et al., 2020; Ramachandran and Srivastava, 2021
					NCT03325556	2021				
	Sargramostim (GM-CSF)	Immune cells	ATG3, ATG7 and GABARAPL2 activation	Improves cognition, Amyloid- β and tau pathology	NCT01409915	2021	NCT04902703	R	2022	Potter et al., 2021; Abdelmoaty et al., 2022
HD	Pridopidine	SIGMAR1 receptor agonist	Facilitates nucleocytoplasmic transport of TFEB	Neuroprotective, improves chorea, motor functions and cognition	NCT02006472	2021	NCT04556656	A	2020	Lundin et al., 2010; de Yebenes et al., 2011; Karl et al., 2013; Wang et al., 2023
					NCT03019289	2021	NCT04388969	R	2020	
					NCT01306929	2022	NCT05287503	R	2022	
PD	Ambroxol	Raise the level of GCa	Facilitates nuclear translocation of TFEB	Neuroprotective, improves chorea, motor functions and cognition			NCT04388969	R	2020	McNeill et al., 2014; Choi et al., 2018; Mullin et al., 2020
							NCT05287503	R	2022	

(Continued)

TABLE 1 (Continued)

Disease	Drug	Drug target	Effect on autophagy	Clinical outcome	Completed trials		Ongoing trials			References	
					ID	Results posted	ID	Status	Study start		
	Atomoxetine	SNRIs	Dose dependent effect on LC3B-II	Improves attention and impulsivity	NCT01738191	2018				Marsh et al., 2009; Hinson et al., 2016; Warner et al., 2018; Corona et al., 2019	
					NCT03651856	2018					
	Cannabidiol	CB1 and CB2 receptors inverse agonist	Prevent JNK MAPK activation	Therapeutic effects in non-motor symptoms, neuroprotective effect	NCT02818777	2019	NCT03944447	R	2018	Yang et al., 2014; Crippa et al., 2019; Huestis et al., 2019; Patricio et al., 2020	
							NCT03639064	R	2020		
							NCT05106504	R	2021		
	Dexmedetomidine	α_2 -adrenoceptor agonist	PI3K/Akt signaling pathway	May slow progression of decline in deep brain activity			NCT05376761	R	2022	Rozet et al., 2006; Martinez-Simon et al., 2017; Yu et al., 2019; Lombardo et al., 2020; Nakajima et al., 2021	
							NCT05197439	NYR	2022		
	Donepezil	AChE inhibitor	BECN1 and LC3B-II induction	Improves cognition	NCT02206620	2019				Aarsland et al., 2002; Ravina et al., 2005; Baik et al., 2021; Baba et al., 2022	
					NCT01521117	2021					
	Exenatide	GLP1 receptor agonist	PKA and PI3K/Akt signaling pathways	Improves motor symptoms, neuroprotective			NCT04232969	A	2020	Aviles-Olmos et al., 2014; Foltynie and Aviles-Olmos, 2014; Athauda et al., 2017	
							NCT04305002	A	2020		
							NCT04269642	A	2020		
							NCT04154072	A	2020		
	Istradefylline	ADORA2A receptor antagonist	Activation of autophagy through AMPK-lysosome induction	Improves depression or cognitive impairment	NCT02610231	2019	NCT05333549	R	2022	Liu Y. et al., 2016; Torti et al., 2018; Chen and Cunha, 2020; Kanzato et al., 2020	
					NCT01968031	2020	NCT05182151	R	2022		
	Pimavanserin	5-HT _{2A} receptor inverse agonist	ULK1, FIP200, ATG101, BECN1, ATG5, and LC3B activation	Improves psychotic symptoms	NCT00550238	2019	NCT03947216	NYR	2020	Hawkins and Berman, 2017; Kitten et al., 2018; Dashtipour et al., 2021	
					NCT01518309	2020	NCT05357612	R	2022		
					NCT03482882	2020					
					NCT03325556	2021					
	Pramipexole	D ₂ /D ₃ receptor agonist	AMPK activation	Improves motor complications and depressive symptoms	NCT03521635	2021	NCT04249544	R	2019	Biglan and Holloway, 2002; Reichmann et al., 2003; Mo et al., 2016; Gencler et al., 2022	

Ongoing clinical trial status: NYR, not yet recruiting; R, recruiting; A, active, not recruiting. 5-HT_{2A}, 5-Hydroxytryptamine 2A; 5-HT₆, 5-Hydroxytryptamine 6; ACh, acetylcholine; AChE, acetylcholinesterase; AD, Alzheimer's disease; ADORA2A, adenosine receptor A_{2A}; AMPK, AMP-activated protein kinase; ApoE4, apolipoprotein E4; BECN1, Beclin-1; CB1 and CB2, cannabinoid receptor 1 and 2; DAG, diacylglycerol; GABA, γ -aminobutyric acid; GABARAPL2, GABA type a receptor associated protein like 2; GCCase, glucocerebrosidase; GLP1, glucagon-like peptide-1; GM-CSF, granulocyte-macrophage colony-stimulating factor; GSK3 β , glycogen synthase kinase 3; HD, Huntington's disease; HMG-CoA, β -hydroxy β -methylglutaryl-CoA; IMPase, inositol monophosphatase; JNK, c-jun N-terminal kinase; LC3 – MAP1LC3B, microtubule-associated proteins 1A/1B light chain 3B; MAPK, mitogen-activated protein kinase; MARCKS, myristoylated alanine-rich c-kinase substrate; mTOR, mammalian target of rapamycin; NMDA, N-methyl-D-aspartate; p62 – SQSTM1, sequestosome-1; PD, Parkinson's disease; PI3K, phosphoinositide 3-kinases; PKA, protein kinase A; PKC ϵ , protein kinase C; SIGMAR1, sigma non-opioid intracellular receptor 1; SNRIs, selective norepinephrine reuptake inhibitor; SV2A, synaptic vesicle glycoprotein 2A; TFEB, transcription factor EB; ULK1, Unc-51 like autophagy activating kinase.

unsuccessful attempts to inhibit the formation of abnormal proteins (tau, amyloid- β) by pharmacological drugs has led researchers to turn toward autophagy-related interventions (Long and Holtzman, 2019; Fu et al., 2021). In the nervous system in particular, the role of autophagy in maintaining protein homeostasis is essential, therefore treatments targeting autophagy offer a promising therapeutic option (He et al., 2012; Karabiyik et al., 2021). Several pharmacological compounds modulating autophagy have shown beneficial effects against various symptoms of AD.

Memantine (NMDA-receptor antagonist) and Donepezil [Acetylcholine-esterase (AChE) inhibitor] are two of the five FDA approved drugs to treat AD affected patients. The autophagy enhancing effects of these agents were recently shown as to contribute to their neuroprotective properties (Dasuri et al., 2016; Hirano et al., 2019). Memantine and Donepezil are still intensively studied autophagy-modulator agents in AD with completed and still ongoing trials from the last five years as specified by ClinicalTrials.gov database (Table 1). Other promising candidates in connection with autophagy, such as Bryostatin, Idalopirdine (Lu AE58054), and Pimavanserin (Meffre et al., 2012; Wilkinson et al., 2014; Nelson et al., 2017; Atri et al., 2018; Ballard et al., 2019; Srinivasan et al., 2020; Ramachandran et al., 2021; Mandic et al., 2022), are still under clinical testing.

Often drugs with other indications exert neuroprotective effects possibly via autophagy-modulation. Levetiracetam an antiepileptic drug inducing BECN1, and LC3B-II expression is currently tested in AD with promising results. In addition, preliminary data from a currently ongoing phase 2 trial report that Levetiracetam can stabilize memory function not just in epileptiform, but in non-seizure AD patients as well (Sen et al., 2021). Metformin, a widely used antidiabetic drug has been shown to act on autophagy via AMPK activation (Farr et al., 2019). Campbell et al. (2018) published a meta-analysis demonstrating that Metformin use in diabetic patients significantly lower the risk of dementia and AD. Sargramostin, an immunomodulator improved cognition and ameliorated A β - and tau-pathology in AD patients, possibly via autophagy induction (Potter et al., 2021).

Huntington's disease

Huntington's disease is a neurodegenerative disorder with an autosomal-dominant inheritance caused by an expansion of CAG repeats that leads to an abnormal polyglutamine strand in the huntingtin protein (HTT). The therapeutic targets that alleviate protein misfolding or promote clearance of misfolded proteins generally slow the progression of the disease in HD models (Pircs et al., 2018, 2022; Brattås et al., 2021; Schumann-Werner et al., 2021). HD is unique in terms of its decisive relationship with autophagy. Wild-type HTT plays an important role in the regulation of autophagy. Autophagy dysfunction, which is a characteristic of HD, not only impairs the clearance of protein aggregates and non-functioning organelles, but mutant HTT also results in the loss of the beneficial regulatory role of HTT in autophagy (Martin et al., 2015; Luo et al., 2020). According to the ClinicalTrials.gov database there are an increasing number of clinical trials in HD targeting distinct steps of autophagy, such as Pridopidine, Memantine, Metformin, and Rilmenidine.

Multiple clinical trials demonstrated the effectivity of Pridopidine in HD especially motor symptoms improvements. Additionally, long-term, high patient number trials showed improvements in cognitive and functional symptoms (Lundin et al., 2010; de Yebenes et al., 2011; Karl et al., 2013). A phase 3 trial is still ongoing involving early-stage HD patients to investigate Pridopidine's effect on disease progression (NCT04556656) (Table 1).

Huntington's disease is a rare disorder with much less registered clinical trials than in AD or PD. Nevertheless, we review some additional autophagy targeting drugs, which did not meet our selection criteria of being tested in more than 1 trial since 2018, but still show promising results.

Memantine is a previously described drug approved for treatment of AD that has also been tested in HD. Previous clinical trials demonstrated the efficacy of Memantine in preventing progression of chorea and motor dysfunctions (Ondo et al., 2007). Some trials suggested that Memantine could also prevent disease progression (Beister et al., 2004; Hjermind et al., 2011). For the past five years, one phase 4 trial has been registered on ClinicalTrials.gov database completed in 2021, with no results published yet (NCT00652457).

Metformin is a type II diabetes drug that inhibits translation of mutant HTT through the MID1/PP2A/mTOR protein complex, thereby preventing its synthesis in Hdh150 mouse models *in vitro* and *in vivo* (Arnoux et al., 2018). A clinical trial started in 2021 using metformin in HD patients is currently in phase 3 and is recruiting patients (NCT04826692).

Imidazoline-1 receptor agonist Rilmenidine is a frequently used antihypertensive agent. Rilmenidine acts as an mTOR-independent autophagy inducer and can attenuate mHTT-related neurotoxicity through this pathway in HD (Rose et al., 2010; Perera et al., 2018, 2021). A two-year open-label study investigated the efficacy of Rilmenidine in mild and moderate HD patients (trial registration: EudraCT number 2009-018119-14) (Underwood et al., 2017). Although the trial faced limitations (low patient number, no placebo arm, open-label) the authors reported a lower rate of generalized brain atrophy, and smaller decline in mental and disease status scores compared to TRACK-HD data (Underwood et al., 2017).

Parkinson's disease

Parkinson's disease is one of the most common neurodegenerative diseases that causes dopamine deficiency through the loss of dopaminergic neurons in the substantia nigra. In postmortem PD brains intracellular α -synuclein protein aggregation can be observed, which leads to the formation of the so-called Lewy bodies (Hartmann, 2004). Mutation in the LRRK2 gene is one of the most frequent cause of late-onset PD. These mutations account for 5–13% of familial PD and 1–5% of idiopathic PD (Rui et al., 2018). In LRRK2 mutation-related PD increased autophagosomal-lysosomal activity can be observed which causes aggregation of accumulating autophagic vesicles and hinder autophagic clearance (Rui et al., 2018). In addition to the abnormal protein aggregates, there is a dysfunctional metabolism resulting from autophagy dysfunction and disruption of the

lysosome degradation pathway (Decressac et al., 2013; Poewe et al., 2017; Hou et al., 2020; Drouin-Ouellet et al., 2022). Despite the high incidence of this incurable disease, current therapies can only delay the progression of PD. Potential autophagy-related therapeutic targets for the treatment of PD are BECN1 and TFEB, which regulate autophagy by degradation of cellular compartments through a specific network called CLEAR (Coordinated Lysosomal Expression and Regulation).

According to the [ClinicalTrials.gov](https://clinicaltrials.gov) database, several drugs with autophagy-modulating properties are involved in more than one trial for PD since 2018.

AMPK-inducer Pramipexole (a D₂/D₃ receptor agonist) and Istradefyllin (an adenosin receptor A_{2A} antagonist) are already FDA-approved drugs for PD with beneficial effects on depression, motor and cognitive functions (Biglan and Holloway, 2002; Reichmann et al., 2003; Liu Y. et al., 2016; Mo et al., 2016; Torti et al., 2018; Chen and Cunha, 2020; Kanzato et al., 2020; Gencler et al., 2022).

There are certain autophagy modifying drugs used in neurological disorders such as Atomoxetine [used in attention deficit hyperactivity disorder (ADHD)], Dexmedetomidine (used as sedative in schizophrenia and bipolar disorders), and Cannabidiol (FDA approved drug for epilepsy); that also seems to be beneficial in PD by improving both motor (e.g., dyskinesia) and non-motor symptoms (concentration, behavior, psychosis, sleeping, etc.) (Rozet et al., 2006; Marsh et al., 2009; Yang et al., 2014; Hinson et al., 2016; Martinez-Simon et al., 2017; Warner et al., 2018; Crippa et al., 2019; Huestis et al., 2019; Yu et al., 2019; Lombardo et al., 2020; Patricio et al., 2020; Nakajima et al., 2021).

Other promising pharmacotherapeutic agents currently under clinical testing for PD which are used since decades for other indications such as bronchitis, chronic obstructive pulmonary disease (Ambroxol) or type II diabetes and metabolic syndrome (Exenatide) (Aviles-Olmos et al., 2014; Foltynie and Aviles-Olmos, 2014; McNeill et al., 2014; Athauda et al., 2017).

In summary, autophagy is a promising pathway for targeting age-related incurable neurodegenerative diseases. Despite the promising outlook of autophagy-based treatments in experimental models, the high number of failed clinical trials call for more reliable pre-clinical models that can capture key aspects of human aging. There is an urgent need to develop human relevant models to study physiological and pathophysiological changes of autophagy during aging and neurodegeneration in order to provide clinically effective therapies.

Cellular reprogramming models to study autophagy

Several studies indicate impaired neuronal autophagy as one of the key elements in neurodegenerative processes (Labbadia and Morimoto, 2015; Aman et al., 2021; Karabiyik et al., 2021). Our current knowledge is mostly based on findings in postmortem and animal models, and while these models are unprecedentedly important in aging research, there is also a pressing need to further investigate neuronal autophagy in preclinical *in vitro* human neuronal models. We review the already established human neuronal models that studied autophagy in aging-related

conditions and the potential new models that capture aging and the role of autophagy in it (see [Figure 1](#)).

In vitro reprogramming of somatic cells allows us to investigate human-derived cells which are rare or hard to access, like neurons (Mertens et al., 2016). The main goal is to use and perform detailed downstream analysis of human-derived cellular model systems with a wide range of techniques [electrophysiology, sequencing, mass spectrometry, Western blot (WB), immunostaining, microscopy etc.] to measure autophagy.

Conventional 2D human-derived induced neuronal stem cell models are derived from either human embryonal stem cells (ESC) ([Figure 1A](#)) or human-derived induced pluripotent stem cells (iPSC) ([Figure 1B](#)). These models have been used in growing numbers for studying autophagy in several late-onset neurodegenerative diseases and revealed autophagic alterations in connection with neurodegeneration (Prajumwongs et al., 2016; Jungverdorben et al., 2017; Mertens et al., 2018; Kolahdouzmohammadi et al., 2021). ESC-derived neuronal models ([Figure 1A](#)) used to study cellular pathogenesis are present almost exclusively in stem cell transplantation experiments for ethical reasons (Singh et al., 2016). On the other hand, since they represent prenatal neural age, they are not suitable for investigating neuronal autophagy in aging (Steg et al., 2021). iPSCs can be generated from adult (ergo aged) somatic cells by forced expression of specific genes responsible for cellular stemness (e.g., POU5F1, SOX2, MYC, KLF4) either with viral transduction, microRNAs or chemical compounds (Ghaedi and Niklason, 2019; [Figure 1B](#)). Through this procedure, iPSCs are reprogrammed to an earlier epigenetic stage from which they can be further differentiated into any somatic cell types of the human body preserving the genetic features of the donor (Rando and Chang, 2012; Mertens et al., 2018; Ghaedi and Niklason, 2019). Although, since iPSC-neurons get rejuvenated, predicted as being fetal-like neurons based on their DNA methylation profile (Steg et al., 2021), they are useful tools to study the role of autophagy in rejuvenation or in mutation-driven neuronal diseases, but their use in neuronal aging research is constrained by their rejuvenated phenotype (Mertens et al., 2018).

Most neuronal reprogramming studies which focus on macroautophagy alterations have been done in human iPSC PD models so far. Studies of LRRK2-G2019S mutant iPSC-derived dopaminergic neurons (DANs) revealed compromised autophagic maturation and clearance accompanied by morphological alterations of PD-DANs (Sánchez-Danés et al., 2012; Reinhardt et al., 2013; Su and Qi, 2013; Borgs et al., 2016). Borgs et al. (2016) identified upregulation of LC3B, ATG5 and ATG7 genes by RT-qPCR. Sánchez-Danés et al. (2012) identified significant increase both in LC3B⁺ and p62⁺ autophagic structures by immunostaining analysis and elevated level of LC3B-II protein by WB. These findings were confirmed by the accumulation of autophagic structures using electron microscopy (EM) (Sánchez-Danés et al., 2012). Consequently, Su and Qi also detected increased LC3B-II level by WB and immunostaining and increased lysosomal activity in PD-DANs (Su and Qi, 2013), while Reinhardt and colleagues reported decline in basal autophagic activity observed as decreased LC3B-II protein level but accumulation of autophagic structures by EM (Reinhardt et al., 2013). Interestingly, other PD-related mutations – LRRK2-I2020T (elevated LC3B-II and p62 protein level (Ohta et al., 2015)), GBA1-N370S (increased LC3B-II

and LAMP1 protein level (Schöndorf et al., 2014); increased LC3B-II, p62, BECN1, LAMP1 and LAMP2 protein level (Fernandes et al., 2016)), SAC1-R258Q (increased number of WIPI2⁺ autophagic structures by immunostaining (Vanhouwaert et al., 2017))—showed similar detrimental effect on autophagic processes in PD-DANs. Present studies have not implicated autophagy impairments in other mutation-related PD, such as PINK1 or PARK2 mutant iPSC-derived neurons. Heman-Ackah et al. (2017) investigated iPSC neurons derived from PD patients with a special SNCA mutation caused by the multiplication of the α -synuclein (SNCA) gene. They found reduced BECN1 protein levels, while GO analysis of transcriptomic data revealed enrichment for autophagic pathways in SNCA mutant PD-neurons (Heman-Ackah et al., 2017). di Domenico et al. (2019) used an exciting new approach to generate iPSC-DANs and iPSC-astrocytes from the same donors and investigated LRRK2-G2019S mutation-driven PD-related changes in the autophagic course using DAN-astrocyte co-culture experiments. The authors emphasized that PD-astrocytes showed even stronger impairment in autophagic clearance than PD-DANs resulting in more robust α -synuclein accumulation. Moreover, these dysfunctional PD-astrocytes were able to impair normal neural functions of healthy control-derived DANs (di Domenico et al., 2019). In hESC-derived PD models no studies could be found up to date where the autophagic process was investigated in detail.

Significant autophagy dysfunction has been also observed in iPSC models of AD. Lee et al. (2014) and Reddy et al. (2016) reported decreased autophagic flux accompanied by accumulation of autophagic vacuoles in iPSC-derived neurons from AD patients. Lee reported decreased p62 and elevated TFEB, LC3B-II and LAMP1 protein level by WB analysis and accumulation of autophagic vacuoles by EM in Presenilin-1 (PS1) mutant AD-neurons (Lee et al., 2014). The authors considered that increased activity of acid sphingomyelinase presented in PS1 mutants caused the impairment in autophagolysosomal processes (Lee et al., 2014). Reddy et al. investigated PS1-depleted iPSC-derived neurons and found decreased LC3B-II/I ratio and decreased p62 level which showed strong correlation with the decreased promoter activity of Sestrin-2 (mediating oxidative stress rescue and AMPK-mTOR signaling (Liang et al., 2016)) accompanied by increased TFEB phosphorylation and mTOR activity (Reddy et al., 2016). According to the work of Verheyen et al. (2015) the induction of autophagy with Rapamycin or Trehalose in iPSC-derived neurons of AD patients reversed tau pathology. Ubina et al. (2019) studied hESC-derived neurons which were genetically modified to induce amyloid- β accumulation to mimic AD proteinopathy. The amyloid- β pathology was concomitant with reduction in LC3B⁺ autophagic structures indicating impairment in the autophagic clearance mechanism of amyloid- β plaques (Ubina et al., 2019).

Numerous studies have investigated autophagy in HD patients-derived iPSC-neuronal models. Malankhanova et al. (2020) used two approaches to model HD neurons by either generating iPSC-striatal medium spiny neurons (iPSC-MSNs) from human embryonic fibroblasts which were genetically modified with CRISPR/Cas9 insertion of expanded 69 CAG repeat long tract or by generating iPSC-MSNs from HD patient-derived blood mononuclear cells with 47 CAG repeats. Large autophagic vacuoles were reported by transmission electron microscopy (TEM) accompanied by an impaired neural morphology (Malankhanova et al., 2020). Camnasio et al. (2012) detected elevated LC3B-II

protein level by WB in HD iPSC-neurons, increased lysosomal activity using LysoTracker assay with flow cytometry and accumulation of lysosomes by immunostaining. Nekrasov et al. (2016) identified accumulation of autophagosomes and morphology impairments in HD patient-derived iPSC-GABA medium spiny-like neurons (hiPSC-GMSLNs) using TEM. These aberrations could be partially or fully restored by autophagy modifying agents, such as Lithium or LY294002 (PI3K inhibitor). Interestingly, treatment of HD iPSC-GMSLNs with EVP4593—which normalizes impaired Ca²⁺-transport—showed beneficial effect on autophagic processes by decreasing the number of autophagosomes (Nekrasov et al., 2016). In recent years, other studies also implicated new targets regulating the autophagic machinery in neurons. Fu and Zhang demonstrated in ESC- and iPSC-neurons that decreased autophagy was associated with increased HIPK3 (Homeodomain-interacting protein kinase 3) level in HD neurons (Fu et al., 2018; Zhang et al., 2022). Functional experiments revealed that HIPK3 activates DAXX (Death domain-associated protein 6), a transcriptional suppressor of autophagic genes (ULK1 and BECN1). Moreover, they identified a positive feedback loop between mHTT and HIPK3 as high level of mHTT induces HIPK3 which in turn inhibits autophagic clearance of mHTT. This process is thought to play an important role in disease progression (Fu et al., 2018; Zhang et al., 2022). Aron and colleges investigated the pathology-improving role of USP12 (Ubiquitin specific peptidase 12) in HD iPSC-neurons (Aron et al., 2018). USP12 increased autophagy via ATG7-dependent way by potentiating LC3B turnover (measured by optical pulse labeling assay) and increased the number of autophagic structures identified by EM. The use of super resolution microscopy and immunoprecipitation assay showed significant colocalization of USP12-p62 and USP12-mHTT-Optineurin (another autophagy receptor). USP12 may promote the degradation of mHTT by delivering mHTT to the autophagosomes (Aron et al., 2018). Guo et al. (2013) implicated the role of p53 and DRP1 induced autophagy-mediated cell death in HD iPSC-neurons which showed higher expression of these proteins. Di Pardo et al. (2017, 2019) showed that sphingosine-1-phosphate (S1P) metabolism is impaired in iPSC-neurons derived from HD patients, which can also play a role in autophagy dysfunction as elevated S1P level induce autophagy (Di Pardo et al., 2017; Di Pardo et al., 2019). A recently published paper by Bailus et al. (2021) identified another potential autophagy suppressor FKBP5 in human neural stem cells (hNSC) and iPSC-MSNs. The authors propose that FKBP5 binds to mHTT (colocalization was detected by immunostaining) and induce conformational changes which prevent mHTT from autophagosomal degradation (Bailus et al., 2021). FKBP5 seems to have autophagy modulating effects too, as pharmacological or siRNA inhibition induced autophagy manifested in increased level of LC3B-II, p62 and ULK1 protein level (Bailus et al., 2021).

Autophagy impairment was also present in HD astrocytes. Juopperi et al. (2012) reported that autophagy is dysfunctional in the astrocytes generated from iPSCs of an adult-onset patient with 50 CAG repeats and his daughter with juvenile HD (109 CAG repeats). iPSC-astrocytes of the juvenile HD patient showed even stronger upregulation in LC3B⁺ autophagic structures (immunostaining) which was confirmed by TEM as well (Juopperi et al., 2012).

These initial studies point clearly towards a clear alteration in neuronal autophagy in AD, PD and HD; however, the limitations of iPSC-derived neuronal models mimicking human neuronal aging and age-related neurodegenerative diseases need to be kept in mind. The pluripotent phase during reprogramming allows the iPSC-derived neuronal cells to get rejuvenated, and as a consequence, the cells lose many of their aging signatures including DNA methylation (Horvath, 2013; Frobel et al., 2014), transcriptome profile (Mertens et al., 2015), telomere length (Marion et al., 2009), mitochondrial dysfunction (Suhr et al., 2010) and senescence (Lapasset et al., 2011). The clonal expansion of these cells further causes the loss of the genetic heterogeneity originally present in patient-derived samples which can bias our findings especially in cases of idiopathic disease modeling (Mertens et al., 2018). Moreover, studies demonstrated that in many cases iPSC-derived disease models don't exhibit disease-associated phenotypes under normal culture condition (Dimos et al., 2008; Soldner et al., 2009; Zhang et al., 2010; HD iPSC Consortium, 2012) only upon introducing interventions to mimic aging-like phenotype (ROS, telomere manipulation, progerin, etc.) (HD iPSC Consortium, 2012; Miller et al., 2013; Vera et al., 2016; Wu et al., 2019; Chao et al., 2021).

There are increasing number of exciting attempts to induce aging in iPSCs. Vera et al. (2016) applied telomerase inhibitor treatment to initiate aging-like processes in iPSCs and iPSC-derived neurons. As a result, they observed age-like features such as shorter telomeres, increased ROS, DNA damage, reduced dendrite numbers and reduced proliferation. Treatment with telomerase inhibitor in PD-patient derived iPSC-neurons could only present preliminary PD-like phenotype [tyrosine hydroxylase (TH) loss] (Vera et al., 2016). Miller et al. (2013) and Machiela et al. (2020) induced overexpression of progerin (a truncated form of lamin A), which elevates with aging. Accelerated aging-like phenotype of iPSC-neurons included dendrite degradation, TH loss, mitochondrial dysfunction, and protein aggregates. Stress-induced aging was investigated by Zhu et al. (2019) in PD patient iPSC-derived neural progenitor cells (NPCs). They reported decreased SIRT1 (a histone-deacetylase responsible for stress resistance) expression accompanied by increased level of senescence-associated proteins like P53, P21, and P16 and autophagy dysfunction via ATG acetylation upon irradiation and MPTP (1-Methyl-4-phenyl-1,2,3,6-tetrahydropyridine) treatment (Zhu et al., 2019).

Altogether, these initial studies indicate that iPSC-derived neurons can capture some aging aspects of the donor but it is important to note that iPSC reprogramming strongly boosts autophagy in the cells, as highly active autophagy machinery is one of the hallmarks of cellular stemness meaning that autophagy induction is inevitable in iPSC generation (He et al., 2012; Wang et al., 2013; Tang, 2014).

Considering that aging is an incredibly complex and not yet fully understood process, an *in vitro* model which can preserve the genotype and the aging phenotype of the donor would be beneficiary to study neuronal autophagy during human aging in detail (Torrent et al., 2015; Mertens et al., 2018). Direct cellular reprogramming, a relatively novel technique can potentially overcome some of the limitations of currently well-known and widely used cellular reprogramming techniques in studying neuronal aging *in vitro* (Drouin-Ouellet et al., 2017; Inagaki et al., 2022; Figure 1C). During direct neural reprogramming,

cells are being transdifferentiated into induced neurons (iNs) without going through a pluripotent or progenitor phase by using a combination of proneuronal transcription factors, microRNAs, growth factors and chemical compounds. The inevitable benefit of this technique is that the generated cells maintain not just the genetic but also the epigenetic—including many of the aging—signature of the parental cells (Drouin-Ouellet et al., 2017; Mertens et al., 2018; Shrigley et al., 2018). This novel technique allowed the generation of *in vitro* physiologically aged human cells which can recapitulate some key aspects of the donors age, such as DNA methylation, transcriptomic aging, DNA damage, mitochondrial dysfunction, accelerated ROS production and oxidized proteins, impaired proteostasis, cellular compartmentalization defects, altered membrane potential and morphology (Jovičić et al., 2015; Mertens et al., 2015; Yang et al., 2015; Huh et al., 2016; Liu M. et al., 2016; Drouin-Ouellet et al., 2017; Tang et al., 2017; Kim et al., 2018; Shrigley et al., 2018; Victor et al., 2018; Pircs et al., 2022).

Altogether, this novel technique is proved to preserve a highly complex epigenetic phenotype. iNs are thus considered as a more realistic representation of the aging-signature of the human donor as iPSC models. Therefore, using direct neural reprogramming in studying human neuronal aging and age-related neurodegenerative diseases can give us fundamental knowledge about the mechanism of epigenetic aging and its role in neuronal diseases (Mertens et al., 2018; Drouin-Ouellet et al., 2022; Pircs et al., 2022). In our latest paper, we investigated neuronal autophagy disturbances using HD-derived induced neurons (HD-iNs) (Pircs et al., 2022). We demonstrated that patient-derived iNs can recapitulate many aspects of the disease phenotype, like accelerated aging, reduced neuronal morphology and autophagy discrepancies (Pircs et al., 2022). HD-iNs showed enhanced epigenetic age based on DNA methylation assay and transcriptional changes. Disease-like phenotype was also manifested in aberrant morphology of HD-iNs having shorter and thinner neurites compared to age-matched healthy iNs. Global proteomic analysis confirmed by WB revealed significant autophagy impairment in HD-iNs affecting the AMPK pathway. Most interestingly, immunocytochemistry staining of autophagic structures (LC3B, p62, and LAMP1) clearly showed that there is a subcellular, compartment-specific impairment of autophagy in HD-iNs characterized by autophagosome accumulation in the neurites (Pircs et al., 2022). Oh et al. (2022) used HD-derived induced medium spiny neurons (iMSNs) generated from healthy donors, symptomatic (HD-iMSNs) and pre-symptomatic HD (preHD-iMSNs) patients using direct reprogramming. They found remarkable age- and disease-related alterations in chromatin accessibility, decrease in LC3B⁺ and increase in p62⁺ autophagic structures and miR-29b-3p miRNA upregulation in HD-iMSNs compared to the control and preHD-iMSN groups (Oh et al., 2022). Target gene pathway analysis of miR-29b-3p revealed the role of miR-29b-3p in senescence and autophagy (Oh et al., 2022). These findings further support the decisive role of autophagy impairments in HD-related neurodegeneration and accelerated aging. Most recently, Drouin-Ouellet et al. (2022) applied the induced neuronal model to study autophagy in idiopathic PD patient-derived induced neurons (iNs) and induced dopaminergic neurons (iDANs). They reported impaired autophagic activity in PD-iDANs, especially at the early steps of the autophagic

process, which was also supported by a downregulation of early autophagy-related genes (Drouin-Ouellet et al., 2022). Consequently, age-dependent accumulation of LC3B⁺, LAMP2⁺, and p62⁺ autophagic structures and phosphorylated α -synuclein could be detected in PD-iDANs (Drouin-Ouellet et al., 2022). Through comparing iDANs with iNs generated from the same PD patient, they could observe neuronal subtype specific autophagy impairments resulting in different neuronal vulnerability of iDANs than iNs, which is in line with the dopaminergic neuronal loss present in the human PD brain (Hartmann, 2004; Drouin-Ouellet et al., 2022). Remarkably, these disease-specific features were not present neither in the parental fibroblasts, nor in iPSC-derived iDANs from the same donor, underlining the importance of the direct reprogramming in idiopathic, late onset neurodegenerative disease modeling (Drouin-Ouellet et al., 2022).

As we have mentioned above, direct neuronal reprogramming-based disease models are great tools to capture the genetic and epigenetic features of aging and age-related neurodegenerative diseases to study them in a human-derived *in vitro* system. The so far published studies underline its capability to reveal age-related and disease-specific neuronal features, which could not be achieved in such complexity in iPSC models. Although, induced neurons also have limitations. Using skin fibroblasts as a cell source for transdifferentiation, skin-specific age-related changes may get carried over into iNs, such as UV irradiation-induced DNA changes; these may bring non-neuronal aging-relevant aspects into the system (Mertens et al., 2018; Piracs et al., 2022). The cell source can also be a limiting factor, as skin biopsy is an invasive procedure necessitating medical contribution and ethical approvals (Vangipuram et al., 2013). From the skin biopsy sample, a certain number of fibroblasts can be separated which need to be expanded for experimental purposes, but high passage number fibroblasts (over 15 passages) tend to lose their transdifferentiation capability (Vangipuram et al., 2013; Piracs et al., 2022). This limitation can be, however, overcome with good cell banking practice. The generation of isogenic controls remain extremely challenging compared to iPSC technology, therefore the selection and size of the cohort becomes very important. However, as the iN technology is much less laborious than the iPSC method, higher number of samples can be studied at a time (Drouin-Ouellet et al., 2017; Piracs et al., 2022).

In summary, conventional 2D culture models are highly suitable for investigating aging and disease phenotype in a simplified, human-origin system using various interventions (starvation, drug administration, viral transduction, CRISPR etc.) and a wide range of techniques for analysis (microscopy, immunostaining, molecular biology techniques, multiomics, etc.). Using 2D neuronal cultures (iPSC-neurons and iNs) we already gained substantial human-relevant knowledge about the role of autophagy processes and impairments in neurons and in neurodegeneration, and this will be surely strengthened in the future.

However, neurons cultivated in monolayer culture clearly miss dimensional and spatial complexity (Duval et al., 2017). Besides the widely used 2D cell culture, in the last decades more and more attempts were made to achieve new cellular model systems which have higher complexity than monolayer cultures. 3D cell culture is a fairly new and fast-developing approach which may bridge

the gap between classic *in vitro* and *in vivo* research modalities by combining advantages from both (Lancaster and Knoblich, 2014; Amin and Paşca, 2018). The most important benefits of the 3D neuronal models are complex structure, high accessibility, and easy handling which are suitable for high throughput screening purposes (Lancaster and Knoblich, 2014; Amin and Paşca, 2018).

Due to the novelty of the 3D technique in neural aging and neurodegeneration research, most of the related publications are still focusing on the development and optimization of reproducible, high efficiency and disease-specific 3D neural models (Brawner et al., 2017; Centeno et al., 2018; Brighi et al., 2020). However, few pioneer studies have been published recently, which demonstrated that brain organoid models can be used to study autophagy in human neural cells in a more complex view than in monolayer systems (Ha et al., 2020; Lee et al., 2020; Jarazo et al., 2022). The human-derived 3D models used in these studies were generated from iPSCs, derived from healthy donors and patients with neurodegenerative diseases (e.g., PD (Ha et al., 2020; Jarazo et al., 2022) and Niemann-Pick lysosomal storage disease type C (NPD) (Lee et al., 2020). Determination of the autophagic flux was achieved by transcriptomics (NPD: TFEB, RAB39A, RAB23, VAMP7, VAMP8, SNAP25) (Lee et al., 2020), proteomics (PD: EIF2S1, RRAGC, AKT1, HMGB1, IGFR1, LAMP2, 14-3-3 ζ , BIRC7) (Jarazo et al., 2022) and detection of autophagy markers by WB (LC3B-II/I, p62) (Ha et al., 2020; Lee et al., 2020). Abnormal autophagy function in patient-derived organoids could be demonstrated in these 3D models (Ha et al., 2020; Lee et al., 2020; Jarazo et al., 2022). The level of LC3B-II was significantly elevated in PD-organoids (Ha et al., 2020) and NPD-derived organoids (Lee et al., 2020). NPD organoids also showed increased p62 expression (Lee et al., 2020). The authors demonstrated the applicability of 3D models for drug testing as they successfully treated the PD-organoids with 2-hydroxypropyl- β -cyclodextrin (HP- β -CD) (Jarazo et al., 2022), and LRRK2 kinase inhibitor PFE-360 (Ha et al., 2020) and used valproic acid (VPA) in the NPD-organoids (Lee et al., 2020). PFE-360 and VPA effectively restored autophagic processes by reducing LC3B-II and p62 levels in PD and NPD patient-derived organoids, respectively, (Ha et al., 2020; Lee et al., 2020). While VPA also enhanced genes involved in autophagy induction (TFEB, RAB39A, RAB23) and fusion (VAMP7, VAMP8, SNAP25) (Lee et al., 2020). With the treatment of PD-organoids with HP- β -CD, autophagic flux could be restored by modulating autophagy regulator proteins LAMP2, 14-3-3 ζ , and BIRC7 (Jarazo et al., 2022).

In summary, these studies demonstrate the potential of 3D neural models to study autophagy in neurodegenerative diseases. However, the investigation of neural aging in 3D models has still not been addressed as iPSC-derived organoids lose the aging signature of the donor (Mertens et al., 2018). Transcriptomic analysis revealed that even four-months old brain organoids (longest cultivation time to date) mimic the transcriptomic profile of a second/third-trimester human fetal tissue (Hartley and Brennand, 2017). An extremely interesting and promising development will be the generation of organoids from aged-iPSCs, or iNs (Figure 1E), which could bypass this problem, however, such models remain to be established.

Conclusion

There is growing evidence of autophagy as a key factor in neuronal aging and health. The autophagy machinery was first described 60 years ago, and several studies have since then demonstrated a strong correlation between autophagic activity and aging with a conserved presence in a wide range of species (Aman et al., 2021). The gradual decline in autophagic activity during aging suggests autophagy has a defining role in youth and age.

As humans age, autophagy declines progressively in the brain (Shibata et al., 2006; Lipinski et al., 2010). Several recent studies have revealed a pivotal role of autophagy impairment in neurodegenerative diseases, especially in late-onset neuronal disorders like PD, AD and HD (Sapp et al., 1997; Zhu et al., 2003; Nixon et al., 2005; Martinez-Vicente et al., 2010; Tanji et al., 2011; Nilsson et al., 2013; Sun et al., 2014; Moors et al., 2016; Chang et al., 2017; Aman et al., 2021; Pircs et al., 2022). Autophagy dysfunction has proven to be a common feature in these age-related neurodegenerative diseases which implicates its definite role in disease development and progression. In preclinical models, restoration of autophagy showed beneficial effects on disease pathology proposing autophagy dysfunction as a key pathogenic focus, which can serve as potential targets for future therapies (Karabiyik et al., 2021). To demonstrate how patients can benefit from autophagy enhancing therapies, we reviewed all ongoing and completed clinical trials using autophagy modulators for the past five years published since 2018. Several drugs have already shown autophagy modulating properties and demonstrated effectiveness in patients with AD, PD and HD (e.g., Donepezil, Memantine, Pramipexole, Pimavanserin). Almost 20% of the drugs tested for the past five years in AD have autophagy modifying effects, while in PD and HD this percentage is even higher, close to 30% and over 35%, respectively. Drug repurposing represents a surprisingly high number of trials published since 2018. Interestingly, many of these “repurposed” drugs with beneficial effects in neurodegeneration induce autophagy (e.g., antidiabetic drugs Metformin and Exenatide or mucolytic drug Ambroxol shown to be effective in PD). A better understanding of the effect of autophagy induction on these repurposed drugs could be more cost and time-effective and potentially help patients affected by age-related disorders. The reviewed preclinical and clinical trials provide strong evidence of the beneficiary role of autophagy in health and disease. However, a remarkable number of clinical studies using autophagy inducing treatments such as Resveratrol (Berman et al., 2017) or Lithium (Hampel et al., 2009; Forlenza et al., 2011; Devanand et al., 2022), fail to fulfill to provide clinically relevant findings. The high number of failed clinical studies highlight the importance of strengthening our understanding of neuronal autophagy by first choosing more appropriate preclinical models and methods to predict drug efficiency in humans. Currently, most of the drug development and preclinical testing are done in animal models, while many age-related diseases are only affecting humans (Dawson et al., 2018). Although these models are inevitably important, their usage in modeling human brain and neuronal aging as well as human-specific neurodegenerative diseases is limited. A better understanding of neuronal autophagy decline in humans during physiological and pathophysiological conditions could be the key for successful clinical interventions.

We reviewed all currently existing human-derived *in vitro* 2D and 3D neuronal models that are able to capture some aspects of human neuronal aging, thus providing a possibility to study autophagy in human aging and age-related diseases in detail (Figure 1). Cellular reprogramming techniques for human neuronal cell generation *in vitro* have allowed the possibility to study evolutionarily conserved cellular processes. There are, however, only a few publications that focus on the alteration of autophagy during aging and age-related diseases in human cellular reprogrammed neuronal models. Stem cell reprogramming models (ESC and iPSC, Figures 1A, B) are useful tools to study mutation-driven autophagy alterations in neurodegenerative diseases, but their juvenile phenotype limits their use in aging-related research. Direct cellular reprogramming (Figure 1C) allows the generation of neurons through transdifferentiation to preserve the genetic profile also in addition to several aspects of the epigenetic age of the donor (Drouin-Ouellet et al., 2017; Mertens et al., 2018). Patient-derived iNs demonstrate disease-specific features including morphological aberrations and autophagy dysfunction in age-related diseases such as HD or idiopathic PD (Oh et al., 2019; Drouin-Ouellet et al., 2022; Pircs et al., 2022). iNs are suitable for testing autophagy targeting therapeutic approaches in a human-relevant model by performing functional experiments and drug screening (Pircs et al., 2022). iNs provide the first possibility to generate patient-specific and epigenetically aged human neurons. This model paves the way to study human neuronal aging in detail and provides great opportunities to better understand how human neuronal aging occurs. These novel findings will serve as a basis for understanding neuronal rejuvenation and aging. This will allow the development of future therapies that may halt or prevent age-related neurodegenerative diseases.

Author contributions

LD and BK: writing—original draft and writing—review and editing. AA: visualization, writing—original draft, and writing—review and editing. KP: supervision, writing—original draft, and writing—review and editing. All authors contributed to the article and approved the submitted version.

Funding

This research was supported by the STIA-KFI-2020, the STIA-PoC-2020, the TKP-NVA-20, the ICGEB CRP/HUN21-05_EC, the ÚNKP-21-4-I-SE-27, and the ÚNKP-22-4-II-SE-5 New National Excellence Programs of the Ministry for Culture and Innovation from the source of the National Research, Development and Innovation Fund, the HD Human Biology Project Fellowship 2022 of Huntington's Disease Society of America, the Swedish Research Council #2020-02247_3, the Swedish Government Initiative for Strategic Research Areas (MultiPark & StemTherapy), the Jeansson's Foundation (# F 2020/1735), the Tore Nilsons Foundation For Medical Research (# 2020-00824), the Åhlen Foundation (# 213009), the Crafoord Foundation (# 20210629), the Neuro Foundation (# F2021/102),

and the Magnus Bergvall Foundation (# 2021-04138). TKP-NVA-20 has been implemented with the support provided by the Ministry of Innovation and Technology of Hungary from the National Research, Development, and Innovation Fund, financed under the TKP-NVA funding scheme. The project has received funding from the EU's Horizon 2020 Research and Innovation Program under grant agreement No. 739593.

Acknowledgments

We are thankful to all members of the HCEMM-SU Neurobiology and Neurodegenerative Diseases Research Group. We are immensely grateful to Kinga Sándor-Bajusz for her excellent comments on the manuscript.

References

- Aarsland, D., Laake, K., Larsen, J., and Janvin, C. (2002). Donepezil for cognitive impairment in Parkinson's disease: A randomised controlled study. *J. Neurol. Neurosurg. Psychiatry* 72, 708–712. doi: 10.1136/jnnp.72.6.708
- Abdelmoaty, M., Machhi, J., Yeapuri, P., Shahjin, F., Kumar, V., Olson, K., et al. (2022). Monocyte biomarkers define sargramostim treatment outcomes for Parkinson's disease. *Clin. Transl. Med.* 12:e958. doi: 10.1002/ctm2.958
- Adelipour, M., Saleth, L., Ghavami, S., Alagarsamy, K., Dhingra, S., and Allameh, A. (2022). The role of autophagy in the metabolism and differentiation of stem cells. *Biochim. Biophys. Acta Mol. Basis Dis.* 1868:166412. doi: 10.1016/j.bbdis.2022.166412
- Adlimoghaddam, A., Neuendorff, M., Roy, B., and Albensi, B. C. (2018). A review of clinical treatment considerations of donepezil in severe Alzheimer's disease. *CNS Neurosci. Ther.* 24, 876–888. doi: 10.1111/cns.13035
- Aman, Y., Schmauck-Medina, T., Hansen, M., Morimoto, R., Simon, A., Bjedov, I., et al. (2021). Autophagy in healthy aging and disease. *Nat. Aging* 1, 634–650. doi: 10.1038/s43587-021-00098-4
- Amin, N., and Paşca, S. (2018). Building models of brain disorders with three-dimensional organoids. *Neuron* 100, 389–405. doi: 10.1016/j.neuron.2018.10.007
- Arnoux, I., Willam, M., Griesche, N., Krummeich, J., Watari, H., Offermann, N., et al. (2018). Metformin reverses early cortical network dysfunction and behavior changes in Huntington's disease. *Elife* 7:e38744. doi: 10.7554/eLife.38744
- Aron, R., Pellegrini, P., Green, E., Maddison, D., Opoku-Nsiah, K., Oliveira, A., et al. (2018). Deubiquitinase Usp12 functions noncatalytically to induce autophagy and confer neuroprotection in models of Huntington's disease. *Nat. Commun.* 9:3191. doi: 10.1038/s41467-018-05653-z
- Athauda, D., MacLagan, K., Skene, S., Bajwa-Joseph, M., Letchford, D., Chowdhury, K., et al. (2017). Exenatide once weekly versus placebo in Parkinson's disease: A randomised, double-blind, placebo-controlled trial. *Lancet* 390, 1664–1675. doi: 10.1016/S0140-6736(17)31585-4
- Atri, A., Frölich, L., Ballard, C., Tariot, P., Molinuevo, J., Boneva, N., et al. (2018). Effect of idalopirdine as adjunct to cholinesterase inhibitors on change in cognition in patients with Alzheimer disease: Three randomized clinical trials. *JAMA* 319, 130–142. doi: 10.1001/jama.2017.20373
- Aviles-Olmos, I., Dickson, J., Kefalopoulou, Z., Djamshidian, A., Kahan, J., Ell, P., et al. (2014). Motor and cognitive advantages persist 12 months after exenatide exposure in Parkinson's disease. *J. Parkinsons Dis.* 4, 337–344. doi: 10.3233/JPD-140364
- Baba, T., Takeda, A., Murakami, A., Koga, T., Isomura, T., Mori, E., et al. (2022). Effect of donepezil for dementia prevention in Parkinson's disease with severe hyposmia (The DASH-PD study): A randomized long-term placebo-controlled trial. *EClinicalMedicine* 51:101571. doi: 10.1016/j.eclinm.2022.101571
- Baik, K., Kim, S., Jung, J., Lee, Y., Chung, S., Yoo, H., et al. (2021). Donepezil for mild cognitive impairment in Parkinson's disease. *Sci. Rep.* 11:4734. doi: 10.1038/s41598-021-84243-4
- Bailus, B., Scheeler, S., Simons, J., Sanchez, M., Tshilenge, K., Creus-Muncunill, J., et al. (2021). Modulating FKBP5/FKBP51 and autophagy lowers HTT (huntingtin) levels. *Autophagy* 17, 4119–4140. doi: 10.1080/15548627.2021.1904489
- Ballard, C., Youakim, J., Coate, B., and Stankovic, S. (2019). Pimavanserin in Alzheimer's disease psychosis: Efficacy in patients with more pronounced psychotic symptoms. *J. Prev. Alzheimers Dis.* 6, 27–33. doi: 10.14283/jpad.2018.30
- Beister, A., Kraus, P., Kuhn, W., Dose, M., Weindl, A., and Gerlach, M. (2004). The N-methyl-D-aspartate antagonist memantine retards progression of Huntington's disease. *J. Neural Transm. Suppl.* 68, 117–122. doi: 10.1007/978-3-7091-0579-5_14
- Berman, A., Motechin, R., Wiesenfeld, M., and Holz, M. (2017). The therapeutic potential of resveratrol: A review of clinical trials. *NPJ Precis. Oncol.* 1:35. doi: 10.1038/s41698-017-0038-6
- Biglan, K., and Holloway, R. G. (2002). A review of pramipexole and its clinical utility in Parkinson's disease. *Expert. Opin. Pharmacother.* 3, 197–210. doi: 10.1517/14656566.3.2.197
- Boada-Rovira, M., Brodaty, H., Cras, P., Baloyannis, S., Emre, M., Zhang, R., et al. (2004). Efficacy and safety of donepezil in patients with Alzheimer's disease: Results of a global, multinational, clinical experience study. *Drugs Aging* 21, 43–53. doi: 10.2165/00002512-200421010-00004
- Borgs, L., Peyre, E., Alix, P., Hanon, K., Grobarczyk, B., Godin, J., et al. (2016). Dopaminergic neurons differentiating from LRRK2 G2019S induced pluripotent stem cells show early neuritic branching defects. *Sci. Rep.* 6:33377. doi: 10.1038/srep33377
- Brattås, P., Hersbach, B., Madsen, S., Petri, R., Jakobsen, J., and Pirce, K. (2021). Impact of differential and time-dependent autophagy activation on therapeutic efficacy in a model of Huntington disease. *Autophagy* 17, 1316–1329. doi: 10.1080/15548627.2020.1760014
- Brawner, A., Xu, R., Liu, D., and Jiang, P. (2017). Generating CNS organoids from human induced pluripotent stem cells for modeling neurological disorders. *Int. J. Physiol. Pathophysiol. Pharmacol.* 9, 101–111.
- Brighi, C., Cordella, F., Chiriatti, L., Soloperto, A., and Di Angelantonio, S. (2020). Retinal and brain organoids: Bridging the gap between in vivo physiology and in vitro micro-physiology for the study of Alzheimer's diseases. *Front. Neurosci.* 14:655. doi: 10.3389/fnins.2020.00655
- Camnasio, S., Delli Carri, A., Lombardo, A., Grad, I., Mariotti, C., Castucci, A., et al. (2012). The first reported generation of several induced pluripotent stem cell lines from homozygous and heterozygous Huntington's disease patients demonstrates mutation related enhanced lysosomal activity. *Neurobiol. Dis.* 46, 41–51. doi: 10.1016/j.nbd.2011.12.042
- Campbell, J., Stephenson, M., de Courten, B., Chapman, I., Bellman, S., and Aromataris, E. (2018). Metformin use associated with reduced risk of dementia in patients with diabetes: A systematic review and meta-analysis. *J. Alzheimers Dis.* 65, 1225–1236. doi: 10.3233/JAD-180263
- Centeno, E., Cimarosti, H., and Bithell, A. (2018). 2D versus 3D human induced pluripotent stem cell-derived cultures for neurodegenerative disease modelling. *Mol. Neurodegener.* 13:27. doi: 10.1186/s13024-018-0258-4
- Chang, D., Nalls, M., Hallgrímsdóttir, I., Hunkapiller, J., van der Brug, M., Cai, F., et al. (2017). A meta-analysis of genome-wide association studies identifies 17 new Parkinson's disease risk loci. *Nat. Genet.* 49, 1511–1516. doi: 10.1038/ng.3955
- Chang, N. (2020). Autophagy and stem cells: Self-eating for self-renewal. *Front. Cell Dev. Biol.* 8:138. doi: 10.3389/fcell.2020.00138

Conflict of interest

The authors declare that the research was conducted in the absence of any commercial or financial relationships that could be construed as a potential conflict of interest.

Publisher's note

All claims expressed in this article are solely those of the authors and do not necessarily represent those of their affiliated organizations, or those of the publisher, the editors and the reviewers. Any product that may be evaluated in this article, or claim that may be made by its manufacturer, is not guaranteed or endorsed by the publisher.

- Chao, C., Shen, P., Tzeng, T., Kung, H., Tsai, T., and Wong, Y. (2021). Human iPSC-derived neurons as a platform for deciphering the mechanisms behind brain aging. *Biomedicine* 9:1635. doi: 10.3390/biomedicine9111635
- Chen, C., Liu, Y., Liu, Y., and Zheng, P. (2009). mTOR regulation and therapeutic rejuvenation of aging hematopoietic stem cells. *Sci. Signal.* 2:ra75. doi: 10.1126/scisignal.2000559
- Chen, J., and Cunha, R. (2020). The belated US FDA approval of the adenosine A2A receptor antagonist istradefylline for treatment of Parkinson's disease. *Purinergic. Signal.* 16, 167–174. doi: 10.1007/s11302-020-09694-2
- Choi, S., Gu, Y., Peters, R., Salgame, P., Ellner, J., Timmins, G., et al. (2018). Ambroxol induces autophagy and potentiates rifampin antimycobacterial activity. *Antimicrob. Agents Chemother.* 62:e01019–18. doi: 10.1128/AAC.01019-18
- Corona, J., Carreón-Trujillo, S., González-Pérez, R., Gómez-Bautista, D., Vázquez-González, D., and Salazar-García, M. (2019). Atomoxetine produces oxidative stress and alters mitochondrial function in human neuron-like cells. *Sci. Rep.* 9:13011. doi: 10.1038/s41598-019-49609-9
- Crippa, J., Hallak, J., Zuadi, A., Guimarães, F., Tumas, V., and Dos Santos, R. (2019). Is cannabidiol the ideal drug to treat non-motor Parkinson's disease symptoms? *Eur. Arch. Psychiatry Clin. Neurosci.* 269, 121–133. doi: 10.1007/s00406-019-00982-6
- Dashtipour, K., Gupta, F., Hauser, R., Karunapuzha, C., and Morgan, J. (2021). Pimavanserin treatment for Parkinson's disease psychosis in clinical practice. *Parkinsons Dis.* 2021:2603641. doi: 10.1155/2021/2603641
- Dasuri, K., Zhang, L., Kim, S., Bruce-Keller, A., and Keller, J. (2016). Dietary and donepezil modulation of mTOR signaling and neuroinflammation in the brain. *Biochim. Biophys. Acta* 1862, 274–283. doi: 10.1016/j.bbdis.2015.11.002
- Dawson, T., Golde, T., and Lagier-Tourenne, C. (2018). Animal models of neurodegenerative diseases. *Nat. Neurosci.* 21, 1370–1379. doi: 10.1038/s41593-018-0236-8
- de Yebenes, J., Landwehrmeyer, B., Squitieri, F., Reilmann, R., Rosser, A., Barker, R., et al. (2011). Pridopidine for the treatment of motor function in patients with Huntington's disease (MermatHD): A phase 3, randomised, double-blind, placebo-controlled trial. *Lancet Neurol.* 10, 1049–1057. doi: 10.1016/S1474-4422(11)70233-2
- Decressac, M., Mattsson, B., Weikop, P., Lundblad, M., Jakobsson, J., and Björklund, A. (2013). TFEB-mediated autophagy rescues midbrain dopamine neurons from α -synuclein toxicity. *Proc. Natl. Acad. Sci. U.S.A.* 110, E1817–E1826. doi: 10.1073/pnas.1305623110
- Devanand, D., Crocco, E., Forester, B., Husain, M., Lee, S., Vahia, I., et al. (2022). Low dose lithium treatment of behavioral complications in Alzheimer's disease: Lit-AD randomized clinical trial. *Am. J. Geriatr. Psychiatry* 30, 32–42. doi: 10.1016/j.jagp.2021.04.014
- Dhanasekaran, D., and Reddy, E. P. (2017). JNK-signaling: A multiplexing hub in programmed cell death. *Genes Cancer* 8, 682–694. doi: 10.18632/genesandcancer.155
- di Domenico, A., Carola, G., Calatayud, C., Pons-Espinal, M., Muñoz, J., Richaud-Patin, Y., et al. (2019). Patient-specific iPSC-derived astrocytes contribute to non-cell-autonomous neurodegeneration in Parkinson's disease. *Stem Cell Rep.* 12, 213–229. doi: 10.1016/j.stemcr.2018.12.011
- Di Pardo, A., Amico, E., Basit, A., Armirotti, A., Joshi, P., Neely, M., et al. (2017). Defective sphingosine-1-phosphate metabolism is a druggable target in Huntington's disease. *Sci. Rep.* 7:5280. doi: 10.1038/s41598-017-05709-y
- Di Pardo, A., Pepe, G., Castaldo, S., Marracino, F., Capocci, L., Amico, E., et al. (2019). Stimulation of sphingosine kinase 1 (SPHK1) is beneficial in a Huntington's disease pre-clinical model. *Front. Mol. Neurosci.* 12:100. doi: 10.3389/fnmol.2019.00100
- Dimos, J., Rodolfa, K., Niakan, K., Weisenthal, L., Mitsumoto, H., Chung, W., et al. (2008). Induced pluripotent stem cells generated from patients with ALS can be differentiated into motor neurons. *Science* 321, 1218–1221. doi: 10.1126/science.1158799
- Drouin-Ouellet, J., Legault, E., Nilsson, F., Pirce, K., Bouquety, J., Petit, F., et al. (2022). Age-related pathological impairments in directly reprogrammed dopaminergic neurons derived from patients with idiopathic Parkinson's disease. *Stem Cell Rep.* 17, 2203–2219. doi: 10.1016/j.stemcr.2022.08.010
- Drouin-Ouellet, J., Pirce, K., Barker, R., Jakobsson, J., and Parmar, M. (2017). Direct neuronal reprogramming for disease modeling studies using patient-derived neurons: What have we learned? *Front. Neurosci.* 11:530. doi: 10.3389/fnins.2017.00530
- Duval, K., Grover, H., Han, L., Mou, Y., Pegoraro, A., Fredberg, J., et al. (2017). Modeling physiological events in 2D vs. 3D cell culture. *Physiology (Bethesda)* 32, 266–277. doi: 10.1152/physiol.00036.2016
- Fang, Y., An, N., Zhu, L., Gu, Y., Qian, J., Jiang, G., et al. (2020). Autophagy-Sirt3 axis decelerates hematopoietic aging. *Aging Cell* 19:e13232. doi: 10.1111/accel.13232
- Farr, S., Roesler, E., Niehoff, M., Roby, D., McKee, A., and Morley, J. (2019). Metformin improves learning and memory in the SAMP8 mouse model of Alzheimer's disease. *J. Alzheimers Dis.* 68, 1699–1710. doi: 10.3233/JAD-181240
- Fernandes, H., Hartfield, E., Christian, H., Emmanouilidou, E., Zheng, Y., Booth, H., et al. (2016). ER stress and autophagic perturbations lead to elevated extracellular α -synuclein in GBA-N370S Parkinson's iPSC-derived dopamine neurons. *Stem Cell Rep.* 6, 342–356. doi: 10.1016/j.stemcr.2016.01.013
- Ferri, C., Prince, M., Brayne, C., Brodaty, H., Fratiglioni, L., Ganguli, M., et al. (2005). Global prevalence of dementia: A Delphi consensus study. *Lancet* 366, 2112–2117. doi: 10.1016/S0140-6736(05)67889-0
- Foltyniec, T., and Aviles-Olmos, I. (2014). Exenatide as a potential treatment for patients with Parkinson's disease: First steps into the clinic. *Alzheimers Dement.* 10(1 Suppl), S38–S46. doi: 10.1016/j.jalz.2013.12.005
- Forlenza, O., Diniz, B., Radanovic, M., Santos, F., Talib, L., and Gattaz, W. (2011). Disease-modifying properties of long-term lithium treatment for amnesic mild cognitive impairment: Randomised controlled trial. *Br. J. Psychiatry* 198, 351–356. doi: 10.1192/bjp.bp.110.080044
- Fröbel, J., Hemeda, H., Lenz, M., Abagnale, G., Jousen, S., Denecke, B., et al. (2014). Epigenetic rejuvenation of mesenchymal stromal cells derived from induced pluripotent stem cells. *Stem Cell Rep.* 3, 414–422. doi: 10.1016/j.stemcr.2014.07.003
- Fu, M., Zhang, X., Zhang, X., Yang, L., Luo, S., and Liu, H. (2021). Autophagy plays a role in the prolongation of the life span of *Caenorhabditis elegans* by astaxanthin. *Rejuvenation Res.* 24, 198–205. doi: 10.1089/rej.2020.2355
- Fu, Y., Sun, X., and Lu, B. (2018). HIPK3 modulates autophagy and HTT protein levels in neuronal and mouse models of Huntington disease. *Autophagy* 14, 169–170. doi: 10.1080/15548627.2017.1393130
- Gencler, O., Oztekin, N., and Oztekin, M. (2022). Comparison of pramipexole versus ropinirole in the treatment of Parkinson's disease. *Ideggyogy. Sz.* 75, 39–49. doi: 10.18071/isz.75.0039
- Ghaedi, M., and Niklason, L. (2019). Human pluripotent stem cells (iPSC) generation, culture, and differentiation to lung progenitor cells. *Methods Mol. Biol.* 1576, 55–92. doi: 10.1007/978-1-4939-9911-1_11
- Guo, X., Disatnik, M., Monbureau, M., Shamloo, M., Mochly-Rosen, D., and Qi, X. (2013). Inhibition of mitochondrial fragmentation diminishes Huntington's disease-associated neurodegeneration. *J. Clin. Invest.* 123, 5371–5388. doi: 10.1172/JCI70911
- Ha, J., Kang, J., Lee, M., Baek, A., Kim, S., Chung, S., et al. (2020). Simplified brain organoids for rapid and robust modeling of brain disease. *Front. Cell Dev. Biol.* 8:594090. doi: 10.3389/fcell.2020.594090
- Hampel, H., Ewers, M., Bürger, K., Annas, P., Mörtberg, A., Bogstedt, A., et al. (2009). Lithium trial in Alzheimer's disease: A randomized, single-blind, placebo-controlled, multicenter 10-week study. *J. Clin. Psychiatry* 70, 922–931.
- Hansen, M., Rubinstein, D., and Walker, D. (2018). Autophagy as a promoter of longevity: Insights from model organisms. *Nat. Rev. Mol. Cell Biol.* 19, 579–593. doi: 10.1038/s41580-018-0033-y
- Hartley, B., and Brennand, K. (2017). Neural organoids for disease phenotyping, drug screening and developmental biology studies. *Neurochem. Int.* 106, 85–93. doi: 10.1016/j.neuint.2016.10.004
- Hartmann, A. (2004). Postmortem studies in Parkinson's disease. *Dialogues Clin. Neurosci.* 6, 281–293. doi: 10.31887/DCNS.2004.6.3/ahartmann
- Hawkins, T., and Berman, B. (2017). Pimavanserin: A novel therapeutic option for Parkinson disease psychosis. *Neurol. Clin. Pract.* 7, 157–162. doi: 10.1212/CPJ.0000000000000342
- HD iPSC Consortium (2012). Induced pluripotent stem cells from patients with Huntington's disease show CAG-repeat-expansion-associated phenotypes. *Cell Stem Cell* 11, 264–278. doi: 10.1016/j.stem.2012.04.027
- He, J., Kang, L., Wu, T., Zhang, J., Wang, H., Gao, H., et al. (2012). An elaborate regulation of mammalian target of rapamycin activity is required for somatic cell reprogramming induced by defined transcription factors. *Stem Cells Dev.* 21, 2630–2641. doi: 10.1089/scd.2012.0015
- Heman-Ackah, S., Manzano, R., Hoozemans, J., Schepers, W., Flynn, R., Haerty, W., et al. (2017). Alpha-synuclein induces the unfolded protein response in Parkinson's disease SNCA triplication iPSC-derived neurons. *Hum. Mol. Genet.* 26, 4441–4450. doi: 10.1093/hmg/ddx331
- Hinson, V., Delambo, A., Elm, J., and Turner, T. A. (2016). Randomized clinical trial of atomoxetine for mild cognitive impairment in Parkinson's disease. *Mov Disord Clin Pract.* 4, 416–423. doi: 10.1002/mdc3.12455
- Hirano, K., Fujimaki, M., Sasazawa, Y., Yamaguchi, A., Ishikawa, K., Miyamoto, K., et al. (2019). Neuroprotective effects of memantine via enhancement of autophagy. *Biochem. Biophys. Res. Commun.* 518, 161–170. doi: 10.1016/j.bbrc.2019.08.025
- Hjermind, L., Law, I., Jønh, A., Stokholm, J., and Nielsen, J. (2011). Huntington's disease: Effect of memantine on FDG-PET brain metabolism? *J. Neuropsychiatry Clin. Neurosci.* 23, 206–210. doi: 10.1176/jnp.23.2.jnp206
- Horvath, S. (2013). DNA methylation age of human tissues and cell types. *Genome Biol.* 14:R115. doi: 10.1186/gb-2013-14-10-r115
- Hou, X., Watzlawik, J., Fiesel, F., and Springer, W. (2020). Autophagy in Parkinson's Disease. *J. Mol. Biol.* 432, 2651–2672. doi: 10.1016/j.jmb.2020.01.037

- Hou, Y., Dan, X., Babbar, M., Wei, Y., Hasselbalch, S., Croteau, D., et al. (2019). Ageing as a risk factor for neurodegenerative disease. *Nat. Rev. Neurol.* 15, 565–581. doi: 10.1038/s41582-019-0244-7
- Huestis, M., Solimini, R., Pichini, S., Pacifici, R., Carlier, J., and Busardò, F. (2019). Cannabidiol adverse effects and toxicity. *Curr. Neuropharmacol.* 17, 974–989. doi: 10.2174/1570159X17666190603171901
- Huh, C., Zhang, B., Victor, M., Dahiya, S., Batista, L., Horvath, S., et al. (2016). Maintenance of age in human neurons generated by microRNA-based neuronal conversion of fibroblasts. *Life* 5:e18648. doi: 10.7554/eLife.18648
- Inagaki, E., Yoshimatsu, S., and Okano, H. (2022). Accelerated neuronal aging in vitro ~melting watch~. *Front. Aging Neurosci.* 14:868770. doi: 10.3389/fnagi.2022.868770
- Jarazo, J., Barmpa, K., Modamio, J., Saraiva, C., Sabaté-Soler, S., Rosety, I., et al. (2022). Parkinson's disease phenotypes in patient neuronal cultures and brain organoids improved by 2-Hydroxypropyl- β -Cyclodextrin treatment. *Mov. Disord.* 37, 80–94. doi: 10.1002/mds.28810
- Jovićić, A., Mertens, J., Boeynaems, S., Bogaert, E., Chai, N., Yamada, S., et al. (2015). Modifiers of C9orf72 dipeptide repeat toxicity connect nucleocytoplasmic transport defects to FTD/ALS. *Nat. Neurosci.* 18, 1226–1229. doi: 10.1038/nn.4085
- Jungverdorben, J., Till, A., and Brüstle, O. (2017). Induced pluripotent stem cell-based modeling of neurodegenerative diseases: A focus on autophagy. *J. Mol. Med. (Berl)* 95, 705–718. doi: 10.1007/s00109-017-1533-5
- Juopperi, T., Kim, W., Chiang, C., Yu, H., Margolis, R., Ross, C., et al. (2012). Astrocytes generated from patient induced pluripotent stem cells recapitulate features of Huntington's disease patient cells. *Mol. Brain* 5:17. doi: 10.1186/1756-6606-5-17
- Kanzato, N., Nakachi, K., Mochizuki, S., Kanda, T., and Mori, A. (2020). Blood hexokinase reduction in de novo Parkinson's disease and remodeling of glycolytic energy homeostasis with L-DOPA/Istradefylline combination therapy. *Parkinsonism Relat. Disord.* 79, e68–e69.
- Karabiyik, C., Frake, R. A., Park, S. J., Pavel, M., and Rubinsztein, D. C. (2021). Autophagy in ageing and ageing-related neurodegenerative diseases. *Ageing Neurodegener. Dis.* 1:2.
- Karl, K., McGarry, A., McDermott, M. P., Kayson, E., Walker, F., Goldstein, J., et al. (2013). A randomized, double-blind, placebo-controlled trial of pridopidine in Huntington's disease. *Mov. Disord.* 28, 1407–1415. doi: 10.1002/mds.25362
- Kaushik, S., Tasset, I., Arias, E., Pampliega, O., Wong, E., Martinez-Vicente, M., et al. (2021). Autophagy and the hallmarks of aging. *Ageing Res. Rev.* 72:101468. doi: 10.1016/j.arr.2021.101468
- Khuanjing, T., Palee, S., Kerdphoo, S., Jaiwongkam, T., Anomasiri, A., Chattipakorn, S., et al. (2021). Donepezil attenuated cardiac ischemia/reperfusion injury through balancing mitochondrial dynamics, mitophagy, and autophagy. *Transl. Res.* 230, 82–97. doi: 10.1016/j.trsl.2020.10.010
- Kim, Y., Zheng, X., Ansari, Z., Bunnell, M., Herdy, J., Traxler, L., et al. (2018). Mitochondrial aging defects emerge in directly reprogrammed human neurons due to their metabolic profile. *Cell Rep.* 23, 2550–2558. doi: 10.1016/j.celrep.2018.04.105
- Kishi, T., Matsunaga, S., Oya, K., Nomura, I., Ikuta, T., and Iwata, N. (2017). Memantine for Alzheimer's disease: An updated systematic review and meta-analysis. *J. Alzheimers Dis.* 60, 401–425. doi: 10.3233/JAD-170424
- Kitten, A., Halliwell, S., Saklad, S., and Evoy, K. (2018). Pimavanserin: A novel drug approved to treat Parkinson's disease psychosis. *Innov. Clin. Neurosci.* 15, 16–22.
- Klionsky, D., Abdelmohsen, K., Abe, A., Abedin, M., Abeliovich, H., Acevedo Arozana, A., et al. (2016). Guidelines for the use and interpretation of assays for monitoring autophagy (3rd edition). *Autophagy* 12, 1–222. doi: 10.1080/15548627.2015.1100356
- Kolahdouzmohammadi, M., Totonchi, M., and Pahlavan, S. (2021). The role of iPSC modeling toward projection of autophagy pathway in disease pathogenesis: Leader or follower. *Stem Cell Rev. Rep.* 17, 539–561. doi: 10.1007/s12015-020-10077-8
- Labbadia, J., and Morimoto, R. (2015). The biology of proteostasis in aging and disease. *Annu. Rev. Biochem.* 84, 435–464. doi: 10.1146/annurev-biochem-060614-033955
- Lancaster, M., and Knoblich, J. (2014). Organogenesis in a dish: Modeling development and disease using organoid technologies. *Science* 345:1247125. doi: 10.1126/science.1247125
- Lapasset, L., Milharet, O., Prieur, A., Besnard, E., Babled, A., Ait-Hamou, N., et al. (2011). Rejuvenating senescent and centenarian human cells by reprogramming through the pluripotent state. *Genes Dev.* 25, 2248–2253. doi: 10.1101/gad.17392.2.111
- Lee, J., Jin, H., Park, M., Kim, B., Lee, P., Nakauchi, H., et al. (2014). Acid sphingomyelinase modulates the autophagic process by controlling lysosomal biogenesis in Alzheimer's disease. *J. Exp. Med.* 211, 1551–1570. doi: 10.1084/jem.20132451
- Lee, S., Shin, N., Kook, M., Kong, D., Kim, N., Choi, S., et al. (2020). Human iNSC-derived brain organoid model of lysosomal storage disorder in Niemann-Pick disease type C. *Cell Death Dis.* 11, 1059. doi: 10.1038/s41419-020-03262-7
- Leeman, D., Hebestreit, K., Ruetz, T., Webb, A., McKay, A., Pollina, E., et al. (2018). Lysosome activation clears aggregates and enhances quiescent neural stem cell activation during aging. *Science* 359, 1277–1283. doi: 10.1126/science.aag3048
- Liang, Y., Zhu, J., Huang, H., Xiang, D., Li, Y., Zhang, D., et al. (2016). SESN2/sestrin 2 induction-mediated autophagy and inhibitory effect of isorhapontigenin (ISO) on human bladder cancers. *Autophagy* 12, 1229–1239. doi: 10.1080/15548627.2016.1179403
- Lipinski, M., Zheng, B., Lu, T., Yan, Z., Py, B., Ng, A., et al. (2010). Genome-wide analysis reveals mechanisms modulating autophagy in normal brain aging and in Alzheimer's disease. *Proc. Natl. Acad. Sci. U.S.A.* 107, 14164–14169. doi: 10.1073/pnas.1009485107
- Liu, M., Zang, T., and Zhang, C. (2016). Direct lineage reprogramming reveals disease-specific phenotypes of motor neurons from human ALS patients. *Cell Rep.* 14, 115–128. doi: 10.1016/j.celrep.2015.12.018
- Liu, Y., Yang, T., Zhao, L., Ni, Z., Yang, N., He, F., et al. (2016). Activation of Adenosine 2A receptor inhibits neutrophil apoptosis in an autophagy-dependent manner in mice with systemic inflammatory response syndrome. *Sci. Rep.* 6:33614. doi: 10.1038/srep33614
- Lombardo, M., DiPiazza, A., Rippey, K., Lubarr, N., Clar, E., and Azmi, H. (2020). Treatment of Acute delirium in a patient with Parkinson's disease by transfer to the intensive care unit and administration of dexmedetomidine. *J. Mov. Disord.* 13, 159–162. doi: 10.14802/jmd.20005
- Long, J., and Holtzman, D. (2019). Alzheimer disease: An update on pathobiology and treatment strategies. *Cell* 179, 312–339. doi: 10.1016/j.cell.2019.09.001
- Lundin, A., Dietrichs, E., Haghighi, S., Göller, M., Heiberg, A., Loutfi, G., et al. (2010). Efficacy and safety of the dopamine stabilizer Pridopidine (ACR16) in patients with Huntington's disease. *Clin. Neuropharmacol.* 33, 260–264. doi: 10.1097/WNF.0b013e3181ebb285
- Luo, F., Sandhu, A., Rungratanawanich, W., Williams, G., Akbar, M., Zhou, S., et al. (2020). Melatonin and autophagy in aging-related neurodegenerative diseases. *Int. J. Mol. Sci.* 21:7174. doi: 10.3390/ijms21197174
- Machiela, E., Jeloka, R., Caron, N., Mehta, S., Schmidt, M., Baddeley, H., et al. (2020). The interaction of aging and cellular stress contributes to pathogenesis in mouse and human huntington disease neurons. *Front. Aging Neurosci.* 12:524369. doi: 10.3389/fnagi.2020.524369
- Malankhanova, T., Suldina, L., Grigor'eva, E., Medvedev, S., Minina, J., Morozova, K., et al. (2020). A human induced pluripotent stem cell-derived isogenic model of Huntington's disease based on neuronal cells has several relevant phenotypic abnormalities. *J. Pers. Med.* 10:215. doi: 10.3390/jpm10040215
- Mandic, M., Misirkic Marjanovic, M., Vucicevic, L., Jovanovic, M., Bosnjak, M., Perovic, V., et al. (2022). MAP kinase-dependent autophagy controls phorbol myristate acetate-induced macrophage differentiation of HL-60 leukemia cells. *Life Sci.* 297:120481. doi: 10.1016/j.lfs.2022.120481
- Marion, R., Strati, K., Li, H., Tejera, A., Schoeftner, S., Ortega, S., et al. (2009). Telomeres acquire embryonic stem cell characteristics in induced pluripotent stem cells. *Cell Stem Cell* 4, 141–154. doi: 10.1016/j.stem.2008.12.010
- Marsh, L., Biglan, K., Gerstenhaber, M., and Williams, J. (2009). Atomoxetine for the treatment of executive dysfunction in Parkinson's disease: a pilot open-label study. *Mov. Disord.* 24, 277–282. doi: 10.1002/mds.22307
- Martin, D., Ladha, S., Ehrnhoefer, D., and Hayden, M. (2015). Autophagy in Huntington disease and huntingtin in autophagy. *Trends Neurosci.* 38, 26–35. doi: 10.1016/j.tins.2014.09.003
- Martinez-Simon, A., Alegre, M., Honorato-Cia, C., Nuñez-Cordoba, J., Cacho-Asenjo, E., Trocóniz, I., et al. (2017). Effect of dexmedetomidine and propofol on basal ganglia activity in Parkinson disease: A controlled clinical trial. *Anesthesiology* 126, 1033–1042. doi: 10.1097/ALN.0000000000001620
- Martinez-Vicente, M., Tallozy, Z., Wong, E., Tang, G., Koga, H., Kaushik, S., et al. (2010). Cargo recognition failure is responsible for inefficient autophagy in Huntington's disease. *Nat. Neurosci.* 13, 567–576. doi: 10.1038/nn.2528
- McNeill, A., Magalhaes, J., Shen, C., Chau, K., Hughes, D., Mehta, A., et al. (2014). Amroxol improves lysosomal biochemistry in glucocerebrosidase mutation-linked Parkinson disease cells. *Brain* 137(Pt 5), 1481–1495. doi: 10.1093/brain/awu020
- McShane, R., Westby, M., Roberts, E., Minakaran, N., Schneider, L., Farrimond, L., et al. (2019). Memantine for dementia. *Cochrane Database Syst. Rev.* 3:CD003154. doi: 10.1002/14651858.CD003154.pub6
- Meffre, J., Chaumont-Dubel, S., Mannoury la Cour, C., Loiseau, F., Watson, D., Dekeyne, A., et al. (2012). 5-HT(6) receptor recruitment of mTOR as a mechanism for perturbed cognition in schizophrenia. *EMBO Mol. Med.* 4, 1043–1056. doi: 10.1002/emmm.201201410
- Menzies, F., Fleming, A., and Rubinsztein, D. (2015). Compromised autophagy and neurodegenerative diseases. *Nat. Rev. Neurosci.* 16, 345–357. doi: 10.1038/nrn3961
- Mertens, J., Marchetto, M., Bardy, C., and Gage, F. (2016). Evaluating cell reprogramming, differentiation and conversion technologies in neuroscience. *Nat. Rev. Neurosci.* 17, 424–437. doi: 10.1038/nrn.2016.46
- Mertens, J., Paquola, A., Ku, M., Hatch, E., Böhnke, L., Ladjevardi, S., et al. (2015). Directly reprogrammed human neurons retain aging-associated transcriptomic

signatures and reveal age-related nucleocytoplasmic defects. *Cell Stem Cell* 17, 705–718. doi: 10.1016/j.stem.2015.09.001

Mertens, J., Reid, D., Lau, S., Kim, Y., and Gage, F. (2018). Aging in a dish: iPSC-derived and directly induced neurons for studying brain aging and age-related neurodegenerative diseases. *Annu. Rev. Genet.* 52, 271–293. doi: 10.1146/annurev-genet-120417-031534

Miller, J., Ganat, Y., Kishinevsky, S., Bowman, R., Liu, B., Tu, E., et al. (2013). Human iPSC-based modeling of late-onset disease via progerin-induced aging. *Cell Stem Cell* 13, 691–705. doi: 10.1016/j.stem.2013.11.006

Mo, Y., Tang, L., Ma, Y., and Wu, S. (2016). Pramipexole pretreatment attenuates myocardial ischemia/reperfusion injury through upregulation of autophagy. *Biochem. Biophys. Res. Commun.* 473, 1119–1124. doi: 10.1016/j.bbrc.2016.04.026

Moors, T., Paciotti, S., Chiasserini, D., Calabresi, P., Parnetti, L., Beccari, T., et al. (2016). Lysosomal dysfunction and α -synuclein aggregation in Parkinson's disease: Diagnostic links. *Mov. Disord.* 31, 791–801. doi: 10.1002/mds.26562

Mullin, S., Smith, L., Lee, K., D'Souza, G., Woodgate, P., Elflein, J., et al. (2020). Amroxol for the Treatment of patients with Parkinson disease with and without glucocerebrosidase gene mutations: A nonrandomized, noncontrolled trial. *JAMA Neurol.* 77, 427–434. doi: 10.1001/jamaneuro.2019.4611

Nakajima, T., Suzuki, Y., and Miyaue, N. (2021). Successful management of Parkinson's disease dyskinesia during local anesthesia with dexmedetomidine. *Cureus* 13:e13739. doi: 10.7759/cureus.13739

Navarro Negredo, P., Yeo, R., and Brunet, A. (2020). Aging and rejuvenation of neural stem cells and their niches. *Cell Stem Cell* 27, 202–223. doi: 10.1016/j.stem.2020.07.002

Nekrasov, E. D., Vigont, V., Klyushnikov, S., Lebedeva, O., Vassina, E., Bogomazova, A., et al. (2016). Manifestation of Huntington's disease pathology in human induced pluripotent stem cell-derived neurons. *Mol. Neurodegener.* 11:27. doi: 10.1186/s13024-016-0092-5

Nelson, T., Sun, M., Lim, C., Sen, A., Khan, T., Chirila, F., et al. (2017). Bryostatins effects on cognitive function and PKC β in Alzheimer's disease phase IIA and expanded access trials. *J. Alzheimers Dis.* 58, 521–535. doi: 10.3233/JAD-170161

Nilsson, P., Loganathan, K., Sekiguchi, M., Matsuba, Y., Hui, K., Tsubuki, S., et al. (2013). A β secretion and plaque formation depend on autophagy. *Cell Rep.* 5, 61–69. doi: 10.1016/j.celrep.2013.08.042

Nixon, R., Wegiel, J., Kumar, A., Yu, W., Peterhoff, C., Cataldo, A., et al. (2005). Extensive involvement of autophagy in Alzheimer disease: An immuno-electron microscopy study. *J. Neuropathol. Exp. Neurol.* 64, 113–122. doi: 10.1093/jnen/64.2.113

Nnah, I., Wang, B., Saqena, C., Weber, G., Bonder, E., Bagley, D., et al. (2019). TFEb-driven endocytosis coordinates MTORC1 signaling and autophagy. *Autophagy* 15, 151–164. doi: 10.1080/15548627.2018.1511504

Noguchi, M., Hirata, N., Tanaka, T., Suizu, F., Nakajima, H., and Chiorini, J. (2020). Autophagy as a modulator of cell death machinery. *Cell Death Dis.* 11:517. doi: 10.1038/s41419-020-2724-5

O'Bryant, S., Zhang, F., Petersen, M., Johnson, L., Hall, J., and Rissman, R. A. (2021). Precision medicine approach to treating Alzheimer's disease using rosiglitazone therapy: A biomarker analysis of the REFLECT trials. *J. Alzheimers Dis.* 81, 557–568. doi: 10.3233/JAD-201610

Oh, J., Lee, J., and Lee, Y. (2019). Evaluation of the Mrp2-mediated flavonoid-drug interaction potential of quercetin in rats and in vitro models. *Asian J. Pharm. Sci.* 14, 621–630. doi: 10.1016/j.ajps.2018.12.003

Oh, Y., Lee, S., Kim, W., Chen, S., Church, V., Cates, K., et al. (2022). Age-related Huntington's disease progression modeled in directly reprogrammed patient-derived striatal neurons highlights impaired autophagy. *Nat. Neurosci.* 25, 1420–1433. doi: 10.1038/s41593-022-01185-4

Ohta, E., Nihira, T., Uchino, A., Imaizumi, Y., Okada, Y., Akamatsu, W., et al. (2015). I2020T mutant LRRK2 iPSC-derived neurons in the Sagamihara family exhibit increased Tau phosphorylation through the AKT/GSK-3 β signaling pathway. *Hum. Mol. Genet.* 24, 4879–4900. doi: 10.1093/hmg/ddv212

Ondo, W., Mejia, N., and Hunter, C. B. (2007). A pilot study of the clinical efficacy and safety of memantine for Huntington's disease. *Parkinsonism Relat. Disord.* 13, 453–454. doi: 10.1016/j.parkrel.2006.08.005

Park, J., Kim, H., Moon, H., Park, B., Park, J., Sim, W., et al. (2021). Human cardiac stem cells rejuvenated by modulating autophagy with MHY-1685 enhance the therapeutic potential for cardiac repair. *Exp. Mol. Med.* 53, 1423–1436. doi: 10.1038/s12276-021-00676-x

Patricio, F., Morales-Andrade, A., Patricio-Martínez, A., and Limón, I. (2020). Cannabidiol as a therapeutic target: Evidence of its neuroprotective and neuromodulatory function in Parkinson's Disease. *Front. Pharmacol.* 11:595635. doi: 10.3389/fphar.2020.595635

Perera, N., Sheean, R., Lau, C., Shin, Y., Beart, P., Horne, M., et al. (2018). Rilmenidine promotes MTOR-independent autophagy in the mutant SOD1 mouse model of amyotrophic lateral sclerosis without slowing disease progression. *Autophagy* 14, 534–551. doi: 10.1080/15548627.2017.1385674

Perera, N., Tomas, D., Wanniarachchilage, N., Cuic, B., Luikinga, S., Rytova, V., et al. (2021). Stimulation of mTOR-independent autophagy and mitophagy by rilmenidine exacerbates the phenotype of transgenic TDP-43 mice. *Neurobiol. Dis.* 154:105359. doi: 10.1016/j.nbd.2021.105359

Pirces, K., Drouin-Ouellet, J., Horváth, V., Gil, J., Rezeli, M., Garza, R., et al. (2022). Distinct subcellular autophagy impairments in induced neurons from patients with Huntington's disease. *Brain* 145, 3035–3057. doi: 10.1093/brain/awab473

Pirces, K., Petri, R., Madsen, S., Brattås, P., Vuono, R., Ottosson, D., et al. (2018). Huntingtin aggregation impairs autophagy, leading to argonaute-2 accumulation and global MicroRNA dysregulation. *Cell Rep.* 24, 1397–1406. doi: 10.1016/j.celrep.2018.07.017

Poewe, W., Seppi, K., Tanner, C., Halliday, G., Brundin, P., Volkmann, J., et al. (2017). Parkinson disease. *Nat. Rev. Dis. Primers* 3:17013. doi: 10.1038/nrdp.2017.13

Potter, H., Woodcock, J., Boyd, T., Coughlan, C., O'Shaughnessy, J., Borges, M., et al. (2021). Safety and efficacy of sargramostim (GM-CSF) in the treatment of Alzheimer's disease. *Alzheimers Dement. (N. Y.)* 7:e12158. doi: 10.1002/trc2.12158

Prajumwongs, P., Weerananantapan, O., Jaroonsitichawan, T., and Noisa, P. (2016). Human embryonic stem cells: A model for the study of neural development and neurological diseases. *Stem Cells Int.* 2016:2958210. doi: 10.1155/2016/2958210

Ramachandran, S., and Srivastava, S. K. (2021). Abstract LB184: Induction of ulk1 regulated autophagy by a novel antipsychotic drug leads to apoptosis in pancreatic cancer cells. *Cancer Res.* 81:LB184.

Ramachandran, S., Kaushik, I., and Srivastava, S. (2021). Pimavanserin: A novel autophagy modulator for pancreatic cancer treatment. *Cancers (Basel)* 13:5661. doi: 10.3390/cancers13225661

Rando, T., and Chang, H. (2012). Aging, rejuvenation, and epigenetic reprogramming: Resetting the aging clock. *Cell* 148, 46–57. doi: 10.1016/j.cell.2012.01.003

Ravina, B., Putt, M., Siderowf, A., Farrar, J., Gillespie, M., Crawley, A., et al. (2005). Donepezil for dementia in Parkinson's disease: A model for the study of neural blind, placebo controlled, crossover study. *J. Neurol. Neurosurg. Psychiatry* 76, 934–939. doi: 10.1136/jnnp.2004.050682

Reddy, K., Cusack, C., Nnah, I., Khayati, K., Saqena, C., Huynh, T., et al. (2016). Dysregulation of nutrient sensing and CLEARance in presenilin deficiency. *Cell Rep.* 14, 2166–2179. doi: 10.1016/j.celrep.2016.02.006

Reichmann, H., Brecht, M., Köster, J., Kraus, P., and Lemke, M. (2003). Pramipexole in routine clinical practice: A prospective observational trial in Parkinson's disease. *CNS Drugs* 17, 965–973. doi: 10.2165/00023210-200317130-00003

Reinhardt, P., Schmid, B., Burbulla, L., Schöndorf, D., Wagner, L., Glatza, M., et al. (2013). Genetic correction of a LRRK2 mutation in human iPSCs links parkinsonian neurodegeneration to ERK-dependent changes in gene expression. *Cell Stem Cell* 12, 354–367. doi: 10.1016/j.stem.2013.01.008

Rose, C., Menzies, F., Renna, M., Acevedo-Aroza, A., Corrochano, S., Sadiq, O., et al. (2010). Rilmenidine attenuates toxicity of polyglutamine expansions in a mouse model of Huntington's disease. *Hum. Mol. Genet.* 19, 2144–2153. doi: 10.1093/hmg/ddq093

Rozet, I., Muangman, S., Vavilala, M., Lee, L., Souter, M., Domino, K., et al. (2006). Clinical experience with dexmedetomidine for implantation of deep brain stimulators in Parkinson's disease. *Anesth. Analg.* 103, 1224–1228. doi: 10.1213/01.ane.0000239331.53085.94

Rui, Q., Ni, H., Li, D., Gao, R., and Chen, G. (2018). The role of LRRK2 in neurodegeneration of parkinson disease. *Curr. Neuropharmacol.* 16, 1348–1357. doi: 10.2174/1570159X16666180222165418

Sánchez-Danés, A., Richaud-Patin, Y., Carballo-Carbajal, I., Jiménez-Delgado, S., Caig, C., Mora, S., et al. (2012). Disease-specific phenotypes in dopamine neurons from human iPS-based models of genetic and sporadic Parkinson's disease. *EMBO Mol. Med.* 4, 380–395. doi: 10.1002/emmm.201200215

Sapp, E., Schwarz, C., Chase, K., Bhide, P., Young, A., Penney, J., et al. (1997). Huntingtin localization in brains of normal and Huntington's disease patients. *Ann. Neurol.* 42, 604–612. doi: 10.1002/ana.410420411

Schöndorf, D., Aureli, M., McAllister, F., Hindley, C., Mayer, F., Schmid, B., et al. (2014). iPSC-derived neurons from GBA1-associated Parkinson's disease patients show autophagic defects and impaired calcium homeostasis. *Nat. Commun.* 5:4028. doi: 10.1038/ncomms5028

Schumann-Werner, B., Dogan, I., Mirzazade, S., Mall, B., Overbeck, R., Honrath, P., et al. (2021). Clinical predictors and neural correlates for compromised swallowing safety in Huntington disease. *Eur J Neurol.* 28, 2855–2862. doi: 10.1111/ene.14953

Sen, A., Akinola, M., Tai, X., Symmonds, M., Davis Jones, G., Mura, S., et al. (2021). An investigation of levetiracetam in Alzheimer's disease (ILIAD): A double-blind, placebo-controlled, randomised crossover proof of concept study. *Trials* 22:508. doi: 10.1186/s13063-021-05404-4

Shibata, M., Lu, T., Furuya, T., Degterev, A., Mizushima, N., Yoshimori, T., et al. (2006). Regulation of intracellular accumulation of mutant Huntingtin by Beclin 1. *J. Biol. Chem.* 281, 14474–14485. doi: 10.1074/jbc.M600364200

- Shrigley, S., Piracs, K., Barker, R., Parmar, M., and Drouin-Ouellet, J. (2018). Simple generation of a high yield culture of induced neurons from human adult skin fibroblasts. *J. Vis. Exp.* 132:56904. doi: 10.3791/56904
- Singh, S., Srivastava, A., Srivastava, P., Dhuriya, Y., Pandey, A., Kumar, D., et al. (2016). Advances in stem cell research- a ray of hope in better diagnosis and prognosis in neurodegenerative diseases. *Front. Mol. Biosci.* 3:72. doi: 10.3389/fmolb.2016.00072
- Soldner, F., Hockemeyer, D., Beard, C., Gao, Q., Bell, G., Cook, E., et al. (2009). Parkinson's disease patient-derived induced pluripotent stem cells free of viral reprogramming factors. *Cell* 136, 964–977. doi: 10.1016/j.cell.2009.02.013
- Srinivasan, S., Tampi, R., Balaram, K., and Kapoor, A. (2020). Pimavanserin for the treatment of psychosis in Alzheimer's disease: A literature review. *World J. Psychiatry* 10, 162–174. doi: 10.5498/wjpv.10.17.162
- Steg, L., Shireby, G., Imm, J., Davies, J., Franklin, A., Flynn, R., et al. (2021). Novel epigenetic clock for fetal brain development predicts prenatal age for cellular stem cell models and derived neurons. *Mol. Brain* 14:98. doi: 10.1186/s13041-021-00810-w
- Su, Y., and Qi, X. (2013). Inhibition of excessive mitochondrial fission reduced aberrant autophagy and neuronal damage caused by LRRK2 G2019S mutation. *Hum. Mol. Genet.* 22, 4545–4561. doi: 10.1093/hmg/ddt301
- Suhr, S., Chang, E., Tjong, J., Alcasid, N., Perkins, G., Goissis, M., et al. (2010). Mitochondrial rejuvenation after induced pluripotency. *PLoS One* 5:e14095. doi: 10.1371/journal.pone.0014095
- Sun, Y., Ji, X., Mao, X., Xie, L., Jia, J., Galvan, V., et al. (2014). Differential activation of mTOR complex 1 signaling in human brain with mild to severe Alzheimer's disease. *J. Alzheimers Dis.* 38, 437–444. doi: 10.3233/JAD-131124
- Tabibzadeh, S. (2023). Role of autophagy in aging: The good, the bad, and the ugly. *Aging Cell* 22:e13753. doi: 10.1111/acel.13753
- Tan, Y., Xu, X., Dai, J., Yin, Y., He, X., Zhang, Y., et al. (2021). Melatonin induces the rejuvenation of long-term ex vivo expanded periodontal ligament stem cells by modulating the autophagic process. *Stem Cell Res. Ther.* 12:254. doi: 10.1186/s13287-021-02322-9
- Tang, B. (2014). mTOR, autophagy, and reprogramming. *Front. Cell Dev. Biol.* 1:4. doi: 10.3389/fcell.2013.00004
- Tang, Y., Liu, M., Zang, T., and Zhang, C. (2017). Direct Reprogramming rather than iPSC-based reprogramming maintains aging hallmarks in human motor neurons. *Front. Mol. Neurosci.* 10:359. doi: 10.3389/fnmol.2017.00359
- Tanji, K., Mori, F., Kakita, A., Takahashi, H., and Wakabayashi, K. (2011). Alteration of autophagosomal proteins (LC3, GABARAP and GATE-16) in lewy body disease. *Neurobiol. Dis.* 43, 690–697. doi: 10.1016/j.nbd.2011.05.022
- Torrent, R., De Angelis Rigotti, F., Dell'Era, P., Memo, M., Raya, A., and Consiglio, A. (2015). Using iPSC cells toward the understanding of Parkinson's disease. *J. Clin. Med.* 4, 548–566. doi: 10.3390/jcm4040548
- Torti, M., Vacca, L., and Stocchi, F. (2018). Istradefylline for the treatment of Parkinson's disease: Is it a promising strategy? *Expert. Opin. Pharmacother.* 19, 1821–1828. doi: 10.1080/14656566.2018.1524876
- Ubina, T., Magallanes, M., Srivastava, S., Warden, C., Yee, J., and Salvaterra, P. M. A. (2019). Human embryonic stem cell model of A β -dependent chronic progressive neurodegeneration. *Front. Neurosci.* 13:1007. doi: 10.3389/fnins.2019.01007
- Underwood, B., Green-Thompson, Z., Pugh, P., Lazic, S., Mason, S., Griffin, J., et al. (2017). An open-label study to assess the feasibility and tolerability of rilmenidine for the treatment of Huntington's disease. *J. Neurol.* 264, 2457–2463. doi: 10.1007/s00415-017-8647-0
- Vangipuram, M., Ting, D., Kim, S., Diaz, R., and Schüle, B. (2013). Skin punch biopsy explant culture for derivation of primary human fibroblasts. *J. Vis. Exp.* 77, e3779. doi: 10.3791/3779
- Vanhuuwaert, R., Kuenen, S., Masius, R., Bademosi, A., Manetsberger, J., Schoovaerts, N., et al. (2017). The SAC1 domain in synaptotagmin is required for autophagosome maturation at presynaptic terminals. *EMBO J.* 36, 1392–1411. doi: 10.15252/embj.201695773
- Vera, E., Bosco, N., and Studer, L. (2016). Generating late-onset human iPSC-based disease models by inducing neuronal age-related phenotypes through telomerase manipulation. *Cell Rep.* 17, 1184–1192. doi: 10.1016/j.celrep.2016.09.062
- Verheyen, A., Diels, A., Dijkmans, J., Oyelami, T., Meneghello, G., Mertens, L., et al. (2015). Using human iPSC-derived neurons to model TAU aggregation. *PLoS One* 10:e0146127. doi: 10.1371/journal.pone.0146127
- Victor, M., Richner, M., Olsen, H., Lee, S., Monteys, A., Ma, C., et al. (2018). Striatal neurons directly converted from Huntington's disease patient fibroblasts recapitulate age-associated disease phenotypes. *Nat. Neurosci.* 21, 341–352. doi: 10.1038/s41593-018-0075-7
- Vossel, K., Ranasinghe, K., Beagle, A., La, A., Ah Pook, K., Castro, M., et al. (2021). Effect of levetiracetam on cognition in patients with Alzheimer disease with and without epileptiform activity: A randomized clinical trial. *JAMA Neurol.* 78, 1345–1354. doi: 10.1001/jamaneurol.2021.3310
- Vucicevic, L., Misirkic, M., Ciric, D., Martinovic, T., Jovanovic, M., Isakovic, A., et al. (2020). Transcriptional block of AMPK-induced autophagy promotes glutamate excitotoxicity in nutrient-deprived SH-SY5Y neuroblastoma cells. *Cell Mol. Life Sci.* 77, 3383–3399. doi: 10.1007/s00018-019-03356-2
- Wang, S., Wu, H., Yasui, Y., Geva, M., Hayden, M., Maurice, T., et al. (2023). Nucleoporin POM121 signals TFEB-mediated autophagy via activation of SIGMAR1/sigma-1 receptor chaperone by pridopidine. *Autophagy* 19, 126–151. doi: 10.1080/15548627.2022.2063003
- Wang, S., Xia, P., Ye, B., Huang, G., Liu, J., and Fan, Z. (2013). Transient activation of autophagy via Sox2-mediated suppression of mTOR is an important early step in reprogramming to pluripotency. *Cell Stem Cell* 13, 617–625. doi: 10.1016/j.stem.2013.10.005
- Wang, Y., Liu, Z., Shu, S., Cai, J., Tang, C., and Dong, Z. (2020). AMPK/mTOR Signaling in autophagy regulation during cisplatin-induced acute kidney injury. *Front. Physiol.* 11:619730. doi: 10.3389/fphys.2020.619730
- Warner, C., Ottman, A., and Brown, J. (2018). The role of atomoxetine for parkinson disease-related executive dysfunction: A systematic review. *J. Clin. Psychopharmacol.* 38, 627–631. doi: 10.1097/JCP.0000000000000963
- Wilkinson, D., Windfeld, K., and Colding-Jørgensen, E. (2014). Safety and efficacy of idalopirdine, a 5-HT6 receptor antagonist, in patients with moderate Alzheimer's disease (LADDER): A randomised, double-blind, placebo-controlled phase 2 trial. *Lancet Neurol.* 13, 1092–1099. doi: 10.1016/S1474-4422(14)70198-X
- Wu, P., Fann, M., Tran, T., Chen, S., Devina, T., Cheng, I., et al. (2019). Assessing the therapeutic potential of *Graptopetalum paraguayense* on Alzheimer's disease using patient iPSC-derived neurons. *Sci. Rep.* 9:19301. doi: 10.1038/s41598-019-55614-9
- Yang, L., Rozenfeld, R., Wu, D., Devi, L., Zhang, Z., and Cederbaum, A. (2014). Cannabidiol protects liver from binge alcohol-induced steatosis by mechanisms including inhibition of oxidative stress and increase in autophagy. *Free Radic. Biol. Med.* 68, 260–267. doi: 10.1016/j.freeradbiomed.2013.12.026
- Yang, Y., Jiao, J., Gao, R., Le, R., Kou, X., Zhao, Y., et al. (2015). Enhanced rejuvenation in induced pluripotent stem cell-derived neurons compared with directly converted neurons from an aged mouse. *Stem Cells Dev.* 24, 2767–2777. doi: 10.1089/scd.2015.0137
- Yu, T., Liu, D., Gao, M., Yang, P., Zhang, M., Song, F., et al. (2019). Dexmedetomidine prevents septic myocardial dysfunction in rats via activation of α 7nAChR and PI3K/Akt-mediated autophagy. *Biomed. Pharmacother.* 120:109231. doi: 10.1016/j.biopha.2019.109231
- Zachari, M., and Ganley, I. (2017). The mammalian ULK1 complex and autophagy initiation. *Essays Biochem.* 61, 585–596. doi: 10.1042/EBC20170021
- Zhang, N., An, M., Montoro, D., and Ellerby, L. (2010). Characterization of human Huntington's disease cell model from induced pluripotent stem cells. *PLoS Curr.* 2:RRN1193. doi: 10.1371/currents.RRN1193
- Zhang, X., Chen, S., Huang, K., and Le, W. (2013). Why should autophagic flux be assessed? *Acta Pharmacol. Sin.* 34, 595–599. doi: 10.1038/aps.2012.184
- Zhang, X., Wen, X., Al-Ramahi, I., Botas, J., Lu, B., and Fu, Y. (2022). Inhibition of HIPK3 by AST487 Ameliorates Mutant HTT-Induced Neurotoxicity and Apoptosis via Enhanced Autophagy. *Neurosci Bull.* 38, 99–103. doi: 10.1007/s12264-021-00783-9
- Zhao, M., Sun, L., Yu, X., Miao, Y., Liu, J., Wang, H., et al. (2013). Acetylcholine mediates AMPK-dependent autophagic cytoprotection in H9c2 cells during hypoxia/reoxygenation injury. *Cell Physiol. Biochem.* 32, 601–613. doi: 10.1159/000354464
- Zheng, X., Zhang, H., Lv, Y., Jin, F., Wu, X., Zhu, J., et al. (2022). Levetiracetam alleviates cognitive decline in Alzheimer's disease animal model by ameliorating the dysfunction of the neuronal network. *Front. Aging Neurosci.* 14:888784. doi: 10.3389/fnagi.2022.888784
- Zhu, J., Guo, F., Shelburne, J., Watkins, S., and Chu, C. (2003). Localization of phosphorylated ERK/MAP kinases to mitochondria and autophagosomes in Lewy body diseases. *Brain Pathol.* 13, 473–481. doi: 10.1111/j.1750-3639.2003.tb00478.x
- Zhu, L., Dong, C., Sun, C., Ma, R., Yang, D., Zhu, H., et al. (2015). Rejuvenation of MPTP-induced human neural precursor cell senescence by activating autophagy. *Biochem. Biophys. Res. Commun.* 464, 526–533. doi: 10.1016/j.bbrc.2015.06.174
- Zhu, L., Sun, C., Ren, J., Wang, G., Ma, R., Sun, L., et al. (2019). Stress-induced precocious aging in PD-patient iPSC-derived NSCs may underlie the pathophysiology of Parkinson's disease. *Cell Death Dis.* 10:105. doi: 10.1038/s41419-019-13



OPEN ACCESS

EDITED BY
Shani Stern,
University of Haifa,
Israel

REVIEWED BY
Consuelo Morgado-Valle,
Universidad Veracruzana,
Mexico
Mark Wagshul,
Albert Einstein College of Medicine,
United States

*CORRESPONDENCE
Rui Chen
✉ chenrui@goodat126.com

[†]These authors have contributed equally to this work and share first authorship

SPECIALTY SECTION
This article was submitted to
Cellular and Molecular Mechanisms of Brain-aging,
a section of the journal
Frontiers in Aging Neuroscience

RECEIVED 05 November 2022
ACCEPTED 10 March 2023
PUBLISHED 31 March 2023

CITATION
Wang J, Li Y, Ji L, Su T, Cheng C, Han F, Cox DJ, Wang E and Chen R (2023) The complex interplay of hypoxia and sleep disturbance in gray matter structure alterations in obstructive sleep apnea patients.
Front. Aging Neurosci. 15:1090547.
doi: 10.3389/fnagi.2023.1090547

COPYRIGHT
© 2023 Wang, Li, Ji, Su, Cheng, Han, Cox, Wang and Chen. This is an open-access article distributed under the terms of the [Creative Commons Attribution License \(CC BY\)](#). The use, distribution or reproduction in other forums is permitted, provided the original author(s) and the copyright owner(s) are credited and that the original publication in this journal is cited, in accordance with accepted academic practice. No use, distribution or reproduction is permitted which does not comply with these terms.

The complex interplay of hypoxia and sleep disturbance in gray matter structure alterations in obstructive sleep apnea patients

Jing Wang^{1,2†}, Yezhou Li^{3†}, Lirong Ji⁴, Tong Su^{1,2},
Chaohong Cheng^{1,2}, Fei Han², Daniel J. Cox⁵, Erlei Wang⁴ and
Rui Chen^{1,2*}

¹Department of Respiratory, The Second Affiliated Hospital of Soochow University, Suzhou, China, ²Department of Sleeping Center, The Second Affiliated Hospital of Soochow University, Suzhou, China, ³School of Biological Sciences, University of Manchester, Manchester, United Kingdom, ⁴Department of Radiology, The Second Affiliated Hospital of Soochow University, Suzhou, China, ⁵Division of Psychology, Communication, and Human Neuroscience, School of Health Sciences, Faculty of Biology, Medicine and Health, University of Manchester, Manchester, United Kingdom

Background: Obstructive Sleep Apnea (OSA) characteristically leads to nocturnal hypoxia and sleep disturbance. Despite clear evidence of OSA-induced cognitive impairments, the literature offers no consensus on the relationship between these pathophysiological processes and brain structure alterations in patients.

Objective: This study leverages the robust technique of structural equation modeling to investigate how hypoxia and sleep disturbance exert differential effects on gray matter structures.

Methods: Seventy-four Male participants were recruited to undergo overnight polysomnography and T1-weighted Magnetic Resonance Imaging. Four structural outcome parameters were extracted, namely, gray matter volume, cortical thickness, sulcal depth, and fractal dimension. Structural equation models were constructed with two latent variables (hypoxia, and sleep disturbance) and three covariates (age, body mass index, and education) to examine the association between gray matter structural changes in OSA and the two latent variables, hypoxia and sleep disturbance.

Results: The structural equation models revealed hypoxia-associated changes in diverse regions, most significantly in increased gray matter volume, cortical thickness and sulcal depth. In contrast, sleep disturbance. Was shown to be largely associated with reduce gray matter volume and sulcal depth.

Conclusion: This study provides new evidence showing significant effects of OSA-induced hypoxia and sleep disturbance on gray matter volume and morphology in male patients with obstructive sleep apnea. It also demonstrates the utility of robust structural equation models in examining obstructive sleep apnea pathophysiology.

KEYWORDS

obstructive sleep apnea, hypoxia, sleep disturbance, gray matter, structural equation models

1. Introduction

Obstructive sleep apnea (OSA) is a highly prevalent multisystem chronic disease, which predisposes patients to diseases including hypertension, diabetes mellitus, stroke, emotional disorders and cognitive impairments such as memory and attention deficits (Chen et al., 2011; Rosenzweig et al., 2015; Benjafield et al., 2019; Bubu et al., 2020; Gottlieb and Punjabi, 2020). The main characteristic of OSA is the repetitive airway collapse, partially reducing or completely blocking the pharyngeal airflow despite respiratory efforts leading to chronic intermittent hypoxia (Dewan et al., 2015). Frequent blocking also may lead to sleep disturbance, manifested by a decrease in the deeper stages of sleep.

Neuroimaging studies have shown that OSA may be associated with gray matter structural alterations. A meta-analysis revealed a clear decrease in gray matter volume (GMV) in middle aged untreated patients with OSA (Shi et al., 2017). However, recently, using more advanced neuroimaging measures, Baril et al. (2017) found a consistent positive relationship between markers of OSA severity (hypoxemia, respiratory disturbances, and sleep structure alteration) and gray matter hypertrophy and thickening, while another large sample study observed lower mean oxygen saturation during sleep was associated with atrophy of both cortical and subcortical brain areas (Marchi et al., 2020). Furthermore, Cross et al. (2018) and his colleagues reported more complex results, that is, hypoxia metrics were shown to be associated with decreased cortical thickness, while sleep disturbance with increased thickness. Although researchers have posited the presence of two counteracting mechanisms (One may indicate cellular damage, while the other may reflect transitory responses) to account for these seemingly contradictory results (Baril et al., 2021), no consensus on the exact pattern of OSA-induced gray matter changes can be drawn from the current literature (Baril et al., 2017; Cross et al., 2018; André et al., 2020; Marchi et al., 2020).

To characterize OSA severity, previous studies often used individual polysomnographic parameters (e.g., apnea-hypopnea index (AHI), mean oxygen saturation) to examine OSA-related gray matter changes. However, such single-parameter analyses are prone to producing spurious results due to the measurement error. Structural equation modeling (SEM) could be used to model the complex relationship between multiple inter-dependent variables in a multi-level variable structure. It permits the exploration of complex relationships among a number of potentially inter-dependent variables (Bentler and Stein, 1992). In the context of this study, using the SEM model accounts for and even takes advantage of the collinearity between variables by extracting the covariance between related variables as physiologically meaningful latent variables. Moreover, it allows for a more principled analysis of the OSA pathophysiological processes, as well as their potentially differential effects on the OSA brain.

Despite the popularity of GMV, it is a coarse measure that captures both a region's surface area and cortical thickness, which might convey distinct pathophysiological implications (Fornito et al., 2008; Winkler et al., 2010). Therefore, the current study also included the use of Surface-Based Morphometry (SBM) to provide measures of cortical thickness and surface complexity. To quantify cortical complexity, fractal dimension (FD) utilizes the concepts of fractals to characterize the nested and hierarchical structures of the

brain (Madan and Kensinger, 2016). Sulcal depth (SD), defined as the Euclidean distance between the central surface and an imaginary convex hull encompassing the surface mesh, has been shown to change significantly in various patient groups such as Parkinson's disease (Wang et al., 2021). To our knowledge, there have not been studies investigating the cortical complexity in the OSA population.

In this study, we constructed an SEM model consisting of two latent variables—hypoxia and sleep disturbance, to examine the effects of these two physiological factors on gray matter structure. Based on previous studies, we hypothesize that there may be a mixture of effects for both hypoxia and sleep disturbance in affecting different regions of the OSA brain.

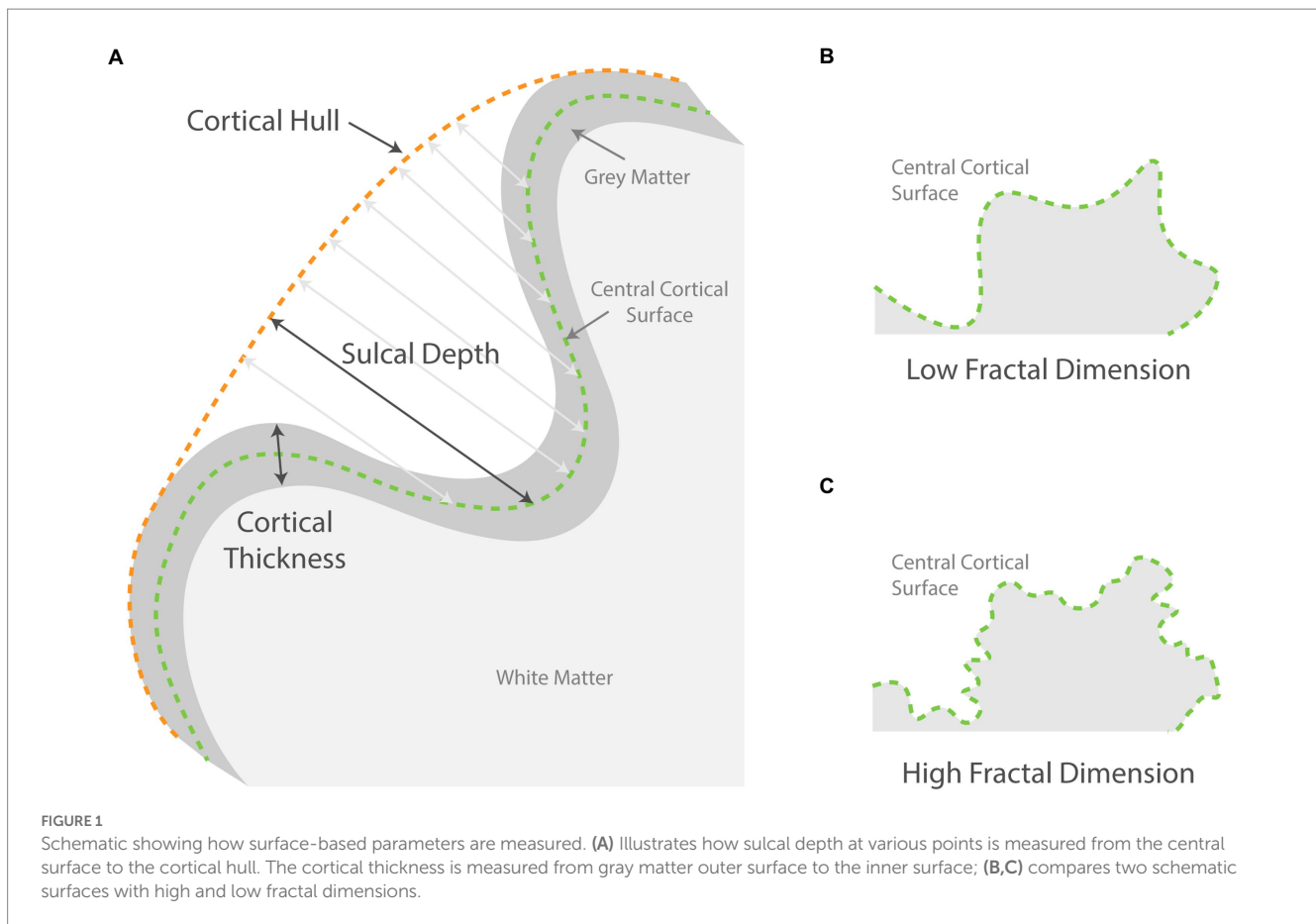
2. Participants and methods

2.1. Participants

This prospective study recruited 74 patients who presented with a primary complaint of snoring and were formally diagnosed with OSA at the sleep center of the Second Affiliated Hospital of Soochow University from August 2020 to September 2021. The OSA diagnosis was confirmed by polysomnography (PSG) with an AHI ≥ 5 (Kapur et al., 2017). Participants were between 25 to 60 years old (median age = 39 years, SD = 9.6 years). In terms of participant genders, as previous large-sample studies found that the clinical phenotype of female patients with OSA differs from that of male patients (Basoglu and Tasbakan, 2018; Bonsignore et al., 2019). Moreover, another study found more severe OSA-related white matter tract damages in female patients than their male counterparts with similar OSA severity (Macey et al., 2012). Therefore, given that OSA is a significantly male-dominant disorder (Young et al., 1993; Franklin and Lindberg, 2015; Theorell-Haglöw et al., 2018) and that the anticipated extent of gray matter structural change is small, the present study chose to include only male patients to reduce sample heterogeneity. Participants with a history of neurological, respiratory, or other medical conditions that might affect sleep were excluded. The participants gave informed consent, and the study protocol was approved by the Research Ethics Committee of the Second Affiliated Hospital of Soochow University, Suzhou, China (JD-LK-2018-004-02).

2.2. PSG

The participants underwent overnight, supervised, laboratory-based video polysomnography (PSG) using the Compumedics Grael multifunctional PSG monitoring system. Sleep staging and sleep-related respiratory analyses were scored manually by registered technician according to the AASM scoring criteria (Kapur et al., 2017). Apnea was defined as any airflow reduction greater than 90% that lasted longer than 10 s. Hypopnea was defined as $>3\%$ desaturation from pre-event baseline or arousal. The AHI was defined as the sum of the number of apnea and hypopnea per hour of sleep. Other measures included total sleep time (TST), sleep efficiency (SE), oxygen desaturation index (ODI), proportion of sleep time with $\text{SaO}_2 < 90\%$ (T90), minimum pulse oxygen saturation (MinSaO₂), arousal index, and proportions of each sleep stage.



2.3. MRI

Magnetic Resonance structural images were collected using a T1-weighted magnetization-prepared rapid-acquisition gradient echo (MPRAGE) sequence on a 3 T Siemens Prisma MRI scanner. The voxel size was $1.0 \times 1.0 \times 1.0 \text{ mm}^3$. The acquired structural MR images were bias-corrected, segmented, normalized, and 8 mm-smoothed using the Statistical Parametric Mapping (SPM12) toolbox¹ and the Computational Anatomy Toolbox (CAT12, neuro-jena.github.io/cat/; Theorell-Haglöw et al., 2018) in MatLab (MathWorks, 2020). The regional average gray matter volumes of a total of 142 ROIs were extracted for each subject using the neuromorphometrics atlas.

A separate CAT12 surface-based pipeline was used to produce a normalized surface mesh for each participant. Using the surface mesh, cortical thickness (Dahnke et al., 2013), sulcal depth, and fractal dimension were estimated (see Figure 1 for an illustration). The images of cortical thickness were smoothed using an isotropic Gaussian kernel of 15 mm and images of the complexity measures were smoothed using a kernel of 20 mm for the filter size to encompass both the sulcal fundus and gyral crown. Finally, mean values for cortical thickness, sulcal depth, and fractal dimension across the 72 surface ROIs were extracted using the Desikan-Killiany DK40 atlas (Desikan et al., 2006).

2.4. SEM

Two latent variables (hypoxia and sleep disturbance) were included in the SEM model (see Figure 2). Hypoxia combined three indicator (observed) variables: minSaO_2 , T90%, and ODI. The latter, sleep disturbance, was constructed from two negatively correlated indicator variables: proportion of sleep time in the NREM1&2 sleep and NREM3 sleep. It was decided that AHI should not be included as indicator variables as it is a measure of the apnea frequency, which is thus not directly measuring hypoxia or sleep disturbance. AHI also correlates strongly with indicator variables for both hypoxia and sleep disturbance, and thus its inclusion in the SEM model would lead to statistical difficulties in the model computations. The four ROI-based V/SBM measures were then entered individually into the SEM model as the outcome measure. Including the three covariates, age, body mass index (BMI), and education, the main regression equation for the SEM model was formulated as follows:

$$\text{Outcome Measure} \sim \text{Hypoxia} + \text{Sleep Disturbance} + \text{Age} + \text{BMI} + \text{Education}$$

where the Outcome Measure can be any of the $142 + 72 \times 3 = 358$ ROI-based parameter means. To account for the potential false discovery effect, p values were corrected using the Benjamini-Hochberg procedure. All statistical analyses apart from the MR image

¹ www.fil.ion.ucl.ac.uk/spm

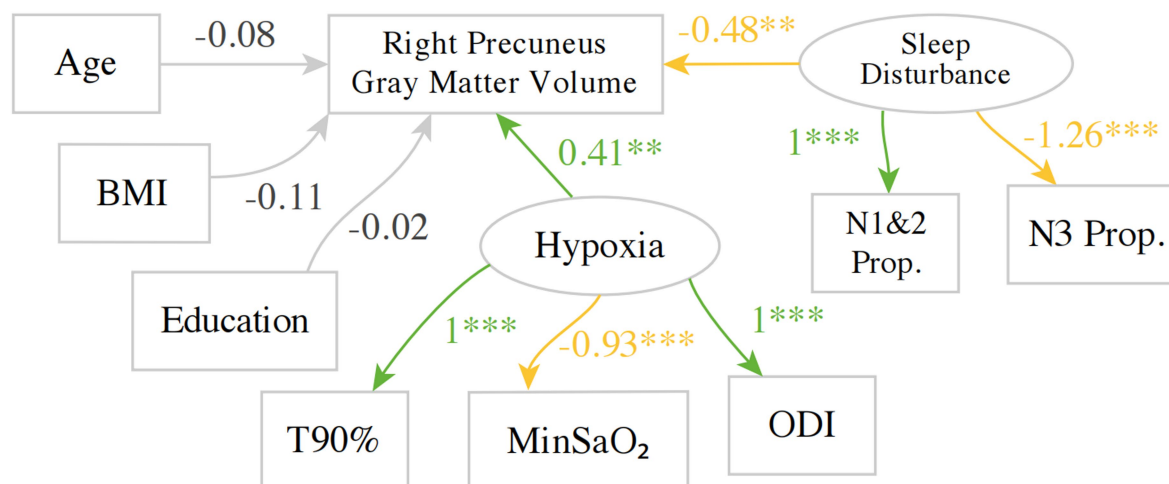


FIGURE 2

An example SEM model investigating the predictors for gray matter volume in the right precuneus. Green indicates a positive estimate, whereas yellow indicates a negative estimate. BMI, body mass index; T90%, Proportion Time with $\text{SaO}_2 < 90\%$; MinSaO₂, Minimum pulse oxygen saturation; ODI, oxygen desaturation index; N1&2P, NREM 1+2 Sleep Proportion; N3P, NREM3 Sleep Proportion. ** $p < 0.01$, *** $p < 0.001$.

TABLE 1 Descriptive characteristics of the study cohort (sample size=74).

	Values (N=74)	Skewness
Demography		
Age, years	39 (33, 43)	0.639
BMI, $\text{kg}\cdot\text{m}^{-2}$	26.4 (24.8, 28.6)	0.491
Hypertension	19 (26%)	1.09
Questionnaires		
ESS	8.0 (4.0, 11.8)	0.306
MOCA	27.0 (25.0, 29.0)	-0.432
Polysomnography		
Total sleep time, min	427 (386, 494)	0.043
Sleep efficiency, %	88 (83, 93)	-0.798
Latency to REM, min	88 (69, 114)	2.46
NREM 1 sleep, %	13 (7, 22)	1.22
NREM 2 sleep, %	54 (43, 59)	-0.176
NREM 1&2 sleep, %	67 (61, 75)	0.325
NREM 3 sleep, %	11 (6, 18)	0.046
REM Sleep, %	20.6 (17.7, 24.2)	-0.404
ODI, $\text{times}\cdot\text{h}^{-1}$	24 (11, 47)	0.617
AHI, $\text{times}\cdot\text{h}^{-1}$	32 (16, 51)	0.577
MinSaO ₂ , %	79 (69, 86)	-0.893
T90, %	4 (1, 18)	1.95
Arousal Index (Resp.), $\text{times}\cdot\text{h}^{-1}$	11 (4, 25)	1.38
Arousal Index (Spont.), $\text{times}\cdot\text{h}^{-1}$	5.9 (3.9, 9.1)	1.96

Values are display as median (Inter-quartile range). BMI, body mass index; ESS, Epworth Sleepiness Scale; MOCA, Montreal Cognitive Assessment; ODI, oxygen desaturation index; AHI, apnea-hypopnea index; MinSaO₂, Minimum pulse oxygen saturation; T90, Proportion Time with $\text{SaO}_2 < 90\%$; Resp., respiratory; Spont., spontaneous; Prop., proportion.

processing were carried out using the R statistical package (version 4.1.1).²

3. Results

3.1. Demographic, clinical, and sleep characteristics

Table 1 shows the clinical characteristics and PSG parameters of this study cohort. Patients with OSA exhibit hypoxia and sleep structural abnormalities as shown by PSG parameters. Data are represented by means and inter-quartile range (IQR).

3.2. SEM modeling

With regards to the hypoxia-related variables, the factor loading for T90% was set to 1 so that the implicit direction of the latent variable hypoxia aligns with T90% to aid interpretation, i.e., higher implicit values for hypoxia indicate more severe hypoxia. As expected, the factor loading for ODI is positive, as higher values of ODI indicate more severe hypoxia, whereas the factor loading for MinSaO₂ was negative. Similarly, the factor loading of NREM1&2 proportion was set to 1, whereas its negative correlate, NREM 3 proportion, was estimated to have a negative factor loading of -1.26.

A total of 357 other SEM models were fitted for each structural measure in each region defined by the neuroanatomical atlases, with multiple testing corrected for using False Discovery Rate (FDR). The principal results of the SEM models are shown in Figure 3 and Supplementary Table 1, where the estimates for two latent variables

² <http://link.springer.com/10.1007/978-3-540-74686-7>

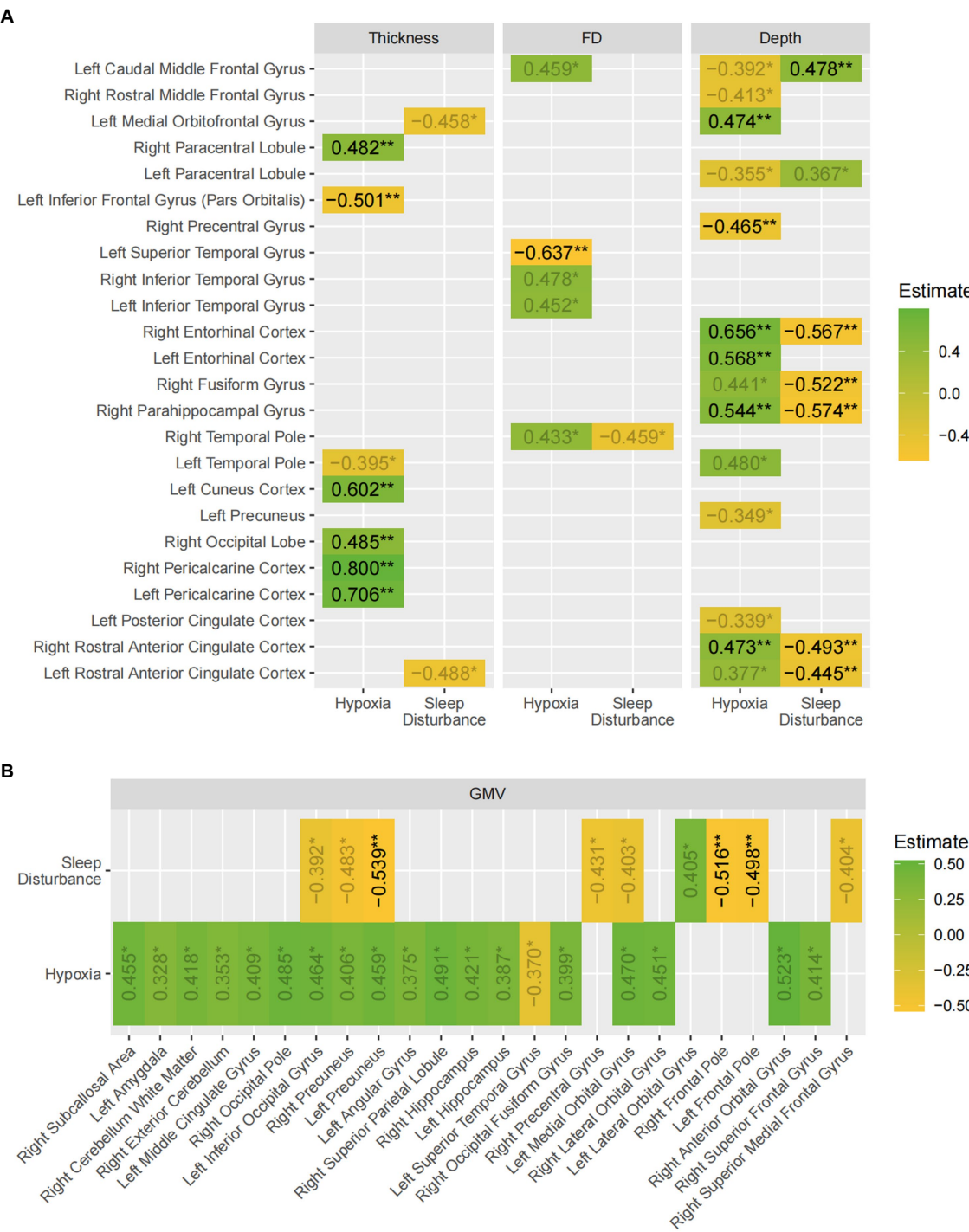


FIGURE 3
A summary of the findings of the SEM models. The values shown are the beta estimates for the latent variables, hypoxia and sleep disturbance (values with $0.01 < p < 0.05$ are displayed in gray). Green indicates a positive estimate, whereas yellow indicates a negative estimate. (A) Shows the results for the three surface-based measures; (B) shows the results for gray matter volume. The asterisks indicate false-discovery rates: * $p < 0.05$ ** $p < 0.01$.

regressing on the outcome measure in the main regression equation are shown alongside the FDRs. As an example, the estimates correspond to the two arrows pointing from Hypoxia and sleep disturbance to the gray matter volume of the right precuneus in Figure 2. The estimates for age were significant with $FDR < 0.05$ in 59 out of 358 (16.5%) of the SEM models and accounting for 57 out of 209

(27.3%) ROIs in the two atlases. The estimates for age were negative for 56 out of 57 SEM models. The estimates for the other regression terms, as well as covariance relations, were similar in magnitude and same in direction as the values shown in Figure 2. Overall, the results demonstrated widespread gray matter volume and sulcal depth differences in multiple brain regions of the frontal,

parietal, and temporal lobe with hypoxia exerting statistically significant effects in more regions than sleep disturbance. Moreover, the effect of hypoxia on most regions was positive where patients experiencing worse hypoxia paradoxically exhibited higher cortical thickness, complexity, and gray matter volume. However, in most cases, the positive effects hypoxia exerted on the regions were balanced, if not inverted by the effects of sleep disturbance, as shown by the larger regression estimates for sleep disturbance in most regions with both latent variables showing significant effects.

4. Discussion

OSA has been known to be associated with changes in the central nervous system, leading to various cognitive impairments. For the first time, structural equation modeling (SEM) was used to analyze the effects of OSA-related hypoxia and sleep structure disruption on gray matter volume, cortical thickness, sulcal depth, and fractal dimension. The main findings of the study can be summarized as: (1) OSA exerted widespread effects on gray matter structures, and the effects were most prominent for sulcal depth and gray matter volume; (2) Overall, hypoxia tends to be associated with gray matter hypertrophy, while sleep disturbance bring about more gray matter atrophy.

In the present study, age, BMI and education were included as covariates. It is widely accepted that the brain shrinks in volume even in healthy aging, most prominently in the frontal and temporal cortex, putamen, and thalamus (Fjell and Walhovd, 2010). BMI has also been reported to modulate brain structural changes both in healthy people (Ho et al., 2011; Bolzenius et al., 2015) and OSA patients (Huang et al., 2019), and given the prevalence of obesity among OSA patients, BMI was entered as a covariate. Although the evidence on education is less well-established, some studies did report higher temporal lobe gray matter volume and reduced age-related changes associated with higher levels of education (Coffey et al., 1999; Ho et al., 2011).

One notable aspect of the results overall is that the impact of hypoxia and sleep disturbance affects the gray matter structures in no consistent manner, with a mixture of hypertrophy and atrophy in different cerebral regions. However, this is reflective of the literature on this subject, where conflicting changes were observed in individual studies showing both gray matter atrophy and hypertrophy (Baril et al., 2021), as well as between studies (Shi et al., 2017). Remarkably, some previous studies have even reported a complete absence of OSA-driven structural changes. For example, a cohort study of 312 participants showed that moderate-to-severe OSA at baseline was not associated with regional brain volume changes 15 years later (Lutsey et al., 2016), although the authors did note a possible self-selection bias where healthy participants were more likely to be present at follow-up. A meta-analysis by Shi has also highlighted the diverse range of regions where OSA-related changes were reported, including all cortical lobes and subcortical structures, though less so in the occipital cortex (Shi et al., 2017). This is in general alignment with the findings of the current study, though the last observation was not reproduced as both hypoxia and sleep disturbance were found to be significantly associated with multiple occipital structures. Checking against the several methodological pitfalls suggested by the authors of the meta-analysis to explain the apparent discordant findings, this study has kept to a high standard of robustness: (1) they suggested that

some studies failed to account for important covariates such as obesity, whereas this study has included three covariates: age, BMI, and education; (2) some studies have not corrected for multiple comparisons, whereas this study used false discovery rates when reporting the SEM results.

To potentially account for this apparent lack of clear patterns of OSA-induced cortical structural alterations, a proposal was put forth by Rosenzweig et al. (2015). The authors proposed that OSA and its associated hypoxia exert its impact on the brain through a combination of adaptive and maladaptive processes, thus resulting in a mixture of gray matter hypertrophy and atrophy, and a mixture of increases and decreases in cortical thickness and complexity in different regions. The relative contribution of these processes is dependent on the dynamic interplay of various factors. Building on this, Baril et al. (2021) further hypothesized that the OSA-related brain structural changes occur in two phases. In the first phase of early and mild OSA, there are inflammatory processes lead to intracellular edema, as well as adaptive compensatory processes that leads to cortical hypertrophy, both contributing to the thickening of the gray matter regions. In the second phase, however, cortical atrophy dominates in the later and more severe patients with OSA. This hypothesis was supported primarily by an earlier study by the same group in a study of older patients with OSA (Baril et al., 2017). In that study, instead of a mixture of gray matter hypertrophy and atrophy found in other studies of younger patient cohorts, the results showed gray matter hypertrophy exclusively, in a diverse range of regions. This led to the authors' suggestion that hypertrophy is more likely seen in studies with older participants, who tended to have just recently developed OSA and were milder in disease severity, where the earlier reactive / adaptive hypertrophic processes dominate. The current study, however, observed a widespread hypoxia-related increase in gray matter volume even in a cohort of young and middle-aged patients. As such, these results do not seem to align with the hypothesis by Cross et al. (2018) and Baril et al. (2021). Nevertheless, the dynamic interplay between adaptive and maladaptive processes, coupled with the within-study heterogeneity and cross-study differences in the patient demographic and OSA phenotypes, may offer a plausible explanation for such divergent findings between studies.

Methodologically, the SEM approach adopted by the study reduced the random measurement error by extracting the covariance of indicator variables into a combined latent variable. Arguably, this offers a more principled way to combine the various PSG-derived parameters, in contrast to the data-driven approach provided by Principal Component Analysis (PCA). The latter has been adopted by a few studies such as one by Cross et al. (2018), where the first two principal components had to be empirically labeled as "oxygen desaturation" (mainly driven by AHI, ODI, T90%, and MinSaO₂) and "sleep disturbance" (mainly driven by sleep efficiency, awakening index, and arousal index). Their results revealed a significant negative association between "oxygen desaturation" and the cortical thickness of bilateral temporal lobes, but a positive association between "sleep disturbance" and thickness in the right postcentral gyrus, pericalcarine, and pars opercularis. A similar PCA-based study by Baril et al. (2017) found a very consistent positive association between each of the three principal components (labeled as "hypoxia," "respiratory disturbances," and "sleep fragmentation") and cortical thickness of various brain regions in the frontal, parietal, and cingulate cortex. Nevertheless, it should also be noted that no results were

directly contradicting, i.e., opposite results in the same brain region, between this study and the two existing studies by Baril et al. (2017) and Cross et al. (2018).

Furthermore, this study was unique in that it examined gray matter cortical complexity in terms of the sulcal depth (SD) and fractal dimension (FD), which has previously rarely been studied. Unlike gray matter volume and cortical thickness, SD and FD can provide nuanced information about the shape of cortical surface. Our study found similarly mixed effects of OSA on cortical complexity, especially as measured by sulcus depth, where hypoxia was associated with increased SD in bilateral anterior cingulate cortices, bilateral rostral anterior cingulate cortices, and right parahippocampal, fusiform and entorhinal cortices and decreased SD in parts of the prefrontal and pre- and paracentral gyri. Sleep disturbance tends to be associated with the opposite effect to that of hypoxia, although in fewer regions. Along with previous studies of sulcal depth and morphological changes in aging and dementia (Kochunov et al., 2005; Im et al., 2008; Yun et al., 2013), schizophrenia (Turetsky et al., 2009) and Williams syndrome (Kippenhan et al., 2005), the results in this study suggests the utility of tapping into nuanced measures of cortical complexity to capture changes potentially overlooked by cortical thickness and gray matter volume in the OSA brain.

There are several limitations to the current study. Firstly, as the participants were drawn from a larger cohort of patients received at a hospital, this study was not able to include healthy control subjects for comparison. However, using various PSG parameters as continuous variables, the study still yielded significant findings on how disease severity moderates OSA's effects on brain structure. As is common for studies of OSA, the duration of disease for patients was unknown, which would be an important covariate influencing the extent of OSA-associated changes, especially in teasing apart patients in the early hypertrophic phase and those in the late atrophic phase.

To conclude, the present study is the first to apply structural equation modeling to the analysis of OSA-associated brain structural changes. The results showed a significant association between hypoxia and increases in gray matter volume, cortical thickness, and cortical complexity in a diverse range of brain regions, as well as an association between altered sleep structure and decreases in the same structural measures, albeit in fewer regions. These results have highlighted the utility of the more fine-grained and advanced surface-based morphometry analysis to reveal the subtle structural differences possibly overlooked by the voxel-based measures commonly adopted by the literature. This study also served as a demonstration of a novel approach to combine the wide array of polysomnographic parameters in a unified SEM analysis of OSA-related brain structural changes.

Data availability statement

The raw data supporting the conclusions of this article will be made available by the authors, without undue reservation.

Ethics statement

The studies involving human participants were reviewed and approved by Research Ethics Committee of the Second Affiliated

Hospital of Soochow University, Suzhou, China (JD-LK-2018-004-02). The patients/participants provided their written informed consent to participate in this study.

Author contributions

JW and YL contributed to the study's conception and design and data acquisition, analysis, and interpretation and drafted the paper. LJ, TS, CC, and FH contributed to data acquisition, analysis, and interpretation. EW contributed to data acquisition and analysis and revised the work critically. DC contributed to data analysis and interpretation and revised the work critically. RC contributed to the study's conception and design and revised the work critically. All authors contributed to the article and approved the submitted version.

Funding

This work was supported by the National Nature Science Foundation of China (grant numbers 81770085 and 82070095) and the Science, Education, and Health of Suzhou Youth Science and Technology Project (grant number KJXW2021016).

Acknowledgments

The authors are grateful to all of the individuals who participated in the present study. We are also grateful to Qiaojun Wang, Xing Xu, Jiubo Wang, at the sleep center of The Second Affiliated Hospital of Soochow University, Suzhou, China, who helped assemble and analyze the data.

Conflict of interest

The authors declare that the research was conducted in the absence of any commercial or financial relationships that could be construed as a potential conflict of interest.

Publisher's note

All claims expressed in this article are solely those of the authors and do not necessarily represent those of their affiliated organizations, or those of the publisher, the editors and the reviewers. Any product that may be evaluated in this article, or claim that may be made by its manufacturer, is not guaranteed or endorsed by the publisher.

Supplementary material

The Supplementary material for this article can be found online at: <https://www.frontiersin.org/articles/10.3389/fnagi.2023.1090547/full#supplementary-material>

References

- André, C., Rehel, S., Kuhn, E., Landeau, B., Moulinet, I., Tournon, E., et al. (2020). Association of Sleep-Disordered Breathing with Alzheimer Disease Biomarkers in community-dwelling older adults: a secondary analysis of a randomized clinical trial. *JAMA Neurol.* 77, 716–724. doi: 10.1001/jamaneurol.2020.0311
- Baril, A. A., Gagnon, K., Brayet, P., Montplaisir, J., De Beaumont, L., Carrier, J., et al. (2017). Gray matter hypertrophy and thickening with obstructive sleep apnea in middle-aged and older adults. *Am. J. Respir. Crit. Care Med.* 195, 1509–1518. doi: 10.1164/rccm.201606-1271OC
- Baril, A. A., Martineau-Dussault, M. È., Sanchez, E., André, C., Thompson, C., Legault, J., et al. (2021). Obstructive sleep apnea and the brain: a focus on gray and white matter structure. *Curr. Neurol. Neurosci. Rep.* 21:11. doi: 10.1007/s11910-021-01094-2
- Basoglu, O. K., and Tasbakan, M. S. (2018). Gender differences in clinical and polysomnographic features of obstructive sleep apnea: a clinical study of 2827 patients. *Sleep Breathing = Schlaf Atmung* 22, 241–249. doi: 10.1007/s11325-017-1482-9
- Benjafield, A. V., Ayas, N. T., Eastwood, P. R., Heinzer, R., Ip, M., Morrell, M. J., et al. (2019). Estimation of the global prevalence and burden of obstructive sleep apnoea: a literature-based analysis. *Lancet Respir. Med.* 7, 687–698. doi: 10.1016/S2213-2600(19)30198-5
- Bentler, P. M., and Stein, J. A. (1992). Structural equation models in medical research. *Stat. Methods Med. Res.* 1, 159–181. doi: 10.1177/096228029200100203
- Bolzenius, J. D., Laidlaw, D. H., Cabeen, R. P., Conturo, T. E., McMichael, A. R., Lane, E. M., et al. (2015). Brain structure and cognitive correlates of body mass index in healthy older adults. *Behav. Brain Res.* 278, 342–347. doi: 10.1016/j.bbr.2014.10.010
- Bonsignore, M. R., Saesranta, T., and Riha, R. L. (2019). Sex differences in obstructive sleep apnoea. *Eur. Respir. Rev.* 28:190030. doi: 10.1183/16000617.0030-2019
- Bubu, O. M., Andrade, A. G., Umasabor-Bubu, O. Q., Hogan, M. M., Turner, A. D., de Leon, M. J., et al. (2020). Obstructive sleep apnea, cognition and Alzheimer's disease: a systematic review integrating three decades of multidisciplinary research. *Sleep Med. Rev.* 50:101250. doi: 10.1016/j.smrv.2019.101250
- Chen, R., Xiong, K. P., Huang, J. Y., Lian, Y. X., Jin, F., Li, Z. H., et al. (2011). Neurocognitive impairment in Chinese patients with obstructive sleep apnoea hypopnoea syndrome. *Respirol Carlton* 16, 842–848. doi: 10.1111/j.1440-1843.2011.01979.x
- Coffey, C. E., Saxton, J. A., Ratcliff, G., Bryan, R. N., and Lucke, J. F. (1999). Relation of education to brain size in normal aging. *Neurology* 53, 189–189. doi: 10.1212/wnl.53.1.189
- Cross, N. E., Memarian, N., Duffy, S. L., Paquola, C., LaMonica, H., D'Rozario, A., et al. (2018). Structural brain correlates of obstructive sleep apnoea in older adults at risk for dementia. *Eur. Respir. J.* 52:1800740. doi: 10.1183/13993003.00740-2018
- Dahnke, R., Yotter, R. A., and Gaser, C. (2013). Cortical thickness and central surface estimation. *Neuroimage* 65, 336–348. doi: 10.1016/j.neuroimage.2012.09.050
- Desikan, R. S., Ségonne, F., Fischl, B., Quinn, B. T., Dickerson, B. C., Blacker, D., et al. (2006). An automated labeling system for subdividing the human cerebral cortex on MRI scans into gyral based regions of interest. *Neuroimage* 31, 968–980. doi: 10.1016/j.neuroimage.2006.01.021
- Dewan, N. A., Nieto, F. J., and Somers, V. K. (2015). Intermittent hypoxemia and OSA: implications for comorbidities. *Chest* 147, 266–274. doi: 10.1378/chest.14-0500
- Fjell, A. M., and Walhovd, K. B. (2010). Structural brain changes in aging: courses, causes and cognitive consequences. *Rev. Neurosci.* 21, 187–221. doi: 10.1515/revneuro.2010.21.3.187
- Fornito, A., Yücel, M., Wood, S. J., Adamson, C., Velakoulis, D., Saling, M. M., et al. (2008). Surface-based morphometry of the anterior cingulate cortex in first episode schizophrenia. *Hum. Brain Mapp.* 29, 478–489. doi: 10.1002/hbm.20412
- Franklin, K. A., and Lindberg, E. (2015). Obstructive sleep apnea is a common disorder in the population—a review on the epidemiology of sleep apnea. *J. Thorac. Dis.* 7, 1311–1322. doi: 10.3978/j.issn.2072-1439.2015.06.11
- Gottlieb, D. J., and Punjabi, N. M. (2020). Diagnosis and Management of Obstructive Sleep Apnea: a review. *JAMA* 323, 1389–1400. doi: 10.1001/jama.2020.3514
- Ho, A. J., Raji, C. A., Becker, J. T., Lopez, O. L., Kuller, L. H., Hua, X., et al. (2011). The effects of physical activity, education, and body mass index on the aging brain. *Hum. Brain Mapp.* 32, 1371–1382. doi: 10.1002/hbm.21113
- Huang, X., Tang, S., Lyu, X., Yang, C., and Chen, X. (2019). Structural and functional brain alterations in obstructive sleep apnea: a multimodal meta-analysis. *Sleep Med.* 54, 195–204. doi: 10.1016/j.sleep.2018.09.025
- Im, K., Lee, J. M., Seo, S. W., Yoon, U., Kim, S. T., Kim, Y. H., et al. (2008). Variations in cortical thickness with dementia severity in Alzheimer's disease. *Neurosci. Lett.* 436, 227–231. doi: 10.1016/j.neulet.2008.03.032
- Kapur, V. K., Auckley, D. H., Chowdhuri, S., Kuhlmann, D. C., Mehra, R., Ramar, K., et al. (2017). Clinical practice guideline for diagnostic testing for adult obstructive sleep apnea: an American Academy of sleep medicine clinical practice guideline. *J. Clin. Sleep Med.* 13, 479–504. doi: 10.5664/jcsm.6506
- Kippenhan, J. S., Olsen, R. K., Mervis, C. B., Morris, C. A., Kohn, P., Meyer-Lindenberg, A., et al. (2005). Genetic contributions to human gyrification: sulcal morphometry in Williams syndrome. *J. Neurosci.* 25, 7840–7846. doi: 10.1523/JNEUROSCI.1722-05.2005
- Kochunov, P., Mangin, J. F., Coyle, T., Lancaster, J., Thompson, P., Rivière, D., et al. (2005). Age-related morphology trends of cortical sulci. *Hum. Brain Mapp.* 26, 210–220. doi: 10.1002/hbm.20198
- Lutsey, P. L., Norby, F. L., Gottesman, R. F., Mosley, T., MacLehose, R. F., Punjabi, N. M., et al. (2016). Sleep apnea, sleep duration and brain MRI markers of cerebral vascular disease and Alzheimer's disease: the atherosclerosis risk in communities study (ARIC). *PLoS One* 11:e0158758. doi: 10.1371/journal.pone.0158758
- Macey, P. M., Kumar, R., Yan-Go, F. L., Woo, M. A., and Harper, R. M. (2012). Sex differences in white matter alterations accompanying obstructive sleep apnea. *Sleep* 35, 1603–1613. doi: 10.5665/sleep.2228
- Madan, C. R., and Kensinger, E. A. (2016). Cortical complexity as a measure of age-related brain atrophy. *Neuroimage* 134, 617–629. doi: 10.1016/j.neuroimage.2016.04.029
- Marchi, N. A., Ramponi, C., Hirotzu, C., Haba-Rubio, J., Lutti, A., Preisig, M., et al. (2020). Mean oxygen saturation during sleep is related to specific brain atrophy pattern. *Ann. Neurol.* 87, 921–930. doi: 10.1002/ana.25728
- MathWorks, T. (2020) MATLAB (R2020b). *The MathWorks Inc.*
- Rosenzweig, I., Glasser, M., Polsek, D., Leschziner, G. D., Williams, S. C., and Morrell, M. J. (2015). Sleep apnoea and the brain: a complex relationship. *Lancet Respir. Med.* 3, 404–414. doi: 10.1016/S2213-2600(15)00090-9
- Shi, Y., Chen, L., Chen, T., Li, L., Dai, J., Lui, S., et al. (2017). A meta-analysis of voxel-based brain Morphometry studies in obstructive sleep apnea. *Sci. Rep.* 7:10095. doi: 10.1038/s41598-017-09319-6
- Theorell-Haglöw, J., Miller, C. B., Bartlett, D. J., Yee, B. J., Openshaw, H. D., and Grunstein, R. R. (2018). Gender differences in obstructive sleep apnoea, insomnia and restless legs syndrome in adults—what do we know? A clinical update. *Sleep Med. Rev.* 38, 28–38. doi: 10.1016/j.smrv.2017.03.003
- Turetsky, B. I., Crutchley, P., Walker, J., Gur, R. E., and Moberg, P. J. (2009). Depth of the olfactory sulcus: a marker of early embryonic disruption in schizophrenia? *Schizophr. Res.* 115, 8–11. doi: 10.1016/j.schres.2009.09.005
- Wang, E., Jia, Y., Ya, Y., Xu, J., Mao, C., Luo, W., et al. (2021). Abnormal topological Organization of Sulcal Depth-Based Structural Covariance Networks in Parkinson's disease. *Front. Aging Neurosci.* 12:575672. doi: 10.3389/fnagi.2020.575672
- Winkler, A. M., Kochunov, P., Blangero, J., Almasy, L., Zilles, K., Fox, P. T., et al. (2010). Cortical thickness or grey matter volume? The importance of selecting the phenotype for imaging genetics studies. *Neuroimage* 53, 1135–1146. doi: 10.1016/j.neuroimage.2009.12.028
- Young, T., Palta, M., Dempsey, J., Skatrud, J., Weber, S., and Badr, S. (1993). The occurrence of sleep-disordered breathing among middle-aged adults. *N. Engl. J. Med.* 328, 1230–1235. doi: 10.1056/NEJM199304293281704
- Yun, H. J., Im, K., Yang, J.-J., Yoon, U., and Lee, J. M. (2013). Automated sulcal depth measurement on cortical surface reflecting geometrical properties of sulci. *PLoS One* 8:e55977. doi: 10.1371/journal.pone.0055977



OPEN ACCESS

EDITED BY

Shong Lau,
Salk Institute for Biological Studies,
United States

REVIEWED BY

Kyong Jin Shin,
Inje University Haeundae Paik Hospital,
Republic of Korea
Eva Sykova,
Institute of Experimental Medicine (ASCR),
Czechia
Seong-il Oh,
Kyung Hee University Medical Center,
Republic of Korea

*CORRESPONDENCE

Seung Hyun Kim
✉ kimsh1@hanyang.ac.kr

SPECIALTY SECTION

This article was submitted to
Cellular and Molecular Mechanisms of Brain-
aging,
a section of the journal
Frontiers in Aging Neuroscience

RECEIVED 20 January 2023

ACCEPTED 20 March 2023

PUBLISHED 12 April 2023

CITATION

Nam J-Y, Chun S, Lee TY, Seo Y, Kim K, Park J,
Sung W, Oh K-W, Lee S, Park J-S, Oh J,
Chung KC, An H, Chu HS, Son B and
Kim SH (2023) Long-term survival benefits of
intrathecal autologous bone marrow-derived
mesenchymal stem cells (Neuronata-R®:
lenzumestrocel) treatment in ALS: Propensity-
score-matched control, surveillance study.
Front. Aging Neurosci. 15:1148444.
doi: 10.3389/fnagi.2023.1148444

COPYRIGHT

© 2023 Nam, Chun, Lee, Seo, Kim, Park, Sung,
Oh, Lee, Park, Oh, Chung, An, Chu, Son and
Kim. This is an open-access article distributed
under the terms of the [Creative Commons
Attribution License \(CC BY\)](#). The use,
distribution or reproduction in other forums is
permitted, provided the original author(s) and
the copyright owner(s) are credited and that
the original publication in this journal is cited,
in accordance with accepted academic
practice. No use, distribution or reproduction is
permitted which does not comply with these
terms.

Long-term survival benefits of intrathecal autologous bone marrow-derived mesenchymal stem cells (Neuronata-R®: lenzumestrocel) treatment in ALS: Propensity-score-matched control, surveillance study

Jae-Yong Nam¹, Sehwan Chun^{1,2}, Tae Yong Lee^{1,3}, Yunjeong Seo¹, Kwijoo Kim¹, Jinseok Park⁴, Wonjae Sung⁴, Ki-Wook Oh⁴, Sanggon Lee^{4,5}, Jin-Sung Park⁶, Juyeon Oh⁷, Kyung Cheon Chung⁸, Hyonggin An⁹, Hyeon Sik Chu¹⁰, Bugyeong Son¹⁰ and Seung Hyun Kim^{4,10*}

¹Central Research Center, CORESTEMCHEMON Inc., Seoul, Republic of Korea, ²Department of Biology, Kyung Hee University, Seoul, Republic of Korea, ³College of Pharmacy, Chungbuk National University, Cheongju, Republic of Korea, ⁴Department of Neurology, College of Medicine, Hanyang University, Seoul, Republic of Korea, ⁵Department of Neurology, Chung-Ang University Gwangmyeong Hospital, Gwangmyeong, Republic of Korea, ⁶Department of Neurology, School of Medicine, Kyungpook National University, Kyungpook National University Chilgok Hospital, Daegu, Republic of Korea, ⁷College of Nursing, Dankook University, Cheonan, Republic of Korea, ⁸Department of Neurology, Bethesda Gospel Hospital, Yangsan, Republic of Korea, ⁹Department of Biostatistics, Korea University College of Medicine, Seoul, Republic of Korea, ¹⁰Cell Therapy Center, Hanyang University Hospital, Seoul, Republic of Korea

Objective: Neuronata-R® (lenzumestrocel) is an autologous bone marrow-derived mesenchymal stem cell (BM-MSC) product, which was conditionally approved by the Korean Ministry of Food and Drug Safety (KMFDs, Republic of Korea) in 2013 for the treatment of amyotrophic lateral sclerosis (ALS). In the present study, we aimed to investigate the long-term survival benefits of treatment with intrathecal lenzumestrocel.

Methods: A total of 157 participants who received lenzumestrocel and whose symptom duration was less than 2 years were included in the analysis (BM-MSC group). The survival data of placebo participants from the Pooled-Resource Open-Access ALS Clinical Trials (PROACT) database were used as the external control, and propensity score matching (PSM) was used to reduce confounding biases in baseline characteristics. Adverse events were recorded during the entire follow-up period after the first treatment.

Results: Survival probability was significantly higher in the BM-MSC group compared to the external control group from the PROACT database (log-rank, $p < 0.001$). Multivariate Cox proportional hazard analysis showed a significantly lower hazard ratio for death in the BM-MSC group and indicated that multiple injections were more effective. Additionally, there were no serious adverse drug reactions found during the safety assessment, lasting a year after the first administration.

Conclusion: The results of the present study showed that lenzumestrocel treatment had a long-term survival benefit in real-world ALS patients.

KEYWORDS

lenzumestrocel, amyotrophic lateral sclerosis, stem cell therapy, survival analysis, mesenchymal stem cell

Introduction

Amyotrophic lateral sclerosis (ALS) is a progressive neurodegenerative disease affecting both the upper and lower motor neuron systems, which eventually results in generalized weakness and, ultimately, death due to respiratory failure (Brown and Al-Chalabi, 2017; Hardiman et al., 2017).

Despite recent advances in determining the genetic and molecular mechanisms of motor neuron cell death in ALS, precise mechanisms of the selective degeneration of motor neurons and heterogeneous clinical phenotypes are not clearly understood (Taylor et al., 2016; Mejjini et al., 2019; Kim et al., 2020; Saez-Atienzar et al., 2021). Additionally, no curative therapeutic agents are currently available for the treatment of ALS. The only two Food and Drug Administration (FDA)-approved drugs are riluzole and edaravone (Miller et al., 2002; Rothstein, 2017). However, they have modest therapeutic effects (Jaiswal, 2019; Saitoh and Takahashi, 2020; Witzel et al., 2022).

Stem cell therapy has shown various potential therapeutic effects in a range of diseases along with safety in recent clinical trials (Hoang et al., 2022). In particular, the immunomodulatory abilities of mesenchymal stem cells are being investigated in many clinical trials as a treatment option for neurodegenerative diseases (Chen et al., 2018). The safety of MSC therapy has been confirmed in many studies, and some studies have shown positive results (Mazzini et al., 2010; Petrou et al., 2016; Šyková et al., 2017; Aljabri et al., 2021; Tavakol-Afshari et al., 2021). There are also active clinical trials investigating the use of mesenchymal stem cell therapy for ALS.

Neuronata-R® (lenzumestrocel) is an autologous bone marrow-derived mesenchymal stem cell (BM-MSC) product, which has been conditionally approved by the Korean Ministry of Food and Drug Safety (KMFDS, December 31, 2013) as an orphan drug for concomitant therapy with riluzole for use in the treatment of patients with ALS. Phase I and II clinical trials (NCT01363401) showed clinically significant improvements in the decline of Revised ALS Functional Rating Scale (ALSFRS-R) scores up to 6 months after the administration of lenzumestrocel (Oh et al., 2015, 2018). Despite the clinical effectiveness of lenzumestrocel administration, which was determined by the decline of ALSFRS-R scores lasting at least 6 months, the lack of a long-term survival benefit in the post-hoc analysis may be associated with the limited number of injections (two doses in a single-cycle) and the gradual loss of MSC itself. Additionally, the number of participants in the phase II trial was relatively small when analyzing the survival data.

After conditional approval from the KMFDS to administer BM-MSC for the treatment of ALS, 257 participants with ALS underwent single-cycle lenzumestrocel treatment (two repeated MSC injections with 1-month interval). Among them, 34 participants with ALS received one or more booster injections at various intervals following the single-cycle treatment to achieve long-lasting benefits.

The present study aimed to provide a long-term survival analysis for lenzumestrocel treatment participants. Propensity-score-matched

external control group from Pooled-Resource Open-Access ALS Clinical Trials (PROACT) were compared with those of the BM-MSC treatment group (Atassi et al., 2014).

Materials and methods

Lenzumestrocel surveillance study

Lenzumestrocel was developed based on the MSC properties to have the capacity to release neurotrophic factors and to show immune-inflammatory modulation in ALS, as described in previous reports (Oh et al., 2018; Nam et al., 2022). Based on the efficacy and safety data in phase I and II clinical trials (NCT01363401), lenzumestrocel was designated as an orphan drug for concomitant therapy with riluzole in patients with ALS under the Revised Rule of Orphan Drug Designation by the KMFDS (December 31, 2013; KMFDS Announcement No. 2013–262). In addition, a new drug application (NDA) for lenzumestrocel as an orphan drug was granted by the KMFDS (July 30, 2014). After NDA approval, according to the risk management plan of lenzumestrocel recommended by the KMFDS, post-marketing surveillance (PMS) was conducted as a complete enumeration survey from March 2, 2015 to January 31, 2022. This study was approved by the Hanyang University Seoul Hospital Institutional Review Board (IRB) (IRB file#: PMS2015-001).

BM-MSC treatment cohort for propensity-score matching

All participants of the BM-MSC treatment group were diagnosed with clinically definite or probable or clinically probable with lab-supported ALS according to the revised El Escorial criteria (Brooks et al., 2000). Clinical data (age, sex, site of onset, etc.) were collected from 257 participants treated with lenzumestrocel. To reduce the heterogeneity of the study population, participants whose symptom duration exceeded 2 years before the BM-MSC injection and who had no serial ALSFRS-R scores for the follow-up period after the first treatment were excluded from the analysis. Finally, 170 participants were included in the propensity-score matching analysis (Figure 1A). Written informed consent was obtained from all participants prior to the first administration.

External control cohort from PROACT database for propensity-score matching

PROACT database contains de-identified records of participants from 23 clinical trials. To compare the survival probability of the BM-MSC treatment group with the placebo-allocated participants'

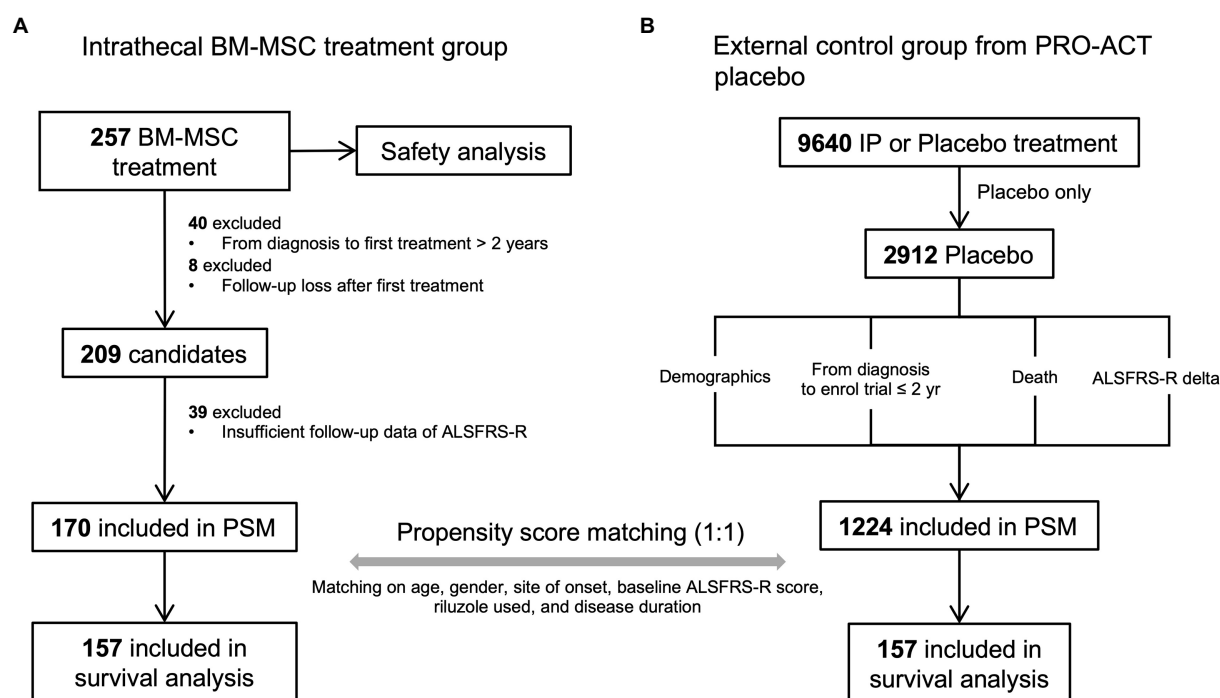


FIGURE 1

The propensity-score-matched participant selection for survival and safety analysis and data pre-processing steps. **(A)** BM-MSc treatment cohort. A total of 257 participants were administered lenzomestrol. Safety evaluation was conducted during a one-year follow-up period after the first treatment. Survival analysis was performed on propensity score matched 157 participants. **(B)** external control group from the PROACT database. Only 2,912 placebo participants were extracted out of 9,640 participants in the treatment group data (treatment.csv). Participants who enrolled in the trial within 2 years from their diagnosis and who had a baseline ALSFRS-R score were assigned as the control group. The clinical information of each participant was extracted from each data source. A total of 157 placebo participants were used for survival analysis.

group, data ($n=2,912$) were extracted from the PROACT database and used as an external control group. First, participants of the external control group whose symptom duration was less than 2 years were selected to match the BM-MSc treatment group. Then, the individuals' death status and time were achieved from the deathdata.csv dataset. If the participant was alive until the end of the trial, the last follow-up time was determined based on the last measured time of the ALSFRS-R score from the alsfrs.csv dataset and was regarded as censored. Demographics and clinical information, such as age, sex, site of onset, and riluzole use, were obtained from other PROACT datasets. Finally, 1,224 participants were included in the propensity-score matching analysis (Figure 1B).

Selection of BM-MSc treatment group and external control group for survival analysis using propensity score matching

Propensity score matching (PSM) is widely used in observational studies to reduce confounding biases in treated and untreated participants (Austin, 2011; Austin et al., 2021). BM-MSc-treated participants were matched to PROACT placebo participants in a ratio of 1:1 (Austin, 2010). PSM was performed

using the nearest neighbor (NN) method on the propensity score, which was calculated by logistic regression, including covariates with age, sex, site of onset, baseline ALSFRS-R score, riluzole used, and disease duration. After matching, 314 participants (157 participants in each group) were included in the survival analysis.

Estimation of initial progression speed

Due to the lack of long-term follow-up data prior to baseline for ALSFRS-R scores in both groups and inaccurate time from the onset for some subjects, accurate disease progression cannot be calculated. Therefore, the initial progression speed was calculated using the following process.

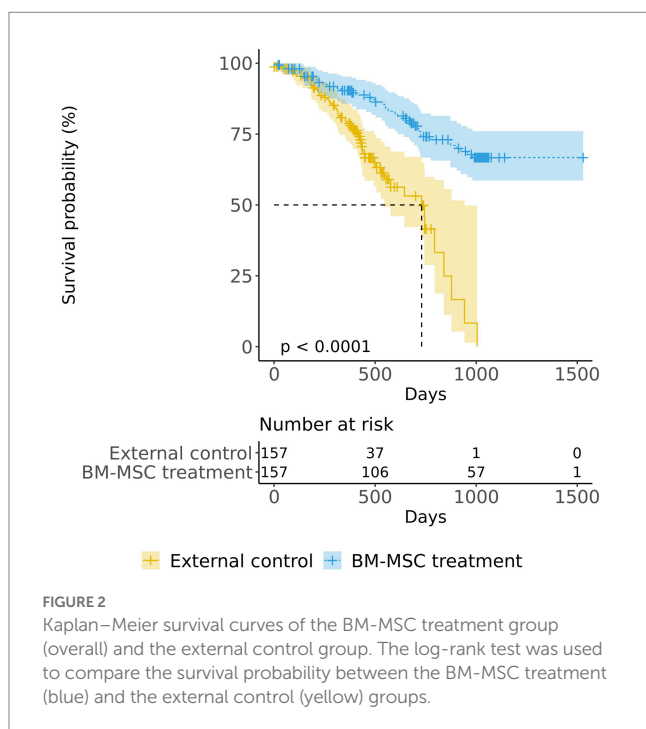
(i) Baseline ALSFRS-R is available for all subjects. (ii) Data on time from diagnosis to baseline are available for all subjects. (iii) According to the results of the PROACT study, the average time from onset to diagnosis is 12 months (Atassi et al., 2014).

$$\text{initial progression speed} = \frac{48 - (\text{baseline ALSFRS-R score})}{\text{time from onset to baseline (months)}}$$

$$\text{time from onset to baseline} = [\text{time from the diagnosis to baseline} + 12] (\text{months})$$

TABLE 1 Baseline characteristics of the propensity score matched the BM-MSc treatment group and the external control group.

	BM-MSc treatment group (<i>n</i> =157)	External control group (PROACT) (<i>n</i> =157)	Value of <i>p</i>
Age (yr)	55.8 ± 10.7	55.7 ± 12.4	0.934
Sex (M: F)	95: 62	94: 63	1.000
Riluzole used	141 (89.8%)	141 (89.8%)	1.000
Baseline ALSFRS-R score	35.5 ± 5.90	35.7 ± 5.75	0.749
Time from diagnosis to baseline (months)	8.34 ± 5.26	8.66 ± 5.72	0.615
Site of symptom onset (Bulbar: Limb)	34: 123	31: 126	0.781



significance was set at 0.05. Survival analysis (time to death) was conducted using Kaplan–Meier curves and log-rank test using the survminer (version 0.4.9) and survival (version 3.1–8) R packages.

The BM-MSc treatment group includes participants treated with a single-cycle (repeated two injections of lenzumestrol, *n* = 134) and a single-cycle with additional booster injections (*n* = 21, minimum three times to maximum ten times). To compare the clinical benefits of multiple treatments with lenzumestrol, we separated the BM-MSc treatment group into a single-cycle injection group and a multiple-injection group. Two participants who were administered only once (one of two repeated injections in a single cycle) were excluded from the analysis.

The Cox proportional hazards model was used to estimate the associations between prognostic clinical variables and survival time. In the Cox model, the BM-MSc treatment group was divided into a single-cycle injection group and a multiple-injection group. We included six factors (sex, site of onset, riluzole used, baseline ALSFRS-R score, age, and treatment group) in the model to adjust for the bias of confounding factors introduced by subgrouping. Two continuous variables, age and baseline ALSFRS-R score, were dichotomized at the age of 54 years and the baseline ALSFRS-R score of 31 points. Propensity score calculations and matching were conducted using MatchIt (version 4.4.0) R package. All statistical analyses were performed using R software (version 3.6.3).

Safety assessment

Safety was evaluated based on the incidence of adverse events (AEs), adverse drug reactions (ADRs), and serious adverse events (SAEs), which were collected during the entire follow-up period from 2015 to 2022 after the first lenzumestrol treatment. Safety analysis was conducted on the AEs that occurred one year after administration in 257 subjects who had received at least one lenzumestrol injection. All AEs and SAEs reported within a year of the lenzumestrol injection were considered ADR unless a causal relationship with lenzumestrol was determined as an ‘unlikely possibility’. In addition, newly advanced neurological symptoms related to the natural progression of ALS were not regarded as AE. All AEs were coded using the Medical Dictionary for Regulatory Activities (MedDRA) version 25 and summarized according to system organ class (SOC) and preferred terms (PT; Brown et al., 1999).

Statistical method

Differences in baseline clinical variables between the two independent groups were analyzed using a T-test (continuous) or Chi-square test (categorical) for appropriate data types. Statistical

Results

Comparison of baseline characteristics in propensity-score-matched groups

Baseline clinical characteristics between the propensity-score-matched (PSM) BM-MSc treatment group and the external control group are summarized in Table 1. There were no statistically significant differences in baseline covariates between the matched groups. The standardized mean differences in all covariates were less than 0.1, which also indicated that the propensity score-based matching groups were well-balanced (Supplementary Figure 1).

Long-term survival analysis

In both the matched groups, we confirmed 40 deaths in the BM-MSc treatment group and 56 deaths in the external control group. The Kaplan–Meier plot of survival data shows a separation of the survival curves with significance (Figure 2). The survival probability was significantly higher in the BM-MSc treatment group compared to that in the external control group (log-rank, *p* < 0.001). The estimated

median survival time of the external control group was 730 days (24 months; CI:17.95–30.97), whereas the BM-MSC treatment group's time was not estimated as the number of death did not exceed half of the group. We also confirmed that the restricted mean survival time of the external control group was 629 days (20.68 months; SE:1.03), and the BM-MSC treatment group was 1,201 days (39.48 months; SE:1.44).

The survival probabilities of both the single-cycle injection group ($p < 0.001$) and the multiple-injection group ($p < 0.001$) were significantly different from those of the external control group (Figure 3). It was also noted that the multiple-injection group showed a higher survival probability than the single-cycle injection group, but the difference was not statistically significant (pairwise log-rank test $p = 0.18$).

Generally, the time to events (use of tracheostomy or ventilator) is more likely to occur earlier than the time to death. The PROACT database only contains information on time to death and does not provide information on time to events. Therefore, we compared the BM-MSC group's time-to-events information with PROACT's time-to-death information. As a result, we confirmed that the survival probability of the BM-MSC group was higher, which was consistent with the analysis of time-to-death (Supplementary Figure 2).

Survival analysis with initial progression speed

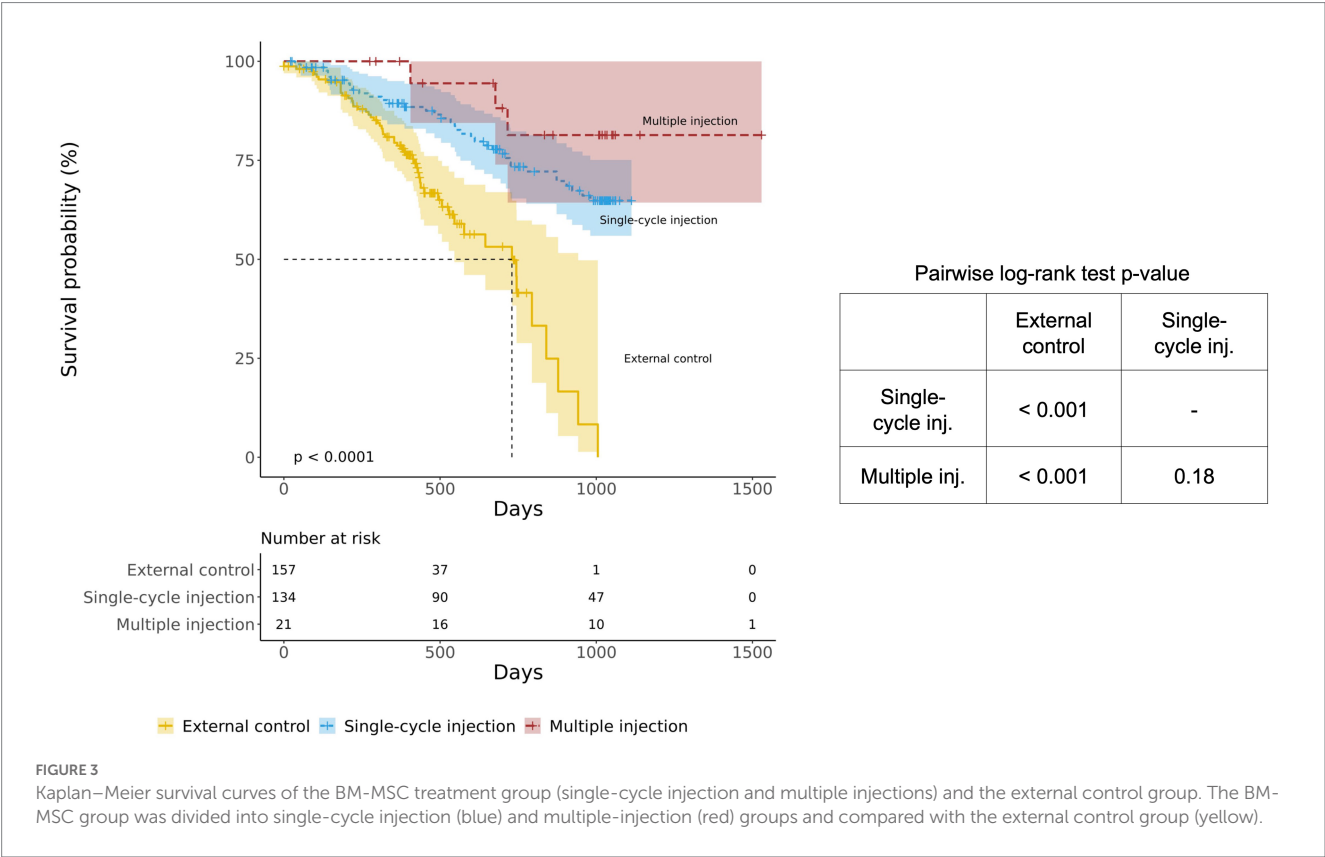
One of the important prognostic factors for predicting survival in ALS is the progression speed of the disease (Kimura et al., 2006; Kjældgaard et al., 2021). The disease progression speed can differ between the subjects in the two groups, which can lead to differences in survival probability. Therefore, we compared the initial progression speed between the two groups to determine whether this factor

contributes to the observed difference in survival probability (see methods). The calculated initial progression speed was 0.78 ± 0.52 /month for the external control group and 0.64 ± 0.32 /month for the BM-MSC treatment group, indicating a difference of 0.14/month with the BM-MSC treatment group being lower (value of $p = 0.005$). The initial progression speed showed a significant difference between the BM-MSC treatment group and the external control group, which could have had an impact on the difference in survival probability. However, we added initial progression speed as a covariate to the existing PSM method and conducted survival analysis in the same manner. The results were consistent with the previous findings (Supplementary Figure 3).

Next, we compared the survival rates between the external control and BM-MSC group using only subjects with intermediate initial progression speed (between the first quartile (1Q) and the third quartile(3Q)) by limiting the range of initial progression speed (Supplementary Figure 4A). Similarly, the survival rate of the BM-MSC group was significantly higher (Supplementary Figure 4B). In conclusion, although there was a difference in initial progression speed in both groups, we confirmed that the survival probability of the BM-MSC treatment group was higher even after controlling for it through PSM or excluding rapid and slow progression.

Hazard ratios for death in multivariate cox proportional hazards regression

We conducted a Cox proportional hazards regression analysis to investigate the association between survival time and several risk factors. A forest plot of the Cox proportional hazards model is shown in Figure 4. The hazard ratios of both the single-cycle injection group ($HR = 0.30$,



95% CI:0.185–0.48, $p<0.001$) and multiple-injection group (HR=0.19, 95% CI:0.059–0.63, $p=0.006$), which were adjusted by sex, site of onset, riluzole used, baseline ALSFRS-R score, and age, were significantly lower than the external control group (i.e., the reductions in risk of death for single-cycle injection and multiple injections were 70 and 81%, respectively). Moreover, the multiple-injection group had a lower hazard ratio than the single-cycle injection group. We found several prognostic factors associated with survival time, including riluzole use (HR=0.50, 95% CI:0.285–0.87, $p=0.015$) and age (HR=3.41, 95% CI:1.975–5.89, $p<0.001$). These results suggest that participants who received lenzumestrocel treatment have a reduced risk of death compared with the propensity-score-matched external control group. Multiple injections may have more effectiveness in patients with ALS.

Comparison of functional assessments

We compared the change in ALSFRS-R scores from baseline to 12 months between the two groups. There was no significant difference in the change of ALSFRS-R scores between the BM-MSc group and the external control group (Supplementary Figure 5). On the other hand, when comparing the multiple-injection group and the single-cycle injection group, we observed that multiple-injection group had a lower decrease in ALSFRS-R scores (Supplementary Figure 6).

Subgroup analysis of the differences between Korean and non-Korean subjects in the BM-MSc group

We analyzed the differences in survival probability and baseline characteristics between Korean and non-Korean subjects in the

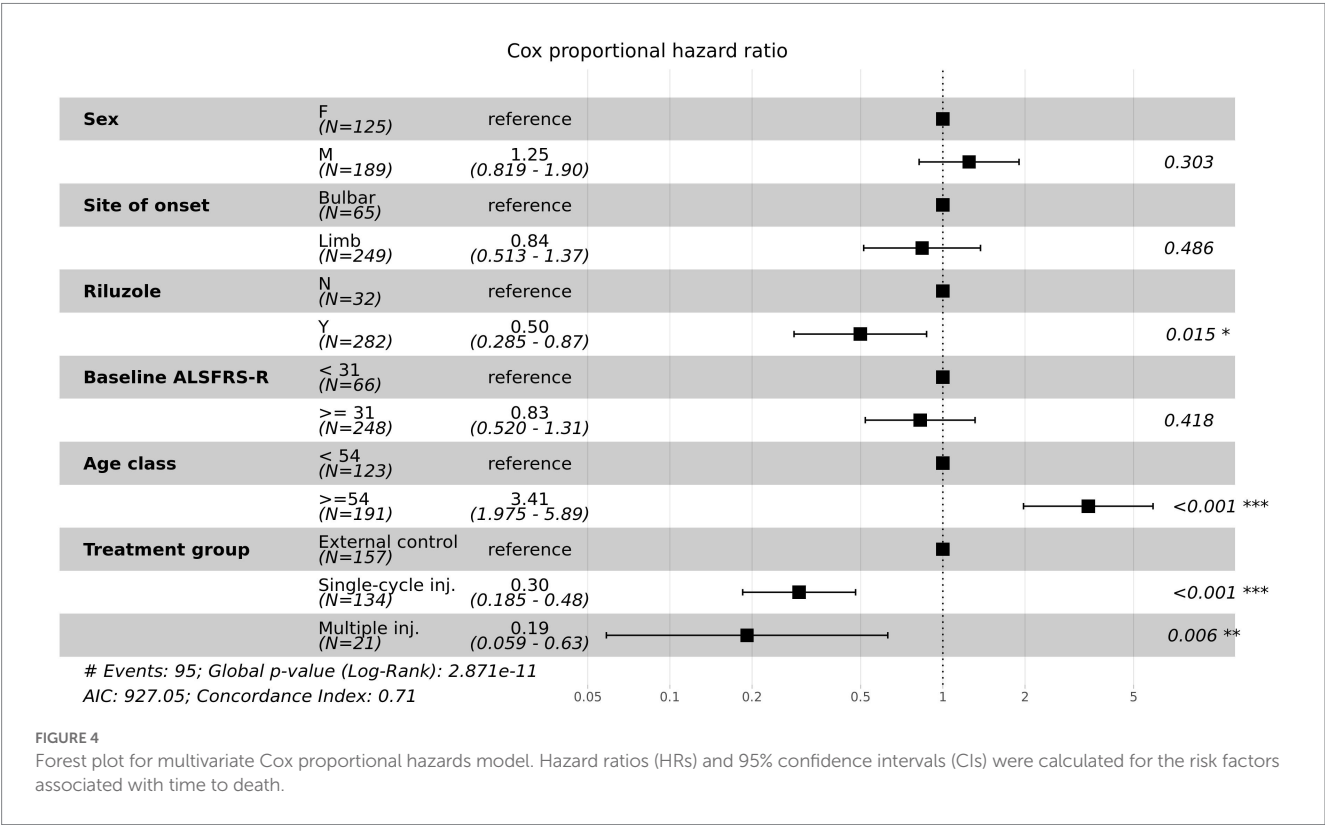
BM-MSc group. There was no significant difference in survival curves between the two groups (Supplementary Figure 7). Non-Korean subjects had a higher initial survival probability, but it decreased after crossover. At baseline, non-Korean subjects were younger (not significant) and had a 2.5-point higher ALSFRS-R score than Korean subjects (Supplementary Table 1). The initial progression speed also showed that non-Korean subjects had a slightly slow progression speed, indicating that overall, non-Korean participants had an advantage in survival. Still, the decrease in survival rate after about 1.6 years may be due to various factors, including the genetic, environmental, lifestyle, and influence of the medical system.

Subgroup analysis of the differences between non-Korean subjects in the BM-MSc group and external control

We compared the non-Korean subjects ($n=25$) in the BM-MSc group with an external control group. The survival probability of the BM-MSc group tended to be higher, but there was no statistically significant difference (Supplementary Figure 8).

Long-term safety assessment

A total of 1,204 adverse events (AEs) were reported during a one-year follow-up period in 257 participants after the first administration of lenzumestrocel. Table 2 lists the AEs experienced by more than 5% of participants. The most common AEs were back



pain ($n=85$; 114 events), headache ($n=80$; 109 events), pyrexia ($n=65$; 91 events), pain ($n=45$; 52 events), and pain in the extremities ($n=44$; 53 events). The incidence of adverse drug reactions (ADRs) was 17.12% (44/257; 92 events; [Table 3](#)). The ADRs included pyrexia ($n=19$; 21 events), headache ($n=19$; 20 events), back pain ($n=12$; 17 events), pain ($n=7$; 8 events), and nausea ($n=6$; 6 events). Most ADRs were mild and transient. However, moderate back pain, coccydynia, or pain in extremities persisting for more than 2 weeks were noted in 13 participants (5.1%; 19 events). And one case of micturition disorder (moderate and continuous) was reported. The incidence of serious adverse events (SAEs) was 26.85% (69/257; 108 events) and accounted for around 9% of AEs. [Table 4](#) lists the SAEs experienced by more than 1% of participants. SAEs included respiratory failure ($n=7$; 7 events), back pain ($n=4$; 4 events), pain ($n=4$; 4 events), coccydynia ($n=3$; 3 events), and musculoskeletal pain ($n=3$; 3 events). A total of 36 events were related to hospitalization, and 20 deaths occurred. All respiratory failure events were related to

natural disease courses and were not considered treatment-related events. However, back pain and coccydynia may be potentially related to BM-MSC treatment due to plausible stem cell-related arachnoiditis. The AEs that were reported during the entire follow-up period are summarized in [Supplementary Table 2](#).

Discussion

Lenzumestrocel is an autologous BM-MSC isolated and expanded *ex vivo* under good manufacturing practice (GMP) conditions at CORESTEMCHEMON Inc. (Seoul, Republic of Korea). It was also conditionally approved by the Korean Ministry of Food and Drug Safety (KMFDS) for the treatment of ALS in 2013. A randomized, open-label phase II clinical trial (NCT01363401) demonstrated that single-cycle (repeated two injections with one-month interval) intrathecal administration of BM-MSCs showed a better clinical outcome (the decline of ALSFRS-R score from baseline) in the

TABLE 2 Summary of adverse events.

System organ class	Number of events	Number of participants	% of total participants
Preferred term			
Gastrointestinal disorders			
Constipation	32	27	10.51%
Nausea	28	24	9.34%
Dyspepsia	17	17	6.61%
Diarrhea	16	15	5.84%
General disorders and administration site conditions			
Pyrexia	91	65	25.29%
Pain	52	45	17.51%
Implant site pain	20	17	6.61%
Investigations			
Alanine aminotransferase increased	14	13	5.06%
Musculoskeletal and connective tissue disorders			
Back pain	114	85	33.07%
Pain in extremity	53	44	17.12%
Arthralgia	38	33	12.84%
Musculoskeletal pain	14	14	5.45%
Nervous system disorders			
Headache	109	80	31.13%
Dizziness	21	19	7.39%
Psychiatric disorders			
Insomnia	18	18	7.00%
Sleep disorder	13	13	5.06%
Respiratory, thoracic and mediastinal disorders			
Cough	17	14	5.45%
Productive cough	16	14	5.45%
Skin and subcutaneous tissue disorders			
Pruritus	19	17	6.61%

Only adverse events that occurred in more than 5% of all participants were listed.

TABLE 3 Summary of adverse drug reactions.

System organ class	Number of events	Number of participants	% of total participants
Preferred term			
Gastrointestinal disorders			
Nausea	6	6	2.33%
Vomiting	2	2	0.78%
General disorders and administration site conditions			
Chills	2	2	0.78%
Injection site pain	1	1	0.39%
Pain	8	7	2.72%
Pyrexia	21	19	7.39%
Injury, poisoning and procedural complications			
Upper limb fracture	1	1	0.39%
Musculoskeletal and connective tissue disorders			
Back pain	17	12	4.67%
Coccydynia	2	2	0.78%
Muscle tightness	1	1	0.39%
Musculoskeletal pain	2	2	0.78%
Myalgia	1	1	0.39%
Pain in extremity	5	5	1.95%
Nervous system disorders			
Headache	20	19	7.39%
Dizziness	2	2	0.78%
Renal and urinary disorders			
Micturition disorder	1	1	0.39%

TABLE 4 Summary of serious adverse events.

System organ class	Number of events	Number of participants	% of total participants
Preferred term			
General disorders and administration site conditions			
Pain	4	4	1.56%
Hepatobiliary disorders			
Cholecystitis acute	3	3	1.17%
Musculoskeletal and connective tissue disorders			
Back pain	4	4	1.56%
Coccydynia	3	3	1.17%
Musculoskeletal pain	3	3	1.17%
Respiratory, thoracic and mediastinal disorders			
Dyspnea	3	3	1.17%
Respiratory arrest	3	3	1.17%
Respiratory failure	7	7	2.72%

Only adverse events that occurred in more than 1% of all participants were listed.

treatment group than in the control group for up to 6 months with no serious adverse drug reactions (Oh et al., 2018). In post-hoc survival analysis of the phase II clinical trial of lenzumestrocel, the estimated mean survival time was 48 (SE = 6) months in the control group and 55 (SE = 4) months in the MSC group with no significance ($p = 0.487$).

The lack of long-term survival benefit may be associated with a small sample size ($n = 64$) and a relatively short observation period in the control group due to using other investigational products (Oh et al., 2018). To overcome limitations, we conducted this pilot study using a propensity-score-matched external control group.

In this study, we conducted a survival analysis of the propensity score-matched BM-MSc ($n=157$) and external control from PROACT placebo ($n=157$) groups to evaluate the long-term survival benefits of BM-MSc treatment in patients with ALS. The survival probability was significantly higher in the BM-MSc group than in the external control group, which is considered to indicate the long-term clinical benefit of BM-MSc treatment. In addition, the Cox proportional hazard model showed a statistically significant lower hazard ratio for both single-cycle injection and multiple injections after adjusting for prognostic covariates (e.g., sex, site of onset, riluzole used, baseline ALSFRS-R score, and age) in comparison to the external control. We also performed the same analysis on all participants before applying the PSM method and confirmed consistent results (Supplementary Figures 9, 10).

It is important to note that there were differences in baseline characteristics between the single-cycle injection and multiple-injection groups (Supplementary Table 3). The multiple-injection group had a significantly higher baseline ALSFRS-R score by approximately 4.1 points ($p=0.005$). Additionally, there was a trend toward younger age in the multiple-injection group, but it was not significant. Furthermore, the multiple-injection group had a higher baseline ALSFRS-R score ($p=0.005$) and a slower initial progression speed ($p<0.001$). Therefore, it is suggested that there may be other factors contributing to the extension of survival besides multiple injections, and further investigation is necessary to identify these factors.

Due to invasive procedures of stem cell therapy, the sham-procedure control group is controversial in the early stage of the clinical trial. However, a comparison with historical control can be helpful in this situation. The age, sex, site of onset, baseline ALSFRS-R score, riluzole use, and disease duration are well-known prognostic factors of ALS. As these prognostic factors did not differ between groups in this study, trial-to-trial variations may be reduced. Therefore, despite a non-randomized study design, the two groups compared in this study seem to be appropriately balanced.

This study has the following limitations. First, the study was not designed as a two-arm randomized trial. The PROACT data is limited to patients with ALS who meet specific inclusion and exclusion criteria, which may limit the generalizability of our findings to other populations. The results provide preliminary evidence that lenzumestrocel has survival benefits. Second, while PROACT provides valuable data on ALS progression and survival, it is limited in the types of outcomes that can be measured. Other important outcomes, such as quality of life and time to events (ventilator or tracheostomy), were not included in the data. Therefore, our findings should be interpreted within the context of the limitations of the PROACT dataset. Third, the Korean healthcare system may have a potential influence. Even though 16% (25/157) of participants were non-Korean, critical treatments in the course of ALS, including riluzole prescription, percutaneous endoscopic gastrostomy (PEG) tube insertion, non-invasive ventilator rental, and tracheostomy care, are covered by the Korean National Health Insurance Service, lowering the patient's out-of-pocket expense to 10% of the overall medical cost (Kim et al., 2021). In addition, considering the cost of lenzumestrocel, the socioeconomic status of the participants is considered to be above-average and, thereby, may contribute to their survival. Fourth, most participants were followed

up in a single center, one of the multidisciplinary ALS clinics in a tertiary hospital in Seoul. It is acknowledged that multidisciplinary care can increase the survival probability (Hardiman et al., 2017), and Seoul and the metropolitan area are recognized to offer superior accessibility and levels of medical service (Jun et al., 2019), which can also contribute to the survival probability. Fifth, the subjects in the multiple-injection group had various injection intervals after single-cycle administration. The analysis of cytokines in CSF of patients with different additional injection periods showed that patients with additional injections at 3–4 months had more benefits in ALSFRS-R score and cytokine levels compared to those with injection intervals of 5–12 months (Supplementary Figures 11–13). The potential difference in clinical benefits depending on the interval of additional injections was not addressed in this study. Sixth, more detailed safety issues, including long-term persistent pain after stem cell therapy, should be more systemically analyzed in larger-scale clinical trials. To overcome these limitations, a phase III trial was required to confirm the long-term efficacy of lenzumestrocel.

Phase III ALSUMMIT clinical trial protocol (NCT04745299) was approved by the U.S. FDA and KMFDS. ALSUMMIT is a randomized, multicenter, double-blind, parallel-group, sham procedure-controlled phase III trial to evaluate the long-term efficacy and safety of repeated BM-MSCs in the treatment of ALS (56-week main study with five BM-MSc injections followed by 24-month observational study) (Nam et al., 2022). The participant recruitment progress nearly reached 90% while preparing this manuscript.

In summary, our analyses revealed a statistically significant long-term survival extension of BM-MSc treatment and suggested that multiple additional booster injections may have more survival benefits in patients with ALS.

Data availability statement

The original contributions presented in the study are included in the article/Supplementary material, further inquiries can be directed to the corresponding author.

Ethics statement

The studies involving human participants were reviewed and approved by the Hanyang University Seoul Hospital Institutional Review Board (IRB file#: PMS2015-001). The participants provided their written informed consent to participate in this study.

Author contributions

J-YN, TL, and SK conceptualized and designed the study. YS, KK, and BS collected the clinical data. J-YN and SC analyzed the data. J-YN, SC, and SK wrote the manuscript. J-YN, JP, WS, J-SP, JO, BS, K-WO, SL, HC, KC, and SK reviewed the manuscript. J-YN, BS, and SK revised the final version of the manuscript. HA conducted statistical analysis and review. All authors have carefully reviewed and agreed to the submitted version of the manuscript.

Acknowledgments

We thank all participants in this study and their families for providing their treatment information. We would also like to thank the members of the Department of Biostatistics at the Korea University College of Medicine for the statistical analysis and review.

Conflict of interest

J-YN, SC, TL, YS, and KK are employees of CORESTEMCHEMON Inc.

The remaining authors declare that the research was conducted in the absence of any commercial or financial relationships that could be construed as a potential conflict of interest.

References

- Aljabri, A., Halawani, A., Bin Lajdam, G., Labban, S., Alshehri, S., and Felemban, R. (2021). The safety and efficacy of stem cell therapy as an emerging therapy for ALS: a systematic review of reported clinical trials. *Front. Neurol.* 12:783122. doi: 10.3389/fneur.2021.783122
- Atassi, N., Berry, J., Shui, A., Zach, N., Sherman, A., Sinani, E., et al. (2014). The PROACT database: design, initial analyses, and predictive features. *Neurology* 83, 1719–1725. doi: 10.1212/WNL.0000000000000951
- Austin, P. C. (2010). Statistical criteria for selecting the optimal number of untreated subjects matched to each treated subject when using many-to-one matching on the propensity score. *Am. J. Epidemiol.* 172, 1092–1097. doi: 10.1093/aje/kwq224
- Austin, P. C. (2011). An introduction to propensity score methods for reducing the effects of confounding in observational studies. *Multivariate Behav Res* 46, 399–424. doi: 10.1080/00273171.2011.568786
- Austin, P. C., Xin Yu, A. Y., Vyas, M. V., Kapral, M. K., and Kapral, M. K. (2021). Applying propensity score methods in clinical research in neurology. *Neurology* 97, 856–863. doi: 10.1212/WNL.0000000000001277
- Brooks, B. R., Miller, R. G., Swash, M., and Munsat, T. L. World Federation of Neurology Research Group on Motor Neuron, D (2000). El Escorial revisited: revised criteria for the diagnosis of amyotrophic lateral sclerosis. *Amyotroph. Lateral Scler. Other Motor Neuron Disord.* 1, 293–299. doi: 10.1080/146608200300079536
- Brown, R. H., and Al-Chalabi, A. (2017). Amyotrophic lateral sclerosis. *N. Engl. J. Med.* 377, 162–172. doi: 10.1056/NEJMr1603471
- Brown, E. G., Wood, L., and Wood, S. (1999). The medical dictionary for regulatory activities (MedDRA). *Drug Saf.* 20, 109–117. doi: 10.2165/00002018-199920020-00002
- Chen, X., Wang, S., and Cao, W. (2018). Mesenchymal stem cell-mediated immunomodulation in cell therapy of neurodegenerative diseases. *Cell. Immunol.* 326, 8–14. doi: 10.1016/j.cellimm.2017.06.006
- Hardiman, O., Al-Chalabi, A., Chio, A., Corr, E. M., Logroscino, G., Robberecht, W., et al. (2017). Amyotrophic lateral sclerosis. *Nat. Rev. Dis. Primers.* 3:17071. doi: 10.1038/nrdp.2017.71
- Hoang, D. M., Pham, P. T., Bach, T. Q., Ngo, A. T. L., Nguyen, Q. T., Phan, T. T. K., et al. (2022). Stem cell-based therapy for human diseases. *Signal Transduct. Target. Ther.* 7:272. doi: 10.1038/s41392-022-01134-4
- Jaiswal, M. K. (2019). Riluzole and edaravone: a tale of two amyotrophic lateral sclerosis drugs. *Med. Res. Rev.* 39, 733–748. doi: 10.1002/med.21528
- Jun, K. Y., Park, J., Oh, K. W., Kim, E. M., Bae, J. S., Kim, I., et al. (2019). Epidemiology of ALS in Korea using nationwide big data. *J. Neurol. Neurosurg. Psychiatry* 90, 395–403. doi: 10.1136/jnnp-2018-318974
- Kim, G., Gautier, O., Tassoni-Tsushima, E., Ma, X. R., and Gitler, A. D. (2020). ALS genetics: gains, losses, and implications for future therapies. *Neuron* 108, 822–842. doi: 10.1016/j.neuron.2020.08.022
- Kim, S. H., Oh, K., and Son, B. (2021). “Public policy in ALS care: South Korea” in *Public policy in ALS/MND care: An international perspective*. eds. R. H. Blank, J. E. Kurent and D. Oliver (Singapore: Springer Singapore), 247–261. doi: 10.1007/978-981-15-5840-5_19
- Kimura, F., Fujimura, C., Ishida, S., Nakajima, H., Furutama, D., Uehara, H., et al. (2006). Progression rate of ALSFRS-R at time of diagnosis predicts survival time in ALS. *Neurology* 66, 265–267. doi: 10.1212/01.wnl.0000194316.91908.8a
- Kjældgaard, A.-L., Pilely, K., Olsen, K. S., Jessen, A. H., Lauritsen, A. Ø., Pedersen, S. W., et al. (2021). Prediction of survival in amyotrophic lateral sclerosis: a nationwide, Danish cohort study. *BMC Neurol.* 21:164. doi: 10.1186/s12883-021-02187-8
- Mazzini, L., Ferrero, I., Luparello, V., Rustichelli, D., Gunetti, M., Mareschi, K., et al. (2010). Mesenchymal stem cell transplantation in amyotrophic lateral sclerosis: a phase I clinical trial. *Exp. Neurol.* 223, 229–237. doi: 10.1016/j.expneurol.2009.08.007
- Mejzini, R., Flynn, L. L., Pitout, I. L., Fletcher, S., Wilton, S. D., and Akkari, P. A. (2019). ALS genetics, mechanisms, and therapeutics: where are we now? *Front. Neurosci.* 13:1310. doi: 10.3389/fnins.2019.01310
- Nam, J. Y., Lee, T. Y., Kim, K., Chun, S., Kim, M. S., Shin, J. H., et al. (2022). Efficacy and safety of Lenzumestrol (Neuronata-R[®] inj.) in patients with amyotrophic lateral sclerosis (ALSUMMIT study): study protocol for a multicentre, randomized, double-blind, parallel-group, sham procedure-controlled, phase III trial. *Trials* 23:415. doi: 10.1186/s13063-022-06327-4
- Oh, K. W., Moon, C., Kim, H. Y., Oh, S. I., Park, J., Lee, J. H., et al. (2015). Phase I trial of repeated intrathecal autologous bone marrow-derived mesenchymal stromal cells in amyotrophic lateral sclerosis. *Stem Cells Transl. Med.* 4, 590–597. doi: 10.5966/sctm.2014-0212
- Oh, K. W., Noh, M. Y., Kwon, M. S., Kim, H. Y., Oh, S. I., Park, J., et al. (2018). Repeated intrathecal mesenchymal stem cells for amyotrophic lateral sclerosis. *Ann. Neurol.* 84, 361–373. doi: 10.1002/ana.25302
- Petrou, P., Gotthelf, Y., Argov, Z., Gotkine, M., Levy, Y. S., Kassis, I., et al. (2016). Safety and clinical effects of mesenchymal stem cells secreting neurotrophic factor transplantation in patients with amyotrophic lateral sclerosis: results of phase 1/2 and 2a clinical trials. *JAMA Neurol.* 73, 337–344. doi: 10.1001/jamaneurol.2015.4321
- Rothstein, J. D. (2017). Edaravone: a new drug approved for ALS. *Cells* 171:725. doi: 10.1016/j.cell.2017.10.011
- Saez-Atienzar, S., Bandres-Ciga, S., Langston, R. G., Kim, J. J., Choi, S. W., Reynolds, R. H., et al. (2021). Genetic analysis of amyotrophic lateral sclerosis identifies contributing pathways and cell types. *Sci. Adv.* 7:eabd9036. doi: 10.1126/sciadv.abd9036
- Saitoh, Y., and Takahashi, Y. (2020). Riluzole for the treatment of amyotrophic lateral sclerosis. *Neurodegener Dis Manag* 10, 343–355. doi: 10.2217/nmt-2020-0033
- Syková, E., Rychmach, P., Drahorádová, I., Konrádová, Š. I., Růžicková, K., Voříšek, I., et al. (2017). Transplantation of mesenchymal stromal cells in patients with amyotrophic lateral sclerosis: results of phase I/IIa clinical trial. *Cell Transplant.* 26, 647–658. doi: 10.3727/096368916X693716
- Tavakoli-Afshari, J., Boroumand, A. R., Farkhad, N. K., Adhami Moghadam, A., Sahab-Negah, S., and Gorji, A. (2021). Safety and efficacy of bone marrow derived-mesenchymal stem cells transplantation in patients with amyotrophic lateral sclerosis. *Regen Ther* 18, 268–274. doi: 10.1016/j.reth.2021.07.006
- Taylor, J. P., Brown, R. H. Jr., and Cleveland, D. W. (2016). Decoding ALS: from genes to mechanism. *Nature* 539, 197–206. doi: 10.1038/nature20413
- The Cochrane Collaboration Miller, R. G., Mitchell, J. D., Lyon, M., and Moore, D. H. (2002). Riluzole for amyotrophic lateral sclerosis (ALS)/motor neuron disease (MND). *Cochrane Database Syst. Rev.* 2:CD001447. doi: 10.1002/14651858.CD001447
- Witzel, S., Maier, A., Steinbach, R., Grosskreutz, J., Koch, J. C., Sarikidi, A., et al. (2022). Safety and effectiveness of long-term intravenous Administration of Edaravone for treatment of patients with amyotrophic lateral sclerosis. *JAMA Neurol.* 79, 121–130. doi: 10.1001/jamaneurol.2021.4893

Publisher's note

All claims expressed in this article are solely those of the authors and do not necessarily represent those of their affiliated organizations, or those of the publisher, the editors and the reviewers. Any product that may be evaluated in this article, or claim that may be made by its manufacturer, is not guaranteed or endorsed by the publisher.

Supplementary material

The Supplementary material for this article can be found online at: <https://www.frontiersin.org/articles/10.3389/fnagi.2023.1148444/full#supplementary-material>



OPEN ACCESS

EDITED BY

Janelle Drouin-Ouellet,
Montreal University,
Canada

REVIEWED BY

Maryam Ardalan,
University of Gothenburg,
Sweden
Kate Beecher,
Queensland University of Technology,
Australia

*CORRESPONDENCE

Miriam Illa
✉ miriamil@clinic.cat

[†]These authors have contributed equally to this work and share last authorship

SPECIALTY SECTION

This article was submitted to
Cellular Neuropathology,
a section of the journal
Frontiers in Cellular Neuroscience

RECEIVED 05 December 2022

ACCEPTED 23 March 2023

PUBLISHED 26 April 2023

CITATION

Kühne BA, Gutierrez-Vázquez L, Sánchez
Lamelas E, Guardia-Escote L, Pla L, Loreiro C,
Gratacós E, Barenys M and Illa M (2023)
Lactoferrin/sialic acid prevents adverse effects
of intrauterine growth restriction on neurite
length: investigations in an *in vitro* rabbit
neurosphere model.
Front. Cell. Neurosci. 17:1116405.
doi: 10.3389/fncel.2023.1116405

COPYRIGHT

© 2023 Kühne, Gutierrez-Vázquez, Sánchez
Lamelas, Guardia-Escote, Pla, Loreiro,
Gratacós, Barenys and Illa. This is an open-
access article distributed under the terms of
the [Creative Commons Attribution License](#)
(CC BY). The use, distribution or reproduction
in other forums is permitted, provided the
original author(s) and the copyright owner(s)
are credited and that the original publication in
this journal is cited, in accordance with
accepted academic practice. No use,
distribution or reproduction is permitted which
does not comply with these terms.

Lactoferrin/sialic acid prevents adverse effects of intrauterine growth restriction on neurite length: investigations in an *in vitro* rabbit neurosphere model

Britta Anna Kühne^{1,2}, Lara Gutierrez-Vázquez¹,
Estela Sánchez Lamelas¹, Laia Guardia-Escote¹, Laura Pla²,
Carla Loreiro^{2,3}, Eduard Gratacós^{2,3,4}, Marta Barenys^{1,5†} and
Miriam Illa^{2,6*†}

¹Grup de Recerca en Toxicologia (GRET) i INSA-UB, Departament de Farmacologia, Toxicologia i Química Terapèutica, Facultat de Farmàcia i Ciències de l'Alimentació, Universitat de Barcelona, Barcelona, Spain, ²BCNatal | Fetal Medicine Research Center (Hospital Clínic and Hospital Sant Joan de Déu), Universitat de Barcelona, Barcelona, Spain, ³Institut d'Investigacions Biomèdiques August Pi i Sunyer (IDIBAPS), Barcelona, Spain, ⁴Center for Biomedical Research on Rare Diseases (CIBER-ER), Barcelona, Spain, ⁵German Centre for the Protection of Laboratory Animals (Bf3R), German Federal Institute for Risk Assessment (BfR), Berlin, Germany, ⁶Institut de Recerca Sant Joan de Déu, Esplugues de Llobregat, Spain

Introduction: Intrauterine growth restriction (IUGR) is a well-known cause of impaired neurodevelopment during life. In this study, we aimed to characterize alterations in neuronal development underlying IUGR and discover strategies to ameliorate adverse neurodevelopment effects by using a recently established rabbit *in vitro* neurosphere culture.

Methods: IUGR was surgically induced in pregnant rabbits by ligation of placental vessels in one uterine horn, while the contralateral horn remained unaffected for normal growth (control). At this time point, rabbits were randomly assigned to receive either no treatment, docosahexaenoic acid (DHA), melatonin (MEL), or lactoferrin (LF) until c-section. Neurospheres consisting of neural progenitor cells were obtained from control and IUGR pup's whole brain and comparatively analyzed for the ability to differentiate into neurons, extend neurite length, and form dendritic branching or pre-synapses. We established for the very first time a protocol to cultivate control and IUGR rabbit neurospheres not only for 5 days but under long-term conditions up to 14 days under differentiation conditions. Additionally, an *in vitro* evaluation of these therapies was evaluated by exposing neurospheres from non-treated rabbits to DHA, MEL, and SA (sialic acid, which is the major lactoferrin compound) and by assessing the ability to differentiate neurons, extend neurite length, and form dendritic branching or pre-synapses.

Results: We revealed that IUGR significantly increased the neurite length after 5 days of cultivation *in vitro*, a result in good agreement with previous *in vivo* findings in IUGR rabbits presenting more complex dendritic arborization of neurons in the frontal cortex. MEL, DHA, and SA decreased the IUGR-induced length of primary dendrites *in vitro*, however, only SA was able to reduce the total neurite length to control level in IUGR neurospheres. After prenatal *in vivo* administration of SAs parent compound LF with subsequent evaluation *in vitro*, LF was able to prevent abnormal neurite extension.

Discussion: We established for the first time the maintenance of the rabbit neurosphere culture for 14 days under differentiation conditions with increasing complexity of neuronal length and branching up to pre-synaptic formation. From

the therapies tested, LF or its major compound, SA, prevents abnormal neurite extension and was therefore identified as the most promising therapy against IUGR-induced changes in neuronal development.

KEYWORDS

fetal growth restriction, neural progenitor cells, *in vitro* techniques, sialic acid, melatonin, DHA, neurite outgrowth, neuroprotective therapies

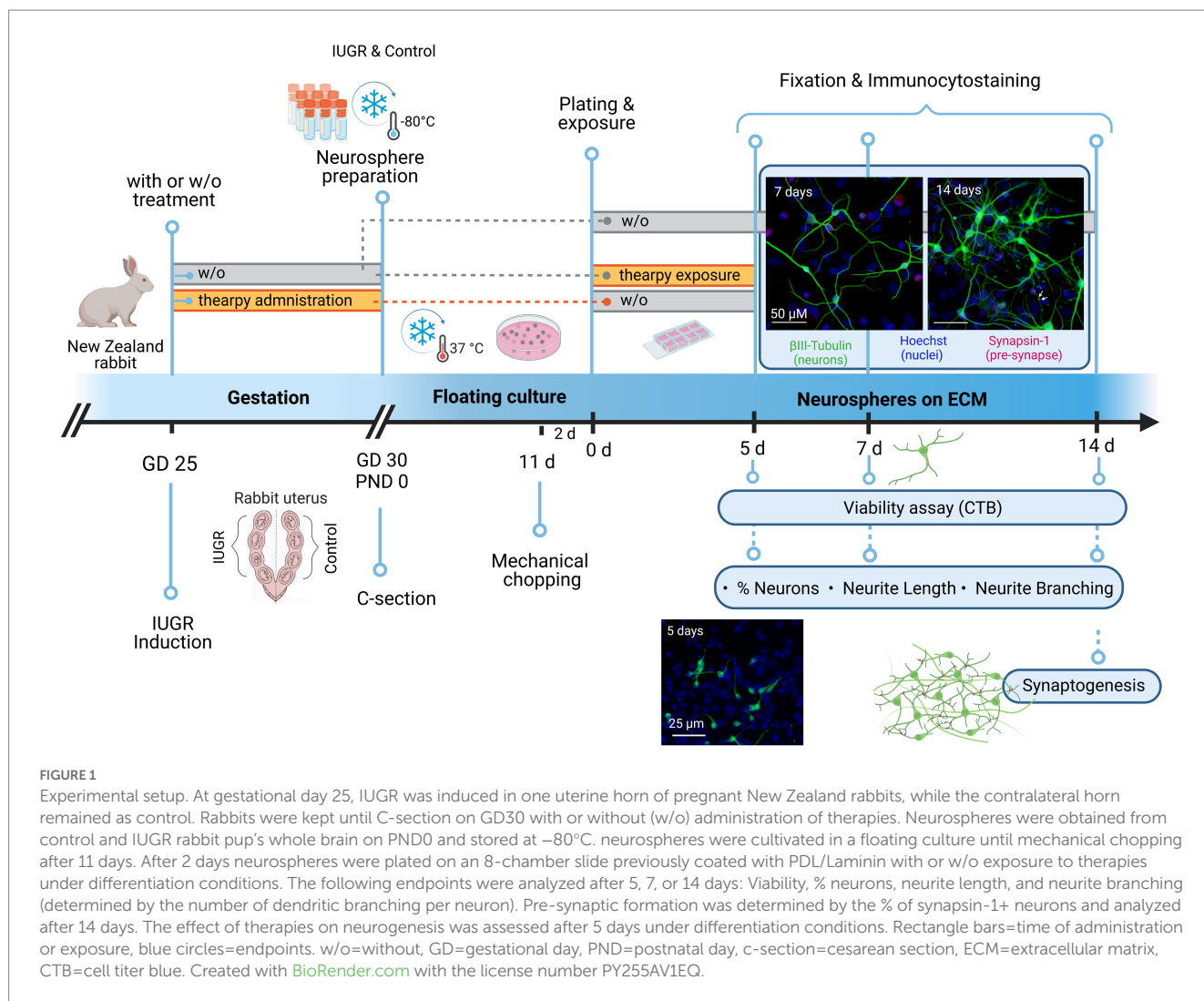
1. Introduction

Intrauterine growth restriction (IUGR) is defined as a significant decrease in fetal growth rate resulting in a birth weight below the 10th percentile of the corresponding gestational age (Sharma et al., 2016). The prevalence accounts for 5–10% of all pregnancies, and amounts to approximately 600,000 cases in Europe, being therefore a serious health problem (Kady and Gardosi, 2004). Placental insufficiency, the main cause of IUGR, chronically decreases the blood flow and nutrient supply to the developing fetus resulting in an unfavorable *in utero* environment with chronic hypoxia conditions. This situation results to a wide range of abnormal trajectories of brain development including grey (GM) and white matter (WM) injury (Esteban et al., 2010; Pla et al., 2020), which are associated with short- and long-term neurodevelopmental damage and cognitive dysfunctions (Mwaniki et al., 2012; Batalle et al., 2014; Eixarch et al., 2016). This WM injury is tightly related to impaired oligodendrocyte development and myelination (Tolcos et al., 2011; Eixarch et al., 2012; Reid et al., 2012; Rideau Batista Novais et al., 2016), while GM impairment is, in this case, related to altered neuronal connectivity, as described in humans (Batalle et al., 2012) including irregular neurite and dendritic processes in cerebellar cortex and hippocampus, as discovered in sheep, guinea pig and rabbit models of IUGR (Dieni and Rees, 2003; Piorkowska et al., 2014; Pla et al., 2020). Previous investigations of our group unraveled IUGR induced impaired oligodendrogenesis in an *in vitro* rabbit neurospheres model, which correlates very well with clinical outcomes of WM injury (Kühne et al., 2022). In the current study, we have focused on investigating neuronal development using the same model but studying differentiation of neurons, their neurite outgrowth followed by dendritic branching and network formation *in vitro*. Besides that, we also used the model to test the potential neuroprotective therapies docosahexaenoic acid (DHA), melatonin (MEL), lactoferrin (LF), and LF's main metabolite sialic acid (SA).

Currently, there is no efficient neuroprotective treatment to avoid deleterious consequences of IUGR in brain development (Lees et al., 2022). Several clinical and experimental assessments give evidence that early postnatal approaches like breastfeeding (Rao et al., 2007), individualized newborn developmental care and assessment program (Als et al., 2012), and environmental enrichment (Illa et al., 2018) can partially ameliorate the neurodevelopmental impairment caused by IUGR. However, all these strategies have been applied after birth, at a time point when adverse effects of IUGR on brain development have already occurred. The application of a treatment during the prenatal period, a “critical window of opportunity” (Andersen, 2003) is a unique chance to complement postnatal approaches which should not be missed. But to discover efficacious prenatal neuroprotective

treatments, it is essential to first deepen the understanding of the mechanisms causing neurostructural changes underlying fetal programming due to IUGR, and for that, to have a good experimental model is indispensable.

Eixarch et al. (2009) developed an experimental IUGR model in pregnant rabbits mimicking placental insufficiency leading to neurodevelopmental symptoms of IUGR which highly correlate with clinical outcomes including postnatal functional and structural discrepancies (Eixarch et al., 2009, 2012). Previous studies using this animal model discovered neonatal as well as long-term persistence of brain reorganization and changes in cerebral network organization induced by IUGR (Eixarch et al., 2012; Illa et al., 2013; Batalle et al., 2014). These results agreed with clinical investigations that 1 year old infants who suffered IUGR also present alterations in structural brain connectivity based on connectomics studies (Batalle et al., 2012). The species rabbit was selected due to its higher similarity to human neurodevelopment compared to other species according to a precocial score established by Workman et al. (2013). Rabbits resemble humans in terms of circulatory changes during gestation, placentation, and brain maturation which occurs primarily postnatally in both species (Derrick et al., 2004; Carter, 2007; Workman et al., 2013). Combining clinical findings with the neurological changes observed in rabbits indicates that the rabbit IUGR model is a suitable model to assess IUGR-induced alterations in humans (Bassan et al., 2000; Eixarch et al., 2009, 2011; Barenys et al., 2021). To understand better, which basic cellular processes are altered during brain development under IUGR, our group established an *in vitro* model based on primary rabbit neuronal progenitor cells (NPCs) (Barenys et al., 2021). In this model, rabbit NPCs obtained from control and IUGR pups are cultured as three-dimensional (3D) cell aggregates known as neurospheres. Neurospheres are able to imitate basic courses of brain development such as NPC proliferation, migration and differentiation into the brain effector cells neurons, oligodendrocytes and astrocytes (Moors et al., 2007, 2009; Breier et al., 2010; Gassmann et al., 2010; Schreiber et al., 2010; Barenys et al., 2017). Because of its 3D structure encompassing multiple cell types, the neurosphere model is a valuable test system for studying a wide range of neurodevelopmental processes guided by a broad variety of cellular pathways (Gassmann et al., 2010, 2014; Baumann et al., 2016; Barenys et al., 2017, 2021; Dach et al., 2017; Masjosthusmann et al., 2019). In a cost-efficient and animal-reduction approach, with this model we were able to test a much wider concentration range of potential therapies *in vitro* compared to classical *in vivo* experiments. After that, and to confirm the findings, on the day of IUGR induction, potential therapies were administered to pregnant animals *in vivo* to subsequently investigate their prenatal effects in the neurosphere model. A detailed description of the experimental setup is displayed in Figure 1.



By using the rabbit neurosphere assay, our group revealed previously IUGR-induced adversity on the differentiation rate of pre-myelinating oligodendrocytes and discovered two therapies, DHA and MEL, reverting the reduced oligodendrocyte differentiation after *in vitro* exposure and preventing it after *in vivo* administration to the pregnant rabbit (Kühne et al., 2022). This previous study demonstrated that the novel rabbit *in vitro* neurosphere assay is able to accurately predict the *in vivo* outcome regarding oligodendrocyte differentiation (Kühne et al., 2022). DHA is also described to facilitate myelin formation, neurotransmitter synthesis, and sustaining synaptogenesis and neuronal network (Greenberg et al., 2008; Gil-Sánchez et al., 2010; Lauritzen et al., 2016), while MEL is depicted to reduce fetoplacental oxidative stress and white- and grey-matter damage in a sheep model of placental insufficiency (Rees et al., 2011; Miller et al., 2014). LF, a SA-rich glycoprotein, was considered as a promising candidate as it enhances neuronal growth, synaptic connectivity as well as placental development (Lopez et al., 2008; Wang, 2016). We selected MEL, DHA and LF due to their promising potential to improve impaired neurogenesis. Due to very limited solubility of LF in the cell culture medium, we used its main metabolite SA for the *in vitro* experiments. Further, we assessed their safety and efficacy on several neuronal endpoints: Neuron differentiation, neurite length, number of dendrites per neuron, as well as cell viability.

2. Materials and methods

2.1. IUGR induction

All animal experimentation procedures were approved by the Ethics Committee for Animal Experimentation (CEEAA) of the University of Barcelona. All protocols were accepted by the Department of Environment and Housing of the Generalitat de Catalunya with the license number 11126, date of approval 24/5/2021, and the procedure CEEA number OB 340/19 SJD. The method of IUGR induction was previously described in Eixarch et al. (2009). Briefly, IUGR was induced at the 25th gestational day (GD) in pregnant New Zealand rabbits by surgical ligation of 40–50% of the uteroplacental vessels of each gestational sac of one uterine horn, while the contralateral horn was left for normal growth. Caesarean section was carried out at GD30 to obtain IUGR and control pups.

2.2. Administration of therapies *in vivo*

On the day of IUGR induction pregnant rabbit mothers were assigned to 4 different groups: without (w/o) administration, or with administration of MEL, DHA, or LF. The therapies were daily

administered to the pregnant rabbit by releasing the solution with a syringe in the throat from the day of IUGR induction (GD 25) until the day of caesarean section (GD 30). Specific doses were determined as followed: MEL (10 mg/kg bw/day), DHA (37 mg/kg bw/day) and Lf (166 mg/kg bw/day). We refer to Kühne et al. (2022) for a detailed description about selection of *in vivo* doses, calculations and suppliers. For all treatment groups, the inclusion criteria for postnatal day 0 (PND0) IUGR pups was a birth weight lower and for control pups higher than the 25th percentile (39.7 g, Barenys et al., 2021). The number and birth weight of PND0 rabbit pups from each group was equal to the animals described in Kühne et al. (2022). Briefly 12 control and 10 IUGR pups from the group w/o were included from 8 rabbit mothers, 2 control and 2 IUGR rabbit pups were included from two different rabbit mothers for each treatment group.

From one rabbit pup's whole brain, at least four independent experiments were performed.

2.3. Neurosphere preparation

The *in vitro* neurosphere culture was generated directly after decapitation at PND0, as described in Pla et al. (2022). Briefly, neural progenitor cells (NPCs) were isolated from rabbits' whole brains by dissection, mechanical dissociation, digestion (20 min incubation with 20 U/ml papain [Worthington #LS003124] at 37°C), mechanical homogenization into a cell suspension, and centrifugation (10 min at 1200 rpm). The cell pellet obtained was resuspended in 1 ml of freezing medium (1:1; volume of pellet: volume of freezing medium [consisting in 70% (v/v) proliferation medium, 20% (v/v) fetal calf serum (FCS [Serva #1192002]), and 10% (v/v) DMSO]) and immediately stored at -80°C. Each cryo-vial was thawed by brief immersion in a 37°C water bath, and cells were transferred to 15 ml of proliferation medium preconditioned at 37°C and 5% CO₂ for 2 h, and gentle resuspension. The cell suspension was centrifuged (10 min, 1,200 rpm), supernatant discarded and cells transferred to Poly-HEMA [Sigma #192066] coated dishes filled with proliferation medium [consisting in DMEM [Gibco #10569010] and Hams F12 [Gibco #31765027] 3:1 supplemented with 2% B27 [Gibco #17504044], and 20 ng/ml human recombinant epidermal growth factor (EGF [Gibco #PHG0313]) and recombinant human fibroblast growth factor 2 (FGF2 [R&D systems #233-FB]), Penicillin–Streptomycin (10,000 U/ml) [Gibco #15140122] supplemented with Rho kinase (ROCK) inhibitor Y-276322 [Tocris #1254] at a final concentration of 10 µM. Half of the volume of proliferation medium per petri dish was exchanged every 2–3 days by proliferation medium without ROCK inhibitor.

2.4. Neurosphere plating

IUGR and control brains derived neurospheres formed for 11 days in proliferation medium were always cultured in parallel. Two days before starting experiments, proliferating neurospheres were mechanically chopped to a size of 0.2 mm (McIlwain tissue chopper) to ensure homogeneous neurosphere size and spherical shape. Neurospheres were not chopped more than once. On the experiment plating day, 0.3 mm diameter neurospheres were selected and transferred in 8-chamber slides (Falcon #354118) previously coated with laminin [Sigma #L2020] and poly-D-lysine (PDL [Sigma #P0899]) containing differentiation medium [consisting in DMEM and Hams F12 3:1 supplemented with N2 [Gibco #17502048], Penicillin–Streptomycin (10,000 U/ml)]. The medium of 7-, and 14-day experiments were supplemented with 1% FCS. Half of the medium was renewed every 2–3 days. NPCs plated on a laminin/PDL coated surface radially migrated out of the sphere core and differentiated into effector cells. Each chamber contained five (5-day experiment) or six (7- and 14-day experiment) neurospheres representing replicates within one experiment, and at least three independent experiments were performed for every endpoint and exposure condition.

2.5. Therapy exposure *in vitro*

Compounds for neuroprotective therapy testing were dissolved in their corresponding vehicle depending on their maximum solubility (Table 1) and subsequently in differentiation medium. The effect of the potential therapies was assessed after 5 days of differentiation.

2.6. Immunocytochemistry

After 5, 7, or 14 days under differentiation conditions, neurospheres were fixed with paraformaldehyde (PFA) 4% for 30 min at 37°C, washed twice with PBS and stored in PBS until immunostained.

2.6.1. Neuronal staining after 5 and 7 days

Neurospheres were incubated with a primary antibody solution containing 10% goat serum [Sigma #G9023] and 1:100 rabbit IgG anti-βIII-tubulin antibody [Sigma T2200] in PBS-T (PBS containing 0.1% Triton X-100) for 1 h at 37°C. After three washing steps with PBS, slides were incubated with secondary antibody solution containing 2% goat serum, 1:100 Hoechst 33258 [Sigma #B1166] and 1:200 Alexa 546 anti-rabbit IgG [Invitrogen #A-11030] in PBS for 30 min at 37°C.

TABLE 1 Therapy exposure *in vitro*.

Therapy (synonym)	CAS Number	Max. Solubility	Concentration <i>in vitro</i>	MTC
MEL	73-31-4	100 µM (in DMSO)	0.1 – 0.3 – 1 – 3 µM	3 µM
DHA	6217-54-5	300 µM (in DMSO)	0.1 – 0.3 – 1 – 3 – 10 µM	10 µM
SA	131-48-6	30 µM (in DMSO)	0.1 – 0.3 – 1 – 3 – 10 µM	30 µM

Summary of the concentration range tested of potential therapies and their maximum solubility is indicated, as well as the maximum tolerated concentration (MTC) established in Kühne et al. (2022). The maximum solvent concentration was 0.1% (v/v) DMSO.

2.6.2. Co-staining of neurons and pre-synapses after 14 days

Neurospheres were incubated for 1 h at 37°C, with a primary antibody solution containing goat serum as blocking solution (10%), rabbit anti- β III-tubulin IgG antibody (1:100), mouse anti-synapsin1 IgG antibody [synaptic system #106011] and PBS-T. After three washes with PBS, slides were incubated with secondary antibody solution containing 2% goat serum, 1:100 Hoechst 33258, 1:100 Alexa 488 anti-rabbit IgG [Invitrogen #A-11008], 1:100 Alexa 546 anti-mouse IgG and PBS for 30 min at 37°C.

After incubation with the respective secondary antibody solution and three washing steps with PBS, slides were mounted with Aqua Poly/Mount (Polyscience #18606) and stored at 4°C until image acquisition.

2.7. Image acquisition and analysis of neuronal endpoints

The endpoints “% of neurons,” “number of dendrites per neuron,” and “neurite length” were analyzed after 5, 7, and 14 days of differentiation, whereas “pre-synaptic formation” was only assessed after at time point 14 days (Figure 1). EGF [20 ng/ml] was used as a positive control for neuronal differentiation. Neurospheres were fixed, immunocyto stained, and image analysis was carried out by taking two images of each migration area with a BX61 microscope (Olympus, Japan) with “UPlanFl 10x/0.30 Ph1” objective lens and using the ImageJ/Fiji 1.53q software. The number of nuclei (Hoechst staining) representing the total amount of cells was automatically counted using ImageJ/Fiji 1.53q software and neurons (β III-tubulin+ cells) were manually counted. To determine the % of neurons the number of neurons was normalized to the number of nuclei.

The number of dendrites/neuron and their distances from the soma (neurite length) were manually measured by using ImageJ 1.53q after 5 days of differentiation. After 7 and 14 days, the number of dendrites/neuron and neurite length were assessed with the “Sholl analysis” of the ImageJ/Fiji 1.53q blinded to the experimental groups (L.G.V. and B.A.K.). The tool “Sholl analysis” was used to trace manually the different paths of dendrites calculating dendritic branching and length, as described in detail in Pla et al. (2020). The 8-bit tracing was constructed by using the Fiji plugins “Segmentation” and “Simple Neurite Tracer” as described in Binley et al. (2014). The total amount of dendrites was classified in primary, secondary, or tertiary dendrites depending on their point of division. The primary dendrites are born from the soma, the secondary ones from the primaries and so on. After 14 days the ability to generate pre-synapses was analyzed. Pre-synaptic puncta were defined as Synapsin-1 (pre-synaptic marker) co-localized with β III-Tubulin+ cells. Pre-synaptic formation (synapsin-1+ neurons [%]) was determined by the number of neurons with synapsin-1+ puncta normalized by the total number of neurons. Analysis was evaluated in 5–6 neurospheres/condition, minimum 10 neurons/neurosphere in at least 3 independent experiments.

2.8. Cell viability

The cell viability was assessed with the CellTiter-Blue® cell viability assay (Promega #G8081). This assay is based on the

measurement of mitochondrial reductase activity of living cells by conversion of resazurin to the fluorescent product resorufin. After 2 h of incubation with the reagent (1:3), medium was placed in a 96-well plate and read with FLUOstar Optima microplate reader. Neurospheres exposed to 10% DMSO (2h) were used as lysis control.

2.9. Statistics

Statistical analysis was performed using GraphPad Prism v9. The difference between two samples was calculated with a two-tailed paired student's *t*-test. Concentration-dependent effects were analyzed using one-way ANOVA. Time-course experiments including the comparisons of more than two groups were assessed by performing a two-way ANOVA. One-way and two-way ANOVA analysis was always followed by post-hoc test Bonferroni's multiple comparison test. The respective statistical analysis is mentioned in each figure legend. The significance threshold was established at $*p \leq 0.05$.

3. Results

3.1. IUGR increases neurite length after 5 days *in vitro*

Neurospheres were prepared from 12 control and 10 IUGR rabbit pups with a significantly reduced body weight in the IUGR group as described in Kühne et al. (2022). Previous results from our group testing the impact of IUGR in the rabbit neurosphere model after 3 days in culture determined no difference between control and IUGR on the endpoint “% neurons” (Barenys et al., 2021). In the current study, we investigated the impact of IUGR on neuronal endpoints after 5 days *in vitro* to unravel if changes may occur at a later time point but we confirmed that the percentage of neurons was also not significantly different between control and IUGR at this time point (Figures 2A,B, Control: $2.25 \pm 0.39\%$ vs. IUGR: $2.34 \pm 0.25\%$, $p = 0.800$). The positive control EGF significantly decreased the % of neurons in both groups (Figure 2B, Control: $0.21 \pm 0.08\%$; IUGR: $0.15 \pm 0.04\%$), and significantly increased the metabolic activity in comparison to the solvent control indicating a proliferative effect as expected for this growth factor (Supplementary Figure S1A) proving that the system is flexible and can react to external stimuli known to keep cells in a proliferating instead of in a differentiating status. The endpoint “neurite length” was measured by the distance from the soma to the neurite end (Figure 2C), and the “number of dendrites per neuron” revealed the degree of dendritic arborization (Figure 2D). After 5 days in culture, neurons of control, and IUGR neurospheres developed mainly primary dendrites and significantly fewer secondary dendrites per neuron (1.39 control primary vs. 0.12 control secondary dendrites/neuron, $p < 0.0001$; Figure 2D). Importantly, the total neurite length was significantly increased in IUGR neurospheres compared to the respective control value (Figure 2C, total control: 29.82 ± 2.84 vs. IUGR: $36.03 \pm 3.46 \mu\text{m}$, $p = 0.011$). This difference was due to the significantly larger primary neurites in IUGR neurospheres (Figure 2C, primary control: 28.50 ± 2.71 vs. IUGR: $34.81 \pm 3.48 \mu\text{m}$, $p = 0.006$), and not to differences in the secondary neurite length

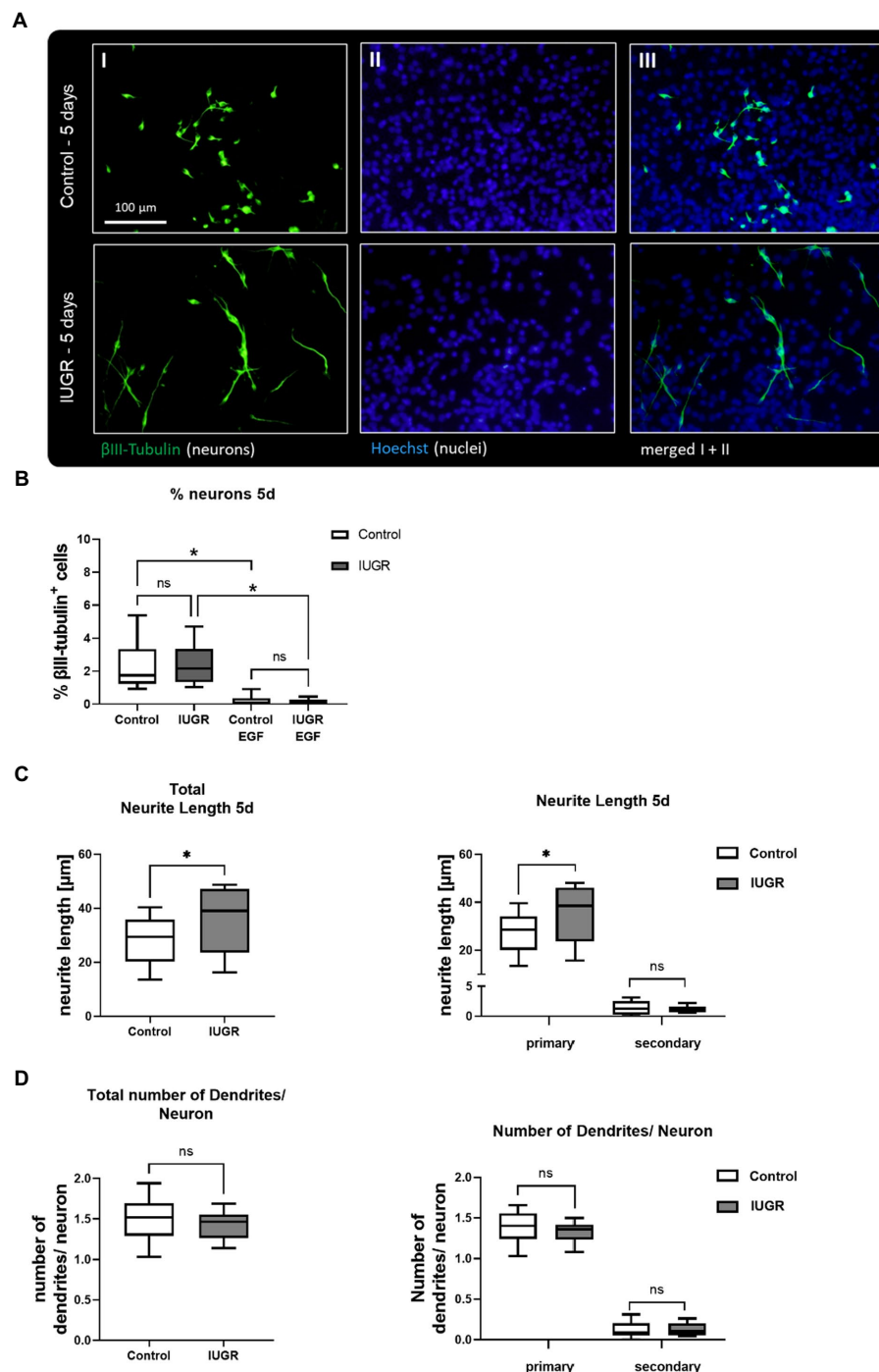


FIGURE 2

Neuronal development after 5 days after 5 days. (A) Representative pictures of neuronal marker βIII-Tubulin (I, green), nuclei marker Hoechst 33258 (II, blue) and merged (III) in control and IUGR neurospheres after 5 days under differentiation conditions. Control and IUGR neurospheres were tested for (B) % neurons, including the positive control EGF [20 ng/ml], (C) neurite length and (D) number of dendrites/neurons. Mean±SEM; * $p \leq 0.05$, ns: not significant. Comparison between two groups was analyzed by two-tailed paired *t*-test. Comparisons of more than two groups were assessed by performing a one-way ANOVA followed by Bonferroni's multiple comparison test.

(Figure 2C, secondary control: 1.36 ± 0.35 vs. IUGR: 1.19 ± 0.16 μm, $p = 0.943$). The number of dendrites per neuron did not vary between control and IUGR after 5 days, neither the total number nor the number of primary or secondary dendrites (Figure 2D, total control: 1.51 ± 0.09 vs. IUGR: 1.44 ± 0.05 dendrites/neuron, $p = 0.353$).

3.2. IUGR increases the % of neurons after 14 days in a time-dependent manner

We established for the very first time the maintenance of rabbit control and IUGR neurospheres under long-term differentiation conditions [maximum time in culture previously described was 5 days

in vitro (Barenys et al., 2021)] and examined the changes in neuronal morphology or network formation over time (Figure 3). Representative pictures of neurospheres cultured for 7 and 14 days *in vitro* revealed that both groups (IUGR and control) continued developing β III-tubulin+ cells. After 7 days both neurosphere groups, control and IUGR, did not develop the pre-synaptic marker synapsin-1 (Supplementary Figures S2), but after 14 days they presented pre-synaptic formation (Figures 3A,B). In a time-course experiment including the time points 5, 7, and 14 days, a significant interaction between time and cases (control and IUGR) was observed ($p=0.0143$). The percentage of β III-tubulin+ cells was only slightly increased in the IUGR group compared to the control after 7 days. But remarkably, after 14 days, the percentage of neurons in IUGR neurospheres exceeded to a significant extent the percentage of neurons in the control group (Figure 3C, Control: $4.43 \pm 0.98\%$ vs. IUGR: $8.82 \pm 2.61\%$, $p=0.005$). By using this time-course approach we discovered that the neuronal differentiation rate is significantly faster in IUGR compared to control (Figure 3C, difference between the slopes of control and IUGR: $p=0.013$), without affecting the viability at any time point indicating a specific effect on neuronal development by excluding a cytotoxic effect (Supplementary Figures S1B,C). The total neurite length and number of dendrites per neuron increased over time in both groups, control and IUGR, demonstrating a more complex neuronal morphology with extended neurites and more branched dendrites from 5 to 14 days (Figures 3D,E). After 14 days, the percentage of neurons developing pre-synaptic puncta (synapsin-1+ neurons) was measured (Figure 3B IV–V arrows, Figure 3F). However, no significant difference in the presynaptic formation between control and IUGR was discovered (Figure 3F, Control: $15.23 \pm 9.97\%$ vs. IUGR: $27.45 \pm 11.36\%$, $p=0.277$).

To investigate the development of neurite length and dendritic arborization in more detail, we measured not only their total number and length but also the number and length of primary, secondary, and tertiary dendrites after 7 and 14 days *in vitro* (Figure 4). While NPCs cultured for 5 days only formed neurons with primary and secondary dendrites (Figures 2C,D), NPCs cultured for 7 and 14 days established a more advanced neuronal phenotype including tertiary dendrites (Figure 4). Representative pictures display the measurement of neurite length and the number of primary, secondary, and tertiary dendrites of control and IUGR neurons after 7 and 14 days using the “Sholl analysis” (Figures 4A,C). Primary dendrites from neurons of both groups (control and IUGR) significantly extended their length over time from 7 to 14 days (Figure 4B), whereas only the IUGR group significantly increased the number of primary dendrites/neuron over time (Figure 4D). Secondary dendrites of neurons of both groups increased their number from 7 to 14 days, while only the control group significantly increased the length of secondary dendrites (Figures 4B,D). Tertiary dendrites from neurons of both groups did not significantly expand their length or number over time.

3.3. Assessment of potential therapies after 5 days *in vitro*

We selected the time point 5 days *in vitro* for further assessments of potential therapies, because our results at this time point correlate very well with the situation described *in vivo* in a previous study investigating structural brain changes in a rabbit model of IUGR (Pla

et al., 2020). This study observed a more advanced dendritic morphology in the frontal cortex of IUGR compared to control animals (Pla et al., 2020).

With the aim to revert adverse effects on neurogenesis induced by IUGR, we evaluated the safety and efficacy of 3 potential therapies MEL, DHA, and SA on the neuronal endpoints “% of neurons,” “neurite length,” and “number of dendrites per neuron,” as well as cell viability. In a previous study of our group using rabbit neurospheres, the maximum tolerated concentration (MTC) from MEL, DHA, and SA was determined in control neurospheres with the following criteria: viability was not lower than 70% of the solvent control (SC), migration distance and % of oligodendrocytes were not significantly reduced (Kühne et al., 2022). In the current approach, the additional criteria to set the MTC was “no significant adverse effect on any on the tested neuronal endpoints” in control neurospheres. Control neurospheres were exposed to potential therapies in a concentration-dependent manner for 5 days under differentiation conditions *in vitro* (Figure 5). None of the tested therapies adversely disturbed the tested endpoints (Figure 5, Supplementary Figure S3) and the MTC of each compound was set at the highest tested concentration for each compound, which was in accordance with the results in Kühne et al. (2022). A summary of these concentrations is presented in Table 1.

The main interest was to find a concentration of the selected therapies which reverts the effects of IUGR. The cell viability determined by metabolic activity was always performed in the same experiments to distinguish between a specific effect and a general cytotoxic effect (Supplementary Figure S3). IUGR neurospheres were exposed to increasing concentrations of the selected therapies up to their MTC (Table 1). MEL, DHA, and SA did not significantly interfere with the % of neurons at any of the tested concentrations neither in control nor in IUGR neurospheres (Figures 5A, 6A). Our focus lied on decreasing the neurite length of the IUGR group because the total neurite length and the length of primary dendrites were significantly increased by IUGR after 5 days *in vitro*. MEL did not significantly reduce the total neurite length in IUGR neurospheres in none of the tested concentrations (Figure 6B). However, the lowest (0.1 μ M) and the highest (3 μ M) concentration of MEL significantly reduced the length of primary dendrites by presenting a stronger effect in the lowest concentration (Figure 6C, 0.1 μ M MEL $20.70 \pm 2.86 \mu$ m vs. SC $34.81 \pm 3.48 \mu$ m, $p=0.004$). MEL induced a non-monotonic response without showing a concentration-dependent effect or impact on the total neurite length, that is why MEL was not considered as the most favorable therapy against IUGR induced adverse effects on neurite length. Likewise, DHA did not present a significant reduction in the total neurite length at any of the tested concentrations (Figure 6B). Nevertheless, DHA showed a concentration-dependent effect on primary dendrites decreasing their length significantly ($p=0.001$, Figure 6C). Even though DHA showed a positive effect on primary dendrites, the total length of neurites could not be improved. On the contrary, the exposure of SA to IUGR neurospheres prompted a concentration-dependent effect on total neurites and primary dendrites by significantly reducing their length. 10 μ M SA significantly decreased the total neurite length ($21.03 \pm 0.75 \mu$ m vs. SC $36.03 \pm 3.46 \mu$ m, $p=0.05$), and 1 and 10 μ M SA significantly reduced the length of primary dendrites (1 μ M SA $22.43 \pm 0.93 \mu$ m, $p=0.022$; 10 μ M SA 19.64 ± 0.5 , $p=0.003$). The total number of dendrites per neuron was not altered by any of the tested therapies (Figure 6D), neither the number of primary nor secondary dendrites per neuron (Figure 6E). Based on these findings, SA was selected to be the best candidate in reverting neurite extension induced by IUGR *in vitro*.

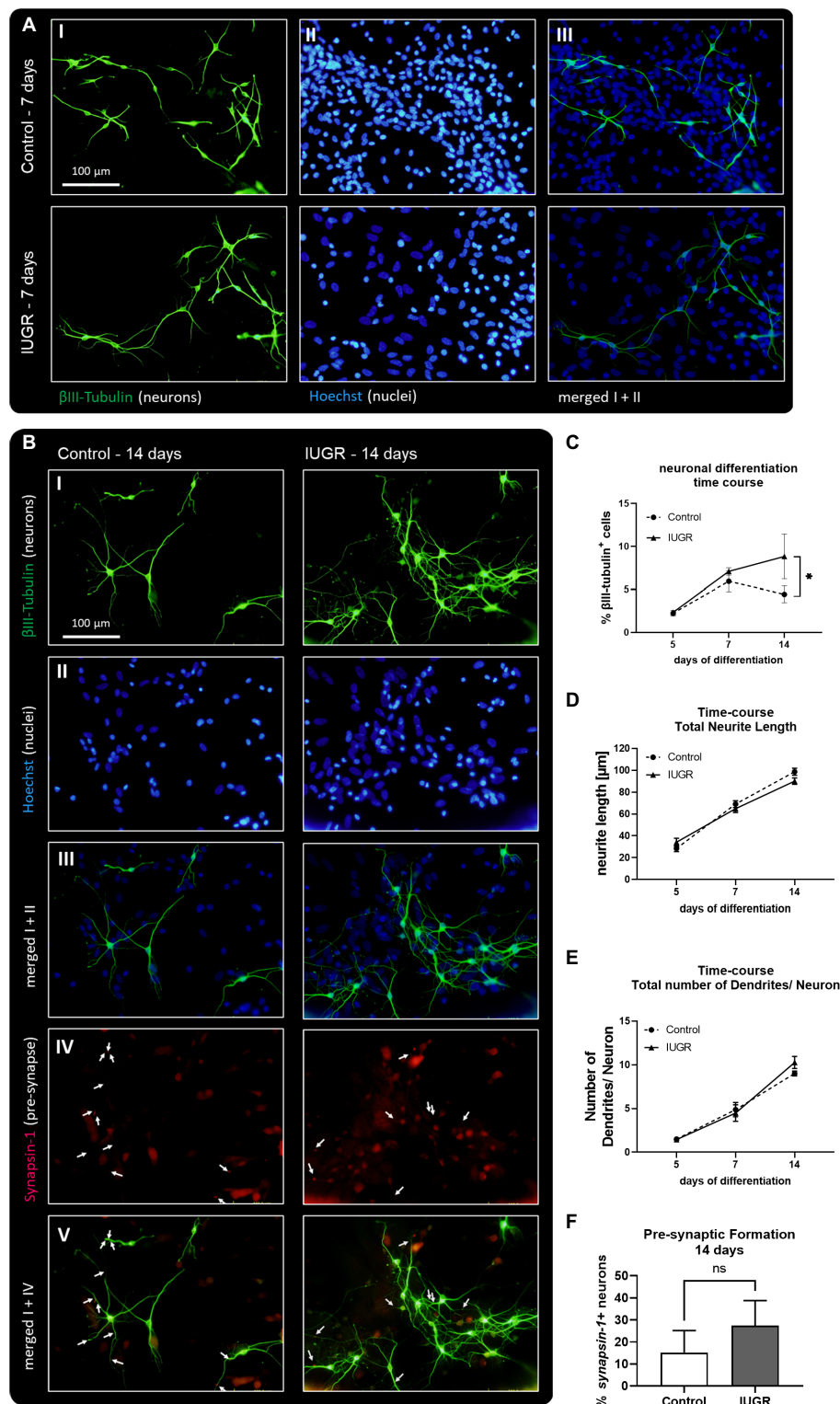


FIGURE 3

Neuronal development and network formation after 5, 7, and 14 days. **(A)** 7 days of neuronal differentiation in control and IUGR neurospheres. Representative pictures of neuronal marker β III-Tubulin (I, green), nuclei marker Hoechst 33258 (II, blue) and merged (III). **(B)** 14 days of neuronal differentiation control and IUGR neurospheres. Representative pictures of (I) Neuronal marker β III-Tubulin (green), (II) nuclei marker Hoechst 33258 (blue), (III) merged picture of neuronal and nuclei staining, (IV) pre-synaptic marker Synapsin-1, (V) merged picture of neuronal and synaptic staining. Scale bar=100 μ m. **(C)** Time course of neuronal differentiation from 3 to 14 days of differentiation [% β III-Tubulin positive cells], **(D)** Time course of total neurite length/ neuron from 5–14 days. **(E)** Time course of total number of dendrites/neuron from 5–14 days. **(F)** Pre-synaptic formation: Rabbit neurospheres obtained from control and IUGR pups were cultured for 14 days and comparatively tested for the ability to generate pre-synapses. Pre-synaptic formation was determined by the number of neurons with synapsin-1 positive puncta normalized by the total number of neurons (synapsin-1+ neurons [%]). Analysis was evaluated in 6 neurospheres/condition, minimum 10 neurons/neurosphere in 3 independent experiments. Mean \pm SEM; * $p \leq 0.05$, ns: not significant. Time-course analysis was performed using two-way ANOVA followed by Bonferroni's multiple comparison. Comparison between two groups was analyzed by two-tailed paired t -test **(F)**.

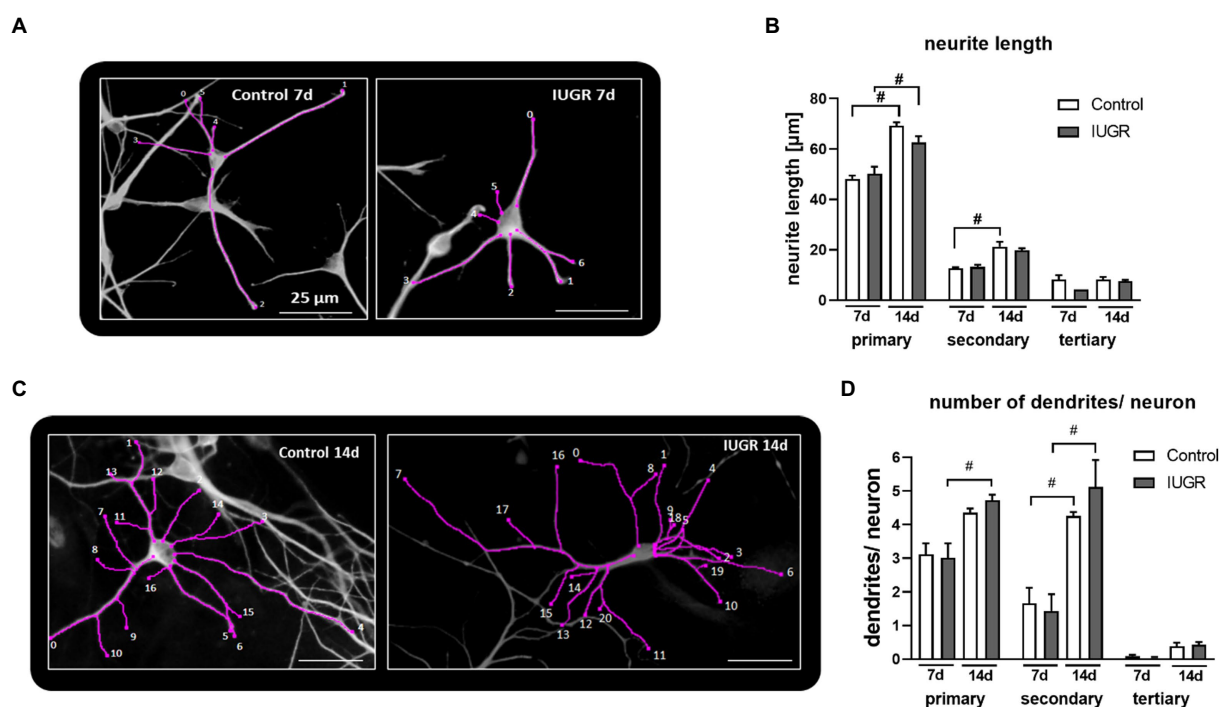


FIGURE 4

Length and number of primary, secondary and tertiary dendrites per neuron after 7 and 14 days. Example of “Sholl analysis” of a control (left) and IUGR (right) neuron, respectively, with traced and counted dendrites, after (A) 7 and (B) 14 days of differentiation, scale bar=25 μm. Control and IUGR neurospheres were cultured for 7 or 14 days and comparatively tested for the (C) neurite length of primary, secondary and tertiary dendrites, (D) number of primary, secondary and tertiary dendrites/neuron. Analysis was evaluated in 6 neurospheres/condition, minimum 10 neurons/neurosphere in at least 3 independent experiments. Mean±SEM; * $p \leq 0.05$ control vs. IUGR. #: $p \leq 0.05$ 7 d vs. 14 d. Analysis was performed using two-way ANOVA followed by Bonferroni's multiple comparison.

3.4. Administration of therapies *in vivo*—evaluation *in vitro*

To investigate the transferability of the *in vitro* results to the *in vivo* situation, we randomly assigned pregnant rabbits to different groups and administered MEL, DHA, or LF daily from the day of IUGR induction until C-section. SA is the main metabolite of LF, and therefore not SA but the parent compound LF was selected for the treatment *in vivo*. The body weight of the PND0-IUGR pups from all groups (with or without treatment; w/o) was significantly lower than the body weight of the respective control group, indicating that the treatments had no effect on the body weight [see Table 1 in Kühne et al. (2022)].

Neurospheres were obtained from control and IUGR pup's whole brain from the different treatment groups and analyzed for neuronal endpoints after 5 days under differentiation condition *in vitro*. The cell viability determined by metabolic activity was not significantly reduced compared to the control value in neurospheres of any treatment group (Supplementary Figure S4). The % of neurons was not significantly different between control and IUGR neurospheres obtained from pups from all treatment groups, which is in accordance with the effect observed *in vitro* (Figure 7A). Neurospheres obtained from IUGR pups prenatally administered to MEL did not display any improvement in neurite length, neither the total neurite length nor the length of primary or secondary dendrites (Figure 7B). Likewise, the prenatal administration of DHA to the pregnant rabbit could not prevent the adverse effect of IUGR on total neurite length, primary, or

secondary dendrites (Figure 7B). However, neurospheres from IUGR pups of LF-treated rabbits presented a significant reduction in the total neurite length compared to the non-treated IUGR group (LF total: $23.71 \pm 0.64 \mu\text{m}$ vs. w/o total: $36.03 \pm 3.46 \mu\text{m}$, $p = 0.049$, Figure 7B). The length of primary dendrites was also significantly reduced in IUGR neurospheres of the LF group compared to primary dendrites of the non-treated IUGR group (LF primary: $22.23 \pm 1.10 \mu\text{m}$ vs. w/o primary: $34.81 \pm 3.48 \mu\text{m}$, $p = 0.0045$), while the length of secondary dendrites remained unaffected. In control neurospheres from the LF group, the neurite length of total and primary dendrites stayed on the level of w/o control neurospheres. Remarkably, these results are in good agreement with the results of the *in vitro* exposure to SA, the main metabolite of LF (Figures 6B,C). Finally, the total number of dendrites per neuron did not differ between any treatment group and w/o group (Figure 7C). None of the *in vivo* tested therapies influenced the number of primary or secondary dendrites per neuron, which was also in line with our *in vitro* results (Figures 6D,E).

Taking into account all results presented, the *in vitro* neurosphere assay correctly predicted the outcome of both, positive and negative results of the *in vivo* administration for the endpoints “% of neurons,” “total neurite length,” and “total number of dendrites” or “number of primary and secondary dendrites.” Merely the *in vitro* results of “length of primary and secondary dendrites” after exposure to MEL and DHA was not in accordance with the results of the prenatal *in vivo* treatment. Our findings revealed LF as the most promising therapy to prevent increased neurite length caused by IUGR.

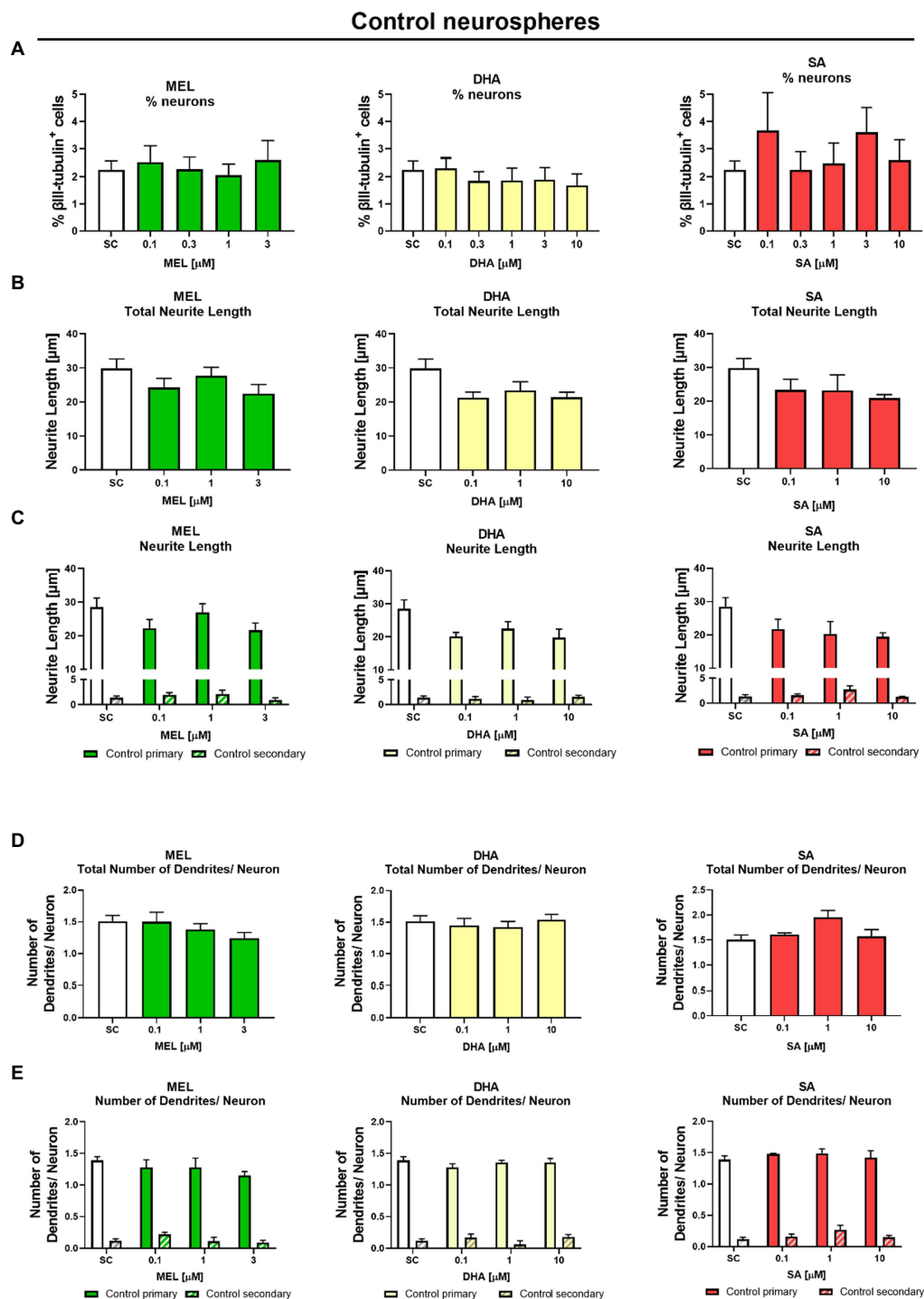


FIGURE 5

Exposure to potential therapies *in vitro* – safety evaluation after 5 days *in vitro*: Safety assessment of therapies on neuronal endpoints. Control neurospheres were tested for (A) % neurons [% β III-tubulin+ cells], (B) total neurite length, (C) length of primary and secondary dendrites, (D) total number of dendrites/neuron, and (E) number of primary and secondary dendrites/neuron and exposed to increasing concentrations of Melatonin (MEL, green), DHA (yellow), or Sialic Acid (SA, red). Mean \pm SEM. Concentration-dependent effects were analyzed using one-way ANOVA followed by Bonferroni's multiple comparison test.

4. Discussion

We used a previously established rabbit neurosphere model mimicking brain development under IUGR conditions (Barenys et al.,

2021). The *in vitro* neurosphere system has been revealed to reproduce the clinical situation of WM injury by reducing the percentage of pre-oligodendrocytes in the IUGR group *in vitro* by accurately predicting the outcome *in vivo* with respect to oligodendrogenesis,

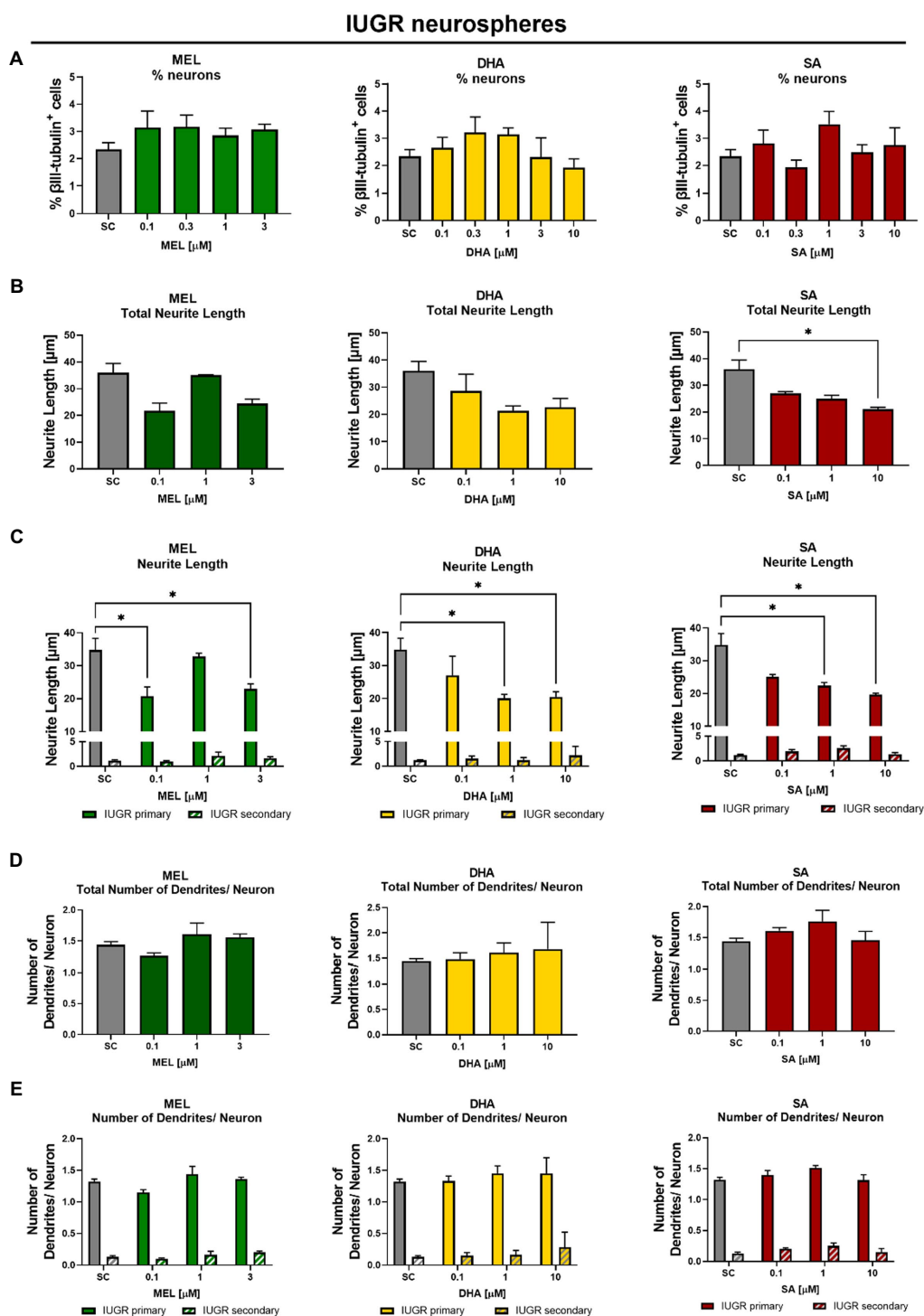


FIGURE 6

Exposure to potential therapies *in vitro* – efficacy evaluation after 5 days *in vitro*: Effect of therapies on neuronal endpoints. IUGR neurospheres were tested for (A) % neurons [% β III-tubulin⁺ cells], (B) total neurite length, (C) length of primary and secondary dendrites, (D) total number of dendrites/ neuron, and (E) number of primary and secondary dendrites/neuron and exposed to increasing concentrations of Melatonin (MEL, green), DHA (yellow), or Sialic Acid (SA, red). Mean \pm SEM; * $p \leq 0.05$ SC vs. treatment. Concentration-dependent effects were analyzed using one-way ANOVA followed by Bonferroni's multiple comparison test. Comparison of more than two groups were assessed by performing a two-way ANOVA followed by Bonferroni's multiple comparison test (C,E).

which makes it a powerful and consistent tool to assess IUGR induced neurological alterations (Kühne et al., 2022). In this study, we assessed the impact of IUGR on neuronal development after 5, 7, and 14 days

and pre-synaptic formation after 14 days *in vitro*, as well as the safety and efficacy of potential therapies *in vitro* and after *in vivo* administration.

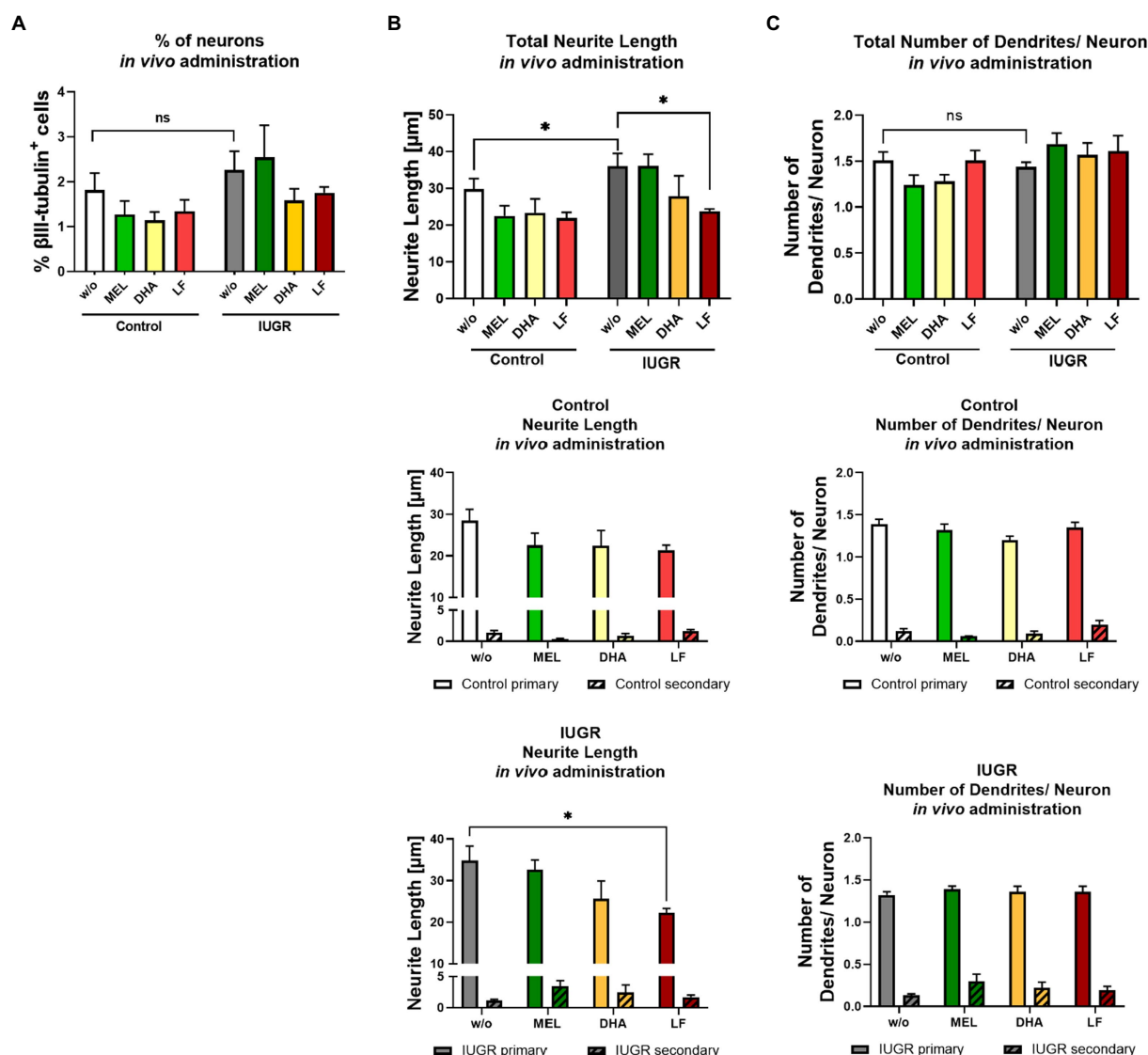


FIGURE 7

Administration of potential therapies *in vivo* – evaluation after 5 days *in vitro*. Pregnant rabbits received no treatment (w/o), MEL (10 mg/kg bw/day, green), DHA (37 mg/kg bw/day, yellow) or LF (166 mg/kg bw/day, red) at the day of IUGR induction until cesarean section. Neurospheres obtained from Control and IUGR pups were tested for (A) % neuronal differentiation (% β III-tubulin+ cells), (B) total neurite length and below length of primary and secondary dendrites in control and IUGR neurospheres (C) total number of dendrites/ neuron and below number of primary and secondary dendrites in control and IUGR neurospheres; Mean \pm SEM; * $p \leq 0.05$, ns: not significant. Upper row: Data was analyzed using one-way ANOVA. Comparison of more than two groups (treatment, primary and secondary dendrites) was assessed by two-way ANOVA. Both followed by Bonferroni's multiple comparison test.

IUGR neurospheres presented a significant increase in the total neurite length as well as in the length of primary dendrites after 5 days *in vitro*. These results correlate very well with a previous *in vivo* study of our group, where IUGR rabbit pups (PND1) presented a more complex branched morphology in frontal cortex neurons. In that study, tertiary, quaternary and quinary dendritic branches were significantly increased in the IUGR versus the control group (Pla et al., 2020). With the same *in vivo* rabbit model, diffusion tensor imaging parameters were assessed revealing reduced fractional anisotropy (FA) in several brain regions of WM and GM including the frontal cortex of IUGR animals (Eixarch et al., 2012). A decrease in cortical FA is associated with an increase in dendritic expansion and branching of neurons (McKinstry et al., 2002) and also correlates well with the increased neurite length present in our IUGR *in vitro* culture.

Although the exact mechanism leading to these changes in neurite branching *in vitro* and *in vivo* is not known yet, a recent study of our group provides evidence of a possible underlying molecular mechanism: IUGR neurospheres present a significant higher expression of the adhesion molecule integrin- β 1 at gene and protein level (Kühne et al., 2022). Integrin- β 1 interacts with the extracellular matrix (ECM) protein laminin allowing the migration of NPCs to a distal destination and the alignment of glial cell in brain and cerebellar cortex (Graus-Porta et al., 2001; Förster et al., 2002; Belvindrah et al., 2007; Barenys et al., 2017; Kühne et al., 2019). But integrin- β 1 is not only involved in migration but also in the extension of neurite length and arborization in the developing brain as studies have shown that integrin- β 1 deficiency in cells from partial knock-out mice were not able to evolve dendritic branching

(Marrs et al., 2006; Belvindrah et al., 2007). Also, integrin- β 1 blocking or inhibition experiments reduced or avoided neurite extension and branching on laminin (Moresco et al., 2005; Warren et al., 2012; Ortiz-Romero et al., 2018). In view of the finding that IUGR neurospheres overexpress integrin- β 1, future experiments to prove if this is the underlying mechanism of the changes observed in neurites, such as plating control and IUGR neurospheres on an ECM with decreasing laminin concentrations to discover whether the extended neurite length decreases with declining laminin concentrations, are needed.

We successfully established for the very first time the maintenance of the rabbit neurosphere culture for 7 and 14 days under differentiation conditions. This is of importance for research groups working with the rabbit model and needing longer-term culture periods to model longer exposure to toxicants or to therapeutic agents. Over that time in culture, both control and IUGR neurospheres developed a more complex neuronal phenotype including more dendrites and longer neurites. This outcome demonstrates that our rabbit neurosphere system is able to reflect spatiotemporal processes of brain development with increasing complexity of the nervous system as described for human neurospheres (Kim et al., 2006).

In the time-course experiment, the percentage of neurons in IUGR significantly exceeded the % of neurons in control neurospheres after 14 days. This increase in percentage of neurons was not previously described in the *in vivo* IUGR model (it was not tested) and therefore needs further confirmation. For this reason, we decided not to focus on the prevention/reversion of this result for the evaluation of the therapies. After 14 days, both groups were able to develop the pre-synaptic marker synapsin-1, suggesting neuronal network formation. Our results indicate a faster network expansion in the rabbit compared to the human neurosphere culture. Neurons of primary human NPCs did not develop synaptic markers until 28 days under differentiation conditions and human induced pluripotent stem cells developed synaptic markers at first after 28 days in culture forming an electrically active neuronal network (Hofrichter et al., 2017; Nimtz et al., 2020). We did not find a difference in pre-synaptic marker formation between control and IUGR, but to our knowledge, IUGR induced disturbance of neuronal function including signal transmissions has never been studied yet in an *in vitro* model of IUGR. In future, it will be necessary to co-label pre- and post-synaptic compartments by including a post-synaptic marker such as PSD-95 to confirm the formation of synapses between neurons. However, it was challenging to maintain rabbit neurospheres for more than 7 days under differentiation conditions, and it was necessary to supplement the medium with FCS, which is known to improve viability but also induce neuronal differentiation in rabbit neurospheres (Barenys et al., 2021). If IUGR neurospheres need to be kept under restricted oxygen and nutrients supply *in vitro* for long-term culture to continue to be a correct model to study IUGR needs further clarification, thus we decided to focus on the differentiation day 5 in the current study.

To date no efficient treatment is available to improve adverse brain development occurring from IUGR, and neuroprotective therapies are urgently needed to be applied prenatally during the “critical window of opportunity” to protect or correct IUGR-induced brain damage (Andersen, 2003). Our rabbit model mimics the situation of late-onset IUGR, which is the most critical instance encompassing the highest incidence of IUGR cases with a very small time window between diagnosis and intervention (Figueras and Gratacos, 2017; Figueras

et al., 2018). For the safety and efficacy testing of potential therapies MEL, DHA, and LF or its main metabolite SA we exposed the neurospheres for 5 days under differentiation conditions, as this time point presented several advantages: i) it is a short-time period in good agreement with the short intervention time described in late-onset IUGR cases in humans, ii) it is the time between IUGR induction *in vivo* and C-section, so the *in vitro* and *in vivo* treatments would be comparably long, and iii) the *in vitro* results on IUGR-induced changes in neurites highly correspond to previous *in vivo* findings (Pla et al., 2020). Regarding the safety of the selected therapies, none of the tested concentrations *in vitro* or after prenatal administration *in vivo* exhibited an adverse effect on viability or neuronal endpoints in control neurospheres indicating safe concentrations *in vitro* and *in vivo*. These results comply with the safety assessment of all tested compounds on the endpoint oligodendrogenesis as previously calculated in Kühne et al. (2022). In this earlier study, we identified MEL and DHA as the most promising therapies to prevent and revert IUGR adverse effects on oligodendrogenesis, while LF did not change impaired oligodendrocyte differentiation after IUGR induction (Kühne et al., 2022). The hormone MEL is a highly effective antioxidant, which readily crosses the placental and blood–brain barrier reducing fetoplacental oxidative stress and decreased white- and grey-matter damage in different models of IUGR (Rees et al., 2011; Miller et al., 2014; Castillo-Melendez et al., 2017). DHA is a long-chain omega-3 polyunsaturated fatty acid that is an important component of brain membrane phospholipids, which contributes to neuronal differentiation and signaling and accelerate myelination (Greenberg et al., 2008; Gil-Sánchez et al., 2010; Lauritzen et al., 2016). By exposure to different concentrations of MEL, DHA, and SA to IUGR neurospheres *in vitro*, all three tested compounds could revert the IUGR-induced length of primary dendrites, however, only SA was able to decrease the total neurite length in IUGR neurospheres. After *in vivo* administration only LF could prevent the neurite elongation in IUGR neurospheres and was therefore considered as the best candidate for the protection of neuronal development.

LF is an iron-binding, SA-rich glycoprotein known to act as anti-bacterial and anti-inflammatory compound protecting the development of brain and cognitive function (Wang, 2016). LF was reported to protect against immature brain injury by recovering cerebral GM and WM destruction in a rat model of hypoxia-ischemia after maternal supplementation with LF (van de Looij et al., 2014). SA is a monosaccharide that plays a key role in the synthesis of brain gangliosides and sialylated glycoproteins including polysialic acid (Poly-SA), which binds to the neural cell adhesion molecule (NCAM) and is crucial for the neurodevelopment (Weinhold et al., 2005; Bonfanti, 2006; Wang, 2016). (Burgess et al., 2007) discovered in an *in vitro* primary embryonic rat cell culture, that poly-SA limits the neurite elongation of septal neurons by preventing the interactions between integrin- β 1 and laminin. The other way around, a removal of poly-SA enhances the laminin and integrin- β 1 interaction, which was responsible for neurite outgrowth. Another group reported that a removal of poly-SA facilitated the development of immature neurons in adult mice (Coviello et al., 2021), thus showing the *in vivo* relevance of this interaction. These results are in line with our investigations revealing an overexpression of integrin- β 1 in IUGR NPCs (Kühne et al., 2022) along with elongated neurite length in IUGR neurospheres, which could be reverted due to SA exposure *in vitro* and prevented by LF administration *in vivo*.

However, it is important to remark that we do not know if the increased neuronal arborization is harmful or is a mechanism compensating other adverse effects of IUGR. In previous *in vivo* experiments using the same rabbit model, IUGR animals did not present severe functional impairments at short-term (PND1) (Pla et al., 2020), but only at later time points (PND70) neurobehavioral and cognitive deficiencies could be evaluated and indeed memory and anxiety traits were detected in the IUGR animals (Illa et al., 2013, 2018). In future, we need studies evaluating long-term effects of LF in GM along with cognitive functional studies, which could not be assessed at the short-term evaluation in our animal species (Illa et al., 2023).

In summary, we established for the first time the sustainment of the rabbit neurosphere culture until 14 days under differentiation conditions with increasing complexity of neuronal length and branching up to pre-synaptic formation, mimicking spatiotemporal characteristics of brain development. IUGR neurospheres presented a significant increase in neurite length compared to control neurospheres after 5 days *in vitro*. The underlying mechanism of this effect in the IUGR group is not known, but we hypothesize that it could be attributed to an increase in the adhesion molecule integrin- β 1, as previously discovered in Kühne et al. (2022). Supporting this hypothesis, SA was able to revert *in vitro*, and LF to prevent *in vivo* the induced neurite length in IUGR neurospheres. Whereas MEL and DHA could not improve the IUGR induced total neurite extension neither *in vitro* nor after prenatal treatment *in vivo*. For future applications in the clinical field it may be of high interest to develop a combined supplementation during pregnancy including DHA and/or MEL as protective agent against impaired oligodendrocyte differentiation (Kühne et al., 2022) and LF to prevent IUGR-induced alterations on neuronal development.

Data availability statement

The original contributions presented in the study are included in the article/Supplementary material, further inquiries can be directed to the corresponding author.

Ethics statement

The animal study was reviewed and approved by the Ethics Committee for Animal Experimentation (CEEa) of the University of Barcelona with the CEEa number OB 340/19 SJD and the Department of Environment and Housing of the Generalitat de Catalunya with the license number 11126. Date of approval 24/5/2021.

References

- Als, H., Duffy, F. H., McAnulty, G., Butler, S. C., Lightbody, L., Kosta, S., et al. (2012). NICAD improves brain function and structure in preterm infants with severe intrauterine growth restriction. *J. Perinatol.* 32, 797–803. doi: 10.1038/jp.2011.201
- Andersen, S. L. (2003). Trajectories of brain development: Point of vulnerability or window of opportunity? *Neurosci. Biobehav. Rev.* 27, 3–18. doi: 10.1016/S0149-7634(03)00005-8
- Barenys, M., Gassmann, K., Baksmeier, C., Heinz, S., Reverte, I., Schmuck, M., et al. (2017). Epigallocatechin gallate (EGCG) inhibits adhesion and migration of neural progenitor cells *in vitro*. *Arch. Toxicol.* 91, 827–837. doi: 10.1007/s00204-016-1709-8
- Barenys, M., Illa, M., Hofrichter, M., Loreiro, C., Pla, L., Klose, J., et al. (2021). Rabbit neurospheres as a novel *in vitro* tool for studying neurodevelopmental effects induced by intrauterine growth restriction. *Stem Cells Transl. Med.* 10, 209–221. doi: 10.1002/scrm.20-0223
- Bassan, H., Leider Trejo, L., Kariv, N., Bassan, M., Berger, E., Fattal, A., et al. (2000). Experimental intrauterine growth retardation alters renal development. *Pediatr. Nephrol.* 15, 192–195. doi: 10.1007/s004670000457
- Batalle, D., Eixarch, E., Figueras, F., Muñoz-Moreno, E., Bargallo, N., Illa, M., et al. (2012). Altered small-world topology of structural brain networks in infants with

Author contributions

BA, MB, and MI contributed to conception and design of the study. BA, LG-E, MB, and MI contributed to data analysis and interpretation of the data. BA, LG-V, ES, LP, and CL performed methodology, generated, and analysed data. EG contributed to resources and funding acquisition. MB and MI administrated and supervised the project. BA wrote the original draft of the manuscript. LG-E, MB, and MI critically revised and edited manuscript. All authors contributed to the article and approved the submitted version.

Funding

This study has been funded by Instituto de Salud Carlos III, PI18/01763 (Co-funded by European Regional Development Fund. ERDF, a way to build Europe) and the ASISA Foundation. BK received a scholarship from Fundació Bosch i Gimpera (project number: 300155).

Acknowledgments

Figure 1 was created with BioRender.com with the license number PY255AV1EQ. CL received the support the Health Department of the Catalan Government (grant no. SLT006/17/00325).

Conflict of interest

The authors declare that the research was conducted in the absence of any commercial or financial relationships that could be construed as a potential conflict of interest.

Publisher's note

All claims expressed in this article are solely those of the authors and do not necessarily represent those of their affiliated organizations, or those of the publisher, the editors and the reviewers. Any product that may be evaluated in this article, or claim that may be made by its manufacturer, is not guaranteed or endorsed by the publisher.

Supplementary material

The Supplementary material for this article can be found online at: <https://www.frontiersin.org/articles/10.3389/fncel.2023.1116405/full#supplementary-material>

intrauterine growth restriction and its association with later neurodevelopmental outcome. *NeuroImage* 60, 1352–1366. doi: 10.1016/j.neuroimage.2012.01.059

Batalle, D., Muñoz-Moreno, E., Arbat-Plana, A., Illa, M., Figueras, F., Eixarch, E., et al. (2014). Long-term reorganization of structural brain networks in a rabbit model of intrauterine growth restriction. *NeuroImage* 100, 24–38. doi: 10.1016/j.neuroimage.2014.05.065

Baumann, J., Gassmann, K., Masjosthusmann, S., DeBoer, D., Bendt, F., Giersiefer, S., et al. (2016). Comparative human and rat neurospheres reveal species differences in chemical effects on neurodevelopmental key events. *Arch. Toxicol.* 90, 1415–1427. doi: 10.1007/s00204-015-1568-8

Belvindrah, R., Graus-Porta, D., Goebels, S., Nave, K. A., and Müller, U. (2007). $\beta 1$ Integrins in radial glia but not in migrating neurons are essential for the formation of cell layers in the cerebral cortex. *J. Neurosci.* 27, 13854–13865. doi: 10.1523/JNEUROSCI.4494-07.2007

Binley, K. E., Ng, W. S., Tribble, J. R., Song, B., and Morgan, J. E. (2014). Sholl analysis: A quantitative comparison of semi-automated methods. *J. Neurosci. Methods* 225, 65–70. doi: 10.1016/j.jneumeth.2014.01.017

Bonfanti, L. (2006). PSA-NCAM in mammalian structural plasticity and neurogenesis. *Prog. Neurobiol.* 80, 129–164. doi: 10.1016/j.pneurobio.2006.08.003

Breier, J. M., Gassmann, K., Kayser, R., Stegeman, H., de Groot, D., Fritsche, E., et al. (2010). Neural progenitor cells as models for high-throughput screens of developmental neurotoxicity: State of the science. *Neurotoxicol. Teratol.* 32, 4–15. doi: 10.1016/j.ntt.2009.06.005

Burgess, A., et al. (2007). “Polysialic acid limits septal neurite outgrowth on laminin,” *Brain Research*, *Brain Research*, 1144, 52–58. doi: 10.1016/j.brainres.2007.01.072

Carter, A. M. (2007). Animal models of human placentation - a review. *Placenta* 28, S41–S47. doi: 10.1016/j.placenta.2006.11.002

Castillo-Melendez, M., Yawno, T., Sutherland, A., Jenkin, G., Wallace, E. M., and Miller, S. L. (2017). Effects of antenatal melatonin treatment on the cerebral vasculature in an ovine model of fetal growth restriction. *Dev. Neurosci.* 39, 323–337. doi: 10.1159/000471797

Coviello, S., Benedetti, B., Jakubecova, D., Belles, M., Klimczak, P., Gramuntell, Y., et al. (2021). Psa depletion induces the differentiation of immature neurons in the piriform cortex of adult mice. *Int. J. Mol. Sci.* 22:5733. doi: 10.3390/ijms22115733

Dach, K., Bendt, F., Huebenthal, U., Giersiefer, S., Lein, P. J., Heuer, H., et al. (2017). BDE-99 impairs differentiation of human and mouse NPCs into the oligodendroglial lineage by species-specific modes of action. *Sci. Rep.* 7, 1–11. doi: 10.1038/srep44861

Derrick, M., Luo, N. L., Bregman, J. C., Jilling, T., Ji, X., Fisher, K., et al. (2004). Preterm fetal hypoxia-ischemia causes hypertonia and motor deficits in the neonatal rabbit: A model for human cerebral palsy? *J. Neurosci.* 24, 24–34. doi: 10.1523/JNEUROSCI.2816-03.2004

Dieni, S., and Rees, S. (2003). Dendritic morphology is altered in hippocampal neurons following prenatal compromise. *J. Neurobiol.* 55, 41–52. doi: 10.1002/neu.10194

Eixarch, E., Batalle, D., Illa, M., Muñoz-Moreno, E., Arbat-Plana, A., Amat-Roldan, I., et al. (2012). Neonatal neurobehavior and diffusion MRI changes in brain reorganization due to intrauterine growth restriction in a rabbit model. *PLoS One* 7:e31497. doi: 10.1371/journal.pone.0031497

Eixarch, E., Figueras, F., Hernández-Andrade, E., Crispi, F., Nadal, A., Torre, I., et al. (2009). An experimental model of fetal growth restriction based on selective ligation of uteroplacental vessels in the pregnant rabbit. *Fetal Diagn. Ther.* 26, 203–211. doi: 10.1159/000264063

Eixarch, E., Hernandez-Andrade, E., Crispi, F., Illa, M., Torre, I., Figueras, F., et al. (2011). Impact on fetal mortality and cardiovascular Doppler of selective ligation of uteroplacental vessels compared with undernutrition in a rabbit model of intrauterine growth restriction. *Placenta* 32, 304–309. doi: 10.1016/j.placenta.2011.01.014

Eixarch, E., Muñoz-Moreno, E., Bargallo, N., Batalle, D., and Gratacos, E. (2016). Motor and cortico-striatal-thalamic connectivity alterations in intrauterine growth restriction. *Am. J. Obstet. Gynecol.* 214, 725.e1–725.e9. doi: 10.1016/j.ajog.2015.12.028

Esteban, F. J., Padilla, N., Sanz-Cortés, M., de Miras, J. R., Bargalló, N., Villoslada, P., et al. (2010). Fractal-dimension analysis detects cerebral changes in preterm infants with and without intrauterine growth restriction. *NeuroImage* 53, 1225–1232. doi: 10.1016/j.neuroimage.2010.07.019

Figueras, F., Caradeux, J., Crispi, F., Eixarch, E., Peguero, A., and Gratacos, E. (2018). Diagnosis and surveillance of late-onset fetal growth restriction. *Am. J. Obstet. Gynecol.* 218, S790–S802.e1. doi: 10.1016/j.ajog.2017.12.003

Figueras, F., and Gratacos, E. (2017). An integrated approach to fetal growth restriction. *Best Pract. Res. Clin. Obstet. Gynaecol.* 38, 48–58. doi: 10.1016/j.bpobgyn.2016.10.006

Förster, E., Tielsch, A., Saum, B., Weiss, K. H., Johanssen, C., Graus-Porta, D., et al. (2002). Reelin, disabled 1, and $\beta 1$ integrins are required for the formation of the radial glial scaffold in the hippocampus. *Proc. Natl. Acad. Sci. U. S. A.* 99, 13178–13183. doi: 10.1073/pnas.202035899

Gassmann, K., Abel, J., Bothe, H., Haarmann-Stemmann, T., Merk, H. F., Quasthoff, K. N., et al. (2010). Species-specific differential AhR expression protects human neural progenitor cells against developmental neurotoxicity of PAHs. *Environ. Health Perspect.* 118, 1571–1577. doi: 10.1289/ehp.0901545

Gassmann, K., Schreiber, T., Dingemans, M. M. L., Krause, G., Roderigo, C., Giersiefer, S., et al. (2014). BDE-47 and 6-OH-BDE-47 modulate calcium homeostasis in primary fetal human neural progenitor cells via ryanodine receptor-independent mechanisms. *Arch. Toxicol.* 88, 1537–1548. doi: 10.1007/s00204-014-1217-7

Gil-Sánchez, A., Larqué, E., Demmelmair, H., Acien, M. I., Faber, F. L., Parrilla, J. J., et al. (2010). Maternal-fetal in vivo transfer of [^{13}C]docosahexaenoic and other fatty acids across the human placenta 12 h after maternal oral intake. *Am. J. Clin. Nutr.* 92, 115–122. doi: 10.3945/ajcn.2010.29589

Graus-Porta, D., Blaess, S., Senften, M., Littlewood-Evans, A., Damsky, C., Huang, Z., et al. (2001). $\beta 1$ -class Integrins regulate the development of laminae and folia in the cerebral and cerebellar cortex. *Neuron* 31, 367–379. doi: 10.1016/S0896-6273(01)00374-9

Greenberg, J. A., Bell, S. J., and Ausdal, W. V. (2008). Omega-3 fatty acid supplementation during pregnancy. *Rev. Obstet. Gynecol.* 1, 162–169.

Hofrichter, M., Nimtz, L., Tigges, J., Kabiri, Y., Schröter, F., Royer-Pokora, B., et al. (2017). Comparative performance analysis of human iPSC-derived and primary neural progenitor cells (NPC) grown as neurospheres in vitro. *Stem Cell Res.* 25, 72–82. doi: 10.1016/j.scr.2017.10.013

Illa, M., Brito, V., Pla, L., Eixarch, E., Arbat-Plana, A., Batallé, D., et al. (2018). Early environmental enrichment enhances abnormal brain connectivity in a rabbit model of intrauterine growth restriction. *Fetal Diagn. Ther.* 44, 184–193. doi: 10.1159/000481171

Illa, M., Eixarch, E., Batalle, D., Arbat-Plana, A., Muñoz-Moreno, E., Figueras, F., et al. (2013). Long-term functional outcomes and correlation with regional brain connectivity by MRI diffusion Tractography metrics in a near-term rabbit model of intrauterine growth restriction. *PLoS One* 8:e76453. doi: 10.1371/journal.pone.0076453

Illa, M., Pla, L., Loreiro, C., Miranda, C., Mayol, M., Kühne, B. A., et al. (2023). Neonatal effects of maternal supplementation with docosahexaenoic acid and Lactoferrin on the fetal brain and placenta in a rabbit model of intrauterine growth restriction. *Obstet. Gynaecol. Res.* 6, 1–14. doi: 10.26502/ogr0108

Kady, S. M., and Gardosi, J. (2004). Perinatal mortality and fetal growth restriction. *Best Pract. Res. Clin. Obstet. Gynaecol.* 18, 397–410. doi: 10.1016/j.bpobgyn.2004.02.009

Kim, H.-T., Kim, I. S., Lee, I. S., Lee, J. P., Snyder, E. Y., and in Park, K. (2006). Human neurospheres derived from the fetal central nervous system are regionally and temporally specified but are not committed. *Exp. Neurol.* 199, 222–235. doi: 10.1016/j.expneurol.2006.03.015

Kühne, B. A., Puig, T., Ruiz-Martínez, S., Crous-Masó, J., Planas, M., Feliu, L., et al. (2019). Comparison of migration disturbance potency of epigallocatechin gallate (EGCG) synthetic analogs and EGCG PEGylated PLGA nanoparticles in rat neurospheres. *Food Chem. Toxicol.* 123, 195–204. doi: 10.1016/j.fct.2018.10.055

Kühne, B. A., Teixidó, E., Ettcheto, M., Puig, T., Planas, M., Feliu, L., et al. (2022). Application of the adverse outcome pathway to identify changes in prenatal brain programming after exposure to EGCG. *Food Chem. Toxicol.* 170:113506. doi: 10.1016/j.fct.2022.113506

Kühne, B. A., Vázquez-Aristizabal, P., Fuentes-Amell, M., Pla, L., Loreiro, C., Gómez-Catalán, J., et al. (2022). Docosahexaenoic acid and melatonin prevent impaired Oligodendrogenesis induced by intrauterine growth restriction (IUGR). *Biomedicine* 10:1205. doi: 10.3390/biomedicine10051205

Lauritzen, L., Brambilla, P., Mazzocchi, A., Harsløf, L. B., Ciappolino, V., and Agostoni, C. (2016). DHA effects in brain development and function. *Nutrients* 8, 1–17. doi: 10.3390/nu8010006

Lees, C. C., Romero, R., Stampalija, T., Dall'Asta, A., DeVore, G., Prefumo, F., et al. (2022). Clinical opinion: The diagnosis and management of suspected fetal growth restriction: an evidence-based approach. *Am. J. Obstet. Gynecol.* 226, 366–378. doi: 10.1016/j.ajog.2021.11.1357

Lopez, V., Kelleher, S. L., and Lönnnerdal, B. (2008). Lactoferrin receptor mediates apo-but not holo-lactoferrin internalization via clathrin-mediated endocytosis in trophoblasts. *Biochem. J.* 411, 271–278. doi: 10.1042/BJ20070393

Marrs, G. S., Honda, T., Fuller, L., Thangavel, R., Balsamo, J., Lilien, J., et al. (2006). Dendritic arbors of developing retinal ganglion cells are stabilized by $\beta 1$ -integrins. *Mol. Cell. Neurosci.* 32, 230–241. doi: 10.1016/j.mcn.2006.04.005

Masjosthusmann, S., Siebert, C., Huebenthal, U., Bendt, F., Baumann, J., and Fritsche, E. (2019). Arsenite interrupts neurodevelopmental processes of human and rat neural progenitor cells: the role of reactive oxygen species and species-specific antioxidative defense. *Chemosphere* 235, 447–456. doi: 10.1016/j.chemosphere.2019.06.123

McKinstry, R. C., Mathur, A., Miller, J. H., Ozcan, A., Snyder, A. Z., Scheff, G. L., et al. (2002). Radial organization of developing preterm human cerebral cortex revealed by non-invasive water diffusion anisotropy MRI. *Cereb. Cortex* 12, 1237–1243. doi: 10.1093/cercor/12.12.1237

Miller, S. L., Yawno, T., Alers, N. O., Castillo-Melendez, M., Supramaniam, V. G., VanZyl, N., et al. (2014). Antenatal antioxidant treatment with melatonin to decrease newborn neurodevelopmental deficits and brain injury caused by fetal growth restriction. *J. Pineal Res.* 56, 283–294. doi: 10.1111/jpi.12121

Moors, M., Cline, J., Abel, J., and Fritsche, E. (2007). ERK-dependent and -independent pathways trigger human neural progenitor cell migration. *Toxicol. Appl. Pharmacol.* 221, 57–67. doi: 10.1016/j.taap.2007.02.018

Moors, M., Rockel, T. D., Abel, J., Cline, J. E., Gassmann, K., Schreiber, T., et al. (2009). Human neurospheres as three-dimensional cellular systems for developmental

- neurotoxicity testing. *Environ. Health Perspect.* 117, 1131–1138. doi: 10.1289/ehp.0800207
- Moresco, E. M. Y., Donaldson, S., Williamson, A., and Koleske, A. J. (2005). Integrin-mediated dendrite branch maintenance requires Abelson (Abl) family kinases. *J. Neurosci.* 25, 6105–6118. doi: 10.1523/JNEUROSCI.1432-05.2005
- Mwaniki, M. K., Atieno, M., Lawn, J. E., and Newton, C. R. J. C. (2012). Long-term neurodevelopmental outcomes after intrauterine and neonatal insults: A systematic review. *Lancet* 379, 445–452. doi: 10.1016/S0140-6736(11)61577-8
- Nimtzt, L., Hartmann, J., Tigges, J., Masjosthusmann, S., Schmuck, M., Keßel, E., et al. (2020). Characterization and application of electrically active neuronal networks established from human induced pluripotent stem cell-derived neural progenitor cells for neurotoxicity evaluation. *Stem Cell Res.* 45:101761. doi: 10.1016/j.scr.2020.101761
- Ortiz-Romero, P., Borralleras, C., Bosch-Morató, M., Guivernau, B., Albericio, G., Muñoz, F. J., et al. (2018). Epigallocatechin-3-gallate improves cardiac hypertrophy and short-term memory deficits in a Williams-Beuren syndrome mouse model. *PLoS One* 13:e0194476. doi: 10.1371/journal.pone.0194476
- Piorkowska, K., Thompson, J., Nygard, K., Matuszewski, B., Hammond, R., and Richardson, B. (2014). Synaptic development and neuronal myelination are altered with growth restriction in fetal Guinea pigs. *Dev. Neurosci.* 36, 465–476. doi: 10.1159/000363696
- Pla, L., Illa, M., Loreiro, C., Lopez, M. C., Vázquez-Aristizabal, P., Kühne, B. A., et al. (2020). Structural brain changes during the neonatal period in a rabbit model of intrauterine growth restriction. *Dev. Neurosci.* 42, 217–229. doi: 10.1159/000512948
- Pla, L., Kühne, B. A., Guardia-Escote, L., Vázquez-Aristizabal, P., Loreiro, C., Flick, B., et al. (2022). Protocols for the evaluation of neurodevelopmental alterations in rabbit models in vitro and in vivo. *Front. Toxicol.* 4:918520. doi: 10.3389/ftox.2022.918520
- Rao, M., Hediger, M. L., Levine, R. J., Naficy, A. B., and Vik, T. (2007). Effect of breastfeeding on cognitive development of infants born small for gestational age. *Acta Paediatr.* 91, 267–274. doi: 10.1111/j.1651-2227.2002.tb01713.x
- Rees, S., Harding, R., and Walker, D. (2011). The biological basis of injury and neuroprotection in the fetal and neonatal brain. *Int. J. Dev. Neurosci.* 29, 551–563. doi: 10.1016/j.ijdevneu.2011.04.004
- Reid, M. V., Murray, K. A., Marsh, E. D., Golden, J. A., Simmons, R. A., and Grinspan, J. B. (2012). Delayed myelination in an intrauterine growth retardation model is mediated by oxidative stress upregulating bone morphogenetic protein 4. *J. Neuropathol. Exp. Neurol.* 71, 640–653. doi: 10.1097/NEN.0b013e31825cfa81
- Rideau Batista Novais, A., Pham, H., van de Looij, Y., Bernal, M., Mairesse, J., Zana-Taieb, E., et al. (2016). Transcriptomic regulations in Oligodendroglial and microglial cells related to brain damage following fetal growth restriction. *Glia* 64, 2306–2320. doi: 10.1002/glia.2307
- Schreiber, T., Gassmann, K., Götz, C., Hübenthal, U., Moors, M., Krause, G., et al. (2010). Polybrominated diphenyl ethers induce developmental neurotoxicity in a human in vitro model: Evidence for endocrine disruption. *Environ. Health Perspect.* 118, 572–578. doi: 10.1289/ehp.0901435
- Sharma, D., Shastri, S., and Sharma, P. (2016). Intrauterine growth restriction: Antenatal and postnatal aspects. *Clin. Med. Insights Pediatr.* 10, 67–83. doi: 10.4137/CMPed.S40070
- Tolcos, M., Bateman, E., O'Dowd, R., Markwick, R., Vrijnsen, K., Rehn, A., et al. (2011). Intrauterine growth restriction affects the maturation of myelin. *Exp. Neurol.* 232, 53–65. doi: 10.1016/j.expneurol.2011.08.002
- van de Looij, Y., Ginet, V., Chatagner, A., Toulotte, A., Somm, E., Hüppi, P. S., et al. (2014). Lactoferrin during lactation protects the immature hypoxic-ischemic rat brain. *Ann. Clin. Transl. Neurol.* 1, 955–967. doi: 10.1002/acn3.138
- Wang, B. (2016). Molecular determinants of milk Lactoferrin as a bioactive compound in early neurodevelopment and cognition. *J. Pediatr.* 173, S29–S36. doi: 10.1016/j.jpeds.2016.02.073
- Warren, M. S., Bradley, W. D., Gourley, S. L., Lin, Y. C., Simpson, M. A., Reichardt, L. F., et al. (2012). Integrin $\beta 1$ signals through Arg to regulate postnatal dendritic arborization, synapse density, and behavior. *J. Neurosci.* 32, 2824–2834. doi: 10.1523/JNEUROSCI.3942-11.2012
- Weinhold, B., Seidenfaden, R., Röckle, I., Mühlenhoff, M., Schertzinger, F., Conzelmann, S., et al. (2005). Genetic ablation of polysialic acid causes severe neurodevelopmental defects rescued by deletion of the neural cell adhesion molecule. *J. Biol. Chem.* 280, 42971–42977. doi: 10.1074/jbc.M511097200
- Workman, A. D., Charvet, C. J., Clancy, B., Darlington, R. B., and Finlay, B. L. (2013). Modeling transformations of neurodevelopmental sequences across mammalian species. *J. Neurosci.* 33, 7368–7383. doi: 10.1523/JNEUROSCI.5746-12.2013

Glossary

CEEA	Ethics Committee for Animal Experimentation
DHA	docosahexaenoic acid
ECM	extracellular matrix
EGF	epidermal growth factor
FA	fractional anisotropy
FCS	fetal calf serum
FGF	fibroblast growth factor
FGR	Fetal Growth Restriction
GD	gestational day
GM	grey matter
IUGR	intrauterine growth restriction
LF	lactoferrin
MEL	melatonin
MTC	maximum tolerated concentration
NCAM	neural cell adhesion molecule
NPCs	neuronal progenitor cells
PDL	poly-D-lysine
PND	postnatal day
ROCK	Rho kinase inhibitor Y-276322
SA	sialic acid
SC	solvent control
WM	white matter

Frontiers in Aging Neuroscience

Explores the mechanisms of central nervous system aging and age-related neural disease

The third most-cited journal in the field of geriatrics and gerontology, with a focus on understanding the mechanistic processes associated with central nervous system aging.

Discover the latest Research Topics

[See more →](#)

Frontiers

Avenue du Tribunal-Fédéral 34
1005 Lausanne, Switzerland
frontiersin.org

Contact us

+41 (0)21 510 17 00
frontiersin.org/about/contact

